Chapter 10: Linking global to regional climate change

Coordinating Lead Authors:
Francisco J. Doblas-Reyes (Spain), Anna Amelia Sörensson (Argentina)

Lead Authors:
Mansour Almazroui (Saudi Arabia), Alessandro Dosio (Italy), William Gutowski (USA), Rein Haarsma (Netherlands), Rafiq Hamdi (Belgium), Bruce Hewitson (South Africa), Won-Tae Kwon (Republic of Korea), Benjamin Lamptey (Niger/Ghana), Douglas Maraun (Austria/Germany), Tannecia Stephenson (Jamaica), Izuru Takayabu (Japan), Laurent Terray (France), Andrew Turner (UK), Zhiyan Zuo (China)

Contributing Authors:
Muhammad Adnan (Pakistan), Muhammad Amjad (Pakistan), Bodo Ahrens (Germany), Farooq Azam (India), Ségolène Berthou (United Kingdom), Melissa Bukovsky (USA), Alex Cannon (Canada), Ana Casanueva (Spain), Marie-Estelle Demory (Switzerland), Leandro Díaz (Argentina), Hervé Douville (France), Sergio Henrique Faria (Spain/Brazil), Laura Gallardo (Chile), Subimal Ghost (India), Nathan Gillett (Canada), Hugues Goose (Belgium), José M. Gutiérrez (Spain), Pandora Hope (Australia), Akm Saiful Islam (Bangladesh), Christopher Jack (South Africa), Martin Jury (Austria/Spain), Gerhard Krinner (France), Asif Khan (Pakistan), Hiroyuki Kusaka (Japan), Stefan Lange (Germany), Flavio Lehner (Switzerland), Fei Liu (China), Dirk Notz (Germany), Carlos Pérez García-Pando (Spain), Jan Polcher (France/Germany), Krishnan Ravaghavan (India), Ingo Richter (Japan/Germany), Ramiro Saurral (Argentina), Reinhard Schiemann (United Kingdom/Germany), Sonia Seneviratne (Switzerland), Ted Shepherd (United Kingdom), Jana Sillmann (Norway/Germany), Didier Swingedouw (France), Victor Venema (Germany), Piotr Wolski (South Africa), Cunde Xiao (China), Jakob Zscheischler (Switzerland)

Review Editors:
Greg Flato (Canada), Fredolin Tangang (Malaysia), Muhammad Irfan Tariq (Pakistan)

Chapter Scientist:
Martin Jury (Spain/Austria)

Date of Draft:
01/03/2020

Notes:
TSU compiled version

Executive Summary

The AR5, SR1.5, SROCC and SRLCC reports underlined the urgent need for regional climate information that is useful and relevant to the decision scale. To help fill this gap, Chapter 10 assesses the foundations of how to move from global information to the regional scales of societal need. The AR6 thus provides foundational knowledge of key factors that frame the formulation, interpretation and application of regional messages of change. This chapter assesses the key foundations for the generation of regional climate change messages with methodologies that are employed in Chapters 11, 12 and the Atlas. This chapter adds to Chapter 2 on the challenges and requirements associated with observations for constructing messages on a regional scale as compared to the global scale. The fitness of different modelling tools in different regional contexts is assessed, starting from the methodologies used at global scale in Chapters 3 and 4. Chapter 3 assesses the human influence on the climate system on a global scale, while in this chapter methodologies of attribution of regional climate change are assessed. Note that regional climate change, which ultimately is the change experienced at each location and the change that society needs to adapt to, is different from the global climate change attributable to human activities assessed in Chapter 3. Regional climate change can also be due to natural internal processes such as atmospheric internal variability and regional climate response to changes in large-scale phenomena and to other external forcings than those related to human activity, such as modulations of the solar cycle, orbital forcing or volcanic eruptions. Additional approaches for messaging assessed in this chapter are the interaction between different actors in the co-production process, the relevance of the context and values, the use of storylines as a tool to convey information, and the distillation process using multiple lines of evidence necessary to produce climate information and messages.

Observations and models as sources of regional information

To increase confidence in future projections of regional climate, there is *high confidence* that multiple sources of observations and tailored diagnostics are needed to evaluate climate model performance. There is *very high confidence* that the availability of multiple observational records at regional scale is fundamental for assessing climate model performance {Section 10.2.2}. There is *high confidence* that complex, multi-variate and process-oriented diagnostics are needed to evaluate whether a climate model realistically simulates required aspects of present-day regional climate, and to increase confidence of future projections of these aspects {Section 10.3.3}.

Observational records for mountainous regions, data sparse regions and cities cause difficulties that pose limits to the assessment of regional climate change. There is *very high confidence* that precipitation measurements, especially of solid precipitation, in mountainous areas are strongly affected by the gauge location and setup. There is *high confidence* on elevation-dependant warming in most of the mountain ranges but field measurements are extremely limited at high elevations {Cross-Chapter-Box 10.3; Section 10.2.2}. It is *virtually certain* that the scarcity and decline of observations (e.g., in southern Mediterranean, Africa, or India) increase the uncertainty of long-term temperature and precipitation estimates {Section 10.2.2, Sections 10.6.2-3-4}. Gridded products of temperature and precipitation are strongly affected by interpolation methods over complex orography and data scarce regions such as the southern Mediterranean {Section 10.2.2, Section 10.6.4}. It is *virtually certain* that uncertainties related to long-term warming estimates at regional scale are reduced using statistical homogenization methods {Section 10.2.2}.

Reducing errors in the model formulations of global climate models is fundamental for improving both global climate model performance at the regional scale and the boundary conditions for dynamical downscaling. There is *very high confidence* that, in spite of these errors, global climate models are an important source of future climate information at the regional scale. There is *medium confidence* that increasing global climate model resolution helps reducing systematic errors, although there is *high confidence* that higher resolution *per se* does not solve all performance limitations. {Section 10.3.3}

Including all relevant forcings in regional climate models, including aerosols, land-use change and ozone concentrations is a prerequisite for reproducing historical trends and to ensure fitness for

purpose for future projections in certain regions (*medium confidence*) {Section 10.3.3, Section 10.4.1, Box 10.2}.

Dynamical downscaling using regional climate models adds value in representing many regional weather and climate phenomena, in particular over complex terrain (*very high confidence*), in spite of errors in model formulation that affects performance. Simulations at kilometre-scale resolution add value to the representation of convection (*high confidence*) and many local-scale phenomena such as land-sea breezes and influences of soil-moisture (*medium confidence*), which are, in turn, relevant for triggering convection. {Section 10.3.3}

Statistical downscaling methods with carefully chosen predictors and an appropriate model structure for a given application realistically represent many characteristics of present-day daily temperature and precipitation (*high confidence*), and plausibly simulate future changes in daily mean temperature (*medium confidence*). There is, however, a lack of research about which predictors are required for plausibly simulating future daily precipitation. Statistical downscaling of spatial fields remains a challenge, especially for daily precipitation. {Section 10.3.3}

Bias adjustment has proven beneficial as an interface between climate model projections and impact modelling, yet it cannot correct for unresolved or fundamentally misrepresented processes that lead to model errors (*high confidence*). Applying bias adjustment to models that substantially misrepresent relevant physical processes leads to severe problems (*medium confidence*). Using bias adjustment as statistical downscaling, in particular of coarse-resolution GCMs, may lead to substantial misrepresentations of regional climate and climate change (*medium confidence*). Instead, dynamical downscaling may be required to resolve relevant local processes prior to bias adjustment. {Section 10.3.3, Cross-Chapter Box 10.2}

At the regional scale, multi-model mean and ensemble spread are not sufficient to characterise low-probability high-impact changes or situations where different models simulate substantially different or even opposite changes (*high confidence*). Storyline approaches are a complementary instrument to aid the representation of climate projection uncertainties. Multi-model ensembles, while excluding models that simulate processes relevant for a given purpose unrealistically, are required to assess regional climate response uncertainty (*very high confidence*), although model spread is in general not a full measure of projection uncertainty. Grand ensembles of many realisations of internal variability are required to separate internal variability from forced changes (*high confidence*). In the construction of global/regional climate model ensembles, computational costs can be reduced by selecting a small number of global/regional climate model combinations such that climate response uncertainty is spanned as comprehensively as possible. {Section 10.3.4}

There is *very high confidence* that all types of urban parameterizations simulate radiation exchanges in a realistic way; they have, however, strong biases when simulating latent heat fluxes. Networks of monitoring stations in urban areas provide key information to enhance the understanding of urban microclimates and their interaction with climate change. A simple single-layer parameterization is sufficient for urban climate modelling focusing on the urban heat island and its interaction with regional climate change (*low confidence*). {Box 10.2}

Attribution of climate changes on regional scales

Anthropogenic forcing has been a major driver of temperature change since 1950 in many sub-continental regions of the world (*high confidence*). {Section 10.4.1}

Anthropogenic forcing has contributed to multi-decadal precipitation changes in several regions (*medium confidence*). Large observational uncertainty and internal variability as well as model errors lead to low confidence with regard to a well-constrained quantification (best estimate and confidence interval) of the total anthropogenic contribution to precipitation changes as well as the relative contributions of greenhouse gases, including ozone, and different aerosol species. {Section 10.4.1}

Based on detection and attribution studies and climate projections from multi-model initial-condition large ensembles, temperature change due to anthropogenic forcing will be the dominant factor to future multi-decadal temperature trends in most land regions of the world under the high-end (SSP5-8.5 and RCP8.5) GHG emission scenarios (*high confidence*) {Section 10.4.2}.

Based on multi-model historical simulations, regional-scale attribution studies and climate projections, in particular those coming from initial-condition large ensembles, it is *very likely* that internal variability will still significantly influence future multi-decadal precipitation trends in many land regions (except Antarctica, Section 9.4.2) until at least the mid-21st century {10.4.2}.

The global annual mean surface-air temperature response to urbanization is negligible (*high confidence*). However, in cities and their surroundings, the observed warming trend can partly be attributed to historical urbanization in rapidly industrialized countries (*very high confidence*). There is *very high confidence* that annual-mean maximum temperature is less affected than annual-mean minimum temperature by historical urbanization. {Box 10.2}

Co-production and distillation of regional climate information and messages

There is *high confidence* that involving diverse expertise from climate scientists and decision makers in the production of regional climate information results in better integration of scientific evidence into decision making. There is *high confidence* that regional climate-change messages are influenced by the values of those constructing, communicating, and receiving the message. There is *high confidence* that including users ensures the correct context in forming the message. {Section 10.5}

There is *high confidence* that distilling climate messages derived from multiple, potentially contrasting, lines of evidence such as observed, palaeoclimate proxy and simulated data, theoretical understanding, diverse analysis methods and expert judgment increases confidence in regional climate change messages {Section 10.5.4, Section 10.6}. Three examples of the distillation process are described next.

A message of a drier future in the Cape Town region will gain confidence by a distillation process that shows agreement among several lines of evidence: the projected precipitation by both global and regional climate models of different spatial resolutions, and the observed and projected changes of circulation patterns consistent with drier conditions. However, the distillation is limited by a lack of information about certain physical relationships, such as whether or not a relationship between Cape Town precipitation and large-scale circulation processes also occurs over longer historical periods than only the post-1979 decades, and how compensating changes in greenhouse gases and Antarctic ozone will influence circulation changes over the twenty-first century. {Section 10.6.2}

The contrast between long-term future increases in Indian monsoon rainfall and declining rainfall in the observational record can be explained using multiple lines of evidence. The observational record and future projections are not contradictory since the trends are attributed to different mechanisms (aerosols and greenhouse gases, respectively). The long-term future changes are generally consistent across global (including at high resolution) and regional climate models, and supported by theoretical arguments; furthermore, while there are subtle differences found in palaeoclimate analogues of the future climate (the mid-Holocene), different physical mechanisms at play suggest that palaeoclimate evidence does not reduce confidence in the future projections. {Section 10.6.3}

The distillation of several lines of evidence provides confidence in Mediterranean warming exceeding Northern Hemisphere mean warming. The lines of evidence include the projected temperature by global and regional climate models, agreement between observational records and understanding of mechanisms. The mechanisms include dynamic and thermodynamic processes and the impact of aerosols.

Despite the robust information of enhanced Mediterranean warming, uncertainties about future amplitude and regional distribution due to differences between the models about the relative contribution of those mechanisms remain. The yet unresolved discrepancy between the warming in the CMIP5 and CMIP6 experiments is an example of this uncertainty, which highlights the need for further investigation and distillation of all available evidence. {Section 10.6.4}

10.1 Foundations for regional climate messages

10.1.1 Preamble

Regional climate is determined by a complex interplay of global external forcings, large-scale internal modes of climate variability and teleconnections, as well as regional-scale climate processes, feedbacks and forcings. Depending on the specific context, regional climates may refer to large areas such as a monsoon region, but they may also be confined to smaller areas such as a coastline, a mountain range or a human settlement like a city. Users (understood as anyone incorporating climate information into their activity) often request climate information to a provider from within this range of scales since regional operating and adaptation decision scales range from the local to the sub-continental level. Hence, the term region is used in this chapter to indicate the range of scales of relevance for impact and adaptation without prescribing any formal regional boundaries.

Given the large number of types of regional climates and the broad range of regional scales, a variety of methodologies and approaches have been developed to construct climate change information for regions. The sources include global (GCM) and regional (RCM) climate models, statistical downscaling and bias adjustment methods, among many others. Regional observations likewise play a key role in the regional climate information formulation process. High quality observations, that allow monitoring the regional aspects of climate, are used to adjust inherent model biases, and are the basis for assessing model performance. Climate information also requires attributing observed changes to large- and regional-scale anthropogenic and natural drivers and forcings. A commonly used source is made of model-based long-term projections of regional climate change, as well as climate simulations for the near-term, understood as the next 30 years (Kushnir et al., 2019; Rössler et al., 2019a).

All these sources, observations and model-based data, are used to distil contextualised regional climate information from multiple evidences (Figure 10.1). This climate information is then further distilled in a co-production process involving the user and the producer resulting in a regional climate message. The distillation process leading to the message considers the specific context of the question at stake, the values of both the user and the producer, and the challenge of communicating across different communities (Figure 10.1).

The main objective of this chapter is to assess the key foundations for the generation of messages about regional climate change. This objective has been partly addressed in previous IPCC reports (Box 10.1), but this chapter assesses the way the regional climate change problem is dealt with from a more methodological point of view. The chapter is closely linked to three other chapters (11, 12 and Atlas), which comprehensively assess regional climate change information, as well as to the chapters that assess global-to-continental scale climate information (2, 3, 4, 6 and 8).

The chapter starts with an introduction of concepts and sources for the generation of regional climate messages (Section 10.1). Section 10.2 addresses the aspects associated with the access to and use of observations in the construction of regional climate information. The different modelling approaches available to construct regional information are introduced and assessed in Section 10.3, which also addresses the performance of models in simulating relevant climate phenomena to estimate the credibility of future projections. Section 10.4 assesses the causes of selected recent climate changes to illustrate the complex interplay of processes shaping regional climate change. Section 10.5 tackles how messages of regional climate are distilled from different sources of information taking into account the context and the values of both the producer and the societal actors to whom messages are destined. Section 10.6 illustrates how the distillation approach to construct regional climate change information and messages works using three case studies. Finally, Section 10.7 lists a number of topics identified as limit to this assessment.

[START FIGURE 10.1 HERE]

Figure 10.1: Simplified view of the construction of a regional climate message including sources, context, values and storylines, with the processes that lead to the distillation of the message. The chapters and sections where the elements entering the message construction can be found are indicated.

[END FIGURE 10.1 HERE]

10.1.2 Space and time scales and uncertainty treatment

The global coupled atmosphere-ocean-land-cryosphere system, including its feedbacks, shows variability over a wide spectrum of temporal and spatial scales (Hurrell et al., 2009). This section discusses concepts and definitions with respect to what can be considered a region, the relevant time scales for regional climate information and region-specific aspects of the baselines used. The section also introduces the sources of uncertainty in model-derived regional climate information and how the quantification of the uncertainties impacts the confidence of the climate information and message.

There is increasing recognition that the evolutions of the weather and climate are linked to the same physical processes in the coupled Earth system operating across multiple space and time scales (outlined in Figure 10.2). The concept of a unified and seamless framework for weather and climate prediction (Brown et al., 2012a; Hoskins, 2013) provides the context for understanding and simulating regional climate across multiple space and time scales. This benefits from the convergence of the methods traditionally used in the two fields, in particular with regard to the initialization of the climate system and towards maximizing the predictability evident at different time scales. Furthermore, there is evidence that errors inherent in the mean climate simulation in GCMs originate within a few days in simulations initialized with the observed state of the climate system (Martin et al., 2010; Cavallo et al., 2016; Sexton et al., 2019). Process interaction in space is pervasive, which means that small spatial scales have an impact on the larger scales. Global and regional models that resolve ocean mesoscale or atmospheric convection processes help understand these multiscale interactions in the climate system (Section 10.3.1). They help identify the processes of greatest importance for the region of interest, and documenting their upscale effects on climate (Hurrell et al., 2006; Allen et al., 2018) (Section 10.3.3).

[START FIGURE 10.2 HERE]

Figure 10.2: Schematic diagram derived from the inventive way of (Orlanski, 1975) displaying relevant interacting space and time scales to regional climate change information. Also indicated are the processes included in the different models and model components considered in Chapter 10 as a function of time and space scales. This figure is a companion of Figure 1.14 in Chapter 1 where the region sets adopted in the report are illustrated as a function of time and space scales.

[END FIGURE 10.2 HERE]

10.1.2.1 Definition of regions

Although climate change is a global phenomenon, its manifestations and consequences are different in different regions. Regional climate is not only controlled by large-scale forcings like greenhouse gases (GHGs), solar radiation, or volcanic aerosols, and processes like the atmospheric general circulation or large-scale oceanic modes of variability, but also by regional and local forcings, such as some natural and anthropogenic aerosols or land use and the associated complex multiscale interactions. Section 10.3 discusses several of these regional processes and their relevance to the models used to generate climate information, while Section 10.4 offers some examples of their expression on some regional climate.

The definition of the regional scale is ambiguous. Chapter 1 provides definitions of the different regional types adopted in the report using the same frame of multiscale processes as those illustrated in Figure 10.2. Among those processes, large-scale climate and phenomena have been defined in Chapter 2 (Cross-Chapter Box 2.1) as ranging from global and hemispheric, to ocean basin and continental. In this chapter, regional scales are defined as those from the sub-continental areas (e.g., the Mediterranean basin) to local scales (e.g., human settlements such as megacities) without prescribing any formal regional boundaries. The relevant driving modes and processes at the regional scale are summarized in Figure 10.2. An example of the relevance of regional scales interacting with each other is offered for the polar-mid-latitude regions in the Cross-Chapter Box 10.1.

To accomplish one of the chapter objectives of assessing the methodologies for producing climate change information on a regional scale and its attribution to a range of drivers, these methodologies are applied on a large variety of examples of regions. These examples are considered representative of specific regions spanning almost all continents (except the Antarctic) and represent regions with very different spatial extension (Figure 10.3).

[START FIGURE 10.3 HERE]

Figure 10.3: Regions used in the chapter. The regions for Section 10.4, illustrative regional attribution examples are in blue: Caribbean small islands, central and eastern Eurasia, East Asia, western Europe, south-western Australia, south-eastern South America, Sahel/West African monsoon region, and south-western North America (AR6 region SWN). The regions for Section 10.6, the comprehensive case studies of constructing regional climate messages, are in black: Cape Town, Mediterranean and South Asian monsoon. The urban areas used in Box 10.2 (urban climate) and the region used in Cross-Chapter Box 10.3 (Hindu-Kush Himalayan climate) are in red and orange, respectively.

[END FIGURE 10.3 HERE]

10.1.2.2 Scales in time and baselines

Climate variability is observed on a continuum from weather to climate time scales, as reflected in the current initiatives across time scales like the subseasonal-to-seasonal (Vitart et al., 2017) and the seasonal-to-multiannual (Smith et al., 2012) predictions. Climate variability emerges from the weather time scale as a combination of slow internal climate processes and external forcings. The relatively short observational time record (Section 10.2) is a primary challenge to estimate the forced signal and to isolate low-frequency, multi-decadal and longer term internal variability (Frankcombe et al., 2015; Overland et al., 2016; Bathiany et al., 2018). Besides, only one realization of internal variability is available for the actual climate and it is nontrivial to extract estimates of its characteristics from the available data (Frankcombe et al., 2015). However approaches that use large observational ensembles produced from models have been alternatively applied (Section 10.4; McKinnon and Deser, 2018).

There is a close relationship between spatial and time scales. New et al. (2001) suggested that larger spatial variations generally occur at longer time scales and are associated with correspondingly large-scale phenomena in the climate system (Figure 10.2). For example, an individual convective storm may exhibit scales of variability from metres and seconds to kilometres and hours, while for El Niño-Southern Oscillation (ENSO) the scales of variability are regional to hemispheric in extent and multi-year in length. Munoz et al. (2015) used extreme rainfall characteristics (i.e., frequency, intensity and location) to highlight that different climate drivers with different spatial and time scales interact with each other. Climate models consider this integrated approach, although their present ability to simulate regional phenomena and even represent large-scale climate drivers still leaves room for improvement (Section 10.3).

Due to the large range of drivers of variability and change (Figure 10.2), quantifying the interplay between internal modes of decadal variability and any externally forced component is crucial in attempts to attribute regional climate changes (e.g., Hoell et al., 2017; Nath et al., 2018). A climate signal could arise purely due to some anthropogenic influence or conversely, entirely due to internal variability, but it is most likely the result of a combination of the two (Section 10.4). The interplay of internal and forced variability of different time scales is particularly relevant to near-term climate prediction, which aims at predicting the phase of the multi-annual variability in the context of changing external factors (Kushnir et al., 2019).

The time characteristics of climate variability has implications for regional impacts (Bathiany et al., 2018). This is true not only because a longer event accumulates more impacts, but also because it can have impacts greater than the sum of its parts. For instance, a long heat wave can have greater impacts on human mortality than the sum of individual hot days (Gasparrini and Armstrong, 2012), while the compounding effect of the three-year drought experienced in Syria commencing in 2006 has been considered to exacerbate water and agricultural insecurity, failure of agricultural systems and widespread migration (Kelley et al., 2015).

It is important to note that in this chapter and subsequent ones the baselines or reference periods used for presentation of climate change may vary from those used in Chapters 1–9 (Section 1.4.1, Cross-Chapter Box 1.2). In those chapters three main time baselines are defined for the past, i.e., pre-industrial (1750), early-industrial (1850–1900) and recent (1995–2014), while the future baseline periods are 2021–2040 (near term), 2041–2060 (mid-century) and 2081–2100 (long term). This choice also poses some difficulties because this chapter assesses results obtained from both GCM and RCM simulations, which often use different baselines. Regional simulations described in the recent literature have been performed using different baselines determined by the availability of the boundary conditions from global simulations such as 1950–2005 for CMIP5 historical and 2006-2100 for CMIP5 future scenarios (Vaittinada Ayar et al., 2016; Dong-feng et al., 2017; Cai et al., 2018), and for older scenarios other periods have been used. These are different from the baselines used in the CMIP6 exercise (Chapter 3). The mismatch needs to be taken into account when assessing results obtained from both RCMs and GCMs in the context of the climate information distillation process, or when linking the results of this chapter to the assessments performed in previous chapters. The choice of baseline provides another source of uncertainty for the use of climate information for climate impacts (e.g., for the response of bird species in Africa; Baker et al., 2016). This also highlights the need to consider a range of different baselines to satisfy the requirements of the variety of users, because the choice of a baseline directly affects the perceived result in impacts studies (Dobor and Hlásny, 2018), as illustrated in Sections 10.4 and 10.6. One way of overcoming the baseline uncertainty is to define the historical reference period for a given model based on a fixed global-mean temperature change from the pre-industrial period (e.g., Sylla et al., 2018a for West Africa; Kjellström et al., 2018 for Europe; Taylor et al., 2018 for the Caribbean; Montroull et al., 2018 for South America).

10.1.2.3 Uncertainty and confidence

Uncertainty and confidence in messages of regional climate change are not different in nature to the way they are used in larger-scale (continental and global) climate problems (Chapter 1). The degree of confidence in climate simulations and in the resulting climate information and message typically depends on the quantification of all the uncertainties associated with the specific set of simulations used as well as with the performance assessment of these simulations. Since the direct verification of simulations of future climate changes is not possible, model performance and reliable (i.e., trustworthy) uncertainty estimates need to be assessed indirectly through process understanding and a systematic comparison with observations of past and current climate (Section 10.3.3; Eyring et al., 2019; Knutti et al., 2010). The uncertainty of the observations also has to be taken into account in this assessment (Section 10.2). These uncertainty estimates are then propagated in the distillation process that uses climate data, among other sources, to generate climate information (Smith and Matthews, 2015).

Uncertainties in model-based future regional climate information arise from different sources and are introduced at various stages in the process (Lehner et al., submitted): 1) forcing uncertainties associated with the future scenario or pathway that is assumed, 2) internal variability sampled by a range of initial conditions, either generated by the model itself (Hawkins et al., 2016; Deser et al., submitted) or as close to the observations as possible (as done in near-term climate prediction), and 3) uncertainties related to imperfections in climate models, also referred to as structural uncertainty. However, the relative role of each one of these sources of uncertainty differs between the global and the regional scales as well as between variables and also between different regions (Lehner et al., submitted). The model uncertainty is among the largest contributors to the uncertainty cascade at the regional scale and arises from limited theoretical understanding, uncertainty in model parameters, structural model uncertainty, and even the inability to accurately describe known processes (McNeall et al., 2016). Additionally, new approaches to estimate the internal variability, like the availability of large ensembles of historical simulations and projections, have illustrated how important it is to obtain reliable estimates of regional climate projections that fully take into account all the variability sources (Dai and Bloecker, 2018; Deser et al., submitted). Specific elements in regional climate information, like the inconsistency between the GCM and RCM physics and dynamics or the observational uncertainty in bias-adjustment methods, also play a role in the uncertainty cascade (Sørland et al., 2018). All these elements affect the overall confidence in regional climate messages with respect to the typical uncertainty level of phenomena and indicators at global scales (Chapters 1–9).

One way to address the internal and structural uncertainties in climate information is to consider results from both multiple models and multiple realizations of the same model (Section 10.3.1; Díaz et al., submitted; Eyring et al., 2016a; Lehner et al., submitted). An implicit assumption is that multiple models provide additional and more reliable information than a single model and that higher confidence could be placed on results that are common to an ensemble, although in principle all models could suffer from similar deficiencies leading to an excess of confidence in some results. This illustrates the relevance of considering the independence of the models contributing to create the climate message, because when the independence of the elements in the multi-model ensemble is reduced, the likelihood of incorrectly sampling the uncertainty grows (Boé, 2018). This problem also strongly affects the decisions on weighting different models in a multi-model ensemble according to their performance to better represent uncertainty (Section 10.3.3; Abramowitz et al., 2018). The complex scene created by the different sources of uncertainty and the range of modelling approaches involved in the generation of regional climate information make the collection of results available from multi-model, multi-member simulations are often most useful when synthesized through a distillation process, as described in Section 10.5.4.

10.1.3 Regional climate messages

Regional climate messages translate climate information synthesized from different lines of evidence into the context of a user vulnerable to climate at regional scales (Baztan et al., 2017) taking into account the values (Corner et al., 2014; Bessette et al., 2017) of both the producer and user (Section 10.5). They allow connecting global climate change to the local and regional scales, where adaptation responses and policy decisions take place through the distillation of the climate information, which is also distilled from different climate sources (Figure 10.1; Sections 10.2–10.4) and play an important role in guiding climate-resilient development (Kruk et al., 2017; Parker and Lusk, 2019).

The approaches adopted in the generation of regional climate messages are diverse and include the simple production and delivery of data as information or the co-production with the user using as many lines of evidence as possible. The choice of the source and the approach has deep ramifications for the usefulness of the message. For instance, it is well established that it is invalid to take a time series from a cell of a GCM simulation as an observational estimate of a point within the cell, due to the lack of representativeness (Section 10.3), and consequently a message building on this type of data source is not useful. The construction of regional climate information (Lourenço et al., 2016) has constraints in terms of achievable spatial and temporal resolution (Lagabrielle et al., 2018; Sayles, 2018), the way of dealing with bias and error, or the impact of non-stationarity on climate statistics. Relevant decisions are usually made about what method is more suitable to a specific application, bringing the question of context to the fore. The regional climate message generation approaches first distil the different data sources into regional climate information that consolidates multiple lines of evidence and co-produce the climate message with the user through a second distillation process (Pettenger, 2016; Verrax, 2017). The specific climate message distillation approach and the way the outcome is communicated define the characteristics and the form of the regional climate message. Messages may be provided in the form of summarised raw data, a set of user-oriented indicators, a set of figures and maps with either a brief description, in the form of a storyline, or formulated as rich and complex climate adaptation plans. In all cases, the messages are intended to meet a specific demand and include a description of the sources and assumptions, estimates of the associated uncertainty and its sources, and guidance to prevent possible misunderstandings in its communication.

The choices made to generate climate messages have typically been part of a linear supply chain, starting from the generation of climate data using often climate simulations only that are transformed into maps or derived data products, and finally formulating statements that are communicated and delivered to a broad range of users (Hewitt et al., 2012; Hewitson et al., 2017). This methodology has proven to be valuable in many cases, but it is equally fraught with dangers of not communicating important assumptions, estimating the relevant uncertainty, and possibly causing misunderstandings in the hand-over from one community to another one. This has led to the emergence of new pathways to generate user-oriented climate messages, many in the context of emerging climate services (Buontempo et al., 2018), that are assessed in Sections 10.5 and 10.6.

10.1.4 Sources of regional climate variability

Regional climate comprises a vast number of weather phenomena and processes across different time and space scales (Figure 10.2). Variability in regional climate arises from natural and anthropogenic forcings, the local expression of large-scale remote forcings (also known as teleconnections), and the feedbacks between them. This section briefly introduces these sources of variability relevant at the regional scale and should be read along with corresponding sections in Chapters 3 and 7. Section 10.4 discusses the relevance for a number of example regions and Section 10.6 makes reference to the sources in specific cases where regional climate messages are built. Section 8.2 offers a companion discussion focussing on changes in the water cycle.

10.1.4.1 Forcings controlling regional climate

10.1.4.1.1 Anthropogenic well-mixed greenhouse gases

This global forcing impacts both land areas (in terms of surface temperature for instance) and ocean basins, where both heat and carbon are stored over long time scales. However, there are important differences in the processes affected over land and ocean. Over the ocean, the increased radiative forcing leads to an increase in latent heat flux and a decrease in sensible heat flux, while over land, water availability is limited and increased radiative energy is therefore converted mostly into sensible heat (Sutton et al., 2007). Consequently, GHGs affect the Northern Hemisphere temperatures more than the Southern ones since the Northern Hemisphere has more continental surfaces. This hemispheric warming asymmetry can also affect rainfall patterns, as it is the case in the Sahel (Section 10.4.1.2.1). The different impact of the GHG forcing also occurs at smaller spatial scales like the elevation-dependent warming in mountain areas (Cross-Chapter Box 10.3; Pepin et al., 2015).

10.1.4.1.2 Solar forcing

Variations in solar forcing can have regional impacts through influences on circulation patterns. The 11-year solar variability impacts on the leading atmospheric circulation modes of the North Atlantic region (Gray et al., 2013; Thiéblemont et al., 2015; Sjolte et al., 2018), and has been suggested as an important source of near-term predictability of the North Atlantic Oscillation (NAO; Kushnir et al., 2019), although the hypothesis is also contested (Ortega et al., 2015; Chiodo et al., 2019). On centennial timescales, solar fluctuations were found to be correlated with the Eastern Atlantic Pattern (Sjolte et al., 2018). Impacts on the winter circulation and temperature over Eurasia (Chen et al., 2015) and North America (Liu et al., 2014b; Li and Xiao, 2018) have also been identified.

10.1.4.1.3 Stratospheric ozone

Stratospheric ozone depletion has been argued to be a driver of the southward expansion of the Southern Hemisphere descending branch of the Hadley cell (Garfinkel et al., 2015; Waugh et al., 2015; Grise et al.,

2019) that has regional impacts in e.g., south-eastern South America (González et al., 2014; Wu and Polvani, 2017). Further discussion of the impacts of stratospheric ozone on regional climate can be found in Section 10.4.1.2.

10.1.4.1.4 Aerosols

Both natural and anthropogenic aerosols are often emitted at a regional scale, have a short atmospheric lifetime (from a few hours to several days; Section 6.1), are dispersed regionally and affect climate at a regional scale through radiative cooling/heating and cloud microphysical effects (Rotstayn et al., 2015; Sherwood et al., 2015; Chapter 8). The majority of aerosols scatter solar radiation, but with strong regional variations (Shindell and Faluvegi, 2009) that leads to regional radiative effects of up to two orders of magnitude larger than the global average (Li et al., 2016b, 2016a; Mallet et al., 2016). Black carbon, instead, is known to absorb solar radiation with a very inhomogeneous spatial distribution, leading to regional atmospheric warming (Gustafsson and Ramanathan, 2016).

Aerosol burden and forcing are generally co-located. However, temperature and precipitation responses are both local and remote (Li et al., 2016c; Kasoar et al., 2018; Liu et al., 2018c; Samset et al., 2018; Thornhill et al., 2018; Westervelt et al., 2018). For instance, changes in aerosol concentrations in the Northern Hemisphere have been reported to modulate monsoon precipitation in West Africa and the Sahel (Undorf et al., 2018; Section 10.4.1.2) and in Asia (Zhang et al., 2018; Section 10.6.3).

10.1.4.1.5 Natural aerosols

Natural aerosols include mineral dust, volcanic aerosol and sea salt. The feedback processes between climate and mineral dust as well as sea salt are described in Section 6.4.

Mineral dust created by wind erosion of arid and semi-arid surfaces dominates the aerosol load over a number of areas and, hence, is a phenomenon essentially regional. The major sources of contemporary dust are located in the arid topographic basins of Northern Africa, Middle East, Central and Southwest Asia, the Indian subcontinent, and East Asia. Relatively smaller sources are found in Australia, Patagonia, North America, and South Africa (Prospero et al., 2002; Ginoux et al., 2012). Dust affects the Earth's energy balance and, therefore, the energy and water cycles, directly by scattering and absorbing radiation, and indirectly by serving as nuclei of warm and cold clouds, thereby altering their properties, lifetime, and reflectivity (Chapter 6). Dust variations are controlled by changes in surface winds, precipitation, and vegetation, which in turn are modulated at multiple time scales by dominant modes of internal climate variability (Ridley et al., 2014; Wang et al., 2015b; DeFlorio et al., 2016; Evan et al., 2016; Pu and Ginoux, 2018). Upon deposition, dust reduces snow surface albedo, initiating snow albedo feedbacks that can exert regionally important impacts upon the hydrological cycle (Skiles et al., 2012). Wind-induced dust storms result in locally intense visibility hazards and potentially hazardous air quality for humans in arid and semi-arid environments as well as over wide areas downwind (Chapter 12).

The sign and magnitude of the global and regional climate response to either the individual or the combined effects of dust remain largely uncertain. The surface direct radiative effect is likely negative over land and ocean, especially when the assumed solar absorption by dust is large (Miller et al., 2014; Strong et al., 2015). Surface temperature and precipitation adjust to the direct radiative effect over the extent of the perturbed circulation in complicated ways, and their sign and magnitude depend sensitively upon the assumed dust absorptive properties. Dust likely cools the surface, but in regions such as the Sahara surface air temperature increases as the prescribed shortwave absorption by dust is increased, despite further dimming of the surface (Miller et al., 2014). Dust likely increases surface temperature over the major reflective dust sources (Miller et al., 2014; Solmon et al., 2015; Strong et al., 2015; Jin et al., 2016; Sharma and Miller, 2017).

Volcanic eruptions load the atmosphere with large amounts of sulphur, which is transformed through chemical reactions and micro-physics processes into sulphate aerosols (Stoffel et al., 2015; LeGrande et al., 2016). If the plume reaches the stratosphere, sulphate aerosols can remain there for a few months to years (about two to three for large eruptions). It is then transported to other areas by the Brower-Dobson circulation. If the eruption occurs in the tropical area, the dispersion is made all over the Earth in a few years, while if the eruption occurs in the high latitudes of one hemisphere, aerosols mainly remain in the same hemisphere (Pausata et al., 2015). Sulphate aerosols impact the radiative forcing of the Earth, backscattering shortwave radiation, limiting the amount of energy reaching the Earth's surface (Timmreck, 2012). The global temperature response observed after the last five major eruptions of the last two centuries is estimated to be around 0.2°C (Swingedouw et al., 2017), in association with a general decrease of precipitation over the continental surfaces (Iles and Hegerl, 2017).

Volcanic eruptions impact regional climate through both their spatial heterogeneous effect on the radiative budget and the dynamical responses triggered, influencing a number of modes of climate variability (Robock and Mao, 1992). Nevertheless, the statistical significance of the regional response remains difficult to evaluate over the historical era (Bittner et al., 2016; Swingedouw et al., 2017) due to the small sampling of large volcanic eruptions over this period and the fact that the signal is superimposed upon relatively large internal variability (Gao and Gao, 2018; Dogar and Sato, 2019). Evidence from paleoclimate observations is therefore crucial to obtain a sufficient signal-to-noise ratio (Sigl et al., 2015). Reconstructions of climate variability modes based on proxy data records allowed evaluating the impact of volcanic eruptions on those modes (Zanchettin et al., 2013; Ortega et al., 2015; Michel et al., 2018; Sjolte et al., 2018).

10.1.4.1.6 Anthropogenic aerosols

Although the global mean optical depth caused by anthropogenic aerosols did not change from the 1975 to 2005, the regional pattern changed dramatically from Europe to eastern Asia, which is now the main polluter (Fiedler et al., 2017, 2019; Stevens et al., 2017). Regional implications of clean air policies that reduce emissions of these types of aerosols are described in the Western Europe summer warming example in Section 10.4.1.2.6.

Aerosol-radiation interactions induce feedbacks on temperature. Under severely polluted conditions, aerosols enhance stratification from morning to daytime and increase their surface concentration leading to a positive feedback loop (Gao et al., 2016; Kajino et al., 2017).

10.1.4.1.7 Land use and management including urbanization

Regional climate is also shaped by small-scale forcings such as land-use changes or the presence and expansion of cities. These features can have local (e.g., irrigation mitigates temperature extremes at the irrigated site; Section 10.3.3.7.2) and non-local impacts (e.g., increased rainfall downwind of a city; Box 10.2).

Anthropogenic changes to the continental land surface such as deforestation, afforestation, conversion to croplands, land management (e.g., irrigation and tillage), urbanization, and construction of artificial dams can have large impacts on local and regional climate (Box 10.1). The impact of a specific land-use change will depend on the background climate. As an example, afforestation can induce local warming in boreal areas in winter since it decreases the albedo over snow covered areas, while in tropical regions afforestation leads to cooling through increased latent heat flux that overrules the decrease in albedo. In this chapter, the potential influence of land management such as irrigation on regional climate change is exemplified in the end-to-end example on the South Asian summer monsoon (Section 10.6.3).

There is *limited evidence* but *high agreement* that the GMST response to urbanization changes is negligible (Zhang et al. 2013; Chen et al., 2016; Hansen et al., 2010; Parker, 2006). However, there is evidence that urbanization may amplify regionally the air temperature response to climate change in different climatic zones (Mahmood et al., 2014) either under present (Doan et al., 2016; Kaplan et al., 2017; Li et al., 2018d) or future conditions (Argüeso et al., 2014; Kim et al., 2016; Kusaka et al., 2016; Grossman-Clarke et al., 2017) with a strong impact on minimum temperatures. For instance, in Flanders (Northern Belgium) Berckmans et al. (2019), found that urbanization scenario for the near future (up to 2035) has an impact on minimum temperature (0.6 °C) that is comparable to the projected climate change signal in the RCP8.5 scenario.

10.1.4.2 Internal drivers and their pathways to shaping regional climate

Internal climate variability on seasonal to multi-decadal time-scales is a strong internal driver of regional climate. This variability arises from internal modes of atmospheric and oceanic variability, the interaction of ocean modes and intrinsically coupled climate modes, and may additionally be forced by other components of the climate system. It also interacts with the forced response of the climate system. A detailed description of various modes of variability can be found in Chapters 2, 3 and 9 while their future projections are assessed in Chapter 4. Here, the focus is on their regional impact.

Mid-latitude climate is strongly affected by the mid-latitude jet and cyclones along the storm tracks. The variability of these phenomena is characterised by large-scale atmospheric modes (Figure 10.2) such as the NAO, the Northern and Southern Annular Modes (NAM and SAM). They show variability on all time scales, including decadal and longer periods.

Modes of variability may have different regional effects in different seasons like with the NAO in European winter (Tsanis and Tapoglou, 2019) and summer (Bladé et al., 2012; Dong et al., 2013). The SAM, which affects the climate of the Southern Hemisphere continents (Hendon et al., 2014a), has variability that can be attributed to natural processes (Smith and Polvani, 2017), while other aspects of the variability are defined by the recent stratospheric ozone changes (Bandoro et al., 2014). The teleconnections between these modes of variability and surface weather exhibit considerable non-stationarities (Hertig et al., 2015).

Due to the large ocean heat capacity and long time scales, multiannual to multi-decadal modes of ocean variability such as the Pacific Decadal Variability (PDV), Interdecadal Pacific Oscillation (IPO), Atlantic Multidecadal Variability (AMV) (Buckley and Marshall, 2016), and Indian Ocean Dipole Mode (IOD) are key drivers of regional climate change. These modes not only affect nearby regions but also remote parts of the globe through atmospheric teleconnections (Meehl et al., 2013; Dong and Dai, 2015) and can act to modulate the impact of the different natural and anthropogenic forcings (Davini et al., 2015; Ghosh et al., 2017; Ménégoz et al., 2018b). This generates a regional response in terms of temperature, wind, and precipitation.

The dynamics of the ocean modes of variability is simultaneously affected by other modes of variability spanning the full range of length and time scales due to non-linearity (Kucharski et al., 2010; Dong et al., 2018) (see Figure 10.1). This mutual interdependence can result in changing characteristics of the connection over time as, for example, for IPV and IOD (Dong and McPhaden, 2017), and of their regional climate impact (Martín-Gómez and Barreiro, 2016, 2017). The link of ocean modes to regional climate should therefore be treated with caution because this can vary over time even in a stationary climate (Sterl et al., 2007; Pinto et al., 2011; Gallant et al., 2013; Brands, 2017). Besides, the strong seasonality of the modes and related teleconnections means that their impact on regional climates can be seasonally dependent (Haarsma et al., 2015).

[START BOX 10.1 HERE]

BOX 10.1: Regional climate in AR5 and the special reports SRCCL, SROCC and SR1.5

This box summarizes the information on linking global and regional climate change information in the Fifth Assessment Report (AR5) and the three special reports to be published prior to the publication of the Sixth Assessment Report (AR6). This information helps framing the treatment of the production of regional climate information in previous reports and identifies some of the gaps that AR6 needs to address.

AR5

In the WGI Chapter 14 (Christensen et al., 2013), regional downscaling methods are mentioned to provide climate information at the scales needed for many climate impact studies. The assessment finds *high confidence* that downscaling adds value both in regions with highly variable topography and for various small-scale phenomena. Regional models necessarily inherit biases from the global models used to provide boundary conditions. Furthermore, the ability to systematically evaluate RCMs, and statistical downscaling schemes, were hampered because coordinated inter-comparison studies were still emerging. However, several studies demonstrated that added value arises from higher resolution of stationary features like topography and coastlines, and from improved representation of small-scale processes like convective precipitation.

The Working Group II (WGII) Chapter 21 (Hewitson et al., 2014b) addressed the regional climate change context from the perspective of impacts, vulnerability and adaptation. This chapter emphasizes that a good understanding of decision-making contexts is essential to define the type and scale of information required from physical climate (*high confidence*). Further, the chapter identifies that the regional climate information is limited by the paucity of comprehensive observations and their analysis along with the different levels of confidence in projections (*high confidence*). Notable was that at the time of the AR5 many studies still rely on global data sets, models, and assessment methods to inform regional decisions, which are not as effective as tailored regional approaches. The regional scale was not defined but instead it was emphasised that climate change responses play out on a range of scales, and the relevance and limitations of information differ strongly from global to local scales, and from one region to another.

The point was made that better understanding of changes in climate processes would strengthen the reliability of emerging messages on future climate change. The reliability of past changes is predicated on the availability and quality of observations, while the reliability of future projections depends on the performance of the models used for the projections in simulating the processes that lead to these changes.

The chapter noted that downscaled information (RCM and statistical empirical) remains weakly coordinated, and that results indicate that high-resolution downscaled reconstructions of the current climate can have significant errors. Key in this is that the increase in downscaled data sets has not narrowed the uncertainty range, and that integrating these data with historical change and process-based understanding remains an important challenge.

With regard to spatial resolution, the chapter identifies the common perception that higher resolution (i.e., more spatial detail) equates to more useable and robust information, which is not necessarily true. As a consequence, it is through the integration of multiple sources of information that robust understanding of change is developed.

Context strongly and differently conditions the entry point. Perspectives have been characterized as top-down (physical vulnerability) and bottom-up perspectives (social vulnerability). The top-down perspective uses climate change impacts as the starting point of how people and/or ecosystems are vulnerable to climate change, and commonly applies global-scale scenario information or refine this to the region of interest through downscaling procedures. Conversely, in the “bottom-up” approach the development context is the starting point, focusing on local scales, and layers climate change on top of this. An impact focus tends to look to the future to see how to adjust to expected changes, whereas a vulnerability-focused approach is centred on addressing the drivers of current vulnerability.

Special Report on Climate Change and Land (SRCCL; IPCC, 2019)

Land surface processes modulate the likelihood, intensity, and duration of many extreme events including heatwaves, droughts, and heavy precipitations. According to the SRCCL, there is *robust evidence and high agreement* that land cover and land use or management exert significant influence on atmospheric states (e.g., temperature, rainfall, wind intensity) and phenomena (e.g., monsoons), at various spatial and temporal scales, through their biophysical impacts on climate. There is *robust evidence* that dry soil moisture anomalies favour summer heat waves. Part of the projected increase in heat waves and droughts can be attributed to soil moisture feedbacks in regions where evapotranspiration is limited by moisture availability (*medium confidence*). Vegetation changes can also amplify or dampen extreme events through changes in albedo and evapotranspiration, which will influence future trends in extreme events (*medium confidence*).

Whatever the land change (e.g., afforestation, urbanization), its location on Earth determines the sign and magnitude of its impacts on climate (*robust evidence, high agreement*). For instance, irrigation may have contributed to a decrease in extreme temperature in strongly irrigated areas (*medium confidence*). The background climate also influences the sign and magnitude of the changes triggered by land-use and land cover change.

Water management and irrigation are generally not accounted by the CMIP5 global models. Additional water can modify regional energy and moisture balance particularly with highly productive agricultural crops with high rate of evapotranspiration. Urbanization increases the risks associated with extreme events (*high confidence*). Urbanization suppresses evaporative cooling and amplifies heatwave intensity (*high confidence*) with a strong impact on minimum temperatures (*very likely*, *high confidence*). Urban areas stimulate storm occurrence and heavy precipitations in part due to the presence of aerosols. Urbanization also increases the risk of flooding during heavy rain events.

Special Report on the Ocean and Cryosphere in a Changing Climate (SROCC; IPCC, 2019b)
Observations and models for assessing changes in the ocean and the cryosphere have been developed considerably during the past century but observations in some key regions remain under-sampled and are very short relative to the timescales of natural variability and anthropogenic changes. Retreat of mountain glaciers and thawing of mountain permafrost continues and will continue due to significant warming in those regions, where it is likely to exceed global temperature increase.

It is *virtually certain* that Antarctica and Greenland have lost mass over the past decade and observed glacier mass loss over the last decades is attributable to anthropogenic climate change (*high confidence*). It is *virtually certain* that projected warming will result in continued loss in Arctic sea ice in summer, but there is *low confidence* in climate model projections of Antarctic sea ice change because of model biases and disagreement with observed trend. Knowledge and observations of the polar regions are sparse compared to many other regions, due to remoteness and challenges of operation in them.

The sensitivity of small islands and coastal areas to increased sea level differs between emission scenarios and regionally and a consideration of local processes is critical for projections of sea level impacts at local scales.

Special Report on Global Warming of 1.5°C (SR1.5; IPCC, 2018)
Most land regions are experiencing greater warming than the global average, with annual average warming already exceeding 1.5°C in many regions. Over one quarter of the global population live in regions that have already experienced more than 1.5°C of warming in at least one season. Land regions will warm more than ocean regions over the coming decades (transient climate conditions).

Transient climate projections reveal observable differences between 1.5°C and 2°C global warming in terms of mean temperature and extremes, both at a global scale and for most land regions. Such studies also reveal detectable differences between 1.5°C and 2°C precipitation extremes in many land regions. Besides, for mean precipitation and various drought measures there is substantially lower risk for human systems and ecosystems in the Mediterranean region at 1.5°C compared to 2°C.

The different pathways to a 1.5ºC warmer world may involve a transition through 1.5°C, with both short and long-term stabilization (without overshoot), or a temporary rise and fall over decades and centuries (overshoot). The influence of these pathways is small for some climate variables at the regional scale (e.g., regional temperature and precipitation extremes) but can be very large for others (e.g., sea level).

Decisions on changes in land use can strongly affect regional climate change through biophysical feedbacks (e.g., changes in land evaporation or surface albedo), potentially affecting regional temperature and precipitation.

[END BOX 10.1 HERE]

[START CROSS-CHAPTER BOX 10.1 HERE]

Cross-Chapter Box 10.1: Influence of the Arctic on mid-latitude climate

Contributors: Francisco Doblas-Reyes (Spain), Hervé Douville (France), Nathan Gillett (Canada), Rein Haarsma (Netherlands), Gerhard Krinner (France), Dirk Notz (Germany), Krishnan Raghavan (India), Sonia Seneviratne (Switzerland), Laurent Terray (France), Cunde Xiao (China)

Mean surface air temperature in the Arctic is rising more than twice as quickly as the global mean surface air temperature (Davy et al., 2018), with the strongest warming during winter. In some seasons and for certain parts of the temperature distribution, the warming is up to three times stronger, such as the warming of the coldest nights (Seneviratne et al., 2016). Several mechanisms are responsible for the enhanced lower troposphere warming of the Arctic (Sections 4.5.1.1 and 7.4.2). These include the ice-albedo, lapse rate, Planck and cloud feedbacks (Pithan and Mauritsen, 2014). The rapid Arctic warming has a strong impact on the ocean, atmosphere and cryosphere in that region (Atlas 5.10.1). To illustrate the latter, late summer and early autumn sea ice extent has decreased by around 13% per decade since 1979 (Section 2.3.2.1). At least half of this recent Arctic sea ice decline is due to anthropogenic forcings (*high confidence*), as is further discussed in Sections 3.4.1.1 and 9.3.1.

In this box, the possible impact of the Arctic warming on the lower latitudes is discussed. This linkage was also the topic of the Box 3.2 of the SROCC. It is a topic that has recently raised wide interest (Ogawa et al., 2018; Wang et al., 2018a). Different hypotheses, which differ between winter and summer, have emerged that describe possible mechanisms of how the Arctic can influence the weather and climate at lower latitudes. They involve changes in the polar vortex, storm tracks, jet stream, planetary waves, stratosphere-troposphere coupling, and eddy-mean flow interactions, thereby affecting the mid-latitude atmospheric circulation, and the frequency and intensity of extremes, like cold spells, heat waves, and floods (Figure 1). These hypotheses and the impact on mid-latitude climate, in particular on the extremes, are, however, strongly debated and criticised. These mechanisms and their criticisms will be discussed here as an extension to the SROCC box.

[START CROSS-CHAPTER BOX 10.1, FIGURE 1 HERE]

Cross-Chapter Box 10.1, Figure 1: Mechanisms of potential impacts of Arctic warming on mid-latitude climate. Mechanisms are different for winter and summer with different associated impacts on mid-latitudes. The mechanisms involve changes in the polar vortex, storm tracks, planetary waves and jet stream.

[END CROSS-CHAPTER BOX 10.1, FIGURE 1 HERE]

Mechanisms for a potential impact in winter

It has been proposed that Arctic amplification, by reducing the equator-pole temperature contrast, could result in a weaker and more meandering jet with Rossby waves of larger amplitude (Francis et al., 2017). This may cause weather systems to travel eastward more slowly and thus, all other things being equal, Arctic amplification could lead to more persistent weather patterns over the mid-latitudes (Francis and Vavrus, 2012). The persistent large meandering flow may increase the likelihood of temperature and precipitation extremes because they frequently occur when atmospheric circulation patterns are persistent, which tends to occur with a strong meridional wind component. Another proposed impact of Arctic warming is on the NAO/AO that shows a negative trend over the past two decades (Robson et al., 2016; Iles and Hegerl, 2017), and has been linked to the reduction of sea ice in the Barents and Kara seas, and the increase in Eurasian snow cover (Cohen et al., 2012a; Nakamura et al., 2015; Yang et al., 2016b). During negative NAO/AO the storm tracks shift equatorward and winters are predominantly more severe across northern Eurasia and the eastern United States, but relatively mild in the Arctic. This temperature pattern is sometimes referred to as the 'warm Arctic–cold continents (WACC)' pattern (Chen et al., 2018). However, Sun et al. (2016a) argue that the WACC is a manifestation of natural variability. Enhanced sea-ice loss in the Barents-Kara Sea has also been related to increased stratospheric polar vortex variability (Kretschmer et al., 2016) that would induce a negative NAO/AO (Kim et al., 2014), the WACC pattern (Kim et al., 2014), and an increase in cold-air outbreaks (Kretschmer et al., 2018). Arctic warming might also increase Eurasian snow cover in autumn caused by the moister air that is advected into Eurasia from the Arctic with reduced sea-ice cover (Cohen et al., 2014; Jaiser et al., 2016), although Peings (2019) suggests a possible influence of Ural blockings on both the fall snow cover and the early winter polar stratosphere. Routson et al. (2019) argue that during the mid-Holocene, the weaker Arctic-Equator meridional temperature gradient and reduced cyclonic activity resulted in less mid-latitude precipitation, suggesting a similar response for the present Arctic warming.

Mechanisms for a potential impact in summer

Similar as in winter, Arctic summer warming may result in a weakening of the westerly jet and mid-latitude storm tracks, as suggested for the recent period of Arctic warming (Coumou et al., 2015; Petrie et al., 2015; Chang et al., 2016). Additional proposed impacts are a southward shift of the jet (Butler et al., 2010) and a double jet structure associated with an increase of the land-ocean thermal gradient at the land-ocean boundary (Coumou et al., 2018). It is hypothesized that weaker jets, diminished meridional temperature contrast, and reduced baroclinicity might induce a larger amplitude in stationary wave response to stationary forcings (Zappa et al., 2011; Petoukhov et al., 2013; Hoskins and Woollings, 2015; Coumou et al., 2018; Mann et al., 2018), and also that a double jet structure would favour wave resonance (Kornhuber et al., 2017; Mann et al., 2017). Some studies suggest that this is corroborated by an observed increase of quasi-stationary waves (Di Capua and Coumou, 2016; Vavrus et al., 2017; Coumou et al., 2018).

Assessment

The above proposed theories are based on concepts of geophysical fluid dynamics and surface coupling and can, in principle, help explain the existence of a link between the Arctic changes and the mid-latitudes (Barnes and Screen, 2015). However, the validity of some dynamical underlying mechanisms, such as reduced meridional temperature contrast inducing enhanced wave amplitude, have been questioned (Hassanzadeh et al., 2014; Hoskins and Woollings, 2015), or on the contrary related to reduced winter temperature variability (Collow et al., 2019).

Studies that support the Arctic influence are mostly based on observational relationships between the Arctic temperature or sea ice extent and mid-latitude anomalies or extremes (Cohen et al., 2012a; Francis and Vavrus, 2012, 2015; Budikova et al., 2017). They are often criticised by the lack of statistical significance and the inability to disentangle cause and effect (Barnes, 2013; Barnes and Polvani, 2013; Screen and Simmonds, 2013; Barnes et al., 2014b; Hassanzadeh et al., 2014; Barnes and Screen, 2015; Sorokina et al., 2016; Douville et al., 2017; Gastineau et al., 2017). Kretschmer et al. (2016) do attempt to disentangle cause and effect using causal inference techniques, and find a relationship with Barents-Kara Sea sea-ice loss, but no evidence of the impact of Eurasian snow cover. Section 9.5.4.6 assesses that there is *low confidence* in the reported relationships between Eurasian snow cover in fall and Northern Hemisphere circulation trends and anomalies in the following winter. The role of the Barents-Kara Sea ice loss is challenged by Blackport et al. (2019) who find a minimal influence of reduced sea ice on severe mid-latitude winters, and by Warner et al. (2019) who suggest that the apparent winter NAO response to the Barents-Kara sea-ice variability is mainly an artefact of the Aleutian Low internal variability and of the co-variability between sea ice and the Aleutian Low originating from tropical-extratropical teleconnections. Mori et al. (2019a) argue that models underestimate the forcing of the Barents-Kara Sea ice loss on the atmosphere, which is disputed by Screen and Blackport (2019). Other studies have stressed the importance of atmospheric variability as a driver of Arctic variability (Lee, 2014; Woods and Caballero, 2016; Olonscheck et al., 2019).

An additional argument in the criticism is the inability of climate models to simulate a significant response, larger than the natural variability (Screen et al., 2014; Walsh, 2014; Chen et al., 2016c; Peings et al., 2017), although some studies find a significant response in summer, because then the internal variability is weaker (Petrie et al., 2015).

Finally, a warmer Arctic climate can, without any additional changes in atmospheric dynamics, reduce cold extremes in winter due to advection of increasingly warmer air from the Arctic into the mid-latitudes

(Screen, 2014; Ayarzagüena and Screen, 2016; Ayarzagüena et al., 2018).

Summarizing, different theories have been developed about the impact of recent Arctic warming on the mid-latitudes in both winter and summer. Although some of the proposed causalities seem to be supported by various studies, such as the link with Barents-Kara Sea ice loss in winter and weakened storm tracks in summer, the underlying mechanisms and relative strength compared to internal climate variability have been questioned. A recent review paper by Cohen et al. (2020) states that divergent conclusions between model and observational studies, and even intramodel studies, continue to obfuscate a clear understanding of how Arctic warming is influencing mid-latitude weather. In agreement with Box 3.2 of SROCC, there is hence *low to medium confidence* in the exact role and quantitative impact of historical Arctic warming and sea-ice loss on mid-latitude atmospheric variability.

Regarding future climate, it is important to note that mid-latitude variability is also affected by many drivers other than the Arctic changes and that those drivers as well as the linkages to mid-latitude variability might change in a warmer world. The AMOC, PDV, ENSO, upper tropospheric tropical heating, polar stratospheric vortex, land-surface processes associated with soil moisture (Miralles et al., 2014; Hauser et al., 2016) are a few examples. A considerable body of literature has shown that changes to the NAO/AO on seasonal and climate change timescales can be driven by variations in the wavelength and amplitude of Rossby waves, mainly of tropical origin (Fletcher and Kushner, 2011; Cattiaux and Cassou, 2013; Ding et al., 2014; Goss et al., 2016). The impact of future Artic warming on mid-latitude circulation is difficult to disentangle from the effect of such a plethora of drivers (Blackport and Kushner, 2017; Li et al., 2018a). One of the impacts of climate change is a poleward shift of the jet (Barnes and Polvani, 2013), which is less obvious in winter especially over North Atlantic (Peings et al., 2018; Oudar et al., submitted), and the increase of the meridional temperature gradient in the upper troposphere, which increases storm track activity (Barnes and Screen, 2015). Although climate models indicate that future Arctic warming and the associated equator-pole temperature gradient could affect mid-latitude climate and variability (Haarsma et al., 2013b; McCusker et al., 2017; Zappa et al., 2018), they do not reveal a dominant impact on extreme weather (Woollings et al., 2014).

In conclusion future climate change will affect mid-latitude variability in a number of ways that are still to be clarified, potentially also including the impact of Arctic warming, but there is *low confidence* in the dominant contribution of Arctic warming compared to other drivers.

[END CROSS-CHAPTER BOX 10.1 HERE]

10.2 Using observations for constructing regional climate messages

10.2.1 Observation types

10.2.1.1 In-situ and remote sensing data

Climate information for the atmosphere and land mainly comes from two different and complementary data sources: direct (including in-situ data and from the instruments launched from the ground such as upper-air stations/radiosondes) and remote observing systems (e.g., space-borne, radar, reflectometry, occultation, and lidar observations). Direct observing systems are a critical component of a global monitoring programme, producing the basic data that is essential for monitoring how climate variability, especially extremes in temperature and precipitation, evolves across different regions. There are more observations over land than over the ocean. The Northern Hemisphere has more observational facilities than the Southern Hemisphere, but how much more depends on the variable (e.g., Harris et al. (2014) for a comparison for a number of surface variables and Schneider et al. (2016) for precipitation). These direct observations are essential to monitor local and regional climate, in ensuring that climate models can be evaluated and for the calibration of satellite sensors. Direct observations are irregularly spaced and are the basis for gridded products (see Section 10.2.1.2) that are needed to assess model performance. Comparing model simulations with individual station data introduces other issues such as comparing point values with model values that represent what happens in an area.

Surface or in-situ observations can come from a variety of networks such as climate reference networks, mesoscale weather and supersite observation networks, citizen science networks, and others, all with their strengths and weaknesses (McPherson, 2013). Supersite observatories are surface observing networks that measure a large amount of atmospheric and soil variables at least hourly over a decade or more (Ackerman and Stokes, 2003; Haeffelin et al., 2005; Xie et al., 2010; Chiriaco et al., 2018). These data are recorded with instruments with an adequate calibration, and undergo quality control and homogenization. They produce some of the most valuable data needed to diagnose processes and changes in regional and local climate. Several climate datasets have been developed from in situ station observations, at different spatial scales and temporal frequencies (see Technical Annex I on observations). These include sub-daily (Lewis et al., 2019; Dumitrescu et al., 2016), daily (Aalto et al., 2016; Funk et al., 2015; Beck et al., 2017a, 2017b; Camera et al., 2014; Chen et al., 2008; Journée et al., 2015; Schneider et al., 2017), and monthly time scales (Aryee et al., 2018; Cuervo-Robayo et al., 2014).

Satellite products provide a valuable complement to in-situ measurements and are particularly useful over regions with none or sparse direct observations. Most satellite products have global coverage. They have been discussed in earlier chapters (e.g., Chapters 2 and 8) for large scale assessment. Currently 54 essential climate variables (ECVs; Bojinski et al., 2014) are defined by the Global Climate Observing System (GCOS) programme, and efforts are integrated in related programmes, such as Copernicus Climate Change Service of the European Union. When considering their application at a regional scale it is important to consider that the spatio-temporal resolution of these products varies considerably, and that there is commonly a trade-off between temporal and spatial resolution. For example, Landsat provides images with a high spatial resolution of around 30 metres, but offers full coverage of the globe once every 8 to 16 days (Wulder et al., 2016), while SMOS (ESA's Soil Moisture Ocean Salinity Earth Explorer mission) has a coarser spatial resolution of 25 km, but covers the full globe each 2.5–3 days (Kerr et al., 2012). Moreover, a simple concatenation of data in time would show non-climatic jumps due to changes in calibration and processing algorithms or artificial trends for a satellite series related to orbit stability or changing performance of the instruments (Barrett et al., 2014). Re-calibration and cross-calibration are then an essential prerequisite to obtain homogenous time series of measurements across different or successive satellites that can then be used to produce long series known as climate data records (Merchant et al., 2017). For example, precipitation estimation from Remotely Sensed Information using Artificial Neural Networks (PERSIANN) is a sub-daily to daily rainfall product which covers 50°S to 50°N globally with 25 km resolution since 2000 to present (Nguyen et al., 2019). Also, the Tropical Rainfall Measurement Mission (TRMM; covering 35°N–35°S, 1997–2016) (Simpson et al., 1996) and Global Precipitation Measurements (GPM; 65°N–65°S, 2014–present) (Skofronick-Jackson et al., 2017) satellite products have provided three-dimensional precipitation radar data with ~5 km pixel size for more than 20 years and feature sub-diurnal sampling. These large scale products can also be used to study for example the characteristics of extreme precipitation systems at a regional scale and to study the relationship with their atmospheric environment (Sohn et al., 2013; Hamada and Takayabu, 2018). Constellation products such as the Global Satellite Mapping of Precipitation (GSMaP) (Kubota et al., 2007) and Integrated Multi-satellitE Retrievals for GPM (IMERG) (Huffman et al., 2007) provide hourly global precipitation data with ~11 km coverage. CPC MORPHing technique (CMORPH) provides 30 min interval global precipitation with ~8 km coverage since 2002 (Joyce et al., 2004). The use of these large scale high-resolution spatio-temporal precipitation products have enhanced our understanding of precipitation process at regional scale such as diurnal cycles in a large river valley (Chen et al., 2012c), in coastal regions (Hassim et al., 2016; Hirose et al., 2017; Yokoi et al., 2017) and in mountainous regions (Hirose et al., 2017). Advanced geostationary satellites such as GOES-East and GOES-17 (Goodman et al., 2018), Meteosat-10 and 11 (Schmetz et al., 2002), Himawari-8 and 9 (Kurihara et al., 2016), and FY-4 (Cao et al., 2014) are valuable for regional applications since they provide images at very high spatiotemporal resolutions, typically 1–2 km, every 10–15 minutes.

The climate science community is moving fast towards the use of a maturity model (related to the technical readiness levels framework for flight hardware and instrumentation) for generating climate data records useful at regional scale that captures best practices from the scientific community, preservation information from the archive community, and software best practices from the engineering community (Bates and

Privette, 2012; Hollmann et al., 2013; Yang et al., 2016a). There is now a network of satellite-based Global Observation System (https://www.wmo.int/pages/prog/www/OSY/GOS.html), mainly for cloud and moisture patterns using the visible or infrared channel sensors. The network has been established in 1987 in the framework of the FGGE (First GARP Global Experiment) project. Initially the network included two GOESs (USA), METEOSAT (Europe), a Russian satellite, and GMS (Japan). The network has been increased including INSAT (India), FY2 (China), and COMS (Korea) with a total number of 10 geostationary satellites. In order to fill the gap around the Polar Regions there are also some sun-synchronous orbit satellites now. During the past 40 years, time, resolution, and the channel sensors have all increased.

10.2.1.2 Derived products

Derived products are the result of modifying an existing one. It is created from raw datasets collected through surface observations, remote-sensing tools, and research vessels using either statistical interpolation techniques (see Section 10.2.2.4) or numerical atmospheric and land-surface models (Bosilovich et al., 2015).

Most global observational datasets are available at coarse temporal or spatial resolution, or do not include all available station data of a particular region due to, among others, availability problems. Therefore, efforts have been made to develop regional or country-scale datasets (see Technical Annex I on observations). Radar and satellite remote sensing are two other sources that can provide a valuable complement to direct measurements at regional scale. Examples for precipitation have been described recently, some of which have been released to the community (Bližňák et al., 2018; Dietzsch et al., 2017; Dinku et al., 2014; Krähenmann S. et al., 2018; Manz et al., 2016; Oyler et al., 2015; Panziera et al., 2018; Shen et al., 2018; Yang et al., 2017). However, some of these datasets are limited by their short length of record, varying between one (Shen et al., 2018) and 64 years (Oyler et al., 2015).

Reanalyses products are designed to merge irregular observations and models that encompass many physical and dynamical processes. They generate a dynamical and coherent estimate of the state of the climate system (often only for the atmosphere and land) on uniform grids either at global (Balsamo et al., 2015; Chaudhuri et al., 2013), regional (Chaney et al., 2014; Dahlgren et al., 2016; Maidment et al., 2014; Mahmood et al., 2018; Attada et al., 2018; Langodan et al., 2017) or country scales (Krähenmann et al., 2018; Mahmood et al., 2018; Rostkier-Edelstein et al., 2014). Recently, reanalyses using-convection permitting RCMs have been published (e.g., Wahl et al. (2017) for central Europe).

Regional reanalyses are valuable for regional assessment, since they can employ higher resolution model simulations due to their small spatial coverage. Their accuracy also improves with respect to global reanalyses since they are often developed over regions with a high density of observational data to be assimilated into the model (e.g., Yamada et al., 2012). Current regional reanalyses datasets cover areas like the Arctic, Europe, North America, South Asia and Australia (see Technical Annex I on observations).

10.2.2 Challenges for regional climate change assessment

10.2.2.1 Quality control

The usefulness of an observational data is conditioned by the availability and outcome of a quality control (QC) process. The objective of the QC is to verify if a reported data value is representative of the measured variable and to what degree the value could be contaminated by unrelated factors. The QC procedure depends strongly on the specific nature of the dataset. It focuses on aspects such as correctly identifying sensor, time and location, having values that reliably reflect the expected conditions, estimate if the uncertainty information is adequate, and assessing the consistency among the observed measurements. Detailed documentation of the data processing is part of the QC procedures and enhances the applicability of the data.

The outcome of the QC should be taken into account when using the observations. For instance, it informs users that many reanalysis datasets may be inconsistent in the long term because they assimilate inhomogeneous observations over the reanalyses period (Kobayashi et al., 2015). As a consequence, the evaluation against independent observations suggests that reanalyses should not be automatically regarded as climate quality products for monitoring trends at the regional level (Manzanas et al., 2014; Torralba et al., 2017). When problems are identified some observational datasets are provided with a quality mask (Contractor et al., 2019) that can be taken into account when using the observations. Quality-controlled data are now produced widely such as sub-daily precipitation records in the United Kingdom (Blenkinsop et al., 2017) and the USA (Nelson et al., 2016). However, many more datasets and variables lack the same level of scrutiny.

QC is also closely related to data scarcity (Section 10.2.2.3), like in cases where the quality of a derived dataset is affected by gaps in time and space to fit the purpose of a specific application. This is often the case in high-resolution dynamical downscaling where high-resolution, gridded observational data may not be available to assess the added value of the increase in resolution (e.g., Di Luca et al., 2016; Zittis et al., 2017; Section 10.3.3). This implies a need for additional efforts to reach quality-controlled, high-resolution observational datasets.

10.2.2.2 Homogenization

Station data are influenced by factors that act at regional scale, from mesoscale and local scale down to the microscale (WMO, 2019), therefore, secular station time series contain inhomogeneities such as artificial jumps or trends, which hamper assessments of regional long-term trends. Typical reasons for this are the urbanization of a station's surroundings (Hamdi, 2010; Adachi et al., 2012; Sun et al., 2016b), or cooling due to its relocation (Tuomenvirta, 2001; Yan et al., 2010; Xu et al., 2013; Dienst et al., 2017, 2019). Another source of inhomogeneity is transitions in measurement methods that affect most instruments of an observational network over a limited time span, such as the transition to Stevenson screens (Parker, 1994; Böhm et al., 2010; Brunet et al., 2011; Auchmann and Brönnimann, 2012) or to automatic weather stations (WMO, 2017). The main approach to reduce the influence of inhomogeneities in station observations is statistical homogenization produced by comparing a candidate station with neighbouring reference stations (Trewin, 2010). This is a challenging task because candidates and their references normally have multiple inhomogeneities.

Three challenges should still be noted. First, most of our understanding of statistical homogenization stems from the homogenization of temperature observations from dense networks. A recent study suggests that our ability to remove biases quickly diminishes for sparse networks (Gubler et al., 2017; Lindau and Venema, 2018a). This affects early instrumental data and observations that are not strongly correlated between stations, such as wind and humidity (Chimani et al., 2018). Second, in addition to systematic errors, homogenized data will also suffer from random errors, which are largest at the station level, but also present in network-average signals (Lindau and Venema, 2018b). They stem from the errors introduced by the homogenization. The uncertainties related to the homogenization procedure are determined both by the break signal, as well as the noise signal and the performance of the homogenization method. These errors are spatially correlated and have an impact on aspects like post-processing, interpolation and downscaling of climate simulations (Section 10.2.3.2). Third, the above discussion pertains to the homogenization of monthly and annual means. Homogenization of daily variability around the mean is more difficult. For daily data, specific correction methods are used (Della-Marta and Wanner, 2006; Mestre et al., 2011; Trewin, 2013) that are able to improve the homogeneity of test cases, but recent independent validation efforts were not able to show much improvement (Chimani et al., 2018). The difference may stem from assumptions on the nature of inhomogeneities for daily data, which are not yet well understood.

It is *virtually certain* that the uncertainties related to long-term warming estimates at regional scale are reduced using statistical homogenization methods. By decomposing the long-term warming RMSE into a bias and a noise uncertainty around the bias, especially the bias, but mostly also the noise uncertainty will be reduced. This is based on our understanding of the causes and nature of inhomogeneities combined with the design principles of statistical homogenization methods, as well as on analytical (Lindau and Venema, 2018b), numerical (Venema et al., 2012; Williams et al., 2012), and empirical validation studies (Hausfather et al., 2016; Gubler et al., 2017).

10.2.2.3 Data scarcity

Even if satellite products have global coverage and can be used over regions with none or sparse observations, their performance at a regional scale vary greatly. For example over complex orography regions the satellite-only products have large systematic and random errors while the gauge-corrected ones perform better (Guo et al., 2017a). Data scarcity arises largely due to the lack of sustainable maintenance of observing stations, inaccessibility of the data held in national networks, and uneven spatial distribution of stations that lead to a low density in many regions. This is particularly damaging when trying to assess regional climate change, for which a high density of observational data is desirable. Although in several regions numerous stations provide (monthly) data covering more than 100 years for both temperature and precipitation (GCOS, 2015), large areas of the world remain sparsely covered. For instance, the geographical and temporal coverage of stations contributing to the Global Precipitation Climatology Centre (GPCC) monthly product vary greatly and the total number of stations providing data declined from 1990 onwards, although this may relate to delays in data acquisition (GCOS, 2015). According to Kidd et al., (2017), assuming each GPCC-available gauge represented a surrounding area of 5-km radius, the total area covered would represent only about 1% of Earth's surface; in addition, only 1.6% of Earth's surface lies within 10 km of a rain gauge and many areas around the world (e.g., northern Canada, Siberia, Tibetan plateau, regions in Africa, Australia and South America) are beyond 100 km from the nearest rain gauge. Data scarcity is especially critical over Africa (Nikulin et al. 2012). For example, over South Africa, where the station density is relatively large compared to the rest of the continent, the number of weather stations collecting daily temperature used in the fourth version of the Climatic Research Unit Temperature dataset (CRUTEM4, Osborn and Jones, 2014) has significantly declined since 1980 (Archer et al., 2018).

Even in Europe, where regional high resolution observational datasets exist, precipitation station density in the widely used E-OBS gridded dataset varies largely in space and time across regions, with Germany offering ten times more stations than France (Prein and Gobiet, 2017). This variability is partly due to the resistance of some data owners to share their data within an international effort. Regardless of the reason behind it, low station density is a major source of uncertainty (Isotta et al., 2015). Using 10-year rainfall measurements from a network of 150 rain gauges over an area of around 300 km^2 Kirchengast et al. (2014) and O and Foelsche (2018) found that for capturing the area-averaged precipitation amount of heavy summertime precipitation events on a daily (hourly) basis with a normalised root mean square error of less than 20%, at least 2 to 5 (12) stations are required. Similarly to the E-OBS dataset, gridded daily temperature and precipitation datasets are being developed for other regions of the world such as Southeast Asia (SA-OBS, van den Besselaar et al., 2017a) and West Africa (WACA&D, Van Den Besselaar et al., 2015). However, stations are unevenly distributed and its number varies over time, with gaps due to missing values. Still, there is value in these initiatives illustrated by the large number of studies where they are used.

Data scarcity results in critical problems for climate monitoring (e.g., trend analysis of extreme events requires high temporal and spatial resolutions) or model evaluation (Section 10.4.2). It is *virtually certain* that the scarcity and decline of observations increase the uncertainty of the long-term temperature and precipitation estimates. As an example Lin and Huybers (2019) found that changes in the number of rain gauges after 1975 resulted in spurious trends in extremes of Indian rainfall in a 0.25°gridded dataset covering the 20th century. In fact, the number of stations used to construct the gridded dataset dropped by half after 1990, leading to inhomogeneity and spurious trends (Section 10.6.3). Over the southern part of the Mediterranean, which is an extended area being sparsely covered by meteorological stations, data scarcity can lead to large uncertainties in the different gridded datasets and strongly affect model evaluation (Section 10.6.4).

10.2.2.4 Gridding

Derived gridded datasets require merging data from different sources of observations and/or reanalysis data on a uniform grid (e.g., Xie and Arkin, 1997; Section 10.2.1.2). However, in-situ observations are distributed irregularly, especially over sparsely populated areas. This leads to an interpolation challenge. Gridded products of temperature and precipitation are strongly affected by the interpolation methods over complex orography and data scarce regions.

There are two main approaches to produce gridded datasets: (1) based on in-situ observations and (2) combining in-situ observations with remote-sensing data. The first approach has been widely employed in regions with high station density using interpolation techniques such as inverse distance weighting, optimal interpolation, and kriging (Chen et al., 2008; Haylock et al., 2008; Frei, 2014; Isotta et al., 2014; Masson and Frei, 2014; Hiebl and Frei, 2016; Inoue et al., 2016). This approach can provide high spatial and temporal resolutions according to the scale of observational data. The second approach has been mainly applied in data sparse regions with low station density, using methods like simple bias adjustment, quantile mapping, and kriging merging in-situ observations and satellite data (Cheema and Bastiaanssen, 2012; Dinku et al., 2014; Abera et al., 2016). Erdin et al. (2012) have been developing gridded rainfall datasets by combining radar and rain gauge data using kriging. Alternatively, Krähenmann et al. (2018) have produced a high resolution gridded dataset from station data, satellite estimation, and standard model outputs using several merging techniques.

Gridding of station data is affected by uncertainties stemming from measurements errors, inhomogeneities, the distribution of the underlying stations and the interpolation error. The dominant factor is station density (Herrera et al., 2018b). Uncertainty due to interpolation is typically small for temperature but substantial for precipitation and its derivatives such as drought indices (Chubb et al., 2015; Hellwig et al., 2018). The largest errors typically occur in sparsely sampled mountain areas (Section 10.1.2.6). Interpolation generally brings about smoothing effects, for instance, the weaker variability of the derived dataset with respect to the in-situ observations (Chen et al., 2019). As a result, the effective resolution of gridded data is typically much lower than its nominal resolution. For instance, a 5 km gridded precipitation dataset for the European Alps has an effective resolution of about 10–25 km (Isotta et al., 2014). In an example for precipitation in Spain, the effective resolution converged to the nominal resolution only when at least 6–7 stations where inside the corresponding grid cell (Herrera et al., 2018b). To account for the smoothing errors, new stochastic ensemble observation data sets have been introduced. In this approach each ensemble member represents one possible observed field, given the station observations (Von Clarmann, 2014).

10.2.2.5 Observations in small islands

A discussion on the specific challenges related to observations, either in-situ or remote sensing, over small island will be developed here with a link to the case study on the Caribbean islands in Section 10.4.1.2.8.

10.2.2.6 Observations in mountain areas

Variability of meteorological parameters observed over mountainous areas is often quite high, indicating strong control of local topography on meteorological parameters (Gultepe et al., 2014). Difficult access, harsh climatic conditions as well as instrumental issues make meteorological measurements extremely challenging at higher elevations (Azam et al., 2018; Beniston et al., 2018). Measurements of wind speed, temperature, relative humidity and radiative fluxes are critical for climate model validation, but difficult to deal with due to complex interactions over mountainous terrain, and often need corrections (Gultepe, 2015). Permanent meteorological stations are limited and current knowledge is mainly based on sporadic valley bottom or low elevation meteorological stations (Qin et al., 2009; Lawrimore et al., 2011; Gultepe, 2015), which, generally, do not represent the higher elevation climate (Immerzeel et al., 2015; Shea et al., 2015). There is *medium evidence* but *high agreement* on elevation-dependent warming (EDW; Cross-Chapter-Box 10.3) in most of the mountain ranges but unfortunately field-measurements supporting EDW are extremely limited from high elevations (Qin et al., 2009; Pepin et al., 2015). Measuring the precipitation amounts, especially solid precipitations, in mountainous areas is one of the most interesting but difficult tasks due to the presence of orographic barriers, its strong vertical and horizontal variability, and representative sites for precipitation measurements (Barry, 2012).

There is *very high confidence* (*robust evidence and high agreement*) that precipitation measurements, especially solid precipitations, in mountainous areas are strongly affected by the gauge location and setup. These measurements are also affected by the type of measurement method, presence/absence of shield, presence/absence of heating system, range of operating meteorological conditions, etc. (Nitu et al., 2018). Solid precipitation measurements generally have errors ranging from 20% to 50%, largely due to under catch in windy, icing and rimming conditions (Rasmussen et al., 2012), and therefore require corrections by applying the transfer functions developed mainly from collected wind speed and temperature data (Kochendorfer et al., 2017). The latest Solid Precipitation Intercomparison Experiment report recommends measurements of wind speed, wind direction and temperature as the minimum standard ancillary data for solid precipitation monitoring (Nitu et al., 2018).

Recent advancements through remote-sensing methods provide an alternative, but they also have limitations over mountainous areas. Different versions of Tropical Rainfall Measuring Mission products were found to perform differently over the mountainous areas (Zulkafli et al., 2014). It was noticed that orographic heavy rainfall over Taiwan associated with typhoon Morakot in 2009 was severely underestimated in all microwave products including TRMM 3B42. The underestimation have been mitigated in the Global Satellite Mapping of Precipitation (GSMaP) product by considering the orographic effects (Shige et al., 2013). Studies have suggested a high accuracy of passive optical satellite (e.g., MODIS, Landsat) snow products under clear skies when comparing with the field observations; however, cloud masking and sub-pixel cloud heterogeneity in these snow cover products considerably restrict their applications (Kahn et al., 2011; Brun et al., 2015; Tang et al., 2017; Stillinger et al., 2019). Gridded datasets (e.g., CRU, GPCC Full Data Product, GPCC Monitoring Product, ERA-Interim, ERA5, MERRA-2, MERRA-2 bias corrected, PERSIANN-CDR) are of paramount importance, yet demand in-situ observations to improve the temporal and spatial distribution of meteorological parameters over complex mountain terrain (Zandler et al., 2019).

10.2.2.7 Other sources of uncertainty

Beyond climate monitoring, the quality and availability of multiple observational references play a central role in the model evaluation assessment. In fact, when using observations for model evaluation, there are multiple examples where inter-observational uncertainty is as large as the inter-model variability. This has been shown for various aspects of the Indian monsoon (Section 10.6.3) (Collins et al., 2013a) and for precipitation uncertainties over Africa (Section 10.6.4) (Nikulin et al., 2012; Sylla et al., 2013; Dosio et al., 2015; Bador et al., submitted). Over the India-Tibet region and East Asia Kim et al. (2015b) and Kim and Park (2016) showed that differences among gridded precipitation datasets can generate significant uncertainties in deriving precipitation characteristics. The uncertainties vary according to regions, seasons, and statistical properties (Cross-Chapter-Box 10.3). Dosio et al. (2015) demonstrated uncertainty between precipitation datasets over parts of East Africa up to 3 mm/day, nearly as large as the inter-model spread. Kotlarski et al. (2017) compared three high-resolution observational temperature and precipitation datasets (E-OBS, a compilation of national/regional high-resolution gridded datasets, and the EURO4M-MESAN 0.22° reanalysis based on a high-resolution limited area model) with five EURO-CORDEX RCMs driven by ERA-Interim. Generally, the differences between RCMs are larger than those between observation datasets, but for individual regions and performance metrics, observational uncertainty can dominate. They also showed that the choice of reference dataset can have an influence in the RCM ranking score. Using a very different perspective, the agreement between model simulations may be used to estimate the uncertainty and quality of observations (Massonnet et al., 2016). There is *very high confidence* (*robust evidence and high agreement*) that multiple observational references at regional scale are fundamental for the model performance assessment.

Another example of uncertainty is related to the fact that global observational products such as remote-sensing derived data or reanalyses have higher uncertainty in data sparse regions when in-situ data are used to tune the algorithm/model. An example is the estimate of evapotranspiration, for which a large variety of methods based on remote sensing exists (Zhang et al., 2016c). Remotely sensed evapotranspiration products are mostly evaluated against the Fluxnet networks, which has a relatively dense coverage over North America, Europe and Japan (Ichii et al., 2017), but only a few sites over other regions. Consequently, evapotranspiration algorithms in surface and boundary layer parameterizations may be not representative for data sparse regions. Satellite products of evapotranspiration have been shown to have very large uncertainties over tropical South America (Sörensson and Ruscica, 2018), in particular for the annual cycle and variability, while uncertainties in the mean are largest over arid areas. Some well-documented agricultural droughts over arid areas were found to be unrepresented in satellite products due to uncertainties in the representation of radiation anomalies in the forcing data (Sörensson and Ruscica, 2018).

10.2.3 Use of observations

Two pathways concerning the fitness-for-purpose in observations can be identified: one is for the development of adaptation strategies (related for example to extreme precipitation in Japan (Shimpo et al., 2019)) and the other is for the evaluation and improvement of climate models and post-processing techniques.

10.2.3.1 Model evaluation and parametrization improvement

Many kinds of observation measurement are used to improve and develop new parameterizations for new generations of climate models. For example, although a parameterization of a land surface model is often developed over a certain soil type and might not be adequate for other types, adjustments can be done by constraining the model with observations. For example, by assimilating satellite brightness temperature observations with their LDAS-UT scheme (Yang et al., 2007) successfully optimized a land-surface model for the Tibetan plateau.

Adequate modelling of precipitation processes, especially for extreme precipitation, is still a challenging issue for regional climate modelling. Recent accumulation of three dimensional radar observations from space (e.g., TRMM and GPM) are utilized to examine regional characteristics of extreme rainfall and its environment (Hamada and Takayabu, 2018; Sohn et al., 2013), based on knowledge from global statistics of extreme rainfall characteristics (Hamada et al., 2015b).

Convective latent heating is an essential part of the diabatic heating of the atmosphere. Observational estimates of latent heating can be used for model evaluation (Section 10.3.3.5). The TRMM precipitation radar with the spectral latent heating algorithm (Shige et al., 2009) and the Convective Stratiform Heating product (Tao et al., 2016) enabled to have an estimate of the three dimensional convective heating. Since the latent heating profiles represent the precipitation characteristics even more directly than precipitation profiles themselves, the SLH product is able to clarify cumulus congestus regimes in subtropical regions aside the South Pacific Convergence Zone in the eastern Pacific ocean (e.g., Takayabu et al., 2010; Takayabu and Tao, 2020).

The scale representativeness is an issue in utilizing soil observations (Taylor et al., 2012, 2013a). Although a variety of technologies to measure soil moisture at the point scale exist (Dobriyal et al., 2012), its spatial representativeness is less than 1 m^2 (Ochsner et al., 2013; Liu et al., 2016b). Therefore, to be able to use in situ soil moisture for validating coarser-scale data from satellites or models, networks of point-scale measurements are used (Crow et al., 2015; Polcher et al., 2016). Smaller networks are typically of the size of a single climate model grid or a satellite pixel and are suitable for monitoring water sheds, while small numbers of those representing larger areas (>100 km^2) are emerging (Ochsner et al., 2013).

10.2.3.2 Statistical downscaling, bias adjustment and weather generators

Statistical downscaling, bias adjustment and weather generators are post-processing methods used to derive climate information from climate simulations. They all require observational data for calibration as well as evaluation (Section 10.3.3.3.3). Typically, the so-called perfect prognosis methods use quasi-observations for the predictors (i.e. reanalyses) and actual observations for the predictands (the surface variables of interest). By contrast, bias adjustment methods use observations only for the predictands. Weather generators typically require only observed predictands, although some are conditioned on predictors as well. Very often these methods operate on the daily scale, because of user needs, but also for the limited availability of sub-daily observations and the limited ability of climate models to realistically simulate sub-daily weather (Iizumi et al., 2012). Some methods are calibrated on the monthly scale, but some of the generated time series are then further disaggregated to the daily scale (e.g., Thober et al., 2014). Some methods, mainly weather generators, represent sub-daily weather (Mezghani and Hingray, 2009; Kaczmarska et al., 2014). Many methods simulate temperature and precipitation only, although some also represent wind, radiation and other variables. The limited availability of high quality and long observational records typically restricts these applications to a few cases (Pryor and Hahmann, 2019).

All limitations and challenges of observational data discussed in Section 10.2.2 apply to the use for post processing of climate model data. High quality and long observational data series are particularly relevant, as all statistical post-processing approaches require observations. Different reanalyses present significant discrepancies when used as key predictor variables at the daily scale (Brands et al., 2012; Dayon et al., 2015), suggesting that this data source may not be suitable for statistical downscaling.

An important issue for bias adjustment is the correct representation of the required spatial scale. Ideally, bias adjustment is calibrated against area-averaged data of the same spatial scale as the climate model output. Hence, high-quality gridded datasets with an effective resolution close to the nominal resolution are required. Driven by the need to generate regional scale information also in station sparse regions, researchers considered derived datasets that blend direct and remote sensing data to produce high-resolution observations to be used as predictands (e.g., Haiden et al., 2011; Wilby and Yu, 2013; Sections 10.2.1.2 and 10.2.2.4). Such developments are particularly important for statistical downscaling and bias adjustment.

10.2.3.3 Assimilation of data, including paleoclimate

Following some early concept studies, the first practical applications of paleoclimate data assimilation over past centuries used only selected data to reconstruct past climate changes for analysis of a specific process or case (Widmann et al., 2010). Recently, assimilation of multiple series from various data sources including tree rings, ice cores, lake cores, corals, and bivalves, has allowed production of reconstructions that can be widely shared and applied to multiple purposes as with modern reanalyses (Franke et al., 2017; Hakim et al., 2016; Steiger et al., 2018, Tardif et al. 2019). Most of these paleo-reanalyses are global but there are products using regional models or targeted at specific regions such as Europe, east Africa and Indian ocean (Fallah et al., 2018; Klein and Goosse, 2018).

Paleo-reanalyses are opening a new range of applications and have already provided useful information on seasonal to multi-decadal climate variability over the past millennia. They are useful tools to study the covariance between variables at interannual to centennial timescales and at regional to global spatial scales. In particular, they have highlighted the processes that can be responsible for change in continental hydrology at multi-decadal timescales (Franke et al., 2017; Klein and Goosse, 2018; Steiger et al., 2018). Paleo-reanalyses have confirmed a large contribution of internal variability in past changes at regional scale during the pre-industrial period, superimposed on a weak common signal due to forcing changes (Goosse et al., 2012; Goosse, 2017) and the absence of globally coherent warm period in the common era before the recent warming (Neukom et al., 2019). The reconstructions of the atmospheric state obtained in the reanalysis also provide a robust evidence of a local enhancement of warming or cooling conditions because of changes in atmospheric circulation, such as during the generally warm Medieval Climate Anomaly (950–1250 CE), the cooling observed in 1809/1810, or the cold and rainy 1816 summer in Europe (Goosse et al., 2012; Hakim et al., 2016; Franke et al., 2017; Schurer et al., 2019).

10.2.4 Outlook for improving observational data for regional climates

An encouraging development for understanding past climate variations over the last 250 years at the regional scale lies in the field of data rescue, in which hitherto hidden archives of meteorological data are brought to the forefront. At the global level, weather rescue is led by the Atmospheric Circulation Reconstructions over the Earth (ACRE) project (Allan et al., 2011). ACRE recovers land and ocean historical instrument data, which, after quality control, is made available for use as inputs or constraints in global or regional reanalyses. An example that benefits from that effort is the 56-member Twentieth Century Reanalyses (20CR; Compo et al., 2011), which is fed entirely by surface pressure observations and the addition of monthly sea surface temperature (SST) or sea-ice as boundary conditions. Alternatively, the ERA-20C reanalysis is a single-member product that assimilates surface pressure and marine winds over 1900–2010 (Poli et al., 2016a, 2016b), whereas CERA-20C provides a 10-member ensemble of coupled reanalysis, accounting for errors in the observational record as well as model error (Laloyaux et al., 2018). All these reanalyses are global, but their availability plays a central role in a large number of regional climate studies.

Particular techniques include the transcription of handwritten logbooks of meteorological observations from merchant shipping (e.g., Brönnimann et al., 2011), aided by participatory "citizen science" projects such as Old Weather (oldweather.org). Other projects include Operation Weather Rescue[1], which includes recent efforts to digitise mountain weather data from an observing outpost on the United Kingdom's highest mountain at the turn of the 20th century, or work to retrieve archives of Australian climate information (both examples reviewed in Ashcroft et al., 2016).

10.3 Using models for constructing regional climate messages

Much of the information available on future regional climate arises from studies based on climate model simulations. In this section, different types of models (Section 10.3.1) and model experiments (Section 10.3.2) for generating regional climate information are discussed, followed by an assessment of the performance, added value, and fitness-for-purpose of different model types (Section 10.3.3). The focus is put on representing large- to local-scale phenomena and processes relevant for regional climate. Finally, uncertainties of regional climate projections and methodologies to manage these are assessed (Section 10.3.4).

10.3.1 Types of models

Regional climate change information may be derived from a hierarchy of different model types covering a wide range of spatial scales and processes (see Figure 10.4 for an overview). The most relevant models will be introduced in the following. The application of any model relies on assumptions, depending on the specific model as well as the application. Table 10.1 gives an overview of the generic assumptions of the different model types discussed here for generating regional climate information. The violation of these assumptions will affect the model performance, which is discussed in Section 10.3.3.

[START FIGURE 10.4 HERE]

Figure 10.4: Typical model types and chains used in modelling regional climate. Grey lines: upstream model output is used without further post-processing. Orange lines: upstream model output is dynamically downscaled. Green lines: upstream model output is further statistically post-processed. The dashed lines indicate

[1] https://www.zooniverse.org/projects/edh/weather-rescue

model chains that might prove useful but have not or only rarely been used.

[END FIGURE 10.4 HERE]

[START TABLE 10.1 HERE]

Table 10.1: Assumptions underlying different model types in simulating regional climate change. Violating these assumptions will affect model performance (see links to different subsections for details). All future assumptions add to the present climate assumptions and are given conditional on the driving GCM simulating a plausible global climate sensitivity (Chapters 4 and 7). The assumptions listed for future climate applications of perfect prognosis (prog) statistical downscaling and bias adjustment are often called "stationarity assumption" **[Placeholder: Links to the chapter subsections need to be added yet.]**.

Model Type	Scale	Present Climate	Future Climate
GCM	Large	GCM includes all relevant large-scale forcings and simulates relevant large-scale circulation realistically.	GCM simulates processes controlling changes realistically. Parameterisations work in different climate.
	Regional	GCM includes all relevant regional forcings and simulates all relevant regional scale processes and feedbacks and their dependence on large-scale climate realistically.	GCM simulates processes controlling changes realistically. Parameterisations work in different climate.
RCM (dynamically downscaled GCM)	Large	As with GCM. The RCM does not deteriorate GCM simulations. Feedbacks from regional into large-scale processes are negligible.	As with GCM.
	Regional	As with GCM.	As with GCM.
Perfect prog statistical downscaling of GCM	Large	GCM simulates all relevant large-scale predictors realistically and bias free. The predictors represent the regional variability at all desired time-scales.	As with GCM. The predictors represent the response to external forcing.
	Regional	The statistical model structure is adequate to represent the predictor influence on regional-scale variability. There are no relevant feedbacks involving the predictands.	The statistical model structure is adequate under the required extrapolation.
Bias adjustment of dynamical model	Large	As with driving model.	As with driving model.
	Regional	As with driving model. The gap between driving model resolution and target resolution is minor.	As with driving model. The chosen bias adjustment is applicable in a future climate.
Delta change approach applied to dynamical model	Large	NA	As with driving model. There are no changes altering the non-changed statistics (e.g., no circulation changes that alter temporal structure)
	Regional	NA	As with driving model.

			There are no changes altering the non-changed statistics. The gap between driving model resolution and target resolution is minor.
Change factor weather generator applied to dynamical model	Large	NA	As with driving model.
	Regional	The weather generator structure is adequate.	As with driving model. The weather generator structure is adequate in a future climate. Change factors are adequately incorporated for all changing weather aspects. The gap between driving model resolution and target resolution is minor.

[END TABLE 10.1 HERE]

10.3.1.1 GCMs, including high-resolution and variable resolution GCMs

State of the art GCMs are generally used to derive climate information at continental to global scales both for the past and future climate (Chapters 3 and 4). Although the nominal horizontal resolution in CMIP5 GCMs is typically 100–200 km, which implies an effective resolution of 600 to 1000 km (Klaver et al., submitted) thereby strongly limiting their ability to resolve local details, their results have also been applied to study past and future regional climate change. There has long been a tension regarding how to best use available simulation resources among choices of increasing model resolution (to capture finer scale processes), enhancing the ensemble size (to better capture internal variability and more accurately determine the response to forcings), improving parameterizations and adding new processes, such as the carbon cycle. Despite these efforts, since AR5 the progress in reducing biases and providing more credible regional projections by GCMs and ESMs has been moderate. Now for AR6, several of the new CMIP6 (Eyring et al., 2016a) model intercomparison projects (MIPs)s address some of these limitations. The list of MIPs is provided in Chapter 3. HighResMIP (High-Resolution MIP, Haarsma et al., 2016) and GMMIP (Global Monsoons MIP, Zhou et al., 2016) specifically address the regional climate challenge using GCMs and ESMs. HighResMIP focuses on producing global climate projections at a horizontal resolution of around 50 km grid spacing or finer and GMMIP aims at better understanding and predicting of monsoons.

Apart from increasing resolution everywhere, variable resolution GCMs, that is, with locally enhanced resolution, have also been developed since the 1970s (Li, 1999), resulting in a first coordinated effort by Fox-Rabinovitz et al., (2006, 2008). An overview of recent developments has been given by McGregor, (2015). This is a rapidly developing field (Krinner et al., 2014; Ferguson et al., 2016; Huang et al., 2016) that will likely contribute to improved future regional projections.

10.3.1.2 RCMs

RCMs are dynamical models similar to GCMs that are run over a limited area, but with a resolution higher than that of standard GCMs. They are the basis for dynamical downscaling but are also often used for process understanding. At the domain boundaries, RCMs take their values from a driving data set, which could be a GCM or a reanalysis. RCMs are typically one-way nested: they do not feed back into the driving model, although two-way nested GCM-RCM simulations have been performed (Lorenz and Jacob, 2005; Harris and Lin, 2013; Junquas et al., 2016).

When RCMs are driven by GCMs, large-scale biases may be inherited through the lateral boundary conditions in addition to any inherent biases of the RCM itself (an issue usually referred to as 'garbage-in, garbage-out'; e.g., Dosio et al., 2015; Hall, 2014; Hong and Kanamitsu, 2014; Takayabu et al., 2016). The consistency between the circulation features simulated by the RCM and those inherited through the boundary conditions depends on two factors: 1) the relative importance of the large-scale forcing compared to local-scale phenomena, and 2) the size of the RCM domain (e.g., Diaconescu and Laprise, 2013). In fact, large (continental scale) domains allow the RCM to generate its own climate, including additional unforced, internal variability (Nikiema et al., 2017, and references therin). An approach to ensure, if desired, consistency with the driving model (e.g., to synchronize internal variability) is spectral nudging (Kida et al., 1991; Waldron et al., 1996; von Storch et al., 2000; Kanamaru and Kanamitsu, 2007) by which selected variables, such as the wind field, are forced to closely follow a prescribed large-scale field over a specified range of spatial scales, whereas smaller scales are generated by the regional model itself.

The CORDEX initiative (COordinated Regional climate Downscaling EXperiment; Giorgi et al., 2009; Giorgi and Gutowski, 2015; Gutowski Jr. et al., 2016) provides ensembles of high-resolution historical (starting as early as 1950) and future climate projections for various regions of the world. RCMs in CORDEX typically have had a horizontal resolution between 10 and 50 km. Much finer spatial resolution is required to fully resolve deep convection, an important cause of precipitation in much of the world. Therefore, an emerging strand in dynamical downscaling employs simulations at convection permitting scales, at horizontal resolutions of a few kilometres, where deep-convection parameterisations can be switched off, approximately resolving deep convection (Prein et al., 2015; Coppola et al., 2018; Stratton et al., 2018). A recent study indicates that explicitly simulating convection may be beneficial also in simulations performed at coarser resolutions (Vergara-Temprado et al., 2019). Alternatively, some RCMs make use of scale-aware parameterizations that are able to adapt to increasing resolution without switching off the convection scheme (Hamdi et al., 2012; De Troch et al., 2013; Plant and Yano, 2015; Giot et al., 2016; Termonia et al., 2018a; Yano et al., 2018).

RCMs often consist of atmospheric and land components that do not include all possible Earth-system processes and therefore neglect important processes such as air-sea coupling (in standard RCMs SSTs are prescribed from GCM simulations) or the chemistry of cloud-aerosol interaction (aerosols prescribed with a climatology), which may influence regional climate projections. Therefore, in recent years, many RCMs were extended by coupling to additional components like interactive oceans, sometimes with sea-ice, (Kjellström et al., 2005; Somot et al., 2008; Van Pham et al., 2014; Sein et al., 2015; Ruti et al., 2016), rivers (Sevault et al., 2014; Lee et al., 2015; Di Sante et al., 2019), glaciers (Kotlarski et al., 2010), and aerosols (Zakey et al., 2006; Zubler et al., 2011; Nabat et al., 2015). The coupling of these components allows for the investigation of additional climate processes such as regional sea-level change (Adloff et al., 2018), ocean-land interactions (Lima et al., 2019; Soares et al., 2019a), or the control of high-frequency ocean-atmosphere coupling on the climatology of Mediterranean cyclones (Flaounas et al., 2018). If such RCMs are extended by additional components (such as the carbon cycle), they may be named Regional Climate System Models (RCSMs; Somot et al., 2018) or Regional Earth System Models (RESMs; Giorgi and Gao, 2018).

10.3.1.3 Sub-component models

A selection of sub-component models developed to represent the influence of sub-grid processes is introduced in this section. The relevance of including these models in GCM or RCM coupled simulations will be assessed in Section 10.3.3.

10.3.1.3.1 Natural aerosols

Dust has traditionally been specified with a climatological estimate in climate simulations. However, interactive dust emission modules that are able to correctly simulate the dust optical depth in most of the key emission regions have only been recently introduced (Pu and Ginoux, 2018). Dust variations are controlled by changes in surface winds, precipitation, and vegetation, which in turn are modulated at multiple time scales by dominant modes of internal climate variability. For instance, the dust increase during the first decade of the 21st Century in the Middle East has been associated with drought conditions in the Fertile Crescent (Yu et al., 2015) that could have been amplified by anthropogenic warming (Kelley et al., 2015).

This complexity points at the importance of including model components that represent the interaction between the atmosphere, the land surface and dust emissions.

The impact of volcanic eruptions on the climate variability modes can shape regional climates for a few years after the eruption and can be seen as a unique source of predictability for climate (Ménégoz et al., 2018a). This requires models to capture these impacts, which still remains a limited ability with model-dependent results. A better integration of the volcanic aerosol in GCMs is evaluated in VolMIP (Zanchettin et al., 2016). The need for a good knowledge of initial conditions is also key, since the response is very sensitive to them (Ménégoz et al., 2018b; Zanchettin et al., 2019). However, a better performance requires taking into account volcanic location (Haywood et al., 2013; Pausata et al., 2015; Stevenson et al., 2016; Liu et al., 2018a), strength (Emile-Geay et al., 2008; Lim et al., 2016c; Liu et al., 2018b), and seasonality (Stevenson et al., 2017; Sun et al., 2019a, 2019b) into consideration. For instance, observations now made available by new satellites (Vernier et al., 2011) have been suggested to be used for the four-dimensional evolution of aerosol clouds in climate models, accounting at the same time for spatial variations (Yang et al., 2019).

10.3.1.3.2 Anthropogenic aerosols

To account for the effects of anthropogenic aerosols on regional climate, these can be represented in climate models (GCMs or RCMs) using modules of differing complexity. Without a fully coupled chemistry module, the radiative forcing can be simulated by specifying the optical properties from observations and prescribe the effect of the aerosols on the cloud droplet number with the single plume parameterization scheme (Fiedler et al., 2017, 2019; Stevens et al., 2017). In models with fully coupled chemistry modules the emissions of anthropogenic aerosols and reactive species are prescribed, and the model simulate the aerosol load and the optical and cloud perturbations that lead to the final spatio-temporal distribution of radiative forcing (Myhre et al., 2013; Ghan et al., 2016).

10.3.1.3.3 Land management models

Land management has been implemented in GCMs and RCMs since AR5, two important examples being irrigation and tillage. Irrigation increases the soil moisture, enhancing the latent heat flux and reducing the sensible heat flux and, in turn, local temperature. The simplest approach to implementing irrigation demand in a model is to define it as the difference between actual and desired soil moisture availability, the latter most commonly set to field capacity (Nazemi and Wheater, 2015). This demand is applied to areas equipped for irrigation and often applied all year round (Pokhrel et al., 2016) resulting in an overestimation of actual irrigation demand. The simplest way to implement supply of water to fill the irrigation demand is to add water from an infinite surface storage until the demand is covered (Tuinenburg et al., 2014; Nazemi and Wheater, 2015; Pokhrel et al., 2016). Another approach forces the model with historical irrigation data constructed from data assessment irrigation data and offline hydrological modelling, which can improve the spatio-temporal heterogeneity of irrigation (Shukla et al., 2014; Wada et al., 2014; Cook et al., 2015b).

Tillage lowers the surface albedo by replacing light-coloured crop residue with darker soil, making the surface absorb more energy. The effect of tillage versus no-tillage systems in coupled simulations has been implemented through changes in albedo and, to account for effects on evaporation, soil resistance (Davin et al., 2014; Hirsch et al., 2017, 2018).

10.3.1.3.4 Lake models

Lakes have very different surface properties in comparison to land (lower surface roughness and albedo, and higher thermal conductance and heat capacity), and their presence in a landscape introduces large heterogeneities of temperature and evapotranspiration. A common way of accounting for the difference between land and lake temperatures has been to put the lake temperature and lake ice conditions equal to those at the closest sea point. This approach is problematic for seasonally ice-covered lakes, sea temperature falls much slower during autumn than the actual lake temperature would and therefore creates an artificial heat and moisture source to the atmosphere (Kirillin et al., 2012; Pietikäinen et al., 2018).

Lake models have been incorporated in RCMs (Martynov et al., 2010; Samuelsson et al., 2010; Gula and Peltier, 2012; Bennington et al., 2014). Most lake models assume that the horizontal gradient of temperature is negligible in comparison to the vertical gradient to justify a 1D approach. Although this can be problematic for large lakes (León et al., 2007), the large computational cost of coupled 2D and 3D lake models prevents this approach (Pietikäinen et al., 2018). A multi-layer model can describe the lake thermocline without parameterization (Xiao et al., 2016), but is computationally expensive. Therefore, the most common approach in RCMs is the two-layer model, including a lake-ice model, with parameterized vertical temperature profiles based on measurements (Mironov et al., 2010; Golosov et al., 2018).

10.3.1.4 Statistical approaches to generate regional climate projections

An alternative or addition to dynamical downscaling is the use of statistical approaches to generate regional projections. In AR5 these methods have been collectively referred to as statistical downscaling, but have received little attention. A major conclusion was that a wide range of different methods exist and a general assessment of their performance is difficult (Flato et al., 2014). Since AR5, several initiatives have been launched to improve the understanding of statistical approaches such as VALUE (which has been merged into the EURO-CORDEX activities; Maraun et al., 2015), STARMIP (Vaittinada Ayar et al., 2016) and BADJAM (Galmarini et al., 2019). The performance of different implementations of these approaches will be assessed in Section 10.3.3.

10.3.1.4.1 Perfect prognosis

Perfect prognosis models are statistical models calibrated between observation-based large-scale predictors (e.g., from reanalysis) and observed local-scale predictands. Regional climate projections are then generated by replacing the quasi-observed predictors by those from climate model (typically GCM) projections. Typical implementations of perfect prognosis models include regression-like models and the analogue method.

Regression-like models rely on a transfer function linking an observed local statistic (such as the temperature at a given day) to some set of large-scale predictors. Recent developments include the development of stochastic regression models to explicitly simulate local variability (San-Martín et al., 2017; those explicitly modelling temporal dependence are assessed in Section 10.3.1.4.4). Recently, the use of machine learning techniques has been proposed, including genetic programming to construct a data-driven model structure (Zerenner et al., 2016) and deep and convolutional neural networks (Reichstein et al., 2019).

Analogue methods (e.g., Maraun and Widmann, 2018b) are based on the assumption that two similar large-scale atmospheric fields typically result in similar local weather fields. Thus, analogue methods compare a simulated large-scale atmospheric field with an archive of observed atmospheric fields and select, by some distance metric, the observed field closest to the simulated field as analogue. The downscaled atmospheric field is then chosen as the local atmospheric field observed on the instant the analogue occurred. New analogue methods have been developed to simulate unobserved values including a rescaling of the analogue (Pierce et al., 2014) or by combining analogues and regression models (Chardon et al., 2018).

10.3.1.4.2 Bias adjustment

Bias adjustment is a statistical post-processing technique used to pragmatically reduce the errors in climate model outputs. The approach estimates the bias or relative error between a chosen simulated statistical property (such as the long-term mean or specific quantiles of the climatological distribution) and the corresponding observed one over a calibration period; the simulated statistic is then adjusted taking into account the simulated deviation. Bias adjustment methods are regularly applied on spatial scales similar to that of the simulation being corrected, but they are often used as a simple statistical downscaling method by calibrating them between coarse resolution (e.g., GCM) model output and finer observations. The most important difference between perfect prognosis and bias adjustment is that, whereas perfect prognosis can link any physically sensible predictor at a given day to any local atmospheric variable, bias adjustment can only link long-term statistics of a simulated atmospheric variable to the same long-term statistic of the same observed atmospheric variable. By construction, the bias of the adjusted statistical property vanishes over the calibration period. In a climate change context this approach assumes that biases are time invariant (Table 10.1 for further specification of this assumption).

Typical implementations of bias adjustment are (1) additive adjustments, where the model data is adjusted by adding a constant, (2) rescaling, where the model data is adjusted by a factor, (3) or more flexible quantile mapping approaches that adjust different ranges of a distribution individually. One strand of research on new bias adjustment methods since AR5 has focused on the development of trend-preserving quantile mapping methods and multi-variable methods. Hempel et al. (2013), Pierce et al. (2015), Switanek et al. (2017), and Lange (2019) developed variants of quantile mapping that preserve trends in the mean or even further distributional statistics. Multivariate bias adjustment extends univariate methods, which adjust statistics of individual variables separately, to joint adjustment of multiple variables simultaneously. Implementations remove biases in (1) specific measures of multivariate dependence, like correlation structure, via linear transformations (Bárdossy and Pegram, 2012; Cannon, 2016), or, more flexibly, (2) the full multivariate distribution via nonlinear transformations (Vrac and Friederichs, 2015; Cannon, 2018; Vrac, 2018; Robin et al., 2019). Other research strands focus on the explicit separation of bias adjustment and a subsequent stochastic downscaling (Volosciuk et al., 2017; Lange, 2019c), or the integration of process understanding (Maraun et al., 2017b), such as by conditioning the adjustment on the occurrence of relevant phenomena (Manzanas and Gutiérrez, 2019). Over recent years, several issues have been identified that may arise when using bias adjustment. These are discussed in Cross-Chapter Box 10.2.

10.3.1.4.3 Delta change approaches

A mathematically similar though conceptually very different approach to bias adjustment is the delta change approach. Here, selected observations are modified according to corresponding changes derived from dynamical model simulations. Traditionally, only long term means have been adjusted, but recently approaches to modify temporal dependence (Webber et al., 2018) have been developed, as well as quantile mapping approaches that individually adjust quantiles of the observed distribution (Willems and Vrac, 2011).

10.3.1.4.4 Weather generators

Weather generators are statistical models that simulate weather time series of arbitrary length. They are calibrated to represent observed weather statistics, in particular temporal day-to-day (or even sub-daily) variability. One variant of these models is conditioned on large-scale atmospheric predictors on a day-by-day basis. These models are advanced stochastic perfect prognosis methods underlying the same assumptions. Recent multisite-examples are based on, for instance, generalised linear models (Chandler, 2019). Another widely used variant is change-factor weather generators: the weather generator parameters are calibrated against present and future climate model simulations, and the climate change signal in these parameters is then applied to the parameters calibrated to observations. Such weather generators evolve randomly on a day-by-day basis and take only long-term changes from the climate model. Recent research has mainly focussed on multi-site Richardson type (Markov-chain) weather generators (Keller et al., 2015; Dubrovsky et al., 2019), some explicitly modelling extremes and extremal dependence (Evin et al., 2018).

10.3.2 Types of experiments

The most commonly used experiments to generate regional climate change information are transient simulations. Alternative experiment types may better serve for a specific purpose. The role of these experiment types for generating regional climate information will be assessed in the following.

10.3.2.1 Transient simulations and time-slice experiments

Transient simulations intend to represent the evolving climate state of the Earth system (Chapter 4). They are typically based on some of the CMIP-type coupled GCM simulations, such as those in the DECK and ScenarioMIP part of CMIP6 covering the period 1850–2100 (Eyring et al., 2016a), and HighResMIP (although covering only the period 1950–2050 due to computational constrains; Haarsma et al., 2016). Global transient climate simulations may be further downscaled by either dynamical or statistical downscaling. Currently available CORDEX RCM simulations (1950–2100) are based on CMIP5 (Gutowski Jr. et al., 2016).

On the contrary, time-slice experiments are designed to represent only a short, specific period of time (typically 30 years). They are often run using GCMs or RCMs in atmosphere-only mode, forced by SSTs derived either from observations, like in the AMIP experiments, or historical simulations and future projections from coupled GCMs. Compared to the transient simulations, they offer advantages in being computationally cheaper (due to the lack of coupled ocean and short duration), which allows for the number of ensemble members (Zhang et al., 2016d), and/or the resolution (Haarsma et al., 2013a; Davini et al., 2017) to be increased. Convection-permitting simulations, both covering the globe or particular regions, are currently conducted for short time slices only (Kendon et al., 2017; Coppola et al., 2018; Hewitt and Lowe, 2018). Some time-slice experiments have been carried out for coupled ocean atmosphere RCMs (Sein et al., 2015; Zou and Zhou, 2016, 2017).

10.3.2.2 Pseudo-global warming experiments

Often, results from downscaling experiments suffer from large-scale circulation biases in the driving GCMs such as misplaced storm tracks (Section 10.3.3.4). Moreover, changes in the atmospheric circulation are often uncertain owing to both climate response uncertainty (Section 10.3.4.2) and internal variability (Section 10.3.4.3). If, in a given application, one can assume that changes in the regional climate aspects of interest are dominated by thermodynamic rather than by circulation changes, so-called pseudo-global warming (PGW) experiments (Schär et al., 1996) may be helpful in mitigating the effects of circulation biases, and to fix the large-scale circulation to present climate. In classical PGW experiments, boundary conditions for the downscaling are taken from reanalysis data, though modified according to the thermodynamic aspects of climate change simulated by GCMs. These changes are added to the reanalysis by modifying the 3-dimensional temperature and moisture fields according to GCM-simulated changes. The large-scale dynamical fields are unchanged, assuming that they are not influenced by the imprinted thermodynamic changes. The boundary conditions thus represent the observed weather sequence as represented by the reanalysis, but with adjusted temperatures, humidity and atmospheric stability. Recent applications of PGW experiments include an assessment of climate change in Japan (Adachi et al., 2012; Kawase et al., 2012, 2013), the Los Angeles area (Walton et al., 2015), Hawaii (Zhang et al., 2016a), and the Alps (Keller et al., 2018). Recently, PGW studies have been generalised to modify GCM simulations with the objective of separating the drivers of regional climate change, such as the Mediterranean amplification (e.g., Brogli et al., 2019; Section 10.3.2.3).

Equivalent simulations can be conducted for individual events, thereby allowing for very high resolution. With counterfactual past climate conditions, such simulations can be used for conditional event attribution (Trenberth et al., 2015; Chapter 11), with hypothetical future conditions to generate storylines of how specific events may manifest in a warmer climate. The approach has been employed to study extreme events that require very high resolution simulations such as tropical cyclones (Lackmann, 2015; Takayabu et al., 2015; Kanada et al., 2017; Gutmann et al., 2018; Patricola and Wehner, 2018) or convective precipitation events (Pall et al., 2017; Hibino et al., 2018). The range of possible events is broader and has included Korean heat waves (Kim et al., 2018) and monsoon onset in West Africa (Lawal et al., 2016). However, if only individual events are simulated, no conclusions can be derived directly on changes in the occurrence probability of these events (Otto et al., 2016a; Shepherd, 2016).

10.3.2.3 Sensitivity studies with selected drivers

Sensitivity studies are used to disentangle and document the impact of a specific driver or process on a given climate change or phenomenon. The influence of a single external forcing can be assessed with transient historical simulations within two different frameworks (Bindoff et al., 2013; Gillett et al., 2016). The former entails performing simulations with prescribed (often observed) changes only in the external forcing of interest, the others being fixed at a constant value (often pre-industrial). The latter is based on simulations in which all external forcings are applied but the one of interest. Both approaches in general do not give the same results as the climate response to a range of forcings is not necessarily identical to the sum of climate responses to individual forcings (Ming and Ramaswamy, 2011; Jones et al., 2013; Schaller et al., 2013; Shiogama et al., 2013; Marvel et al., 2015; Deng et al., 2019).

To study the influence of internal variability, new approaches such as partial coupling simulations are now routinely used since AR5. These are coupled ocean-atmosphere simulations in which the interaction between the atmosphere and the ocean is only one-way over an oceanic basin or sub-basin and two-way everywhere else. Different implementations have been used such as SST anomaly Newtonian relaxation at the air-sea interface or prescribing daily or higher frequency wind stress anomalies from reanalysis (Kosaka and Xie, 2013, 2016; England et al., 2014; McGregor et al., 2014; Douville et al., 2015; Deser et al., 2017a). Such simulations have been applied to identify the regional impacts of the AMV (Ruprich-Robert et al., 2017, 2018).

Another framework is used to evaluate the impact land conditions have on a climate phenomenon. The modelling framework consists of a pair of model experiments, with one simulation serving as control run, and a perturbed simulation with prescribed land conditions (i.e., soil moisture, leaf area index, and surface albedo) characterizing a specific state of the land surface. The difference between the perturbed and control simulations enables a robust assessment of the possible impact of land conditions on e.g., large-scale droughts and heatwaves (Seneviratne et al., 2013; Stegehuis et al., 2015; Hauser et al., 2016, 2017; Vogel et al., 2017; Rasmijn et al., 2018).

RCM sensitivity simulations have been used in a similar way to assess the contribution of different large-scale drivers to projected regional climate change (Brogli et al., 2019b, 2019a) and the influence of selected drivers on observed extreme events (Meredith et al., 2015b; Wang et al., 2017a; Ardilouze et al., 2019).

10.3.2.4 Control simulations

Over recent years, the role of internal variability has become clearer in the interpretation of climate projections, in particular at the regional scale (Section 10.3.4.3). A considerable fraction of CMIP5 and CMIP6 resources has therefore been invested in generating an ensemble of control simulations with prescribed constant external forcings. These are often several hundred years long, and sometimes much longer (Pedro et al., 2016; Rackow et al., 2018). As part of the CMIP6 DECK (Eyring et al., 2016a) pre-industrial control (piControl) simulations have been conducted (Menary et al., 2018).

Similarly, control simulations with present-day conditions (pdControl) have been performed to represent internal variability under more recent concentrations of forcing agents (Pedro et al., 2016; Williams et al., 2018). Control simulations have been used to study the role of internal variability, teleconnections and many other fundamental aspects of climate models (Wang et al., 2015c; Krishnamurthy and Krishnamurthy, 2016). Unforced internal variability is a fundamental aspect of regional climate as any response to external forcings in experiments with variable forcings will interact with this type of variability (Thompson et al., 2015; Deser et al., 2017b). These simulations are also used along with large ensembles of historical or scenario simulations to assess the characteristics of the regional internal climate variability (Olonscheck and Notz, 2017).

10.3.2.5 Simulations for evaluating downscaling methods

Since AR5, reanalysis-driven RCMs have been extensively evaluated for many regions of the world, especially in the framework of the CORDEX project (see the examples in the Atlas). Experiments driven by perfect boundary conditions or predictors (observations or reanalysis) can be useful to evaluate downscaling performance (Frei et al., 2003; Laprise et al., 2013). In such a setting, any discrepancy between the modelled and observed climate arises only from errors in the downscaling method (Laprise et al., 2013) or internal climate variability generated by the downscaling method.

A comprehensive inter-comparison of statistical downscaling, bias adjustment and weather generators is lacking, although several methodologies have been evaluated over specific regions. Over Europe, the VALUE initiative assessed the performance of statistical downscaling for marginal, temporal, and spatial aspects of temperature and precipitation including extremes, and performed a process based evaluation of specific climatic phenomena (Gutiérrez et al., 2018; Maraun et al., 2018). Alternatively, statistical downscaling can be evaluated in the so-called perfect model or pseudo reality simulations (Charles et al., 1999), where a high-resolution climate model simulation is used as proxy for a hypothetical present and future reality. A statistical downscaling model is first calibrated with this pseudo present-day climate and, subsequently, assessed whether it correctly reproduces the future conditions (Dixon et al., 2016).

10.3.3 Model performance and added value in simulating and projecting regional climate

Assessing model performance is a prerequisite for characterizing confidence in regional climate projections. This section sets out with a discussion of evaluation diagnostics and the concept of added value, followed by an overall performance assessment to simulate regional climate with different model types. A key part of the subsection addresses performance to simulate relevant phenomena and processes at both large and small scales as well as the representation of past regional trends. The subsection closes with an assessment of approaches to link model performance in present climate to the model fitness for simulating future regional climate.

10.3.3.1 Evaluation diagnostics

Model evaluation compares simulated aspects of the climate system with the corresponding observed ones. The comparison involves two components: what is compared, typically measured by a quantitative statistic or index (referred to as diagnostic; see Chapter 1), and the quantification of the mismatch between model and an observational reference (referred to as performance measure or metric; Gleckler et al., 2008; Maraun et al., 2018).

Since AR5, model evaluation has made use of a broad combination of diagnostics (Kotlarski et al., 2014; Eyring et al., 2016b; Gleckler et al., 2016; Ivanov et al., 2017, 2018), ranging from long-term means to indices of extreme events (Zhang et al., 2011; Sillmann et al., 2013) or a combination of those (Dittus et al., 2016). More complex diagnostics are used to characterize specific meteorological phenomena (Sprenger et al. 2017), such as ENSO feedbacks (Bellenger et al., 2014), Madden-Julian Oscillation (MJO) characteristics (Ahn et al., 2017; Benedict et al., 2014; Jiang et al., 2015; Kim et al., 2015), extra-tropical modes of variability (Lee et al., 2019), cyclone tracking (Neu et al., 2013), or front detection (Hope et al., 2014; Schemm et al., 2015). However, the mismatch between observations and a model simulation might be caused solely by internal variability, particularly in the case of teleconnections and trends, especially for diagnostics calculated over short time periods (Notz, 2015; Deser et al., 2017c).

Diagnostics are a complex set. To characterise compound events (Zscheischler et al., 2018), a family of events defined by several variables that might not be extreme individually, new diagnostics for multivariate dependencies are needed (Hobaek Haff et al., 2015; Wahl et al., 2015; Sippel et al., 2016, 2017; Tencer et al., 2016; Bevacqua et al., 2017; Careto et al., 2018). Their success depends on the availability of relevant observational data (Section 10.2.2). Multivariate dependences discovered in compound events can also be used for designing and evaluating multivariate bias correction and statistical downscaling. Process-based diagnostics are useful for identifying the cause of models errors, although it is not always possible to associate a systematic error with a specific cause (Eyring et al., 2019). AR5 discussed two main approaches of process-based evaluation: 1) the isolation of physical components or parameterizations by dedicated experiments (as discussed in Section 10.3.2.4) and 2) diagnostics conditioned on relevant regimes, usually synoptic-scale weather patterns. The regime-based approach has been used with both GCMs (e.g., Catto et al., 2015) and RCMs (Endris et al., 2016; Whan and Zwiers, 2017; Pinto et al., 2018), but also with perfect prognosis and bias adjustment methods (Kjellström et al., 2013; Marteau et al., 2015; Addor et al., 2016; Beranová and Kyselý, 2016; Soares and Cardoso, 2018; Soares et al., 2019b).

Recent studies highlight the importance of user-defined or user-relevant diagnostics for model evaluation (Maraun et al., 2015; Rössler et al., 2019b). Diagnostics have been used to assess the performance of climate models to produce useful input data for impact models as in the comparison between RCMs and convection permitting models to capture flood generating precipitation events in the Alps (Reszler et al., 2018). Alternatively, the observed impact can be compared to that simulated by an impact model with input from both observations and climate models. This approach has been used to evaluate the influence of statistical downscaling and bias adjustment on hydrological (Rojas et al., 2011; Chen et al., 2012c; Gutiérrez et al., 2018; Rössler et al., 2019b), agricultural (Ruiz-Ramos et al., 2016; Galmarini et al., 2019), forest and wildfire (Abatzoglou and Brown, 2012; Migliavacca et al., 2013), and regional ocean modelling (e.g., Macias et al., 2018).

10.3.3.2 Model improvement and added value

Obtaining regional information from global simulations may involve a range of different methods (see Section 10.3.1). An approach with higher complexity or resolution is useful if it adds further, useful information to that of a reference model (such as a standard GCM). This further useful information is often referred to as added value and is a function of variables, processes, and the temporal and spatial scales targeted taking into account the needs of specific users (Di Luca et al., 2012; Ekström et al., 2015; Giorgi and Gutowski, 2015; Torma et al., 2015; Rummukainen, 2016; Falco et al., 2018). There is no common definition of added value. Added value is considered here to be a characteristic that arises when one methodology attempts to give further value to what another methodology yields. The added value of downscaling GCM simulations is most likely where regional- and local-scale processes play an important role in the climate of a region, for example in complex or heterogeneous terrain such as mountains (Lee and Hong, 2014; Prein et al., 2016a), along coastlines (Feser et al., 2011; Herrmann et al., 2011), or where convective processes are important (Prein et al., 2015). Precipitation, in particular, is a variable where downscaling potentially can provide a substantial added value, because precipitation events are often regional in scale and short in duration.

Most frequently, added value is discussed in terms of downscaling methods when adding value to the GCM output that yields useful added detail. Assessment of the further detail added to GCM output and the value of attaining it depends in part on the particular interests of the user (Di Luca et al., 2016). However, a common baseline expectation is that the downscaling method should give improved representation of the climate of a region compared to the driving data from the GCM (Di Luca et al., 2015), though arguably, there should be a clear physical reason for the improvement. Depending on the chosen definition, different statistical approaches may or may not add value to dynamical model simulations (Maraun et al., 2018). Perfect prognosis incorporates process information and may, in principle, add value. Bias adjustment and change factor weather generators intrinsically cannot improve the representation of processes and only add detail to long-term climatologies.

A variety of performance measures can provide assessment of added value, such as errors versus observations on fine spatial scales (Di Luca et al., 2016), coherence of simulated versus observed spatial patterns (Di Luca et al., 2016), matching of probability distribution functions (Soares and Cardoso, 2018), and field-significance tests of spatially distributed errors (Wilks, 2016; Ivanov et al., 2017, 2018). The added value likely depends on the region, season, and governing physical processes (Lenz et al., 2017; Schaaf and

Feser, 2018).

A first step in determining added value in downscaling is to analyse whether or not the downscaling procedure gives detail on spatial or temporal scales not well-resolved by a GCM, thus indicating the potential to represent climatic features missing in the GCM output. This added detail, referred to as potential added value (PAV; Di Luca et al., 2012), is not in itself sufficient to demonstrate added value in downscaling (Takayabu et al., 2016), but lack of PAV indicates that the downscaling method lacks usefulness. An advantage of a PAV analysis is that it sidesteps the challenge of having high resolution observations available to assess if there is true added value. Instead, relatively simple simulation experiments with fine and coarse-resolution simulations by the same model are used to see how well applying downscaling to the coarse simulation produces output that agrees with the fine-resolution simulation. Because the evaluation rests on model simulations only, one can assess the PAV for multiple fields and determine if there are physically consistent outcomes that help identify the processes yielding the PAV. Such analysis can provide a physical basis for examining whether or not added value exists with respect to observed and projected climates. Simulations known as “big brother” experiments (Di Luca et al., 2012) have demonstrated PAV and reasons for its occurrence for some regions (Di Luca et al., 2012; Lenz et al., 2017).

Evaluating added value contributes to estimating the quality of regional information. Several studies have demonstrated the added value of downscaling in specific contexts, both for current climate and for climate projections (Sections 10.3.3.4 to 10.3.3.10). However, added value is not guaranteed simply by producing model output at finer resolution; it can depend on several factors, such as general framework of the simulation and the specific climatic variables analysed (Di Luca et al., 2012; Hong and Kanamitsu, 2014; Xue et al., 2014). Unforced, internal variability and sampling methodologies can obscure the climate signals being evaluated (Laprise, 2014).

A further challenge, especially for increasingly higher resolutions, is that adequate observational data may not be available to assess added value (e.g., Di Luca et al., 2016; Zittis et al., 2017; Section 10.2). This implies a need for additional efforts to obtain and quality-control higher resolution observational (or observation-based) data sets. Univariate demonstration of added value is necessary, but even that may not be sufficient, as better agreement with observations in the downscaled variable may be a consequence of compensating errors that are not guaranteed to compensate similarly as climate changes. Multivariate analysis of added value is more able to demonstrate physical consistency between observed and simulated behaviour (Prein et al., 2013a; Meredith et al., 2015a; Reboita et al., 2018).

10.3.3.3 Overall performance of different model types

The ability to simulate regional climate realistically is a formidable challenge and while improvements to do so, as measured by performance measures (Section 10.3.3.1), have been steady, progress has also been very slow (Fernández et al., 2019). The first level of performance assessment for the construction of regional climate messages tackles the evaluation of the fitness of the most common user variables such as temperature and precipitation. Model performance addresses not only the assessment of a single model, but also the evolution of multi-model ensembles, which are one of the most common tools to build regional climate messages for the future. As an example, Sillmann et al. (2013) found that the spread of metrics among CMIP5 models for several extreme temperature indices are reduced compared to CMIP3 models. In a multi-model context, climate models exhibit large inter-model differences (Matte et al., 2019). This occurs due to the substantial variety in model biases, which largely dominate model performance. They are a symptom of processes not represented correctly in the models and complicate the extraction of useful climate change information. In certain cases, systematic errors are common across a model class, performance metrics highlighting pervasive problems in the models (Wang et al., 2015a; Nikiema et al., 2017). In the following, the performance of the different model types described in Section 10.3.1, GCMs, RCMs and statistical models, will be discussed. The role of sub-component models will be discussed where appropriate. An illustration of dynamical model performance can be found in Figures 10.5 and 10.6, while examples for statistical model performance are in Table 10.2.

[START FIGURE 10.5 HERE]

Figure 10.5: Illustration of some systematic errors in simulations performed with dynamical models. (a) Top row: Mean summer (June to August) near-surface air temperature (in °C) over the Mediterranean area in two observational datasets with the first panel for Berkeley surface temperature dataset (BEST) (Rohde et al., 2013) and the second panel for E-OBS v19.0e (Cornes et al., 2018), and mean bias for five multi-model experiments with GCMs (CMIP5, CMIP6 and HighResMIP) and RCMs (CORDEX EUR-44 and EUR-11). Biases of the CMIP ensembles are shown with respect to BEST, HighResMIP and CORDEX ensembles with respect to E-OBS. Bottom row: Box-and-whisker plot of the yearly mean summer near-surface temperature averaged over the western Mediterranean area (33°N–45°N, 10°W–10°E, black quadrilateral in the first panel of the top row) for a set of references and single model runs of the five multi-model experiments (one simulation per model). Additional observation and reanalysis data included in the bottom row are CRU TS v4.02, E-OBS v17, ERA-Interim, EWEMBI, HadCRUT4, JRA-55, NCEP/NCAR (Kalnay et al., 1996; Dee et al., 2011; Morice et al., 2012; Harris et al., 2014; Kobayashi and Iwasaki, 2016; Cornes et al., 2018; Lange, 2019b). As (a) but for precipitation rate (mm day^{-1}) and showing Global Precipitation Climatology Centre (GPCC) version 2018 (Schneider et al., 2017) in the first panel of the top row. Biases of the CMIP ensembles are shown in respect to GPCC. Additional observation and reanalysis data included in the bottom row are CRU TS v4.02, E-OBS v17, ERA-Interim, EWEMBI, GHCN (Jones and Moberg, 2003; Dee et al., 2011; Harris et al., 2014; Cornes et al., 2018; Lange, 2019b). All results correspond to the period 1986–2005. **[Placeholder: The maps for EUR-44 and EUR-11 need to be completed]**

[END FIGURE 10.5 HERE]

[START FIGURE 10.6 HERE]

Figure 10.6: Probability density function of the winter (December to February, top) and summer (June to August, bottom) daily precipitation in the HighResMIP, CMIP5 (eight models), CORDEX EUR-44 (27 models) and EUR-11 (36 models) multi-model simulations for different European regions: France (FR), Central Europe (CE), Mediterranean (MD) and Scandinavia (SC). **[Placeholder: Observations will be added]**

[END FIGURE 10.6 HERE]

10.3.3.3.1 GCMs

GCMs are known for having pervasive systematic errors in some aspects of their large-scale behaviour (e.g., Oueslati and Bellon, 2015; see Section 10.3.4 and Chapter 3). They also show substantial systematic errors in precipitation and temperature at different regional scales: continental (Prasanna, 2016), national (Lovino et al., 2018) and local (Jiang et al., 2015). The systematic errors, which appear both in the mean and in higher order moments (Ren et al., 2019) of the climatological distribution of the variable (Figure 10.5), can be as high as 100% and have been considered an important limiting factor in model usability (Palmer, 2016). Performance at the regional scale is assessed in terms of the time or spatial averages (Prasanna, 2016), the ability to reproduce the seasonal cycle (Hasson et al., 2016), or a set of extreme indicators. In many cases, the performance estimates have been used to select models for an application or more in depth study (Lovino et al., 2018), to select the models that provide boundary conditions to perform RCM simulations (McSweeney et al., 2015) or to weight the results of the GCM simulations (Sanderson et al., 2015). Regional biases could occur even if all the relevant large-scale processes are correctly represented, but not their interaction.

The special class of high-resolution GCMs (Prodhomme et al., 2016) are expected to improve some of the regional processes that are not appropriately represented in standard GCMs, such as the drought forcing by the circulation (van Haren et al., 2015). There is general agreement that increasing global model resolution improves some long-standing biases (Schiemann et al., 2014; Dawson and Palmer, 2015; Feng et al., 2017; Fabiano et al., submitted), although the resolution increase is not a guarantee of overall improvement. For instance, increasing resolution at GCM scale has been shown to improve Asian monsoon rainfall anchored to orography and the monsoon circulation (Johnson et al., 2016). However, it fails to solve the major dry bias.

Some efforts have been undertaken to obtain similar improvements in performance using stochastic parameterisations in standard resolution models (MacLeod et al., 2016; Zanna et al., 2017, 2019; Strømmen et al., 2018).

Despite the known systematic errors in temperature and precipitation that affect model performance, there is *high confidence* that GCMs provide useful information for the generation of future climate messages at the regional scale. There is *robust evidence and high agreement* that the increase of global model resolution can help in reducing a number of the systematic errors limiting performance, although resolution per se does not automatically solve all performance limitations shown by GCMs.

10.3.3.3.2 RCMs

GCMs tend to have difficulties in simulating climate over regions with complex topography or strong surface gradients, as well as the upscale cascade of energy from unresolved scales (Zanna et al., 2019). This is because small-scale interactions and local feedbacks that take place at small, unresolved scales are missing and result in a degradation of the model performance compared to models with higher resolution. In this case, RCMs (and variable resolution GCMs) can resolve part of these processes in the regions of interest at an acceptable computational cost. Usually, the performance assessment focused mainly on temperature and precipitation climatology, including trends and extremes (Chapter 11 and Atlas). However, some studies have also investigated the ability of RCMs to correctly reproduce processes and phenomena (Sections 10.3.3.4 to 10.3.3.7).

The performance assessment of RCMs is carried out by evaluating simulations of the current climate with boundary forcings provided by both reanalysis products and GCM historical simulations in a comparison with the best observations available. RCM simulations driven by reanalyses (Section 10.3.2.5) have been extensively used to evaluate many aspects of the downscaling capability (including added value with respect to the driving reanalysis) and are used to identify the errors intrinsic to the RCM (Section 10.3.3.5 and Atlas).

When RCMs are driven by GCMs, they are typically not able to mitigate GCM biases in large-scale dynamical processes. Thus, if such biases are substantial, and if the corresponding large-scale processes are important drivers of regional climate, downscaling is questionable (Section 10.3.3.4). However, when GCMs have weak circulation biases and regional climate change is controlled mainly by regional-scale processes and feedbacks, dynamical downscaling has the potential to add substantial value to GCM simulations (Hall, 2014, Section 10.3.3.5 and Atlas).

There is *robust evidence* and *high agreement* that RCMs have the potential to add value for the generation of future climate messages at the regional scale and have the potential to add value to GCM simulations especially over regions of complex orography or with heterogeneous surface characteristics.

[START TABLE 10.2 HERE]

Table 10.2: Performance of different statistical methods in representing local weather at daily resolution. REG: (generalised) linear model; ANA: analogue; QM: quantile mapping, RI: Richardson-type; POI: Poisson clustering; HM: hidden Markov; SS: single-site; MS: multisite; U: unconditional; C: conditional; "+": should work reasonably well based on empirical evidence and/or expert judgement; “o”: problems may arise depending on the specific context; "-": weak performance either by construction or inferred from empirical evidence; "?": not studied. The categorisation assumes that predictors are provided by a well performing dynamical model. Statements about extremes refer to moderate events occurring at least once every 20 years. Adopted and extended from (Maraun and Widmann, 2018b), **[Note: References will be added after the SOD. Each reference will receive a label, which will be referred to in each entry. The +/0/- will be replaced by colour codes.]**

Aspect	Perfect Prog				Bias Adjustment				Weather generators			
	REG deterministic	REG inflated	REG white noise	ANA SS/MS	Additive/Scaling	QM empirical	QM parametric	QM extremes	RI U SS/MS	RI C SS/MS	POI SS/MS	HM U/C
Temperature												
Mean	+	+	+	○	+	+	+	+	+	+	+	+
Variance	-	○	+	○	○	+	+	+	+	+	+	+
Extremes	-	○	+	+	○	+	+	+	+	+	+	+
Temperature, temporal variability												
Autocorrelation	+	+	-	-	+	+	+	+	+	+	+	+
Mean spells	○	○	-	-	+	+	+	+	+	+	+	+
Extreme spells	+	+	-	○	+	+	+	+	+	+	+	+
Interannual variance	-	○	-	-	+	○	○	○	-	○	-	-/○
Climate change	+	-	+	-	+	○	○	○	+	+	+	+
Temperature, spatial variability												
Means	○	○	-	-/+	+	+	+	+	-/?	-/?	-/?	?
Extremes	-	-	-	-/+	+	+	+	+	-/?	-/?	-/?	?
Precipitation, marginal												
Wet-day probabilities	-	-	+	+	+	+	+	+	+	+	+	+
Mean intensity	-	-	+	+	+	+	+	+	+	+	+	+
Extremes	-	-	+	+	○	+	○	+	○	○	○	○
Precipitation, temporal variability												
Transition probabilities	-	-	+	+	○	+	+	+	+	+	+	+
Mean spells	-	-	+	+	○	+	+	+	○	+	○	○/+
Extreme spells	-	-	+	+	+	+	+	+	-	○	-	-/○
Interannual variance	-	○	○	○	+	○	○	○	-	○	-	-/○
Climate change	+	-	+	○	+	○	○	○	+	+	+	+
Precipitation, spatial variability												
Means	-	-	-	-/+	○	+	+	+	-/○	-/○	-/○	○
Extremes	-	-	-	-/+	○	○	○	○	-/?	-/?	-/?	?
Multi variable												
Bulk	-	-	-	+	+	+	+	+	+	+	+	+

[END TABLE 10.2 HERE]

10.3.3.3.3 Statistical downscaling, bias adjustment and weather generators

The performance of statistical downscaling models, bias adjustment and weather generators is very much determined by the chosen model structure (e.g., to representing variability and extremes or spatial dependence) and, when used, the predictors selected (Maraun et al., 2018). The VALUE initiative has assessed the performance of a range of perfect prognosis methods, bias adjustment methods, and weather generators in a perfect predictor experiment where the predictors are taken from reanalysis data (Maraun et al., 2015, 2018; Gutiérrez et al., 2018). Table 10.2 shows an overview comprising performance results from VALUE and other studies.

Perfect prognosis methods can perform well when the synoptic forcing (i.e., the explanatory power of large-scale predictors) is strong (Schoof, 2013). Using this approach, downscaling of precipitation is particularly skilful in the presence of strong orographic forcing. The representation of daily variability and extremes requires the use of analogue methods or stochastic regression models, although the former typically do not extrapolate to unobserved values (Gutiérrez et al., 2018; Hertig et al., 2018). Temporal variability in precipitation is well represented by analogue methods and stochastic regression, but analogue methods typically underestimate temporal dependence of temperature (Maraun et al., 2017a). Spatial dependence in both temperature and precipitation is only well represented by analogue methods, for which analogues are defined jointly across stations, and by stochastic regression methods explicitly representing spatial dependence (Widmann et al., 2019). Overall, there is *high confidence* that analogue methods and stochastic regression are able to represent many aspects of daily temperature and variability, but the analogue method is inherently limited in representing climate change (Gutiérrez et al., 2013).

Bias adjustment methods, if driven with reanalysis predictors, in principle adjust well all the aspects that they are intended to (Maraun and Widmann, 2018b). For temperature, all univariate methods are good to adjust means, variance, and high quantiles (Gutiérrez et al., 2018; Hertig et al., 2018). For precipitation, means, intensities, wet-day frequencies, and wet-dry and dry-wet transitions are well adjusted (Maraun et al., 2017a; Gutiérrez et al., 2018). The representation of high quantiles depends on the method chosen. In this case flexible quantile mapping performs best (Hertig et al., 2018). Empirical (non-parametric) methods perform better than parametric methods over the observed range, but it is unclear how this translates into extrapolation to unobserved values (Hertig et al., 2018; Stocker et al., 2015). Many quantile mapping methods overestimate interannual variability (Maraun et al., 2017a). Temporal and spatial dependence are usually not adjusted and thus inherited from the driving model (Maraun et al., 2017a; Widmann et al., 2019). Spatial fields are thus typically too smooth in space, also after bias adjustment (Widmann et al., 2019). Multivariate bias adjustment methods are good to adjust all statistical aspects of the multivariate distribution that they intend to adjust. Depending on the method, this includes correlation structure or all aspects of multivariate dependence structure (Cannon, 2016, 2018; Vrac, 2018). Often, marginal distributions are corrected using quantile mapping and hence univariate performance characteristics generally follow those mentioned above. However, adjustment of multivariate dependence necessarily modifies the temporal sequencing of the driving model (Cannon, 2016). Hence, there will be a loss of coherence between the modelled and bias adjusted chronology of events, and temporal dependence is no longer fully inherited from the driving model. The extent of the modification depends on the chosen method (Vrac and Friederichs, 2015; Cannon, 2016; Vrac, 2018). If multivariate adjustment includes a spatial dimension, then spatial dependence is adjusted well (Vrac, 2018). There is *high confidence* that bias adjustment can improve the marginal distribution of simulated climate variables, if applied to a climate model that adequately represents the processes relevant for a given application (Box 10.2).

Weather generators represent well most aspects that are explicitly calibrated. This typically includes mean, variance, high quantiles (for precipitation, if explicitly modelled), and short-term temporal variability for both temperature and precipitation, whereas interannual variability is strongly underestimated (Frost et al., 2011; Hu et al., 2013a; Keller et al., 2015; Maraun et al., 2017a; Gutiérrez et al., 2018; Hertig et al., 2018; Dubrovsky et al., 2019; Widmann et al., 2019). There is growing evidence that some spatial weather generators fairly realistically capture the spatial dependence of temperature and precipitation (Frost et al., 2011; Hu et al., 2013a; Keller et al., 2015; Evin et al., 2018; Dubrovsky et al., 2019). There is *high confidence* that weather generators can realistically simulate a wide range of local weather characteristics at single locations, but there is *limited evidence* and *limited agreement* of the ability of weather generators to realistically simulate the spatial dependence of atmospheric variables across multiple sites.

10.3.3.3.4 Comparison of dynamical downscaling and statistical methods

Several studies have addressed the relative performance of dynamical downscaling and statistical approaches in simulating various aspects of regional climate. A general outcome is that statistical downscaling, bias adjustment and weather generators, as they are calibrated, outperform uncorrected output of RCMs and GCMs for a range of statistical aspects at single locations, but RCMs are superior when spatial fields are relevant (Mehrotra et al., 2014; Vaittinada Ayar et al., 2016; Maraun et al., 2018). Similarly, there is some evidence that bias adjustment is comparable in performance when applied to GCMs and dynamically downscaled GCMs only for single locations, but dynamical downscaling prior to bias adjustment clearly adds value once spatial dependence is relevant (Maraun et al., 2018). These results may explain why dynamical downscaling does not add value to GCM simulations for (single-site) agricultural modelling, when both GCM and RCM are bias adjusted (Glotter et al., 2014), but dynamical downscaling adds value compared to bias adjusted GCM output for spatially distributed hydrological models (Qiao et al., 2014).

10.3.3.4 Performance at simulating large-scale phenomena and teleconnections relevant for regional climate

Regional climate is often controlled by large-scale weather phenomena and teleconnections. In particular extreme events are often caused by specific, in some cases persistent, circulation patterns (Chapter 11). The ability of climate models to accurately represent such phenomena is therefore important to reasonably represent not only continental, but also regional climate and its variability. Standard resolution GCMs can suffer from biases in the location, occurrence frequency or intensity of large-scale phenomena. In such cases, any statements about regional climate and climate change will be highly uncertain. In fact, when these biases have large amplitude, RCMs over their limited domains cannot reduce their signature but merely add detail to an unrealistic large-scale field. In some cases, however, RCMs run over a large-domain may improve large-scale circulation features. Due to their enhanced representation of complex topography and coastlines that can lead to a better representation of the interaction between large-scale phenomena and local features, RCMs may also, in principle, add value to simulating the regional manifestation of teleconnections. This subsection illustrates this aspect with selected examples from the mid-to-high latitudes and tropics.

10.3.3.4.1 Mid-to-high latitude atmospheric variability phenomena: blocking and extratropical cyclones

A major phenomenon for mid-to-high latitude mean and extreme climate is atmospheric blocking, known to lead to extreme cold conditions in winter and warmth and drought during summer and determining the seasonal regional climate in certain years (Sousa et al., 2017, 2018b). Atmospheric blocking is characterized by a quasi-stationary long-lasting, high pressure system that blocks and diverts the movement of synoptic cyclones. An overview of model performance in simulating blocking is given in Figure 10.7. The longitudinal distribution of blocking frequency and its seasonality is reasonably well reproduced in the CMIP5 multi-model mean. However, CMIP5 climate models often underestimate winter blocking frequency over Europe and the north-eastern Atlantic (Anstey et al., 2013; Cattiaux et al., 2013; Dunn-Sigouin and Son, 2013; Masato et al., 2013; Davini and D'Andrea, 2016), an aspect still appearing in the CMIP6 experiments (Davini and D'Andrea, submitted). This underestimation is dominated by short-lived blocking events with duration shorter than ten days. In contrast, North Pacific blocking frequency is overestimated by most models over broad regions and in all seasons, particularly on the poleward side of the observed blocking frequency maximum (Anstey et al., 2013; Dunn-Sigouin and Son, 2013). Summertime blocking frequency is slightly overestimated over the subpolar oceans, while it is underestimated over Eurasia (Masato et al., 2013). CMIP5 climate models also underestimate decadal variability of Greenland summer blocking, which has seen a record rise in the observations since the 1990s while models indicate a decrease in the recent past and 21st century (Hanna et al., 2018). With regard to the Southern Hemisphere, CMIP5 models have differing large biases with opposite sign in austral winter, while they systematically simulate too little blocking to the south of Australia during summer (Parsons et al., 2016; Patterson et al., 2019). This underestimation is probably related to the overly equatorward jets found in most CMIP5 models (Bracegirdle et al., 2013) involving shortwave cloud forcing biases, underestimated low-level orographic drag, and/or a too persistent SAM (Ceppi et al., 2012; Pithan et al., 2016; Simpson et al., 2013). Blocking underestimation is highly region- and season-dependent and not necessarily an intrinsic property of the CMIP5 models (Masato et al., 2013; Patterson et al., 2019). In general, blocking biases result from lack of vertical (both tropospheric and stratospheric) and/or horizontal resolution, mean state biases, in particular, biases related to the parameterization of orographic effects, the misrepresentation of the Gulf Stream SST front (Anstey et al., 2013; Berckmans et al., 2013; Davini and D'Andrea, 2016; O'Reilly et al., 2016; Pithan et al., 2016; Schiemann et al., 2017). Overall SST biases have been suggested to have only a weak relevance (Davini and D'Andrea, 2016).

Based on 13 RCMs driven by ERA40, (Sanchez-Gomez et al., 2009) show that RCMs reproduce the European weather regimes, including blocking, behaviour in terms of composite pattern, mean frequency of occurrence and persistence reasonably well as well as the long-term trends and the interannual variability of the frequency of occurrence. In a study of five ERA-Interim-driven RCMs, Jury et al., (2018) showed that RCMs typically simulate fewer blocking events over Europe than are present in the driving data, irrespective of the RCM horizontal resolution.

[START FIGURE 10.7 HERE]

Figure 10.7: **[Placeholder**: Characteristics of summer (June to August) blocking over the North Atlantic in the HighResMIP experiment (seven models) as a function of resolution along with the CMIP5 and CMIP6 multi-model results and a reference from ERA-Interim for (left) global climate model and (right) atmospheric global climate model simulations using observed sea surface temperature and sea ice. Top row: area mean blocking frequency; middle row: spatial correlation between simulated and observed frequencies; bottom row: root mean squared error between simulated and observed frequencies.**]**

[END FIGURE 10.7 HERE]

Other related key mid-latitude phenomena are the storm tracks of Atlantic and Pacific extratropical cyclones (Shaw et al., 2016). Similar to CMIP3, most CMIP5 models simulate climatological storm tracks that are too weak and displaced equatorward (Chang et al., 2012). Zappa et al. (2013) evaluated the North Atlantic storm track in CMIP5 models and found that the winter storm track tends to be either too zonal or displaced southward, resulting in too many cyclones in central Europe. The position of the summer North Atlantic storm track is generally well captured, but some models underestimate the number of cyclones. In both summer and winter, the intensity of cyclones is often too weak. Yang et al. (2018) found that half of thirteen selected CMIP5 models are able to reproduce the spatial pattern of the winter North Pacific storm-track climatology, but most of them underestimate its strength and spatial variation. They also found that most CMIP5 models are unable to reproduce interannual variability in storm-track strength and spatial pattern. In the Southern Hemisphere, most CMIP5 climate models have large equatorward biases in storm-track latitude leading to larger projected poleward shifts of the storm tracks for models with the largest bias (Chang et al., 2012). Many causes of storm track biases have been suggested, such as misrepresented orography (Berckmans et al., 2013), in particular inadequate parameterisations of low-level drag (Pithan et al., 2016), SST biases (Booth et al., 2017), and a missing representation of mesoscale atmospheric features and mesoscale ocean eddies (Willison et al., 2013; Foussard et al., 2019).

In general, RCMs cannot mitigate large-scale circulation errors of the driving GCM. If run over large-domains, reanalysis-driven RCMs can, for specific regions, significantly improve the representation of storm characteristics compared to the driving reanalysis near areas with marked orography and regions with large water masses (Poan et al., 2018). However, this is not necessarily true if the domain is large enough as the RCM and its biases will then control the circulation leading to a biased performance with regard to storm characteristics (Pontoppidan et al., 2019). Flaounas et al. (2018) investigated the ability of 12 RCMs and RESMs to reproduce the climatology of Mediterranean cyclones based on different cyclone tracking methods. All RCMs reasonably reproduce the main areas of high cyclone occurrence. Air-sea coupling has a rather weak impact on cyclone climatology and intensity. Sánchez-Gómez and Somot (2018) showed that the effect of RCM internal variability on density of cyclone tracks is very significant and larger than for other variables such as precipitation. It is larger in summer than in winter, in particular over the Iberian Peninsula, countries in northern Africa and the eastern Mediterranean, which are regions of enhanced cyclogenesis during the warm season.

10.3.3.4.2 Tropical phenomena: ENSO teleconnections, Madden-Julian oscillation

The assessment of model performance in simulating ENSO characteristics, including ENSO spatial pattern, frequency, asymmetry between warm and cold events, and diversity, is discussed in Chapter 3. Here the ability of the recent generation of GCMs to adequately simulate ENSO-related teleconnections is reviewed.

The model assessment is a challenge due to the different types of ENSO and model errors in ENSO spatial patterns, non-stationary aspects of the teleconnection, as well as the strong influence of atmospheric internal variability at mid-to-high latitudes (Coats et al., 2013; Polade et al., 2013; Capotondi et al., 2015; Deser et al., 2017c; Garcia-Villada et al., submitted).

Langenbrunner and Neelin (2013) showed that there is little improvement in the CMIP5 ensemble relative to CMIP3 in amplitude and spatial patterns of the ENSO influence on boreal winter precipitation (with model-observation spatial pattern correlation coefficients typically less than 0.5). However, the CMIP5 ensemble accurately represents the amplitude of the precipitation response in regions where observed teleconnections are strong. Moreover, a *high agreement* between models on the teleconnection sign indicates a good performance in representing the observed teleconnections. Hurwitz et al. (2014) showed that CMIP5 models broadly simulate the expected (as seen in the MERRA reanalysis) upper tropospheric responses to central equatorial Pacific or eastern equatorial Pacific ENSO events in boreal autumn and winter. They also show that CMIP5 models do simulate the correct sign of Arctic stratospheric response, which consists in the polar vortex weakening during eastern and central Pacific Niño events and vortex strengthening during both types of La Niña events. In contrast, most CMIP5 models do not capture the observed weakening of the polar vortex in response to central Pacific ENSO events. This is due to a weak poleward planetary wave response linked to a weak South Pacific Convergence Zone convective response to central Pacific ENSO events that originates from a poor representation of the south-eastern tilted portion of the South Pacific Convergence Zone in the CMIP5 models (Brown et al., 2013).

In RCMs, the effects of tropical large-scale modes and teleconnections are inherited through the boundary conditions and influenced by the size of the numerical domain. For instance, Done et al. (2015) and Erfanian and Wang (2018) claim that large domains that include teleconnected oceanic regions are required, although, without spectral nudging, this can lead to biased synoptic-scale patterns (Prein et al., 2019). RCMs generally reproduce the regional precipitation responses to ENSO forcing, and improve the representation of these teleconnections compared to the driving reanalysis (Endris et al., 2013; Fita et al., 2017). Chandrasa and Montenegro (2019) and Endris et al. (2016) showed that the RCM response to different ENSO phases is largely determined by the quality of the forcing data (either reanalysis of GCMs) rather than the model internal dynamics. However, Whan and Zwiers (2017) argued that the differences in the physical schemes in two RCMs driven by the same reanalysis can lead to large differences in the response of extreme precipitation to ENSO teleconnection in North America.

The MJO (Technical Annex VI) has a strong influence on a range of tropical phenomena from the onset and breaks of the Asian and Australian monsoon systems, the triggering and termination of ENSO events, and tropical cyclone activity. Significant extratropical surface air temperature variations can also arise as a result of teleconnections triggered by the MJO. Temperature variations over North America and Europe can arise in response to MJO-induced heating and horizontal temperature advection by northerlies or southerlies associated with a meridionally propagating Rossby wave train (Cassou, 2008; Lin et al., 2009; Henderson et al., 2016; Mundhenk et al., 2016; Seo et al., 2016; Jiang et al., 2017).

In agreement with results from previous model generations, most CMIP5 models still underestimate MJO amplitude, and struggle to generate a coherent precipitation/convection and wind field eastward propagation (Hung et al., 2013; Jiang et al., 2015; Ahn et al., 2017). This underestimation affects the regional surface climate both in the tropics and extra-tropics. Additionally, most CMIP5 models simulate an MJO that propagates too fast compared to observations and intra-seasonal precipitation variability remains poorly simulated among CMIP5 models (Ahn et al., 2017). However, the propagation speed of some CMIP5 models in the Indian Ocean tends to be slower than observed due to a too strong persistence of equatorial precipitation (Hung et al., 2013; Jiang et al., 2015). Improvements in moisture-convection coupling and gross moist stability (i.e., the efficiency of vertical advection to export moist static energy out of the convective column) representation might be the most fruitful means to improving simulations of the MJO (Ahn et al., 2017; Kim and Maloney, 2017). Though the GCM representation of the MJO has advanced in recent decades, there is *high confidence* that most models from the current generation of GCMs still have difficulties in achieving a robust and physically-coherent MJO simulation.

10.3.3.5 Performance at simulating regional phenomena and processes

Regional climate is shaped by a wide range of weather phenomena occurring at scales from about 2,000 km to 2 km (Figure 10.2). These modulate the influence of large-scale atmospheric phenomena and create the characteristic and potentially severe weather conditions experienced regionally. The climate in different regions will be affected by different mesoscale phenomena, and in a given application, several of these may be relevant. A skilful representation of these phenomena is a necessary condition for providing credible and relevant climate change information for a given region and application. Therefore, it is important to understand the strengths and weaknesses of different model types in simulating these phenomena. Here, the performance of different climate model types to simulate a selection of relevant mesoscale weather phenomena is assessed.

10.3.3.5.1 Convection including tropical cyclones

Convection is the process of vertical mixing due to atmospheric instability. Deep moist convection is associated with thunderstorms and related severe weather such as heavy precipitation and strong wind gusts. Convection may occur in single locations, in spatially extended severe events such as supercells, and organised into larger mesoscale convective systems such as squall lines or tropical cyclones (Section 10.3.3.5.1), and embedded in fronts (Section 10.3.3.5.4).

Shallow and deep convection are not explicitly simulated but parameterized in standard GCMs and RCMs. As a consequence, these models suffer from several biases in the representation of convection and related phenomena. AR5 has stated that many CMIP3 and CMIP5 models simulate the peak in the diurnal cycle of precipitation too early, but increasing resolution and better parameterisations help to mitigate this problem (Flato et al., 2014). Similar issues arise for RCMs with parameterised deep convection (Prein et al., 2015). Such standard RCMs also tend to overestimate high cloud cover (Langhans et al., 2013; Keller et al., 2016).

Simulations with non-hydrostatic RCMs at convection-permitting resolution (at 3 km and finer) improve the representation of phenomena associated with deep convection, such as the initiation and diurnal cycle of convection (Zhu et al., 2012; Prein et al., 2013a, 2013b; Fosser et al., 2015; Berthou et al., 2018; Sugimoto et al., 2018; Finney et al., 2019), the triggering of convection by orographic lifting (Langhans et al., 2013; Fosser et al., 2015), spatial patterns of precipitation (Prein et al., 2013a, 2013b), precipitation intensities (Prein et al., 2015; Fumière et al., 2019), the scaling of precipitation with temperature (Ban et al., 2014), cloud cover (Böhme et al., 2011; Langhans et al., 2013), and maximum vertical wind speeds (Meredith et al., 2015a). Phenomena such as supercells, mesoscale convective systems, or the local weather associated with squall lines are not captured by GCMs and standard RCMs. Convection-permitting RCM simulations, however, have been shown to realistically simulate supercells (Trapp et al., 2011), mesoscale convective systems, their life cycle and motion (Prein et al., 2017; Crook et al., 2019), and heavy precipitation associated with a squall line (Kendon et al., 2014). There is *high confidence* that simulations at convection permitting resolution add value to the representation of deep convection and related phenomena.

Convection is the key ingredient of tropical cyclones. An inter-comparison study of high-resolution atmospheric global climate model (AGCM) simulations (Shaevitz et al., 2014) showed that tropical cyclone intensities appeared in general to be better represented with increasing model resolution. Takayabu et al. (2015) have compared simulations of typhoon Hayan at different resolutions ranging from 20 km to 1 km (Figure 10.7). While the eyewall structure in the precipitation pattern was strongly smoothed in the coarse resolution simulations, it was well resolved at the highest resolution. Gentry and Lackmann (2010) found similar improvements in simulating hurricane Ivan for horizontal resolutions between 8 km and 1 km. There is *high confidence* that convection permitting resolution is required to realistically simulate the three-dimensional structure of tropical cyclones.

[START FIGURE 10.8 HERE]

Figure 10.8: Hourly accumulated precipitation profiles (mm hour^{-1}) around the eye of Typhoon Haiyan, represented by (a) GSMaP satellite observation data, (b) Guiuan radar (PAGASA), (c) meso-ensemble forecast (60 km), (d) NHRCM (20 km), (e) NHRCM (5 km), and (f) WRF (1 km) models. Adapted from Takayabu et al. (2015).

[END FIGURE 10.8 HERE]

10.3.3.5.2 Mountain wind systems

Mountain slope and valley winds are localised thermally generated diurnal circulations that have a strong influence on regional temperature and precipitation patterns in mountain regions. During the day, heating of mountain slopes compared to the free atmosphere induces upslope winds; during the night this circulation reverses. This phenomenon is not resolved by GCMs and coarse-resolution RCMs. A reanalysis-driven RCM simulation at 4 km resolution showed good skill in simulating the diurnal cycle of temperature and wind on days of weak synoptic forcing in the Rocky Mountains (Letcher and Minder, 2017). Similarly the mountain-plain wind circulation over the Tianshan mountains in Central Asia is well simulated by a model running at 4 km resolution (Cai et al. 2019). In the Alps, a 1 km resolution has been required (Zängl, 2004).

Föhn winds are regional-scale synoptically-driven winds that cause orographic precipitation in the windward side of a mountain range, and as a result of the raised condensation level, adiabatic warming in the downwind side. In an RCM study for the Japanese Alps, Ishizaki and Takayabu (2009) found that at least a 10 km resolution was required to realistically simulate Föhn events.

Synoptically-forced winds may be channelled and accelerated in long valleys. For instance, the Tramontana, Mistral and Bora are northerly winds blowing down-valley from central France and the Balkans into the Mediterranean (Flaounas et al., 2013). In winter, these winds may cause severe cold air outbreaks along the coast. Flaounas et al. (2013) have shown that a GCM with a horizontal resolution of roughly 3.75° longitude/1.875° latitude is unable to reproduce these winds because of the coarse representation of orography, whereas a 0.44° resolution RCM resolves these winds. Nevertheless, 0.44° RCM simulations did not realistically represent the Mistral (Obermann et al., 2018) and Bora winds (Belušić et al., 2018), but simulations at 0.11° resolution added substantial value. Similarly, Cholette et al. (2015) found that a 0.27° RCM resolution was not sufficient to adequately simulate the channelling of winds in the St. Lawrence River Valley in eastern Canada, whereas a 0.09° resolution was.

There is *very high confidence* that climate models with resolutions of around 10 km or finer are necessary for better simulating mountain wind systems such as slope and valley winds and the channelling of winds in valleys.

10.3.3.5.3 Coastal winds and lake effects

Simulating coastal climates and the influence of big lakes are a modelling challenge, due to the complex coastlines, the different heat capacities of land and water, the resulting wind system, and the differential evaporation. Regional features are often not well resolved by GCMs. The AR5 concluded that RCMs can add value to the simulation of coastal climates.

The summer coastal low-level jets in the mid-latitude western continental coasts are forced by the eastern branch of the semi permanent ocean anticyclones which drive equatorward coastal parallel winds, an inland thermal low, a strong cross-shore thermal contrast associated to the oceanic upwelling and high coastal topography. They are important factors in shaping regional climate by, for instance, preventing onshore advection of humidity and thereby causing aridity (Soares et al., 2014), or by transporting moisture towards regions of precipitation as in the North American monsoon (Bukovsky et al., 2013).

Reanalyses and most GCMs do not well resolve the details of coastal low-level jets (Bukovsky et al., 2013;

Soares et al., 2014), but they are still able to represent annual and diurnal cycles and interannual variability (Cardoso et al., 2016; Lima et al., 2019). Bukovsky et al. (2013) found RCM simulations at a 50 km resolution to improve the representation of the coastal low-level jet in the Gulf of California and the associated precipitation pattern compared to the driving GCM. Lucas-Picher et al. (2017) find indirect evidence via precipitation patterns that 12 km simulations further improve the representation. In a study of the Iberian coastal low-level jet, Soares et al. (2014) dynamically downscaled the ERA-Interim reanalysis to an 8 km resolution. The simulations show a realistic three-dimensional jet structure, and the surface winds compare well with observations. Lucas-Picher et al. (2017) showed that a 0.44°-resolution RCM underestimated winds along the Canadian east coast, whereas a 0.11°-resolution version better represented the coastline, orography, surface roughness and local atmospheric circulation and thereby simulated more realistic 10-metre wind speed. Also, the Etesian winds in the Aegean Sea were realistically simulated by 0.11°-resolution RCMs (Dafka et al., 2018).

A particularly relevant coastal phenomenon is the sea breeze, which is caused by the differential heating of water and land during the course of the day and typically reaches several tens of kilometres inland. Reanalyses and GCMs have too coarse a resolution to represent this phenomenon, such that they typically underestimate precipitation over islands and misrepresent its diurnal cycle (Lucas-Picher et al., 2017). RCMs simulate sea breezes and thereby improve the representation of precipitation in coastal areas and islands. Over Cuba and Florida, a long peninsula, only a 0.11°-resolution RCM is able to realistically simulate the inland propagation of precipitation during the course of the day. RCM simulations at a 20 km horizontal resolution realistically represented the sea breeze circulation in the Mediterranean Gulf of Lions including the intensity, direction and inward propagation (Drobinski et al., 2018). Even though a coupled ocean-atmosphere simulation improved the representation of diurnal SST variations, the sea breeze representation itself was not enhanced.

Big lakes modify the downwind climate. In particular during winter they are relatively warm compared to the surrounding land, provide moisture, destabilize the passing air column and produce convective systems; the increase in friction when moving air reaches land causes convergence and uplift, and may trigger precipitation. Gula and Peltier, (2012) found that a state-of-the-art GCM does not realistically simulate these effects over the North American Great Lakes, but a 10 km RCM better represents them and thereby simulates realistic downwind precipitation patterns, in particular enhanced snowfall during the winter season. Similar results were found by Wright et al. (2013) and Lucas-Picher et al. (2017). In a convection permitting simulation of the Lake Victoria region, a too strong nocturnal land-breeze resulted in unrealistically high precipitation (Finney et al., 2019).

There is *high confidence* that climate models with sufficiently high resolution are necessary for better simulating lake and coastal weather including low-level jets, lake and sea breezes, as well as lake effects on rainfall and snow.

In regions like Fenno-Scandinavia or central-eastern Canada, very large fractions of land are covered by small and medium sized lakes. Other regions have fewer but larger lakes, such as central-eastern Africa, the eastern border between the US and Canada, and central Asia. In these regions it has been considered essential to include a lake model in an RCM to realistically represent regional temperatures (Deng et al., 2013; Mallard et al., 2014; Pietikäinen et al., 2018; Samuelsson et al., 2010; Thiery et al., 2015), as well as remote effects (Spero et al., 2016). For the Caspian Sea, which can be considered a large lake, it is found that a coupled ocean-atmosphere RCM improved, in addition to representing the circulation in the sea, the simulation of SST fields compared to simulations with a simpler coupled lake model (Turuncoglu et al., 2012).

There is *medium evidence* and *high agreement* that it is important to include interactive lake models in RCMs to improve the simulation of regional temperature, in particular in seasonally ice-covered areas with large fractions of lakes. There is *medium evidence* of the local influence of lakes on snow and rainfall as well as the importance of including lakes in regional climate simulations.

10.3.3.5.4 Fronts

Weather fronts are two-dimensional surfaces separating air masses of different characteristics and are a key element of mid-latitude cyclones. In particular cold fronts are regions of relatively strong uplift and hence often associated with severe weather (e.g., Schemm et al., 2016). Stationary or slowly moving fronts may cause extended heavy precipitation. Research on how climate models represent fronts, however, is still limited.

Catto et al. (2014) found in both ERA-Interim and CMIP5 models that frequency and strength of fronts were realistically simulated, albeit with some biases in the location of front occurrence maxima. In a follow-up study, Catto et al. (2015) investigated the representation of frontal precipitation for boreal and austral winter. The frequency of frontal precipitation is too high and the intensity is too low, but these compensating biases approximately cancelled out such that the total precipitation bias was small. Blázquez and Solman (2018) found similar results for the Southern Hemisphere during austral winter, and also showed that CMIP5 models typically overestimate the fraction of frontal precipitation compared to total precipitation. The bias also appears in the observational reference. The ERA-Interim reanalysis misrepresents conditional symmetric instability associated with fronts, and the corresponding precipitation (Glinton et al., 2017).

Only few studies evaluating fronts in RCMs have been conducted. Kawazoe and Gutowski (2013) diagnosed strong temperature gradients associated with extreme wintertime precipitation events in the framework of the North American Regional Climate Change Assessment Program (NARCCAP) RCM ensemble (Mearns et al., 2012) and found the models agreed well with observation-based gradients in a reanalysis of comparable resolution. De Jesus et al. (2016) diagnosed the representations of cold fronts over southern Brazil by two RCMs, and found that across the year, cold fronts were only underestimated by about 5%, but in one of the RCMs, cold fronts during summer were underestimated by 17%. An RCM-based reanalysis suggests that high resolution RCM simulations improve the representation of orographic influences on fronts (Jenkner et al., 2009).

10.3.3.6 Performance at simulating regional feedbacks

Both the SRCCL (Jia et al., 2019) and the SROCC (Hock et al., 2019) highlight the weaknesses of climate models in simulating atmosphere-land feedbacks. The performance in simulating some of these feedbacks is assessed below.

The snow-albedo effect is an important process contributing to enhanced warming at high elevations (Pepin et al., 2015). In complex terrain, GCMs often do not represent the orography well enough to realistically simulate the snow-albedo feedback (Hall, 2014; Walton et al., 2015). RCMs have the potential for considerably improving the representation of the snow-albedo effect in complex terrain, but the performance appears to depend strongly on the specific model. Over Europe, some of the EURO-CORDEX RCMs simulate a springtime snow albedo feedback close to that observed, whereas other models considerably overestimate it (Winter et al., 2017). In a multi-physics ensemble based on the WRF RCM, the simulated snow-atmosphere interaction causes a cold bias in north-eastern Europe, which is amplified by the albedo feedback (García-Díez et al., 2015). For the Rocky Mountains, WRF simulations generally reproduce the observed spatial and seasonal variability in snow cover, but exhibit a strong overestimation of snow albedo (Minder et al., 2016). The elevation dependence of historical warming, which is partly caused by the snow-albedo effect, is realistically represented across Europe by the ENSEMBLES RCMs (Kotlarski et al., 2015). There is *medium confidence* that RCMs considerably improve the representation of the snow albedo effect in complex terrain.

Soil-moisture feedbacks both influence changes in temperature and precipitation. More than 30% of CMIP5 models overestimate the influence of preceding precipitation (a measure of soil moisture) on temperature extremes in Europe and the USA (Donat et al., 2018), and many CMIP5 models simulate an unrealistic influence of evaporation on temperature extremes for European and US wet regions (Ukkola et al., 2018). For the EURO-CORDEX RCMs, Knist et al. (2017) found that the simulated coupling strength agrees well with observations in Northern Europe (weak) and Southern Europe (strong), but in Central Europe many

RCMs tend to overestimate the coupling strength. Global reanalysis-driven land-surface models agreed relatively well with observations. However, the strength of coupling varied strongly across models at the regional scale, and a realistic partitioning of the incoming radiation into latent and sensible heat fluxes did not necessarily result in a realistic soil-moisture temperature coupling (Gevaert et al., 2018).

Evaluating the representation of soil-moisture precipitation feedbacks in climate models is challenging as different processes may induce feedbacks including moisture recycling, boundary-layer dynamics and mesoscale circulations. Moreover, the effects of soil-moisture on precipitation have a spatial and a temporal aspect with different possible feedbacks, and the feedbacks may be region and scale dependent and may even change sign depending on the strength of the background flow (Taylor et al., 2013a; Froidevaux et al., 2014; Guillod et al., 2015; Tuttle and Salvucci, 2016). On seasonal-to-interannual time scales, six CMIP5 models showed a stronger soil-moisture precipitation feedback than estimated by satellite data (Levine et al., 2016). Taylor et al. (2013) found that convection-permitting RCMs could simulate well surface-induced mesoscale circulations in day-time convection and the observed negative soil moisture feedback, whereas an RCM with parameterised convection, even when run at the same resolution, simulated an unrealistic positive feedback. There is *medium evidence* and *high agreement* that simulations at convection permitting resolution are required to realistically represent soil-moisture precipitation feedbacks.

Ocean-atmosphere RCMs have successfully been used to simulate phenomena involving strong regional feedbacks like tropical cyclones in the Indian Ocean (Samson et al., 2014), near-coastline intense precipitation in the Mediterranean (Berthou et al., 2015), or snow bands in the Baltic region (Pham et al., 2017). The positive impact of ocean-coupling on the simulation of strongly convective phenomena such as Medicanes, a class of severe cyclones in the Mediterranean, can only be diagnosed when using relatively fine horizontal grid-resolutions in the atmosphere of about 10 km (Akhtar et al., 2014; Flaounas et al., 2018; Gaertner et al., 2018). A positive impact of ocean coupling has been quantified in marginal sea regions with reduced large-scale influence (e.g., in the Baltic sea area during weak phases of the NAO and thus weak influence of Atlantic westerlies in the area (Kjellström et al., 2005; Pham et al., 2018). There is some evidence available that coupled ocean-components also positively impact RCM simulations of inland climates such as precipitation extremes in Central Europe (Ho-Hagemann et al., 2017; Akhtar et al., 2019). There *is high confidence* that coupled ocean-atmosphere RCMs improve the representation of ocean-atmosphere feedbacks and related phenomena.

10.3.3.7 Performance at simulating regional drivers of climate and climate change

10.3.3.7.1 Aerosols

In CMIP5 models, the influence of vegetation changes on mineral dust is largely underestimated while the influence of surface wind and precipitation are overestimated, resulting in a low bias of dust load (Pu and Ginoux, 2018). Simulations of future changes in dust are hindered by the uncertainties in future regional wind and precipitation as the climate warms (Evan et al., 2016), in the effect of CO_2 fertilization on source extent (Huang et al., 2017), in the dust feedbacks (Evans et al., 2019), and in the effect of human activities that change the land use and disturb the soil, including cropping and livestock grazing, recreation and urbanization, and water diversion for irrigation (Ginoux et al., 2012).

Both proxy analyses and simulations have demonstrated reduced Asian monsoon after tropical and Northern Hemisphere eruptions due to reduced humidity and divergent circulation (Man and Zhou, 2014; Zhuo et al., 2014; Liu et al., 2016a; Stevenson et al., 2016). For the NAO, GCM experiments (Zanchettin et al., 2013; Ortega et al., 2015; Michel et al., 2018; Sjolte et al., 2018) have confirmed that tropical volcanic eruptions (larger than Mt Pinatubo in 1991) may lead to a positive phase of the NAO in the following few years (with an uncertainty on the exact years impacted). Nevertheless, such an effect is not well reproduced in climate models (Driscoll et al., 2012; Toohey et al., 2014; Swingedouw et al., 2017; Ménégoz et al., 2018b). For near-term time scales, a few decadal prediction systems have evaluated the impacts that volcanic eruptions may have on the predictability of regional climate and found a significant increase in forecast quality (Swingedouw et al., 2017; Illing et al., 2018; Ménégoz et al., 2018a).

It has been argued that some recent regional climate changes can only be represented by climate models if anthropogenic aerosols are included. Some examples are the recent enhanced warming over Europe (Nabat et al., 2014; Dong et al., 2017), the cooling over the East Asia monsoon region, leading to a weakening of the monsoon (Song et al., 2014; Wang et al., 2017c), as well as the observed monsoon precipitation in West Africa and South Asia (Undorf et al., 2018).

10.3.3.7.2 Land management

The inclusion of irrigation in GCMs and RCMs over the South Asian monsoon region has been found to be important to represent the monsoon circulation and rainfall correctly (Lucas-Picher et al., 2011; Guimberteau et al., 2012; Shukla et al., 2014; Tuinenburg et al., 2014; Cook et al., 2015a). Similarly, the inclusion of irrigation over northern India and western Pakistan could be important for the correct simulation of precipitation over the Upper Indus Basin in northern Pakistan (Saeed et al., 2013). Irrigation over East African Sahel inhibits rainfall over the irrigated region and enhances instead rainfall to the east, coherent with both observations and theoretical understanding of the local circulation anomalies induced by the lower air surface temperatures over the irrigated region (Alter et al., 2015). Although many studies on how modelled irrigation help reduce daytime temperature or alternatively elevates nighttime temperatures are available, few compare modelled results with observations. An exception is the study over the North China Plain, showing that a RCM represented the observed nighttime warming when introducing an irrigation scheme (Chen and Jeong, 2018).

There is *medium evidence* and *high agreement* that representing irrigation is important for a realistic simulation of South Asian monsoon precipitation. There is *limited evidence* that including irrigation in climate models improves the simulation of maximum and minimum daily temperatures as well as precipitation outside of the South Asian monsoon region.

Regional land radiation management, including modifying the albedo through e.g., no-tillage practices, have been suggested as a measure to decrease maximum daily temperatures regionally (see review in Seneviratne et al., 2018), but although modelled results and theoretical understanding are coherent, few studies have verified the realism of the modelled results comparing with observations. Hirsch et al. (2018) is an exception, showing that implementing conservation agriculture in a GCM over regions where it is practiced, improves the simulation of surface heat fluxes.

10.3.3.8 Process-based evaluation of statistical downscaling and bias adjustment

Perfect prognosis methods typically bridge mesoscales by directly linking synoptic and local scales, and bias adjustment simply adjusts the output of the dynamical model. Within the VALUE initiative, Soares et al. (2018) analysed whether statistically downscaled and bias-adjusted model data could represent the observed sensitivity of local weather to a range of phenomena relevant to European climate. The performance of perfect prognosis methods strongly depends on the method, the chosen predictors, and the scale at which the predictors are defined. Bias adjustment was, as expected, not able to represent any sensitivity to a phenomenon that was not resolved by the driving model, and quantile mapping could even exaggerate well-represented sensitivities.

10.3.3.9 Performance at simulating historical regional climate changes

As an important precondition for credibly projecting regional climate change, climate models are required to realistically simulate historical regional trends. This section assesses how well GCMs and different downscaling approaches perform this task. Caveats of performance evaluations will be discussed. Region-by-region assessments may be found in the Atlas.

Trends in climate variables even on multi-decadal time scales are a superposition of forced signals and internal climate variability (Chapter 3 and Section 10.4.1). Comparing simulated and observed historical trends is therefore relevant for two reasons: first, to attribute observed regional changes to different drivers and forcings, and second to evaluate how well climate models ultimately simulate regional trends. The attribution aspect will be discussed in depth in Section 10.4. Here, the focus is on model evaluation.

10.3.3.9.1 Performance of GCMs at simulating regional historical trends

At the regional scale the forced signal may be small compared to the internal variability (Section 10.3.4.3), especially for variables other than temperature. In these instances, given the limited ability to predict internal variability at multi-decadal time scales, an agreement between observed and individual simulated trends would therefore be expected to occur only by chance (Laprise, 2014). Thus, the AR5 has assessed the consistency of observed trends with those simulated by climate model ensembles as a whole (Kirtman et al., 2014). For regional trends, AR5 concluded that the CMIP5 ensemble cannot be taken as a reliable representation of reality and that the true uncertainty can be larger than the simulated model spread (Kirtman et al., 2014). These findings have been corroborated and extended since then. Misrepresented trends have been attributed to an underestimation of trends in large-scale circulation patterns (van Haren et al., 2013), missing trends in both SST, and the occurrence of tropical cyclones (Saha et al., 2014; Roxy et al., 2015).

10.3.3.9.2 Performance of downscaling at simulating regional historical trends

In the context of downscaling, the following questions could be addressed: (1) whether downscaling methods can reproduce observed trends when driven with observed boundary conditions or predictors, and (2) whether downscaling can add value to the trends simulated by the GCMs.

For temperature in the continental US, Bukovsky (2012) found that an ensemble of RCMs driven with the NCEP reanalysis skilfully simulated recent spring and, by and large, winter trends, but did not reproduce summer and autumn trends. Three RCMs with ERA-Interim boundary conditions reproduced the observed warming trend over Central America, though with lower strength (Cavazos et al., 2019). Similar studies have been carried out for statistical downscaling and bias adjustment using predictors from reanalyses (or in case of bias adjustment, dynamically downscaled reanalyses). For a range of different perfect prognosis methods Huth et al. (2015) found that simulated temperature trends were too strong for winter and too weak for summer. The performance was similar for the different methods, indicating the importance of choosing sensible predictors. Similarly, Maraun et al. (2017) found that the performance of perfect prognosis methods depends mostly on the predictor and domain choice (for instance, temperature trends were only captured by those methods including surface temperature as predictor). Bias adjustment methods reproduced the trends of the driving reanalysis, apart from quantile mapping methods, which deteriorated these trends.

Regarding the added value of downscaling, Racherla et al. (2012) found no improvement in the simulation of regional-scale temperature and precipitation trends in a dynamically downscaled GCM compared to the actual GCM itself. Laprise (2014), however, argues that the experiment was ill-designed: because the weak forced signal was masked by internal variability, the GCM simulated trend cannot be expected to follow the observed trend, and the RCM cannot be expected to decrease the deviation between simulated and observed trends.

Including all relevant regional forcings is important to realistically simulate historical trends. RCM experiments are often set up in such a way that changes in forcing agents are included only via the boundary conditions, but not explicitly included inside the domain. Jerez et al. (2018) demonstrated that not including time-varying GHG concentrations within the RCM domain may misrepresent temperature trends by 1–2 ºC per century. Including anthropogenic sulphate aerosols in reanalysis-driven RCM simulations substantially improved the representation of recent brightening and warming trends in Europe (Nabat et al., 2014 , Section 10.3.3.7). Similarly, Bukovsky (2012) argued that RCMs may not capture observed summer temperature trends in the US because changes in land cover are not taken into account. Barlage et al. (2015) have revealed that including the behaviour of groundwater in land schemes increases the performance of the WRF model to represent climate variability in the central US. Hamdi et al. (2014) found that an RCM that did not incorporate the historical urbanization in the land-use, land-cover scheme is not able to reproduce the warming trend observed in urban stations with a larger bias for the minimum temperature trend.

Overall, there is *low evidence* that dynamical downscaling adds value in simulating regional trends, but there is *high confidence* that including all relevant forcings is a prerequisite for reproducing historical trends.

10.3.3.10 Fitness of climate models for projecting regional climate

AR5 stated that confidence in climate model projections is based on the physical understanding of the climate system and its representation in climate models. A climate model credibility is increased if the model is able to simulate past variations in climate (Flato et al., 2014), as discussed, for instance, in Section 10.3.3.9. In particular, the credibility of downscaled information depends on both the quality of the downscaling method itself and that of the GCM providing the large-scale boundary conditions (Flato et al., 2014). Credibility is closely linked to the concept of adequacy or fitness for purpose (Parker, 2009, Chapter 1). From a regional perspective, one may ask whether a climate model is adequate for the purpose of simulating future changes of specific aspects of a specific regional climate. A key challenge is to link performance in simulating present and past climate (Sections 10.3.3.3 to 10.3.3.9) to the confidence in future projections (Section 1.3.4; Baumberger et al., 2017). The following discussion is an assessment of how the preceding model performance evaluation can be used into the generation of climate information.

10.3.3.10.1 Assessing the fitness-for-purpose of regional projections

A general idea of model fitness for a given application may already be obtained by checking whether relevant large-scale (Section 10.3.3.4) and regional scale (Sections 10.3.3.5 and 10.3.3.6) processes are explicitly resolved (Figure 10.2). The basis for confidence in climate projection is a solid process understanding (Flato et al., 2014; Baumberger et al., 2017). Thus, the key to assessing the fitness for purpose of a model is the evaluation of how relevant processes controlling regional climate are represented (Collins et al., 2018). A process-based evaluation may even be more appropriate than an evaluation of the variables of interest (e.g., temperature, precipitation), because biases in the latter may in principle be reduced if the underlying processes are realistically simulated (Cross-Chapter Box 10.2), while individual variables may appear as well represented because of compensating errors (Flato et al., 2014; Baumberger et al., 2017). Fitness-for-purpose can also be assessed by comparing the simulated response of a model with simulations of higher resolution models that better represent relevant processes (Baumberger et al., 2017). For instance, Giorgi et al. (2016) have corroborated their findings on precipitation changes comparing standard RCM simulations with convection permitting simulations.

The evaluation of historical variability and long-term changes provides further relevant information (Flato et al., 2014). Trend evaluation may provide very useful insight, but has limitations in particular at the regional scale, mainly due to multi-decadal internal climate variability (Section 10.3.3.8), observational uncertainty (Section 10.2), and the fact that often not all regional forcings are known (Section 10.4.1).

The fitness of statistical downscaling and bias adjustment for regional climate projections has been scarcely addressed. Perfect model experiments (Section 10.3.2.5) have been used to assess whether a given model structure with a chosen set of predictors is capable of reproducing the simulated future climates (Gutiérrez et al., 2013; Räty et al., 2014; Dayon et al., 2015; Dixon et al., 2016; San-Martín et al., 2017). Importantly, it is found that standard analogue methods inherently underestimate future warming trends (Gutiérrez et al., 2013). Emerging discussions on bias adjustment are assessed in the Cross-Chapter Box 10.2.

10.3.3.10.2 Increasing the fitness of models for regional projections

Increasing resolution (Haarsma et al., 2016) or carrying out downscaling may be particularly important when it modifies the climate change signal of a lower resolution model in a physically plausible way (Hall, 2014). Improvements may result from a better representation of regional processes, upscale effects, as well as the possibility of a region-specific model tuning (Sørland et al., 2018). For instance, Gula and Peltier (2012) showed that a higher resolution allows for a more realistic simulation of lake induced precipitation, resulting in a more credible projection of changes in the snow belts of the North American Great Lakes. Similarly, Giorgi et al. (2016) demonstrated that an ensemble of RCMs better represents high-elevation surface heating and in turn increased convective instability. As a result, the summer convective precipitation response was opposite to that simulated by the driving GCMs (Figure 10.8). Walton et al. (2015) showed that a kilometre-scale resolution RCM enables a more realistic representation of the snow-albedo feedback in mountainous terrain compared to standard resolution GCMs, leading to a more plausible simulation of elevation-dependent warming.

[START FIGURE 10.9 HERE]

Figure 10.9: Projected changes in summer (June to August) precipitation (in percent with respect to the mean precipitation) over the Alps between the periods 2070–2099 and 1975–2004. (a) Mean of four GCMs regridded to a common 1.32°x1.32° grid resolution; (b) mean of six RCMs driven with these GCMs. The grey contours show elevation at 500 m intervals from the digital elevation model of the SMHI-RCA EUR11, regridded to the GCM resolution for panel b. Adapted from Giorgi et al. (2016).

[END FIGURE 10.9 HERE]

Besides, including additional components and feedbacks can substantially modify the simulated future climate. For example, Kjellström et al. (2005) and Somot et al. (2008) have shown that an RESM can significantly modify the SST response to climate change of its driving GCM with implications for the climate change signal over both the sea and land. In particular, coupled ocean-atmosphere RCMs may increase the credibility of projections in regions of strong air-sea coupling such as the East Asia-western North Pacific domain (Zou and Zhou, 2016, 2017).

Of course, a difference between the climate changes simulated by two models does not automatically imply the more complex or higher resolution model is superior (e.g., Dosio et al., 2019). For instance, most studies comparing high-resolution, convection permitting RCM simulations that explicitly simulate deep convection with simulations of hydrostatic RCMs with parameterized convection find, at least for some regions, a qualitatively different response of short duration extreme summer precipitation (Chan et al., 2014b, 2014a; Ban et al., 2015; Tabari et al., 2016; Vanden Broucke et al., 2018), whereas other studies do not (Fosser et al., 2017). Process studies of convection under warming conditions provide evidence that convection permitting simulations simulate physically more plausible heavy precipitation changes (Meredith et al., 2015a), but further research is required to determine the agreement in these findings.

Overall, there is *high confidence* that increasing model resolution, downscaling and adding relevant model components can increase the fitness for some aspects of regional projections when are accompanied by a process-understanding analysis.

10.3.4 Managing uncertainties in regional climate projections

Regional climate projections are affected by mainly three sources of uncertainty (Section 10.2.2): unknown future external forcings, imperfect knowledge and implementation of the response of the climate system to external forcings, and internal variability (Lehner et al., submitted). In a regional downscaling context, uncertainties arise in every step of the modelling chain. Additionally, the calibration of statistical downscaling methods is affected by observational uncertainty (Section 10.2.3.3). Here the propagation of uncertainties, the management of uncertainties, the role of the internal variability for regional projections, and the design and use of ensembles to account for uncertainties will be assessed.

10.3.4.1 Propagation of uncertainties

Modelling chains for generating regional climate information range from the definition of forcing scenarios to the global modelling, and potentially to dynamical or statistical downscaling and bias adjustment (Figure 10.2). The propagation and potential accumulation of uncertainties along the chain has been coined the cascade of uncertainty (Wilby and Dessai, 2010). Even within one model, like a GCM, uncertainty propagates across scales. These uncertainties are related to forcings and global climate sensitivity, and errors in the representation of the large-scale circulation (Section 10.3.3.4) and regional processes (Section 10.3.3.5), feedbacks (Section 10.3.3.6) and drivers (Section 10.3.3.7). Statistical downscaling, bias adjustment and weather generators express mesoscale to convective-scale atmospheric processes by a simplified and uncertain statistical model (Maraun and Widmann, 2018b). The overall uncertainty can be statistically decomposed into the individual sources (Evin et al., 2019), although there might be non-linear dependences between them.

The uncertainty propagation often increases the spread in regional climate projections when comparing GCM and downscaled results, which has been used by some authors as an argument against top-down approaches to climate information (Prudhomme et al., 2010), but increased uncertainties in the modelling chain may in principle arise from a more comprehensive sampling of previously unknown or underrepresented uncertainties (Maraun and Widmann, 2018b). The spread increase is then an expression of a better understanding and increased model fitness for purpose (Section 10.3.3.10).

10.3.4.2 Representing and reducing uncertainties

Climate response uncertainties (Chapter 1) can be represented by multi-model ensembles, although the sampled uncertainty typically underestimates the full range of uncertainty (Collins et al., 2013b; Shepherd et al., 2018). Traditionally, climate response uncertainty has been characterized by the multi-model mean change and associated ensemble spread. The change has then further been qualified in terms of the agreement across models and the significance compared to internal climate variability (Collins et al., 2013b). Since AR5, several limitations of this “quasi-probabilistic” approach have been identified (Madsen et al., 2017). Such a treatment fails to address physically plausible, but unlikely high-impact scenarios (Chapter 1; Sutton, 2018). Moreover, in particular at the regional scale, qualitatively different or even opposite changes may be equally plausible (Shepherd, 2014). In a multi-model mean these different responses would be lumped together, strongly dampened, and qualified as non-robust, whereas in fact high impacts might be expected. Even more, the multi-model mean itself is often implausible, because it is a statistical construct, and may not manifest at all (Zappa and Shepherd, 2017). Overall, there is *high confidence* that some regional future climate changes may not be well characterised by multi-model mean and spread, and that additional approaches may be required.

Since AR5, physical climate storyline approaches (see also Chapter 1, Section 10.5.3, and Atlas 6.1.3) have therefore been developed to better characterise and communicate uncertainties in regional climate projections (Shepherd, 2019). A special class of storylines attempts to attribute regional uncertainties to uncertainties in remote drivers. For instance, the Dutch Meteorological Service has presented precipitation projections for the Netherlands for different plausible changes of the mid-latitude atmospheric circulation and different levels of European warming (Attema et al., 2014). Manzini et al. (2014) have quantified the impact of uncertainties in tropical upper troposphere warming, polar amplification, and stratospheric wind change on Northern Hemisphere winter climate change. Based on these results, Zappa and Shepherd (2017) separated the multi-model ensemble into physically consistent sub-groups or storylines of qualitatively different projections in relevant remote drivers of the atmospheric circulation.

These storyline approaches help to physically explain contradicting projections at the regional scale and thus make the conveyed information a better representation of the true uncertainty (Hewitson et al., 2014a). Additionally, the attribution of regional uncertainties to drivers may in principle help to reduce uncertainties in the case where some storylines can be ruled out because the projected changes in the driving processes appear to be physically implausible (Zappa and Shepherd, 2017). There is hence *high confidence* that storylines attributing uncertainties in regional projections to uncertainties in changes of remote drivers aid the representation of climate projection uncertainties.

Another approach that has been developed over recent years to characterise and reduce projection uncertainties are emergent constraints (Hall et al., 2019; Chapter 1). The idea is to link the spread in climate model projections via a regression to the spread in present climate model biases for relevant driving processes. Models with lower biases are assigned higher weight in the projections, which in turn reduces the spread of the projection in a physical way and may additionally reduce projection uncertainty. For instance, Simpson et al. (2016) have reduced the spread in projections of North American winter hydroclimate by linking this spread to model biases in the representation of relevant stationary wave patterns. Other examples of using emergent constraints (Chapter 4) in a regional context are Brown et al. (2016), Li et al. (2017), and Giannini and Kaplan (2019).

10.3.4.3 Role of internal variability

A regional climate projection based on a single simulation from a single GCM or driving a single RCM alone will inevitably be affected by internal variability due to the chaotic nature of the climate system (Figure 10.10). This is mainly due to the dominant influence of the chaotic atmospheric circulation on regional climate variability, in particular at mid-to-high latitudes. Internal variability is an irreducible source of uncertainty for mid-to-long-term projections (Chapter 1).

There is *very high confidence* that the role of internal variability has likely been underestimated in previous assessments of regional climate projections as shown by a large body of literature based on initial condition, single-model large ensembles (Deser et al., 2012b, 2014; Kay et al., 2015; Dai and Bloecker, 2018; Maher et al., 2019). Initial-condition large ensembles allow quantification of the influence of internal variability on GCM-based regional climate projections for all simulated variables and spatial and temporal scales (see also Section 1.4.4). Another related development is the more frequent use of observation-based statistical models to assess the influence of internal variability on regional-scale GCM and RCM projections (Thompson et al., 2015; Salazar et al., 2016).

Since AR5, several large (of size 30 or more) initial condition ensembles have been constructed and used to assess signal-to-noise diagnostics, mainly limited to GCMs (Deser et al., 2012b; Kay et al., 2015; Sigmond and Fyfe, 2016; Bengtsson and Hodges, 2018), but more recently also involving dynamical downscaling (von Trentini et al., 2019b, 2019a). Standard diagnostics include a simple assessment of the signal-to-noise ratio that can be defined as the forced response (ensemble mean) to the noise (ensemble spread) ratio, or the time of emergence, which indicates the time at which a forced climate signal emerges from the secular/decadal "noise" of an internal climate variability estimate (Hawkins and Sutton, 2012; Mahlstein et al., 2012; Lehner et al., 2017a). The time of emergence diagnostic can be based on the signal-to-noise ratio exceedance of a subjective threshold or a level of significance for rejecting a null hypothesis of no change in a given climate variable probability density function between two different periods. The time of emergence can also be assessed with regard to the mean change and/or changes in variability including extremes and records (Maraun, 2013b; King et al., 2015; Bador et al., 2016), although Maraun (2013) argued that the time of emergence can be misleading for the assessment of rare events, as the associated hazard may increase even when the signal-to-noise ratio is low (as indicated by the envelope of grey lines in Figure 10.10). The time of emergence is a subjective diagnostic with different sources of uncertainty as it can be affected by model biases, internal variability, definition of the base period (pre-industrial runs and/or late 19th century), time filtering choices, and spatial scale aggregation diagnostics records (Hawkins and Sutton, 2012; Maraun, 2013b; King et al., 2015; Bador et al., 2016; Lehner et al., 2017a).

[START FIGURE 10.10 HERE]

Figure 10.10: Observed and projected changes in seasonal mean (December to February in the left column and June to August in the right one) precipitation. Observations based on Global Precipitation Climatology Centre (GPCC) version 2018 (Schneider et al., 2017) and Climate Research Unit (CRU TS) version 4.02 (Harris et al., 2014) datasets, projections based on the Max-Planck Institute Grand-Ensemble (MPI-GE) (Maher et al., 2019) with 100 simulations starting from different initial conditions. (a)-(d) 55-year trends (2016–2070) from ensemble members with the minimum (a,c) and maximum (b,d) area mean change in the trend. (e) and (f) Time series of seasonal mean precipitation with the red (blue) lines corresponding to the ensemble member with strongest (weakest) 55-year trend and the grey lines to all remaining ensemble

members. Box-and-whisker plots show changes relative to the base period across all ensemble members for three future time slices (near, mid, and long term). The top panels show global averages, the middle panels averages across the domains marked in (a)-(d), and the bottom panels results for grid boxes close to the cities mentioned.

[END FIGURE 10.10 HERE]

Based on the MPI-GE large-ensemble with an ensemble size of 100, Maher et al., (2019) show that a minimum of 40–50 members are needed to capture both the 21st century SLP-forced trend pattern and the variability of the trend, confirming previous results from Deser et al. (2012). Some regional-scale studies show that both large-scale internal variability and local-scale internal variability together can still represent a substantial fraction of the total uncertainty related to hydrological cycle variables, even at the end of the 21st century (Lafaysse et al., 2014; Aalbers et al., 2018; Gu et al., 2018).

There is *high confidence* that internal variability introduces substantial irreducible uncertainty in regional-scale climate change attribution and climate change projections. This problem applies to all regions and time scales (from a decade up to a century) and is more acute in the extra-tropics and for climate variables other than temperature, such as precipitation or for atmospheric circulation.

10.3.4.4 Designing and using ensembles for regional climate change assessments to take uncertainty into account

As noted in Sections 10.3.4.2 and 10.3.4.3, ensembles of climate simulations play an important role in quantifying uncertainties in the simulation output. In addition to providing information on internal variability, ensembles of simulations can estimate scenario uncertainty and model (structural) uncertainty. Chapter 4, especially Box 4.1, discusses issues involved with evaluating ensembles of GCM simulations and their uncertainties.

In a downscaling context, further considerations are necessary, such as the selection of GCM-RCM combinations when performing dynamical downscaling. This is a relevant issue when resources are limited. The structural uncertainty of both the GCM and the downscaling method can be important (e.g., Dosio, 2017; Mearns et al., 2012), as well as further potential uncertainty created by inconsistencies between the GCM and the downscaling method (e.g., Dosio et al., 2019), which could include, for example, differences in topography or the way to model precipitation processes (Mearns et al., 2013).

An important consideration is which set of GCMs should be used for the combination. Some RCM-based initiatives consider a matrix of GCM-RCM combinations or one RCM to downscale multiple GCMs. If adequate resources exist, then large numbers of GCM-RCM combinations are possible, as in the ENSEMBLES project (Déqué et al., 2012). However, coordinated downscaling programmes can be limited by the resources available, both human and computational, for producing ensembles of downscaled output, which limits the number of feasible GCM-RCM combinations. With this limitation in mind, a small set of GCMs needs to be chosen that span the range of equilibrium climate sensitivity (e.g., Inatsu et al., 2015; Mearns et al., 2012, 2013) or some other relevant measure of sensitivity, such as the projected range of tropical SSTs (Suzuki-Parker et al., 2018). These GCMs may also be selected to represent physically self-consistent changes in regional climate (Zappa and Shepherd, 2017). Statistical methods can provide estimates of outcomes from missing GCM-RCM combinations in a large matrix (Déqué et al., 2012; Heinrich et al., 2014).

However, even using a relatively small set of GCMs can still involve substantial computation that strains available resources, both for performing the simulations and for using all simulations in the ensemble for further impacts assessment. The NARCCAP programme (Mearns et al., 2012) used only a subset of its possible GCM-RCM combinations that balanced comprehensiveness of sampling the matrix with economy of computation demand (Mearns et al., 2013). If information from all possible combinations is still desired, one can apply statistical methods to a well-balanced, but incompletely filled matrix and extract climatological information for the missing combinations. An advantage of the sparse, but balanced matrix for those using the downscaling output for further studies, such as vulnerability, impacts and adaptation assessments is that they have a smaller, yet comprehensive set of GCM-RCM combinations to work with. Alternatively, data-clustering methods can clump together downscaling simulations featuring similar climate-change characteristics, so that only one representative simulation from each cluster may be needed for further impacts analysis, again systematically reducing the necessary number of simulations to work with (Mendlik and Gobiet, 2016; Wilcke and Bärring, 2016).

Whatever the resources, participation of multiple models in a simulation programme such as CORDEX for RCMs or CMIP for GCMs creates ensembles of opportunity, which are ensembles populated by models that participants chose to use for simulation without there necessarily being an overarching guiding principle for an optimum choice. As discussed in Chapter 4, these ensembles are likely suboptimal for assessing sources of uncertainty. An important contributor to the suboptimal character of such an ensemble is that the models are not independent. Some may also have larger biases than others. Yet often, the output from models in these ensembles has received equal weight when viewed collectively, as was the case in much of the AR5 assessment (e.g., Collins et al., 2013; Flato et al., 2014; Kirtman et al., 2014; Knutti et al., 2013).

One approach to emphasize independent models is to combine models with the same origins into families, effectively an a priori weighting, and create ensemble averages giving equal weight to each of these families of models. A variation of this approach lumps together models that use similar parameterizations for some processes (Chapter 4). Much of the work with these approaches has been done using GCMs, which can be a basis for selecting relatively independent GCMs as contributors to a GCM-RCM matrix, for example. Evans et al. (2014) have also used RCM independence as a guiding principle for selecting RCMs to include in their matrix. Alternatively, some have proposed a posteriori weighting, wherein weights are based on a measure of simulation accuracy. Räisänen and Palmer (2001) and Giorgi and Mearns (2002) developed initial applications of this approach to GCM/RCM ensembles. Accuracy weighting has continued to be used for analysing GCMs (see Chapter 4) and RCMs (Déqué et al., 2012). However, the choice of accuracy measure can be somewhat arbitrary, and if applying the weighting to projections, it assumes that the models replicating present climate the best have the least error in their future scenario climates. Therefore, there is growing support for a process-based binary weighting, i.e., that GCMs should be discarded that unrealistically represent processes controlling the regional climate of interest (McSweeney et al., 2015; Maraun et al., 2017b; Eyring et al., 2019). Box 4.1 offers a more detailed discussion of the issues surrounding these approaches and their implications for ensemble evaluation and weighting.

There is *high confidence* that ensembles for regional climate projections should be selected such that models unrealistically simulating processes relevant for a given application are discarded, but at the same time, the chosen ensemble spans an appropriate range of projection uncertainties.

[START CROSS-CHAPTER BOX 10.2 HERE]

Cross-Chapter Box 10.2: Issues in bias adjustment

Contributors: Ana Casanueva (Spain), Alessandro Dosio (Italy), José M. Gutiérrez (Spain), Stefan Lange (Germany), Douglas Maraun (Austria/Germany)

Bias adjustment was not assessed in AR5 (Flato et al., 2014) in spite of being commonly used at the interface between climate model projections and the assessment of climate hazards and impacts. Over recent years, however, several issues have been identified that may arise from an uncritical use of bias adjustment. This Cross-Chapter Box first discusses the rationale behind using bias adjustment, and then assesses these issues and potentially adverse consequences. The box extends the assessment in Section 10.3.3.4, where the performance of different bias adjustment methods is assessed when applied to perfect predictors.

Justification and need for bias adjustment

Bias adjustment has become widely used in climate hazard and impact studies (Gangopadhyay et al., 2011;

Hagemann et al., 2013; Warszawski et al., 2014) and national assessment reports (Cayan et al., 2013; Georgakakos et al., 2014). However, some authors question its validity when applied to climate change studies, as bias adjustment may alter the spatial-temporal and inter-variable consistency of the model data, violating conservation principles and neglecting feedback mechanisms (Ehret et al., 2012). In addition, the underlying assumption of whether biases are time-invariant or not is still debated (Vannitsem, 2011; Ehret et al., 2012).

However, following a more pragmatic approach, and acknowledging the underlying shortcomings, other studies argue that climate model biases are severe enough to, in principle, justify the use of bias adjustment prior to impact modelling (Maraun et al., 2017b). A key argument made for the use of bias adjustment is the fact that impact models commonly react very sensitively, often non linearly, to the input climatic variables and their biases. Examples of impact modelling studies showing an improvement in simulating present day hazard, when fed with bias-adjusted climate model output, include the assessment of hydrological impacts such as river discharge (Rojas et al., 2011; Muerth et al., 2013; Montroull et al., 2018), forest fires (Migliavacca et al., 2013), crop production (Ruiz-Ramos et al., 2016), and regional ocean modelling (Macias et al., 2018). The use of bias-adjusted model outputs is also particularly beneficial when threshold-based climate indices are required (Dosio, 2016). There are, however, cases where bias adjustment may not be necessary or useful, such as:

- when only qualitative statements are required,
- when only changes in mean climate are considered (however, some authors argue that bias adjustment may improve the change, see below),
- when percentile-based indices are used.

Time-invariance assumption and modifications of the climate change signal by bias adjustment

The AR5 has already presented examples of state-dependent climate model biases with examples where the time-invariance assumption, which implies that biases are the same in both the present and future climates, of the biases is violated (Flato et al., 2014). Further research since then addressed this issue by means of perfect model experiments (Section 10.3.2.5) and process understanding. Perfect model studies with GCMs found that circulation, energy, and water-cycle biases are roughly state-independent (Krinner and Flanner, 2018), whereas temperature biases depend linearly on temperature (Kerkhoff et al., 2014). Other studies show that regional temperature biases may depend on soil moisture and albedo, and may thus be state-dependent (Maraun, 2012; Bellprat et al., 2013; Maraun et al., 2017b). The state-dependence implies time-varying biases, meaning that there will be different biases in present and future climate. For present climate, Teutschbein and Seibert (2013) argue that bias adjustment with quantile mapping methods may account for such state-dependence.

[START CROSS-CHAPTER BOX 10.2, FIGURE 1 HERE]

Cross-Chapter Box 10.2, Figure 1: Modification of simulated climate change signals by different bias-adjustment methods in different settings over the Iberian Peninsula. Climate change signal (deltas, Δ) for the 2071–2100 (RCP8.5) period with respect to the baseline 1971–2000 for global (G-RAW, 1.125º horizontal resolution) and regional (R-RAW, 0.2º) model outputs (first two boxplots in each panel) together with bias-adjusted results (rest of boxplots). Results are shown for two similar bias-adjustment experiments with high-resolution (0.2º, left column) and coarse (1.125º, right column) observational reference data from two different datasets: Iberia01 (IB) and E-OBS (E). In the left column the GCM outputs are "downscaled" to the high resolution, whereas the RCM outputs have the same target resolution (so there is no associated downscaling). However, in the right column all datasets are upscaled to the GCM resolution (no downscaling effect). Results are shown for seven bias-adjustment methods with four results (boxplots) for each method (G-IB-code, G-E-code, R-IB-code, R-E-code, for global 'G' and regional 'R' model outputs adjusted using Iberia01 'IB' or E-OBS 'E' observational references). Adapted from Casanueva et al. (submitted).

[END CROSS-CHAPTER BOX 10.2, FIGURE 1 HERE]

It has been shown that bias adjustment methods like quantile mapping can modify simulated climate change trends, with notable impacts on changes to climate indices (Figure 1), in particular, extremes (Haerter et al., 2011; Dosio et al., 2012; Ahmed et al., 2013; Hempel et al., 2013; Maurer and Pierce, 2014; Cannon et al., 2015; Dosio, 2016). Some authors argue that these trend modifications are implicit corrections of state-dependent biases (Boberg and Christensen, 2012; Gobiet et al., 2015). However, others argue that quantile mapping is calibrated on high-frequency (like daily values) variability and cannot necessarily correct long-term trends (Maraun et al., 2017b). Similar arguments have led to the development of trend preserving quantile mapping methods (Section 10.3.1.4.2). Other authors claim that bias adjustment has no overwhelming negative or positive effect on future precipitation changes, and there is no clear advantage in using a trend-preserving bias adjustment (Maurer and Pierce, 2014). Further research is still required to fully understand the time and state-dependence of climate model biases in bias adjustment, and the validity of trend modifications by quantile-mapping approaches.

Bias adjustment in the presence of large-scale circulation errors

Recent research has investigated the influence on bias adjustment of circulation errors, such as biases in the frequency of precipitation-relevant weather types (Addor et al. 2016). In this case, a standard bias adjustment (i.e. not accounting for this frequency bias) would remove the overall climatological bias, but residual precipitation biases for individual weather types would remain. Conversely, a bias adjustment applied separately for each weather type would remove weather-type specific biases, but not the overall climatological bias. Other works showed that the attempt to correct such frequency biases, by e.g., adjusting the number of wet days, may artificially deteriorate the spell-length distribution and either delete or artificially introduce long dry spells (Maraun et al., 2017b).

In presence of biases in the location of dominant circulation patterns, bias adjustment may introduce physically inconsistent and implausible solutions (e.g., a northward-moving North Atlantic storm track accompanied by a southward moving precipitation pattern (Maraun et al., 2017b)). Bias adjusting the location of circulation features has been proposed (Levy et al., 2013) but this may introduce inconsistencies with the model orography, land-sea contrasts, and SSTs (Maraun et al., 2017b). Other authors therefore suggest bias adjustment during the simulation (Guldberg et al., 2005; Kharin et al., 2012; Krinner et al., 2019).

There is *medium confidence* that the selection of climate models with low biases in the synoptic-scale atmospheric circulation may increase the validity of bias adjustment.

Bias adjustment prior to dynamical downscaling

Some authors suggest to mitigate the influence of large-scale temperature or circulation biases by performing a bias adjustment of the driving fields prior to dynamical downscaling (e.g., Colette et al., 2012; Hernández-Díaz et al., 2013). For present climate, this approach has been shown to substantially reduce the RCM biases in mean temperature and precipitation. In a case study for South Africa, White and Toumi (2013) demonstrated that bias adjustment reduces the bias in downscaled monthly mean precipitation, but quantile mapping artificially amplifies its interannual variability. This approach may introduce dynamical inconsistencies because the adjustment corrects the location of long-term mean patterns, but not the location of day-to-day variability (Maraun et al., 2017b). A modified version therefore corrects GCM-simulated SSTs and uses these as surface boundary conditions for an AGCM simulation, which in turn provides the boundary conditions for dynamical downscaling (Hernández-Díaz et al., 2019). Further research is required to understand the validity of bias-adjusted GCM outputs prior to dynamical downscaling.

Representativeness issues and the use of bias adjustment as statistical downscaling

Bias adjustment assumes that the simulated variable is representative of the observed target variable, which is not always the case. Maraun et al., (2017b) investigated a case where observed precipitation was closely correlated with ENSO variability, but GCM-simulated precipitation was essentially uncorrelated with the simulated ENSO variability. In complex terrain, the simulated regional flow may be substantially shifted compared to reality because of, among other things, the coarse representation of topography in the climate model (Maraun and Widmann, 2015). In both cases, standard bias adjustment is not appropriate.

Bias adjustment is often used to downscale climate model results from gridbox to point scale or finer resolution. For instance, several authors apply bias adjustment directly to GCM outputs instead of using an intermediate dynamical downscaling step (e.g., Johnson and Sharma, 2012). Bias adjustment of coarse simulations may lead to representativeness issues, as the climate in one location may substantially differ from the climate of the closest model cells. For precipitation, long-term trends may be artificially modified and area-aggregated extremes may be overestimated (Maraun, 2013a; Gutmann et al., 2014; Maraun et al., 2017b). Similarly, temperature inversions in unresolved valleys, as well as sub-grid elevation dependent-warming due to unresolved snow-albedo feedbacks are not represented (Maraun et al., 2017b) (Figure 2). It has therefore been suggested to account for local random variability by combining bias adjustment with stochastic downscaling (Volosciuk et al., 2017; Lange, 2019c), although this approach still does not account for local modifications of the climate change signal. Statistical emulators of high-resolution RCMs have been proposed to account for local modifications of the climate change signal (Walton et al., 2015).

Overall, there is *high confidence* that the use of bias adjustment for statistical downscaling, in particular of coarse resolution GCMs, has limitations and that dynamical downscaling may be required to resolve relevant local processes prior to bias adjustment. Examples of such added value of RCMs are given in Sections 10.3.3.3 and 10.3.3.5.

[START CROSS-CHAPTER BOX 10.2, FIGURE 2 HERE]

Cross-Chapter Box 10.2, Figure 2: Boreal spring (March to May) daily mean temperature in the Sierra Nevada region in California. (a) Present climate (1981–2000 average) in the GFDL-CM3 GCM, interpolated to 8 km (left), GCM bias adjusted (using quantile mapping) to observations at 8 km resolution (middle) and WRF RCM at 3 km horizontal resolution (right). (b) Climate change signal (2081–2100 average minus 1981–2000 average according to RCP8.5) in the GCM (left), the bias adjusted GCM (middle) and the RCM (right). As the GCM does not resolve the snow-albedo feedback, it simulates an implausible regional warming signal. The bias adjustment cannot improve the missing feedback. Only the high-resolution RCM simulation simulates a plausible elevation-dependent climate change signal. Adapted from Maraun et al. (2017b).

[END CROSS-CHAPTER BOX 10.2, FIGURE 2 HERE]

Calibrating and evaluating bias adjustment in the presence of observational uncertainty and internal variability

Observational uncertainties and internal variability may introduce substantial uncertainty in the estimation of biases and thus in the calibration of bias-adjustment methods. Dobor and Hlásny (2018) found a considerable influence of the choice of the observational dataset and calibration period on the bias adjustment for some regions in Europe. Similarly, Kotlarski et al. (2017) found that RCM biases are typically larger than observational uncertainties, but in some regions, and in particular for wet-day frequencies, spatial patterns and the intensity distribution of daily precipitation, the situation may reverse. Switanek et al. (2017) found a strong influence of internal variability and thus of the choice of calibration period on the calibration of quantile mapping and ultimately even on the modification of the climate change signal.

Bias adjustment is typically evaluated using cross-validation, i.e. by calibrating the adjustment function to one period of the observational record, and by evaluating it on a different one. Some studies highlight the difficulties of evaluating bias adjustment using this approach (Maraun et al., 2017b). Maraun and Widmann (2018) demonstrated that, for climate-change simulations, multi-decadal internal climate variability may lead to a rejection of a valid bias adjustment or even lead to a positive evaluation of an invalid bias adjustment. The authors therefore argued that, in the presence of substantial internal variability, bias adjustment of climate cannot sensibly be evaluated by cross-validation, but instead by evaluating aspects that have not been adjusted, such as temporal, spatial, or multi-variable dependence.

Recommendations for the use of bias adjustment

In the light of these issues, several attempts have been made to provide guidelines for the use of bias adjustment, the most important ones are summarised in the following. Ehret et al. (2012) recommend that when using bias adjustment, the raw model output should always be provided alongside the bias adjusted data. This recommendation was backed up by Stocker et al. (2015). Maraun et al., (2017b) argued that the target resolution should be similar to the model resolution to avoid representativeness issues. Stocker et al. (2015) and Maraun et al. (2017) both highlighted the relevance of understanding model biases and the misrepresentations of the underlying physical processes prior to any bias adjustment, and encourage the development of physics-informed bias adjustment methods, and the collaboration between bias adjustment users, experts in climate modelling and experts in the considered regional climate (Galmarini et al., 2019).

[END CROSS-CHAPTER BOX 10.2 HERE]

10.4 Interplay between anthropogenic change and internal variability at regional scales

This section assesses the physical causes of past and future regional climate change in the context of the ongoing anthropogenic influence on the global climate. In this section, regional climate change refers to a transient change in the state of the climate that can be identified by changes in the mean and/or higher moments, and persists for an extended period, typically a few decades or longer. Regional climate change as interpreted here may be due to natural internal processes such as atmospheric internal variability and local climate response to low-frequency modes of climate variability such as the AMV and the PDV. Regional climate change can also be due to changes in external forcings such as modulations of the solar cycle, orbital forcing, volcanic eruptions, and persistent anthropogenic changes in the composition of the atmosphere or in land use ((IPCC, 2018) glossary; Section 10.1.4; Cross-Chapter Box 3.1). Note that this differs from the United Nations Framework Convention on Climate Change (UNFCCC) Article 1 definition, which defines climate change as a change attributable to human activities altering the atmospheric composition. This different perspective is in line with the enhanced perception since the AR5 of the importance on internal variability as a driver of multi-decadal regional climate changes (Section 1.4.1).

The assessment focuses on eight illustrative examples that span a wide range of regions, time scales, attribution methods and issues (Figure 10.11), and that without aiming at being comprehensive, offer the possibility to illustrate a number of methodological aspects. Here, the examples are defined by a geographical spatial domain as well as a past period (from a couple to several decades) during which the specific regional climate has undergone a substantial change. Note that substantial does not refer here to significantly rejecting a specific statistical null hypothesis. Instead, it is loosely used to describe a change that can have one or more of the following properties: large amplitude and/or spatial extent, a rare occurrence, high-impact in terms of consequence for human and natural systems, thus making a relevant link with the WGII assessment report. Elements about two specific WGII regions, mountains and cities, are also included (Cross-Chapter Box 10.3 and Box 10.2). The list of all selected illustrative examples roughly follows the order of the regional chapters of the WGII report. Section 10.4.1 describes regional-scale attribution methodologies and provides an assessment of the main causal factors underlying the observed changes for each example region. Section 10.4.2 focuses on the interplay between internal variability and external forcing in shaping future regional climate change, and its geographical and seasonal variations. A complete assessment of future regional climate change for all regions considered in the report (as defined in Box 1.1) can be found in the Atlas chapter.

[START FIGURE 10.11 HERE]

Figure 10.11: Time series of surface air temperature (in °C, blue and red colours) or precipitation (in mm per month, green and ochre colours) anomalies (relative to the 1951–1980 period) area-averaged over appropriate regions of the selected illustrative examples. The regions are broadly defined by the green (precipitation) and magenta (temperature) rectangles. The precise region boundaries and examples are from top to bottom and left to right: (a) The south-western North America (28°N–40°N, 105°W–120°W) drought. (b) The Caribbean small islands (15°N–27°N, 65°W–85°W) summer (June to August) drought. (c) The south-eastern South America (26.25°S–38.75°S, 56.25°W–66.25°W) Austral summer (December to February) drought. (d) The Sahel and the West African summer (June to September) monsoon (10°N–20°N, 20°W–40°E) drought and recovery. (e) The south-western Australia (25°S–39°S, 110°E–122°E) Austral autumn and winter rainfall decline. (f) The East Asia summer (June to August) monsoon weakening and recovery; here the time series is the difference of mean precipitation between two regions: (110°E–125°E, 35°N–45°N) – (105°E–125°E, 20°N–35°N). (g) The central and eastern Eurasia (40°N–65°N, 40°E–140°E) winter (January to March) cooling. (h) The western Europe (35°N–70°N, 15°W–20°E) summer (June to August) warming. Temperature data is from the Berkeley surface temperature dataset (BEST) (Rohde et al., 2013) and precipitation from Global Precipitation Climatology Centre (GPCC) version 2018 (Becker et al., 2013; Schneider et al., 2017). The light-grey area on each graphic represents the period of interest for attribution. The black line is a simple low-pass filter that has been used in AR4, Chapter 3, Appendix 3.A. It has five weights 1/12 [1-3-4-3-1] and for annual data, its half-amplitude point is for a six-year period, and the half-power point is near 8.4 years.

[END FIGURE 10.11 HERE]

10.4.1 Attributing past regional changes to multiple causal factors

This section focuses on recent research on attribution of past regional climate change for the selected illustrative examples. In this chapter, attribution is defined as the process of evaluating the relative contributions of multiple causal factors (or drivers) to a regional climate change (Box 1.3; Rosenzweig and Neofotis, 2013; Shepherd, 2019). Note that this slightly differs from the usual definition of attribution used in the AR5 (Hegerl et al., 2010; Box 3.1). In particular, the preliminary detection step is not required to perform attribution since causal factors may also include drivers of internal variability, such as the AMV or PDV among many others, in addition to external natural and anthropogenic forcing. Indeed, to understand changes in climate and attribute cause at the regional scale it is also vital to consider internal variability that might be considered as a noise problem at global scale. In order to make this distinction clear, the term regional-scale (or process-based) attribution will be used in this section (Cross-Chapter Box 1.4). Importantly, regional-scale attribution also seeks to determine the physical processes and uncertainties involved in the driver's influence. Therefore, this section builds on the detection and attribution work of Chapter 3 by focusing on regional-scale changes arising from both internal variability and external forcing drivers.

Firstly, in Section 10.4.1.1, methodologies in the attribution of regional climate change and links to drivers of climate change at the global and regional scale as outlined in Section 10.1.4 are assessed. Next, in Section 10.4.1.2 a series of examples in which the attribution of regional climate changes in the historical period involves the interplay between the action of large- and local-scale anthropogenic drivers and internal variability are assessed.

10.4.1.1 Methodologies for regional climate change attribution

Attribution at sub-continental and regional scales are usually more complicated than at the global scale due to various factors: a larger contribution of internal variability drivers, an increased degeneracy among the responses to different external forcings, the importance at local scale of some omitted forcings in GCM simulations, and larger model errors related to the representation of small-scale phenomena (Zhai et al., 2018). In addition to standard optimal fingerprint regression-based approaches (Section 3.2.1 and Zhai et al. (2018)), several emerging methodologies have been increasingly used for regional climate change attribution. These include three statistical approaches, namely, dynamical adjustment techniques, the univariate detection and attribution method, and the ensemble empirical mode decomposition method that are often combined with dynamical model-based large ensembles (including both initial condition ensembles and perturbed physics ensembles; Section 1.4.4). Details are provided below.

Standard optimal fingerprint methods have been applied to detection and attribution of climate change mean temperature signal in several regions of the world such as Canada, India, Central Asia, Northern China, Australia, and North Africa (Li et al., 2017a; Dileepkumar et al., 2018; Wang et al., 2018c; Peng et al., 2019; Wan et al., 2019). The influence of anthropogenic forcing, and in particular that of GHGs, is robustly detected in annual and seasonal mean temperatures for all the considered regions. The contribution of the GHG forcing to the observed temperature change varies among the different regions, ranging between 60 to more than 100%. While the influence of external natural forcing can often be detected as well, its contribution to observed changes is usually much smaller (Li et al., 2017a; Wan et al., 2019). Detection of precipitation changes due to human influence is much more difficult, due to a larger amount of internal variability at regional to local scales, as well as substantial modelling and observational uncertainty (Wan et al., 2015; Sarojini et al., 2016; Li et al., 2017a). It is noteworthy that these methods require a very significant reduction of spatial and temporal dimensions in order to reliably estimate the covariance matrix of internal variability (an entire region is thus often considered as being only one or a few spatial points that represent the spatial average of the whole region or a few sub-regions; time samples are often 5- or 10-year averages). Finally, model error is rarely included in the statistical model used in detection and attribution regional studies, while it has been shown to have a strong impact on the stability of scaling factors and confidence intervals when increasing the spatial dimension (Ribes and Terray, 2013). New statistical methods are emerging to provide some alternative to standard optimal fingerprinting but they have not yet been evaluated and applied at regional scales (Section 3.2.2).

The dynamical adjustment method (Smoliak et al., 2015; Deser et al., 2016) seeks to isolate changes in surface air temperature or precipitation that are due purely to atmospheric circulation changes. The residual can then be analysed and attributed to internal changes in both land or ocean surface conditions and the thermodynamical response to external forcing. Smoliak et al. (2015) performed their dynamical adjustment using partial least squares regression of temperature to remove variations arising from sea-level pressure changes. Deser et al. (2016) used constructed atmospheric circulation analogues and resampling to estimate the dynamical contribution to changes in temperature. Removing temperature or any other variable changes associated with circulation patterns allows a cleaner, simplified residual time series of the regional climate variable to be assessed, in order to more easily determine the influence of local and remote ocean and land internal drivers or external forcing agents. It is noteworthy that the dynamical adjustment method by itself cannot account for the component of the forced response associated with circulation changes that project onto atmospheric internal variability. However, this component can be estimated within a model framework by averaging the dynamical contribution across multiple members of an initial condition large ensemble (Deser et al., 2016).

Dynamical adjustment methods have been used by, for instance, Deser et al. (2016), O'Reilly et al. (2017), Gong et al. (2019), and Guo et al. (2019). Deser et al. (2016) focused on the causes of observed and simulated multi-decadal trends in North American temperature. A 30-member model ensemble was used, with differing initial states, to identify forced and internally generated components. They demonstrated that the main advantage of this technique is to narrow the spread of temperature trends found by the model ensemble and to bring the dynamically-adjusted observational trend much closer to the forced response estimated by the model ensemble mean. Similarly, O'Reilly et al. (2017) applied dynamical adjustment techniques to more carefully determine the influence of the AMV on continental climates. Variations in summer temperature and the AMV from 1901 to 2010 were measured, while three sea-level pressure datasets were used to construct the patterns of internal circulation variability. Over Europe, summer temperature anomalies induced thermodynamically by the warm phase of the AMV are further reinforced by circulation anomalies; meanwhile, precipitation signals are largely controlled by dynamical responses to the AMV. Based on a partial least-squares approach, Gong et al. (2019) showed that recent winter temperature 30-year trends over northern East Asia are strongly influenced by internal variability linked to decadal changes of the Arctic Oscillation. Using dynamical adjustment purely on precipitation observations, Guo et al. (2019)

showed that human influence has led to increased wintertime precipitation across north-eastern North America, as well as a small region of north-western North America, and to an increase in precipitation across much of north-western and north central Eurasia.

The univariate detection method does not use spatial pattern information, but compares observed trends in gridded datasets with distributions of trends from ensembles of simulations during the historical period using natural forcing-only versus all forcings combined with distributions of internal variability trends from long simulations with pre-industrial constant external forcing (Knutson et al., 2013; Knutson and Zeng, 2018). Consistency between observed and historical simulation trends is also assessed with statistical tests that can be applied independently over a large number of grid points. The fraction of area classified as detectable, attributable, or consistent/inconsistent is then finally estimated. The method can be viewed as a simple consistency test for both amplitude and pattern of observed versus simulated trends. Its application to CMIP3 and CMIP5 models suggests that 80% of the Earth surface has a detectable anthropogenic warming signal (Knutson et al., 2013).

The ensemble empirical mode decomposition method (Wu and Huang, 2009; Wilcox et al., 2013; Ji et al., 2014; Qian and Zhou, 2014) decomposes data, such as time series of historical temperature and precipitation, into independent oscillatory modes of decreasing frequency. The last step of the method leaves behind a nonlinear residual time series with no further oscillations. Typically, the nonlinear trend (e.g., of 20th-century temperature) can be reconstructed by summing the long-term mean, the residual, and eventually the lowest-frequency mode to account for a multi-decadal forced signal, for instance associated with the anthropogenic aerosol forcing. The ensemble empirical mode decomposition method is an example of a data-driven, non-parametric approach that can be used to directly provide an estimate of the forced response without the need for model data (Qian, 2016). Lehner et al. (2018b) have employed it directly on observations, together with dynamical adjustment, and initial condition and multi-model ensembles, designing a step-by-step attribution framework to tackle attribution of temperature and precipitation climate trends in the mid-to-high latitude regions.

An additional regional attribution technique is based on the similarity between observations and one or several simulations of a large ensemble. Huang et al. (submitted, b) used a perturbed physics ensemble to attribute the drying trend of the Indian monsoon over the latter half of the 20th century to decadal forcing from the PDV (see detailed case study in Section 10.6). The ensemble members predicted different trends in PDV behaviour across the 20th century and the negative precipitation trend was only replicated in those members with a strong negative-to-positive PDV transition across the 1970s, consistent with the observed PDV behaviour. In a similar manner, Cvijanovic et al. (2017) addressed the possible influence of Arctic sea-ice loss on the North Pacific pressure ridge and, consequently, on south-western United States precipitation. They used a coupled atmosphere-ocean mixed layer setup, rather than the fully coupled set up of Huang et al. (submitted, b). They sampled the uncertainties in selected sea-ice physics parameters (varying parameters within a realistic range) to achieve a "low Arctic sea-ice" state in their perturbed simulations. They then compared the latter with control simulations representative of sea-ice conditions at the end of the 20th century to assess changes purely due to sea-ice loss.

Finally, new methods aiming at removing underlying model biases before performing detection and attribution, for instance related to precipitation changes, are beginning to emerge based on image transformation techniques such as warping (Levy et al., 2014a). By correcting location and seasonal precipitation biases in CMIP5 models, Levy et al. (2014b) showed that the agreement between observed and fingerprint patterns can be improved, further enhancing the ability to attribute observed precipitation changes to external forcings. The improvement mainly relies on the assumption that precipitation changes are tied to the underlying climatology, which has been shown to be a reasonable assumption in regions of the world where an intensification of the hydrological cycle is expected (Held and Soden, 2006).

Finally, evidence that the models employed in regional-scale attribution are fit for purpose is essential in order to estimate the degree of confidence one can have in the attribution results (Section 10.3.3). For example, models need to be evaluated and assessed in their simulation of internal variability modes which are known through their teleconnections to be important drivers of regional climate change (Section 3.7).

Models are likely to have different performance in different regions and therefore their evaluation assessment in terms of key physical processes and mechanisms needs to be adapted to the regional climate change under consideration.

10.4.1.2 Regional climate change attribution examples

10.4.1.2.1 The Sahel and the West African monsoon drought and recovery

The West African monsoon (10°N–20°N, 10°W–20°E) from 1950 to the present has experienced some of the most severe multi-decadal rainfall variations in the world, including excessive rainfall in the 1950s–1960s, followed by two decades of deficient rainfall, leading to a large negative trend until the mid-to-late 1980s. In a study of rain gauge data over the Sahel (11°N–18°N; 20°W–10°E) since 1950, Panthou et al. (2018) also demonstrated trends towards longer dry spells and greater rainfall intensity or higher frequency of heavy rains. Some authors use the term Sahel interchangeably with the West African monsoon, although others consider the Sahel to cover the whole width of northern tropical Africa broadly within the 10–20°N band. Since the mid-1980s, there has been a partial recovery of annual rainfall amounts (Wang et al., submitted), more significant over the central rather than the western Sahel from August to October (Lebel and Ali, 2009; Sanogo et al., 2015; Maidment et al., 2015). The period since the mid-1980s is also characterized by fewer rainy days with a rise in extreme rainfall occurrence, suggesting an intensification of the hydrological cycle (Giannini et al., 2013; Panthou et al., 2014). This finding was supported by rainfall records from an observatory in Niger since 1990, in which annual maximum sub-hourly rainfall intensities are found to have increased by 2–6% per decade. Bichet and Diedhiou (2018b, 2018a) used CHIRPS merged satellite/gauge data to show a wetter western Sahel since 1981, but with shorter and more frequent dry spells, while over the Guinea Coast, they showed less frequent and more intense rainfall. These distinct changes in precipitation characteristics suggest a greater complexity than merely a modulation of mean rainfall over several decades.

In this example the drivers of the long-term drought in the West African monsoon region are assessed, spanning the decades from the 1950s up to the 1990s, in which annual rainfall fell between 20 and 30% (Hulme, 2001) (Figure 10.12a,b). The subsequent recovery of these rains is also explained (Figure 10.12a). The role of GHG and aerosol emissions as well as SST variability in different ocean basins on these changes in West African monsoon and Sahel precipitation are discussed. The interested reader is also referred to Section 8.3.2.4.

[START FIGURE 10.12 HERE]

Figure 10.12: Attribution of historic precipitation change in the West African monsoon and Sahel region during June to August: (a) Time series of GPCC version 2018 (Schneider et al., 2017) precipitation anomalies (mm day^{-1}, baseline 1955–1984) in the Sahel box (10°N–20°N, 20°W–40°E) indicated in panel (b) (same as Figure 10.11) with a five-year weighted mean applied (see Figure 10.11). The two periods used for difference diagnostics are shown in grey columns. (b) Precipitation change (mm day^{-1}) in GPCC data for the 1980–1990 minus the 1950–1960 periods. (c) Precipitation difference (mm day^{-1}) averaged over 1955–1984 and four ensemble members of HadGEM3 experiments between 1.5x and 0.2x historical aerosol emissions scaling factors after Shonk et al. (2019). (d) Precipitation anomaly time series (mm day^{-1}, baseline 1955–1984) over the Sahel in the CMIP6 multi-model database for 26 historical simulations with all forcings (in red), ten with greenhouse gas-only forcing (in light blue) and eight with aerosol-only forcing (in grey). (e) Precipitation change (% (29 years)$^{-1}$) for the (left) decline period (1955–1984) and (right) recovery period (1985–2014) for ensemble means and in 26 individual models of the CMIP6 historical experiment, ten with greenhouse gas-only forcing, eight with aerosol-only forcing, 34 CMIP5 models (in dark blue) and in individual members of the Database for Policy Decision Making for Future Climate Change Grand-Ensemble (d4PDF-GE) (Mizuta et al., 2017) (pink histogram) and the Max-Planck Institute Grand-Ensemble (MPI-GE) (Maher et al., 2019) (violet histogram). The two black crosses represent observational estimates from GPCC and the Climate Research Unit Time-Series (CRU TS) version 4.02 (Harris et al., 2014). Trends are estimated using ordinary least squares.

[END FIGURE 10.12 HERE]

For the attribution of the rainfall decline, the impact of the different ocean basin SSTs on the West African monsoon decline is assessed first. Nicholson (2013) reviewed competing mechanisms from equatorial Atlantic SSTs and interhemispheric SST gradients in regulating interannual and decadal variability of the Sahel. Rodríguez-Fonseca et al. (2015) reviewed evidence determining that on interannual time scales, the tropical ocean warming results in reduced Sahelian rainfall, while positive SST anomalies over the Mediterranean Sea tend to be associated with increased rainfall. Similarly, at decadal time scales, warming over the tropics leads to Sahel drought, whereas North Atlantic warming promotes increased rainfall. This suggests the general importance of meridional temperature gradients in supporting the West African monsoon.

Several papers have formalised the SST influence on the West African monsoon in the framework of the AMV. Martin et al. (2014), Martin and Thorncroft (2014), and Park et al. (2015b) suggested that changes in the SST gradient between the tropics and extratropical Atlantic increased the Northern Hemisphere differential warming and in turn drive Sahel rainfall. This suggested influence of AMV on the West African monsoon has been supported by results from CMIP5 decadal experiments (Gaetani and Mohino, 2013; Mohino et al., 2016; Sheen et al., 2017) showing that initialized decadal hindcasts outperform empirical predictions based on persistence (some skill is also attributed to a non-negligible contribution from external radiative forcing). The influence of PDV has also been studied but to a lesser extent. In a correlation/regression analysis of observations and CMIP5 models, Villamayor and Mohino (2015) suggested that the positive phase of the PDV has a negative impact on Sahel rainfall anomalies regardless of changes induced by anthropogenic forcing.

Other studies have highlighted the role of anthropogenic aerosol forcing rather than internal modes of climate variability alone. In terms of regional emissions, Dong et al. (2014) used HadGEM2-ES simulations to study the impacts of European and Asian anthropogenic sulphur dioxide on summer Sahel rainfall. European emissions led to an increase in shortwave scattering by increased sulphate burden, leading to a decrease in surface downward shortwave radiation and thus surface cooling over North Africa. This weakens the Saharan heat low and Sahel precipitation. The remote effects of Asian emissions led to a smaller change in sulphate burden over North Africa, but they induce adjustment of the Walker circulation, which again leads to a weakening of the monsoon circulation and a decrease in Sahel precipitation.

The effects of anthropogenic aerosol can also be considered at the hemispheric scale in an interaction with the effects of GHG, leading to a hemispheric asymmetry in temperature change that in turn shifts the inter-tropical convergence zone position. Based on a coupled atmosphere-slab ocean model and following Biasutti and Giannini (2006), Ackerley et al. (2011) showed that increases in GHG alone cause an increase in Northern Hemisphere precipitation, particularly in the Sahel, while increases in aerosol loading cause a reduction in Sahel rainfall. Ackerley et al. (2011) further supported their hypothesis by comparing very large perturbed physics ensembles of all-historical forcings and altered aerosols in a coupled GCM. They concluded that aerosol changes were the main driver of observed drying over 1950–1980. This is consistent with Polson et al. (2014) who used CMIP5 aerosol and GHG single-forcing experiments to show that aerosol emissions, which are larger and more widespread in the Northern Hemisphere, have led to declining rainfall across the Northern Hemisphere monsoons, including in West Africa. Likewise, Hwang et al. (2013) found the consistent timing of the southward shift of the inter-tropical convergence zone in CMIP3 and CMIP5 historical simulations to support the role of external forcing. Their atmospheric energetics approach attributed this to anthropogenic aerosol cooling of the Northern Hemisphere. By sampling the impact of uncertain aerosol radiative forcing across the CMIP5 archive and applying different aerosol scaling factors to a single-model study of the historical period, an impact on rainfall at the Gulf of Guinea coast was noted (Shonk et al., submitted), with differences of 0.5 mm day^{-1} between the strongest and weakest aerosol forcings. This is illustrated in Figure 10.12c, although the signal is shifted southwards with respect to the observations due to model bias.

The recovery in West African monsoon and Sahel rainfall since the late 1980s raises the question of whether similar mechanisms apply. Atmospheric internal variability possibly plays a role in the trend: a five member ensemble of AGCM simulations forced with observed SSTs predicted a Sahel rainfall recovery from the 1980s–2000s with a large spread, ranging from 6% to 21% (Roehrig et al., 2013). A detection study based on three reanalyses (Cook and Vizy, 2015) suggests that the recent recovery in Sahel rainfall is concomitant with the increase of Sahara surface temperature, which is 2–4 times greater than the tropical-mean; the amplified Saharan warming with maximum from July to October was confirmed by Vizy and Cook (2017) and subsequently in the review of Cook and Vizy (2019). The warmer Sahara drives a stronger thermal low and more intense West African monsoon flow with more moisture, enhancing convection over the central and eastern Sahel while it weakens over the western Sahel. The Saharan temperature increase over the last 30 years was forced by anomalous night time longwave heating of the surface by water vapour (Evan et al., 2015). Such a result is supported by the ensemble mean of 15 CMIP5 models (Lavaysse et al., 2016), although not all models are able to simulate a rainfall-heat low regression pattern as in observations. Sahel rainfall is also incorrectly located in preliminary CMIP6 models, relating to errors in the simulated tropospheric temperature gradient (Martin et al., 2017). Taylor et al. (2017) attributed the change to a different mechanism: the frequency of extreme Sahelian storms (mesoscale convective systems) which have tripled since 1982 in satellite observations. While this increase in storms was only weakly correlated to the recovery of Sahel rainfall, it was attributed to the increase in global land temperatures and the increased temperature gradient southward from the Sahara, increasing the wind shear.

Recent work also suggests the prominent influence of the Mediterranean Sea on the recovery of the West African monsoon and Sahel rains, such as Park et al. (2016) who analysed observational and multi-model datasets and conducted SST-sensitivity experiments with two AGCMs. Stronger evaporation and moist air advection from the Mediterranean southward into the Sahel give enhanced low-level moisture convergence and increased rainfall. However, the AGCM nature of the study could not (by design) identify whether the Mediterranean Sea SST warming is caused by external forcing or if internal factors have also contributed.

Advancing on this, Dong and Sutton (2015) used the HadGEM3-A AGCM to investigate the role of SST, GHG and aerosol in climate changes over 1964–2011. They suggested that the GHG direct radiative influence is the main cause of Sahel rainfall recovery, with an additional role for changes in anthropogenic aerosol. They also found that recent changes in SSTs, although substantial, did not seem to have a significant impact on the recovery, which is expected to be sustained or amplified in the near-term future. CMIP6 attribution analysis results for a limited range of historical simulations with all and single forcings are represented in Figure 10.12d.

Giannini and Kaplan (2018) determined that since the CMIP5 multi-model mean over the historical period largely follows observations of the decline and recovery in Sahel rainfall (defined by the authors as the full width of tropical northern Africa, 10°N–20°N, 20°W–40°E, as in Figure 10.12), then there must be an externally forced driver. Similarly, Knutson and Zeng (2018) were able to demonstrate a coherent Sahel drying signal in the CMIP5 multi-model mean over the extended 1901–2010 period, although the observed drying trend was of larger magnitude. However, Vellinga et al. (2016) caution that the full magnitude of decadal variability is not captured in most CMIP5 models, arguing that the models are not capable of reproducing heavy rainfall events associated with a teleconnection to the AMV and therefore internal variability still plays a role. Giannini and Kaplan (2019) attempted to unify the above driving mechanisms based on a singular value decomposition of observed and modelled SSTs, themselves forced by a combination of changing anthropogenic aerosol and GHG emissions. Using the resulting singular vectors as predictors in a bivariate regression of Sahel rainfall, they demonstrated the mapping of the GHG-forced SST pattern onto the combined sum of tropical and North Atlantic SSTs, while the anthropogenic aerosol pattern projected onto cooling in the North Atlantic. Thus, since the 1950s, tropical warming arising from GHG and North Atlantic cooling from aerosol led to regional stabilization, suppressing Sahel rainfall. The subsequent reduction in regional aerosol emissions led to warming in the North Atlantic, and a recovery in the Sahel. Such findings are continued into the near-term future, with Scannell et al. (2019) noting that scenarios featuring more aggressive reductions in aerosol emissions cause a northward shift of rainfall across the Sahel that exceed internal variability even 10 or 20 years after the change. The closer match between observed trends and the d4PDF large ensemble, in which SSTs are matched to observations, compared to the MPI-GE in which they are not, strongly suggests that the underlying ocean surface is essential in driving variability in both the decline and recovery period (Figure 10.12e).

On the basis of these elements, there is *very high confidence* (*robust evidence and high agreement*) that patterns of 20th century surface temperature variability have caused the Sahel drought and subsequent recovery, and that Saharan warming has contributed to this recovery. There is *medium confidence* (*robust evidence and medium agreement*) that patterns of SST variability are themselves driven by anthropogenic emissions: warming in the tropics and subsequently in the North Atlantic by GHG emissions; the cooling and subsequent warming of the North Atlantic by emissions of anthropogenic sulphate aerosols and their eventual removal.

10.4.1.2.2 The East Asia summer monsoon weakening and recovery

Since the late 1970s, the East Asian summer monsoon (EASM) has exhibited a considerable weakening trend, including the southward shift of the main rain belt, known as the southern flooding and northern drought (SFND) pattern (Figure 10.13a). Figure 10.13c shows that summer (June to August; JJA) precipitation differences from observations between two areas, 110°E–125°E, 35°N–45°N and 105°E–125°E, 20°N–35°N, in the region are smaller than -30 mm month^{-1} over the period 1961–2005. The major features of the weakened EASM are as follows: weakening of the southerly flow, a cooling trend of tropospheric temperature in East Asia, westward extension of the western North Pacific subtropical high, zonal expansion of the South Asia high, and a weakening of the land-sea thermal contrast across the East Asian continent and adjacent marginal seas (Hsu et al., 2014). Changes in the EASM have been significantly affected by a range of factors including land and oceanic thermal conditions (Zhou et al., 2009a; Zhang, 2015a), and the associated atmospheric teleconnections (Wang et al., 2017b). Recently a few studies have suggested a recovery in the strength of the EASM circulation since the 2000s (Kwon et al., 2007; Zhou et al., 2017b; Zhu et al., 2018).

[START FIGURE 10.13 HERE]

Figure 10.13:(a) Mean boreal summer (from June to August) precipitation spatial linear trend (mm month^{-1} (44 years)$^{-1}$) over the East Asia Summer Monsoon (EASM) region from 1961 to 2005. Trends are estimated using ordinary least squares. Top row: Observed trends from GPCC version 2018 (Schneider et al., 2017), CRU TS version 4.02 (Harris et al., 2014) and the Asian Precipitation-Highly Resolved Observational Data Integration Towards Evaluation of Water Resources (APHRODITE V1101) (Yatagai et al., 2012). Middle and bottom rows: Simulated trends corresponding to the East Asia-South (105°E–125°E, 20°N–35°N) wettest (left) and mean (middle) and East Asia-North (110°E–125°E, 35°N–45°N) wettest (right) over the EASM region using the 100 ensemble simulations of the MPI-GE (Maher et al., 2019) (middle row) and from the 100 members of the d4PDF-GE (Mizuta et al., 2017) (bottom row). (b) Precipitation difference (mm month^{-1}, baseline 1961–2005) between East Asia-North and East Asia-South for GPCC (grey bar charts). The lines show low-pass filtered time series of this difference for GPCC (in black) and for the East Asia-South wettest (in green) and East Asia-North wettest (in brown) MPI-GE members. The filter is the same as the one used in Figure 10.11. (c) Distribution of trends of the summer precipitation difference between the two regions in panel (b) for MPI-GE (violet histogram), d4PDF-GE (pink histogram), observations (back crosses), historical simulations from a set of 26 CMIP6 models (red circles) and ensemble mean trends.

[END FIGURE 10.13 HERE]

Among various contributing factors, inter-decadal changes of SSTs in different ocean basins play an important role in weakening tendency of the EASM since the late 1970s. Several studies have shown that the EASM weakening is accompanied by inter-decadal changes of Pacific SST that show warming in the tropical central and eastern Pacific but cooling in the central North Pacific, which is similar to the positive phase of the PDV (Ding et al., 2009; Li et al., 2010; Wu et al., 2016c; Zhou et al., 2017b). Li et al. (2010) showed that AGCMs forced with SSTs representing the positive phase of PDV can reasonably reproduce the observed EASM weakening. The proposed mechanisms are the reduced large-scale land-sea thermal contrast (Li et al., 2010) and the Pacific-Japan/East-Asian-Pacific-like atmospheric teleconnection pattern, which develops locally in response to the PDV-associated warm SST anomalies (Qian and Zhou, 2014). The impact of the PDV on the inter-decadal EASM changes is also noted by the recent recovery of EASM circulation in association with the phase transition of PDV from positive to negative (Zhou et al., 2017b). Zhu et al. (2011)

attributed decreased rainfall in southern China and increased rainfall in northern China during 2000–2008 in comparison to 1979–1999 to the shift of PDV to the negative phase based on AGCM experiments. Several studies have pointed out that the thermal forcing over the Tibetan Plateau during the preceding winter and spring associated with snow cover and sensible heating also plays a considerable role in regulating the EASM (Ding et al., 2009; Duan et al., 2013; Si and Ding, 2013) In addition to the PDV influence, the warming in the tropical Indian Ocean also has been found to be influential on the weakening of EASM (Yang and Lau, 2004; Ding et al., 2009). Zhou et al. (2009b) conducted the climate model experiment forced by Indian Ocean warming to show the westward extension of the western North Pacific subtropical high, which is responsible for SFND pattern. However, Fu and Li (2013) revealed that SSTs in the tropical Pacific Ocean exert a more significant influence on the EASM compared to those in the Indian Ocean. Several studies have also pointed out the influence of the AMV on the EASM through the circumglobal teleconnection pattern propagating from the North Atlantic through the westerly jet (Zuo et al., 2013; Wu et al., 2016a, 2016b). This North Atlantic influence has contributed to the strong summertime warming in Northeast Asia occurring in the mid-1990s (Monerie et al., 2018) and the increase of precipitation over the Huaihe-Huanghe valley since the late 1990s (Li et al., 2017c). Yang et al. (2017a) showed with idealised AGCM experiments that the PDV plays a dominant role in driving the SFND pattern whereas the AMV plays a secondary role enhancing the SFND pattern when PDV and AMV are in opposite phase.

Anthropogenic factors such as GHGs and aerosols may also have an influence on the EASM (Song et al., 2014; Zhou et al., 2017b; Tian et al., 2018). Wang et al. (2013) explained the effect of GHGs on the EASM via two pathways using a multi-model ensemble of GCM simulations. On one hand, GHGs induce notable Indian Ocean warming that causes a westward shift of the western North Pacific subtropical high and a southward displacement of the upper tropospheric East Asia westerly jet, leading to increased precipitation in the Yangtze River valley. On the other hand, the surface cooling effects of anthropogenic aerosols in eastern China and evaporative cooling from stronger convection in the Yangtze River valley, lead to a reduced land-sea thermal contrast, which results in weakening of the EASM circulation and hence a drier climate in northern China. Recent papers have argued that GHG and aerosol forcing have different contributions to different parts of the SFND pattern. Changes in GHGs lead to increasing precipitation over southern China, whilst changes in anthropogenic aerosols over East Asia are the dominant factors determining drought conditions over northern China (Song et al., 2014; Tian et al., 2018). The increase in anthropogenic aerosols may result in weakening of the EASM circulation (Jiang et al., 2013; Wang et al., 2015a, 2017d; Xie et al., 2016; Zhang and Li, 2016; Su et al., 2018; Liu et al., 2019). Song et al. (2014) revealed that aerosol forcing in CMIP5 simulations reasonably reproduce the observed weakening trend of low-level EASM circulation due to the surface cooling effect of aerosol reducing land-sea thermal contrast. Recent observational studies indicate that the summertime local-scale rainfall frequency experienced significant declining trend throughout the whole eastern China in recent decades, which is most likely due to the increases in the aerosol burden (Guo et al., 2017b). Although the anthropogenic forcing has led to an overall decrease in total monsoon rainfall, Burke and Stott (2017b) suggested using model simulations that the most extreme heavy rainfall events become shorter in duration and more intense. Zhao and Wu (2017) suggested land use and land cover change as another possible driver of EASM weakening, using an RCM simulation. The roughness changes associated with land use changes over China between the 1980s and 2010s led to a strengthening of the SFND pattern during the monsoon withdrawal. Jiang et al. (2017) also showed that the combined effect of aerosol and urbanization weakens the EASM. In their model experiment, the aerosol cooling effect was partially offset by the urban heating, however their combined effect on the circulation was dominated by the aerosol forcing, which further weakens the EASM circulation.

However, the magnitude of the EASM weakening under anthropogenic forcing alone (i.e., GHGs and aerosols) is much weaker than in the observations. Figure 10.13c has illustrated large differences in trend values between observations and ensembles. This discrepancy suggests that internal variability may play a major role in monsoon weakening with aerosol and GHG forcing playing a secondary role (Li et al., 2010; Zhou et al., 2017b). It should also be noted that the simulated changes in the EASM may largely depend on the sensitivity of the models to GHGs and aerosols and thus the role of anthropogenic factors on EASM change remains uncertain (Zhang, 2015b). Knutson and Zeng (2018) found little evidence for a large-scale anthropogenic weakening of the EASM based on the comparison of observed precipitation trends over 1901–2010. This further supports the notion that internal variability has dominated over anthropogenic influence in this region, as least in terms of trends over the past century.

There is *high confidence* (*robust evidence* and *medium agreement*) that the anthropogenic forcing has been influencing historical EASM changes, but there is *low confidence* (*medium evidence* and *low agreement*) in the magnitude of the anthropogenic influence on historical changes in the EASM. There is *high confidence* (*robust evidence* and *high agreement*) that the transition towards a positive PDV phase has been one of the main drivers of the EASM weakening since the 1970s.

10.4.1.2.3 The southern Australian rainfall decline

In this case study, the drivers of the precipitation trends across southern Australia in recent decades are assessed, extending the assessment done in the AR5 (Christensen et al., 2013). A recent review summarises much of the new research (Dey et al., 2019) that reveals nuances in the processes driving the observed changes. On average, southern Australian annual rainfall totals continue to trend downward, and temperatures are rising in agreement with many land regions worldwide.

Southern Australia has a moderate climate, generally cooler in the south and with average seasonal temperatures ranging up to 33°C in the north of the region in summer and 18°C in winter. Frost occurs in the cooler seasons and there is seasonal snow on the mountains. The westward facing regions of the mainland have a Mediterranean climate with wet winters and very dry summers. The annual average rainfall in the southwest exceeds 600 mm. Inland from this region, annual average rainfall drops to less than 200 mm, and this region of very low annual rainfall extends across the south. In the southeast, the annual average rainfall is also above 600 mm and has a reasonably even seasonal cycle, aside from the westward-facing regions that have higher rainfall totals in winter. There are mountainous regions in the southeast that generally receive more precipitation (including snow) than the surrounding plains (Pepler et al., 2017).

The southwest was known for its reliable rain, and rainfall is generally brought by fronts and cut-off lows (Pook et al., 2012; Hope et al., 2014). Large-scale climate drivers such as ENSO have some influence in the region, but these associations are strongly modulated by their dynamical links with the SAM (Lim and Hendon, 2015). Given southern Australia's latitudinal location on the equatorward edge of the mid-latitude storm track, the region can be very sensitive to shifts in the storm track.

In the southeast, rainfall is also associated with fronts and lows, including intense east coast lows, which can bring a great deal of rainfall (Pepler et al., 2014). Thunderstorm activity is also important for rainfall in the east of the region (Dowdy and Catto, 2017). ENSO and the Indian Ocean Dipole play an important role in driving interannual rainfall variability (Risbey et al., 2009), again modulated by interactions with SAM (Hendon et al., 2014b). Rainfall and temperature are intimately linked in these locations (e.g., Hope and Watterson (2018)). The Antarctic polar vortex has also been found to influence temperatures across southern Australia (Lim et al., 2018), and accounting for this component of the climate system has clarified the linkage between ENSO and SAM.

Maximum daily average temperatures have increased in both the cool (from May to October) and warm (from November to April) half-years by about 1.1°C from 1900 to 2018 in south-eastern Australia (south of 33°S, east of 135°E), and slightly more in south-western Australia (the land southwest of the line joining 30°S–115°E and 35°S–120°E), as measured by the Australian Climate Observations Reference Network-Surface Air Temperature (Trewin, 2013). Individual month-long heat events have also been attributed to increasing levels of atmospheric GHGs (Black et al., 2015; Hope et al., 2016).

Across southern Australia, there has been a downward trend in rainfall since widespread, reliable records began in 1900. In the southwest, this was seen as a downward shift in the late 1960s (Figure 10.14), with an absence of very wet winters, resulting in a decline in average annual rainfall of 11% (from 1970 to 2018 compared to 1900 to 1969) (Hope et al., 2006, 2015). In the southeast, there have been significant drought periods (Gergis et al., 2012; Freund et al., 2017), but there has also been a consistent downward trend in rainfall. Rainfall has been generally low since the start of the Millennium drought in 1997, interspersed with two wet spring/summer periods (2010–2011 and 2016–2017) associated with strong La Niña events. The influence of anthropogenic forcing on the rainfall changes in the southeast is complex because of the varying influences on the relevant large-scale drivers, and climate models can give mixed results (Chiew et al., 2011; Cai et al., 2014). The trends in different seasons provide insight into the drivers, as influences from the higher latitudes are important in winter while tropical drivers and their interactions are more important in the warm season. For instance, the rainfall response to the positive phase of SAM varies strongly by season in this region (Hendon et al., 2007; Hope et al., 2017). The difference in response between the warm and cool seasons is amplified in trends in the mountainous regions of the southeast. Grose et al. (2019) found a seasonally enhanced rainfall decrease on the windward slopes in the cool season and a rainfall increase over peaks in summer due to an increase in convective rainfall (also found by Giorgi et al. (2016) in the European Alps). The rainfall changes in the southeast align with those in the southwest on a range of timescales (Hope et al., 2009), suggesting the shifts to a more positive SAM are also important for rainfall trends in the southeast. Since 1970, the downward trend in autumn and winter rainfall has continued in both the southwest and southeast (Figure 10.14).

[START FIGURE 10.14 HERE]

Figure 10.14: (a) Mean austral autumn and winter (March to August) precipitation spatial linear trend (% (55 year)$^{-1}$) over Australia from 1960 to 2014. Trends are estimated using ordinary least squares. Top row: Observed trends from the GPCC version 2018 (Schneider et al., 2017) and CRU TS version 4.00 (Harris et al., 2014). Middle row: Driest, mean and wettest trends (relative to the region enclosed in the black quadrilateral, left panel of bottom row) from the 100 members of the MPI-GE (Maher et al., 2019). Bottom row: Driest, mean and wettest trends (relative to the above region from the 40 members of the National Center for Atmospheric Research grand ensemble (NCAR-GE) (Kay et al., 2015). (b) Time series of austral autumn and winter precipitation anomalies (%, baseline 1971–2000) over the south-western Australia region delimited by the black quadrilateral for GPCC (grey bar charts). Black, brown and green lines show low-pass filtered time series for GPCC, driest and wettest members of NCAR-GE, respectively. The filter is the same as the one used in Figure 10.11. (c) Distribution of south-western Australia region-averaged austral autumn and winter precipitation 1960–2014 trends (% (55 year)$^{-1}$) for MPI-GE (violet histogram), NCAR-GE (pink histogram), observations (GPCC and CRUTS, dark grey open-filled circles) and historical simulations from a set of 22 CMIP6 models (yellow open-filled circles). Coloured triangles refer to ensemble mean trends of their respective ensemble. Brown and green open-filled circles refer to the driest and wettest NCAR-GE ensemble members.

[END FIGURE 10.14 HERE]

GCM simulations and projections agree that the anthropogenic forcing will drive the region to drier conditions during the cool season (Christensen et al., 2013), generally believed to be associated with a contraction of the storm track around Antarctica and the SAM shifting to a more positive phase (Cai et al., 2014). Related to the rainfall decline, and supporting the hypothesis of a shift to positive SAM, there has been a significant increase in pressure across southern Australia (Hope et al., 2015), with reduced baroclinicity (Frederiksen et al., 2017) and an increase in the number of high pressure systems (Pepler et al., 2019). These factors combine to suggest that the rainfall decline is, at least partially, an anthropogenically-forced response. Based on all and single-forcing simulation ensembles with a high-resolution model, (Delworth and Zeng, 2014) found that the observed long-term regional austral autumn and winter rainfall decline over southern and particularly southwest Australia is partially reproduced in response to anthropogenic changes in levels of GHGs and ozone in the atmosphere, whereas anthropogenic aerosols do not contribute to the simulated precipitation decline. However, the numbers of ensemble members for the all and single forcing simulations are only five and three, respectively, making a robust and quantitative attribution to specific drivers difficult (not to mention the additivity issue, Section 10.3.2.3). The precipitation pattern seen in the model simulated changes for the 1981–2012 period amplifies and expands in the future projections under the RCP8.5 GHG scenario to reach a 40% decline, which strengthens the conclusion that anthropogenic forcing has contributed to the recent precipitation decline in southwest Australia. Based on an atmospheric circulation storyline approach applied to CMIP5 models, Mindlin et al. (submitted) have suggested that tropical upper tropospheric warming is the main driver of southern Australia future drying. Application of the univariate detection method based on CMIP5 models confirms attributable anthropogenic drying in the far southwest Australia over the 1901–2010 and 1951–2010 periods (Knutson and Zeng, 2018). It also suggests detectable wetting annual mean trends in northern Australia over the 1951–2010 period. A robust estimation of the externally-forced contribution to the southwest Australia precipitation decline remains difficult due to observational and model uncertainty. Based on a single model, Delworth and Zeng (2014) estimate that at least 50% of the recent precipitation decline is externally forced while two recent large ensembles suggest a smaller contribution (Figure 10.14).

It is noteworthy that extreme precipitation climate events can occur along with a long-term drying trend. In 2016, two climate event attribution studies found minimal influence from anthropogenic forcing to the record high spring rainfall in the southeast (Hope et al., 2018). However, it was also found that the interaction between La Niña and a high-magnitude SAM was amplified by the global observed SST trends (Lim et al., 2016a) that probably have a component of anthropogenic climate change in them. It is also entirely plausible that a seasonal rainfall extreme event might be influenced by anthropogenic forcing (Guerreiro et al., 2018), even in the presence of a background trend towards less mean rainfall.

There is *high confidence* (*medium agreement* and *robust evidence*) that anthropogenic forcing has contributed to southwest Australia autumn and winter rainfall decline since the early 1970s. There is *low confidence* (*low agreement and medium evidence*) in the magnitude of the human influence and role of specific anthropogenic drivers on the autumn and winter precipitation decline.

10.4.1.2.4 The south-eastern South America summer wetting

One of the few regions where a robust positive trend in precipitation has been detected since the beginning of the 20th century is south-eastern South America (Gonzalez et al., 2013; Vera and Díaz, 2015). This region is the most densely populated and agriculturally productive area of South America and has several large cities. The positive rainfall trend has, together with socio-economic and technological changes, enabled expansion of agriculture into semi-arid areas and has resulted in deforestation and increased crop yields in Argentina (Zak et al., 2008; Barros et al., 2015). On the other hand, large parts of the agricultural regions in the Argentinean Pampas are naturally flood-prone due to the flat topography and poor drainage (Kuppel et al., 2015), which has possibly been aggravated by agricultural expansion leading to decreased transpiration and rising water tables (Nosetto et al., 2015; García et al., 2018). The main rivers of the la Plata Basin in central-northern south-eastern South America have increased their mean flows and extreme discharges since the 1970s (Barros et al., 2004, 2015). While in the upper basin this is mainly due to heavy deforestation, in the southern basin it is mainly due to the increase of precipitation (Saurral et al., 2008; Barros et al., 2015). Urban and agricultural expansion together with increased extreme precipitation has led to higher risks for human systems and ecosystems associated with floods from the early 1980s (Barros et al., 2015).

[START FIGURE 10.15 HERE]

Figure 10.15:(a) Mechanisms that have been suggested to contribute to south-eastern South America summer wetting since the beginning of the 20th century. (b) Mean austral summer (December to February) precipitation spatial linear 1951–2014 trends (mm per season and decade) from GPCC version 2018 (Schneider et al., 2017) and CRU TS version 4.02 (Harris et al., 2014). Trends are estimated using ordinary least squares. (c) Time series of austral summer precipitation anomalies (%, baseline 1995–2014) over the south-eastern South American region (black in (b))for GPCC (bar charts). Black, brown and green lines show low-pass filtered time series for GPCC, driest and wettest members of GFDL-CM3, respectively. The filter is the same as the one used in Figure 10.11. (d) Distribution of precipitation 1951–2014 trends over south-eastern South America from 12 grand ensembles (adapted from Díaz et al. (submitted)). The six grand ensembles to the left reproduce reasonably well the observed spatial patterns of mean precipitation and interannual variability (better performing), while the six grand ensembles to the right have a considerably worse performance (poor performing) (Díaz et al., submitted). The grey horizontal lines show the mean trend of each of these two subsets of grand ensembles. Dashed grey lines show GPCC and CRU TS trends and the red circles to the right show trends of 26 individual CMIP6 models.

[END FIGURE 10.15 HERE]

The dominant contribution to the positive annual mean precipitation trend is an increase in summer (December to February; DJF) precipitation (Rusticucci and Penalba, 2000; Gonzalez et al., 2013, 2014; Vera and Díaz, 2015; de Barros Soares et al., 2017; Díaz and Vera, 2017; Saurral et al., 2017). The trend for the period 1951–2014 using GPCC and CRUTS is illustrated in the maps of Figure 10.15b, and for the black rectangle it amounts to 7.3–8.5 mm per season and decade (see grey dashed horizontal lines in Figure 10.15d) while the mean seasonal precipitation for the same period is 312 (CRUTS) –320 (GPCC) mm. The trend is also detectable in daily and monthly extremes (Re and Barros, 2009; Marengo et al., 2010; Penalba and Robledo, 2010; Doyle et al., 2012; Donat et al., 2013; Lorenz et al., 2016).

The influence of SST anomalies on south-eastern South America precipitation have been studied extensively on interannual to multi-decadal time scales (Paegle and Mo, 2002). The positive phase of ENSO is related to stronger mean and extreme rainfall over south-eastern South America (Ropelewski and Halpert, 1987; Grimm and Tedeschi, 2009; Robledo et al., 2016). For multi-decadal variability, of interest for long term trends, it has been suggested that the ENSO influence is affected by the PDV (Kayano and Andreoli, 2007; Fernandes and Rodrigues, 2018) and the AMV (Kayano and Capistrano, 2014). PDV and AMV also influence the south-eastern South American climate independently of ENSO (Barreiro et al., 2014; Grimm and Saboia, 2015; Robledo et al., 2019). While Pacific SSTs dominate the total influence of oceanic variability in the region, the Atlantic variability seems to dominate on multi-decadal time scales and has been proposed as a driver for the long term positive trend (Seager et al., 2010; Barreiro et al., 2014). Based on an ensemble of season-length model experiments designed to test how south-eastern South America precipitation is modulated by tropical Atlantic SSTs, Seager et al. (2010) showed that cold anomalies in the tropical Atlantic favoured wetter conditions by inducing an upper-tropospheric flow towards the equator, which, via advection of vorticity, led to ascending motion over south-eastern South America (Figure 10.15a). They concluded that a large part of the wetting trend from the mid-20th century was forced by cooling of the tropical Atlantic resulting from the AMV cold phase (Seager et al., 2010). Monerie et al. (2019) supported this argument showing the negative relationship between south-eastern South America precipitation and the AMV index (Huang et al., 2015) in an AGCM coupled to an ocean mixed layer model with nudged SSTs. The idealized AMV warming experiments in Monerie et al. (2019) also supported the results by Seager et al. (2010) in that the mechanism for AMV control on precipitation is associated with the tropical Atlantic part of the AMV pattern.

However, in contrast to these findings, other studies have attributed the positive precipitation trend to anthropogenic GHG emissions. Junquas et al. (2013) attributed the rainfall increase in the region to a non-zonally uniform pattern of SST warming induced by anthropogenic GHG emissions using a stretched-grid AGCM. This warming pattern includes a warming pattern over the Indian and Pacific Oceans that excites wave responses over South America (Figure 10.15a). In fact, zonally uniform SST patterns of warming alone would lead to opposite rainfall signals to those observed. This suggests that the cause of the increased precipitation trend is anthropogenic in origin, with the mechanism mediated by uneven warming patterns in the tropical oceans. Using an ensemble of 59 CMIP5 historical simulations from 14 models, Vera and Díaz (2015) concluded that only the simulations including anthropogenic forcing showed a positive precipitation trend, although weaker than the observed one. The main features of the present summer mean rainfall and variability of South America are still not well represented in all CMIP5 and CMIP6 models (Gulizia and Camilloni, 2015; Díaz and Vera, 2017; Díaz et al., submitted), motivating the construction of ensembles that exclude the worst performing models (Knutti et al., 2010; Section 10.3.4.4). Díaz and Vera (2017) used a ensemble based on 33 CMIP5 models, each one contributing to the ensemble with 1-20 simulations. Sub-ensembles of historical simulations with realistic representation of the rainfall dipole with anomalies of opposite sign over south-eastern South America and eastern Brazil were selected. In these simulations, the trend since the 1950s could be related to changes in rainfall characteristics, favouring the wet dipole phase over south-eastern South America, only when simulations included anthropogenic drivers. Zhang et al. (2016) attributed the wetting to anthropogenic GHG emissions by conducting a suite of experiments with two high-resolution GCMs. The authors explain the attribution with a mechanism in which the radiative forcing drives an expansion of the Hadley cell, so that its descending branch moves poleward from the region, generating anomalous ascending motion and precipitation (Figure 10.15a). A similar result was obtained by Saurral et al. (2019) using a GCM of medium complexity to examine the sensitivity to GHG and ozone concentrations. They found that increased GHG increased precipitation in the region through an intensification of the ascending branch of the Hadley cell (Figure 10.15a).

Mindlin et al. (submitted) developed future atmospheric circulation storylines for Southern Hemisphere mid-latitudes with the CMIP5 models and related these to changes in precipitation. For south-eastern South America summer precipitation increases are related to the storyline based on a late springtime breakdown of the stratospheric polar vortex. The connecting mechanism between the late breakdown of the polar vortex and the increased summer rainfall over the region is a lagged southward shift of the jet stream (Saggioro and Shepherd, 2019) which enhances cyclonic activity over the region (Wu and Polvani, 2017). As depicted in Figure 10.15a, both stratospheric ozone depletion and increased GHG have contributed to the later breakdown of the polar vortex in recent decades (Ceppi and Shepherd, 2019; McLandress et al., 2010; Wu and Polvani, 2017).

A common feature among the above discussed studies is that even if GCMs simulate positive trends, these are in general much smaller in magnitude than the observed trend (see also CMIP6 trends in red open circles in Figure 10.15d). Díaz et al. (submitted) showed that to capture the correct magnitude of the trend it is necessary to use a multi-model ensemble of large initial condition ensembles. Out of the 12 large ensembles that they examined (16–100 members), only 7 simulated the observed trend within their range. This could partly be explained by the model biases of mean precipitation and its interannual variability. In the sub-ensemble of six models that reproduce reasonably well the observed spatial patterns of mean precipitation and interannual variability, the model uncertainty is lower, the trend is closer to observations but the dispersion due to internal variability is higher than for the 6 models with very poor performance.

There is *high confidence* that south-eastern South America summer precipitation has increased during the 20th century and the beginning of the 21st century. This is based on both in situ and gridded observations and is also supported by an understanding of the mechanisms associated with the influence of SST variability and by modelling studies driven by observed concentrations of GHG and ozone. Since AR5, science has advanced in the identification of the drivers of the precipitation increase in south-eastern South America, including GHG, ozone depletion, Pacific and Atlantic variability, but there is still not a consensus on how much each driver has contributed to the wetting. There is *medium confidence* (*medium evidence and medium agreement*) in the possible drivers of south-eastern South America summer precipitation increase during the 20th century, but *low confidence* (*limited evidence and low agreement*) on the relative contribution of each driver to the wetting.

10.4.1.2.5 The central and eastern Eurasian winter cooling

A key example of mid-latitude regional climate change across the historical period is the winter central and eastern Eurasia land cooling of the late-20th century until around 2014. This recent cooling episode disrupted the warming trend that started in the early 1970s (Figure 10.16) and is in striking contrast to the concurrent Arctic amplification (the propensity for greater surface warming in the Arctic region than at other latitudes) and sea-ice decline. The occurrence of this dipolar near-surface air temperature (temperature thereafter) anomalous pattern has been termed the warm Arctic cold Eurasia (or Siberia) pattern (Inoue et al. 2012; Mori et al. 2014) and is the second empirical orthogonal function mode of mid-to-high latitude Eurasian winter temperature variability (Sorokina et al., 2016).

[START FIGURE 10.16 HERE]

Figure 10.16: (a) Winter (January to March) near-surface air temperature spatial linear trend (in °C (12 year)$^{-1}$) over Eurasia from 2001 to 2012. Trends are estimated using ordinary least squares. Top row: Observed trends from the BEST dataset (Rohde et al., 2013), the Cowtan and Way dataset (Cowtan and Way, 2014) and the Global Historical Climatology Network version 2 and the Climate Anomaly Monitoring System (GHCN-CAMS) dataset (Fan and van den Dool, 2008). Middle row: Coldest, mean and warmest trends (relative to the region enclosed in the black quadrilateral, left panel of middle row) from the 100 members of the MPI-GE (Maher et al., 2019). Bottom row: coldest, mean and warmest trends relative to the above region from the 100 members of the d4PDF-GE (Mizuta et al., 2017). (b) Time series of BEST winter temperature anomalies (%, baseline 1971–2000) over the Eurasian region delimited by the black

quadrilateral in (a) (grey bar charts). Black, brown and green lines show low-pass filtered time series for BEST, coldest and warmest members of d4PDF-GE, respectively. The filter is the same as the one used in Figure 10.11. (c) Distribution of Eurasia region-averaged winter temperature 2001-2012 trends (in °C (12 year)$^{-1}$) for MPI-GE (violet histogram), d4PDF (pink histogram), four observational datasets (BEST, GHCN-CAMS, Cowtan and Way and National Oceanic and Atmospheric Administration Merged land ocean global surface temperature analysis version 5 (Vose et al., 2012; Huang et al., 2015; Menne et al., 2018), dark grey open-filled circles) and historical simulations from a set of 22 CMIP6 models (yellow open-filled circles). Coloured triangles refer to ensemble mean trends of their respective ensemble. Blue and dark-red open-filled circles refer to the coldest and warmest d4PDF-GE ensemble members.

[END FIGURE 10.16 HERE]

The Eurasian winter cooling has made an important contribution to the 1998–2012 hiatus in global mean surface temperature (Cohen et al., 2012b; Li et al., 2015; Deser et al., 2017a). Li et al. (2015) used five observational datasets to show that the Eurasian winter cooling trend from 1998 to 2012 dominated the global warming hiatus in terms of a latitudinal contribution. Deser et al. (2017a) showed that Eurasian cooling represented about 70% of the winter temperature hiatus in both observations and a close model analogue drawn from eastern Pacific SST partial coupling experiments (Section 10.3.2.4). The recent Eurasian winter cooling is also related to the re-amplification of the East Asian winter monsoon in the mid-2000s (Wang and Chen, 2014).

Eurasian cold temperature anomalies are tightly coupled to recurrent and/or persistent anticyclonic sea level pressure anomalies corresponding to the intensification of the surface Siberian High (Luo et al., 2017; Gong et al., 2018). Attribution of the Eurasian cooling is then closely related to attribution of the recent increase in Eurasian blocking (Wang and Chen, 2014) and recovery of the Siberian High (Jeong et al., 2011). In turn, as strong western Siberian sea level pressure events are precursors of weak polar vortex states, the recovery of the Siberian High is possibly associated with the recent trend of the polar vortex towards a weaker state (Kretschmer et al., 2018). Based on a simple linear regression model, Kretschmer et al. (2018) suggest that the shift in mid-winter polar vortex states can account for 60% of the recent (1990–2015) mid-winter cooling trends over Eurasian mid-latitudes.

Based on observed correlation/regression analysis and modelling sensitivity experiments, a number of studies since the AR5 have suggested that this anomalous circulation pattern is due to a remote influence of Arctic sea-ice loss, in particular, in the Barents-Kara Seas (Chen et al. 2016; Inoue et al. 2012; Kug et al. 2015; Mori et al. 2014, 2019; Tang et al. 2013). A first category of proposed mechanisms invokes a weaker meridional temperature gradient leading to weakened zonal winds and reduced Atlantic heat transport, altered cyclone pathways and a wavier atmospheric flow (Francis and Vavrus, 2015). An alternative mechanism suggests an amplification of the Siberian High by a stationary Rossby wave train triggered by anomalous heat fluxes (enhanced ocean heat loss) due to sea-ice retreat. Based on simulations targeting the response to future sea-ice loss with a single AGCM with a well resolved stratosphere, Zhang et al. (2018) suggested that the stratospheric response to future sea ice loss is crucial in the development of cold conditions over Siberia, indicating the dominant role of the stratospheric pathway. In particular, the downward influence of the stratospheric circulation anomaly significantly intensifies the ridge near the Ural Mountains and the trough over East Asia. The persistently intensified ridge and trough favour more frequent cold air outbreaks and colder winters over Siberia.

Mori et al. (2014) studied the repeating severe winters of mid-latitude Eurasia that have occurred despite ongoing anthropogenic warming. In a model assessment, they found no robust atmospheric response (by looking at the Arctic Oscillation) to declining sea ice. Instead, they used a 100-member ensemble of atmospheric simulations to demonstrate a doubled likelihood of extreme winters in central Eurasia given the loss of ice and due to more frequent Eurasian blocking episodes. Likewise, Kug et al. (2015) used single-model GCM simulations with SST-restoring at northern latitudes to constrain sea-ice loss over the Arctic during the 1980–2013 period. They found that the model response reproduced the observed regression pattern between a Barents-Kara Seas sea-ice concentration index, as well as temperature and sea level pressure over East Eurasia. Mori et al. (2019) applied maximum covariance analysis to detrended winter temperature from observations combined with a multi-model ensemble of atmospheric simulations in order to extract the forced response due to observed SST and sea-ice concentration changes. They then used single-model sensitivity experiments to assess the relative roles of SST and sea-ice. Their results suggested that Barents-Kara Seas ice loss can explain a substantial fraction (44%) of the 1995–2014 central Eurasia cooling and that atmospheric models systematically underestimate sea-ice forced atmospheric variability. These results might be affected by the fact that the ocean and sea-ice conditions cannot respond to the sea-ice induced atmospheric changes in AGCM experiments (Mori et al., 2019b; Screen and Blackport, 2019). In an alternative explanation, a series of observational and modelling studies have questioned whether there is adequate evidence that Arctic sea-ice loss can significantly influence atmospheric circulation, blocking, and Eurasian winter temperatures. Woollings et al. (2014) found no agreement among a set of 12 CMIP5 models on a significant link at interannual time scales between Eurasian blocking and Barents-Kara Seas temperature during both historical and future periods. Based on their set of AGCM experiments, Li et al. (2015) showed that Arctic sea-ice loss did not drive the associated regional circulation changes, which can instead be related to internal atmospheric variability. Similarly, both Peings and Magnusdottir (2014) and Screen et al. (2014) failed to detect a significant winter atmospheric circulation response over Eurasia to recent sea-ice loss based on large ensembles of sea-ice forced atmospheric simulations with three different AGCMs. Sun et al. (2016a) employed multi-model ensembles of AGCM and coupled GCM simulations to show that the observed Eurasian cooling was the consequence of an extreme event of internal atmospheric decadal variability. This is also suggested by the absence of any significant forced response simulated by two initial-condition large ensembles and the rank of the observed trends among the two model distributions (Figure 10.16). McCusker et al. (2016) also considered the decreasing temperature over central Eurasia since around 1990 in the face of increased anthropogenic forcing and Arctic amplification. Their 600 years of AGCM simulations forced by different sea-ice loss patterns showed no evidence that Arctic sea-ice loss has led to the central Eurasian cooling. They also used a large ensemble of coupled historical simulations in which Eurasian cooling of the same magnitude as the observed one was found only in a single ensemble member. However, it was shown to be unrelated to Barents-Kara Seas sea-ice loss. Hence, they concluded that internal atmospheric variability is the cause of the Eurasian temperature decline, a view shared by Sorokina et al. (2016). The latter study investigated causality by looking at lead-lag relationships between detrended Barents-Kara Seas sea-ice and heat fluxes, and the warm Arctic cold Eurasia pattern on daily, monthly and seasonal time scales in the ERA-Interim reanalysis. The findings showed that the warm Arctic cold Eurasia pattern was associated with a weak reduction in Barents-Kara Seas ice and reduced Barents-Kara Seas heat flux, suggesting that the warm Arctic cold Eurasia pattern might primarily be an expression of internal atmospheric variability that could largely determine the Barents-Kara Seas ice distribution. These findings are confirmed by Blackport et al. (2019) who show, based on two independent and complementary methods of inferring causality from interannual variability in both observations and climate models, that anomalous atmospheric circulation simultaneously drive cold mid-latitude winters and Arctic sea-ice loss. Finally, based on large initial-condition historical and pacemaker ensembles, Deser et al. (2017a) showed that internal variability driven by tropical Pacific SSTs and intrinsic atmospheric dynamics contributed almost equally to the dynamically-induced Eurasian cooling, largely offsetting the radiatively induced warming trend.

In an explanation focusing on the role of the tropics, Trenberth et al. (2014) have suggested that many of the regional circulation patterns associated with the 1999–2012 climate hiatus can be blamed on long-term forcing from central and east Pacific SSTs. They used an AGCM forced with the negative PDV-like SST forcing similar to that observed over the same period and demonstrated the excitation of teleconnections to the Atlantic and Northern Hemisphere high latitudes.

Another hypothesis suggested that Barents-Kara Seas ice reduction may also be related to a larger teleconnection pattern associated with the position of the Gulf Stream in the northwest Atlantic (Sato et al., 2014). Northward shifts in the SST front associated with the Gulf Stream would generate a remote planetary wave response that could favour enhanced advection of warm air and wave energy into the Barents-Kara Seas region (Liu et al., 2014a). The induced warming and sea-ice melting would then amplify the wave train, promoting the warm Arctic cold Eurasia pattern (Sato et al., 2014; Simmonds and Govekar, 2014).

Studies based on observations and reanalysis do find significant linear correlations between Barents-Kara

Seas ice and mid-to-high latitude atmospheric circulation variability including Eurasian blocking, although they do not necessarily agree on the causality direction (Kretschmer et al., 2016; McGraw and Barnes, 2020). Furthermore, even with the use of causal effect networks, causality is challenging to prove because of the complexity of the possibly nonlinear mechanisms involved, non-stationarity and basic state dependence, as well as the relatively few degrees of freedom given the shortness of the observed record (Overland, 2016; Overland et al., 2015; Walsh, 2014). For instance, blocking over Eurasia might lead to warm southerly winds and moisture intrusions over the Barents-Kara Seas region, which have been shown to play a major role in recent Barents-Kara Seas temperature and ice concentration changes due to the associated increase in downwelling longwave radiation (Woods et al., 2013; Park et al., 2015a; Woods and Caballero, 2016). Furthermore, statistical robustness of lead-lag correlation analysis based on high-frequency data is difficult to achieve due to the large persistence of Barents-Kara Seas sea-ice anomalies and, in addition, results can be sensitive to the detrending methodology (Chen et al., 2016b).

Studies based on modelling experiments forced by SST and/or sea-ice concentration boundary conditions do find an atmospheric response by design when using sufficient ensemble size and/or perturbation amplitude. The differing results and the lack of agreement among all model studies based on uncoupled simulations may be due to multiple reasons in addition to model structural differences: opposing influence of regional patterns of sea-ice and SST forcing (Chen et al., 2016b) and non-additivity of the response (Sun et al., 2015), influence of season definition, non-linearity of the atmospheric response (Chen et al., 2016c), different and/or limited ensemble sizes (Screen et al., 2014). Further complicating the regional-scale attribution is the presence of tremendous internal variability in large-scale atmospheric circulation and complex three-way ocean-ice-atmosphere interactions in the Earth climate system (Cohen et al., 2020). This may lead to conditional dependence of the Barents-Kara Seas warm Arctic cold Eurasia pattern linkages on the large-scale circulation regime, in addition to other remote tropical and mid-latitude influence (Overland, 2016; Wang et al., 2019). Further discussion of Arctic-mid-latitude linkages can be found in the Cross-Chapter Box 10.1.

An emerging picture for the Arctic influence on the Eurasian cooling is that of an episodic and regional influence that could conditionally amplify the temperature changes due to internal modes of atmospheric circulation. While there is *high confidence* (*robust evidence* and *medium agreement*) that a significant (at least 50%) fraction of the recent Eurasian cooling has been caused by internal atmospheric variability associated with a weakening of the polar vortex, the persistent diversity of results and disagreement among them result in *low confidence* (*robust evidence* and *low agreement*) in the exact role and quantitative impact of Arctic warming and sea-ice loss on the recent Eurasian cooling.

10.4.1.2.6 Western Europe summer warming

Rapid European summer warming has occurred since around 1990 (Figure 10.17d) (Ruckstuhl et al., 2008; Philipona et al., 2009; van Oldenborgh et al., 2009; van der Schrier et al., 2013; Bador et al., 2016) at a rate of around 2.5 times the global mean temperature increase (van Oldenborgh et al., 2009). This warming was largest in western and central Europe and in the Mediterranean. In the last two millennia of reconstructed observed temperature records for Europe, there has not been any 30-year period with summer temperatures exceeding those of the last three decades (Luterbacher et al., 2016), where record-breaking heat waves and extreme temperatures also occurred (Russo et al., 2015; Lehner et al., 2018a).

[START FIGURE 10.17 HERE]

Figure 10.17: (a) European historical summer (June to August) near-surface air temperature spatial linear trend (in °C (64 years)$^{-1}$) from 1950 to 2014. Trends are estimated using ordinary least squares. Observed trends from E-OBS v19.0e (Cornes et al., 2018) (left) and the coldest (middle) and warmest (right) trends from the 100 members of the MPI-GE (Maher et al., 2019). Trends are estimated using ordinary least-squares. (b) Time series of European area mean (15ºW–20ºE, 35ºN–70ºN) summer temperature anomalies (in °C, baseline 1995–2014) applying the same filter used in Figure 10.11 for different observational datasets: E-OBS, BEST (Rohde et al., 2013), CRU TS v4.02 (Harris et al., 2014) and HadCRUT4 (Morice et al., 2012) (black, dark blue, turquois and brown line, respectively) and model ensemble means of CMIP6, HighResMIP and the MPI-GE (red, light blue and violet line, respectively). (c) European area mean

summer 1950–2014 warming trends (in °C (64 years)$^{-1}$) for ensemble means and individual members of CMIP6 (28 members, red circles), HighResMIP (7 members, blue circles) and MPI-GE (violet histogram). The observational data sets are indicated by black crosses.

[END FIGURE 10.17 HERE]

Several mechanisms have been proposed for this warming, but their relative importance and possible interplays are not yet fully understood. Enhanced warming over land compared to the sea is expected due to the lapse-rate feedback associated with tropospheric moisture contrasts (Kröner et al., 2017; Brogli et al., 2019a), and the globally enhanced land-sea contrast in near surface temperature is a robust result in CMIP5 and CMIP6 models. In addition, the decrease of anthropogenic aerosols over Europe resulting from air pollution policies (Turnock et al., 2016) has been pointed out as an important contributor to the enhanced western European summer warming (Ruckstuhl et al., 2008; Philipona et al., 2009; De Laat and Crok, 2013; Nabat et al., 2014; Besselaar et al., 2015; Dong et al., 2017). Also, Turnock et al. (2015) and Zubler et al. (2011) found a brightening and increase of solar radiation over Europe. Pfeifroth et al. (2018) argues that this brightening is mainly due to cloud changes caused by the indirect aerosol effect with a minor role for the direct aerosol effect, in contrast to Nabat et al. (2014) and Boers et al. (2017) who attribute it to the direct aerosol effect.

Also, circulation changes might have contributed to the enhanced warming. Sutton and Dong (2012) argued that AMV induced a shift around the 1990s towards warmer southern European (and wetter northern European) summers. Ghosh et al. (2017) linked the central and Eastern Europe warming to the AMV that showed a shift from its negative to its positive phase coinciding with the European warming trend. This mechanism is associated with a linear baroclinic atmospheric response to the AMV-related surface heat flux. Also O'Reilly et al. (2017) related warm European summer decades to the AMV, but the connection was shown to be mainly thermodynamic, whereas Peña-Ortiz et al. (2015) found a link between the length of European summers and AMV multi-decadal variability.

Soil moisture feedback has amplified the increase in summer temperatures in particular during drought spells (Seneviratne et al., 2010; Jaeger and Seneviratne, 2011; Miralles et al., 2014; Brulebois et al., 2015; Whan et al., 2015), which are related to unusual circulation regimes, in particular blocking patterns (Pfahl and Wernli, 2012; Pfahl, 2014; Horton et al., 2015; Brunner et al., 2017). However, according to Barnes et al. (2014), there is no robust evidence that the occurrence of blocking has changed during recent decades. Cahynová and Huth (2014) and Vautard and Yiou (2009) argue that European summer warming is not associated with changes in the circulation and that local surface and radiative feedbacks are the main drivers.

Several studies argue that both GCMs and RCMs underestimate the observed trend (Lorenz and Jacob, 2010; Ceppi et al., 2012b; Dosio, 2016; Boé et al., submitted), indicating that essential processes are missing or that the natural variability is not correctly sampled (Dell'Aquila et al., 2018). The model ability to represent circulation multi-decadal trends is assessed in Boé et al. (submitted). They showed that differences in model ensemble mean and observed temperature trends are explained, to a large extent, by a spatial anti-correlation of sea level pressure trends over the North Atlantic and European domains between almost all models and observations. With respect to missing essential processes, in particular the role of aerosols is discussed (Allen et al., 2013; Bartók, 2017), and the inability to simulate the observed trend is attributed to an underestimation of the anthropogenic aerosol effect in the CMIP protocols (Cherian et al., 2014). Nabat et al. (2014) argued that including realistic aerosol variations enables climate models to correctly reproduce the summer warming trend. However, other studies showed models to be sensitive also to local effects, such as land surface processes, convection, microphysics, and snow albedo effect (Ceppi et al., 2012b; Vautard et al., 2013; Davin et al., 2016). The role of aerosols in recent European warming is also discussed in Section Atlas.5.6.2. Finally, it is noteworthy that temperature differences between the Medieval Warm Period, the recent period, and the Little Ice Age are also larger in the reconstructions than in the simulations (Luterbacher et al., 2016).

Figure 10.17 reveals that the observed European warming, compared with the trend distribution from an initial-condition large ensemble over the 1950–2014 period, does not reveal a clear disagreement, although over limited periods there are large deviations due to natural variability (Figure 10.17d). Large ensembles are required for a reliable sampling of the natural variability and robust attribution of past trends (Deser et al., 2016). Figure 10.17 panels a, b, c and e reveal that the observed western European summer warming falls within the distribution simulated by the MPI large ensemble (Maher et al., 2019), indicating that natural variability strongly has affected the historical warming and that large ensembles are necessary for a correct estimation of the forced signal versus natural variability (Lehner et al., submitted).

There is *high confidence* (*strong evidence, high agreement*) that the lapse-rate feedback has contributed to the western European summer warming. There is *medium confidence* (*medium evidence, strong agreement)* that the AMV and atmospheric circulation changes have contributed to the summer warming. There is *medium confidence* (*medium evidence, medium agreement*) that the decrease of anthropogenic aerosols over Europe has been a dominant factor for the enhanced European summer warming. There is *high confidence* (*strong evidence, high agreement*) that local feedbacks, such as the soil-moisture feedback, have contributed to the increase in extreme temperature variability and consequently, frequency and intensity of heat-waves and *medium confidence* (*medium evidence, strong agreement*) that it has contributed to the increase of seasonal mean summer temperature. There is *medium confidence* (*medium evidence, low agreement*) in the ability of GCMs and RCMs to correctly simulate the observed warming trend. A robust assessment is hampered by the small ensemble size of most experiments.

10.4.1.2.7 The south-western North America drought

Persistent hydroclimatic drought in south-western North America remains a much-studied event. Drought is a regular feature of the south-western North America's climate regime, as can be seen in both the modern record, and through paleoclimate reconstructions (Cook et al., 2010; Woodhouse et al., 2010), as well as in future climate model projections (Cook et al., 2015a). Since the early 1980s, which were relatively wet in terms of precipitation and streamflow, the region has experienced major multiyear droughts such as the turn-of-the-century drought that lasted from 1999 to 2005, and the most recent 2012–2014 drought that is perhaps unprecedented within the past 10,000 years (Griffin and Anchukaitis, 2014; Robeson, 2015). Shorter dry spells also happened between these multiyear droughts making the 1980 to present a period with an exceptionally steep trend from wet to dry (Figure 10.18), leading to strong declines in Rio Grande and Colorado river flows (Lehner et al., 2017b; Udall and Overpeck, 2017). While robust attribution of this trend is complicated by the large natural variability in this region, the 20th century warming has been suggested to increase the chances for hydrological drought periods through lowering runoff efficiency (Woodhouse et al., 2016; Lehner et al., 2017b; Woodhouse and Pederson, 2018). There is some evidence suggesting that the Last Glacial Maximum, a period of low atmospheric CO_2, ~21 ka, is a reverse analogue of current, relatively high CO_2 levels (Morrill et al., 2018; Lowry and Morrill, 2019). Pluvial conditions at that time and a reduction in precipitation from the Last Glacial Maximum to the pre-industrial period are consistent with drying trends for the region in models with GHGs exceeding pre-industrial levels. However, the conclusion of the Last Glacial Maximum drying versus wetting seems to strongly depend on the physical property of interest, hydrologic or vegetation indicators (Scheff et al., 2017). Droughts are characterized by deficits in total soil moisture content that can be caused by a combination of decreasing precipitation and warming temperature, which promotes greater evapotranspiration. Regional-scale attribution of the south-western North America drought prevalence since 1980 then mostly focuses on the attribution of change in these two variables.

The observed south-western North America drying fits the narrative of what might happen in response to increasing GHGs concentrations due to the poleward expansion of the subtropics, that is conducive to drying trends over subtropical to mid-latitude regions (Hu et al., 2013b; Birner et al., 2014; Lucas et al., 2014). However, several studies based on modern reanalyses and CMIP5 models have recently shown that the current contribution of GHGs to Northern Hemisphere tropical expansion is much smaller than in the Southern Hemisphere and will remain difficult to detect due to large internal variability, even by the end of the 21st century (Garfinkel et al., 2015; Allen and Kovilakam, 2017; Grise et al., 2018, 2019). In addition, the widening of the Northern Hemisphere tropical belt exhibits strong seasonality and zonal asymmetry, particularly in autumn and the North Atlantic (Amaya et al., 2018; Grise et al., 2018). Thereby, it seems that the recent tropical expansion results from the interplay of internal and forced modes of tropical width variations and that the forced response has not robustly emerged from internal variability (Section 3.3.3).

A second possible causal factor is the role for ocean-forced or internal atmospheric circulation change. Analysis of observed and CMIP5-simulated precipitation indicates that the drought prevalence since 1980 is linked to natural, internal variability in the climate system (Knutson and Zeng, 2018). Based on observations and ensembles of SST-driven atmospheric simulations, Seager and Hoerling (2014) suggested that robust tropical Pacific and tropical North Atlantic forcing drove an important fraction of annual mean precipitation and soil moisture changes and that early 21st century multiyear droughts could be attributed to natural decadal swings in tropical Pacific and North Atlantic SSTs. A cold state of the tropical Pacific would lead by well-established atmospheric teleconnections to anomalous high pressure across the North Pacific and southern North America, favouring a weaker jet stream and a diversion of the Pacific storm track away from the southwest (Seager and Ting, 2017). The multiyear drought of 2012–2016 has been linked to the multiyear persistence of anomalously high atmospheric pressure over the north-eastern Pacific Ocean, which deflected the Pacific storm track northward and suppressed regional precipitation during California's rainy season (Swain et al., 2017). Going into more detail, Prein et al. (2016) used an assessment of changing occurrence of weather regimes to judge that changes in the frequency of certain regimes during 1979–2014 have led to a decline in precipitation by about 25%, chiefly related to the prevalence of anticyclonic circulation patterns in the northeast Pacific. Finally, the moderate model performance in representing Pacific SST decadal variability and its remote influence (Section 3.7.6) as well as its change under warming may affect attribution results of observed and future precipitation changes (Seager et al., 2019).

It has also been suggested that this ocean-controlled influence is limited and internal atmospheric variability has to be invoked to fully explain the observed history of drought on decadal time scales (Seager and Hoerling, 2014; Seager and Ting, 2017). Lasting from roughly 1980 to the present, the regional climate signals show an interesting mix between forced and internal variability. Lehner et al. (2018b) used a dynamical adjustment method and large ensembles of coupled and SST-forced atmospheric experiments to suggest that the observed south-western North America rainfall decline mainly results from the effects of atmospheric internal variability, which is in part driven by a PDV-related phase shift in Pacific SST around 2000 (Figure 10.18). Based upon two very large ensembles (one using a GCM and another one an AGCM constrained by observed SSTs) and a CMIP6 multi-model suite constrained by observed external forcing, Figure 10.18 shows, in agreement with Lehner et al. (2018b), that observed SSTs with their associated atmospheric response are the main drivers of the south-western North America precipitation decrease during the 1983–2014 period. It also suggests that the contribution of natural and anthropogenic forcings to the precipitation decline is extremely small.

[START FIGURE 10.18 HERE]

Figure 10.18:(a) Water year (October to September) precipitation spatial linear trend (in percent (32 year)$^{-1}$) over North America from 1983 to 2014. Trends are estimated using ordinary least squares. Top row: Observed trends from GPCC version 2018 (Schneider et al., 2017), CRU TS version 4.00 (Harris et al., 2014) and the Global Precipitation Climatology Project (GPCP) (Huffman et al., 2009) version 2.3. Middle row: Driest, mean and wettest trends (relative to the region enclosed in the black quadrilateral, middle row) from the 100 members of the MPI-GE (Maher et al., 2019). Bottom row: Driest, mean and wettest trends relative to the above region from the 100 members of the d4PDF-GE (Mizuta et al., 2017). (b) Time series of water year precipitation anomalies (%, baseline 1971–2000) over the above south-western North America region for GPCC (grey bar charts). Black, brown and green lines show low-pass filtered time series for GPCC, driest and wettest members of d4PDF-GE, respectively. The filter is the same as the one used in Figure 10.11. (c) Distribution of south-western region-averaged water-year precipitation 1983–2014 trends (in percent (32 year)$^{-1}$) for MPI-GE (violet histogram), d4PDF (pink histogram), observations (GPCC, CRUTS and GPCP, dark grey open-filled circles) and historical simulations from a set of 22 CMIP6 models (yellow open-filled circles). Coloured triangles refer to ensemble mean trends of their respective ensemble. Brown and green open-filled circles refer to the driest and wettest d4PDF-GE ensemble members.

[END FIGURE 10.18 HERE]

Once aspects of the internal variability are removed by dynamical adjustment, the observed precipitation-change signal and simulated anthropogenically-forced components look much more similar. Unlike the precipitation deficit, the south-western North America accompanying warming is driven primarily by anthropogenic forcing from GHGs rather than atmospheric circulation variability and may help to enhance the drought through increased evapotranspiration (Williams et al., 2015; Lehner et al., 2018b).

There is *high confidence* (*robust evidence* and *high agreement*) that an important fraction (> 50%) of the anomalous atmospheric circulation that caused the south-western North America negative precipitation trend can be attributed to teleconnections arising from tropical Pacific SST variations related to PDV. There is *medium confidence* (*medium evidence* and *medium agreement*) that anthropogenic forcing has made a substantial contribution (~50%) to the south-western North America warming since 1980.

10.4.1.2.8 The Caribbean small islands summer drought

Climate variability over the Caribbean region impacts its agriculture, fisheries, health, tourism, water availability, recreation, energy usage, and other socioeconomic activities. Due to the region's location, it is influenced by synoptic features over the tropical Atlantic and tropical Pacific basins including the migration of the North Atlantic subtropical high and the Inter-Tropical Convergence Zone, easterly winds, the Atlantic warm pool, the intrusion of cold fronts, and the passage of tropical depressions, easterly waves, storms and hurricanes (Ashby et al., 2005; Taylor et al., 2013b).

Caribbean small islands exhibit a climatological mid-summer drought (also termed mid-summer drying) around June/July within a rainfall season from May to October. This mid-summer drought is particularly evident over the western/northern Caribbean and Central America. A negative trend in boreal summer (JJA) precipitation over the Caribbean Sea and parts of Central America has been identified since 1979 in satellite observations, and since 1950 at land stations (Figure 10.19) (Neelin et al., 2006). Differences in calculated trends emerge as a result of the shorter temporal span and absence of orographic rainfall from satellite observations though they enable greater spatial coverage, while some land observations have a longer temporal range but are limited in spatial coverage. This is characteristic of some regions including Mexico, Central America, the Caribbean, and Pacific islands (Wright et al., 2016; Cavazos et al., 2019). Notably, Cavazos et al. (2019) show positive trends in JJA rainfall over Cuba and Jamaica for CRU and parts of Cuba and eastern Hispaniola for CHIRPS, but negative trends over Cuba for GPCC and eastern Hispaniola for CRU for 1980-2010 and similar to patterns observed in Figure 10.19. Using grid-point based detection and attribution analysis, Knutson and Zeng (2018) show detectable anthropogenically-forced decreasing precipitation trends over 1901–2010 for some grid-points in the general region of the Caribbean, including south of Cuba, in the northern Bahamas, and in the Windward Islands, while for shorter periods (1951–2010 and 1981–2010) no attributable trend was found. The drying trend has also been identified in studies undertaken for individual islands. Declines in summer rainfall (-4.4% per decade) and maximum five-day rainfall (-32.6 mm per decade) over 1960–2005 were reported for Jamaica from linear regression analyses on station data (Chen et al., 2012a). A slight decrease in summer precipitation accumulations was observed for Cuba for 1960 to 1995 (Naranjo-Diaz and Centella, 1998). Three of four stations examined for Puerto Rico exhibited declining JJA rainfall over 1955–2009 with the trend statistically significant at the 95% level for Canóvana (Méndez-Lázaro et al., 2019). Recent work also suggests that summer drought events may be intensifying. The 2015 Caribbean drought event was part of a pan-Caribbean drought occurring in 2013–2016 (Herrera et al., 2018a). Herrera and Toby (2017) noted that the summer drought of 2015 was record breaking in terms of its spatial extent with 99% of the Caribbean experiencing drought conditions, and in terms of its severity for 17% of a domain that includes the Caribbean, South America and Central America.

[START FIGURE 10.19 HERE]

Figure 10.19: (a) Observed trends in June to August precipitation (mm day^{-1} decade^{-1}) from GPCC version 2018 (Schneider et al., 2017) and CRU TS version 4.02 (Harris et al., 2014) over the Caribbean from 1979 to 2014. (b) Trends in June to August zonal winds at 925 hPa (m s^{-1} decade^{-1}, in colour) and sea level pressure (solid (dashed) line contours indicate positive (negative) trends in 0.1 hPa decade^{-1} steps) over the tropical North Atlantic from MERRA (Rienecker et al., 2011) and ERA-Interim (Dee et al., 2011)

with the area for the Caribbean low-level jet highlighted (12.5°N–17.5°N, 70°W–80°W). (c) As (a) but for model simulations. Top row: Driest, mean and wettest trends (in the mean over the four indicated station locations in the bottom left panel) from the 100 members of the MPI-GE (Maher et al., 2019). Middle row: Driest, mean and wettest trends relative to the above station locations from the 100 members of the d4PDF-GE (Mizuta et al., 2017). Bottom row: Driest, median and wettest trends relative to the above station locations from historical simulations of 26 CMIP6 models. (d) Time series of average June to August precipitation for four stations (Bahamas in dark red, Cuba in light red, Cayman in brown, Jamaica in orange) and the mean over this four stations (in black) as well as the station location mean extracted from GPCC and CRU TS gridded data. The filter is the same as the one used in Figure 10.11. (e) Distribution of mean precipitation trends for the four station locations between 1979 and 2014 for MPI-GE (violet histogram), d4PDF-GE (pink histogram), historical simulations from a set of 26 CMIP6 models (red circles), observations (means over station observations, GPCC and CRU TS, black crosses) and ensemble mean trends. All trends are estimated using ordinary least squares.

[END FIGURE 10.19 HERE]

JJA rainfall trends over 1980–2010 from PRECIS, RCA4, RegCM4.0-G and RegCM4.5-T suggest disparate trends over Jamaica, Cuba, and eastern Hispaniola (Cavazos et al., 2019) where, for example, some weak positive trends are shown over Cuba but with different magnitudes and spatial distributions. Figure 10.19 shows weak negative trends over much of the Caribbean for 1979-2014 with some weak positive trends over Cuba for MPI-GE ensemble mean. However, weak positive trends are evident over much of the domain for the d4PDF-GE ensemble mean but with some drying trend still evident over Cuba, Jamaica and Hispaniola while a stronger drying trend is observed from the CMIP6 ensemble mean trend. The limited number of available downscaled simulations for this region is a challenge to robust evaluation of trends.

The climatological mid-summer drying is associated with an intensification and westward shift of the North Atlantic subtropical high, and a related increase in the strength of the low-level easterlies over the Gulf of Mexico and the Caribbean Sea (Hastenrath, 1966; Waylen et al., 1996; Knaff, 1997; Magana et al., 1999; Giannini et al., 2000; Rauscher et al., 2008), and a semi-annual strengthening of the Caribbean low level jet (Amador, 1998; Wang, 2007; Wang and Lee, 2007). The mid-summer drought has also been linked to warm SST anomalies in the tropical Atlantic and cool eastern equatorial Pacific SST anomalies through their combined modulation of the Caribbean low level jet (Whyte et al., 2008). Some studies have suggested that the intensifying mid-summer drying occurs alongside a general intensification and poleward movement of the subtropical high pressure cells (Christensen et al., 2007), with an equatorward contraction of tropical convective regions due to the suppression of convection in a more stable atmosphere (Neelin et al., 2003). Rauscher et al. (2011) and Whyte et al. (2008) note that the SST warming over the Atlantic, though smaller than the warming observed over global tropical areas, has been associated with enhanced divergence and increasing strength of the North Atlantic subtropical high and potentially the strength of the Caribbean low level jet. Figure 10.19 suggests a strengthening of the Caribbean low level jet over 1979–2014. Falarz (2019) indicated slight increases in sea level air pressure at the centre of the North Atlantic subtropical high in July for 1948–2018 with a southwest shift in its location for 1998–2018. Figure 10.19 suggests that observed SSTs play a key role in the trends observed given that the histogram spread for d4PDF is smaller than for the fully coupled models and the d4PDF mean is closer to the means from the observation datasets. The histogram also suggests that observational uncertainty is important. These factors taken together imply that there is currently *limited evidence* to conclusively suggest the responsible mechanisms for the summer drying.

Méndez-Lázaro et al. (2014) indicated that the summer drying trend could also be linked to the combined effect of ENSO and the NAO rather than to the anthropogenic forcing. A warm ENSO and positive NAO phase have been shown to result in negative summer rainfall anomalies (Giannini et al., 2000). The mid-summer drought and its intensity have also been associated with the AMV, PDV and ENSO (Maldonado et al., 2016) where, for example, a positive PDV and a warm ENSO are linked to drier mid-summer events. The work of Herrera et al. (2018) suggested that for the 2013–2016 pan-Caribbean drought, anthropogenic warming accounted for ~15–17% of the drought's severity and ~7% of its spatial extent. This indicates that anthropogenic warming may be influencing the drying trends in summer rainfall, though no additional studies to date have presented this case. There is *limited evidence* and *low agreement* for the cause of the drying trend over the Caribbean in mid-summer since 1950 and whether this trend is mainly caused by either decadal-scale internal variability or anthropogenic forcing.

10.4.1.3 Assessment summary

Attribution results from regression-based standard optimal fingerprinting and from the above examples are very different depending on whether one is interested in regional-scale attribution of temperature or precipitation changes. While the influence of anthropogenic forcing on regional temperature long-term change has been detected and attributed in several regions, a robust emergence of human influence on regional precipitation change has not occurred yet for most regions. This lack of emergence for precipitation is likely due to larger observational uncertainty and model error, as well as stronger internal variability. Attribution results can also be very sensitive to the period length and spatial size of the region under scrutiny. Even in the case of temperature and multi-decadal time scale, internal variability can still be the main driver of regional changes due to cancellation between different external forcings (Nath et al., 2018). Based on a non-parametric trend analysis of both CMIP3 and CMIP5 models compared to a large ensemble, Kumar et al. (2016) have found that at global scale, the contribution of internal variability to temperature trend uncertainty increases from 24% for the twentieth century (1901–1998) to 76% for the recent hiatus period (1999–2013) and at regional scales (based on 22 regions from Giorgi (2002)) from 43% to almost 100% during the corresponding time periods.

There is *high confidence* (*robust evidence* and *medium agreement*) that anthropogenic forcing has been a major driver of temperature change since 1950 in many sub-continental regions of the world. While there is *medium confidence* (*medium evidence* and *medium agreement*) that anthropogenic forcing has contributed to multi-decadal precipitation changes in several regions, large observational uncertainty and internal variability as well as model errors lead to *low confidence* (*medium evidence* and *low agreement*) with regard to a well-constrained quantification (best estimate and confidence interval) of the total anthropogenic contribution to precipitation changes as well as the relative contributions of GHGs, including ozone and different aerosol species.

10.4.2 Future regional changes and interplay between internal variability and response to external forcing

The fitness for purpose of regional climate projections to support adaptation policies is often questioned (Section 10.5). This is mainly due to the combination of three different sources of uncertainty (Lehner et al., submitted): uncertainty about the future GHGs and aerosol emissions as well land-use changes (scenario uncertainty, Section 4.2.5), the weakness of process understanding about the multi-scale interactions of large-scale and regional phenomena (also named model or structural uncertainty, Section 10.3), and uncertainty related to the lack of predictability of low-frequency internal variability due the chaotic nature of the climate system (Section 4.4). This section mostly focuses on the latter and its interplay with the model uncertainty associated with the forced climate response to anthropogenic radiative forcing. The different methodologies that are used to estimate and quantify the influence of internal variability and its interplay with the forced response on future regional climate projections are reviewed first. Next, the use of these methods, applied either globally or regionally, is assessed with a focus on our selected examples.

The assessment is necessarily emission scenario and time-dependent, on a region-by-region basis. Depending on the emission scenario, period and/or regions, internal variability can counteract, be neutral, or exacerbate the forced response due to anthropogenic forcing (Deser et al., 2012b; Maher et al., 2019). The response to anthropogenic forcing can also project on internal modes of variability leading to difficulty in identifying the forced response and its spatial pattern. Analysis of multi-model archives such as CMIP-type simulations cannot easily disentangle structural model uncertainty and uncertainty related to internal variability. Only multi-models of (GCM and/or RCM) large initial-condition ensembles allow a clean separation between the two uncertainty sources (Kay et al., 2015; Aalbers et al., 2018; Leduc et al., 2019; Maher et al., 2019; von

Trentini et al., 2019b). The use of multi-model large ensembles is emerging as a promising way to robustly assess the respective contribution of internal variability and model uncertainty to future regional climate changes (Deser et al., submitted; Lehner et al., submitted). It is noteworthy that the use of multi-model initial-condition large ensembles assumes that they have a credible representation of internal variability (McKinnon et al., 2017; McKinnon and Deser, 2018; Chen and Brissette, 2019). Assessing the credibility of simulated internal variability remains an active research field that is still limited by the shortness and uncertainties of the observed record, in particular in data-scarce regions (Section 10.2.2.3).

While other methodologies using internal variability from pre-industrial simulations to assess the role of internal variability in future climate change (Thompson et al., 2015) have been suggested, they implicitly assume that regional-scale internal variability does not change under anthropogenic forcing, which is a strong assumption that does not seem to hold at regional scales (LaJoie and DelSole, 2016; Dai and Bloecker, 2018). Finally, the attribution of past changes is useful but not sufficient to robustly infer the relative contribution of the relevant drivers to future regional climate changes (Section 10.3.3). The relative importance of internal variability and anthropogenic factors is not constant in time as external anthropogenic and natural forcing can vary, as well as internal variability and the interaction between the different drivers (Nath et al., 2019), including a possible modulation of internal variability modes by external forcing (Thiéblemont et al., 2015).

As described in Section 10.3.4.3, the influence of internal variability on climate projections can be quantified based on simple diagnostics such as signal-to-noise ratio and time of emergence. Signal-to-noise ratio and time of emergence global studies are first briefly assessed before focusing on a few selected regions. Based on a temperature variance ratio analysis of five CMIP5 models (each with 4 to 10 members), Lyu et al. (2015) have shown that the unbiased ratio of forced to total variance over the historical period is strongest in the tropics (30–40% in average, up to 70% locally) and decreases poleward (with a range of 5–30%). For temperature, the large variance ratio in tropical areas is mainly due to the forced climate change signal, which is dominant compared with the internal variability background. In contrast, the lower ratio in extratropical areas results from the larger internal variability. The larger ratio of forced variance to total variance generally corresponds to earlier emergence of forced signals from internal variability. The temperature variance ratio, over time intervals with the starting time being fixed at 1860 and the end time increasing from 1870 to 2100, shows that the globally averaged ratios of forced to total variance continue to increase with time under all three radiative concentration pathway GHG scenarios, reflecting the cumulative effect of externally forced climate change. Based on a 40-member ensemble constrained by the SRES-A1B scenario over 2005–2060 and using a simple signal-to-noise metric, the interplay between internal variability and the forced response to GHGs was assessed for surface air temperature, precipitation and sea level pressure (Deser et al., 2012a, 2012b). It was found that for temperature, only one realization is needed to detect a significant (at the 95% confidence level) warming in the 2050s decade compared to the 2010s at nearly all locations, compared to approximately 3–6 (15) ensemble members for tropical and high latitude (middle latitude) precipitation, and approximately 3–6 (9–30) members for tropical (extra-tropical) sea-level pressure, depending on location and season. They also underscored the low signal-to-noise (ratio of ensemble mean trend by standard deviation of ensemble member trends less than 1) in the large-scale patterns (e.g., annular modes) of extra-tropical atmospheric circulation response that are primarily due to intrinsic atmospheric dynamics (Deser et al., 2017b; Maher et al., 2019). Most of the random uncertainty in temperature and precipitation in the extra-tropics is associated with the annular mode variability in both seasons and hemispheres. Finally, they show that the magnitude of random uncertainty associated with internal variability is rarely less than half that due to model uncertainty for forced linear climate trends during 2005–2060. Similar analyses based on the same large ensemble and more recent ones were also conducted for sea level, the Hadley Cell and Arctic sea ice (Hu and Deser, 2013; Kang et al., 2013; Wettstein and Deser, 2014; Maher et al., 2019). Large ensemble simulations from Kay et al. (2015) and Sigmond and Fyfe (2016) were used to quantify the internal variability influence on trends in annual surface air temperature and precipitation over different time periods from 1950 up to 2100 (Dai and Bloecker, 2018). Results indicate that regional precipitation trends due to anthropogenic forcing may not be detectable over most of the globe until the later part of the 21st century even under a high-emission scenario (Figure 10.20), while forced temperature trends since 1979 are already detectable over many low-latitude regions (Hawkins et al., submitted) and are projected to emerge from internal variability over most of the globe by the 2030s under the high-end GHG emission scenarios (Figure 10.20).

[START FIGURE 10.20 HERE]

Figure 10.20: (a) Time series of simulated decadal mean air temperature anomalies (baseline 1995–2014) for regions of Eurasia, Himalaya and western Europe (see Figure 10.11 for the exact regional boundaries). Box plots indicate simulated decadal mean temperature anomalies averaged over near-term (2021–2040) and long-term (2081–2100) future periods. Models include seven initial-condition large ensembles, as in (Deser et al., submitted), 39 CMIP5 and 22 CMIP6 models that all have pre-industrial, historical and scenario simulations (RCP8.5 for CMIP5 and SSP5-8.5 for CMIP6 models). (b) As in (a) but for precipitation anomalies. The regions are sub-regions of North America, East Asia, South America, Africa, Caribbean and Australia (as in Figure 10.11).

[END FIGURE 10.20 HERE]

Based on detection and attribution studies and climate projections based on multi-model initial-condition large ensembles, it is *extremely likely* that temperature change due to anthropogenic forcing will have emerged from internal variability in most land regions of the world by 2050 under the high-end (SSP5-8.5 and RCP8.5) GHG emission scenarios. Based on multi-model historical simulations, regional-scale attribution studies, and climate projections, in particular those coming from initial-condition large ensembles, it is *very likely* that internal variability will still significantly influence future multi-decadal precipitation trends in many land regions (except Antarctica; Section 9.4.2) until at least the mid 21st century.

[START BOX 10.2 HERE]

BOX 10.2: Urban climate

Urban areas extend typically from a few kilometres to hundreds of kilometres, but their internal features influence the air flow at scales down to the street-canyon scale of a few metres (Oke et al., 2017). Urban centres and cities are often several degrees warmer compared to the surrounding rural area due to what is known as the urban heat island effect (Bader et al., 2018; Kuang, 2019). Urban areas and cities affect the local weather by perturbing the wind, temperature, moisture, turbulence, and surface energy budget field. Another unique feature of cities is the release of the anthropogenic heat flux from building energy consumption and direct emission from traffic (Ichinose et al., 1999; Bohnenstengel et al., 2014; Chow et al., 2014; Ma et al., 2017). Three main factors contribute to the establishment of the urban heat island: 3-D urban geometry, thermal characteristics of impervious surfaces, and anthropogenic heat release. There is also a strong contribution of local background climate to the urban heat island magnitude (Zhao et al., 2014; Ward et al., 2016). Cities can also experience other phenomenon, such as the urban dryness island, which refers to conditions where lower relative humidity is observed in cities relative to nearby rural locations (Kuttler et al., 2007; Lokoshchenko, 2017b) and the urban wind island where cities experience slower wind speeds compared to their adjacent suburbs and countryside (Wu et al., 2017; Bader et al., 2018).

Monitoring network

Although the urban heat island is well documented and studied (FAQ 10.2), climate data in urban areas remain very limited. This is in part due to the standards set by the World Meteorological Organization (WMO, 2019) that cannot be met in an urban environment due to the high density of buildings and other obstacles. Especially long-term datasets (a year or more) are very scarce (Bader et al., 2018; Caluwaerts et al., 2020). City-scale climate monitoring networks can enhance the understanding of urban microclimate and their interaction with climate change, and provide key information for end-users such us urban planners, decision-makers such as city mayors, stakeholders and the general public (Chen et al., 2012b; Barlow et al., 2017; Bader et al., 2018). Recently, networks of weather monitoring stations and both satellite and ground-based remote sensing instruments have been established in different cities around the world (see Technical

Annex I on observations). However, there is still a lack of harmonization of collection practices, instrumentations, station locations, and quality control methodologies across cities to facilitate collaborative research (Muller et al., 2013; Barlow et al., 2017). Over the past decade, more crowdsourcing data in real time is becoming available through the use of cheap sensors (using internet of things technology) that are incorporated in various platforms like cars, amateur weather stations, and smartphones (Sosko and Dalyot, 2017). They are collected in citizen science projects (Muller et al., 2015). This technological trend could prove very useful and the regional climate community is making efforts to understand the extent to which these methods can be exploited as a complement to traditional datasets (Meier et al., 2017; Zheng et al., 2018; Langendijk et al., 2019).

Urban modules in climate models

In order to calculate the exchanges of heat, water and momentum between the urban surface and its overlying atmosphere, specific surface-atmosphere exchange schemes dedicated to urban areas must be implemented. Urban schemes were developed in the last 20 years and vary considerably in complexity. In general, three different types, in order of increasing complexity, can be distinguished (Masson, 2006; Grimmond et al., 2010, 2011; Chen et al., 2011; Best and Grimmond, 2015): (1) The simplest is the slab or bulk approach, where urban areas are represented by modifying soil and vegetation parameters within land surface models (e.g., Best et al., 2006; Dandou et al., 2005; Liu et al., 2006; Seaman et al., 1989). They usually feature parameters based on the observation that roughness length and displacement height are large over cities. The energy balance is also often modified to account for the radiation trapped by the urban canopy, heat storage, evaporation, and anthropogenic heat fluxes. However, the three-dimensional structure of the city is not resolved. (2) Single-layer urban canopy modules represent cities with a simplified geometry (urban canyon, with three surface types: roof, road and wall) that can approximately capture the main 3D dynamical and thermal physical processes influencing radiative and energy fluxes (Masson, 2000; Kusaka et al., 2001). (3) In multi-layer urban canopy modules, urban effects are computed vertically throughout the urban canopy, allowing a direct interaction with the planetary boundary layer (Brown, 2000; Martilli et al., 2002; Hagishima et al., 2005; Dupont and Mestayer, 2006; Hamdi and Masson, 2008; Schubert et al., 2012). As a sub-model of urban canopy modules, building-energy models that estimate anthropogenic heat from a building for given atmospheric conditions have also been developed (e.g., Bueno et al., 2012; Kikegawa et al., 2003; Lipson et al., 2018).

Many regional modelling groups are now beginning to implement the three types of urban parameterizations within the land-surface component of their RCMs (Daniel et al., , 2019; Halenka et al., 2019; Hamdi et al., 2014; Kusaka et al., 2012; McCarthy et al., 2012; Oleson et al., 2011; Trusilova et al., 2016).

There is *very high confidence* (*robust evidence* and *high agreement*) that while all types of urban parameterizations generally simulate radiation exchanges in a realistic way, they have, however, strong biases when simulating latent heat fluxes. There is *medium evidence* but *high agreement* (Kusaka et al., 2012a; McCarthy et al., 2012; Hamdi et al., 2014; Trusilova et al., 2016; Jänicke et al., 2017; Daniel et al., 2019) that a simple single-layer parameterization is sufficient for urban climate modelling focusing on the urban heat island and its interaction with the regional climate change at the city scale.

Observed climate in cities

There is *medium evidence* but *high agreement* (Parker, 2010; Zhang et al., 2013; Chen et al., 2016d) that the global annual mean surface air temperature response to urbanization is negligible. At the city scale, there is *very high confidence* (*robust evidence* and *high agreement*) that a percentage of the observed warming trend is linked to historical urbanization in rapidly industrialized countries (Figure 1), although large differences exist between different attribution methods (Park et al., 2017).

[START BOX 10.2, FIGURE 1 HERE]

Box 10.2, Figure 1: Change in the annual mean surface temperature over the period 1950–2018 based on local linear trend retrieved from the GISTEMP data (Lenssen et al., 2019). This background warming is added to the local warming that has been reported during 1950–2018 in the literature from historical urbanization in different cities and plotted on top of the background as hexagon for each city. The colour of the circles refers to the magnitude of the urban warming calculated as the background warming plus the historical urbanization warming. This map has been compiled using the following studies: (Ajaaj et al., 2018; Alizadeh-Choobari et al., 2016; Bader et al., 2018; Chen et al., 2016; Chrysanthou et al., 2014; Doan et al., 2016; Dou et al., 2015; Elagib, 2011; Founda et al., 2015; Fujibe, 2009; Gaffin et al., 2008; Hinkel and Nelson, 2007; ; Li et al., 2018; Liao et al., 2017; Lokoshchenko, 2017; Polydoros et al., 2018; Sun et al., 2016; ; Wang et al., 2018; Zhou et al., 2016, 2017). The bottom left panel shows the low-pass filtered time series of the annual mean temperature anomalies observed in the urban station of Tokyo and the rural reference station in Choshi (Japan) (°C, baseline 1887-1917). The filter is the same as the one used in Figure 10.11.

[END BOX 10.2, FIGURE 1 HERE]

There is *very high confidence* (*robust evidence* and *high agreement*) that the annual-mean maximum temperature is less affected by urbanization than the minimum temperature. It is *virtually certain* that if observations of near-surface air temperatures in growing cities are used in the assessment of global warming trends, these trends are overestimated by the urban warming, while this urban warming is smaller for a station that originally was established in a densely built-up area (Ezber et al., 2007; Fujibe, 2009; Hamdi, 2010; Elagib, 2011; Camilloni and Barrucand, 2012; Robaa, 2013; Hausfather et al., 2013; Argüeso et al., 2014; Alghamdi and Moore, 2015; Alizadeh-Choobari et al., 2016; Sachindra et al., 2016; Liao et al., 2017; Lokoshchenko, 2017; Wang et al., 2017a; Arsiso et al., 2018).

There is *medium confidence* (*medium evidence* and *medium agreement*) (Schlünzen et al., 2010; Ganeshan et al., 2013; Ganeshan and Murtugudde, 2015; Haberlie et al., 2015; Daniels et al., 2016; Liang and Ding, 2017; McLeod et al., 2017) that urban areas induce increases in mean but also in extreme precipitation over and downwind of the city in different climate regions of the world and especially in the afternoon and early evening.

Moreover, since many of the world’s largest cities are located along the coast, this will introduce additional complexity to urban hydrology due to the local sea level rise. The process of subsidence and groundwater withdrawal accelerate local sea level rise faster than the global average (Hallegatte et al., 2013; Bader et al., 2018; Kulp and Strauss, 2019).

Future climate projection

It is *very uncertain* to estimate how the urban heat island will evolve under climate change conditions because several studies using different methods report contrasting results. However, there is *very high confidence* (*robust evidence* and *high agreement*) that the projected change of the urban heat island under climate change conditions is one order of magnitude less than the projected warming in both urban and rural areas under simulation constraints of no urban growth (Adachi et al., 2012; Arsiso et al., 2018; Früh et al., 2011; Hamdi et al., 2014; Hatchett et al., 2016; Hoffmann et al., 2018; Kusaka et al., 2012; McCarthy et al., 2010, 2012; Oleson, 2012; Oleson et al., 2011; Sachindra et al., 2016).

Therefore, climate change will, on average, have a limited impact on the magnitude of the urban heat island. In some studies the regionally downscaled data using a RCM is used to force an off-line urbanized land surface scheme (Lemonsu et al., 2013; Lauwaet et al., 2015; Rafael et al., 2017). These studies report also contrasting results about the changes in the urban heat island magnitude under climate change. However, the contribution and feedback processes by urban heat island and climate change are not accounted for in these offline simulations.

There is *very high confidence* (*robust evidence* and *high agreement*) that future urbanization will amplify the projected air temperature under different background climate, with a strong impact on minimum temperatures, that could be comparable in magnitude to the global warming (Berckmans et al., 2019). There is *very high confidence* (*robust evidence* and *high agreement*) that large impact is expected from the combination of future urban development and more frequent occurrence of extreme climatic events, such as heat waves (Hamdi et al., 2016; Bader et al., 2018). Finally, Kusaka et al. (2016) provided the first attempt in quantifying the uncertainties arising from choice of RCM or of future urban planning scenarios. The results showed that the impacts of urban planning scenario and RCM differences are larger during nighttime, but at most 0.6°C. The results indicate that the uncertainties related to both the RCM and urban planning scenario are significantly less than those arising from global emission scenarios or GCM projections. However, it is worth mentioning that there is a large uncertainty from the RCM with and without urban land use, indicating that this impact is comparable to the differences between GCMs. Impact assessments and adaptation plans will require high spatial resolution climate projections along with models that represent urban processes, ensemble dynamical and statistical downscaling, and local-impact models (Masson et al., 2014; Duchene et al., submitted).

[END CHAPTER BOX 10.2 HERE]

[START CROSS-CHAPTER BOX 10.3 HERE]

Cross-Chapter Box 10.3: Climate Change over the Hindu Kush Himalaya

Contributors: Muhammad Adnan (Pakistan), Muhammad Amjad (Pakistan), Subimal Ghost (India), Akm Saiful Islam (Bangladesh), Martin Jury (Spain/Austria), Asif Khan (Pakistan), Krishnan Raghavan (India), Laurent Terray (France), Andrew Turner (UK), Zhiyan Zuo (China)

The Hindu Kush Himalaya (HKH), with the largest collection of glaciers and snow cover outside the poles, provides the headwaters for several major rivers in Asia (Sharma et al., 2019). Global warming has caused significant glacial retreat, snowmelt, and permafrost degradation in HKH (Yao et al., 2012b, 2012a; Azam et al., 2018; Bolch et al., 2019). Since the 1960s, the HKH has experienced significant trends in the mean and extremes of temperature and precipitation, corresponding to frequent devastating landslides, heavy cloudbursts, flash floods, monsoonal floods/drought, glacial avalanches, glacier lake outburst floods, and hailstorms (Krishnan et al., 2019b). These incidents caused sudden and severe damage to life and property in many parts of the region (Bhardwaj et al., 2019). The change is challenging to predict but will have major consequences, not just in the region, but globally. There was little presence in the complex HKH in previous IPCC assessments due to the lack of consistent high-quality datasets and the simulation performance assessment being hampered by the observational uncertainties. Therefore, there is a critical need to assess the changes in the HKH. These are changes and assessment difficulties common to many other mountain areas. In this box, uncertainty in observational datasets and model performance are first discussed, followed by the key features of the observed climate change and the possible attribution to a number of drivers.

Observational uncertainty and model performance

The key causes of uncertainty in temperature and precipitation datasets for the HKH (e.g., APHROTEMP/APHRODITE, CRU and GPCC) have been identified as the sparseness of observational data and choice of interpolation method (Immerzeel et al., 2015; Ghimire et al., 2018) (Figure 1). In spite of the scarce observations, it can be estimated that the CORDEX South Asia RCMs and their driving CMIP5 GCMs feature a large cold bias in the Himalayas (Mishra, 2015). Using 13 CORDEX South Asia RCMs Sanjay et al. (2017) showed that the downscaled seasonal mean temperatures have relatively larger cold biases than their driving CMIP5 GCMs over the HKH. Despite the cold bias, the ensemble of CORDEX South Asia RCMs shows a significant spatial correlation with the APHROTEMP (Nengker et al., 2018). The CORDEX South Asia RCMs also generally feature a dry bias along the Himalayan foothills and a wet bias at higher elevations in summer (Hasson et al., 2019).

Elevation-dependent warming (EDW)

A key process for the HKH is EDW, as reviewed in Pepin et al. (2015). Xu et al. (2016b) described observed surface warming over the HKH region of between 2°C and 2.5°C at 5,000 m from 1961 to 2006, but considerably lower (0.5°C) at sea level. The SROCC reports that there is not a uniform pattern of EDW since the EDW varies by region, season and temperature indicator (e.g., daily mean, minimum or maximum temperature). The largest warming trend occurred on the Tibetan Plateau while the weakest was over north India (Ren et al., 2017). The annual mean surface temperature in the Tibetan Plateau has accelerated since the 1980s (You et al., 2016). However, a summer cooling trend over the Karakoram (western HKH) for 1960–2010 was reported by Forsythe et al. (2017). Observational analysis and model simulations have attributed EDW to increased GHG and black carbon aerosol emissions over Asia since the 1980s (Xu et al. 2016b). The resulting snow-albedo feedback occurs due to the deposition of light-absorbing aerosols, which accelerate warming (Ming et al., 2012; Gautam et al., 2013; Lau and Kim, 2018; Yan et al., 2016; Zhang et al., 2018). Beside the GHGs and light-absorbing aerosols, Zeng et al. (2015) reported increasing cooling-effect aerosols also lead to the EDW in the HKH because the cooling effect is more pronounced at low elevation than at high elevation. Therefore, there is *high confidence* (*robust evidence* and *high agreement*) that the eastern and central Himalayan region has exhibited rising temperatures, and that the rate of warming is amplified with elevation. There is *high confidence* (*robust evidence* and *high agreement*) that a large fraction of the warming can be attributed to increases in GHG (Figure 1).

[START CROSS-CHAPTER BOX 10.3, FIGURE 1 HERE]

Cross-Chapter Box 10.3, Figure 1: Historical annual-mean surface air temperature linear trend (°C decade^{-1}) and its attribution over the Hindu Kush Himalaya (HKH) region. (a) Top row: Observed trends from the Berkeley surface temperature (BEST) dataset (Rohde et al., 2013), Climatic Research Unit Time Series (CRU TS) version 4.02 (Harris et al., 2014), the Japanese 55-year Reanalysis (JRA-55) (Kobayashi and Iwasaki, 2016) for 1961–2014 and from Asian Precipitation-Highly-Resolved Observational Data Integration Towards Evaluation (APHRODITE) V1204R1 (Yasutomi et al., 2011) for 1961–2007. Second row: Coldest, mean, and warmest trends (relative to the region enclosed in the black quadrilateral, fifth row) from the 100 members of the Max-Planck Institute grand ensemble (MPI-GE) (Maher et al., 2019). Third row: coldest, median, and warmest trends from CMIP6 historical 29 members. Fourth and fifth rows: coldest, median, and warmest trends from CMIP6 aerosol-only nine members and greenhouse gas-only ten members, respectively. The black shape in the last row second column map is the HKH boundary. (b) Time series of annual-mean surface air temperature anomalies (°C, baseline 1961–1980) over the region enclosed in the black quadrilateral (25°N–40°N, 75°E–105°E) in (a) bottom left map. Black, brown, orange, red, dark red, grey, and blue lines show low-pass filtered time series for BEST, CRU TS, JRA-55, APHRODITE, CMIP6 all-forcing historical mean, CMIP6 aerosol-only mean, and CMIP6 greenhouse gas-only mean, respectively. The filter is the same as the one used in Figure 10.11. (c) Distribution of annual mean surface air temperature trends (°C decade^{-1}) over the region enclosed in the black quadrilateral (25°N–40°N, 75°E–105°E) from 1961 to 2017 for ensemble means, the MPI-GE (violet histogram), and individual members of CMIP6 all-forcing historical (red circles), CMIP6 greenhouse gas-only (blue triangles), CMIP6 aerosols-only (grey triangles), and observations (black cross).

[END CROSS-CHAPTER BOX 10.3, FIGURE 1 HERE]

Precipitation

Yao et al. (2012) used GPCP data to show that central-eastern HKH annual precipitation exhibits a decreasing trend from 1979 to 2010, a result repeated in summer in multiple observed datasets (Palazzi et al., 2013; Roxy et al., 2015). This negative trend has been attributed to a weakening South Asian monsoon (Yao et al., 2012b; Palazzi et al., 2013; Roxy et al., 2015; Shrestha et al., 2019). There is much contradictory evidence for precipitation trends in the western HKH. Meher et al. (2018a) used rain gauge data to show significant declining trends in winter rainfall and the number of rainy days over the western HKH over 1902–2005. Li et al. (2018) used four datasets in northern India to show that summer precipitation exhibited a positive trend during 1981–2008. Azmat et al. (2017) suggested that the precipitation has a slightly increasing tendency over the Jhelum river basin in the western HKH for 1961–2013. Hunt et al. (2019) reported that the frequency of western disturbances (WDs) exhibits a slight negative trend from 1970 onwards, leading to a falling trend in winter precipitation over northern India and Pakistan, while Kumar et al. (2015) reported that winter WD frequency over Himachal Pradesh (central Himalayas) during 1977–2007 has experienced a significant declining trend. In contrast, by using the variance of band-pass filtered 200 hPa geopotential height to represent WDs activity, Krishnan et al. (2018) found a rising trend of WDs activity in both reanalysis data and climate model outputs, resulting in enhanced orographic precipitation over the western HKH in recent decades. Therefore, there is *medium confidence* (*medium evidence* but *high agreement*) that the eastern-central HKH has experienced a decrease in summer precipitation. There is *medium confidence* (*medium evidence* but *high agreement*) that the decrease in summer precipitation in the eastern-central HKH can be mainly attributed to the weakening South Asian monsoon (Section 10.6.3). There is *low confidence* (*robust evidence* but *low agreement*) in the precipitation trend and the impact of WDs on the precipitation trend over the western HKH in recent decades.

Extreme events

Using the global land-surface daily air temperature dataset developed by the Chinese Meteorological Administration (Ren et al., 2017), many studies have reported that the HKH has featured a significant rising trend of extreme warm events over 1961–2015, alongside a falling trend of extreme cold events (Wester et al., 2019b; Krishnan et al., 2019a). Sun et al. (2017) reported that the decrease in Tibetan Plateau extreme cold events is smaller than the increase in extreme warm events after 1961. Using the Global Land Monthly and Daily Precipitation datasets developed recently by the Chinese Meteorological Administration, Zhan et al. (2017) found more frequent intense precipitation and less frequent light rain after 1990 in the HKH. Over the central and western HKH, there is an increase in frequency and intensity of extreme precipitation events while no clear trend is observed over the eastern HKH, where contrasting evidence exists (Sheikh et al., 2015; Adnan et al., 2016; Dimri et al., 2017; Talchabhadel et al., 2018). Extreme precipitation events occur during both summer and winter in the western HKH; summer extremes are generally associated with tropical lows (Hurley and Boos, 2015) and their interactions with WDs, whereas winter extremes are associated with only WDs (Dimri et al., 2015). Western HKH summer extremes show an increasing trend associated with weakening southwest monsoon circulation and increased activity of westerly upper-air troughs (Ridley et al., 2013; Madhura et al., 2015; Priya et al., 2017). Therefore, there is *high confidence* (*robust evidence* and *high agreement*) in the increase of extreme warming events and in the decrease of extreme cold events over the eastern Himalayas over the last five decades. There is *medium confidence* (*medium evidence* but *high agreement*) in the increase of summer extreme precipitation over the western HKH. There is *low confidence* (*limited evidence*) that the increasing summer extreme precipitation can be attributed to declining monsoon circulation.

Flood hazards

Intense floods have become more frequent in the HKH region during 2001–2013 (Elalem and Pal, 2015). However, You et al. (2017) suggested that limited observational data availability over HKH may lower the confidence in the result. HKH floods are complex geophysical phenomena associated with extreme precipitation events (Devrani et al., 2015; Dimri et al., 2017), complex topography, glacier lake outburst floods (Kropáček et al., 2015; Das et al., 2015; Cook et al., 2018), and contributions from glaciers and snow-melt due to rising temperature (Immerzeel et al., 2014). These intense floods can be linked to climate change (Adnan et al., 2017; Hunt et al., 2018). Nevertheless, based on the recent attribution studies of discharge in 2017 in the Brahmaputra basin (Philip et al., 2018), the 2013 extreme precipitation in Uttarakhand, extreme precipitation in Srinagar valley in 2014, and extreme rainfall in Bangladesh in 2017 (Rimi et al., 2019), there is no significant increase in the likelihood of these events attributable to anthropogenic climate change (Patil et al., 2019; Rimi et al., 2019). Therefore, there is *medium confidence* (*medium evidence* and *medium agreement*) in the increased frequency of intense floods over the central and western HKH in recent decades. There is *low confidence* (*limited evidence*) in the attribution of anthropogenic climate change to the increasing floods.

[END CROSS-CHAPTER BOX 10.3 HERE]

10.5 Combining approaches to constructing regional climate messages

This section assesses approaches and challenges for producing climate information and climate messages to inform adaption and policy decisions at regional scales (Section 10.1.2.1). An overview of the different sources and approaches to develop regional climate information including the role of climate services is given in Section 10.5.1. A more extensive discussion of climate services can be found in Section 12.6 and in Cross-Chapter Box 12.2. The role of the context in the construction of a climate message is discussed in Section 10.5.2. Narratives and storylines are important approaches in constructing climate change messages, which is the topic of Section 10.5.3. Finally, the distillation process from multiple lines of evidence is discussed in Section 10.5.4.

10.5.1 Sources of and approaches to regional information and climate services

The rise in demand for relevant climate information (Lourenço et al., 2016) has resulted in diverse approaches that include various open-access, web-portal delivery services of data as information (Hewitson et al., 2017), commercialization of climate services (Webber and Donner, 2017), and moves toward the fully tailored distillation of information drawing on and reconciling multiple sources of information (Figure 10.21), where the context is defined through co-design with users. The constructed information is then the basis for the development of a regional climate message that translates the factual information into the context and values of the user (Figure 10.1 and Sections 10.5.3 and 10.5.4).

[START FIGURE 10.21 HERE]

Figure 10.21: Illustration of how using different tools can result in different and potentially conflicting information. Change in daily precipitation (2071–2100 RCP8.5 relative to 1981–2010) over West Africa as simulated by an ensemble of GCM-driven RCMs. (a) Change in daily precipitation (mm) for April to September, as mean of 17 CORDEX models (Dosio et al., submitted) (b-e) Time-latitude diagram of daily precipitation change for four selected RCM-GCM combinations. For each month and latitude, model results are averaged along the longitude between 10°W–10°E (blue box in a). Different CGM-RCM combinations can produce substantially different and contrasting results, when the same RCM is used to downscale different GCMs (b, d), or the same GCM is downscaled by different RCMs (d, e). GCM1=IPSL-IPSL-CM5A, GCM2=ICHEC-EC-EARTH, RCM1=RCA4, RCM2=REMO2009.

[END FIGURE 10.21 HERE]

10.5.1.1 Sources of climate information

Regional climate information may be constructed from a range of sources, each resting on different assumptions and affected by different methodological limitations (Sections 10.2, 10.3 and 10.4). Depending on whether users of climate information select and analyse these sources themselves, or whether they engage with climate scientists in the construction of information, certain products may either be a source of information or an intermediate product in the construction process. Widely used sources are:

- Extrapolation of observed historical trends into the future (e.g., Livezey et al., 2007; Laaha et al., 2016). Given the role of internal variability for regional trends (Section 10.4), this approach is difficult to defend without other supporting evidence (Westra et al., 2010).
- Direct use of the numerical output from GCMs, including high-resolution GCMs (Section 10.3.1). Model data may or may not be bias adjusted (Section 10.3.1.4 and Cross Chapter Box 10.2) or weighted (Section 10.3.4.4 and Box 4.1).
- Use of the numerical output from dynamically (10.3.1.2) or statistically (10.3.1.4) downscaled GCM simulations. Model data may or may not be bias adjusted (in the case of RCMs, Section 10.3.1.4) or weighted (Section 10.3.4.4 and Box 4.1).
- Use of process understanding about the drivers of regional climate variability and change, resting in theory about e.g., dynamics and thermodynamics of the climate system as a basis for process-based evaluation, or to better understand changes in relevant regional weather (Sections 10.1.4, 10.3.3.4, 10.4.2).
- Use of idealized scenarios of possible future climates (e.g., Hallegatte, 2014) to explore the implications and consequences of such scenarios. This approach has been used to explore the response to geoengineering (Cao et al., 2016), as well as alternative scenarios where model

projections are highly uncertain (Brown et al., 2016).

- Access to information from the scientific and not peer-reviewed literature, including the engagement with climate scientists and local communities who may provide indigenous information (Rosenzweig and Neofotis, 2013). The scientific literature captures projections of climate change in a range of forms, and these may be directly accessed by users, incorporated in climate services, or form the foundations for experts consulted by users such as, for example, in communities of practice (Parker and Lusk, 2019), in a meta-analysis of papers to assess future heat mortality (Sanderson et al., 2017), or drawing on the communications to the UNFCCC about national adaptation.

In addition to the difference in models used as sources, the resulting model data may stem from a range of different experiment types targeting different purposes (Section 10.3.2). Depending on the resources, one may even design model experiments specifically for a given use case such as for the construction of event storylines (Section 10.3.2.2).

The diversity of sources may partly be explained by the large range of purposes (Sections 10.1–10.3), such that different sources of regional information may be adequate to represent different aspects of the constructed information (Sections 10.3.3.4–10.3.3.10). Regional climate information is also affected by substantial uncertainties in observational data (Section 10.2) and climate model simulations (Section 10.3). In addition, the complex interplay of different regional climate drivers and the internal variability play an important role (Section 10.4). Combinations of sources and hierarchies of model ensembles are thus required to address different aspects of the problem and to sample uncertainties as comprehensively as possible (Section 10.3.4).

However, users of climate information may face the so-called practitioner's dilemma: often a plethora of different and potentially incompatible datasets (Figure 10.21) are provided without a comprehensive and user relevant evaluation, as well as lacking a transparent and easily understandable explanation of underlying assumptions, strengths and limitations (Barsugli et al., 2013; Hewitson et al., 2014a). Often, the choice of information source is therefore not guided by selecting the most adequate sources of information, but rather determined by practical constraints such as accessibility and ease of use and may be limited to extreme cases like the use of just one model (Rössler et al., 2019a). In some contexts, the availability of information sources may also be strongly limited (section 10.5.2).

10.5.1.2 Approaches to climate information and climate messages

Historically, the construction of climate information has been embedded in a linear supply chain: extracting the source data, processing into maps or secondary data products, preparing the material for communication, and delivering to users. Such a chain, although it is intended to meet a demand for regional climate information, contains many assumptions that are not obvious to the recipients and that may introduce unforeseen propagation and growth of error, uncertainty and possible misunderstandings in the hand-over from one community to the next (Meinke et al., 2006; Lemos et al., 2012; Haines, 2019). This has led to the emergence of two new pathways for the production of regional climate information: the distillation from multiple lines of evidence in relation to the context of the information requirements (Section 10.5.4). and bottom-up approaches, also referred to as scenario-neutral impact studies (Brown et al., 2012, Prudhomme et al., 2010, Culley et al., 2016, Culley et al., 2016). The latter begins with the user's articulation of vulnerability in the context of climatic and non-climatic stressors, follows with the definition of key system thresholds of climatic variables, and only incorporates climate data to assess the likelihood of threshold exceedances. Bottom-up approaches are special cases of robust decision making (Lempert et al., 2006; Lempert and Collins, 2007; Walker et al., 2013; Weaver et al., 2013), which are designed to account for uncertainties not represented by climate models as well as non-climatic stressors. Maraun and Widmann (2018) point out the danger of producing misleading results with these approaches, if not all relevant characteristics of climatic drivers of a given impact system are accounted for. As a response, regional climate change information is increasingly being developed through participatory and context-specific dialogues that bring together producers and users across disciplines, and define climate impacts as one of the many stressors shaping user decisions (Brown and Wilby, 2012; Lemos et al., 2012).

Thus, provision of climate change information for the integration in decision making (Brown and Wilby, 2012; Lemos et al., 2012), from the perspective of the provider, relates to specific contexts of information requirements. This is increasingly recognized as paramount (e.g., Kruk et al., 2017) to construct information relevant for decisions at the regional scale and to include the user values in connecting the science with users (Parker and Lusk, 2019).

10.5.1.3 Climate services in the context of the production of regional climate information

"A climate service can be considered as the provision of climate information in such a way as to assist decision-making. The service needs to be based on scientifically credible information and expertise, have appropriate engagement from users and providers, have an effective access mechanism and meet the users' needs" (Hewitt et al., 2012). Thus, climate services include the synthesis of context-relevant climate information (Guido et al., 2012) addressing a wide range of time scales that go beyond operational weather services (Brasseur and Gallardo, 2016). From this point of view, climate services are an instrument for the production of climate information in a co-production process that is inclusive, collaborative and flexible (Vincent et al., 2018). The historical development and role of climate services is discussed in Chapter 12.

Different climate service providers use different approaches for constructing regional information. For example, the Swedish climate services (Kjellström et al., 2016) is focused on producing country-scale, high-resolution climate projections using the Rossby Centre RCM RCA4. On the other hand, Cordex.be (Termonia et al., 2018b), an initiative for the foundation of climate services in Belgium, created a multi-model small ensemble of high-resolution projections over Belgium at convection-permitting resolution and also used these to drive seven local impact models. Ekström et al. (2016) illustrated the potential pitfalls of GCM sub-sampling or the use of a single downscaled product when conducting impact, adaptation, and vulnerability research in Australia. They suggested the use of the widest range of climate change signals from all available model sources to best characterize the future and avoid possible mal-adaptation. Other examples of using high resolution downscaling products in a climate services context are the dynamical and statistical downscaling of global seasonal forecasts over Ethiopia (Nikulin et al., 2018; Tucker et al., 2018) or, at the urban scale, the future projection of extreme precipitation intensity-duration-frequency curves for climate adaptation in New York state (DeGaetano and Castellano, 2017). These examples suggest that there is *high confidence (medium evidence, high agreement)* that the development and value of climate services benefits from working in close collaboration with stakeholders and practitioners in a solution-oriented co-development approach to generate climate information (Vincent et al., 2018). In this concept of climate services users can also participate in the underpinning research by defining their needs and by developing specific requests. The experience with climate services suggests that while there exists a diversity of perspectives around what constitutes co-production of climate information (Bremer and Meisch, 2017), there is a *medium evidence* and *high agreement* that processes that support collaborative learning and knowledge production involving a diversity of expertise including both climate scientists and decision makers, results in enhanced integration of science evidence into decision (Lemos et al., 2012; Bremer and Meisch, 2017).

Climate services, apart from providing a mechanism or framework for the generation of climate messages, reports also entail a platform for the operational generation of climate information and messages. Climate services can also assist in decision-making, by periodic reports such as national assessment reports (Vincent et al., 2017) or even IPCC reports.

10.5.2 How context frames the message construction

10.5.2.1 Consideration of different contexts

Climate messages seek to build knowledge for informing adaptation and policy through a process of distilling climate information that takes account of the context of both the producer and the user and their values. Hence, without a context for the message, the distillation of the climate information cannot meet the goal of informing adaptation and policy (Baztan et al., 2017; Cash et al., 2003; Lemos et al., 2012). Section

10.1.3 identifies three implicit framing issues to construct regional messages: practical issues arising from the climate information sources, issues involving the context for constructing the messages, and difficulties in constructing messages by complex networks of practitioners. Of these, the social context leads the framing of subsequent decisions about the message construction. This requires a nuanced and holistic approach to recognize the complexity of a coupled social and physical system (Daron et al., 2014). For example, urban water managers must recognize the dependency of the city on different water resources and the interplay of both local and national government legislation that can involve a range of different constituencies and decision makers (Scott et al., 2018).

Context plays a role in determining the risks that may affect human systems and ecosystems and consequently the information needs. Context may also limit the access to information. Hence, the context brings inherent constraints on how climate messages are constructed to be optimally aligned with the application purpose. Although contexts are unlimited in variety, some key contextual elements are:

- Whether the problem formulation needs to be constructed through consultative activities that, for instance, help setting thresholds of vulnerability in complex urban or rural systems (Baztan et al., 2017; Willyard et al., 2018) or is a more a matter of addressing a generic vulnerability already identified as in the case of the frequency of flood events or recurrence intervals of multi-year droughts (Hallegatte et al., 2013).
- Societal capacity, such as cultural or institutional flexibility and willingness to respond to different messages (e.g., Hart and Nisbet, 2012; Kahan, 2012b, 2013).
- The operational capacity of the different actors, which includes users, producers, and communicators (e.g., Gorddard et al., 2016; Sarewitz, 2004).
- Potential contrasts in value systems like the different views of western countries compared to those of economies in transition or countries under development (Henrich et al., 2010a, 2010b).
- The relative importance of climate change in relation to climate variability and non-climate stressors on the time/space scales of interest to the user, which at times are not the ones initially assumed by the producers (Otto et al., 2015).
- Availability, timing and accessibility of the required climate information, including the availability of sources like observations, model simulations, literature and experts of the relevant regional climate (Mulwa et al., 2017). In developing countries, the availability of all or some of these sources may be limited (Dinku et al., 2014).

These and other contextual issues frame subsequent decisions about the regional climate message construction. For example, an engineer typically seeks quantitative information, while the policy community may be more responsive to (complex) storylines (Section 1.4.3) and how messages are positioned within an identified risk framework (Figure 10.22). Multiple contexts can coexist and potentially result in competing approaches (for example, in relation to urban governance versus regional water resource management).

[START FIGURE 10.22 HERE]

Figure 10.22: Schematic of regional climate storylines consistent with a particular climate impact of concern (red), which is associated with a meteorological hazard such as a long-term trend or a short-term event. The hazard involves a combination of thermodynamic factors linked to regional warming and particular dynamical conditions. Storylines express the fact that the same antecedent conditions could have more than one explanation in terms of the role of greenhouse gas forcing, other forcings affecting the dynamical conditions that do not scale with global-mean warming (e.g. ozone depletion, regional aerosol forcing), and natural variability. The dark blue elements represent the specified elements that define the storyline. The thicker arrows indicate that regional warming is mainly determined by greenhouse gas forcing, whilst the dynamical conditions are mainly determined by natural variability. Adapted from Shepherd (2019).

[END FIGURE 10.22 HERE]

10.5.2.2 Conditioning by values and expertise of different actors and communities

Climate messaging is inherently influenced by the values of all parties: those constructing the message, those communicating the message, those receiving the message, and critically those who construct the problem statement which the message seeks to inform. Discussion here focuses on messages targeting regions. A discussion of how values in the scientific community shape climate research appears in Section 1.2. A programme of research spanning several decades, 44 nations and over 25,000 respondents (Schwartz et al., 2012) has identified that certain types of values cluster together. Research into climate change communication has confirmed that certain clusters of values are consistently associated with positive engagement with climate science messaging (Zia and Todd, 2010; Kahan, 2012a; Corner et al., 2014). However, for a message on regional climate change to be effective it needs to recognize and respond to the values of all parties (Figure 10.23), including those of the scientists, (e.g., Bessette et al., 2017; Cash et al., 2003). Values introduce in the message construction the fact that the world is culturally, socially and economically heterogeneous, while until now the construction of messages has been mainly led by the scientific community of developed nations. The dialogue implied by Figure 10.23 is important for giving the message saliency and relevance, most notably when informing the complexity of risks for human systems and ecosystems and resilience in developing nations (e.g., Baztan et al., 2017). Part of the challenge with climate messages, especially for messages of impactful change, is that they can be based on a variety of disciplines and target people with a variety of backgrounds, which could give them differing sets of experiences, capabilities, and values, so that the messages may need to accommodate a range of normative lenses (Sarewitz, 2004; Rosenzweig and Neofotis, 2013; Gorddard et al., 2016). Lack of this recognition can make the message ineffective even if the climate information it is based on is of the highest quality.

[START FIGURE 10.23 HERE]

Figure 10.23: Effective messaging requires shared development of the actionable information that engages all parties involved and the values that guide their engagement. Participants in the development of climate messages come from varying perspectives, based in part on their professions and communities. Each of the three broad categories shown in the Venn diagram (U, P, R) is not a homogenous group, and often has a diversity of perspectives, values and interests among its members. The subheadings in each category are illustrative and not all-inclusive. The arrows connecting those categories represent the distillation process of providing context and sharing climate relevant information. The arrows that point toward the centre represent the distillation of climate messages that involves all three categories.

[END FIGURE 10.23 HERE]

There is a substantial body of evidence that shows that the receptivity of individuals to climate messages is strongly conditioned by motivated reasoning (Hart and Nisbet, 2012; Kahan, 2012b, 2013), wherein a person's reception of climate information is influenced by the values of the community with which the person identifies. This can affect people of any political persuasion, which in turn affects how critically or approvingly they accept statements provided by the scientific community. Adherence to a community's values forms part of an individual's social identity (Hart and Nisbet, 2012). Fear of losing membership of the community can easily outweigh considerations of how believable statements about climate change might be (Hart and Nisbet, 2012). Individuals thus frame their analysis and understanding of climate messages in the context of cultural values espoused by their community (Hart and Nisbet, 2012; Kahan, 2012b, 2013; Campbell and Kay, 2014; Bessette et al., 2017; Tschakert et al., 2017; Vezér et al., 2018). In addition, political activists may purposely skew messages to motivate support of their partisans (Hamilton, 2011).

Overcoming resistance to receiving a climate message is not simply a matter of presenting more information. However, simply presenting more information without recognizing the contextual elements of climate messaging listed in Section 10.5.2.1 is ineffective (Kahan, 2013). Rather, giving more information can harden an aversion to climate messages and the aversion, if present, can become stronger for people who are more scientifically literate: they feel more confident sifting through all sources of information to find support for their positions (Kahan, 2012b). Divisions over the uptake of climate messages can thus become stronger with increased knowledge and, notably, with increased capacity for reflection (Kahan, 2013). A challenge of messaging, then, is that if it is not framed carefully, it may make the sceptical person less receptive to further messages about climate change (Hart and Nisbet, 2012; Shalev, 2015).

Successful framing of climate messages thus seeks to identify interests in targeted groups that yield a common ground between the messenger and the recipients for viewing the messages and responding to them. Audiences may view climate change as a problem distant in time and space (Spence et al., 2012). Linking to climate-change impacts more immediate and local can overcome this psychological distancing (Wiest et al., 2015; Polk, 2018). However, audiences may deny the messaging considered highly threatening (Brügger et al., 2015; McDonald et al., 2015). In addition, an important factor is recognizing that an aversion to climate change solutions, such as those that pose economic challenges (e.g. Bessette et al., 2017), may be a greater cause of a person's negative response to climate messages than the message itself (Campbell and Kay, 2014). The proposed response measures may violate personal or community values, regardless of the level of acceptance of the message of climate change. Recognising this problem, successful framing and response have occurred when climate information is presented in a region-focused context with respect to a local challenge posed by climate change. Thus, two states in the United States of America with fairly conservative leadership, which tend to be more sceptical about climate change, have passed initiatives that respond to specific, local impacts of climate change: rising sea level in Florida and water-resource shortfalls in Arizona (Kahan, 2013). Key factors were recognizing a serious impact and avoiding a central motivation of fighting global climate change. Identifying positive outcomes of adaptation and mitigation efforts also appears to promote successful climate messaging (Bain et al., 2012).

The effectiveness of climate messages can increase if developed in partnership with the communities for which the message is intended (Tschakert et al., 2016) (Figure 10.23), an approach that can inspire trust among all parties and at the same time promote a co-production process (Cash et al., 2003). Trust in the messenger thus acts as a heuristic shortcut, allowing the recipient to make decisions about what messages to believe (Slovic et al., 2004), and audiences have the greatest trust in messengers perceived to understand their context and share their values and identity (Corner et al., 2014). Such partnerships are expedited if the relevant climate information generation that leads to the messaging is transparent and accessible (Vezér et al., 2018). This is not always possible with climate and climate impacts simulation, but developing mental models can help, provided they are informed by values (Bessette et al., 2017). This does not preclude the climate-research community from taking steps to develop and convey messages. Indeed, communicating expert consensus about contested scientific issues is beneficial (Goldberg et al., 2019). Climate services, in particular, can become an effective means for taking messages from the climate community and crafting them to be consistent with the needs, interests and values of stakeholder communities.

A regional message on climate change is intended to inform decision makers. There is *high confidence* (*medium evidence* and *high agreement*) that including users ensures that the context contributes to formulating the message, especially when the messaging involves complex, contextual details. As such, the context and values (of both users and producers) become a central component in the development of effective regional information for a number of applications.

10.5.2.3 The relative roles of spatial and temporal resolution in relation to decision scale

Climate processes occur on a range of spatial and temporal scales, from global to local, from centuries and longer to days or less (Section 10.1.2 and Figure 10.2). Similarly, decisions by stakeholders cover a range of spatial and temporal scales that can vary with the size of their jurisdiction and scope of activity, which determine their (spatial and temporal) decision scales. However, the link between decision scales and the spatial and temporal resolution of climate and related natural-system information is not straightforward, and failure to recognize mismatches between the two can undermine the effectiveness of messages (Cumming et al., 2006; Sayles, 2018).

The scale of regional climate information does not have to be the same as the decision scale. For example, process-based storylines valid at large scales can be used to create messages that are relevant to making local decisions. Thus, an expectation of increased multi-year drought episodes over a subcontinental region due to changes in circulation patterns can be relevant to decisions by an individual farmer. On the other hand, extreme precipitation processes can occur on scales of tens of kilometres and smaller and thus require high resolution climate information when projected future changes (e.g., Xie et al., 2015). An important factor to develop effective climate messages is matching through the distillation process the vulnerability of the social and economic systems, which range from, for instance, a farmer to a national agricultural ministry, with the most prominent changes in the natural system (Andreassen et al., 2018; O'Higgins et al., 2019). Thus, more sophisticated matching of spatial and temporal resolution of climate information with decision scales might require engagement across a hierarchy of governance structures at national, regional and local level (e.g., Lagabrielle et al., 2018).

10.5.2.4 Addressing compound events and non-traditional variables

Users often require and need information from compound events such as concurrent drought and heat waves (Zscheischler and Seneviratne, 2017) or concurrent precipitation and wind extremes (Martius et al., 2016) in the form of non-traditional diagnostics. These diagnostics are post-processed output from models and observations also known as hazards (Chapter 12) that are regional in nature: heat stress, heating degree days, cooling degree days, growing degree days, drought indices, fire-weather indices, or evaporation surplus. Compound events refer to the combination of multiple drivers and/or hazards that contribute to societal or environmental risk (Zscheischler et al., 2018). Because large impacts are often not linked to single climate extremes, a good understanding of compound events is critical for managing the climate-related risks for human systems and ecosystems (Leonard et al., 2014). Awareness for correlated hazards is increasing in the research community and crucial for risk assessment because compound hazards often lead to disproportionate damages. This has been shown for compound precipitation and wind extremes and their impacts on infrastructure (Martius et al., 2016), compound storm surge and rainfall extremes and associated flood damage (Wahl et al., 2015) and compound drought and heat and their effect on terrestrial carbon uptake (Zscheischler et al., 2014).

Non-traditional variables here refers to those that are not part of standard climate model output (e.g. CMIP archives (Eyring et al., 2016a)) and that depend on multiple climate variables. Many, however, can directly be computed from the available climate model output. For instance, heat-stress indicators are typically based on some combination of temperature and humidity (Lee, 1980). Many impact assessments rely on absolute values of non-traditional variables. For instance, a heat index (i.e., an apparent temperature taking into account both air temperature and relative humidity) larger than 40.6°C is considered dangerous (e.g. Anderson et al., 2013). Similarly, energy consumption for heating and cooling of buildings relies on precise estimates of heating and cooling degree days. Crop models rely on the number of growing degree days. Fire warnings are issued when a specific fire-related indicators exceed a certain threshold (de Jong et al., 2016). Due to biases in climate models, assessing risks associated with climate through projections of non-traditional variables is not straightforward and typically requires some sort of bias adjustment (Cross-Chapter Box 10.2) of either the standard climate variables or the non-traditional variable.

When events are very complex or rare, it is often difficult to assign likelihood to them. In such cases, storylines (Sections 1.4.3 and 10.5.3) can be used to explore potentially devastating events that would have low or unknown probabilities (Sutton, 2018). These are particularly helpful for studying compound and cascading events, which can often not be addressed by standard probabilistic frameworks. This is accomplished by presenting physically self-consistent unfolding of past events, or plausible future events or pathways, which frame risk for human systems and ecosystems in an event-oriented rather than a probabilistic manner, while providing a physical basis for partitioning uncertainty and explore the boundaries of plausibility (Shepherd et al., 2018).

10.5.3 Narratives and storylines

Narratives and storylines are approaches that can be used to communicate climate change messages (e.g., Dessai et al., 2018; Fløttum & Gjerstad, 2017; Moezzi et al., 2017; Scott et al., 2018), or integrate climate information into an impact assessment (e.g., Strasser et al., 2019) (Figure 10.22; Section 1.4.3). Narratives/storylines have a purpose to develop evidence-based textual descriptions of some state of the past, present, and future climate, out of which many possible storylines of evolution and events may be constructed. For example, one may have a narrative based on evidence from CMIP5 or CMIP6, and there may be many storylines that connect the narrative to the user context in terms of pathways, events, impacts or consequences. It is recognized that there is need for expert judgment of projections of changing climate when using climate model output for adaptation and mitigation planning (Lempert et al., 2006; Thompson et al., 2016; Dessai et al., 2018). Storylines built on narratives of the projected change that can arise in many ways, allow tailoring them for their intended use (e.g., Zappa and Shepherd, 2017; James et al., 2015; Stevens et al., 2016; Hazeleger et al., 2015). Storylines may also be a core element in future thinking in decision making when messages are timed to support the application of new information in decision cycles or in a framework for future thinking (Corballis, 2019), or even as an approach to conveying information from climate models (Corballis, 2019). It is worth mentioning that, in a broader IPCC context, the term scenario storyline is used as a narrative description of a scenario (or family of scenarios) highlighting their main characteristics, relationships between key driving forces and the dynamics of their evolution as indicated in Chapter 1.

The use of the terms narratives and storyline is not consistent in the literature. They could refer to using climate processes and expert elicitation to convey information and/or messages on regional precipitation (Dessai et al., 2018), plausible storylines of atmospheric circulation change and other physical processes (Hazeleger et al., 2015; Zappa and Shepherd, 2017) (Figure 10.22) or the interchangeable use of concepts beyond analytical approaches (Moezzi et al., 2017). The use of these terms ranges from early compound phrasing of narrative storylines (Schneider, 2001) to emergent transdisciplinary narrative framing (Scott et al., 2018) and storylines derived from mutually exclusive but equally plausible changes in the atmospheric circulation (Zappa and Shepherd, 2017).

Storylines are complementary to data-based approaches such as ensemble means and probabilistic projections. They are especially valuable for recognizing, for instance, risks associated with the emergence of projected low-probability high-impact events. Storylines can be tailored to recognize the values and interests of the intended audiences (Kok et al., 2014; Hazeleger et al., 2015; Bhave et al., 2018), providing the sequences of weather and climate events, such as drought or pluvial episodes, that are part of the climate change scenario in a succinct, physically plausible manner (Hazeleger et al., 2015).

Climate-related risks for human systems and ecosystems are typically greater in developing countries, owing in part to their greater vulnerability and lower capacity for adaptation (e.g. Bhave et al., 2016). Storyline development, however, can engage experts on a region's climate (Dessai et al., 2018) and/or stakeholders (Bhave et al., 2018; Scott et al., 2018) to co-produce storylines that foster adaptive responses to efficiently account for the climate information needs of the region.

10.5.4 Distillation and multiple lines of evidence

The preceding sections laid out the diversity of sources of climate information (Section 10.5.1) and decision contexts (Section 10.5.2). Similar diversity also exists in the way users interact with climate science, ranging from data delivery with a focus on visualisation and user-friendly interfaces (e.g. portals), through to intensive long-term engagement with user communities deploying trans-disciplinary principles. As a result, also a range of approaches to distilling a climate message from different sources of information in a given context exist; Section 10.5.4.1 (below) provides examples. For simulations, in particular, confidence in projections of regional climate can be increased when comparing the response of processes at different scales across hierarchies of models. Recent coordinated modelling efforts spanning GCMs (CMIP; Eyring et al., 2016), high-resolution GCMs (HighResMIP; Haarsma et al., 2016), standard RCMs (CORDEX; Giorgi and

Gutowski, 2015) and convection-permitting RCMs (Coppola et al., 2018) provide unprecedented opportunities to study the response of processes across a broad range of scales and thereby substantially increase our understanding of which models are adequate for which purpose.

The term distillation lacks a clear definition yet speaks to the challenges of constructing or distilling messages of value to society from a diverse range of evidence that may contain disparate elements. In principle, distillation has two aspects, namely the construction of (potentially user-targeted) information and the construction of a climate message in a specific context, targeting a specific purpose and set of values. The former involves data distilled from multiple lines of evidence, using knowledge from experts and with uncertainties comprehensively assessed to give physically plausible climate information. The latter translates the information explicitly into the user context, such as by linking to experience, by formulating a narrative, by highlighting the relevance for the user context, or by putting into the context of non-climatic stressors.

Distilling climate messages for a specific purpose involves including non-climate-scientists in the process of making assumptions, or at least guiding assumptions about the climate research conducted (Collins and Ison, 2009; Wildschut, 2017; Bhave et al., 2018). Importantly, the application of trans-disciplinary engagement processes that emphasise the role of non-scientists in the learning and knowledge production process builds relationships and trust between information users and producers, which is arguably as important for the uptake of climate science into decision making as the nature of the climate information itself (Section 10.5.2). Although there are multiple practical issues involving communication (Rössler et al., 2019), such as providing data in a format that users can read, being mindful of the contextual issues raised in Section 10.5.2 allows non-scientists to be involved in decisions about approaches and assumptions for the distillation and thus take ownership of the resultant information and make informed decisions based on the distilled information and messages (Pettenger, 2016; Verrax, 2017).

10.5.4.1 Information construction

Data, either from observations or models, is in general not information, but may contain relevant information if interpreted appropriately (Hewitson et al., 2017). Relevance is controlled by a given user context and relates to the required time and space scales (Section 10.5.2.3), the characteristics of required variables, and the meteorological and climatic phenomena driving these variables (Section 10.1.3). For example, if climate information for driving impact models is sought (e.g., McSweeney et al., 2015), the impact modelling analysis is the specific user context.

Reconciling different sources of information has two aims: first, assessing the adequacy of different sources in the given context and thereby potentially omitting (or down-weighting) selected sources (Sections 10.3.3), and, second, integrating different sources into a broader picture within a context (Sections 10.3.4). The first aim may in principle lead to a reduction of uncertainty, whereas the second serves to sample uncertainty of different aspects of the given problem as comprehensively as possible.

A non-comprehensive selection of approaches that may contribute to the construction of information is:

- preselection of models based on a priori knowledge on their adequacy for a given context, e.g., based on resolution or structure (e.g. coupled vs. uncoupled model components, simulated processes, structure of statistical downscaling and bias adjustment methods);
- overall assessment and inter-comparison of different sources of information, including hierarchies of models, identification of potentially conflicting results (Figure 10.21);
- testing whether differences in simulations can be explained by internal variability, ideally by initial condition grand ensembles (Section 10.3.4.3);
- assessing the interdependence of chosen models to identify the amount of independent information (Section 10.3.4.4);
- process-based evaluation with focus on those processes that are relevant for the specific application, resulting in an assessment of fitness-for-purpose (Sections 10.3.4–10.3.10);
- tracing differences in projections to the representation of fundamental processes, e.g. by using storylines (Sections 10.3.4.2 and 10.5.3) or sensitivity simulations (Section 10.3.2.3);

- producing event storylines to explore uncertainties not sampled by available model ensembles (Shepherd et al., 2018), for example in pseudo-global warming experiments (Section 10.3.2.2);
- comparing observed trends with projected trends, potentially to constrain projections with, for instance, the Allen-Stott-Kettleborough method (Allen et al., 2000; Stott and Kettleborough, 2002; Stott et al., 2013) to explain drivers of past observed trends (Section 10.4.2) to understand future trends;
- integrating present-day performance via emergent constraints to reduce projection uncertainty (Section 10.3.2);
- sub-selecting ensembles for further impact studies while sampling as much uncertainty as possible (Section 10.3.4.4);
- possibly weighting or omitting models depending on the outcome of the evaluation (Section 10.3.4.4);
- constructing information on different physical aspects of the problem (e.g., changes in driving large-scale circulation (Section 10.3.3.4) or changes in local convective precipitation (Section 10.3.3.5)) from potentially different sources of information;
- using process understanding to develop possible events/storylines that have never happened before (Lin and Emanuel, 2016);
- complementing the sources with expert judgement (e.g. integrating knowledge from theory or experience that is available from experts or the literature).

These approaches can be used in combination to increase confidence in the climate information (Hewitson et al., 2017). The first step in the climate information distillation process is interrogating the user context to determine the best approaches, although there can be cases where the use context is essentially unknown.

The provision of complete climate information includes explanations on the potential use and misuse of the product (Arnold; Street, 2016; Lamb, 2017) and documentation of the assumptions and choices made in producing the information. This is particularly relevant if the information is provided as a generic, publicly accessible product without a specific context (Hewitson et al., 2017).

10.5.4.2 Barriers to message construction

As implied by Section 10.5.2, meeting the needs of users can be a substantial challenge for climate scientists if they misunderstand user needs and context (Porter and Dessai, 2017). Several barriers in user communities can trigger and sustain this challenge. This can include an institutional aversion to incorporating new tools into decision making (Callahan et al., 1999). Coincident with this factor, there may be limited staff capacity, lack of management support and lack of a mandate to plan for climate change (Lee and Whitely Binder, 2010).

Following from those challenges, climate information and messaging production often occurs under the overarching assumption that uncertainty is a problem and reducing uncertainty is the priority (Eisenack et al., 2014; Otto et al., 2016b). This is both a psychological barrier (Morton et al., 2011), as well as pragmatic barrier in cases where uncertainty appears to limit the ability to make decisions (Mukheibir and Ziervogel, 2007). However, where in-depth engagements with decision contexts are undertaken, these initial barriers are often dismantled to reveal a more complex, nuanced and potentially more productive intersection with climate uncertainty (e.g., Lemos et al., 2012c; Moss, 2016b; Rice et al., 2009). Specifically, disclosure of all uncertainties in the climate information and messages, transparency about the sources of these uncertainties, and tailoring the uncertainty information to specific decision frameworks has the potential for reducing problems of distilling a message with uncertain climate information (Otto et al., 2016b).

10.6 Comprehensive examples of constructing regional climate messages

10.6.1 Introduction

Section 6 presents three comprehensive examples of constructing regional climate messages that integrate the multiple sources of regional climate information presented in this chapter. Examining the activities for constructing these messages exposes the strengths and challenges in linking the different sources, while also exposing the assumptions behind and consequences of decisions made in the process. The examples are framed within a human dimension to provide context for their regional climate messages. The recent Cape Town drought, the South Asian monsoon and the Mediterranean summer warming have been chosen, since most of the components for constructing regional climate messages outlined thus far in Chapter 10 are directly relevant to each case.

The three comprehensive examples follow a similar structure:

- Motivation and regional context
- The region's climate
- Observational issues
- Relevant anthropogenic and natural drivers
- Model simulation and attribution over the historical period
- Future climate information from global simulations
- Future climate information from regional downscaling
- Potential for abrupt change
- Storyline and narrative approaches
- Messages distilled from multiple lines of evidence

Following this structure, construction of the regional climate message presented in these examples depends on an assessment of observational uncertainty (Section 10.2) and its role in determining the realism of a climate signal, the evaluations of model bias to judge the adequacy for purpose of a given model (Section 10.3), and expert judgement. Accounting for these factors can lead to attribution of historical climate-change signals (Section 10.4). At the regional scale, attribution must also account for the interplay between externally forced signals and unforced, internal modes of variability; confirmation that an internal mode of variability has driven change at the regional scale is just as valuable for a stakeholder as any attribution to an external source. The sources of information that provide multiple lines of evidence for the messages may conflict, thus requiring distillation of the evidence (Section 10.5) to arrive at the most confident statements. When moving from global climate information to messages at the regional scale, following the structure above provides a basis for arriving at relevant, credible, salient and actionable climate messages. The comprehensive examples of distilling climate messages thus show the value of working with multiple lines of evidence to discern robust messages of climate change for a region.

10.6.2 Cape Town drought

10.6.2.1 Motivation and regional context

Cape Town's "Day Zero" water crisis in 2018 threatened a shut-down of water supply to 3.4 million inhabitants of the city and resulted in domestic water use restriction of 50 litres per person per day lasting for 9 months, punitive water tariffs, and temporary closure of irrigation systems. Problems with water supply in many large cities in developing countries are endemic and rarely reported internationally. The water crisis in Cape Town attracted considerable international attention to a city with functional government structures, well developed services (compared to other urban centres in Africa), a centre of international tourism, and an economic hub with GDP of USD22 billion (~USD 6,000 per capita) (CoCT, 2018) that exceeds that of many developing countries. The crisis was widely seen as a harbinger of future problems to be faced by the city, and a highlight of vulnerability of many cities in the world resulting from interplay of three factors: 1) the fast urban-population growth, 2) the economic, policy, infrastructural and water resource paradigms and constraints, and 3) anthropogenic climate change.

The Cape Town's crisis was a result of a combination of a strong multi-year meteorological drought (Figure 10.24), the severity of which is estimated at 1 in 300 years (Wolski, 2018), and factors related to the nature of the water supply system, operational water management and water resource policies. Cape Town was very successful in implementing water saving actions after the previous drought of 2000–2003, reducing water losses from over 22% to 15.2% (Frame and Killick, 2007; DWA, 2013), in effect decoupling a previous link between population and growth in water demand. As a consequence, Cape Town won a Water Smart City award only three years prior to the crisis. The water-saving actions, together with changing priorities in water resource provision from infrastructure-oriented towards resource and demand management, have likely led to delays in implementation of the expansion of water supply infrastructure (Muller, 2018). The expansion plan, formulated a decade prior to the crisis, fully anticipated long-term climate change-related drying in the region (DWAF, 2007). The crisis also exposed structural deficiencies of water management and inadequacy of the policy model where decisions about local water resources are taken at a national level, particularly in a situation of political tension (Visser, 2018).

[START FIGURE 10.24 HERE]

Figure 10.24: Historical and projected rainfall and Southern Annular Mode (SAM) over the Cape Town region. (a) Yearly accumulation of rainfall (in mm) obtained by summing monthly totals between January and December, with the drought years 2015–2017 highlighted in color. (b) Monthly rainfall for the drought years (in color) compared with the 1981–2014 climatology (grey line). Rainfall in (a) and (b) is the average of 20 quality controlled and gap-filled series from stations within the Cape Town region (31ºS–35ºS, 18ºW–20.5ºW). (c) Time series of historical and projected rainfall anomalies (%, baseline 1980–2010) over Cape Town region and SAM index. Observed data presented as 30-year running means of relative total annual rainfall over the Cape Town region for station-based data (black line, average of 20 stations as in (a) and (b)), and gridded data (average of all grid cells falling within 31ºS–35ºS, 18ºW–20.5ºW): the Global Precipitation Climatology Centre (GPCC) version 2018 (Schneider et al., 2017) (brown line) and the Climate Research Unit (CRU TS) version 4.03 (Harris et al., 2014) (green line). Model ensemble results presented as the 90th-percentile range of relative 30-year running means of 39 CMIP5 (blue shading), 12 CMIP6 (red shading), 6 COREX driven by 1 to 10 GCMs (orange shading) and 6 CCAM (green shading) individual ensemble member's rainfall, respectively. SAM calculated from sea-level pressure reanalysis and GCM data as per Gong and Wang (1999) and averaged over the aforementioned bounding box. The orange, green and grey lines correspond to NCEP/NCAR (Kalnay et al., 1996), ERA20C (Poli et al., 2016b) and 20CR v3 (Slivinski et al., 2019), respectively. (d) Historical and projected trends in rainfall over the Cape Town region and in SAM index. Observations and gridded data processed as in (c). Trends calculated as Theil-Sen trend with block-bootstrap confidence interval estimate. Markers show median trend, bars 95% confidence interval. GCMs in each CMIP group ordered according to the magnitude of trend in rainfall, and the same order is maintained in panels showing trends in SAM.

[END FIGURE 10.24 HERE]

Economic and social impacts of the crisis were significant. Loss of revenue of companies of all sizes resulted from the scaling down of water-dependent activities, but also from the need to invest in water efficient technologies and processes. The upside, however, is that the latter likely increased city's resilience in the long-term. Tourism was affected too through reduced arrivals and bookings, although only temporarily (CTT, 2018). In the agricultural sector, 30,000 people were laid-off and production dropped by 20% (Piennaar and Boonzaaier, 2018). The crisis initially polarized the society, with conflict emerging between various water users and erosion of trust in the government, but eventually social cohesion and an acute awareness of water resource emerged (Robins, 2019).

10.6.2.2 The region's climate

An evaluation of the relative role of rainfall and temperature signal in the 2015–2017 hydrological drought gives a strong indication that lack of rainfall was the primary driver (Otto et al., 2018). Thus, the remainder of this section focuses on rainfall.

Cape Town is located at the south-western tip of Africa, with an approximately 100 km x 300 km region receiving 80% of its rainfall during the austral winter, spanning March to October, with the largest portion in JJA. The region is surrounded by arid and semi-arid regions with summer rainfall regime. In the vicinity of Cape Town, rainfall is strongly heterogeneous, ranging from ~300 mm/year in coastal plains to >2,000 mm/year in mountain ranges. The Cape Town water supply relies on surface water reservoirs located in and supplied from a few small (~800 km^2 in total) mountain catchments. Cape Town's region receives 85% of its rainfall from a series of cold fronts forming within the mid-latitude cyclones. The remainder is brought in by infrequent cut-off lows that occur throughout the year (Favre et al., 2013). This creates a very strong water resource dependency on a single rainfall delivery mechanism, which is potentially strongly affected by anthropogenic climate change (Section 10.6.2.3).

The climatic event underlying the crisis was a multi-year drought, with strong rainfall anomalies in shoulder seasons (March to May, MAM, and less strongly in September to November), and average rainfall in June and July (Sousa et al., 2018a; Mahlalela et al., 2019). The anomaly resulted from fewer rainfall events and lower average intensity of events. The anomaly was strongest in the mountainous region where water supply system's catchments are located (Wolski et al., submitted).

Although the 2015–2017 drought was unprecedented in the historical record, Cape Town has experienced other droughts of substantial magnitude, notably in the 1930s, 1970s and more recently in 2000–2003. Long term (>90 years) rainfall trends are mixed in sign, location-dependent, and weak (Kruger and Nxumalo, 2017; Wolski et al., submitted), and mixed in sign in mid-term (~50 years; MacKellar et al., 2014). In the south-western part of the region, rainfall is mostly decreasing in the post 1981 period, particularly in DJF and MAM, although there is no trend or a weak wetting in JJA (Sousa et al., 2018; Wolski et al., submitted). Rainfall trends of similar magnitude and duration to the post-1981 trend accompanied previous strong droughts in the region (Wolski et al., submitted).

10.6.2.3 Observational issues

Compared to other African countries, South Africa and the Cape Town region have good instrumental weather data. Records start in late 1800s, with in excess of 10 gauges reporting since 1920s, expanding to ~80 gauges in 1980s, and reduction in number or rain gauges since. Few records are available in the mountains receiving more than 1,000 mm/year. In view of strong heterogeneity of rainfall, the changes in number of stations contributing to datasets such as CRU and GPCP results in their unreliability in the region (Wolski et al., submitted) (Figure 10.25).

Paleoclimate studies reveal that long-term rainfall variability in the winter rainfall region of South Africa is consistent with the general model relating it to the warming/cooling-induced latitudinal migration of the westerlies and transformation of the sub-tropical high pressure belt and associated hemispherical processes (Section 10.2.3.3 for further discussion of paleoclimate analysis). Winter and summer rainfall regions are characterized by opposite rainfall anomalies, with higher rainfall in the former associated with lower rainfall in the latter, and vice versa, which reflects the mid-latitude and tropical control respectively (Hahn et al., 2016). The synchronicity of winter rainfall with Antarctic ice core-derived polar temperature anomalies is consistently revealed in studies using different paleo-climate proxies and time scales of 1.4k (Stager et al., 2012), ~3k (Hahn et al., 2016) and 12k years (Weldeab et al., 2013). This general pattern is consistent with patterns detected in other austral winter rainfall regions (South America and Australia/New Zealand) as shown by the common drying trend during the Medieval Climate Anomaly (900–1400 AD) and wetting during Little Ice Age (1400–1800 AD). However, region-to-region differences in rainfall regimes arise at shorter (decadal) time scales that likely reflect influence of locally-relevant processes in each of the southern ocean's basins affecting these regions and modifying the influence of the position of the westerlies (Stager et al., 2012). In the case of South African winter rainfall region, these specific factors likely include the Agulhas current's interaction with the Atlantic, resulting in changes in SST and coastal upwelling, as well as modification of the wind tracks by topography (Stager et al. 2012).

10.6.2.4 Relevant anthropogenic and natural drivers

Considering the primary rainfall delivery mechanism, frontal rain, the dominant large-scale drivers of relevance are those that affect the cyclogenesis, frontogenesis and the latitudinal position and moisture supply of the mid-latitude westerlies. From that perspective, the region's rainfall is linked to the Antarctic Oscillation (AAO; Reason and Rouault, 2005) or Southern Annual Mode (SAM), the dominant monthly and interannual mode of Southern Hemisphere atmospheric variability, and a measure of the pressure gradient between high and mid-latitudes. The Cape Town region's rainfall is also potentially linked to other hemispheric phenomena, such as the expansion of the tropics and, specifically, the South Atlantic high-pressure system and the position of the subtropical and polar jets that although influenced by the SAM/AAO also vary independently of it.

The relationships between these phenomena and Cape Town rainfall have not been thoroughly investigated outside of the context of the 2015–2017 drought, but the drought itself was associated with the poleward expansion of the subtropical anticyclones in the South Atlantic and South Indian Oceans and (a resulting) poleward displacement in the moisture corridor across the South Atlantic (Sousa et al. 2018), as well as a weaker subtropical jet (Mahlalela et al., 2019). Burls et al. (2019) also link the decline in rainfall days to the increase in sea-level pressure along the poleward flank of the South Atlantic high-pressure system and the intensity of the post- frontal ridging high. Additionally, there is a possible linkage between rainfall and near-shore SST cold anomalies arising due to upwelling driven by Ekman transport related to the reduction of westerly and increase in the south-easterly winds. These might lead to suppression of convection and reduction of rainfall over land (Rouault et al., 2010). All these phenomena are conceptually consistent with the poleward migration of the westerlies and expansion of the tropics.

Rainfall in the Cape Town region also responds to SST anomalies in the Southeast Atlantic, including the Agulhas Current retroflection region, which may drive intensification of the low-pressure systems, leading to the trailing front strengthening as it makes landfall over the Cape Town region (Reason and Jagadheesha, 2005). There are also linkages at seasonal time scale between the Cape Town region's rainfall and Antarctic sea ice (Blamey and Reason, 2007).

In addition to the mid-latitude controls, sub-tropical processes also play the role in the Cape Town region's rainfall variability. The 10˚–30˚S region of sub-tropical Atlantic, parts of South American continent and even parts of the African continent north of Cape Town are sources of moisture to atmospheric river events contributing to frontal rainfall (Blamey et al., 2018; Ramos et al., 2019), with implications for the 2015–2017 drought (Sousa et al., 2018a). Also, the second major rainfall contributing system, cut-off-lows, is conditional on moisture supply from the sub-tropics (Abba Omar and Abiodun, 2020).

In spite of evidence linking the drought and recent rainfall trends to the hemispheric process of poleward migration of the westerlies, at annual time scale, correlations between the Cape Town region's rainfall and the main index expressing that process, i.e., the SAM/AAO, are, however, weak and suggest domination of local circulation anomalies over hemispheric forcing (e.g., Seager et al., 2019), with stronger relationships at near-decadal time scales (Reason and Rouault, 2005). Note also that, while in the post-1930 period, the SAM/AAO displays a long-term trend, the Cape Town region's rainfall does not, and only the post-1979 trends of rainfall and SAM/AAO are conceptually consistent (i.e. upward trend in the SAM/AAO is associated with a downward trend in rainfall (Section 10.6.2.5 and Figure 10.24). Also, there is good agreement between the seasonality of the SAM/AAO and rainfall trends in the post-1979 period: a drying trend appears strongly in DJF and MAM, but not in JJA and September to November (Wolski et al., submitted), and trends in the SAM/AAO have similar seasonal dependence (Lim et al., 2016b). Additionally, there is a similar seasonal pattern in the post-1979 trends in indices capturing the southern edge of the tropical high pressure cell (Grise et al., 2018).

In the longer-term, Cape Town region rainfall is characterized by a multi-decadal scale quasi-periodicity (Figure 10.24; Dieppois et al., 2019; Wolski et al., submitted), with the 2015–2017 drought, and previous strong droughts (1930s and 1970s) occurring during its low phases. However, the studies linking the Cape Town 2015–2017 drought to the hemispheric processes expressed by the SAM/AAO (Sousa et al., 2018a; Burls et al., 2019; Mahlalela et al., 2019) focused almost exclusively on the post-1979 period, when global reanalyses are available. The detailed understanding of drivers of previous (1930s and 1970s) Cape Town region droughts and the role of hemispheric processes expressed by the SAM/AAO in the pre-1979 period is missing.

The SAM/AAO varies with a characteristic decorrelation time of ~2 weeks, but its low frequency variability is influenced by GHGs (Fyfe et al., 2012), stratospheric ozone (Arblaster et al., 2011; Thompson et al., 2011) and ENSO (Lim et al., 2016a). The historical trend in the SAM/AAO is related to ozone depletion, and the influence of GHGs on the SAM/AAO is similar in nature to that resulting from the depletion of ozone in the Antarctic. The ongoing ozone recovery compensates for the GHG increase, but the GHG increase is projected to dominate after 2045 (Barnes et al., 2014a). The influence of ozone, however, appears mostly in the austral summer the SAM/AAO state, and it is thus uncertain whether or not ozone dynamics have impacts on austral winter rainfall in general, and the Cape Town region's winter and early winter rainfall in particular.

The relationship between ENSO and Cape Town's rainfall is weak and time-inconsistent, showing the strongest impact in May to June (Philippon et al., 2012). During the drought, there was an El Niño event in the 2015–2016 season, but during the rest of the drought period ENSO was in a neutral state, and no relationship between ENSO on the drought has been elucidated (Sousa et al., 2018a; Mahlalela et al., 2019). ENSO, however, influences large scale processes and phenomena described earlier that are of relevance from the drought perspective. The relationship between ENSO and the SAM/AAO is complex, with various ENSO "flavours" influencing the SAM/AAO differently in different seasons (Ding et al., 2012). Similarly, ENSO impacts meridional circulation and thus the subtropical anticyclone as well as the polar and sub-tropical jets (Seager et al., 2019), however, modifying rather than driving their role in Cape Town's rainfall.

10.6.2.5 Model simulation and attribution over the historical period

Due to the small scale of the Cape Town region, it is difficult to robustly compare CMIP5 GCM simulations to observations. However, in general, the CMIP5 models capture well the nature of seasonality, such as the dominance of austral winter rains, although they overestimate the peak and underestimate the shoulder season rainfall (Mahlalela et al., 2019). Trends in rainfall are particularly difficult to assess as they are generally weak and depend strongly on the time period and dataset adopted for the analyses. Throughout the 20th century, ~50% of CMIP5 and CMIP6 GCMs simulate a significant decline in total annual rainfall, which is not consistent with the lack of robust long-term trend in observations (Figure 10.24).

Models capture the overall manifestations of the observed main hemispherical processes, such as the expansion of tropics, positive trend in the SAM/AAO and the poleward shift of the westerly jet. However, they fail to capture details of their observed climatology and variability (Simpson and Polvani, 2016), and the magnitudes of simulated trends vary, though the models typically underestimate observed trends (Purich et al., 2013; Staten et al., 2018). In general, although CMIP5 models fail to capture the influence of ENSO on the SAM/AAO on a month-to-month basis, they do capture the SAM/AAO-regional rainfall association, although not consistently across all seasons (Purich et al., 2013; Lim et al., 2016b).

10.6.2.6 Future climate information from global simulations

CMIP5 and CMIP6 models show strong consistency in a drying signal for the Cape Town region, with the reduction in total annual rainfall ranging up to 20% by the end of the twenty-first century (Almazroui et al. (submitted); Figure 10.24). This is a robust signal across the ensembles compared to the summer rainfall region of southern Africa, where the climate change signal varies spatially: stronger drying in the west and moderate drying or weak wetting in the east (DEA, 2013, 2018) (see Atlas.5.2 for further discussion of southern Africa precipitation projections). Rainfall changes projected for the Cape Town region are consistent with projected changes in hemispherical-scale processes and regional scale dynamics that point toward reduced frequency of frontal systems affecting that region. There is a robust signal in CMIP5 models for the Southern Hemisphere in terms of poleward expansion of the tropics (Hu et al., 2013b), poleward displacement of mid-latitude storm tracks (Chang et al., 2012), increase in strength and a poleward shift of the westerly winds (Bracegirdle et al., 2018) and sub-tropical jet-streams (Chenoli et al., 2017), and a shift toward a more positive phase of the SAM/AAO (Lim et al., 2016b).

However, there is also a substantial increase in the frequency of atmospheric rivers and integrated water vapour transport towards the Southwest coast of southern Africa in the projected climate (Espinoza et al., 2018). This behaviour has strong implications for the region, as most topographically high locations receive rainfall from persistent atmospheric rivers (Blamey et al., 2018), and reduction of tropical moisture transport was identified by Abba Omar and Abiodun (2020) as one of the significant drivers of the 2015–2017 drought. A thorough understanding of the role of atmospheric rivers in the Cape Town region under changing climate is missing.

10.6.2.7 Future climate information from regional downscaling

Dynamical downscaling studies implemented with a stretched-grid CCAM model (Engelbrecht et al., 2009) revealed a signal compatible with the GCM ensemble, i.e., consistent drying throughout the region, amplifying in time, irrespective of the considered GHG emission scenario and the generation of GCMs (DEA, 2013, 2018). More recent high-resolution (8 km) simulations confirm a similar direction of future change. A multi-model CORDEX ensemble indicates a robust signal of reduction of total annual rainfall in the future, although there is less agreement on how changes in rainfall occurrence may evolve in the region, such as whether through fewer consecutive rain days or longer dry spells (Abiodun et al., 2017; Maúre et al., 2018). For the end of the century under RCP8.5, Dosio et al. (2019) compared a CORDEX ensemble with its driving GCMs and showed that the drying is associated with an increase in the number of consecutive dry days and a reduction in number of rainy days. These results are consistent with the driving GCMs for all the precipitation indices, and they are robust independently of the choice of the RCM or GCM.

Statistical downscaling results using a perfect-prog method (Hewitson and Crane, 2006; Section 10.3.1.4.1), in contrast to the overall drying simulated by GCMs, indicate possible wetting in the region, particularly in the mountainous catchments (DEA, 2013). While the result is theoretically justifiable by thermodynamic considerations in a warming climate, it is possible that this is a spurious effect resulting from the fact that the method was applied using predictor variables that inadequately reflect drivers of rainfall variability in the region (Wolski et al., 2018). There is not enough understanding of the interplay of dynamic and thermodynamic effects on rainfall in the strongly topographically diverse region of Cape Town, however, to dismiss the perfect-prog projections outright, although they remain discounted in view of other sources of information.

10.6.2.8 Potential for abrupt change

Since the rainfall delivery mechanisms in the region are strongly conditional on the latitudinal position of the mid-latitude westerlies and storm track, a question arises as to whether it is possible for the region to experience a threshold-controlled rainfall regime shift, and whether the 2015–2017 drought is simply a manifestation of such as shift. Such a situation might have occurred in Perth, Australia, which is located in a climatological setting almost identical to that of Cape Town. In Perth, patterns in the 120-year river runoff record have been interpreted as several events of step change (as for example illustrated in Figure 11.3 of Hennessy et al., 2007) shifting the region to a "permanent drought" situation. However, Bates et al. (2010), Hughes et al. (2012), and Smith and Power (2014) showed that the decline in the annual inflow is more consistent with a smooth declining trend than with a sequence of sharp breaks (see Section 10.4.1.2.3 for further discussion of past behaviour of southern Australia precipitation trends).

In terms of paleoclimate indicators of regime shifts, multi-proxy and modelling studies indicate that mid-Holocene and more recent climate evolution in the winter South African rainfall region had a character of gradual desertification and wetting, with no abrupt changes (Weldeab et al., 2013). In these multi-proxy analyses, Weldeab et al., (2013) found that the gradual aridification was accompanied by an increase in an easterly hot wind flowing off the edge of South Africa's interior plateau, a weakening of the southern Benguela Current upwelling and Agulhas Current leakage into the southern Atlantic from the Indian Ocean. These effects are consistent with a southward migration of the mid-latitude westerlies. The behaviour indicates that at least within range of the climate variability experienced in the last 12k years, an abrupt shift of the rainfall regime in the Cape Town region is unlikely.

10.6.2.9 Storyline and narrative approaches

There is a consistency in rainfall projections with projections of drivers of rainfall, and with the general understanding of the influence of warming on the circulation dynamics and rainfall patterns in the region. Thus, the expansion of the south Atlantic high-pressure system, related to widespread warming of the tropics and poleward shift of the subsiding limb of the Hadley cell, is associated with the southward displacement of the sub-tropical jet, and southward migration of mid-latitude westerlies and storm tracks, in addition to changes in the SAM/AAO. These effects are also relatively consistent with recent (post-1980s) declines in rainfall in the Cape Town region. There is, however, little consistency in the long-term, with previous droughts in the 20th century not clearly reflecting GHG-related trends, and with an overall weak or increasing rainfall at the time scale of 90 or more years (Kruger and Nxumalo, 2017; Wolski et al., submitted; Figure 10.24). In spite of this inconsistency, the overall message is that of a drier future, with either a warmer and drier climate or a much warmer and considerably drier climate. These messages are reinforced by results of a 2015–2017 drought multi-method attribution study (Otto et al., 2018), which estimated the probability of the event to have increased by a factor of 3 since pre-industrial times (although with a wide 95% confidence interval of 1.5 to 6), and to have a further factor of 3 increase in a world experiencing further warming to 2˚C above pre-industrial levels.

10.6.2.10 Messages distilled from multiple lines of evidence

There is *medium confidence* that the recent (post-1979) downward trend in the Cape Town region's rainfall leading to the 2015–2017 drought is related to hemispheric processes of poleward shift in the westerlies and expansion of the tropical high-pressure cell, supported by a *high agreement* among observational data and reanalyses, but less so in historical CMIP5 and CMIP6 model experiments.

There is *high agreement* among multiple sources giving *high confidence* that precipitation in the Cape Town region will *likely* decrease toward the end of the 21st century. This conclusion is supported by the *high agreement* in projections of key circulation mechanisms, including the southward shift in the Southern Hemisphere of the mid-latitude westerlies, storm tracks, subtropical jet and subsiding branch of the Hadley cell. A potentially counteracting feature is the behaviour of atmospheric rivers, whose impact on the region's precipitation needs further study.

The message of a drier future in the Cape Town region gains confidence by a distillation process that shows agreement among several lines of evidence: the projected precipitation by GCMs and RCMs of different spatial resolutions, and the observed and projected changes of circulation patterns consistent with dryer conditions. However, the distillation is limited by a lack of information about certain physical relationships, such as whether or not a relationship between Cape Town precipitation and large-scale circulation processes also occurs over longer historical periods than just the post-1979 decades, and how compensating changes in GHGs and Antarctic ozone will influence circulation changes over the twenty-first century.

10.6.3 Indian summer monsoon

10.6.3.1 Motivation and regional context

Societies in South Asia are finely attuned to the summer monsoon; for India alone, the monsoon between June and September provides 80% of the annual rainfall, supplying the majority of water resources for agriculture, industry, drinking and sanitation of over a billion people. As such, any variations in the monsoon on time scales from days to decades can have large impacts (Challinor et al., 2006; Gadgil and Gadgil, 2006). There is therefore a pressing need to understand if the monsoon will change in the future under anthropogenic forcing and to quantify any such changes.

In studies going back several decades, the monsoon has been suggested to increase in strength in future projections under idealised enhanced CO_2 forcing, supported by the theory of greater availability of moisture in a warmer climate. It was therefore puzzling that little trend was observed in central India up to the turn of the 21st century, with increases in extreme rainfall events compensating for decreases in light and moderate rain (Goswami et al., 2006b). Further analysis of trends in a variety of datasets has shown consistent negative trends since the 1950s until the turn of the century (Bollasina et al., 2011; Jin and Wang, 2017). This opposition between idealised or theoretical future projections and observed historical trends makes the region an ideal topic for the more in-depth assessment described here.

Simulation of the Indian monsoon over the historical period in CMIP-class GCMs is poor, with consistent deficiencies in summer rainfall in CMIP3 and CMIP5 models (Sperber et al., 2013; also Chapter 8). The region is also the subject of coordinated modelling under the Global Monsoon MIP (GMMIP; Zhou et al., 2016) and regional efforts such as CORDEX South Asia (Gutowski Jr. et al., 2016; Choudhary et al., 2018), sometimes with contradictory outcomes. Research has begun to apply emergent-constraint techniques to the Indian monsoon (Li et al., 2017b), while alternatively, narratives approaches are also beginning to be employed (Dessai et al., 2018).

10.6.3.2 The regional climate of India

The geography of India gives rise to distinct differences in societal experience of the monsoon and its impacts. India is bounded on its west coast by the Western Ghats mountain range, leading to orographic enhancement and heavy rains as the monsoon flow (known as the Somali jet) hits from the southwest; these rains supply rivers with water for much of the southern peninsula. To the east of the Western Ghats, south-eastern India sits under a rain shadow (this is the only major part of India to receive more rainfall during the winter monsoon season). The northern plains region contains the Ganges river basin and has India's most intensive agriculture, the crops either being rainfed or irrigated from the Ganges, associated canals, or groundwater pumping. Synoptic systems known as monsoon depressions are incident upon India's northeast coast, bringing much of the rain to the northern plains. Further north, the Himalayas also experience heavy precipitation; in the eastern Himalayas, this is dominated by the summer monsoon, while the western Himalayas receive most precipitation from western disturbances during winter (Palazzi et al., 2013).

10.6.3.3 Observational issues for India

India has an extensive network of rain gauges dating back to the 19th century. This has led to the production of several gridded products for model evaluation (Prakash et al., 2015) and analysis of climate trends (e.g. around 2,000 quality controlled gauges consistently reporting since the early 1950s, Rajeevan et al., 2006). A smaller subset of 306 stations has operated since the early 19th century and reveals pronounced decadal variability (e.g., Sontakke et al., 2008). A more recent 0.5°-gridded dataset begins in the 1970s, but it is clearly acknowledged as unsuitable for climate trend analysis, since there are critical inhomogeneities in station distribution and reporting over time (Rajeevan and Bhate, 2009). Such data are suitable for use in mesoscale analysis only. Spatial inhomogeneity in the input data also presents challenges; an example snapshot of the uneven distribution of rain gauges into a common data product is shown in Figure 10.25a.

More recently, a 0.25°-gridded dataset has been introduced covering the period from 1901 onwards (Pai et al., 2014, 2015) based on Shepard's interpolation method for gridding irregularly-spaced station data (Shepard, 1968). Findings include the increased intensity of daily rainfall and extreme events over four analysed regions, especially in the latter half of the 20th century. However, as discussed in Section 10.2.2.3, critical assessment of the methods used in conjunction with the inhomogeneities in the input data, in particular their variation over time, leads to the suggestion (Lin and Huybers, 2019) that changes in the input gauges have introduced an artificial jump in higher frequencies of more extreme rainfall since 1975 over central India. At its worst, Lin and Huybers (2019) stated that this may have acted to mask declines in mean rainfall; they highlighted the desire for openness of raw meteorological information to allow improved assessments. While trends for India over the extended period of 1901 to 2010 are inconclusive (Knutson and Zeng, 2018), the number of competing drivers acting over such a long period (Section 10.6.3.5) makes this unsurprising.

Finally, the large number of locally and internationally produced observational products for India and differences between them can indicate some of the uncertainty in observational datasets, which might pose challenges when evaluating climate models (as suggested in Section 10.3.3.3; Prakash et al., 2015). Collins et al., (2013) found evidence of cases (such as the seasonal mean monsoon rainfall) in which large biases clearly separated CMIP5 models from the available observational products. However, in other cases, such as measures of variability or teleconnections, the spread across observational products overlaps with that in the CMIP5 ensemble, with a significant portion of the models within the observational range. Such observational uncertainty presents difficulties in evaluating models.

10.6.3.4 Relevant anthropogenic and natural drivers

Numerous studies in the AR5 and before have shown the relevance of various anthropogenic and natural drivers for the Indian monsoon. While the attribution of observed changes in the monsoon to these drivers and the implications for future projections will be discussed later in Sections 10.6.3.5 and 10.6.3.6 the drivers are summarised briefly here:

- The increase in GHG concentrations (chiefly of CO_2) are suggested as a strong contributor to changes in the Indian monsoon, with potential impacts on the meridional temperature contrast driving the monsoon circulation (Ueda et al., 2006; Roxy et al., 2015), on the monsoon winds in the lower troposphere (Cherchi et al., 2011), or on the availability of moisture, chiefly derived from the Indian Ocean (May, 2011).
- Anthropogenic aerosol emissions can potentially alter the monsoon from both remote regions and locally. Preferential emissions of sulphate aerosol from industrial processes in the Northern Hemisphere could lead to changes in the inter-hemispheric energy transports and weakening of the monsoon (Polson et al., 2014; Undorf et al., 2018). Meanwhile, India has large emissions of sulphate aerosols and also black carbon (soot) from extensive use of cooking fires (Wallack and Ramanathan, 2009; Rehman et al., 2011; Kaskaoutis et al., 2012; Babu et al., 2013; Pandey et al., 2017), although the effect of black carbon on the monsoon is uncertain (Lau and Kim, 2006; Nigam and Bollasina, 2010).
- While natural drivers such as arid and semi-arid desert dust emissions and dust storms from the Arabian peninsula, Iraq, Syria and Iran have a role to play in heating the troposphere locally (Vinoj et al., 2014), their interaction with anthropogenic black carbon aerosols may also drive change in the monsoon (Lau, 2014).
- Over the late-20th century, India underwent considerable land-use change, including a green revolution with massive expansion of agriculture, culminating in the loss of natural vegetation such as forest and shrublands and its replacement with crops. To support the agricultural expansion, India's northern plains have some of the most widespread irrigation in the world; model studies have shown it to be a region of strong land-atmosphere coupling (Koster et al., 2004).
- Increasingly, human migration to urban areas has led to their expansion (another land-use change), potentially with local climate impacts (Shastri et al., 2015; Singh et al., 2016) such as altered sensitivity of extreme rainfall to circulation.
- Finally, internal modes of variability in the oceans such as AMV and PDV are known to yield

decadal forcing on the Asian monsoon (Krishnan and Sugi, 2003; Goswami et al., 2006a), which may interfere with the interpretation of climate signals.

10.6.3.5 Model simulation and attribution of drying over the historical period

That rainfall in India was not increasing over the course of the 20th century had been regarded as a puzzle (Goswami et al., 2006b), because the trend was not in line with the expected wetter trend arising from future projections under GHG emission scenarios (e.g., Kitoh, 2017; Kitoh et al., 2013a; Turner and Annamalai, 2012). Answering the attribution and projection question for changes in Indian monsoon rainfall is complicated by long-standing large dry biases in historical coupled GCM simulations (Sperber et al., 2013), persisting through CMIP3 and CMIP5, and as demonstrated for CMIP6 in Figure 10.25b. These dry biases are connected to a lower tropospheric circulation that is too weak (Sperber et al., 2013) and wet biases in the equatorial Indian Ocean (Bollasina and Ming, 2013).

Various studies have suggested that aerosol forcing is the cause for the declining rainfall trend. Attribution work using single-forcing historical experiments in CMIP5 has suggested this for the Northern Hemisphere monsoons generally (Polson et al., 2014) and specifically for the Asian monsoon region (Guo et al., 2015, 2016; Shawki et al., 2018). This is due to the dominance of aerosol emissions in industrialized regions of the Northern Hemisphere, cooling it relative to the Southern Hemisphere and thus increasing northward energy transport at the expense of moisture transport towards India (Bollasina et al., 2011, albeit in a single GCM). The aerosol hypothesis is supported by Salzmann et al. (2014), who noted a negative monsoon rainfall trend in 15 CMIP5 GCMs forced by aerosol and GHG, compared to a positive trend when forced by GHG only. Takahashi et al. (2018) supported this finding using an experiment in the MIROC-ESM in which aerosols were scaled back to pre-industrial levels, while aerosol removal experiments in remote regions and locally to India have added robustness to this conclusion, particularly for sulphate aerosols (Guo et al., 2016; Shawki et al., 2018). Some caution needs to be taken regarding the impacts of aerosol, since Takahashi et al. (2018) noted the uncertainty surrounding aerosol-cloud interactions, which could change the sign of long-term trends in precipitation. Furthermore, the large spread in effective radiative forcing of aerosol in GCMs could have an impact on the monsoon response to aerosol. Dittus et al. (submitted) forced a single GCM with separate historical experiments in which aerosol emissions were scaled between 0.2 and 1.5 times their observed values, representing the spread in CMIP5 effective radiative forcing. The impact of this on the Indian monsoon over the late-20th century was a spread of around 0.5 mm day^{-1} less rainfall in the strongest aerosol forcing experiment (Shonk et al., submitted). Salzmann et al. (2014) also cautioned that over small regions such as northern-central India, there was a large spread between individual model realisations of comparable magnitude to the purported aerosol-induced signal, suggesting that internal variability may also play a role.

Alternatively, the impact of rapidly warming Indian Ocean SSTs, themselves mainly arising due to radiative forcing from GHG (Guemas et al., 2016), has been blamed for declining Indian rainfall over the historical period. Roxy et al. (2015) forced a coupled GCM in the equatorial Indian Ocean (the region of strongest SST warming signal) by nudging SST to demonstrate a weakening response of the Indian monsoon. Annamalai et al. (2013) used a coupled climate model to suggest instead that preferential warming of the western North Pacific may lead to a Rossby wave response to its west that produces dry advection and descending motion over India, weakening the monsoon. A different viewpoint for the decreasing rainfall lies in the relative cooling of the troposphere over the Asian landmass compared to that of the adjacent Indian Ocean (e.g., Zuo et al., 2012, 2013), following the mechanism of Ueda et al. (2006) in which the thickness of the troposphere over the equator increases, decreasing the meridional temperature gradient. The cause for the relative cooling may lie in robust multi-decadal variations over the Asian landmass, which is related to internal variability, especially the AMV (Zuo et al., 2013, Zuo et al., 2018).

Internal variability in the Pacific could also be a significant driver. Huang et al. (submitted, b) compared 57 members of a perturbed physics ensemble of the coupled HadCM3C model run over the historical period, as well as the MPI 100-member initial condition ensemble. Those members in which the Indian negative rainfall trend was replicated were accompanied by a strong phase change in the IPO from negative to positive, consistent with the observed trend in SST. In parallel with the decline and recovery of the West African monsoon (Section 10.4.2.2.1), Jin and Wang (2017) have demonstrated increasing Indian monsoon rainfall since 2002 in a variety of observed datasets, suggesting the increase is due either to a change in dominance of a particular forcing (for example from aerosol to GHG) or to a phase change in a mode of internal variability such as the IPO. Huang et al. (submitted, b) also partially attribute this increase in rainfall to a phase change in the IPO; likewise the study of Ha et al. (submitted), using the CESM large ensemble and a combination of reanalyses, attributes the positive change to internal variability.

Finally, other authors have raised the possibility that local land-use/land-cover changes and land management are drivers of Indian monsoon drying. For example, Paul et al. (2016) forced the regional WRF model with land cover patterns from 1987 and 2005, representing a shift from forest cover to agricultural land, and found a weakening of summer monsoon rainfall especially in central and eastern India, due to a decrease in local evapotranspiration. Ramarao et al. (2015) have noted the overall anthropogenic impact on the drying trend and noted the potential for the warmer surface to decrease evapotranspiration as a result, potentially feeding back on the supply of moisture. India is the world's most irrigated region with around 0.5 mm/day on an annual basis across parts of the country, although peaks are higher in summer (Cook et al., 2015b; McDermid et al., 2017); including irrigation in GCMs and RCMs slows the monsoon circulation and diminishes the rainfall (Lucas-Picher et al., 2011; Guimberteau et al., 2012; Shukla et al., 2014; Tuinenburg et al., 2014; Cook et al., 2015b). However, the methodologies used to implement irrigation in these studies were simplified relative to actual practice and did not take into account spatial heterogeneity or they overestimated both demand and supply (Nazemi and Wheater, 2015; Pokhrel et al., 2016; see also Section 10.3.1.3.3).

Krishnan et al. (2016) tried to unify some of the above mechanisms. Using all-forcings and natural-forcings historical simulations in the LMDZ4 model, they demonstrated the positive influence of increased GHG concentrations (and GHG-associated SST patterns) on rainfall. Meanwhile the influence of the radiative effect of GHG forcing, together with imposed SSTs, a slight weakening of the monsoon circulation was found, related to an increase in the static stability. When the monsoon was driven by all forcings other than GHGs, declining rainfall was found. Based on other literature, Krishnan et al. (2016) hypothesized that the combination of anthropogenic aerosol, land-use change, and rapid Indian Ocean warming may be to blame for the declining Indian monsoon.

Thus, understanding the 20th century Indian monsoon drying trend relies on a mixture of control exerted from anthropogenic forcing and internal variability (supported by the review of Wang et al. (submitted). Common factors are the relative cooling of the Eurasian land mass or Northern Hemisphere, and relative equatorial warming in the Indian Ocean. Understanding the interplay between these controls will be important for understanding future change in the region.

10.6.3.6 Future climate information from global simulations

In the AR5, Christensen et al. (2013) concluded that Indian monsoon rainfall is likely to strengthen under future climate scenarios (Figure 10.25c), while the circulation will weaken. More recent work has examined changes in the future mean-state monsoon rainfall at RCP4.5 and RCP8.5. Latif et al. (2018) found increased June-to-September rainfall over the Indo-Pakistan region, attributed to strengthened northward moisture transport over the Indian Ocean. However, they selected a subset of models given their agreement at simulating the pattern of observed rainfall trends in the 20th-century historical period. Since the trend over the 20th century is likely to have been driven by other drivers than GHG (Section 10.6.3.5) and the dominant forcing at the end of the 21st century in RCPs is GHG emissions, the result might be different if using different criteria (e.g., the performance in terms of mean circulation patterns) to select the subset of models.

[START FIGURE 10.25 HERE]

Figure 10.25: Changes in the Indian monsoon in the historical and future periods: (a) Observational uncertainty demonstrated by a snapshot of rain-gauge density in the APHRODITE V1101 (Yatagai et al., 2012) 0.5°-daily precipitation dataset for June to September 1956. (b) Multi-model ensemble (MME) mean bias of 16 CMIP6 models for June to September precipitation (mm day^{-1}) compared to GPCC v2018 (Schneider et al., 2017; doi:10.5676/DWD_GPCC/FD_M_V2018_100) observations for the 1985-2010 period. (c) Time series of June to September precipitation averaged over the central India box (15°N–25°N, 75°E–85°E) shown in panel (b) in GPCC (black line) since 1950 in comparison with the MME-mean from the all-forcings historical experiments in 16 CMIP6 models (red line), and with changes in aerosol-only (hist-aer, 8 models, blue line) and greenhouse gas-only (hist-GHG, 9 models, grey line). MME-mean change in the SSP5-8.5 experiment for future projections out to 2100. CMIP6 results are compared with historical and future simulations of the MPI Grand Ensemble (MPI-GE historical-RCP85, violet line) (Maher et al., 2019). Anomalies are computed with respect to the 1995–2014 baseline and a weighted 13-year low-pass filter is applied. The low-pass filter has been used in AR4, Chapter 3, Appendix 3.A. It has 13 weights 1/576 [1-6-19-42-71-96-106-96-71-42-19-6-1] and for annual data, its half-amplitude point is about a 12-year period, and the half-power point is 16 years. (d) Maps of rainfall trends (mm day^{-1} decade^{-1}) in GPCC observations, the CMIP6 MME-mean of hist-aer runs, the CMIP6 MME-mean of greenhouse gas-only runs over the 1950–2000 period and an example MME-mean future projection from CMIP6 SSP5-8.5 for 2015–2100. (e) Histogram to illustrate the role of internal variability for historical 1950–2000 (left) and future 2015–2100 (right) trends in South Asian monsoon rainfall (% decade^{-1}) in the MPI-GE (expressed as percentage of simulations showing a trend in each bin, violet histogram). Individual members as well as ensemble means of CMIP6 historical-SSP5-8.5 (all-forcings, red circles), hist-aer (grey triangles) and hist-GHG (light blue triangles) are also shown, along with observed estimates from GPCC and CRU TS v4 (doi: 10.5285/edf8febfdaad48abb2cbaf7d7e846a86). All trends are estimated using ordinary least squares.

[END FIGURE 10.25 HERE]

Mechanisms for Indian monsoon change were explored in more detail by Li and Ting (2017), in order to determine the relative impacts of SST change and direct radiative forcing from GHG, using CMIP5 coupled and AGCM output. Rainfall increases were found to be dominated by the fast radiative response to GHG increase. However, in response to SST forcing, there was much greater model spread, likely arising from a competition between dynamic and thermodynamic responses in the moisture budget. While the thermodynamic response was found to be robust between models, the dynamic one is not. Li and Ting (2017) therefore conclude that the weak multi-model ensemble mean response of Indian monsoon rainfall in CMIP5 emerges from the combination of different processes arising on different time scales.

More detail of changes to the overall rainy season was examined by Sabeerali and Ajayamohan (2018), who used the CMIP5 RCP8.5 multi-model ensemble to project shortening of the rainy season, due to alteration of onset and withdrawal dates, in contrast to the single-model study of Singh and AchutaRao (2018) who found considerable increases in rainfall during September to November, which could be interpreted as an extension to the monsoon. Most models were found to exhibit preferential warming over the western tropical Indian Ocean, leading to tropospheric warming aloft and reducing the upper tropospheric meridional temperature gradient. This was found to be coincident with weakened easterly wind shear in the vertical, also reducing the period in which the tropospheric meridional temperature gradient is favourable for the monsoon.

Endo et al. (2018) explored the changing meridional temperature gradient in more detail in nine CMIP5 GCMs. In coupled experiments, lower tropospheric monsoon winds are found to move northwards and strengthen over land, in response to the stronger land-sea temperature contrast in RCP8.5 experiments. Meanwhile the tropical easterly jet in the upper troposphere was found to weaken, consistent with weakening of the meridional gradient at upper levels. AMIP experiments were then used to isolate the role of the SST, finding that the strengthened meridional temperature gradient in the lower troposphere can be explained by the GHG radiative forcing alone.

Sooraj et al. (2015) selected a subset of seven CMIP5 models that well simulated the monsoon during the historical period. In RCP4.5, they found a robust reduction in the large-scale upper-tropospheric meridional temperature gradient, ascribed to tropospheric heating and enhanced ascent over the tropical Pacific. This combined with an increase in atmospheric stability to weaken the Asian monsoon circulation. By decomposing the climate signal into dynamic and thermodynamic components, the dynamic part was found to give a tendency for decreasing monsoon rainfall, while the thermodynamic part gave a positive tendency; the positive tendency was greater in magnitude. By testing the impact of CO2 radiation forcing and plant physiological changes separately in quadrupled CO2 experiments in four ESMs, Cui et al. (submitted) showed little impact of plant physiology on annual rainfall, although they exert a negative influence on evapotranspiration and a positive influence on runoff.

The RCP4.5 experiments of Krishnan et al. (2016) in the LMDZ AGCM forced by coupled-model derived future warming patterns superimposed onto AMIP SSTs, showed the 20th century drying of India to continue into the 21st century, before a rainfall recovery in the second half of that period, suggesting a change in the dominant forcing. The switch in forcing will be partially controlled by the rate at which aerosol emissions decline in future scenarios. In a comparison of RCP8.5 with an alternative in which aerosol emissions are held at (high) 2005 values, the version maintaining present day aerosol is shown to feature lower Indian monsoon rainfall at the end of the 21st century (Zhao et al., 2019). The spatial distribution of continuing aerosol emissions is also likely to play a role in near-term projections of the Indian monsoon, indicated by the spread of emissions in SSP1–3 (Samset et al., 2019). In particular SSP3 under weak air-quality policies features a dipole of declining sulphate emissions for China but increases over India, leading to suppression of GHG-related precipitation increases for India (Wilcox et al., submitted).

For the near-term future, consideration must be made of the interplay between internal modes of variability and external forcing in determining the response of the monsoon. Singh and AchutaRao (2018) aimed to quantify sources of uncertainty in Indian regions using the 40-member CESM1 large ensemble. They show that internal variability remains quite large and comparable to model uncertainty until at least the latter part of the 21st century. Much of the rainfall uncertainty is found for the more arid northwest region, with the west-central region exhibiting lower uncertainties. Similarly, Huang et al. (submitted, a) used the 100-member MPI-ESM and 50-member CanESM2 large ensembles to suggest that internal variability can overcome the forced upward trend in the SAM-related rainfall at least to 2045, which they attribute to PDV.

In summary, future scenarios dominated by GHG increases such as the RCPs tend to suggest likely increases in monsoon rainfall, dominated by thermodynamic mechanisms leading to increases in the available moisture. However, there is large uncertainty as to how the rainfall evolution is spatially distributed, which is explored further in the subsequent text on downscaling studies.

10.6.3.7 Future climate information from regional downscaling

While the studies previously mentioned used GCM output directly for attributing past climate trends or projecting the future, others attempted to add value to the results based on GCMs by employing downscaling methods (Section 10.3.3).

Starting with statistical downscaling, Akhter et al. (2019) used principal component-based linear regression to test a variety of large-scale fields from the NCEP-NCAR re-analysis to determine their suitability for downscaling precipitation in seven different regions of India. Fields such as precipitable water and relative humidity seem to be consistently good predictors. Their finding that increasing the domain size leads to worsened results points to the complex nature of India's hydroclimatic zones. Applying statistical methods to the future, albeit in older SRES A2 projections, Vigaud et al. (2013) used a variant of quantile mapping to bias adjust (Section 10.3.1.4.2 and Cross-Chapter Box 10.2) GCM outputs for southern India. The method is applied month-wise to maintain seasonality. During the historical validation period, using India Meteorological Department gauge observations for comparison, the method was shown to improve the pattern, mean and seasonal cycle of modelled rainfall versus the GCMs used. Increases in monsoon rainfall were found for the future in southern India.

Salvi et al. (2013) attempted statistical downscaling for the whole of India at 0.5°-resolution based on five ensemble members of the CCCMA model in SRES scenarios for the 21st century and using a regression-based perfect prognosis method (Section 10.3.1.4.1). They noted increases over the heavy rainfall regions of the west coast and northeast India, while decreases were found in the north, west and southeast regions. Madhusoodhanan et al. (2018) used statistical downscaling at 0.05°-resolution to provide added detail in future rainfall projections over India based on inputs from 20 CMIP5 models. While their method provided *medium confidence* of rainfall change over the Western Ghats, Himalayan foothills and central India, with most models in agreement, they found significant inter-model differences in the pattern of change. However, the accuracy of their method is dependent on the quality of the observational data used for training that, as explained above, offers substantial challenges. In addition, the large disparity in resolution between the output and driving GCM suggest that the downscaled product may provide high spatial detail at the expense of neglecting key physical processes that cannot be resolved at the GCM scale, such as topographically determined circulation distributions.

Given ongoing concerns about the added value of dynamical downscaling for regional climate projection, Singh et al. (2017) raised this issue in relation to the Indian monsoon. They compared nine RCMs from CORDEX South Asia against their driving CMIP5 models, with respect to present-day (1951 or 1970 to 2005) monsoon rainfall patterns and processes related to intraseasonal variability such as northward propagation. They found no consistent improvement in any present-day monsoon characteristics other than the spatial pattern (e.g. the representation of rainfall close to better-resolved orography); some characteristics were made worse.

In contrast, Varikoden et al. (2018) assessed the 1951–2005 historical period in the CORDEX South Asia models and found considerable improvement in the representation of historical rainfall patterns compared to the five driving GCMs. In particular, they noted better simulation of the long-term mean specifically over the Western Ghats mountains (consistent with Singh et al., 2017), reducing the dry bias; but improvements were not found over the northern plains, which are dominated by synoptic variability known as monsoon depressions.

Similarly, Sabin et al. (2013) used the variable-resolution LMDZ model to compare two ten-member ensembles: one operating with a uniform 1°-resolution and a second using a version zoomed to ~35 km over South Asia, while coarsening the grid outside and conserving the total number of grid points. Such modifications led to an improved simulation of orographic precipitation as well as the monsoon trough.

For the future, a combination of the WRF regional model and a surrogate approach (like pseudo-global warming, see Section 10.3.2.2) has been used to demonstrate the separate and combined impacts of warming and moistening on monsoon depressions (Sørland and Sorteberg, 2016; Sørland et al., 2016). The depressions are found to give more precipitation in future, dominated by the warming mechanism which strengthens the synoptic circulation.

Finally, by using a GCM to produce a perturbed parameter ensemble (HadCM3-QUMP) with the PRECIS RCM, Bal et al. (2016) made projections under SRES A1B for the 2020s, 2050s and 2080s in a continuous integration since 1970. They noted increases in rainfall of 15–24% for India.

There are mixed messages as to whether downscaling methods add value to climate projections of the Indian monsoon; it is a common theme however that rainfall patterns tied to orography are better represented by dynamical downscaling, giving *high confidence* to the precipitation changes tied to orography.

10.6.3.8 Potential for abrupt change

Given the interest in physically plausible high impact scenarios (Sutton, 2018), it is worth considering whether the Indian monsoon may undergo abrupt change, which hypothetically could involve failure to establish the meridional tropospheric temperature gradient during spring, collapse of the monsoon circulation and thus considerable weakening of the monsoon rains for a season or more. Such ideas pertaining to collapse of the monsoon were explored in the wider review of Lenton et al. (2008), where it was suggested that monsoon collapse could occur if regional planetary albedo exceeded 0.5, perhaps pertaining to aerosol emissions or land-use change. This finding was based entirely on the results from a single conceptual box model (Zickfeld et al., 2005). As reported in Hoegh-Guldberg et al. (2018), given the small radiative forcing in 1.5°C or 2°C equilibrium scenarios, or the absence of large aerosol emissions at the end of the 21st century in RCPs, there is *limited evidence* of abrupt changes in the Indian monsoon. There has been no credible evidence for abrupt monsoon collapse under the radiative forcings present in the RCP scenarios.

The palaeoclimate record may reveal large magnitude shifts in monsoon behaviour. However, evidence from palaeoclimate proxy observations and model experiments (e.g. of the mid-Holocene) may be unsuitable for constraining future projections of the Indian monsoon (D'Agostino et al., 2019) since the mechanisms involved are different. D'Agostino et al. (2019) argue that in the mid-Holocene dynamic changes arising from the increased obliquity (axial tile) act in concert with thermodynamic changes to enhance the monsoon, whereas in future climate experiments thermodynamic increases oppose and overcome weakening from dynamic mechanisms. This finding is supported by Hill (2019) who found the same mechanisms for change might not be at play on different time scales.

10.6.3.9 Storyline and narrative approaches for India

Since the AR5, considerable focus has been given to understanding regional climate impacts in future scenarios at target levels of global-mean warming in line with the Paris Agreement; such comparisons are often made between 1.5°C and 2°C above pre-industrial conditions. The IPCC Special Report on Global Warming of 1.5˚C (SR15; Hoegh-Guldberg et al., 2018), suggested that since the radiative forcings involved in these time-slice scenarios are rather lower than those at the end of the 21st century in the typical RCP4.5 and RCP8.5 scenarios, then there is only *low confidence* in projections of monsoon change at 1.5°C and 2°C, and of any differences between them. However, in further literature examining equilibrium-temperature experiments for monsoon regions, Chevuturi et al. (2018) compared five AGCMs from HAPPI (Half a degree Additional warming, Prognosis and Projected Impacts) data, forced by SST patterns representative of 1.5˚C and 2.0˚C warming. Despite considerable model spread, the mean and extreme monsoon rainfall both amplify. Persistent daily rainfall extremes are *likely* to become more frequent with the additional half-degree warming.

The only study so far to have examined climate narratives for the Indian monsoon is Dessai et al. (2018). Using an expert elicitation approach, they constructed physically plausible futures of the monsoon substantiated by climate processes, focusing on the Cauvery river basin in southern India. Possible outcomes of the monsoon were provided based on the changes in two drivers: the availability of moisture from the Arabian Sea and the strength of the low-level flow. The key outcome is that the mechanistic narratives identified in the expert elicitation process were able to explain 70% of the variance in monsoon rainfall over 1979–2013, the implication being that climate uncertainties could be easily communicated to stakeholders.

10.6.3.10 Messages distilled from multiple lines of evidence

There is *very high confidence* (*robust evidence*, *high agreement*) that both internal variability and anthropogenic aerosol emissions over the Northern Hemisphere have contributed to the negative rainfall trend in the Indian monsoon over the 20th century. There is *limited evidence* of the spatial distribution of historical and projected changes, made worse by the substantial observational uncertainty. There is *high confidence* (*robust evidence*, *medium agreement*) that Indian monsoon rainfall will increase at the end of the 21st century in response to increased GHG forcing; this arises due to the dominance of thermodynamic mechanisms. No contradictory evidence is found from downscaling methods. There is *low agreement* on how the monsoon onset might change in the future.

10.6.4 Mediterranean summer warming

10.6.4.1 Motivation and regional context

The Mediterranean region is historically loosely denoted as the region that surrounds the Mediterranean Sea. It is a culturally rich area that has experienced significant climate variability over the past decades. The region is characterized by complex orography and strong land-sea contrasts. It also contains a dense and growing human population. Within the Mediterranean region, large regional differences exist: whereas the population of the European Mediterranean countries has been relatively stable or even declining during the last decade, the population of countries in Mediterranean areas of the Middle East and North Africa has quadrupled between 1960 and 2015, and the degree of urbanization has risen from 35 to 64% during the same period (World Bank Group, 2017; Cramer et al., 2018). Agricultural land management is intensifying, particularly through enhanced irrigation; as many southern and eastern land systems seem to have the potential for further increase in yields (Mueller et al., 2012), agricultural management is likely to change further, with consequences for water resources, biodiversity and landscape functioning (Cramer et al., 2018).

The Mediterranean climate is characterized by mild humid winters and dry hot summers. As a consequence, water scarcity is a recurrent problem for the region especially in summer, requiring substantial infrastructural efforts, like dams and irrigation systems (Saadi et al., 2015). The dry hot Mediterranean climate is also a potential factor of risk for wildfires, which are the most important natural threat to forests and wooded areas of the Mediterranean basin. The region also suffers from severe heatwaves causing a mortality-risk in particular for older adults, young children and people with pre-existing and chronic medical conditions.

10.6.4.2 The region's climate

The Mediterranean has a heterogeneous climate, that is partly semi-arid, especially along the southern coast (Lionello et al., 2012). Dry summers are associated with large scale subsidence that is partly related to the downward branch of the Hadley circulation, but also other factors affect the Mediterranean circulation such as the monsoon heating over Asia (Rodwell and Hoskins, 1996) and circulation anomalies induced by middle-east topography (Simpson et al., 2015). Seasonal variability is strongly linked to the NAO in winter and the summer NAO in summer (Folland et al., 2009; Bladé et al., 2012). During positive summer NAO phase the Mediterranean is anomalously wet, associated with an upper level through over the Balkans (Bladé et al., 2012). The Mediterranean Sea acts as an evaporation source that dominates the hydrological cycle of the region but also of remote locations such as the Sahel (Park et al., 2016). Strong storms can develop over the Mediterranean: the most intense ones, known as Medicanes, are particular destructive and exhibit several similarities with tropical cyclones (Cavicchia et al., 2014). Due to its semi-arid climate, the Mediterranean region is characterized by strong land-atmosphere coupling and feedbacks (Seneviratne et al., 2006) generating prolonged droughts and intense heatwaves, which can also affect other European regions (Zampieri et al., 2009).

10.6.4.3 Observational issues

The Mediterranean region spans a wide variety of countries and economies. This has led to large differences in the existence and availability of observations, with the southern part of the area being sparsely covered by meteorological stations (Figure 10.26b). In addition, political problems and civil strife have undermined the continuity of observational records. As a consequence, basin-wide, homogeneous, quality controlled observational datasets are lacking, especially before the advent of substantial satellite observations in the 1970s.

Large differences up to 7°C between CRU and UDEL (see technical annex on observations) datasets have been found over the region especially over mountainous area, such as the Atlas in Morocco (Zittis and Hadjinicolaou, 2017; Strobach and Bel, 2019). Bucchignani et al., (2016b, 2016a) compared three different datasets (CRU, UDEL, and MERRA) with the available ground observations and found that even if the geographical distribution of the bias is qualitatively similar for the three datasets, absolute values of bias are generally lower in MERRA especially over North-Africa during the summer and winter season. There is *high confidence (robust evidence, high agreement)* that the sparse monitoring network in this region strongly affects the interpolation in the different gridded datasets (Section 10.2).

10.6.4.4 Relevant anthropogenic and natural drivers

As discussed in Section 10.4.1.2.6, apart from the increase in GHGs, the anthropogenic decrease in aerosol concentration, resulting from air pollution policies (Turnock et al., 2016), has been an important driver of enhanced summer warming especially over western Europe. This is to a lesser extend also true for the Mediterranean region (Besselaar et al., 2015; Dong et al., 2017). The AMV affecting Western Europe (Section 10.4.1.2.6) also impacts the Mediterranean region. Another driver is the Asian monsoon by inducing adiabatic descent over the Mediterranean (Rodwell and Hoskins, 1996).

10.6.4.5 Model simulation and attribution over the historical period

The European part of the Mediterranean region has been warming faster than the global mean in recent decades. Part of this warming of about 1ºC can be ascribed to the enhanced warming over land associated with the lapse-rate feedback (Kröner et al., 2017). Basin-wide, annual mean temperatures are in 2018 1.4°C above late-19th-century levels (van der Schrier et al., 2013; Cramer et al., 2018; Lionello and Scarascia, 2018). For the last two decades, the surface air temperature of the Mediterranean including the Sea has warmed by around 0.4°C per decade (Macias et al., 2013). Figure 10.26e shows the historical warming over the land points of the Mediterranean. The enhanced Mediterranean warming is related to the enhanced western European warming discussed in Section 10.4.1.2.6.

Several studies have linked the enhanced Mediterranean warming to a shift to the positive phase of the AMV around the 1990s (Sutton and Dong, 2012; Macias et al., 2013; O'Reilly et al., 2017), with the underlying mechanism either being thermodynamical, where the enhanced North Atlantic warming directly warms the Mediterranean, or dynamical, with a linear atmospheric response downstream over Europe (Figure 10.26a). However, the recent warming has also been linked to reduced aerosol concentrations. As discussed in Section 10.4.1.2.6, there is *medium confidence* that reduction of aerosol concentrations, an outcome of air pollution control legislation, has also been a dominant factor for the enhanced warming by changing the optical properties of clouds (Besselaar et al., 2015; De Laat and Crok, 2013; Dong et al., 2017; Philipona et al., 2009; Ruckstuhl et al., 2008; Turnock et al., 2015, 2016). By means of model sensitivity experiments, Nabat et al., (2014) also associated the increase in Mediterranean SST to the decrease in aerosol concentrations.

An analysis of observed vs. modelled surface temperature trends at gridbox scale over 1901–2010 (Knutson et al., 2013) shows for the Mediterranean region observed warming trends that are detectable (highly unusual compared to CMIP5 simulated natural variability) and partly attributable to anthropogenic forcing, being either consistent with or greater than simulated by the CMIP5 model runs that included both anthropogenic and natural forcings. The ensemble-mean trends of CMIP5, CMIP6, HighResMIP and CORDEX over the period 1960-2014 are less than observed (Figure 10.26g). However, there is a large spread among the different models and due to natural variability also among the different ensemble members of an individual model, of which some encompass the observations (Figure 10.26f).

Due to its semi-arid climate, strong atmosphere-land coupling has contributed to the larger increase of mean summer temperature compared to the increase of the annual mean temperature (Seneviratne et al., 2006). In particular, during drought spells, soil moisture limitation of evaporation provides a positive feedback and enhances the intensity of heat waves (Lorenz et al., 2016). By comparing reanalysis-driven RCM simulations with observations, Knist et al. (2017) found that RCMs are able to reproduce soil moisture interannual variability, spatial patterns, and annual cycles of surface fluxes over the period 1990–2008, revealing a strong land-atmosphere coupling especially in southern Europe in summer. Other key mechanisms are the enhanced land-sea temperature contrast which leads to relative humidity and soil moisture feedbacks (Rowell and Jones, 2006). The increased Mediterranean summer drying is also related to the increased moisture divergence associated with enhanced pressure over the Atlantic and Northern Europe (Seager et al., 2014).

ERA-Interim-driven RCM simulations show in general a cold bias over the southern part of the Mediterranean/ Middle East and North Africa region (Almazroui, 2016; Almazroui et al., 2016b, 2016a; Ozturk et al., 2018; Zittis and Hadjinicolaou, 2017), although higher resolution, new bare soil albedo and modified aerosol parametrization significantly improve the results (Bucchignani et al., 2016b, 2016a, 2018).

In their analysis of the effect of model resolution and air-sea coupling in Med-CORDEX RCMs, Panthou et al. (2018) found that models reproduce well the observed spatial patterns of hot days and droughts, although they tend to overestimate extreme return levels of hot days. In particular, higher resolution simulations showed a clear improvement in the representation of droughts, while the additional degrees of freedom in coupled simulations did not downgrade the performance. Similarly, Akhtar et al. (2018) argued that higher resolution improved the wind speed (particularly near coastal areas) and subsequently the turbulent heat flux simulations. Both fields were also better simulated with an interactive ocean model, compared to simulations with prescribed SST.

Finally, Macias et al. (2018) argued that simulated SST in RCMs are significantly improved when wind speed values were bias-corrected towards observed values, whereas other variables like air temperature and cloud cover had a more marginal importance in reducing the SST bias.

10.6.4.6 Future climate information from global simulations

The Mediterranean is expected to be one of the most prominent and vulnerable climate change hotspots (Diffenbaugh and Giorgi, 2012). CMIP5, CMIP6, HighResMIP and CORDEX (Section 10.6.4.7) simulations all project an enhanced future warming for the 21st century compared to global mean and enhanced drying (Figure 10.26h ; Mariotti et al., 2015). In particular, summer warming is projected to reach values up to 40–50% larger than the global warming, with local values up to 100% larger than global warming for the land areas located north of the basin (Lionello and Scarascia, 2018). Peculiar to the Mediterranean is that daily maximum temperature is projected to warm more than daily minimum one. Consequently, the difference between daytime maxima and night-time minima is expected to increase, particularly in summer (Lionello and Scarascia, 2018). Simulations also project a northward and eastward expansion of the Mediterranean climate and the southern part becoming more arid with an increased summer drying in both old and newly established Mediterranean climates (Alessandri et al., 2015; Barredo et al., 2018).

CMIP5 results (Lelieveld et al., 2016) show that warming is strongest in summer in the southern part of the Mediterranean region with warming exceeding 6°C by the end of the century under RCP8.5 scenario compared to the reference period 1986–2005. No positive soil moisture-temperature feedback is found due to the arid background climate, which is governed by the radiative cooling. The CMIP6 dataset also show robust summer warming in the southern parts of Mediterranean and adjacent North Africa regions by the end of the 21st century (Figure 10.26h; Almazroui et al., submitted), although magnitudes differ from CMIP5. The reasons for the apparent discrepancy between the still incomplete CMIP6 data set and CMIP5 are as yet unknown and under investigation.

[START FIGURE 10.26 HERE]

Figure 10.26: Aspects of Mediterranean summer warming. (a) Mechanisms and feedbacks involved in enhanced Mediterranean summer warming. (b) Locations of observing stations in E-OBS v19e (Cornes et al., 2018) and Donat et al. (2014). (c) Differences in temperature observational data sets with respect to E-OBS for the land points between the Mediterranean Sea and 46°N and west of 30°E. (d) Observed summer (June to August) surface air temperature trends (°C decade^{-1}) over the 1960–2014 period from BEST (Rohde et al., 2013) dataset. (e) Time series of area averaged (25°N–50°N, 10°W–40°E) land point summer

temperature anomalies (°C, baseline 1995–2014). Black, brown, orange and violet lines show low-pass filtered temperature of BEST, CRU TS v4.02 (Harris et al., 2014), HadCRUT4 (Morice et al., 2012) and the MPI-GE (Maher et al., 2019), respectively. Dark blue, red and light blue lines and shadings show low-pass filtered ensemble means and standard deviations of CMIP5 (30 members), CMIP6 (15 members) and HighResMIP (7 members), respectively. The filter is the same as the one used in Figure 10.11. (f) Distribution of 1960–2014 summer temperature trends (°C decade^{-1}) for observations (black crosses), the MPI-GE (violet histogram) and for ensemble means and single runs of CMIP5 (dark blue circles), CMIP6 (red circles) and HighResMIP (light blue circles). (g) Bias in ensemble mean 1960–2014 trends (°C decade^{-1}) of CMIP5, CMIP6, HighResMIP and CORDEX in reference to BEST. (h) Projections of ensemble mean 2014–2050 trends (°C decade^{-1}) of CMIP5, CMIP6, HighResMIP and CORDEX. All trends are estimated using ordinary least-squares. **[Placeholder: The CORDEX and HighResMIP panels need to be completed.]**

[END FIGURE 10.26 HERE]

The Mediterranean climate model projections are also characterised by reduced precipitation in all seasons (Lionello and Scarascia, 2018; Mariotti et al., 2015). During summer this is predominantly caused by the warming land-sea contrast (Joshi et al., 2008; Byrne and O'Gorman, 2013a, 2013b) and the lapse rate feedback (Brogli et al., 2019a, 2019b) rather than circulation changes. Land-surface feedbacks increase this drying thereby contributing to the enhanced warming (Whan et al., 2015; Lorenz et al., 2016; Russo et al., 2019). An additional mechanism for Mediterranean drying, with a feedback on summer temperatures, is the "monsoon-desert mechanism" that relates diabatic heating associated with the South Asian summer monsoon rainfall with subsidence over the eastern Mediterranean (Cherchi et al., 2016). Waha et al. (2017) projects a pronounced increase in aridity under RCP8.5 over the Mediterranean coastal areas by the end of the 21st century.

The Mediterranean summer climate is affected by large-scale circulation patterns of which the summer NAO is the most important (Folland et al., 2009; Bladé et al., 2012). It is also connected with the Hadley circulation. These large-scale drivers of the Mediterranean summer climate often show large biases in global models decreasing confidence in the regional projections (Bladé et al., 2012). Correctly simulating their impact on the Mediterranean climate can partly offset the anthropogenic warming signal (Barcikowska et al., 2019).

10.6.4.7 Future climate information from regional downscaling

To unravel the complex interactions and feedbacks involving ocean-atmosphere-land-biogeochemical processes that modulate the climate and environment of the Mediterranean region on a range of spatial and temporal scales, regional downscaling projects are being developed to provide an integrated view on the future of the Mediterranean. A recent example is Med-CORDEX (Ruti et al., 2016; Somot et al., 2018), but earlier activities have included ENSEMBLES (Fernández et al., 2019) and ESCENA (Jiménez-Guerrero et al., 2013) and the ongoing EURO-CORDEX (Jacob et al., 2014).

From an analysis of EURO-CORDEX results, studies showed that southern Europe is projected to face a robust non-linear increase in temperature larger than the global mean, especially for both hot and cold extremes (Jacob et al., 2018; Kjellström et al., 2018; Maule et al., 2017). In particular, Dosio and Fischer (2018) showed that the increase in the number of tropical nights is more than 60% larger in many places in southern Europe and the Mediterranean under 2°C warming compared to 1.5°C. Over the region, the projected temperature increase, including a higher probability of severe heat waves (Russo et al., 2015), together with a reduction in precipitation (Jacob et al., 2014; Dosio, 2016; Rajczak and Schär, 2017) results in projected increase of drought frequency and severity (Spinoni et al., 2018, 2019). Also, the frequency and severity of marine heat waves of the Mediterranean sea are projected to increase (Darmaraki et al., 2019). RCM simulations with the CORDEX-Middle East and North Africa domain under RCP8.5 project a change in hot days (i.e. those with maximum temperature > 50°C) for 2070–2099 with respect to 1971–2000 of about five days in the northern Mediterranean (southern Europe), but up to about 70 days in the southern

Mediterranean (Almazroui, 2019).

For the southern part of the Mediterranean, RCM simulations project a warming for the period 2070-2100 between 3°C and 9°C depending on the RCP4.5 and RCP8.5 scenarios (Bucchignani et al., 2018; Ozturk et al., 2018). Bucchignani et al. (2018) using COSMO-CLM driven by CMCC-CM projects a decrease in precipitation up to 30% in the Mediterranean coastal areas by the end of the 21st century.

Despite the large efforts of these regional downscaling projects, the GCM-RCM matrix is still sparse and lacking a systematic design to explore the uncertainty sources (e.g., GCM, RCM, scenario, resolution). Focusing on the Iberian peninsula, Fernández et al. (2019) argued that the driving GCM is the main contributor to uncertainty in the grand-ensemble. Consistent but implausible temperature changes in RCMs can occur. An example is a strong temperature increase over the Pyrenees due to excessive snow cover in the present climate (Fernández et al., 2019). Based on an older set of RCMs simulations (ENSEMBLES), Déqué et al. (2012) also argued that the largest source of uncertainty in the temperature response over Southern Europe is the choice of the driving GCM (whereas for summer precipitation the choice of the RCM dominates the uncertainty). Similarly, Macias et al., (2018) claimed that the choice of the GCM has the largest impact on the simulated SST bias exhibited by the RCM. Finally, Bartók et al. (2017) found that RCMs projected a change in surface solar radiation (on average, -0.60 W/m^2 per decade over Europe) opposite to that of the driving GCMs, with the large discrepancies being over spring and summer, due mainly to different trends in cloud cover in global and RCMs.

In addition, statistical downscaling studies for the Mediterranean exist that confirm the results obtained from GCM and RCM studies, however with some regional variations (Jacobeit et al., 2014; Hertig and Tramblay, 2017).

10.6.4.8 Potential for abrupt change

A growing number of studies are investigating the impacts of warming levels above the Paris Agreement (which would limit warming to 1.5°C above the pre-industrial level) on the hydrological cycle, vegetation and their socio-economic consequences. Based on EURO-CORDEX results, Barredo et al. (2018) showed that, by the end of the century under RCP8.5, the present land area of the Mediterranean climate zone is projected to contract by 16%, mainly due to the expansion of the arid zone, which is projected to increase by more than twice its present extent, equivalent to three times the size of Greece. In addition, under RCP8.5, the land area of the Mediterranean climate zone is projected to expand to other zones by an area equivalent to 50% of its present extent. The region of heat stress and extreme precipitation extends from southern Europe at 1.5 ºC global warming to heavenly populated regions across Europe at 3 ºC global warming (Pfeifer et al., 2019). Combining Holocene pollen profiles and CMIP5 climate scenarios, Guiot and Cramer (2016) argued that above 2°C of warming, climatic change will generate Mediterranean land ecosystem changes that are unmatched in the Holocene, a period characterized by recurring precipitation deficits rather than temperature anomalies. The changes will likely lead to substantial expansion of deserts in much of southern Europe and northern Africa. Samaniego et al., (2018), using an ensemble of hydrological and land-surface models, estimated that a warming of 3˚C will increase the drought area by 40% affecting up to 42% more of the population. It is important to note that the highest population densities and the location of major cities are largely concentrated along the cost of the Mediterranean (Lange, 2019a). The south European and north African countries are projected to become hot spots for drought by the end of the 21st century (Waha et al., 2017).

10.6.4.9 Storyline and narrative approaches

The atmospheric circulation is influenced by large scale, often slowly varying components of the climate system, such as ocean, sea-ice and soil moisture. Historical and future changes of the atmospheric circulation depend, among other factors, on how these drivers have changed and will change. Zappa and Shepherd (2017) have analysed this for the Mediterranean region and identified different possible evolutions of those drivers and their impact on the Mediterranean winter climate. Important identified drivers are tropical and polar amplification of global warming and the polar stratospheric vortex (Manzini et al., 2014; Simpson et al., 2018), with implications for precipitation. Brogli et al. (2019a, 2019b) and Kröner et al. (2017) have done this for the Mediterranean summer climate, revealing the relative importance of thermodynamic processes, lapse rate and circulation.

10.6.4.10 Messages distilled from multiple lines of evidence

The Mediterranean has a semi-arid climate with a dense and growing human population and various environmental pressures. There is *high confidence (high agreement, robust evidence)* that the Mediterranean region has experienced a summer temperature increase in recent decades that is faster than the increase for the Northern Hemisphere summer mean. There is also *high confidence* (*high agreement, robust evidence*) that the projected summer temperature increase will be larger than the Northern Hemisphere mean, resulting in an increase in frequency and intensity of heat waves with possible socio-economic consequences.

There is *robust evidence* and *high agreement* and, thus, *high confidence* that summer precipitation in the Mediterranean region will decrease toward the end of the 21st century. One reason for the *high confidence* in projected future drying is the finding of prominent detectable and at least partly attributable (to anthropogenic forcing) century-scale decreasing precipitation trends in the region. There is *high confidence* that this will substantially affect the hydrological cycle and vegetation, with implications for the socio-economic structure. Due to the biases in GCMs and RCMs, there is *low to medium confidence* in the spatial distribution of projections of precipitation for the Mediterranean region. Natural variability on decadal time scales enhances this uncertainty.

10.7 Limits to the assessment

A number of challenges have been identified that limit the assessment of regional climate change:

- There is a need to monitor climate in poorly observed regions. Some regions such as the poles, northern Canada, Siberia, Tibetan plateau, southern Mediterranean and large areas in Africa, Australia and South America have only sparse in situ observational networks. Climate is changing fast with a high impact on cities, mountains and forests. However, these locations are undersampled due to the strict WMO standards that do not necessarily promote reference stations in those areas. Furthermore, access to relevant observational data remains a problem since some countries do not make their data available to the research community or charge substantial fees for access. In all these cases, the confidence in messages reliant mainly on numerical models might be low due to the lack of observational validation and support (Sections 10.2 and 10.6).
- There is a substantial shortage of observed variables needed for both validation and model development other than temperature and precipitation, such as evaporation and soil moisture. Climate messages also require high-density, homogeneous, long observational records for a large number of variables. For instance, estimating crop-yield change or potential for generation of renewable energy require data for radiation, wind and relative humidity to elaborate the corresponding climate information and messages (Sections 10.2 and 10.6).
- There is a disproportionate amount of climate change literature available across regions. Literature plays a central role as an information source when climate change messages are produced at the regional level. In addition, large bodies of literature (e.g., local and regional reports) are often overlooked when performing assessments and constructing climate messages. Furthermore, although the quality of the assessment is dependent on the amount of literature dealing with regional climate, research agendas are dominated by the priorities of the global north. As a consequence, aspects relevant to other regions of the planet, some of which are also suffering from climate impacts, may not be given the attention they require (Sections 10.2, 10.3 and 10.6).
- There is a shortage of process-based evaluation at regional scales compared to the increasing number of large-scale evaluations. Such analyses are required to assess the fitness of the chosen models for the given purpose and are the basis for our confidence in climate projections. The relevant processes

cover a wide range of scales from planetary to synoptic to mesoscale and potentially even to local. Yet, there is a lack of regional climate change studies addressing the representation of large-scale processes in GCMs relevant for downscaling. Such studies are particularly important for the design of GCM/RCM ensembles that span the range of projection uncertainty and realistically represent the climate over the region of interest. Moreover, the fitness of statistical methods for climate change studies has received only very limited attention, such as pseudo-reality studies to assess which predictors, change factors and model structures are required for downscaling a given aspect of a variable in a future climate (Section 10.3).

- Internal variability is an important contributor to the climate uncertainty at regional scales, especially for variables other than temperature. To construct near-term regional climate messages there is therefore a need for a better understanding of the processes governing internal variability, such as the oceanic modes of variability, and the teleconnections that connect them to the regions around the world (Sections 10.3, 10.4 and 10.6).
- Methodologies on how to propagate climate uncertainties from global, regional, and up to the human settlement scale are still under development and more investigations are needed for the assessment. For the moment, the production of a climate message at this scale relies mainly on GCMs or RCMs that often do not incorporate urban parametrizations in their land-surface components. In some cases, bias adjustment methods are used with a substantial lack of the physical process involved at this scale. There is also a strong limitation to constraint the uncertainties due to the reduced availability of long-term monitoring stations in cities, as mentioned above. These difficulties limit the usefulness of current climate messages at the urban scale (Box 10.2).
- There is limited literature about the construction of regional climate messages. Regional and local climate messages developed by governmental institutions therefore follow different approaches, thus not being necessarily coherent in the messages produced and communicated. This could be improved implementing a quality control system. Regional and local climate communications are not always available in English and there is need for a database collecting these messages. The climate research community also needs to work further with the social sciences and humanities to better understand how potential users of regional climate messages perceive and respond to them, as well as to translate their requirements to be understood by researchers (Section 10.5).
- There is a shortage of regional climate change studies based on multiple lines of evidence. Most studies rely on either GCMs (potentially bias-adjusted) or downscaled GCMs. But there are only few studies combining information obtained from observations, process understanding and hierarchies of models comprehensively evaluated to address relevant aspects at different spatial scales (Sections 10.5 and 10.6).

Frequently Asked Questions

FAQ 10.1: How can we provide useful climate information for regional stakeholders?

The world is physically and culturally diverse, and the challenges posed by climate change vary by region and location. Because climate change affects so many aspects of people's daily work and living, information about climate change can help with decision-making, but only when the information is relevant for the people involved in making those decisions. Users of climate information may be highly diverse, ranging from professionals in areas such as human health, agriculture or water management to a broader community that experiences the impacts of changing climate. Providing useful, actionable information thus requires an awareness of local contexts, agreement on the appropriate formulation of the information, and a mutual understanding of limitations and uncertainties.

The development, delivery, and use of climate change information are inherently influenced by the values of all parties involved: those providing the information, those communicating the information, those hearing the information, and those who need the information in order to make decisions or solve problems Consequently, partnerships between these participating communities, especially involving those for whom the information is intended, can help ensure that the appropriate information is delivered and provided in ways that are accessible and usable by decision-makers.

Effective partnerships recognize and respond to the values of all parties involved, especially when they involve culturally diverse communities. This is particularly true for climate change – a global issue posing challenges that vary by region. Challenges like this require exchanging information between groups that may be culturally diverse and from different disciplines and domains of expertise. By recognizing this diversity, climate information can be made more relevant and credible, most notably when conveying the complexity of risks for human systems and ecosystems and for building resilience in developing nations, which may be more vulnerable to damaging impacts of climate change.

Useful climate information can come in many different forms and from many different sources. For example, climate scientists can provide information on future changes by extending historical trends forward into the future, using model simulations of the global and/or regional climate change, and inferring regional change by evaluating changes in the weather behaviour that influences a region. Constructing useful climate information requires considering all available sources in order to capture the fullest possible representation of projected changes and distil the information in a way that meets needs of the stakeholders and communities impacted by the changes. Ideally, the distillation process (FAQ 10.1, Figure 1) engages with the intended recipients of the information, especially stakeholders whose work involves non-climatic factors, such as human health, agriculture or water resources. The distillation should evaluate the accuracy of all information sources (observations, simulations, expert judgement), weigh the credibility of possible conflicting information, and arrive at climate information that also estimates the confidence a user should have the information. Information providers should further recognize that the geographic regions and time periods governing stakeholders' interest (for example, the growing season of an agricultural zone) may not align well with the time and space resolution of available climate data, and thus additional development may be required to extract useful climate information.

Successfully framing information on climate impacts and effective societal responses requires presenting information in the context of the local challenges posed by climate change. For example, the U.S. state of Arizona passed an initiative that responded to a specific, local impact of climate change—water-resource shortfalls in Arizona – even though some of the state's government leaders were unsure about global climate change. The success of this effort was the result of recognizing a serious impact while avoiding the central, but likely controversial, motivation of fighting global climate change. Similarly, city officials of Lusaka in Zambia engaged in a sustained dialogue with climate scientists. The result was a partnership that constructs and communicates climate information relevant to governing an African city vulnerable to climate change, such as changes in rain seasons.
Stakeholders often need information about complex, compound events—such as floods following a period of drought – and the information they need, such as data on heat-stress conditions or a drought index, may not

be a primary concern for scientists focused on projecting changes in the physical climate system

One way to link complex information to stakeholder applications is through stories. Storylines give climate change information in a form that connects with the recipients' experiences of existing weather and climate. These storylines can make climate information more accessible and physically comprehensible. For example, a storyline may take a common experience like the arrival and duration of a winter storm and show how the storm's snowfall and winds will change in the future. The development of storylines uses the experience and expertise of stakeholders who seek to develop appropriate response measures, such as water-resource managers and health professionals. With appropriate choices, storylines can engage nuances of the climate information in a meaningful way by building on common experiences, thus enhancing the information's usefulness.

[START FAQ 10.1, FIGURE 1 HERE]

FAQ 10.1, Figure 1: [Placeholder, the figure will be updated: Climate information for decision makers is more useful if the physical and cultural diversity across the world is considered. The figure illustrates schematically the broad range of knowledge that must be blended with the diversity of users to distil information that will have relevance and credibility.**]**

[END FAQ 10.1, FIGURE 1 HERE]

FAQ 10.2: How does the growth of cities interact with climate change?

Urban areas with buildings in close proximity to each other "trap" heat, reduce the natural ventilation and modify the local radiation and energy balance. Combined with less vegetation and heat released by human activities, cities are creating the so-called "urban heat island" (UHI), which causes cities to experience higher than average temperatures than their surrounding areas. Urbanization and the increasing severity of heat waves under climate change further amplify this effect.

Cities are on front line in both the causes and the effects of climate change. On one hand, cities are responsible for up to 70% of current emissions of GHGs yet occupy less than 1% of global land mass. By 2030, almost 60% of the world's population will live in urban areas and every year sees the addition of 67 million new urban dwellers, 90% of these is added to cities in developing countries. On the other hand, cities and their inhabitants are highly vulnerable to climate extremes, including more frequent, longer and more intense heat waves. Urban areas are already vulnerable to increased thermal stress during heat-waves and projected rates of urban growth means that vulnerability will increase. This became apparent in 2003 in Paris, France, when daily mortality tripled during a heat wave in early August (around 30,000 causalities), or in 2010, in Ahmedabad, India, when a heatwave killed more than 1,100 people.
Due to the low albedo (reflectivity) of impervious surfaces, such as rooftops and asphalt roadways, differential heat storage (big heat capacity of building materials), anthropogenic heat, reduced wind speed (greater surface roughness), and light trapping within the canyons formed by taller structures, cities 'trap' heat (see FAQ10.2 Figure 1). They are therefore often associated with elevated surface air temperature, a phenomenon referred to as the urban heat island, where night-time urban air temperature is substantially higher (several degrees) than corresponding temperatures in the surrounding rural areas. In different cities around the world with different background climate, it has been found that during heat waves episodes, the urban heat islands gets intensified compared to its climatological mean values.

Although the urban heat island phenomenon is well documented and better understood, important measurements of meteorological and external climatic drivers across urban areas remain are lacking, due to the scarcity of high-density, in-situ measurement networks. Especially, long-term datasets (a year or more) are very scarce but invaluable because they allow more in-depth research on the seasonal evolution of the urban climate. In many cities, especially in the developing world, the historical record is too short, discontinuous, or the quality too uncertain to support trend analysis and climate change attribution.

Estimating how the urban heat island will evolve under climate change conditions is uncertain because several studies, which use a variety of methods, report contrasting results. However, there is *clear evidence* that future urbanization amplifies the projected air temperature under different background climate *with a strong impact on minimum temperatures that could be comparable in magnitude to the global warming*.

Climate change will, on average, have a limited impact on the magnitude of the urban heat island but urbanization together with more frequent extreme climatic events (e.g. heat waves) will strongly affect cities.

[START FAQ 10.2, FIGURE 1 HERE]

FAQ 10.2, Figure 1: [Placeholder, the figure will be updated: Various factors contribute to either warm up or cool down urban areas, compared to their surroundings. Overall, cities tend to be warmer than their surroundings. This is called the "urban heat island" effect. Values are taken from the recent literature.**]**

[START FAQ 10.2, FIGURE 1 HERE]

References

Aalbers, E. E., Lenderink, G., van Meijgaard, E., and van den Hurk, B. J. J. M. (2018). Local-scale changes in mean and heavy precipitation in Western Europe, climate change or internal variability? *Clim. Dyn.* 50, 4745–4766. doi:10.1007/s00382-017-3901-9.

Aalto, J., Pirinen, P., and Jylhä, K. (2016). New gridded daily climatology of Finland: Permutation-based uncertainty estimates and temporal trends in climate. *J. Geophys. Res. Atmos.* 121, 3807–3823. doi:10.1002/2015JD024651.

Abatzoglou, J. T., and Brown, T. J. (2012). A comparison of statistical downscaling methods suited for wildfire applications. *Int. J. Climatol.* 32, 772–780. doi:10.1002/joc.2312.

Abba Omar, S., and Abiodun, B. J. (2020). Characteristics of cut-off lows during the 2015–2017 drought in the Western Cape, South Africa. *Atmos. Res.* 235, 104772. doi:10.1016/j.atmosres.2019.104772.

Abera, W., Brocca, L., and Rigon, R. (2016). Comparative evaluation of different satellite rainfall estimation products and bias correction in the Upper Blue Nile (UBN) basin. *Atmos. Res.* 178–179, 471–483. doi:10.1016/j.atmosres.2016.04.017.

Abiodun, B. J., Adegoke, J., Abatan, A. A., Ibe, C. A., Egbebiyi, T. S., Engelbrecht, F., et al. (2017). Potential impacts of climate change on extreme precipitation over four African coastal cities. *Clim. Change* 143, 399–413. doi:10.1007/s10584-017-2001-5.

Abramowitz, G., Herger, N., Gutmann, E., Hammerling, D., Knutti, R., Leduc, M., et al. (2018). Model dependence in multi-model climate ensembles: weighting, sub-selection and out-of-sample testing. *Earth Syst. Dyn. Discuss.*, 1–20. doi:10.5194/esd-2018-51.

Ackerley, D., Booth, B. B. B., Knight, S. H. E., Highwood, E. J., Frame, D. J., Allen, M. R., et al. (2011). Sensitivity of Twentieth-Century Sahel rainfall to sulfate aerosol and CO2 forcing. *J. Clim.* doi:10.1175/JCLI-D-11-00019.1.

Ackerman, T. P., and Stokes, G. M. (2003). The Atmospheric Radiation Measurement Program. *Phys. Today* 56, 38–44. doi:10.1063/1.1554135.

Adachi, S. A., Kimura, F., Kusaka, H., Inoue, T., and Ueda, H. (2012). Comparison of the Impact of Global Climate Changes and Urbanization on Summertime Future Climate in the Tokyo Metropolitan Area. *J. Appl. Meteorol. Climatol.* 51, 1441–1454. doi:10.1175/JAMC-D-11-0137.1.

Addor, N., Rohrer, M., Furrer, R., and Seibert, J. (2016). Propagation of biases in climate models from the synoptic to the regional scale: Implications for bias adjustment. *J. Geophys. Res. Atmos.* 121, 2075–2089. doi:10.1002/2015JD024040.

Adloff, F., Jordà, G., Somot, S., Sevault, F., Arsouze, T., Meyssignac, B., et al. (2018). Improving sea level simulation in Mediterranean regional climate models. *Clim. Dyn.* 51, 1167–1178. doi:10.1007/s00382-017-3842-3.

Adnan, M., Rehman, N., Ali, S., Mehmood, S., Mir, K. A., Khan, A. A., et al. (2017). Prediction of summer rainfall in Pakistan from global sea-surface temperature and sea-level pressure. *Weather* 72, 76–84. doi:10.1002/wea.2784.

Ahmed, K. F., Wang, G., Silander, J., Wilson, A. M., Allen, J. M., Horton, R., et al. (2013). Statistical downscaling and bias correction of climate model outputs for climate change impact assessment in the U.S. northeast. *Glob. Planet. Change* 100, 320–332. doi:10.1016/j.gloplacha.2012.11.003.

Ahn, M.-S., Kim, D., Sperber, K. R., Kang, I.-S., Maloney, E., Waliser, D., et al. (2017). MJO simulation in CMIP5 climate models: MJO skill metrics and process-oriented diagnosis. *Clim. Dyn.* 49, 4023–4045. doi:10.1007/s00382-017-3558-4.

Ajaaj, A. A., Mishra, A. K., and Khan, A. A. (2018). Urban and peri-urban precipitation and air temperature trends in mega cities of the world using multiple trend analysis methods. *Theor. Appl. Climatol.* 132, 403–418. doi:10.1007/s00704-017-2096-7.

Akhtar, N., Brauch, J., and Ahrens, B. (2018). Climate modeling over the Mediterranean Sea: impact of resolution and ocean coupling. *Clim. Dyn.* 51, 933–948. doi:10.1007/s00382-017-3570-8.

Akhtar, N., Brauch, J., Dobler, A., Béranger, K., and Ahrens, B. (2014). Medicanes in an ocean–atmosphere coupled regional climate model. *Nat. Hazards Earth Syst. Sci.* 14, 2189–2201. doi:10.5194/nhess-14-2189-2014.

Akhtar, N., Krug, A., Brauch, J., Arsouze, T., Dieterich, C., and Ahrens, B. (2019). European marginal seas in a regional atmosphere–ocean coupled model and their impact on Vb-cyclones and associated precipitation. *Clim. Dyn.* 53, 5967–5984. doi:10.1007/s00382-019-04906-x.

Akhter, J., Das, L., Meher, J. K., and Deb, A. (2019). Evaluation of different large-scale predictor-based statistical downscaling models in simulating zone-wise monsoon precipitation over India. *Int. J. Climatol.* 39, 465–482. doi:10.1002/joc.5822.

Alessandri, A., De Felice, M., Zeng, N., Mariotti, A., Pan, Y., Cherchi, A., et al. (2015). Robust assessment of the expansion and retreat of Mediterranean climate in the 21 st century. *Sci. Rep.* 4, 7211. doi:10.1038/srep07211.

Alghamdi, A. S., and Moore, T. W. (2015). Detecting Temporal Changes in Riyadh's Urban Heat Island. *Pap. Appl. Geogr.* 1, 312–325. doi:10.1080/23754931.2015.1084525.

Alizadeh-Choobari, O., Ghafarian, P., and Adibi, P. (2016). Inter-annual variations and trends of the urban warming in Tehran. *Atmos. Res.* 170, 176–185. doi:10.1016/j.atmosres.2015.12.001.

Allan, R., Brohan, P., Compo, G. P., Stone, R., Luterbacher, J., and Brönnimann, S. (2011). The International Atmospheric Circulation Reconstructions over the Earth (ACRE) Initiative. *Bull. Am. Meteorol. Soc.* 92, 1421–

1425. doi:10.1175/2011BAMS3218.1.
Allen, M. R., Dube, O. P., Solecki, W., Aragón–Durand, F., Cramer, W., Humphreys, S., et al. (2018). "Framing and Context," in *Global warming of 1.5°C. An IPCC Special Report on the impacts of global warming of 1.5°C above pre-industrial levels and related global greenhouse gas emission pathways, in the context of strengthening the global response to the threat of climate change*, eds. V. Masson-Delmotte, P. Zhai, H.-O. Pörtner, D. Roberts, J. Skea, P. R. Shukla, et al. (Geneva, Switzerland: In Press).
Allen, M. R., Stott, P. A., Mitchell, J. F. B., Schnur, R., and Delworth, T. L. (2000). Quantifying the uncertainty in forecasts of anthropogenic climate change. *Nature* 407, 617–620. doi:10.1038/35036559.
Allen, R. J., and Kovilakam, M. (2017). The Role of Natural Climate Variability in Recent Tropical Expansion. *J. Clim.* 30, 6329–6350. doi:10.1175/JCLI-D-16-0735.1.
Allen, R. J., Norris, J. R., and Wild, M. (2013). Evaluation of multidecadal variability in CMIP5 surface solar radiation and inferred underestimation of aerosol direct effects over Europe, China, Japan, and India. *J. Geophys. Res. Atmos.* 118, 6311–6336. doi:10.1002/jgrd.50426.
Almazroui, M. (2016). RegCM4 in climate simulation over CORDEX-MENA/Arab domain: selection of suitable domain, convection and land-surface schemes. *Int. J. Climatol.* 36, 236–251. doi:10.1002/joc.4340.
Almazroui, M. (2019). Temperature Changes over the CORDEX-MENA Domain in the 21st Century Using CMIP5 Data Downscaled with RegCM4: A Focus on the Arabian Peninsula. *Adv. Meteorol.* doi:10.1155/2019/5395676.
Almazroui, M., Islam, M. N., Al-Khalaf, A. K., and Saeed, F. (2016a). Best convective parameterization scheme within RegCM4 to downscale CMIP5 multi-model data for the CORDEX-MENA/Arab domain. *Theor. Appl. Climatol.* 124, 807–823. doi:10.1007/s00704-015-1463-5.
Almazroui, M., Islam, M. N., Alkhalaf, A. K., Saeed, F., Dambul, R., and Rahman, M. A. (2016b). Simulation of temperature and precipitation climatology for the CORDEX-MENA/Arab domain using RegCM4. *Arab. J. Geosci.* 9, 13. doi:10.1007/s12517-015-2045-7.
Almazroui, M., Saeed, S., Islam, M., and Al., E. (submitted). CMIP6 simulated changes of projected temperature and precipitation over Africa CMIP6. *Earth Syst. Environ.* (submitted).
Alter, R. E., Im, E.-S., and Eltahir, E. A. B. (2015). Rainfall consistently enhanced around the Gezira Scheme in East Africa due to irrigation. *Nat. Geosci.* 8, 763–767. doi:10.1038/ngeo2514.
Amador, J. A. (1998). A climatic feature of the tropical Americas : The trade wind easterly jet The Intra-Americas Sea Low-level Jet Overview and Future Research. doi:10.1196/annals.1446.012.
Amaya, D. J., Siler, N., Xie, S.-P., and Miller, A. J. (2018). The interplay of internal and forced modes of Hadley Cell expansion: lessons from the global warming hiatus. *Clim. Dyn.* 51, 305–319. doi:10.1007/s00382-017-3921-5.
Anderson, G. B., Bell, M. L., and Peng, R. D. (2013). Methods to Calculate the Heat Index as an Exposure Metric in Environmental Health Research. *Environ. Health Perspect.* 121, 1111–1119. doi:10.1289/ehp.1206273.
Andreassen, H. P., Gangaas, K. E., and Kaltenborn, B. P. (2018). Matching social-ecological systems by understanding the spatial scale of environmental attitudes. *Nat. Conserv.* 30, 69–81. doi:10.3897/natureconservation.30.28289.
Annamalai, H., Hafner, J., Sooraj, K. P., and Pillai, P. (2013). Global warming shifts the monsoon circulation, drying South Asia. *J. Clim.* 26, 2701–2718. doi:10.1175/JCLI-D-12-00208.1.
Anstey, J. A., Davini, P., Gray, L. J., Woollings, T. J., Butchart, N., Cagnazzo, C., et al. (2013). Multi-model analysis of Northern Hemisphere winter blocking: Model biases and the role of resolution. *J. Geophys. Res. Atmos.* 118, 3956–3971. doi:10.1002/jgrd.50231.
Arblaster, J. M., Meehl, G. A., and Karoly, D. J. (2011). Future climate change in the Southern Hemisphere: Competing effects of ozone and greenhouse gases. *Geophys. Res. Lett.* 38. doi:10.1029/2010GL045384.
Archer, E., Engelbrecht, F., Hänsler, A., Landman, W., Tadross, M., and Helmschrot, J. (2018). Seasonal prediction and regional climate projections for southern Africa. *Biodivers. Ecol.* 6, 14–21. doi:10.7809/b-e.00296.
Ardilouze, C., Batté, L., Déqué, M., van Meijgaard, E., and van den Hurk, B. (2019). Investigating the impact of soil moisture on European summer climate in ensemble numerical experiments. *Clim. Dyn.* 52, 4011–4026. doi:10.1007/s00382-018-4358-1.
Argüeso, D., Evans, J. P., Fita, L., and Bormann, K. J. (2014). Temperature response to future urbanization and climate change. *Clim. Dyn.* 42, 2183–2199. doi:10.1007/s00382-013-1789-6.
Arnold, D. G. "Introduction: climate change and ethics," in *The Ethics of Global Climate Change*, ed. D. G. Arnold (Cambridge: Cambridge University Press), 1–15. doi:10.1017/CBO9780511732294.001.
Arsiso, B. K., Mengistu Tsidu, G., Stoffberg, G. H., and Tadesse, T. (2018). Influence of urbanization-driven land use/cover change on climate: The case of Addis Ababa, Ethiopia. *Phys. Chem. Earth*. doi:10.1016/j.pce.2018.02.009.
Aryee, J. N. A., Amekudzi, L. K., Quansah, E., Klutse, N. A. B., Atiah, W. A., and Yorke, C. (2018). Development of high spatial resolution rainfall data for Ghana. *Int. J. Climatol.* 38, 1201–1215. doi:10.1002/joc.5238.
Ashby, S. a., Taylor, M. A., and Chen, A. A. (2005). Statistical models for predicting rainfall in the Caribbean. *Theor. Appl. Climatol.* 82, 65–80. doi:10.1007/s00704-004-0118-8.
Ashcroft, L., Allan, R., Bridgman, H., Gergis, J., Pudmenzky, C., and Thornton, K. (2016). Current climate data rescue activities in Australia. *Adv. Atmos. Sci.* 33, 1323–1324. doi:10.1007/s00376-016-6189-5.
Ashouri, H., Hsu, K.-L., Sorooshian, S., Braithwaite, D. K., Knapp, K. R., Cecil, L. D., et al. (2015). PERSIANN-CDR:

Daily Precipitation Climate Data Record from Multisatellite Observations for Hydrological and Climate Studies. *Bull. Am. Meteorol. Soc.* 96, 69–83. doi:10.1175/BAMS-D-13-00068.1.
Attada Raju, and Parekh, A., and Chowdary J S., and and Gnanaseelan C (2018). Reanalysis of the Indian summer monsoon: four dimensional data assimilation of AIRS retrievals in a regional data assimilation and modeling framework. *Clim. Dyn.* 50, 2905–2923. doi:10.1007/s00382-017-3781-z.
Attema, J., Bakker, A., Beersma, J., Bessembinder, J., Boers, R., Brandsma, T., et al. (2014). KNMI'14: Climate Change scenarios for the 21st Century–A Netherlands perspective. *Sci. Rep. WR2014-01*. Available at: http://www.klimaatscenarios.nl/brochures/images/KNMI_WR_2014-01_version26May2014.pdf.
Auchmann, R., and Brönnimann, S. (2012). A physics-based correction model for homogenizing sub-daily temperature series. *J. Geophys. Res. Atmos.* 117. doi:10.1029/2012JD018067.
Ayarzagüena, B., Polvani, L. M., Langematz, U., Akiyoshi, H., Bekki, S., Butchart, N., et al. (2018). No robust evidence of future changes in major stratospheric sudden warmings: a multi-model assessment from CCMI. *Atmos. Chem. Phys.* 18, 11277–11287. doi:10.5194/acp-18-11277-2018.
Ayarzagüena, B., and Screen, J. A. (2016). Future Arctic sea ice loss reduces severity of cold air outbreaks in midlatitudes. *Geophys. Res. Lett.* 43, 2801–2809. doi:10.1002/2016GL068092.
Azam, M. F., Wagnon, P., Berthier, E., Vincent, C., Fujita, K., and Kargel, J. S. (2018). Review of the status and mass changes of Himalayan-Karakoram glaciers. *J. Glaciol.* 64, 61–74. doi:10.1017/jog.2017.86.
Azmat, M., Liaqat, U. W., Qamar, M. U., and Awan, U. K. (2017). Impacts of changing climate and snow cover on the flow regime of Jhelum River, Western Himalayas. *Reg. Environ. Chang.* 17, 813–825. doi:10.1007/s10113-016-1072-6.
Babu, S. S., Manoj, M. R., Moorthy, K. K., Gogoi, M. M., Nair, V. S., Kompalli, S. K., et al. (2013). Trends in aerosol optical depth over Indian region: Potential causes and impact indicators. *J. Geophys. Res. Atmos.* 118, 11,794-11,806. doi:10.1002/2013JD020507.
Bader, D. A., Blake, R., Grimm, A., Hamdi, R., Kim, Y., Horton, R., et al. (2018). "Urban Climate Science," in *Climate Change and Cities*, eds. C. Rosenzweig, P. Romero-Lankao, S. Mehrotra, S. Dhakal, S. Ali Ibrahim, and W. D. Solecki (Cambridge: Cambridge University Press), 27–60. doi:10.1017/9781316563878.009.
Bador, M., Boé, J., Terray, L., and et al. (submitted). Impact of higher spatial atmospheric resolution on precipitation extremes over land in global climate models. *J. Geophys. Res. Atmos.* (submitted).
Bador, M., Terray, L., and Boé, J. (2016). Emergence of human influence on summer record-breaking temperatures over Europe. *Geophys. Res. Lett.* 43, 404–412. doi:10.1002/2015GL066560.
Bain, P. G., Hornsey, M. J., Bongiorno, R., and Jeffries, C. (2012). Promoting pro-environmental action in climate change deniers. *Nat. Clim. Chang.* 2, 600–603. doi:10.1038/nclimate1532.
Baker, D. J., Hartley, A. J., Butchart, S. H. M., and Willis, S. G. (2016). Choice of baseline climate data impacts projected species' responses to climate change. *Glob. Chang. Biol.* 22, 2392–2404. doi:10.1111/gcb.13273.
Bal, P. K., Ramachandran, A., Palanivelu, K., Thirumurugan, P., Geetha, R., and Bhaskaran, B. (2016). Climate change projections over India by a downscaling approach using PRECIS. *Asia-Pacific J. Atmos. Sci.* 52, 353–369. doi:10.1007/s13143-016-0004-1.
Balsamo, G., Albergel, C., Beljaars, A., Boussetta, S., Brun, E., Cloke, H., et al. (2015). ERA-Interim/Land: a global land surface reanalysis data set. *Hydrol. Earth Syst. Sci.* 19, 389–407. doi:10.5194/hess-19-389-2015.
Ban, N., Schmidli, J., and Schär, C. (2014). Evaluation of the convection-resolving regional climate modeling approach in decade-long simulations. *J. Geophys. Res. Atmos.* 119, 7889–7907. doi:10.1002/2014JD021478.
Ban, N., Schmidli, J., and Schär, C. (2015). Heavy precipitation in a changing climate: Does short-term summer precipitation increase faster? *Geophys. Res. Lett.* 42, 1165–1172. doi:10.1002/2014GL062588.
Bandoro, J., Solomon, S., Donohoe, A., Thompson, D. W. J., and Santer, B. D. (2014). Influences of the Antarctic Ozone Hole on Southern Hemispheric Summer Climate Change. *J. Clim.* 27, 6245–6264. doi:10.1175/JCLI-D-13-00698.1.
Barcikowska, M. J., Kapnick, S. B., Krishnamurty, L., Russo, S., Cherchi, A., and Folland, C. K. (2019). Changes in the future summer Mediterranean climate: contribution of teleconnections and local factors. *Earth Syst. Dyn. Discuss.*, 1–43. doi:10.5194/esd-2018-85.
Bárdossy, A., and Pegram, G. (2012). Multiscale spatial recorrelation of RCM precipitation to produce unbiased climate change scenarios over large areas and small. *Water Resour. Res.* 48. doi:10.1029/2011WR011524.
Barlage, M., Tewari, M., Chen, F., Miguez-Macho, G., Yang, Z. L., and Niu, G. Y. (2015). The effect of groundwater interaction in North American regional climate simulations with WRF/Noah-MP. *Clim. Change*. doi:10.1007/s10584-014-1308-8.
Barlow, J., Best, M., Bohnenstengel, S. I., Clark, P., Grimmond, S., Lean, H., et al. (2017). Developing a Research Strategy to Better Understand, Observe, and Simulate Urban Atmospheric Processes at Kilometer to Subkilometer Scales. *Bull. Am. Meteorol. Soc.* 98, ES261–ES264. doi:10.1175/BAMS-D-17-0106.1.
Barnes, E. A. (2013). Revisiting the evidence linking Arctic amplification to extreme weather in midlatitudes. *Geophys. Res. Lett.* 40, 4734–4739. doi:10.1002/grl.50880.
Barnes, E. A., Barnes, N. W., and Polvani, L. M. (2014a). Delayed Southern Hemisphere Climate Change Induced by Stratospheric Ozone Recovery, as Projected by the CMIP5 Models. *J. Clim.* 27, 852–867. doi:10.1175/JCLI-D-

13-00246.1.
Barnes, E. A., Dunn-Sigouin, E., Masato, G., and Woollings, T. (2014b). Exploring recent trends in Northern Hemisphere blocking. *Geophys. Res. Lett.* 41, 638–644. doi:10.1002/2013GL058745.
Barnes, E. A., and Polvani, L. (2013). Response of the Midlatitude Jets, and of Their Variability, to Increased Greenhouse Gases in the CMIP5 Models. *J. Clim.* 26, 7117–7135. doi:10.1175/JCLI-D-12-00536.1.
Barnes, E. A., and Screen, J. A. (2015). The impact of Arctic warming on the midlatitude jet-stream: Can it? Has it? Will it? *Wiley Interdiscip. Rev. Clim. Chang.* 6, 277–286. doi:10.1002/wcc.337.
Barredo, J. I., Mauri, A., Caudullo, G., and Dosio, A. (2018). Assessing Shifts of Mediterranean and Arid Climates Under RCP4.5 and RCP8.5 Climate Projections in Europe. *Pure Appl. Geophys.* 175, 3955–3971. doi:10.1007/s00024-018-1853-6.
Barreiro, M., Díaz, N., and Renom, M. (2014). Role of the global oceans and land–atmosphere interaction on summertime interdecadal variability over northern Argentina. *Clim. Dyn.* 42, 1733–1753. doi:10.1007/s00382-014-2088-6.
Barrett, B., Nitze, I., Green, S., and Cawkwell, F. (2014). Assessment of multi-temporal, multi-sensor radar and ancillary spatial data for grasslands monitoring in Ireland using machine learning approaches. *Remote Sens. Environ.* 152, 109–124. doi:https://doi.org/10.1016/j.rse.2014.05.018.
Barros, V., Chamorro, L., Coronel, G., and Baez, J. (2004). The Major Discharge Events in the Paraguay River: Magnitudes, Source Regions, and Climate Forcings. *J. Hydrometeorol.* 5, 1161–1170. doi:10.1175/JHM-378.1.
Barros, V. R., Boninsegna, J. A., Camilloni, I. A., Chidiak, M., Magrín, G. O., and Rusticucci, M. (2015). Climate change in Argentina: trends, projections, impacts and adaptation. *Wiley Interdiscip. Rev. Clim. Chang.* 6, 151–169. doi:10.1002/wcc.316.
Barry, R. G. (2012). Recent advances in mountain climate research. *Theor. Appl. Climatol.* 110, 549–553. doi:10.1007/s00704-012-0695-x.
Barsugli, J. J., Guentchev, G., Horton, R. M., Wood, A., Mearns, L. O., Liang, X.-Z., et al. (2013). The Practitioner's Dilemma: How to Assess the Credibility of Downscaled Climate Projections. *Eos, Trans. Am. Geophys. Union* 94, 424–425. doi:10.1002/2013EO460005.
Bartók, B. (2017). Aerosol radiative effects under clear skies over Europe and their changes in the period of 2001-2012. *Int. J. Climatol.* 37, 1901–1909. doi:10.1002/joc.4821.
Bartók, B., Wild, M., Folini, D., Lüthi, D., Kotlarski, S., Schär, C., et al. (2017). Projected changes in surface solar radiation in CMIP5 global climate models and in EURO-CORDEX regional climate models for Europe. *Clim. Dyn.* 49, 2665–2683. doi:10.1007/s00382-016-3471-2.
Bates, B. C., Chandler, R. E., Charles, S. P., and Campbell, E. P. (2010). Assessment of apparent nonstationarity in time series of annual inflow, daily precipitation, and atmospheric circulation indices: A case study from southwest Western Australia. *Water Resour. Res.* 46. doi:10.1029/2010WR009509.
Bates, J. J., and Privette, J. L. (2012). A maturity model for assessing the completeness of climate data records. *Eos, Trans. Am. Geophys. Union* 93, 441–441. doi:10.1029/2012EO440006.
Bathiany, S., Dakos, V., Scheffer, M., and Lenton, T. M. (2018). Climate models predict increasing temperature variability in poor countries. *Sci. Adv.* 4, 1–11. doi:10.1126/sciadv.aar5809.
Baumberger, C., Knutti, R., and Hirsch Hadorn, G. (2017). Building confidence in climate model projections: an analysis of inferences from fit. *Wiley Interdiscip. Rev. Clim. Chang.* 8, e454. doi:10.1002/wcc.454.
Baztan, J., Cordier, M., Huctin, J.-M., Zhu, Z., and Vanderlinden, J.-P. (2017). Life on thin ice: Insights from Uummannaq, Greenland for connecting climate science with Arctic communities. *Polar Sci.* 13, 100–108. doi:10.1016/j.polar.2017.05.002.
Beck, H. E., van Dijk, A. I. J. M., de Roo, A., Dutra, E., Fink, G., Orth, R., et al. (2017a). Global evaluation of runoff from 10 state-of-the-art hydrological models. *Hydrol. Earth Syst. Sci.* 21, 2881–2903. doi:10.5194/hess-21-2881-2017.
Beck, H. E., Vergopolan, N., Pan, M., Levizzani, V., van Dijk, A. I. J. M., Weedon, G. P., et al. (2017b). Global-scale evaluation of 22 precipitation datasets using gauge observations and hydrological modeling. *Hydrol. Earth Syst. Sci.* 21, 6201–6217. doi:10.5194/hess-21-6201-2017.
Becker, A., Finger, P., Meyer-Christoffer, A., Rudolf, B., Schamm, K., Schneider, U., et al. (2013). A description of the global land-surface precipitation data products of the Global Precipitation Climatology Centre with sample applications including centennial (trend) analysis from 1901–present. *Earth Syst. Sci. Data* 5, 71–99. doi:10.5194/essd-5-71-2013.
Bellenger, H., Guilyardi, E., Leloup, J., Lengaigne, M., and Vialard, J. (2014). ENSO representation in climate models: from CMIP3 to CMIP5. *Clim. Dyn.* 42, 1999–2018. doi:10.1007/s00382-013-1783-z.
Bellprat, O., Kotlarski, S., Lüthi, D., and Schär, C. (2013). Physical constraints for temperature biases in climate models. *Geophys. Res. Lett.* 40, 4042–4047. doi:10.1002/grl.50737.
Belušić, A., Prtenjak, M. T., Güttler, I., Ban, N., Leutwyler, D., and Schär, C. (2018). Near-surface wind variability over the broader Adriatic region: insights from an ensemble of regional climate models. *Clim. Dyn.* 50, 4455–4480. doi:10.1007/s00382-017-3885-5.
Benedict, J. J., Maloney, E. D., Sobel, A. H., and Frierson, D. M. W. (2014). Gross Moist Stability and MJO Simulation

Skill in Three Full-Physics GCMs. *J. Atmos. Sci.* 71, 3327–3349. doi:10.1175/JAS-D-13-0240.1.
Bengtsson, L., and Hodges, K. I. (2018). Can an ensemble climate simulation be used to separate climate change signals from internal unforced variability? *Clim. Dyn.* doi:10.1007/s00382-018-4343-8.
Beniston, M., Farinotti, D., Stoffel, M., Andreassen, L. M., Coppola, E., Eckert, N., et al. (2018). The European mountain cryosphere: a~review of its current state, trends, and future challenges. *Cryosph.* 12, 759–794. doi:10.5194/tc-12-759-2018.
Bennington, V., Notaro, M., and Holman, K. D. (2014). Improving Climate Sensitivity of Deep Lakes within a Regional Climate Model and Its Impact on Simulated Climate. *J. Clim.* 27, 2886–2911. doi:10.1175/JCLI-D-13-00110.1.
Beranová, R., and Kyselý, J. (2016). Links between circulation indices and precipitation in the Mediterranean in an ensemble of regional climate models. *Theor. Appl. Climatol.* 123, 693–701. doi:10.1007/s00704-015-1381-6.
Berckmans, J., Hamdi, R., and Dendoncker, N. (2019). Bridging the gap between policy-driven land use changes and regional climate projections. *J. Geophys. Res.* doi:10.1029/2018JD029207.
Berckmans, J., Woollings, T., Demory, M.-E., Vidale, P.-L., and Roberts, M. (2013). Atmospheric blocking in a high resolution climate model: influences of mean state, orography and eddy forcing. *Atmos. Sci. Lett.* 14, 34–40. doi:10.1002/asl2.412.
Berthou, S., Kendon, E. J., Chan, S. C., Ban, N., Leutwyler, D., Schär, C., et al. (2018). Pan-European climate at convection-permitting scale: a model intercomparison study. *Clim. Dyn.* doi:10.1007/s00382-018-4114-6.
Berthou, S., Mailler, S., Drobinski, P., Arsouze, T., Bastin, S., Béranger, K., et al. (2015). Sensitivity of an intense rain event between atmosphere-only and atmosphere-ocean regional coupled models: 19 September 1996. *Q. J. R. Meteorol. Soc.* 141, 258–271. doi:10.1002/qj.2355.
Besselaar, E. J. M., Sanchez-Lorenzo, A., Wild, M., Klein Tank, A. M. G., and Laat, A. T. J. (2015). Relationship between sunshine duration and temperature trends across Europe since the second half of the twentieth century. *J. Geophys. Res. Atmos.* 120, 10,810-10,836. doi:10.1002/2015JD023640.
Bessette, D. L., Mayer, L. A., Cwik, B., Vezér, M., Keller, K., Lempert, R. J., et al. (2017). Building a Values-Informed Mental Model for New Orleans Climate Risk Management. *Risk Anal.* 37, 1993–2004. doi:10.1111/risa.12743.
Best, M. J., and Grimmond, C. S. B. (2015). Key Conclusions of the First International Urban Land Surface Model Comparison Project. *Bull. Am. Meteorol. Soc.* 96, 805–819. doi:10.1175/BAMS-D-14-00122.1.
Best, M. J., Grimmond, C. S. B., and Villani, M. G. (2006). Evaluation of the urban tile in MOSES using surface energy balance observations. *Boundary-Layer Meteorol.* 118, 503–525. doi:10.1007/s10546-005-9025-5.
Bevacqua, E., Maraun, D., Hobæk Haff, I., Widmann, M., and Vrac, M. (2017). Multivariate statistical modelling of compound events via pair-copula constructions: analysis of floods in Ravenna (Italy). *Hydrol. Earth Syst. Sci.* 21, 2701–2723. doi:10.5194/hess-21-2701-2017.
Bhardwaj, A., Wasson, R. J., Ziegler, A. D., Chow, W. T. L., and Sundriyal, Y. P. (2019). Characteristics of rain-induced landslides in the Indian Himalaya: A case study of the Mandakini Catchment during the 2013 flood. *Geomorphology* 330, 100–115. doi:10.1016/j.geomorph.2019.01.010.
Bhave, A. G., Conway, D., Dessai, S., and Stainforth, D. A. (2016). Barriers and opportunities for robust decision making approaches to support climate change adaptation in the developing world. *Clim. Risk Manag.* 14, 1–10. doi:10.1016/j.crm.2016.09.004.
Bhave, A. G., Conway, D., Dessai, S., and Stainforth, D. A. (2018). Water Resource Planning Under Future Climate and Socioeconomic Uncertainty in the Cauvery River Basin in Karnataka, India. *Water Resour. Res.* 54, 708–728. doi:10.1002/2017WR020970.
Biasutti, M., and Giannini, A. (2006). Robust Sahel drying in response to late 20th century forcings. *Geophys. Res. Lett.* 33, L11706. doi:10.1029/2006GL026067.
Bichet, A., and Diedhiou, A. (2018a). Less frequent and more intense rainfall along the coast of the Gulf of Guinea in West and Central Africa (1981-2014). *Clim. Res.* 76, 191–201. doi:10.3354/cr01537.
Bichet, A., and Diedhiou, A. (2018b). West African Sahel has become wetter during the last 30 years, but dry spells are shorter and more frequent. *Clim. Res.* 75, 155–162. doi:10.3354/cr01515.
Bindoff, N. L., Stott, P. A., AchutaRao, K. M., Allen, M. R., Gillett, N. P., and Gutzler, D., et al. (2013). "Detection and Attribution of Climate Change: from Global to Regional," in *Climate Change 2013 - The Physical Science Basis*, ed. Intergovernmental Panel on Climate Change (Cambridge: Cambridge University Press), 867–952. doi:10.1017/CBO9781107415324.022.
Birner, T., Davis, S. M., and Seidel, D. J. (2014). The changing width of Earth's tropical belt. *Phys. Today* 67, 38–44. doi:10.1063/PT.3.2620.
Bittner, M., Schmidt, H., Timmreck, C., and Sienz, F. (2016). Using a large ensemble of simulations to assess the Northern Hemisphere stratospheric dynamical response to tropical volcanic eruptions and its uncertainty. *Geophys. Res. Lett.* 43, 9324–9332. doi:10.1002/2016GL070587.
Black, M., Karoly, D., and King, A. (2015). The contribution of anthropogenic forcing to the Adelaide and Melbourne, Australia, heat waves of January 2014. *Bull. Am. Meteorol. Soc.* 96, S145–S148.
Blackport, R., and Kushner, P. J. (2017). Isolating the Atmospheric Circulation Response to Arctic Sea Ice Loss in the Coupled Climate System. *J. Clim.* 30, 2163–2185. doi:10.1175/JCLI-D-16-0257.1.

Blackport, R., Screen, J. A., van der Wiel, K., and Bintanja, R. (2019). Minimal influence of reduced Arctic sea ice on coincident cold winters in mid-latitudes. *Nat. Clim. Chang.* 9, 697–704. doi:10.1038/s41558-019-0551-4.
Bladé, I., Liebmann, B., Fortuny, D., and van Oldenborgh, G. J. (2012). Observed and simulated impacts of the summer NAO in Europe: implications for projected drying in the Mediterranean region. *Clim. Dyn.* 39, 709–727. doi:10.1007/s00382-011-1195-x.
Blamey, R. C., Kolusu, S. R., Mahlalela, P., Todd, M. C., and Reason, C. J. C. (2018). The role of regional circulation features in regulating El Niño climate impacts over southern Africa: A comparison of the 2015/2016 drought with previous events. *Int. J. Climatol.* 38, 4276–4295. doi:10.1002/joc.5668.
Blamey, R., and Reason, C. (2007). Relationships between Antarctic sea-ice and South African winter rainfall. *Clim. Res.* 33, 183–193. doi:10.3354/cr033183.
Blázquez, J., and Solman, S. A. (2018). Fronts and precipitation in CMIP5 models for the austral winter of the Southern Hemisphere. *Clim. Dyn.* 50, 2705–2717. doi:10.1007/s00382-017-3765-z.
Blenkinsop, S., Lewis, E., Chan, S. C., and Fowler, H. J. (2017). Quality-control of an hourly rainfall dataset and climatology of extremes for the UK. *Int. J. Climatol.* 37, 722–740. doi:10.1002/joc.4735.
Bližňák, V., Kašpar, M., and Müller, M. (2018). Radar-based summer precipitation climatology of the Czech Republic. *Int. J. Climatol.* 38, 677–691. doi:10.1002/joc.5202.
Boberg, F., and Christensen, J. H. (2012). Overestimation of Mediterranean summer temperature projections due to model deficiencies. *Nat. Clim. Chang.* 2, 1–4. doi:10.1038/nclimate1454.
Boé, J. (2018). Interdependency in Multimodel Climate Projections: Component Replication and Result Similarity. *Geophys. Res. Lett.* 45, 2771–2779. doi:10.1002/2017GL076829.
Boé, J., Terray, L., Moine, M.-P., Valcke, S., and et al. (submitted). Recent summer warming over western Europe in new generation climate models and errors in large-scale circulation trends. *Environ. Res. Lett.* (submitted).
Boers, R., Brandsma, T., and Siebesma, A. P. (2017). Impact of aerosols and clouds on decadal trends in all-sky solar radiation over the Netherlands (1966–2015). *Atmos. Chem. Phys.* 17, 8081–8100. doi:10.5194/acp-17-8081-2017.
Böhm, R., Jones, P. D., Hiebl, J., Frank, D., Brunetti, M., and Maugeri, M. (2010). The early instrumental warm-bias: A solution for long central European temperature series 1760-2007. *Clim. Change*. doi:10.1007/s10584-009-9649-4.
Böhme, T., Stapelberg, S., Akkermans, T., Crewell, S., Fischer, J., Reinhardt, T., et al. (2011). Long-term evaluation of COSMO forecasting using combined observational data of the GOP period. *Meteorol. Zeitschrift* 20, 119–132. doi:10.1127/0941-2948/2011/0225.
Bohnenstengel, S. I., Hamilton, I., Davies, M., and Belcher, S. E. (2014). Impact of anthropogenic heat emissions on London's temperatures. *Q. J. R. Meteorol. Soc.* 140, 687–698. doi:10.1002/qj.2144.
Bojinski, S., Verstraete, M., Peterson, T. C., Richter, C., Simmons, A., and Zemp, M. (2014). The Concept of Essential Climate Variables in Support of Climate Research, Applications, and Policy. *Bull. Am. Meteorol. Soc.* 95, 1431–1443. doi:10.1175/BAMS-D-13-00047.1.
Bolch, T., Shea, J. M., Liu, S., Azam, F. M., Gao, Y., Gruber, S., et al. (2019). "Status and Change of the Cryosphere in the Extended Hindu Kush Himalaya Region," in *The Hindu Kush Himalaya Assessment* (Cham: Springer International Publishing), 209–255. doi:10.1007/978-3-319-92288-1_7.
Bollasina, M. A., and Ming, Y. (2013). The general circulation model precipitation bias over the southwestern equatorial Indian Ocean and its implications for simulating the South Asian monsoon. *Clim. Dyn.* 40, 823–838. doi:10.1007/s00382-012-1347-7.
Bollasina, M. A., Ming, Y., and Ramaswamy, V. (2011). Anthropogenic Aerosols and the Weakening of the South Asian Summer Monsoon. *Science* 334, 502–505. doi:10.1126/science.1204994.
Booth, J. F., Kwon, Y.-O., Ko, S., Small, R. J., and Msadek, R. (2017). Spatial Patterns and Intensity of the Surface Storm Tracks in CMIP5 Models. *J. Clim.* 30, 4965–4981. doi:10.1175/JCLI-D-16-0228.1.
Bosilovich, M. G., Chern, J.-D., Mocko, D., Robertson, F. R., and da Silva, A. M. (2015). Evaluating Observation Influence on Regional Water Budgets in Reanalyses. *J. Clim.* 28, 3631–3649. doi:10.1175/JCLI-D-14-00623.1.
Bracegirdle, T. J., Hyder, P., and Holmes, C. R. (2018). CMIP5 Diversity in Southern Westerly Jet Projections Related to Historical Sea Ice Area: Strong Link to Strengthening and Weak Link to Shift. *J. Clim.* 31, 195–211. doi:10.1175/JCLI-D-17-0320.1.
Bracegirdle, T. J., Shuckburgh, E., Sallee, J.-B., Wang, Z., Meijers, A. J. S., Bruneau, N., et al. (2013). Assessment of surface winds over the Atlantic, Indian, and Pacific Ocean sectors of the Southern Ocean in CMIP5 models: historical bias, forcing response, and state dependence. *J. Geophys. Res. Atmos.* 118, 547–562. doi:10.1002/jgrd.50153.
Brands, S. (2017). Which ENSO teleconnections are robust to internal atmospheric variability? *Geophys. Res. Lett.* 44, 1483–1493. doi:10.1002/2016GL071529.
Brands, S., Gutiérrez, J. M., Herrera, S., and Cofiño, A. S. (2012). On the Use of Reanalysis Data for Downscaling. *J. Clim.* 25, 2517–2526. doi:10.1175/JCLI-D-11-00251.1.
Brasseur, G. P., and Gallardo, L. (2016). Climate services: Lessons learned and future prospects. *Earth's Futur.* 4, 79–89. doi:10.1002/2015EF000338.
Bremer, S., and Meisch, S. (2017). Co-production in climate change research: reviewing different perspectives. *Wiley Interdiscip. Rev. Clim. Chang.* 8, e482. doi:10.1002/wcc.482.

Brogli, R., Kröner, N., Sørland, S. L., Lüthi, D., and Schär, C. (2019a). The Role of Hadley Circulation and Lapse-Rate Changes for the Future European Summer Climate. *J. Clim.* 32, 385–404. doi:10.1175/JCLI-D-18-0431.1.
Brogli, R., Sørland, S. L., Kröner, N., and Schär, C. (2019b). Causes of future Mediterranean precipitation decline depend on the season. *Environ. Res. Lett.* 14, 114017. doi:10.1088/1748-9326/ab4438.
Brönnimann, S., Compo, G. P., Spadin, R., Allan, R., and Adam, W. (2011). Early ship-based upper-air data and comparison with the Twentieth Century Reanalysis. *Clim. Past* 7, 265–276. doi:10.5194/cp-7-265-2011.
Brown, A., Milton, S., Cullen, M., Golding, B., Mitchell, J., and Shelly, A. (2012a). Unified Modeling and Prediction of Weather and Climate. *Bull. Amer. Meteor. Soc.* 93, 1865–1877. doi:10.1175/BAMS-D-12-00018.1.
Brown, C., Ghile, Y., Laverty, M., and Li, K. (2012b). Decision scaling: Linking bottom-up vulnerability analysis with climate projections in the water sector. *Water Resour. Res.* 48, 1–12. doi:10.1029/2011WR011212.
Brown, C., and Wilby, R. L. R. L. (2012). An Alternate Approach to Assessing Climate Risks. *Eos, Trans. Am. Geophys. Union* 93, 401–402. doi:10.1029/2012EO410001.
Brown, J. R., Moise, A. F., and Colman, R. A. (2013). The South Pacific Convergence Zone in CMIP5 simulations of historical and future climate. *Clim. Dyn.* 41, 2179–2197. doi:10.1007/s00382-012-1591-x.
Brown, J. R., Moise, A. F., Colman, R., and Zhang, H. (2016). Will a Warmer World Mean a Wetter or Drier Australian Monsoon? *J. Clim.* 29, 4577–4596. doi:10.1175/JCLI-D-15-0695.1.
Brown, M. J. (2000). Urban parameterizations for mesoscale meteorological models. *Mesoscale Atmos. Dispers.* 9, 193–255.
Brügger, A., Dessai, S., Devine-Wright, P., Morton, T. A., and Pidgeon, N. F. (2015). Psychological responses to the proximity of climate change. *Nat. Clim. Chang.* 5, 1031–1037. doi:10.1038/nclimate2760.
Brulebois, E., Castel, T., Richard, Y., Chateau-Smith, C., and Amiotte-Suchet, P. (2015). Hydrological response to an abrupt shift in surface air temperature over France in 1987/88. *J. Hydrol.* 531, 892–901. doi:https://doi.org/10.1016/j.jhydrol.2015.10.026.
Brun, F., Dumont, M., Wagnon, P., Berthier, E., Azam, M. F., Shea, J. M., et al. (2015). Seasonal changes in surface albedo of Himalayan glaciers from MODIS data and links with the annual mass balance. *Cryosph.* 9, 341–355. doi:10.5194/tc-9-341-2015.
Brunet, M., Asin, J., Sigró, J., Bañón, M., García, F., Aguilar, E., et al. (2011). The minimization of the screen bias from ancient Western Mediterranean air temperature records: an exploratory statistical analysis. *Int. J. Climatol.* 31, 1879–1895. doi:10.1002/joc.2192.
Brunner, L., Hegerl, G. C., and Steiner, A. K. (2017). Connecting Atmospheric Blocking to European Temperature Extremes in Spring. *J. Clim.* 30, 585–594. doi:10.1175/JCLI-D-16-0518.1.
Bucchignani, E., Cattaneo, L., Panitz, H.-J., and Mercogliano, P. (2016a). Sensitivity analysis with the regional climate model COSMO-CLM over the CORDEX-MENA domain. *Meteorol. Atmos. Phys.* 128, 73–95. doi:10.1007/s00703-015-0403-3.
Bucchignani, E., Mercogliano, P., Panitz, H. J., and Montesarchio, M. (2018). Climate change projections for the Middle East–North Africa domain with COSMO-CLM at different spatial resolutions. *Adv. Clim. Chang. Res.* doi:10.1016/j.accre.2018.01.004.
Bucchignani, E., Mercogliano, P., Rianna, G., and Panitz, H. J. (2016b). Analysis of ERA-Interim-driven COSMO-CLM simulations over Middle East – North Africa domain at different spatial resolutions. *Int. J. Climatol.* 36, 3346–3369. doi:10.1002/joc.4559.
Buckley, M. W., and Marshall, J. (2016). Observations, inferences, and mechanisms of the Atlantic Meridional Overturning Circulation: A review. *Rev. Geophys.* 54, 5–63. doi:10.1002/2015RG000493.
Budikova, D., Ford, T. W., and Ballinger, T. J. (2017). Connections between north-central United States summer hydroclimatology and Arctic sea ice variability. *Int. J. Climatol.* 37, 4434–4450. doi:10.1002/joc.5097.
Bueno, B., Pigeon, G., Norford, L. K., Zibouche, K., and Marchadier, C. (2012). Development and evaluation of a building energy model integrated in the TEB scheme. *Geosci. Model Dev.* 5, 433–448. doi:10.5194/gmd-5-433-2012.
Bukovsky, M. S. (2012). Temperature Trends in the NARCCAP Regional Climate Models. *J. Clim.* 25, 3985–3991. doi:10.1175/JCLI-D-11-00588.1.
Bukovsky, M. S., Gochis, D. J., and Mearns, L. O. (2013). Towards Assessing NARCCAP Regional Climate Model Credibility for the North American Monsoon: Current Climate Simulations*. *J. Clim.* 26, 8802–8826. doi:10.1175/JCLI-D-12-00538.1.
Buontempo, C., Hanlon, H. M., Bruno Soares, M., Christel, I., Soubeyroux, J. M., Viel, C., et al. (2018). What have we learnt from EUPORIAS climate service prototypes? *Clim. Serv.* 9, 21–32. doi:10.1016/j.cliser.2017.06.003.
Burke, C., and Stott, P. (2017). Impact of Anthropogenic Climate Change on the East Asian Summer Monsoon. *J. Clim.* 30, 5205–5220. doi:10.1175/JCLI-D-16-0892.1.
Burls, N. J., Blamey, R. C., Cash, B. A., Swenson, E. T., Fahad, A. al, Bopape, M.-J. M., et al. (2019). The Cape Town "Day Zero" drought and Hadley cell expansion. *npj Clim. Atmos. Sci.* 2, 27. doi:10.1038/s41612-019-0084-6.
Butler, A. H., Thompson, D. W. J., and Heikes, R. (2010). The Steady-State Atmospheric Circulation Response to Climate Change–like Thermal Forcings in a Simple General Circulation Model. *J. Clim.* 23, 3474–3496. doi:10.1175/2010JCLI3228.1.

Byrne, M. P., and O'Gorman, P. A. (2013a). Land–Ocean Warming Contrast over a Wide Range of Climates: Convective Quasi-Equilibrium Theory and Idealized Simulations. *J. Clim.* 26, 4000–4016. doi:10.1175/JCLI-D-12-00262.1.
Byrne, M. P., and O'Gorman, P. A. (2013b). Link between land-ocean warming contrast and surface relative humidities in simulations with coupled climate models. *Geophys. Res. Lett.* 40, 5223–5227. doi:10.1002/grl.50971.
Cahynová, M., and Huth, R. (2014). Atmospheric circulation influence on climatic trends in Europe: an analysis of circulation type classifications from the COST733 catalogue. *Int. J. Climatol.* 36, 2743–2760. doi:10.1002/joc.4003.
Cai, L., Alexeev, V. A., Arp, C. D., Jones, B. M., Liljedahl, A. K., and Gädeke, A. (2018). The Polar WRF Downscaled Historical and Projected Twenty-First Century Climate for the Coast and Foothills of Arctic Alaska. 5, 1–15. doi:10.3389/feart.2017.00111.
Cai, P., Hamdi, R., He, H., Luo, G., Wang, J., Zhang, M., et al. Numerical study of the interaction between oasis and urban areas within an arid mountains-desert system in Xinjiang, China using ALARO-SURFEX 3.
Cai, W., Purich, A., Cowan, T., van Rensch, P., and Weller, E. (2014). Did Climate Change–Induced Rainfall Trends Contribute to the Australian Millennium Drought? *J. Clim.* 27, 3145–3168. doi:10.1175/JCLI-D-13-00322.1.
Callahan, B., Miles, E., and Fluharty, D. (1999). Policy implications of climate forecasts for water resources management in the Pacific Northwest. *Policy Sci.* 32, 269–293. doi:10.1023/1004604805647.
Caluwaerts, S., Hamdi, R., Top, S., Lauwaet, D., Berckmans, J., Degrauwe, D., et al. (2020). The urban climate of Ghent, Belgium: A case study combining a high-accuracy monitoring network with numerical simulations. *Urban Clim.* 31, 100565. doi:https://doi.org/10.1016/j.uclim.2019.100565.
Camera, C., Bruggeman, A., Hadjinicolaou, P., Pashiardis, S., and Lange, M. A. (2014). Evaluation of interpolation techniques for the creation of gridded daily precipitation (1×1 km^2); Cyprus, 1980–2010. *J. Geophys. Res. Atmos.* 119, 693–712. doi:10.1002/2013JD020611.
Camilloni, I., and Barrucand, M. (2012). Temporal variability of the Buenos Aires, Argentina, urban heat island. *Theor. Appl. Climatol.* doi:10.1007/s00704-011-0459-z.
Campbell, T. H., and Kay, A. C. (2014). Solution aversion: On the relation between ideology and motivated disbelief. *J. Pers. Soc. Psychol.* 107, 809–824. doi:10.1037/a0037963.
Cannon, A. J. (2016). Multivariate Bias Correction of Climate Model Output: Matching Marginal Distributions and Intervariable Dependence Structure. *J. Clim.* 29, 7045–7064. doi:10.1175/JCLI-D-15-0679.1.
Cannon, A. J. (2018). Multivariate quantile mapping bias correction: an N-dimensional probability density function transform for climate model simulations of multiple variables. *Clim. Dyn.* 50, 31–49. doi:10.1007/s00382-017-3580-6.
Cannon, A. J., Sobie, S. R., and Murdock, T. Q. (2015). Bias Correction of GCM Precipitation by Quantile Mapping: How Well Do Methods Preserve Changes in Quantiles and Extremes? *J. Clim.* 28, 6938–6959. doi:10.1175/JCLI-D-14-00754.1.
Cao, D., Huang, F., and Qie, X. (2014). Development and Evaluation of detection algorithm for FY-4 Geostationary Lightning Imager (GLI) measurement. *XV Int. Conf. Atmos. Electr.*, 15–20.
Cao, L., Duan, L., Bala, G., and Caldeira, K. (2016). Simulated long-term climate response to idealized solar geoengineering. *Geophys. Res. Lett.* 43, 2209–2217. doi:10.1002/2016GL068079.
Capotondi, A., Wittenberg, A. T., Newman, M., Di Lorenzo, E., Yu, J.-Y., Braconnot, P., et al. (2015). Understanding ENSO Diversity. *Bull. Am. Meteorol. Soc.* 96, 921–938. doi:10.1175/BAMS-D-13-00117.1.
Cardoso, R. M., Soares, P. M. M., Lima, D. C. A., and Semedo, A. (2016). The impact of climate change on the Iberian low-level wind jet: EURO-CORDEX regional climate simulation. *Tellus A Dyn. Meteorol. Oceanogr.* 68, 29005. doi:10.3402/tellusa.v68.29005.
Careto, J. A. M., Cardoso, R. M., Soares, P. M. M., and Trigo, R. M. (2018). Land-Atmosphere Coupling in CORDEX-Africa: Hindcast Regional Climate Simulations. *J. Geophys. Res. Atmos.* 123, 11,048-11,067. doi:10.1029/2018JD028378.
Casanueva, A., Herrera, S., Iturbide, M., Lange, S., Jury, M., Dosio;, A., et al. (submitted). Testing Bias Adjustment Methods for Regional Climate Change Applications under Observational Uncertainty and Resolution Mismatch. *Atmos. Sci. Lett.* (submitted). doi:submitted.
Cash, D. W., Clark, W. C., Alcock, F., Dickson, N. M., Eckley, N., Guston, D. H., et al. (2003). Knowledge Systems for Sustainable Development. *Proc. Natl. Acad. Sci.* 100, 8086–8091. doi:10.1073/pnas.1231332100.
Cassou, C. (2008). Intraseasonal interaction between the Madden–Julian Oscillation and the North Atlantic Oscillation. *Nature* 455, 523–527. doi:10.1038/nature07286.
Cattiaux, J., and Cassou, C. (2013). Opposite CMIP3/CMIP5 trends in the wintertime Northern Annular Mode explained by combined local sea ice and remote tropical influences. *Geophys. Res. Lett.* 40, 3682–3687. doi:10.1002/grl.50643.
Cattiaux, J., Douville, H., and Peings, Y. (2013). European temperatures in CMIP5: origins of present-day biases and future uncertainties. *Clim. Dyn.* 41, 2889–2907. doi:10.1007/s00382-013-1731-y.
Catto, J. L., Jakob, C., and Nicholls, N. (2015). Can the CMIP5 models represent winter frontal precipitation? *Geophys. Res. Lett.* 42, 8596–8604. doi:10.1002/2015GL066015.

Catto, J. L., Nicholls, N., Jakob, C., and Shelton, K. L. (2014). Atmospheric fronts in current and future climates. *Geophys. Res. Lett.* 41, 7642–7650. doi:10.1002/2014GL061943.
Cavallo, S. M., Berner, J., and Snyder, C. (2016). Diagnosing Model Errors from Time-Averaged Tendencies in the Weather Research and Forecasting (WRF) Model. *Mon. Weather Rev.* 144, 759–779. doi:10.1175/MWR-D-15-0120.1.
Cavazos, T., Luna-Niño, R., Cerezo-Mota, R., Fuentes-Franco, R., Méndez, M., Pineda Martínez, L. F., et al. (2019). Climatic trends and regional climate models intercomparison over the CORDEX-CAM (Central America, Caribbean, and Mexico) domain. *Int. J. Climatol.*, joc.6276. doi:10.1002/joc.6276.
Cavicchia, L., von Storch, H., and Gualdi, S. (2014). A long-term climatology of medicanes. *Clim. Dyn.* 43, 1183–1195. doi:10.1007/s00382-013-1893-7.
Cayan, D., Kunkel, K., Castro, C., Gershunov, A., Barsugli, J., Ray, A., et al. (2013). “Future climate: Projected average,” in *Assessment of Climate Change in the Southwest United States: A Report Prepared for the National Climate Assessment* (Island Press), 101–125.
Ceppi, P., Hwang, Y.-T., Frierson, D. M. W., and Hartmann, D. L. (2012a). Southern Hemisphere jet latitude biases in CMIP5 models linked to shortwave cloud forcing. *Geophys. Res. Lett.* 39, n/a-n/a. doi:10.1029/2012GL053115.
Ceppi, P., Scherrer, S. C., Fischer, A. M., and Appenzeller, C. (2012b). Revisiting Swiss temperature trends 1959-2008. *Int. J. Climatol.* 32, 203–213. doi:10.1002/joc.2260.
Ceppi, P., and Shepherd, T. G. (2019). The Role of the Stratospheric Polar Vortex for the Austral Jet Response to Greenhouse Gas Forcing. *Geophys. Res. Lett.* 46, 6972–6979. doi:10.1029/2019GL082883.
Challinor, A., Slingo, J., Turner, A., and Wheeler, T. (2006). Indian Monsoon: Contribution to the Stern Review.
Chan, S. C., Kendon, E. J., Fowler, H. J., Blenkinsop, S., and Roberts, N. M. (2014a). Projected increases in summer and winter UK sub-daily precipitation extremes from high-resolution regional climate models. *Environ. Res. Lett.* 9, 084019. doi:10.1088/1748-9326/9/8/084019.
Chan, S. C., Kendon, E. J., Fowler, H. J., Blenkinsop, S., Roberts, N. M., and Ferro, C. A. T. (2014b). The value of high-resolution Met Office regional climate models in the simulation of multihourly precipitation extremes. *J. Clim.* 27, 6155–6174. doi:10.1175/JCLI-D-13-00723.1.
Chandler, R. E. (2019). Multisite, multivariate weather generation based on generalised linear models.
Chandrasa, G. T., and Montenegro, A. (2019). Evaluation of regional climate model simulated rainfall over Indonesia and its application for downscaling future climate projections. *Int. J. Climatol.*, joc.6316. doi:10.1002/joc.6316.
Chaney, N. W., Sheffield, J., Villarini, G., and Wood, E. F. (2014). Development of a High-Resolution Gridded Daily Meteorological Dataset over Sub-Saharan Africa: Spatial Analysis of Trends in Climate Extremes. *J. Clim.* 27, 5815–5835. doi:10.1175/JCLI-D-13-00423.1.
Chang, E. K. M., Guo, Y., and Xia, X. (2012). CMIP5 multimodel ensemble projection of storm track change under global warming. *J. Geophys. Res. Atmos.* 117, n/a-n/a. doi:10.1029/2012JD018578.
Chang, E. K. M., Ma, C.-G., Zheng, C., and Yau, A. M. W. (2016). Observed and projected decrease in Northern Hemisphere extratropical cyclone activity in summer and its impacts on maximum temperature. *Geophys. Res. Lett.* 43, 2200–2208. doi:10.1002/2016GL068172.
Chardon, J., Hingray, B., and Favre, A.-C. (2018). An adaptive two-stage analog/regression model for probabilistic prediction of small-scale precipitation in France. *Hydrol. Earth Syst. Sci.* 22, 265–286. doi:10.5194/hess-22-265-2018.
Charles, S., Bates, B., Whetton, P., and Hughes, J. (1999). Validation of downscaling models for changed climate conditions: case study of southwestern Australia. *Clim. Res.* 12, 1–14. doi:10.3354/cr012001.
Chaudhuri, A. H., Ponte, R. M., Forget, G., and Heimbach, P. (2013). A Comparison of Atmospheric Reanalysis Surface Products over the Ocean and Implications for Uncertainties in Air–Sea Boundary Forcing. *J. Clim.* 26, 153–170. doi:10.1175/JCLI-D-12-00090.1.
Cheema, M. J. M., and Bastiaanssen, W. G. M. (2012). Local calibration of remotely sensed rainfall from the TRMM satellite for different periods and spatial scales in the Indus Basin. *Int. J. Remote Sens.* 33, 2603–2627. doi:10.1080/01431161.2011.617397.
Chen, A. A., Taylor, M. A., Brown, P., and Campbell, J. D. (2012a). *State of the Jamaican Climate 2012 [State of the Jamaican Climate 2012].*
Chen, B., Dong, L., Liu, X., Shi, G. Y., Chen, L., Nakajima, T., et al. (2016a). Exploring the possible effect of anthropogenic heat release due to global energy consumption upon global climate: a climate model study. *Int. J. Climatol.* 36, 4790–4796. doi:10.1002/joc.4669.
Chen, F., Bornstein, R., Grimmond, S., Li, J., Liang, X., Martilli, A., et al. (2012b). Research Priorities in Observing and Modeling Urban Weather and Climate. *Bull. Am. Meteorol. Soc.* 93, 1725–1728. doi:10.1175/BAMS-D-11-00217.1.
Chen, F., Kusaka, H., Bornstein, R., Ching, J., Grimmond, C. S. B., Grossman-Clarke, S., et al. (2011). The integrated WRF/urban modelling system: development, evaluation, and applications to urban environmental problems. *Int. J. Climatol.* 31, 273–288. doi:10.1002/joc.2158.
Chen, H., Ma, H., Li, X., and Sun, S. (2015). Solar influences on spatial patterns of Eurasian winter temperature and atmospheric general circulation anomalies. *J. Geophys. Res. Atmos.* 120, 8642–8657. doi:10.1002/2015JD023415.

Chen, H. W., Alley, R. B., and Zhang, F. (2016b). Interannual Arctic sea ice variability and associated winter weather patterns: A regional perspective for 1979-2014. *J. Geophys. Res. Atmos.* 121, 14,433-14,455. doi:10.1002/2016JD024769.
Chen, H. W., Zhang, F., and Alley, R. B. (2016c). The Robustness of Midlatitude Weather Pattern Changes due to Arctic Sea Ice Loss. *J. Clim.* 29, 7831–7849. doi:10.1175/JCLI-D-16-0167.1.
Chen, H., Xu, C.-Y., and Guo, S. (2012c). Comparison and evaluation of multiple GCMs, statistical downscaling and hydrological models in the study of climate change impacts on runoff. *J. Hydrol.* 434–435, 36–45. doi:10.1016/j.jhydrol.2012.02.040.
Chen, H., Zhang, Y., Yu, M., Hua, W., Sun, S., Li, X., et al. (2016d). Large-scale urbanization effects on eastern Asian summer monsoon circulation and climate. *Clim. Dyn.* 47, 117–136. doi:10.1007/s00382-015-2827-3.
Chen, J., and Brissette, F. P. (2019). Reliability of climate model multi-member ensembles in estimating internal precipitation and temperature variability at the multi-decadal scale. *Int. J. Climatol.* 39, 843–856. doi:10.1002/joc.5846.
Chen, L., Francis, J., and Hanna, E. (2018). The "Warm-Arctic/Cold-continents" pattern during 1901–2010. *Int. J. Climatol.* 38, 5245–5254. doi:10.1002/joc.5725.
Chen, M., Shi, W., Xie, P., Silva, V. B. S., Kousky, V. E., Wayne Higgins, R., et al. (2008). Assessing objective techniques for gauge-based analyses of global daily precipitation. *J. Geophys. Res.* 113, D04110. doi:10.1029/2007JD009132.
Chen, S., Hamdi, R., Ochege, F. U., Du, H., Chen, X., Yang, W., et al. (2019). Added value of a dynamical downscaling approach for simulating precipitation and temperature over Tianshan mountains area, Central Asia. *J. Geophys. Res. Atmos.* 0. doi:10.1029/2019JD031016.
Chen, X., and Jeong, S.-J. (2018). Irrigation enhances local warming with greater nocturnal warming effects than daytime cooling effects. *Environ. Res. Lett.* 13, 024005. doi:10.1088/1748-9326/aa9dea.
Chenoli, S. N., Ahmad Mazuki, M. Y., Turner, J., and Samah, A. A. (2017). Historical and projected changes in the Southern Hemisphere Sub-tropical Jet during winter from the CMIP5 models. *Clim. Dyn.* 48, 661–681. doi:10.1007/s00382-016-3102-y.
Cherchi, A., Alessandri, A., Masina, S., and Navarra, A. (2011). Effects of increased CO2 levels on monsoons. *Clim. Dyn.* 37, 83–101. doi:10.1007/s00382-010-0801-7.
Cherchi, A., Annamalai, H., Masina, S., Navarra, A., and Alessandri, A. (2016). Twenty-first century projected summer mean climate in the Mediterranean interpreted through the monsoon-desert mechanism. *Clim. Dyn.* 47, 2361–2371. doi:10.1007/s00382-015-2968-4.
Cherian, R., Quaas, J., Salzmann, M., and Wild, M. (2014). Pollution trends over Europe constrain global aerosol forcing as simulated by climate models. *Geophys. Res. Lett.* 41, 2176–2181. doi:10.1002/2013GL058715.
Chevuturi, A., Klingaman, N. P., Turner, A. G., and Hannah, S. (2018). Projected Changes in the Asian-Australian Monsoon Region in 1.5°C and 2.0°C Global-Warming Scenarios. *Earth's Futur.* 6. doi:10.1002/2017EF000734.
Chiew, F. H. S., Young, W. J., Cai, W., and Teng, J. (2011). Current drought and future hydroclimate projections in southeast Australia and implications for water resources management. *Stoch. Environ. Res. Risk Assess.* 25, 601–612. doi:10.1007/s00477-010-0424-x.
Chimani, B., Venema, V., Lexer, A., Andre, K., Auer, I., and Nemec, J. (2018). Inter-comparison of methods to homogenize daily relative humidity. *Int. J. Climatol.* 38, 3106–3122. doi:10.1002/joc.5488.
Chiodo, G., Oehrlein, J., Polvani, L. M., Fyfe, J. C., and Smith, A. K. (2019). Insignificant influence of the 11-year solar cycle on the North Atlantic Oscillation. *Nat. Geosci.* 12, 94–99. doi:10.1038/s41561-018-0293-3.
Chiriaco, M., Dupont, J.-C., Bastin, S., Badosa, J., Lopez, J., Haeffelin, M., et al. (2018). ReOBS: a new approach to synthesize long-term multi-variable dataset and application to the SIRTA supersite. *Earth Syst. Sci. Data* 10, 919–940. doi:10.5194/essd-10-919-2018.
Cholette, M., Laprise, R., and Thériault, J. (2015). Perspectives for Very High-Resolution Climate Simulations with Nested Models: Illustration of Potential in Simulating St. Lawrence River Valley Channelling Winds with the Fifth-Generation Canadian Regional Climate Model. *Climate* 3, 283–307. doi:10.3390/cli3020283.
Choudhary, A., Dimri, A. P., and Maharana, P. (2018). Assessment of CORDEX-SA experiments in representing precipitation climatology of summer monsoon over India. *Theor. Appl. Climatol.* 134, 283–307. doi:10.1007/s00704-017-2274-7.
Chow, W. T. L., Salamanca, F., Georgescu, M., Mahalov, A., Milne, J. M., and Ruddell, B. L. (2014). A multi-method and multi-scale approach for estimating city-wide anthropogenic heat fluxes. *Atmos. Environ.* 99, 64–76. doi:https://doi.org/10.1016/j.atmosenv.2014.09.053.
Christensen, J. H., Hewitson, B., Busuioc, A., Chen, A., Gao, X., Held, I., et al. (2007). "Regional Climate Projections," in *Climate Change 2007: The Physical Science Basis*, ed. IPCC (Cham: Cambridge University Press), 847–940. doi:10.1007/978-3-319-68418-5_10.
Christensen, J. H., Kumar, K. K., Aldrian, E., An, S.-I., Cavalcanti, I. F. A., de Castro, M., et al. (2013). "Climate Phenomena and their Relevance for Future Regional Climate Change," in *Climate Change 2013: The Physical Science Basis. Contribution of Working Group I to the Fifth Assessment Report of the Intergovernmental Panel on Climate Change*, eds. T. F. Stocker, D. Qin, G.-K. Plattner, M. Tignor, S. K. Allen, J. Boschung, et al.

(Cambridge: Cambridge University Press), 1217–1308.
Chrysanthou, A., van der Schrier, G., van den Besselaar, E. J. M., Klein Tank, A. M. G. G., and Brandsma, T. (2014). The effects of urbanization on the rise of the European temperature since 1960. *Geophys. Res. Lett.* 41, 7716–7722. doi:10.1002/2014GL061154.
Chubb, T., Manton, M. J., Peace, A. D., and Bilish, S. P. (2015). Estimation of Wind-Induced Losses from a Precipitation Gauge Network in the Australian Snowy Mountains. *J. Hydrometeorol.* 16, 2619–2638. doi:10.1175/jhm-d-14-0216.1.
Coats, S., Smerdon, J. E., Cook, B. I., and Seager, R. (2013). Stationarity of the tropical pacific teleconnection to North America in CMIP5/PMIP3 model simulations. *Geophys. Res. Lett.* 40, 4927–4932. doi:10.1002/grl.50938.
CoCT (2018). Economic Performance Indicators for Cape Town. Cape Town Available at: http://resource.capetown.gov.za/documentcentre/Documents/City research reports and review/CCT EPIC 2018Q1 FINAL 20180702.pdf%0A%0A.
Cohen, J. L., Furtado, J. C., Barlow, M. A., Alexeev, V. A., and Cherry, J. E. (2012a). Arctic warming, increasing snow cover and widespread boreal winter cooling. *Environ. Res. Lett.* 7, 014007. doi:10.1088/1748-9326/7/1/014007.
Cohen, J. L., Furtado, J. C., Barlow, M., Alexeev, V. A., and Cherry, J. E. (2012b). Asymmetric seasonal temperature trends. *Geophys. Res. Lett.* 39. doi:10.1029/2011GL050582.
Cohen, J., Screen, J. A., Furtado, J. C., Barlow, M., Whittleston, D., Coumou, D., et al. (2014). Recent Arctic amplification and extreme mid-latitude weather. *Nat. Geosci.* 7, 627–637. doi:10.1038/ngeo2234.
Cohen, J., Zhang, X., Francis, J., Jung, T., Kwok, R., Overland, J., et al. (2020). Divergent consensuses on Arctic amplification influence on midlatitude severe winter weather. *Nat. Clim. Chang.* 10, 20–29. doi:10.1038/s41558-019-0662-y.
Colette, A., Vautard, R., and Vrac, M. (2012). Regional climate downscaling with prior statistical correction of the global climate forcing. *Geophys. Res. Lett.* 39, n/a-n/a. doi:10.1029/2012GL052258.
Collins, K., and Ison, R. (2009). Jumping off Arnstein's ladder: social learning as a new policy paradigm for climate change adaptation. *Environ. Policy Gov.* 19, 358–373. doi:10.1002/eet.523.
Collins, M., AchutaRao, K., Ashok, K., Bhandari, S., Mitra, A. K., Prakash, S., et al. (2013a). Observational challenges in evaluating climate models. *Nat. Clim. Chang.* 3, 940–941. doi:10.1038/nclimate2012.
Collins, M., Knutti, R., Arblaster, J., Dufresne, J., Fichefet, T., Friedlingstein, P., et al. (2013b). "Long-term Climate Change: Projections, Commitments and Irreversibility," in doi:10.1002/mds.26688.
Collins, M., Minobe, S., Barreiro, M., Bordoni, S., Kaspi, Y., Kuwano-Yoshida, A., et al. (2018). Challenges and opportunities for improved understanding of regional climate dynamics. *Nat. Clim. Chang.* 8, 101–108. doi:10.1038/s41558-017-0059-8.
Collow, T. W., Wang, W., and Kumar, A. (2019). Reduction in Northern Midlatitude 2-m Temperature Variability due to Arctic Sea Ice Loss. *J. Clim.* 32, 5021–5035. doi:10.1175/JCLI-D-18-0692.1.
Compo, G. P., Whitaker, J. S., Sardeshmukh, P. D., Matsui, N., Allan, R. J., Yin, X., et al. (2011). The Twentieth Century Reanalysis Project. *Q. J. R. Meteorol. Soc.* 137, 1–28. doi:10.1002/qj.776.
Contractor, S., Donat, M. G., Alexander, L. V., Ziese, M., Meyer-Christoffer, A., Schneider, U., et al. (2019). Rainfall Estimates on a Gridded Network (REGEN) – A global land-based gridded dataset of daily precipitation from 1950–2013. *Hydrol. Earth Syst. Sci. Discuss.*, 1–30. doi:10.5194/hess-2018-595.
Cook, B. I., Ault, T. R., and Smerdon, J. E. (2015a). Unprecedented 21st century drought risk in the American Southwest and Central Plains. *Sci. Adv.* 1, e1400082. doi:10.1126/sciadv.1400082.
Cook, B. I., Shukla, S. P., Puma, M. J., and Nazarenko, L. S. (2015b). Irrigation as an historical climate forcing. *Clim. Dyn.* 44, 1715–1730. doi:10.1007/s00382-014-2204-7.
Cook, E. R., Seager, R., Heim, R. R., Vose, R. S., Herweijer, C., and Woodhouse, C. (2010). Megadroughts in North America: placing IPCC projections of hydroclimatic change in a long-term palaeoclimate context. *J. Quat. Sci.* 25, 48–61. doi:10.1002/jqs.1303.
Cook, K. H., and Vizy, E. K. (2015). Detection and analysis of an amplified warming of the Sahara Desert. *J. Clim.* doi:10.1175/JCLI-D-14-00230.1.
Cook, K. H., and Vizy, E. K. (2019). Contemporary Climate Change of the African Monsoon Systems. *Curr. Clim. Chang. Reports* 5, 145–159. doi:10.1007/s40641-019-00130-1.
Cook, K. L., Andermann, C., Gimbert, F., Adhikari, B. R., and Hovius, N. (2018). Glacial lake outburst floods as drivers of fluvial erosion in the Himalaya. *Science* 362, 53–57. doi:10.1126/science.aat4981.
Coppola, E., Sobolowski, S., Pichelli, E., Raffaele, F., Ahrens, B., Anders, I., et al. (2018). A first-of-its-kind multi-model convection permitting ensemble for investigating convective phenomena over Europe and the Mediterranean. *Clim. Dyn.* doi:10.1007/s00382-018-4521-8.
Corballis, T. (2019). Populating the Climate. *Environ. Philos.* 16, 275–289. doi:10.5840/envirophil201981284.
Corner, A., Markowitz, E., and Pidgeon, N. (2014). Public engagement with climate change: the role of human values. *Wiley Interdiscip. Rev. Clim. Chang.* 5, 411–422. doi:10.1002/wcc.269.
Cornes, R. C., Schrier, G., Besselaar, E. J. M., and Jones, P. D. (2018). An Ensemble Version of the E-OBS Temperature and Precipitation Data Sets. *J. Geophys. Res. Atmos.* 123, 9391–9409. doi:10.1029/2017JD028200.
Coumou, D., Di Capua, G., Vavrus, S., Wang, L., and Wang, S. (2018). The influence of Arctic amplification on mid-

latitude summer circulation. *Nat. Commun.* 9, 2959. doi:10.1038/s41467-018-05256-8.
Coumou, D., Lehmann, J., and Beckmann, J. (2015). The weakening summer circulation in the Northern Hemisphere mid-latitudes. *Science* 348, 324–327. doi:10.1126/science.1261768.
Cowtan, K., and Way, R. G. (2014). Coverage bias in the HadCRUT4 temperature series and its impact on recent temperature trends. *Q. J. R. Meteorol. Soc.* 140, 1935–1944. doi:10.1002/qj.2297.
Cramer, W., Guiot, J., Fader, M., Garrabou, J., Gattuso, J.-P., Iglesias, A., et al. (2018). Climate change and interconnected risks to sustainable development in the Mediterranean. *Nat. Clim. Chang.* 8, 972–980. doi:10.1038/s41558-018-0299-2.
Crippa, M., Janssens-Maenhout, G., Dentener, F., Guizzardi, D., Sindelarova, K., Muntean, M., et al. (2016). Forty years of improvements in European air quality: regional policy-industry interactions with global impacts. *Atmos. Chem. Phys.* 16, 3825–3841. doi:10.5194/acp-16-3825-2016.
Crook, J., Klein, C., Folwell, S., Taylor, C. M., Parker, D. J., Stratton, R., et al. (2019). Assessment of the Representation of West African Storm Lifecycles in Convection-Permitting Simulations. *Earth Sp. Sci.*, 2018EA000491. doi:10.1029/2018EA000491.
Crow, W. T., Lei, F., Hain, C., Anderson, M. C., Scott, R. L., Billesbach, D., et al. (2015). Robust estimates of soil moisture and latent heat flux coupling strength obtained from triple collocation. *Geophys. Res. Lett.* 42, 8415–8423. doi:10.1002/2015GL065929.
CTT (2018). Cape Town Tourism Research Report. Cape Town.
Cuervo-Robayo, A. P., Téllez-Valdés, O., Gómez-Albores, M. A., Venegas-Barrera, C. S., Manjarrez, J., and Martínez-Meyer, E. (2014). An update of high-resolution monthly climate surfaces for Mexico. *Int. J. Climatol.* 34, 2427–2437. doi:10.1002/joc.3848.
Cui, J., Piao, S., Huntingford, C., Wang, X., Lian, X., Chevuturi, A., et al. (submitted). Vegetation forcing modulates global land monsoon and water resources in a CO2-enriched climate. *Nat. Commun.* (submitted).
Cumming, G. S., Cumming, D. H. M., and Redman, C. L. (2006). Scale Mismatches in Social-Ecological Systems : Causes, Consequences, and Solutions. *Ecol. Soc.* 11, 14. Available at: http://www.ecologyandsociety.org/vol11/iss1/art14/.
Cvijanovic, I., Santer, B. D., Bonfils, C., Lucas, D. D., Chiang, J. C. H., and Zimmerman, S. (2017). Future loss of Arctic sea-ice cover could drive a substantial decrease in California's rainfall. *Nat. Commun.* 8, 1947. doi:10.1038/s41467-017-01907-4.
D'Agostino, R., Bader, J., Bordoni, S., Ferreira, D., and Jungclaus, J. (2019). Northern Hemisphere Monsoon Response to Mid-Holocene Orbital Forcing and Greenhouse Gas-Induced Global Warming. *Geophys. Res. Lett.* 46, 1591–1601. doi:10.1029/2018GL081589.
Dafka, S., Toreti, A., Luterbacher, J., Zanis, P., Tyrlis, E., and Xoplaki, E. (2018). On the ability of RCMs to capture the circulation pattern of Etesians. *Clim. Dyn.* 51, 1687–1706. doi:10.1007/s00382-017-3977-2.
Dahlgren, P., Landelius, T., Kållberg, P., and Gollvik, S. (2016). A high-resolution regional reanalysis for Europe. Part 1: Three-dimensional reanalysis with the regional HIgh-Resolution Limited-Area Model (HIRLAM). *Q. J. R. Meteorol. Soc.* 142, 2119–2131. doi:10.1002/qj.2807.
Dai, A., and Bloecker, C. E. (2018). Impacts of internal variability on temperature and precipitation trends in large ensemble simulations by two climate models. *Clim. Dyn.* 52, 289–306. doi:10.1007/s00382-018-4132-4.
Dandou, A., Tombrou, M., Akylas, E., Soulakellis, N., and Bossioli, E. (2005). Development and evaluation of an urban parameterization scheme in the Penn State/NCAR Mesoscale Model (MM5). *J. Geophys. Res. D Atmos.* 110. doi:10.1029/2004JD005192.
Daniel, M., Lemonsu, A., Déqué, M., Somot, S., Alias, A., and Masson, V. (2019). Benefits of explicit urban parameterization in regional climate modeling to study climate and city interactions. *Clim. Dyn.* 52, 2745–2764. doi:10.1007/s00382-018-4289-x.
Daniels, E. E., Lenderink, G., Hutjes, R. W. A., and Holtslag, A. A. M. (2016). Observed urban effects on precipitation along the Dutch West coast. *Int. J. Climatol.* 36, 2111–2119. doi:10.1002/joc.4458.
Darmaraki, S., Somot, S., Sevault, F., Nabat, P., Cabos Narvaez, W. D., Cavicchia, L., et al. (2019). Future evolution of Marine Heatwaves in the Mediterranean Sea. *Clim. Dyn.* doi:10.1007/s00382-019-04661-z.
Daron, J. D., Sutherland, K., Jack, C., and Hewitson, B. C. (2014). The role of regional climate projections in managing complex socio-ecological systems. *Reg. Environ. Chang.* 15, 1–12. doi:10.1007/s10113-014-0631-y.
Davin, E. L., Maisonnave, E., and Seneviratne, S. I. (2016). Is land surface processes representation a possible weak link in current Regional Climate Models? *Environ. Res. Lett.* 11, 074027. doi:10.1088/1748-9326/11/7/074027.
Davin, E. L., Seneviratne, S. I., Ciais, P., Olioso, A., and Wang, T. (2014). Preferential cooling of hot extremes from cropland albedo management. *Proc. Natl. Acad. Sci.* 111, 9757–9761. doi:10.1073/pnas.1317323111.
Davini, P., and D'Andrea, F. (2016). Northern Hemisphere Atmospheric Blocking Representation in Global Climate Models: Twenty Years of Improvements? *J. Clim.* 29, 8823–8840. doi:10.1175/JCLI-D-16-0242.1.
Davini, P., and D'Andrea, F. (submitted). From CMIP-3 to CMIP-6: Northern Hemisphere atmospheric blocking simulation in present and future climate. *J. Clim.* (submitted).
Davini, P., Hardenberg, J. von, and Corti, S. (2015). Tropical origin for the impacts of the Atlantic Multidecadal Variability on the Euro-Atlantic climate. *Environ. Res. Lett.* 10, 094010. doi:10.1088/1748-9326/10/9/094010.

Davini, P., von Hardenberg, J., Corti, S., Christensen, H. M., Juricke, S., Subramanian, A., et al. (2017). Climate SPHINX: evaluating the impact of resolution and stochastic physics parameterisations in the EC-Earth global climate model. *Geosci. Model Dev.* 10, 1383–1402. doi:10.5194/gmd-10-1383-2017.
Davy, R., Chen, L., and Hanna, E. (2018). Arctic amplification metrics. *Int. J. Climatol.* 38, 4384–4394. doi:10.1002/joc.5675.
Dawson, A., and Palmer, T. N. (2015). Simulating weather regimes: impact of model resolution and stochastic parameterization. *Clim. Dyn.* 44, 2177–2193. doi:10.1007/s00382-014-2238-x.
Dayon, G., Boé, J., and Martin, E. (2015). Transferability in the future climate of a statistical downscaling method for precipitation in France. *J. Geophys. Res. Atmos.* 120, 1023–1043. doi:10.1002/2014JD022236.
de Barros Soares, D., Lee, H., Loikith, P. C., Barkhordarian, A., and Mechoso, C. R. (2017). Can significant trends be detected in surface air temperature and precipitation over South America in recent decades? *Int. J. Climatol.* 37, 1483–1493. doi:10.1002/joc.4792.
de Jesus, E., da Rocha, R., Reboita, M., Llopart, M., Mosso Dutra, L., and Remedio, C. A. R. (2016). Contribution of cold fronts to seasonal rainfall in simulations over the southern La Plata Basin. *Clim. Res.* 68, 243–255. Available at: https://www.int-res.com/abstracts/cr/v68/n2-3/p243-255/.
de Jong, M. C., Wooster, M. J., Kitchen, K., Manley, C., Gazzard, R., and McCall, F. F. (2016). Calibration and evaluation of the Canadian Forest Fire Weather Index (FWI) System for improved wildland fire danger rating in the United Kingdom. *Nat. Hazards Earth Syst. Sci.* 16, 1217–1237. doi:10.5194/nhess-16-1217-2016.
De Laat, A. T. J., and Crok, M. (2013). A late 20th century European climate shift: fingerprint of regional brightening? *Atmos. Clim. Sci.* 3, 291.
De Troch, R., Hamdi, R., Van de Vyver, H., Geleyn, J.-F., and Termonia, P. (2013). Multiscale Performance of the ALARO-0 Model for Simulating Extreme Summer Precipitation Climatology in Belgium. *J. Clim.* 26, 8895–8915. doi:10.1175/JCLI-D-12-00844.1.
DEA (2013). Long-Term Adaptation Scenarios Flagship Research Programme (LTAS) for South Africa. Climate Trends and Scenarios for South Africa. Pretoria, South Africa Available at: www.environment.gov.za.
DEA (2018). South Africa's Third National Communication under the United Nations Framework Convention on Climate Change. Pretoria, South Africa Affairs Available at: https://unfccc.int/sites/default/files/resource/South African TNC Report to the UNFCCC_31 Aug.pdf.
Dee, D. P., Uppala, S. M., Simmons, A. J., Berrisford, P., Poli, P., Kobayashi, S., et al. (2011). The ERA-Interim reanalysis: Configuration and performance of the data assimilation system. *Q. J. R. Meteorol. Soc.* 137, 553–597. doi:10.1002/qj.828.
DeFlorio, M. J., Goodwin, I. D., Cayan, D. R., Miller, A. J., Ghan, S. J., Pierce, D. W., et al. (2016). Interannual modulation of subtropical Atlantic boreal summer dust variability by ENSO. *Clim. Dyn.* 46, 585–599. doi:10.1007/s00382-015-2600-7.
DeGaetano, A. T., and Castellano, C. M. (2017). Future projections of extreme precipitation intensity-duration-frequency curves for climate adaptation planning in New York State. *Clim. Serv.* 5, 23–35. doi:10.1016/J.CLISER.2017.03.003.
Dell'Aquila, A., Mariotti, A., Bastin, S., Calmanti, S., Cavicchia, L., Deque, M., et al. (2018). Evaluation of simulated decadal variations over the Euro-Mediterranean region from ENSEMBLES to Med-CORDEX. *Clim. Dyn.* 51, 857–876. doi:10.1007/s00382-016-3143-2.
Della-Marta, P. M., and Wanner, H. (2006). A Method of Homogenizing the Extremes and Mean of Daily Temperature Measurements. *J. Clim.* 19, 4179–4197. doi:10.1175/JCLI3855.1.
Delworth, T. L., and Zeng, F. (2014). Regional rainfall decline in Australia attributed to anthropogenic greenhouse gases and ozone levels. *Nat. Geosci.* 7, 583–587. doi:10.1038/ngeo2201.
Deng, B., Liu, S., Xiao, W., Wang, W., Jin, J., and Lee, X. (2013). Evaluation of the CLM4 Lake Model at a Large and Shallow Freshwater Lake*. *J. Hydrometeorol.* 14, 636–649. doi:10.1175/JHM-D-12-067.1.
Deng, J., Dai, A., and Xu, H. (2019). Nonlinear Climate Responses to Increasing CO 2 and Anthropogenic Aerosols Simulated by CESM1. *J. Clim.*, JCLI-D-19-0195.1. doi:10.1175/JCLI-D-19-0195.1.
Denis, B., Laprise, R., Caya, D., and Côté, J. (2002). Downscaling ability of one-way nested regional climate models: the Big-Brother Experiment. *Clim. Dyn.* 18, 627–646. doi:10.1007/s00382-001-0201-0.
Déqué, M., and Piedelievre, J. P. (1995). High resolution climate simulation over Europe. *Clim. Dyn.* 11, 321–339. doi:10.1007/BF00215735.
Déqué, M., Somot, S., Sanchez-Gomez, E., Goodess, C. M., Jacob, D., Lenderink, G., et al. (2012). The spread amongst ENSEMBLES regional scenarios: regional climate models, driving general circulation models and interannual variability. *Clim. Dyn.* 38, 951–964. doi:10.1007/s00382-011-1053-x.
Deser, C., Guo, R., and Lehner, F. (2017a). The relative contributions of tropical Pacific sea surface temperatures and atmospheric internal variability to the recent global warming hiatus. *Geophys. Res. Lett.* 44, 7945–7954. doi:10.1002/2017GL074273.
Deser, C., Hurrell, J. W., and Phillips, A. S. (2017b). The role of the North Atlantic Oscillation in European climate projections. *Clim. Dyn.* 49, 3141–3157. doi:10.1007/s00382-016-3502-z.
Deser, C., Knutti, R., Solomon, S., and Phillips, A. S. (2012a). Communication of the role of natural variability in

future North American climate. *Nat. Clim. Chang.* 2, 775–779. doi:10.1038/nclimate1562.
Deser, C., Lehner, F., Rodgers, K. ., and et al. (submitted). Strength in Numbers: Insights from Initial-condition Large Ensembles with Multiple Earth System Models and Future Prospects. *Nat. Clim. Chang.* (submitted).
Deser, C., Phillips, A., Bourdette, V., and Teng, H. (2012b). Uncertainty in climate change projections: the role of internal variability. *Clim. Dyn.* 38, 527–546. doi:10.1007/s00382-010-0977-x.
Deser, C., Phillips, A. S., Alexander, M. A., and Smoliak, B. V. (2014). Projecting North American Climate over the Next 50 Years: Uncertainty due to Internal Variability*. *J. Clim.* 27, 2271–2296. doi:10.1175/JCLI-D-13-00451.1.
Deser, C., Simpson, I. R., McKinnon, K. A., and Phillips, A. S. (2017c). The Northern Hemisphere Extratropical Atmospheric Circulation Response to ENSO: How Well Do We Know It and How Do We Evaluate Models Accordingly? *J. Clim.* 30, 5059–5082. doi:10.1175/JCLI-D-16-0844.1.
Deser, C., Terray, L., and Phillips, A. S. (2016). Forced and Internal Components of Winter Air Temperature Trends over North America during the past 50 Years: Mechanisms and Implications. *J. Clim.* 29, 2237–2258. doi:10.1175/JCLI-D-15-0304.1.
Dessai, S., Bhave, A., Birch, C., Conway, D., Garcia-Carreras, L., Gosling, J. P., et al. (2018). Building narratives to characterise uncertainty in regional climate change through expert elicitation. *Environ. Res. Lett.* 13, 074005. doi:10.1088/1748-9326/aabcdd.
Devrani, R., Singh, V., Mudd, S. M., and Sinclair, H. D. (2015). Prediction of flash flood hazard impact from Himalayan river profiles. *Geophys. Res. Lett.* 42, 5888–5894. doi:10.1002/2015GL063784.
Dey, R., Lewis, S. C., Arblaster, J. M., and Abram, N. J. (2019). A review of past and projected changes in Australia's rainfall. *Wiley Interdiscip. Rev. Clim. Chang.*, e00577. doi:10.1002/wcc.577.
Di Capua, G., and Coumou, D. (2016). Changes in meandering of the Northern Hemisphere circulation. *Environ. Res. Lett.* 11, 094028. doi:10.1088/1748-9326/11/9/094028.
Di Luca, A., Argüeso, D., Evans, J. P., de Elía, R., and Laprise, R. (2016). Quantifying the overall added value of dynamical downscaling and the contribution from different spatial scales. *J. Geophys. Res. Atmos.* 121, 1575–1590. doi:10.1002/2015JD024009.
Di Luca, A., de Elía, R., and Laprise, R. (2012). Potential for added value in precipitation simulated by high-resolution nested Regional Climate Models and observations. *Clim. Dyn.* 38, 1229–1247. doi:10.1007/s00382-011-1068-3.
Di Luca, A., de Elía, R., and Laprise, R. (2015). Challenges in the Quest for Added Value of Regional Climate Dynamical Downscaling. *Curr. Clim. Chang. Reports*, 10–21. doi:10.1007/s40641-015-0003-9.
Di Sante, F., Coppola, E., Farneti, R., and Giorgi, F. (2019). Indian Summer Monsoon as simulated by the regional earth system model RegCM-ES: the role of local air–sea interaction. *Clim. Dyn.* doi:10.1007/s00382-019-04612-8.
Diaconescu, E. P., and Laprise, R. (2013). Can added value be expected in RCM-simulated large scales? *Clim. Dyn.* 41, 1769–1800. doi:10.1007/s00382-012-1649-9.
Díaz, L. B., Saurral, R. I., and Vera, C. S. (submitted). Assessment of South America summer rainfall climatology and trends in a set of Large Ensembles. *Int. J. Climatol.* (submitted).
Díaz, L. B., and Vera, C. S. (2017). Austral summer precipitation interannual variability and trends over Southeastern South America in CMIP5 models. *Int. J. Climatol.* 37, 681–695. doi:10.1002/joc.5031.
Dienst, M., Lindén, J., Engström, E., and Esper, J. (2017). Removing the relocation bias from the 155-year Haparanda temperature record in Northern Europe. *Int. J. Climatol.* 37, 4015–4026. doi:10.1002/joc.4981.
Dienst, M., Lindén, J., Saladié, Ò., and Esper, J. (2019). Detection and elimination of UHI effects in long temperature records from villages – A case study from Tivissa, Spain. *Urban Clim.* 27, 372–383. doi:https://doi.org/10.1016/j.uclim.2018.12.012.
Dieppois, B., Pohl, B., Rouault, M., New, M., Lawler, D., and Keenlyside, N. (2016). Interannual to interdecadal variability of winter and summer southern African rainfall, and their teleconnections. *J. Geophys. Res. Atmos.* 121, 6215–6239. doi:10.1002/2015JD024576.
Diffenbaugh, N. S., and Giorgi, F. (2012). Climate change hotspots in the CMIP5 global climate model ensemble. *Clim. Change* 114, 813–822. doi:10.1007/s10584-012-0570-x.
Dileepkumar, R., AchutaRao, K., and Arulalan, T. (2018). Human influence on sub-regional surface air temperature change over India. *Sci. Rep.* 8, 8967. doi:10.1038/s41598-018-27185-8.
Dimri, A. P., Chevuturi, A., Niyogi, D., Thayyen, R. J., Ray, K., Tripathi, S. N., et al. (2017). Cloudbursts in Indian Himalayas: A review. *Earth-Science Rev.* 168, 1–23. doi:10.1016/j.earscirev.2017.03.006.
Dimri, A. P., Niyogi, D., Barros, A. P., Ridley, J., Mohanty, U. C., Yasunari, T., et al. (2015). Western Disturbances: A review. *Rev. Geophys.* 53, 225–246. doi:10.1002/2014RG000460.
Ding, Q., Steig, E. J., Battisti, D. S., and Wallace, J. M. (2012). Influence of the Tropics on the Southern Annular Mode. *J. Clim.* 25, 6330–6348. doi:10.1175/JCLI-D-11-00523.1.
Ding, Q., Wallace, J. M., Battisti, D. S., Steig, E. J., Gallant, A. J. E., Kim, H.-J., et al. (2014). Tropical forcing of the recent rapid Arctic warming in northeastern Canada and Greenland. *Nature* 509, 209–212. doi:10.1038/nature13260.
Ding, Y., Sun, Y., Wang, Z., Zhu, Y., and Song, Y. (2009). Inter-decadal variation of the summer precipitation in China

and its association with decreasing Asian summer monsoon Part II: Possible causes. *Int. J. Climatol.* 29, 1926–1944. doi:10.1002/joc.1759.
Dinku, T., Hailemariam, K., Maidment, R., Tarnavsky, E., and Connor, S. (2014). Combined use of satellite estimates and rain gauge observations to generate high-quality historical rainfall time series over Ethiopia. *Int. J. Climatol.* 34, 2489–2504. doi:10.1002/joc.3855.
Dittus, A. J., Hawkins, E. H., Wilcox, L. J., Sutton, R., Smith, C. J., Andrews, M., et al. (submitted). Sensitivity of historical climate simulations to uncertain aerosol forcing. *Geophys. Res. Lett.* (submitted).
Dittus, A. J., Karoly, D. J., Lewis, S. C., Alexander, L. V., and Donat, M. G. (2016). A Multiregion Model Evaluation and Attribution Study of Historical Changes in the Area Affected by Temperature and Precipitation Extremes. *J. Clim.* 29, 8285–8299. doi:10.1175/JCLI-D-16-0164.1.
Dixon, K. W., Lanzante, J. R., Nath, M. J., Hayhoe, K., Stoner, A., Radhakrishnan, A., et al. (2016). Evaluating the stationarity assumption in statistically downscaled climate projections: is past performance an indicator of future results? *Clim. Change* 135, 395–408. doi:10.1007/s10584-016-1598-0.
Doan, Q. Van, Kusaka, H., and Ho, Q. B. (2016). Impact of future urbanization on temperature and thermal comfort index in a developing tropical city: Ho Chi Minh City. *Urban Clim.* 17, 20–31. doi:10.1016/j.uclim.2016.04.003.
Dobor, L., and Hlásny, T. (2018). Choice of reference climate conditions matters in impact studies: Case of bias-corrected CORDEX data set. *Int. J. Climatol.* doi:10.1002/joc.5930.
Dobriyal, P., Qureshi, A., Badola, R., and Hussain, S. A. (2012). A review of the methods available for estimating soil moisture and its implications for water resource management. *J. Hydrol.* 458–459, 110–117. doi:https://doi.org/10.1016/j.jhydrol.2012.06.021.
Dogar, M. M., and Sato, T. (2019). Regional Climate Response of Middle Eastern, African, and South Asian Monsoon Regions to Explosive Volcanism and ENSO Forcing. *J. Geophys. Res. Atmos.* 124, 7580–7598. doi:10.1029/2019JD030358.
Donat, M. G., Alexander, L. V., Yang, H., Durre, I., Vose, R., Dunn, R. J. H., et al. (2013). Updated analyses of temperature and precipitation extreme indices since the beginning of the twentieth century: The HadEX2 dataset. *J. Geophys. Res. Atmos.* 118, 2098–2118. doi:10.1002/jgrd.50150.
Donat, M. G., Peterson, T. C., Brunet, M., King, A. D., Almazroui, M., Kolli, R. K., et al. (2014). Changes in extreme temperature and precipitation in the Arab region: long-term trends and variability related to ENSO and NAO. *Int. J. Climatol.* 34, 581–592. doi:10.1002/joc.3707.
Donat, M. G., Pitman, A. J., and Angélil, O. (2018). Understanding and Reducing Future Uncertainty in Midlatitude Daily Heat Extremes Via Land Surface Feedback Constraints. *Geophys. Res. Lett.* 45, 10,627-10,636. doi:10.1029/2018GL079128.
Done, J. M., Holland, G. J., Bruyère, C. L., Leung, L. R., and Suzuki-Parker, A. (2015). Modeling high-impact weather and climate: lessons from a tropical cyclone perspective. *Clim. Change* 129, 381–395. doi:10.1007/s10584-013-0954-6.
Dong-feng, Z., Zhen-yu, H. A. N., and Ying, S. H. I. (2017). ScienceDirect Comparison of climate projections between driving CSIRO-Mk3 . 6 . 0 and downscaling simulation of RegCM4 . 4 over China. *Adv. Clim. Chang. Res.* 8, 245–255. doi:10.1016/j.accre.2017.10.001.
Dong, B., and Dai, A. (2015). The influence of the Interdecadal Pacific Oscillation on Temperature and Precipitation over the Globe. *Clim. Dyn.* 45, 2667–2681. doi:10.1007/s00382-015-2500-x.
Dong, B., Dai, A., Vuille, M., and Timm, O. E. (2018). Asymmetric Modulation of ENSO Teleconnections by the Interdecadal Pacific Oscillation. *J. Clim.* 31, 7337–7361. doi:10.1175/JCLI-D-17-0663.1.
Dong, B., and Sutton, R. (2015). Dominant role of greenhouse-gas forcing in the recovery of Sahel rainfall. *Nat. Clim. Chang.* 5, 757–760. doi:10.1038/nclimate2664.
Dong, B., Sutton, R. T., Highwood, E., and Wilcox, L. (2014). The impacts of European and Asian anthropogenic sulfur dioxide emissions on Sahel rainfall. *J. Clim.* 27, 7000–7017. doi:10.1175/JCLI-D-13-00769.1.
Dong, B., Sutton, R. T., and Shaffrey, L. (2017). Understanding the rapid summer warming and changes in temperature extremes since the mid-1990s over Western Europe. *Clim. Dyn.* 48, 1537–1554. doi:10.1007/s00382-016-3158-8.
Dong, B., Sutton, R. T., Woollings, T., and Hodges, K. (2013). Variability of the North Atlantic summer storm track: mechanisms and impacts on European climate. *Environ. Res. Lett.* 8, 034037. doi:10.1088/1748-9326/8/3/034037.
Dong, L., and McPhaden, M. J. (2017). Why Has the Relationship between Indian and Pacific Ocean Decadal Variability Changed in Recent Decades? *J. Clim.* 30, 1971–1983. doi:10.1175/JCLI-D-16-0313.1.
Dosio, A. (2016). Projections of climate change indices of temperature and precipitation from an ensemble of bias-adjusted high-resolution EURO-CORDEX regional climate models. *J. Geophys. Res. Atmos.* 121, 5488–5511. doi:10.1002/2015JD024411.
Dosio, A. (2017). Projection of temperature and heat waves for Africa with an ensemble of CORDEX Regional Climate Models. *Clim. Dyn.* 49, 493–519. doi:10.1007/s00382-016-3355-5.
Dosio, A., and Fischer, E. M. (2018). Will Half a Degree Make a Difference? Robust Projections of Indices of Mean and Extreme Climate in Europe Under 1.5°C, 2°C, and 3°C Global Warming. *Geophys. Res. Lett.* 45, 935–944. doi:10.1002/2017GL076222.
Dosio, A., Jones, R. G., Jack, C., Lennard, C., Nikulin, G., and Hewitson, B. (2019). What can we know about future

precipitation in Africa? Robustness, significance and added value of projections from a large ensemble of regional climate models. *Clim. Dyn.* 53, 5833–5858. doi:10.1007/s00382-019-04900-3.
Dosio, A., Panitz, H.-J., Schubert-Frisius, M., and Lüthi, D. (2015). Dynamical downscaling of CMIP5 global circulation models over CORDEX-Africa with COSMO-CLM: evaluation over the present climate and analysis of the added value. *Clim. Dyn.* 44, 2637–2661. doi:10.1007/s00382-014-2262-x.
Dosio, A., Paruolo, P., and Rojas, R. (2012). Bias correction of the ENSEMBLES high resolution climate change projections for use by impact models: Analysis of the climate change signal. *J. Geophys. Res. Atmos.* 117, n/a-n/a. doi:10.1029/2012JD017968.
Dosio, A., Turner, A. G., Tamoffo, A. T., Sylla, M. B., Lennard, C., Jones, R. G., et al. (submitted). A tale of two futures: contrasting scenarios of future precipitation for West Africa from an ensemble of Regional Climate Models. *Environ. Res. Lett.* (submitted). doi:Submitted.
Dou, J., Wang, Y., Bornstein, R., and Miao, S. (2015). Observed Spatial Characteristics of Beijing Urban Climate Impacts on Summer Thunderstorms. *J. Appl. Meteorol. Climatol.* 54, 94–105. doi:10.1175/JAMC-D-13-0355.1.
Douville, H., Peings, Y., and Saint-Martin, D. (2017). Snow-(N)AO relationship revisited over the whole twentieth century. *Geophys. Res. Lett.* 44, 569–577. doi:10.1002/2016GL071584.
Douville, H., Voldoire, A., and Geoffroy, O. (2015). The recent global warming hiatus: What is the role of Pacific variability? *Geophys. Res. Lett.* 42, 880–888. doi:10.1002/2014GL062775.
Dowdy, A. J., and Catto, J. L. (2017). Extreme weather caused by concurrent cyclone, front and thunderstorm occurrences. *Sci. Rep.* 7, 40359. doi:10.1038/srep40359.
Doyle, M. E., Saurral, R. I., and Barros, V. R. (2012). Trends in the distributions of aggregated monthly precipitation over the La Plata Basin. *Int. J. Climatol.* 32, 2149–2162. doi:10.1002/joc.2429.
Driscoll, S., Bozzo, A., Gray, L. J., Robock, A., and Stenchikov, G. (2012). Coupled Model Intercomparison Project 5 (CMIP5) simulations of climate following volcanic eruptions. *J. Geophys. Res. Atmos.* 117. doi:10.1029/2012JD017607.
Drobinski, P., Bastin, S., Arsouze, T., Béranger, K., Flaounas, E., and Stéfanon, M. (2018). North-western Mediterranean sea-breeze circulation in a regional climate system model. *Clim. Dyn.* 51, 1077–1093. doi:10.1007/s00382-017-3595-z.
Duan, A., Wang, M., Lei, Y., and Cui, Y. (2013). Trends in Summer Rainfall over China Associated with the Tibetan Plateau Sensible Heat Source during 1980–2008. *J. Clim.* 26, 261–275. doi:10.1175/JCLI-D-11-00669.1.
Dubrovsky, M., Huth, R., Dabhi, H., and Rotach, M. W. (2019). Parametric gridded weather generator for use in present and future climates: focus on spatial temperature characteristics. *Theor. Appl. Climatol.* doi:10.1007/s00704-019-03027-z.
Duchene et al. (submitted). A statistical-dynamical methodology to downscale regional climate projections to urban scale. *J. Appl. Meteorol. Climatol.* (submitted).
Dumitrescu, A., Birsan, M.-V., and Manea, A. (2016). Spatio-temporal interpolation of sub-daily (6 h) precipitation over Romania for the period 1975–2010. *Int. J. Climatol.* 36, 1331–1343. doi:10.1002/joc.4427.
Dunn-Sigouin, E., and Son, S.-W. (2013). Northern Hemisphere blocking frequency and duration in the CMIP5 models. *J. Geophys. Res. Atmos.* 118, 1179–1188. doi:10.1002/jgrd.50143.
Dupont, S., and Mestayer, P. G. (2006). Parameterization of the urban energy budget with the submesoscale soil model. *J. Appl. Meteorol. Climatol.* doi:10.1175/JAM2417.1.
DWA (2013). Metropolitan Municipality Non-Revenue /Water Loss Assessment. Retrieved from www.dwa.gov.za/wsks/UserControls/Do. Available at: www.dwa.gov.za/wsks/UserControls/DownloadImportFiles.aspx?FileID=211.
DWAF (2007). WESTERN CAPE WATER SUPPLY SYSTEM RECONCILIATION STRATEGY STUDY. Cape Town Available at: http://www.dwa.gov.za/Projects/RS_WC_WSS/Docs/Reconciliation Strategy.pdf.
Ehret, U., Zehe, E., Wulfmeyer, V., Warrach-Sagi, K., and Liebert, J. (2012). HESS Opinions "Should we apply bias correction to global and regional climate model data?" *Hydrol. Earth Syst. Sci.* 16, 3391–3404. doi:10.5194/hess-16-3391-2012.
Eisenack, K., Moser, S. C., Hoffmann, E., Klein, R. J. T., Oberlack, C., Pechan, A., et al. (2014). Explaining and overcoming barriers to climate change adaptation. *Nat. Clim. Chang.* 4, 867–872. doi:10.1038/nclimate2350.
Ekström, M., Grose, M., Heady, C., Turner, S., and Teng, J. (2016). The method of producing climate change datasets impacts the resulting policy guidance and chance of mal-adaptation. *Clim. Serv.* 4, 13–29. doi:10.1016/J.CLISER.2016.09.003.
Ekström, M., Grose, M. R., and Whetton, P. H. (2015). An appraisal of downscaling methods used in climate change research. *Wiley Interdiscip. Rev. Clim. Chang.* 6, 301–319. doi:10.1002/wcc.339.
Elagib, N. A. (2011). Evolution of urban heat island in Khartoum. *Int. J. Climatol.* 31, 1377–1388. doi:10.1002/joc.2159.
Elalem, S., and Pal, I. (2015). Mapping the vulnerability hotspots over Hindu-Kush Himalaya region to flooding disasters. *Weather Clim. Extrem.* 8, 46–58. doi:10.1016/j.wace.2014.12.001.
Emile-Geay, J., Seager, R., Cane, M. A., Cook, E. R., and Haug, G. H. (2008). Volcanoes and ENSO over the Past Millennium. *J. Clim.* 21, 3134–3148. doi:10.1175/2007JCLI1884.1.

Endo, H., Kitoh, A., and Ueda, H. (2018). A Unique Feature of the Asian Summer Monsoon Response to Global Warming: The Role of Different Land–Sea Thermal Contrast Change between the Lower and Upper Troposphere. *SOLA* 14, 57–63. doi:10.2151/sola.2018-010.
Endris, H. S., Lennard, C., Hewitson, B., Dosio, A., Nikulin, G., and Panitz, H.-J. (2016). Teleconnection responses in multi-GCM driven CORDEX RCMs over Eastern Africa. *Clim. Dyn.* 46, 2821–2846. doi:10.1007/s00382-015-2734-7.
Endris, H. S., Omondi, P., Jain, S., Lennard, C., Hewitson, B., Chang'a, L., et al. (2013). Assessment of the Performance of CORDEX Regional Climate Models in Simulating East African Rainfall. *J. Clim.* 26, 8453–8475. doi:10.1175/JCLI-D-12-00708.1.
Engelbrecht, F. A., McGregor, J. L., and Engelbrecht, C. J. (2009). Dynamics of the Conformal-Cubic Atmospheric Model projected climate-change signal over southern Africa. *Int. J. Climatol.* 29, 1013–1033. doi:10.1002/joc.1742.
England, M. H., McGregor, S., Spence, P., Meehl, G. A., Timmermann, A., Cai, W., et al. (2014). Recent intensification of wind-driven circulation in the Pacific and the ongoing warming hiatus. *Nat. Clim. Chang.* 4, 222–227. doi:10.1038/nclimate2106.
Erdin, R., Frei, C., and Künsch, H. R. (2012). Data Transformation and Uncertainty in Geostatistical Combination of Radar and Rain Gauges. *J. Hydrometeorol.* 13, 1332–1346. doi:10.1175/jhm-d-11-096.1.
Erfanian, A., and Wang, G. (2018). Explicitly Accounting for the Role of Remote Oceans in Regional Climate Modeling of South America. *J. Adv. Model. Earth Syst.* 10, 2408–2426. doi:10.1029/2018MS001444.
Espinoza, V., Waliser, D. E., Guan, B., Lavers, D. A., and Ralph, F. M. (2018). Global Analysis of Climate Change Projection Effects on Atmospheric Rivers. *Geophys. Res. Lett.* 45, 4299–4308. doi:10.1029/2017GL076968.
Evan, A. T., Flamant, C., Gaetani, M., and Guichard, F. (2016). The past, present and future of African dust. *Nature* 531, 493–495. doi:10.1038/nature17149.
Evan, A. T., Flamant, C., Lavaysse, C., Kocha, C., and Saci, A. (2015). Water vapor-forced greenhouse warming over the Sahara desert and the recent recovery from the Sahelian drought. *J. Clim.* doi:10.1175/JCLI-D-14-00039.1.
Evans, J. P., Ji, F., Lee, C., Smith, P., Argüeso, D., and Fita, L. (2014). Design of a regional climate modelling projection ensemble experiment – NARCliM. *Geosci. Model Dev.* 7, 621–629. doi:10.5194/gmd-7-621-2014.
Evans, S., Malyshev, S., Ginoux, P., and Shevliakova, E. (2019). The Impacts of the Dust Radiative Effect on Vegetation Growth in the Sahel. *Global Biogeochem. Cycles* n/a. doi:10.1029/2018GB006128.
Evin, G., Favre, A.-C., and Hingray, B. (2018). Stochastic generation of multi-site daily precipitation focusing on extreme events. *Hydrol. Earth Syst. Sci.* 22, 655–672. doi:10.5194/hess-22-655-2018.
Evin, G., Hingray, B., Blanchet, J., Eckert, N., Morin, S., and Verfaillie, D. (2019). Partitioning Uncertainty Components of an Incomplete Ensemble of Climate Projections Using Data Augmentation. *J. Clim.* 32, 2423–2440. doi:10.1175/JCLI-D-18-0606.1.
Eyring, V., Bony, S., Meehl, G. A., Senior, C. A., Stevens, B., Stouffer, R. J., et al. (2016a). Overview of the Coupled Model Intercomparison Project Phase 6 (CMIP6) experimental design and organization. *Geosci. Model Dev.* 9, 1937–1958. doi:10.5194/gmd-9-1937-2016.
Eyring, V., Cox, P. M., Flato, G. M., Gleckler, P. J., Abramowitz, G., Caldwell, P., et al. (2019). Taking climate model evaluation to the next level. *Nat. Clim. Chang.* 9, 102–110. doi:10.1038/s41558-018-0355-y.
Eyring, V., Righi, M., Lauer, A., Evaldsson, M., Wenzel, S., Jones, C., et al. (2016b). ESMValTool (v1.0) – a community diagnostic and performance metrics tool for routine evaluation of Earth system models in CMIP. *Geosci. Model Dev.* 9, 1747–1802. doi:10.5194/gmd-9-1747-2016.
Ezber, Y., Lutfi Sen, O., Kindap, T., and Karaca, M. (2007). Climatic effects of urbanization in istanbul: a statistical and modeling analysis. *Int. J. Climatol.* 27, 667–679. doi:10.1002/joc.1420.
Fabiano, F., Christensen, H. M., Strommen, K., Corti, S., Athanasiadis, P., Baker, A., et al. (submitted). Euro-Atlantic Weather Regimes in the PRIMAVERA coupled climate simulations: impact of resolution and mean state biases on model performance. *Clim. Dyn.* (submitted).
Falarz, M. (2019). Azores High and Hawaiian High: correlations, trends and shifts (1948–2018). *Theor. Appl. Climatol.* 138, 417–431. doi:10.1007/s00704-019-02837-5.
Falco, M., Carril, A. F., Menéndez, C. G., Zaninelli, P. G., Li, L. Z. X., and Falco M., Carril A.F., Menéndez C., Zaninelli P.G., L. L. Z. . (2018). Assessment of CORDEX simulations over South America: added value on seasonal climatology and resolution considerations. *Clim. Dyn.* doi:10.1007/s00382-018-4412-z.
Fallah, B., Russo, E., Acevedo, W., Mauri, A., Becker, N., and Cubasch, U. (2018). Towards high-resolution climate reconstruction using an off-line data assimilation and COSMO-CLM 5.00 model. *Clim. Past* 14, 1345–1360. doi:10.5194/cp-14-1345-2018.
Fan, Y., and van den Dool, H. (2008). A global monthly land surface air temperature analysis for 1948–present. *J. Geophys. Res. Atmos.* 113. doi:10.1029/2007JD008470.
Favre, A., Hewitson, B., Lennard, C., Cerezo-Mota, R., and Tadross, M. (2013). Cut-off Lows in the South Africa region and their contribution to precipitation. *Clim. Dyn.* 41, 2331–2351. doi:10.1007/s00382-012-1579-6.
Feng, X., Huang, B., Kirtman, B. P., Kinter, J. L., and Chiu, L. S. (2017). A multi-model analysis of the resolution influence on precipitation climatology in the Gulf Stream region. *Clim. Dyn.* 48, 1685–1704. doi:10.1007/s00382-

016-3167-7.
Ferguson, J. O., Jablonowski, C., Johansen, H., McCorquodale, P., Colella, P., and Ullrich, P. A. (2016). Analyzing the Adaptive Mesh Refinement (AMR) Characteristics of a High-Order 2D Cubed-Sphere Shallow-Water Model. *Mon. Weather Rev.* 144, 4641–4666. doi:10.1175/MWR-D-16-0197.1.
Fernandes, L. G., and Rodrigues, R. R. (2018). Changes in the patterns of extreme rainfall events in southern Brazil. *Int. J. Climatol.* 38, 1337–1352. doi:10.1002/joc.5248.
Fernández, J., Frías, M. D., Cabos, W. D., Cofiño, A. S., Domínguez, M., Fita, L., et al. (2019). Consistency of climate change projections from multiple global and regional model intercomparison projects. *Clim. Dyn.* 52, 1139–1156. doi:10.1007/s00382-018-4181-8.
Feser, F., Rockel, B., von Storch, H., Winterfeldt, J., and Zahn, M. (2011). Regional Climate Models Add Value to Global Model Data: A Review and Selected Examples. *Bull. Am. Meteorol. Soc.* 92, 1181–1192. doi:10.1175/2011BAMS3061.1.
Fick, S. E., and Hijmans, R. J. (2017). WorldClim 2: new 1-km spatial resolution climate surfaces for global land areas. *Int. J. Climatol.* 37, 4302–4315. doi:10.1002/joc.5086.
Fiedler, S., Kinne, S., Huang, W. T. K., Räisänen, P., O'Donnell, D., Bellouin, N., et al. (2019). Anthropogenic aerosol forcing – insights from multiple estimates from aerosol-climate models with reduced complexity. *Atmos. Chem. Phys.* 19, 6821–6841. doi:10.5194/acp-19-6821-2019.
Fiedler, S., Stevens, B., and Mauritsen, T. (2017). On the sensitivity of anthropogenic aerosol forcing to model-internal variability and parameterizing a Twomey effect. *J. Adv. Model. Earth Syst.* 9, 1325–1341. doi:10.1002/2017MS000932.
Finney, D. L., Marsham, J. H., Jackson, L. S., Kendon, E. J., Rowell, D. P., Boorman, P. M., et al. (2019). Implications of Improved Representation of Convection for the East Africa Water Budget Using a Convection-Permitting Model. *J. Clim.* 32, 2109–2129. doi:10.1175/JCLI-D-18-0387.1.
Fita, L., Evans, J. P., Argüeso, D., King, A., and Liu, Y. (2017). Evaluation of the regional climate response in Australia to large-scale climate modes in the historical NARCliM simulations. *Clim. Dyn.* 49, 2815–2829. doi:10.1007/s00382-016-3484-x.
Flaounas, E., Drobinski, P., and Bastin, S. (2013). Dynamical downscaling of IPSL-CM5 CMIP5 historical simulations over the Mediterranean: benefits on the representation of regional surface winds and cyclogenesis. *Clim. Dyn.* 40, 2497–2513. doi:10.1007/s00382-012-1606-7.
Flaounas, E., Kelemen, F. D., Wernli, H., Gaertner, M. A., Reale, M., Sanchez-Gomez, E., et al. (2018). Assessment of an ensemble of ocean–atmosphere coupled and uncoupled regional climate models to reproduce the climatology of Mediterranean cyclones. *Clim. Dyn.* 51, 1023–1040. doi:10.1007/s00382-016-3398-7.
Flato, G., Marotzke, J., Abiodun, B., Braconnot, P., Chou, S. C., Collins, W., et al. (2014). *Climate Change 2013 - The Physical Science Basis.* , ed. Intergovernmental Panel on Climate Change Cambridge: Cambridge University Press doi:10.1017/CBO9781107415324.
Fletcher, C. G., and Kushner, P. J. (2011). The Role of Linear Interference in the Annular Mode Response to Tropical SST Forcing. *J. Clim.* 24, 778–794. doi:10.1175/2010JCLI3735.1.
Fløttum, K., and Gjerstad, Ø. (2017). Narratives in climate change discourse. *Wiley Interdiscip. Rev. Clim. Chang.* 8, e429. doi:10.1002/wcc.429.
Folland, C. K., Knight, J., Linderholm, H. W., Fereday, D., Ineson, S., and Hurrell, J. W. (2009). The Summer North Atlantic Oscillation: Past, Present, and Future. *J. Clim.* 22, 1082–1103. doi:10.1175/2008JCLI2459.1.
Forsythe, N., Fowler, H. J., Li, X. F., Blenkinsop, S., and Pritchard, D. (2017). Karakoram temperature and glacial melt driven by regional atmospheric circulation variability. *Nat. Clim. Chang.* 7, 664–670. doi:10.1038/nclimate3361.
Fosser, G., Khodayar, S., and Berg, P. (2015). Benefit of convection permitting climate model simulations in the representation of convective precipitation. *Clim. Dyn.* 44, 45–60. doi:10.1007/s00382-014-2242-1.
Fosser, G., Khodayar, S., and Berg, P. (2017). Climate change in the next 30 years: What can a convection-permitting model tell us that we did not already know? *Clim. Dyn.* 48, 1987–2003. doi:10.1007/s00382-016-3186-4.
Founda, D., Pierros, F., Petrakis, M., and Zerefos, C. (2015). Interdecadal variations and trends of the Urban Heat Island in Athens (Greece) and its response to heat waves. *Atmos. Res.* 161–162, 1–13. doi:https://doi.org/10.1016/j.atmosres.2015.03.016.
Foussard, A., Lapeyre, G., and Plougonven, R. (2019). Storm Track Response to Oceanic Eddies in Idealized Atmospheric Simulations. *J. Clim.* 32, 445–463. doi:10.1175/JCLI-D-18-0415.1.
Fox-Rabinovitz, M., Côté, J., Dugas, B., Déqué, M., and McGregor, J. L. (2006). Variable resolution general circulation models: Stretched-grid model intercomparison project (SGMIP). *J. Geophys. Res.* 111, D16104. doi:10.1029/2005JD006520.
Fox-Rabinovitz, M., Cote, J., Dugas, B., Deque, M., McGregor, J. L., and Belochitski, A. (2008). Stretched-grid Model Intercomparison Project: decadal regional climate simulations with enhanced variable and uniform-resolution GCMs. *Meteorol. Atmos. Phys.* 100, 159–178. doi:10.1007/s00703-008-0301-z.
Frame, J., and Killick, M. (2007). Integrated water resource planning in the city of Cape Town. *Water SA* 30. doi:10.4314/wsa.v30i5.5188.
Francis, J. A., and Vavrus, S. J. (2012). Evidence linking Arctic amplification to extreme weather in mid-latitudes.

Geophys. Res. Lett. 39. doi:10.1029/2012GL051000.
Francis, J. A., and Vavrus, S. J. (2015). Evidence for a wavier jet stream in response to rapid Arctic warming. *Environ. Res. Lett.* 10, 014005. doi:10.1088/1748-9326/10/1/014005.
Francis, J. A., Vavrus, S. J., and Cohen, J. (2017). Amplified Arctic warming and mid-latitude weather: new perspectives on emerging connections. *Wiley Interdiscip. Rev. Clim. Chang.* 8, e474. doi:10.1002/wcc.474.
Frankcombe, L. M., England, M. H., Mann, M. E., and Steinman, B. A. (2015). Separating internal variability from the externally forced climate response. *J. Clim.* 28, 8184–8202. doi:10.1175/JCLI-D-15-0069.1.
Franke, J., Brönnimann, S., Bhend, J., and Brugnara, Y. (2017). A monthly global paleo-reanalysis of the atmosphere from 1600 to 2005 for studying past climatic variations. *Sci. data* 4, 170076. doi:10.1038/sdata.2017.76.
Frederiksen, C. S., Frederiksen, J. S., Sisson, J. M., and Osbrough, S. L. (2017). Trends and projections of Southern Hemisphere baroclinicity: the role of external forcing and impact on Australian rainfall. *Clim. Dyn.* 48, 3261–3282. doi:10.1007/s00382-016-3263-8.
Frei, C. (2014). Interpolation of temperature in a mountainous region using nonlinear profiles and non-Euclidean distances. *Int. J. Climatol.* 1605, 1585–1605. doi:10.1002/joc.3786.
Frei, C., Christensen, J. H., Déqué, M., Jacob, D., Jones, R. G., and Vidale, P. L. (2003). Daily precipitation statistics in regional climate models: Evaluation and intercomparison for the European Alps. *J. Geophys. Res. Atmos.* 108, n/a-n/a. doi:10.1029/2002JD002287.
Freund, M., Henley, B. J., Karoly, D. J., Allen, K. J., and Baker, P. J. (2017). Multi-century cool- and warm-season rainfall reconstructions for Australia's major climatic regions. *Clim. Past* 13, 1751–1770. doi:10.5194/cp-13-1751-2017.
Froidevaux, P., Schlemmer, L., Schmidli, J., Langhans, W., and Schär, C. (2014). Influence of the Background Wind on the Local Soil Moisture–Precipitation Feedback. *J. Atmos. Sci.* 71, 782–799. doi:10.1175/JAS-D-13-0180.1.
Frost, A. J., Charles, S. P., Timbal, B., Chiew, F. H. S., Mehrotra, R., Nguyen, K. C., et al. (2011). A comparison of multi-site daily rainfall downscaling techniques under Australian conditions. *J. Hydrol.* 408, 1–18. doi:10.1016/j.jhydrol.2011.06.021.
Früh, B., Becker, P., Deutschländer, T., Hessel, J.-D., Kossmann, M., Mieskes, I., et al. (2011). Estimation of Climate-Change Impacts on the Urban Heat Load Using an Urban Climate Model and Regional Climate Projections. *J. Appl. Meteorol. Climatol.* 50, 167–184. doi:10.1175/2010JAMC2377.1.
Fu, J., and Li, S. (2013). The influence of regional SSTs on the interdecadal shift of the East Asian summer monsoon. *Adv. Atmos. Sci.* 30, 330–340. doi:10.1007/s00376-012-2062-3.
Fujibe, F. (2009). Detection of urban warming in recent temperature trends in Japan. *Int. J. Climatol.* 29, 1811–1822. doi:10.1002/joc.1822.
Fumière, Q., Déqué, M., Nuissier, O., Somot, S., Alias, A., Caillaud, C., et al. (2019). Extreme rainfall in Mediterranean France during the fall: added value of the CNRM-AROME Convection-Permitting Regional Climate Model. *Clim. Dyn.* doi:10.1007/s00382-019-04898-8.
Fyfe, J. C., Gillett, N. P., and Marshall, G. J. (2012). Human influence on extratropical Southern Hemisphere summer precipitation. *Geophys. Res. Lett.* 39, n/a-n/a. doi:10.1029/2012GL054199.
Gadgil, S. S., and Gadgil, S. S. (2006). The Indian monsoon, GDP and agriculture. *Econ. Polit. Wkly.* doi:10.2307/4418949.
Gaertner, M. Á., González-Alemán, J. J., Romera, R., Domínguez, M., Gil, V., Sánchez, E., et al. (2018). Simulation of medicanes over the Mediterranean Sea in a regional climate model ensemble: impact of ocean–atmosphere coupling and increased resolution. *Clim. Dyn.* 51, 1041–1057. doi:10.1007/s00382-016-3456-1.
Gaetani, M., and Mohino, E. (2013). Decadal prediction of the sahelian precipitation in CMIP5 simulations. *J. Clim.* 26, 7708–7719. doi:10.1175/JCLI-D-12-00635.1.
Gaffin, S. R., Rosenzweig, C., Khanbilvardi, R., Parshall, L., Mahani, S., Glickman, H., et al. (2008). Variations in New York city's urban heat island strength over time and space. *Theor. Appl. Climatol.* 94, 1–11. doi:10.1007/s00704-007-0368-3.
Gallant, A. J. E., Phipps, S. J., Karoly, D. J., Mullan, A. B., and Lorrey, A. M. (2013). Nonstationary Australasian Teleconnections and Implications for Paleoclimate Reconstructions. *J. Clim.* 26, 8827–8849. doi:10.1175/JCLI-D-12-00338.1.
Galmarini, S., Cannon, A. J., Ceglar, A., Christensen, O. B., de Noblet-Ducoudré, N., Dentener, F., et al. (2019). Adjusting climate model bias for agricultural impact assessment: How to cut the mustard. *Clim. Serv.* doi:10.1016/j.cliser.2019.01.004.
Ganeshan, M., and Murtugudde, R. (2015). Nocturnal propagating thunderstorms may favor urban "hot-spots": A model-based study over Minneapolis. *Urban Clim.* 14, 606–621. doi:10.1016/j.uclim.2015.10.005.
Ganeshan, M., Murtugudde, R., and Imhoff, M. L. (2013). A multi-city analysis of the UHI-influence on warm season rainfall. *Urban Clim.* 6, 1–23. doi:https://doi.org/10.1016/j.uclim.2013.09.004.
Gangopadhyay, S., Pruitt, T., Brekke, L., and Raff, D. (2011). Hydrologic projections for the western United States. *Eos, Trans. Am. Geophys. Union* 92, 441–442. doi:10.1029/2011EO480001.
Gao, C. C., and Gao, Y. J. (2018). Revisited Asian Monsoon Hydroclimate Response to Volcanic Eruptions. *J. Geophys. Res. Atmos.* 123, 7883–7896. doi:10.1029/2017JD027907.

Gao, M., Carmichael, G. R., Wang, Y., Saide, P. E., Yu, M., Xin, J., et al. (2016). Modeling study of the 2010 regional haze event in the North China Plain. *Atmos. Chem. Phys.* 16, 1673–1691. doi:10.5194/acp-16-1673-2016.

García-Díez, M., Fernández, J., and Vautard, R. (2015). An RCM multi-physics ensemble over Europe: multi-variable evaluation to avoid error compensation. *Clim. Dyn.* 45, 3141–3156. doi:10.1007/s00382-015-2529-x.

Garcia-Villada, L. P., Donat, M. G., Angélil, O., and Taschetto, A. S. (submitted). Temperature and Precipitation responses to El Niño-Southern Oscillation in a hierarchy of datasets with different levels of observational constraints. *Clim. Dyn.* (submitted).

García, P. E., Menénendez, A. N., Podestá, G., Bert, F., Arora, P., and Jobbágy, E. (2018). Land use as possible strategy for managing water table depth in flat basins with shallow groundwater. *Int. J. River Basin Manag.* 16, 79–92. doi:10.1080/15715124.2017.1378223.

Garfinkel, C. I., Waugh, D. W., and Polvani, L. M. (2015). Recent Hadley cell expansion: The role of internal atmospheric variability in reconciling modeled and observed trends. *Geophys. Res. Lett.* 42, 10,824-10,831. doi:10.1002/2015GL066942.

Gasparrini, A., and Armstrong, B. (2012). UKPMC Funders Group The impact of heat waves on mortality. *Epidemiology* 22, 68–73. doi:10.1097/EDE.0b013e3181fdcd99.The.

Gastineau, G., García-Serrano, J., and Frankignoul, C. (2017). The Influence of Autumnal Eurasian Snow Cover on Climate and Its Link with Arctic Sea Ice Cover. *J. Clim.* 30, 7599–7619. doi:10.1175/JCLI-D-16-0623.1.

Gautam, R., Hsu, N. C., Lau, W. K.-M., and Yasunari, T. J. (2013). Satellite observations of desert dust-induced Himalayan snow darkening. *Geophys. Res. Lett.* 40, 988–993. doi:10.1002/grl.50226.

GCOS (2015). *Status of the Global Observing System for Climate*. doi:10.13140/RG.2.2.23178.26566.

Gentry, M. S., and Lackmann, G. M. (2010). Sensitivity of Simulated Tropical Cyclone Structure and Intensity to Horizontal Resolution. *Mon. Weather Rev.* 138, 688–704. doi:10.1175/2009MWR2976.1.

Georgakakos, A., Fleming, P., Dettinger, M., Peters-Lidard, C., Richmond, T. C., Reckhow, K., et al. (2014). “Water Resources,” in *Climate Change Impacts in the United States: The Third National Climate Assessment* (U.S. Global Change Research Program), 69–112.

Gergis, J., Gallant, A. J. E., Braganza, K., Karoly, D. J., and Allen, K. (2012). On the long-term context of the 1997–2009 “Big Dry” in South-Eastern Australia: insights from a 206-year multi-proxy rainfall reconstruction. *Clim. Change* 111, 923–944. doi:10.1007/s10584-011-0263-x.

Gevaert, A. I., Miralles, D. G., de Jeu, R. A. M., Schellekens, J., and Dolman, A. J. (2018). Soil Moisture-Temperature Coupling in a Set of Land Surface Models. *J. Geophys. Res. Atmos.* doi:10.1002/2017JD027346.

Ghan, S., Wang, M., Zhang, S., Ferrachat, S., Gettelman, A., Griesfeller, J., et al. (2016). Challenges in constraining anthropogenic aerosol effects on cloud radiative forcing using present-day spatiotemporal variability. *Proc. Natl. Acad. Sci.* 113, 5804–5811. doi:10.1073/pnas.1514036113.

Ghimire, S., Choudhary, A., and Dimri, A. P. (2018). Assessment of the performance of CORDEX-South Asia experiments for monsoonal precipitation over the Himalayan region during present climate: part I. *Clim. Dyn.* 50, 2311–2334. doi:10.1007/s00382-015-2747-2.

Ghosh, R., Müller, W. A., Baehr, J., and Bader, J. (2017). Impact of observed North Atlantic multidecadal variations to European summer climate: a linear baroclinic response to surface heating. *Clim. Dyn.* 48, 3547–3563. doi:10.1007/s00382-016-3283-4.

Giannini, A., and Kaplan, A. (2019). The role of aerosols and greenhouse gases in Sahel drought and recovery. *Clim. Change* 152, 449–466. doi:10.1007/s10584-018-2341-9.

Giannini, A., Kushnir, Y., and Cane, M. A. (2000). Interannual variability of the Carribbean rainfall ENSO and the Atlantic Ocean. *J. Clim.* 13, 297–311. doi:Doi 10.1175/1520-0442(2000)013<0297:Ivocre>2.0.Co;2.

Giannini, A., Salack, S., Lodoun, T., Ali, A., Gaye, A. T., and Ndiaye, O. (2013). A unifying view of climate change in the Sahel linking intra-seasonal, interannual and longer time scales. *Environ. Res. Lett.* 8, 024010. doi:10.1088/1748-9326/8/2/024010.

Gillett, N. P., Shiogama, H., Funke, B., Hegerl, G., Knutti, R., Matthes, K., et al. (2016). The Detection and Attribution Model Intercomparison Project (DAMIP v1.0) contribution to CMIP6. *Geosci. Model Dev.* 9, 3685–3697. doi:10.5194/gmd-9-3685-2016.

Ginoux, P., Prospero, J., Gill, T., Hsu, N., and Zhao, M. (2012). Global-scale attribution of anthropogenic and natural dust sources and their emission rates based on MODIS Deep Blue aerosol products. *Rev. Geophys.* 50, 3005. doi:10.1029/2012RG000388.

Giorgi, F. (2002). Variability and trends of sub-continental scale surface climate in the twentieth century. Part I: observations. *Clim. Dyn.* 18, 675–691. doi:10.1007/s00382-001-0204-x.

GIORGI, F., and GAO, X.-J. (2018). Regional earth system modeling: review and future directions. *Atmos. Ocean. Sci. Lett.* 11, 189–197. doi:10.1080/16742834.2018.1452520.

Giorgi, F., and Gutowski, W. J. (2015). Regional Dynamical Downscaling and the CORDEX Initiative. *Annu. Rev. Environ. Resour.* 40, 467–490. doi:10.1146/annurev-environ-102014-021217.

Giorgi, F., Jones, C., and Asrar, G. R. (2009). Addressing climate information needs at the regional level: the CORDEX framework. *WMO Bull.* 58, 175–183.

Giorgi, F., and Mearns, L. O. (2002). Calculation of Average, Uncertainty Range, and Reliability of Regional Climate

Changes from AOGCM Simulations via the "Reliability Ensemble Averaging" (REA) Method. *J. Clim.* 15, 1141–1158. doi:10.1175/1520-0442(2002)015<1141:COAURA>2.0.CO;2.

Giorgi, F., Torma, C., Coppola, E., Ban, N., Schär, C., and Somot, S. (2016). Enhanced summer convective rainfall at Alpine high elevations in response to climate warming. *Nat. Geosci.* 9, 584–589. doi:10.1038/ngeo2761.

Giot, O., Termonia, P., Degrauwe, D., De Troch, R., Caluwaerts, S., Smet, G., et al. (2016). Validation of the ALARO-0 model within the EURO-CORDEX framework. *Geosci. Model Dev.* 9, 1143–1152. doi:10.5194/gmd-9-1143-2016.

Gleckler, P., Doutriaux, C., Durack, P., Taylor, K., Zhang, Y., Williams, D., et al. (2016). A More Powerful Reality Test for Climate Models. *Eos (Washington. DC).* 97. doi:10.1029/2016EO051663.

Gleckler, P. J., Taylor, K. E., and Doutriaux, C. (2008). Performance metrics for climate models. *J. Geophys. Res.* 113, D06104. doi:10.1029/2007JD008972.

Glinton, M. R., Gray, S. L., Chagnon, J. M., and Morcrette, C. J. (2017). Modulation of precipitation by conditional symmetric instability release. *Atmos. Res.* 185, 186–201. doi:10.1016/j.atmosres.2016.10.013.

Glotter, M., Elliott, J., McInerney, D., Best, N., Foster, I., and Moyer, E. J. (2014). Evaluating the utility of dynamical downscaling in agricultural impacts projections. *Proc. Natl. Acad. Sci.* 111, 8776–8781. doi:10.1073/pnas.1314787111.

Gobiet, A., Suklitsch, M., and Heinrich, G. (2015). The effect of empirical-statistical correction of intensity-dependent model errors on the temperature climate change signal. *Hydrol. Earth Syst. Sci.* 19, 4055–4066. doi:10.5194/hess-19-4055-2015.

Goldberg, M. H., Linden, S., Ballew, M. T., Rosenthal, S. A., and Leiserowitz, A. (2019). The role of anchoring in judgments about expert consensus. *J. Appl. Soc. Psychol.* 49, 192–200. doi:10.1111/jasp.12576.

Golosov, S., Zverev, I., Shipunova, E., and Terzhevik, A. (2018). Modified parameterization of the vertical water temperature profile in the FLake model. *Tellus A Dyn. Meteorol. Oceanogr.* 70, 1–7. doi:10.1080/16000870.2018.1441247.

Gong, D., and Wang, S. (1999). Definition of Antarctic Oscillation index. *Geophys. Res. Lett.* 26, 459–462. doi:10.1029/1999GL900003.

Gong, H., Wang, L., Chen, W., and Wu, R. (2019). Attribution of the East Asian Winter Temperature Trends During 1979–2018: Role of External Forcing and Internal Variability. *Geophys. Res. Lett.* 46, 10874–10881. doi:10.1029/2019GL084154.

Gong, H., Wang, L., Zhou, W., Chen, W., Wu, R., Liu, L., et al. (2018). Revisiting the Northern Mode of East Asian Winter Monsoon Variation and Its Response to Global Warming. *J. Clim.* 31, 9001–9014. doi:10.1175/JCLI-D-18-0136.1.

Gonzalez, P. L. M., Goddard, L., and Greene, A. M. (2013). Twentieth-century summer precipitation in South Eastern South America: comparison of gridded and station data. *Int. J. Climatol.* 33, 2923–2928. doi:10.1002/joc.3633.

Gonzalez, P. L. M., Polvani, L. M., Seager, R., and Correa, G. J. P. (2014). Stratospheric ozone depletion: a key driver of recent precipitation trends in South Eastern South America. *Clim. Dyn.* 42, 1775–1792. doi:10.1007/s00382-013-1777-x.

Goodman, S. J., Schmit, T. J., Daniels, J., Denig, W., and Metcalf, K. (2018). "GOES: Past, Present, and Future," in *Comprehensive Remote Sensing* (Elsevier), 119–149. doi:10.1016/B978-0-12-409548-9.10315-X.

Goosse, H. (2017). Reconstructed and simulated temperature asymmetry between continents in both hemispheres over the last centuries. *Clim. Dyn.* 48, 1483–1501. doi:10.1007/s00382-016-3154-z.

Goosse, H., Crespin, E., Dubinkina, S., Loutre, M.-F., Mann, M. E., Renssen, H., et al. (2012). The role of forcing and internal dynamics in explaining the "Medieval Climate Anomaly." *Clim. Dyn.* 39, 2847–2866. doi:10.1007/s00382-012-1297-0.

Gorddard, R., Colloff, M. J., Wise, R. M., Ware, D., and Dunlop, M. (2016). Environmental Science & Policy Values , rules and knowledge : Adaptation as change in the decision context. *Environ. Sci. Policy* 57, 60–69. doi:10.1016/j.envsci.2015.12.004.

Goss, M., Feldstein, S. B., and Lee, S. (2016). Stationary Wave Interference and Its Relation to Tropical Convection and Arctic Warming. *J. Clim.* 29, 1369–1389. doi:10.1175/JCLI-D-15-0267.1.

Goswami, B. N., Madhusoodanan, M. S., Neema, C. P., and Sengupta, D. (2006a). A physical mechanism for North Atlantic SST influence on the Indian summer monsoon. *Geophys. Res. Lett.* 33, L02706. doi:10.1029/2005GL024803.

Goswami, B. N., Venugopal, V., Sangupta, D., Madhusoodanan, M. S., and Xavier, P. K. (2006b). Increasing trend of extreme rain events over India in a warming environment. *Science* 314, 1442–1445. doi:10.1126/science.1132027.

Goudenhoofdt, E., and Delobbe, L. (2016). Generation and Verification of Rainfall Estimates from 10-Yr Volumetric Weather Radar Measurements. *J. Hydrometeorol.* 17, 1223–1242. doi:10.1175/JHM-D-15-0166.1.

Gray, L. J., Scaife, A. A., Mitchell, D. M., Osprey, S., Ineson, S., Hardiman, S., et al. (2013). A lagged response to the 11 year solar cycle in observed winter Atlantic/European weather patterns. *J. Geophys. Res. Atmos.* 118, 13,405-413,420. doi:10.1002/2013JD020062.

Griffin, D., and Anchukaitis, K. J. (2014). How unusual is the 2012-2014 California drought? *Geophys. Res. Lett.* 41,

9017–9023. doi:10.1002/2014GL062433.
Grimm, A. M., and Saboia, J. P. J. (2015). Interdecadal Variability of the South American Precipitation in the Monsoon Season. *J. Clim.* 28, 755–775. doi:10.1175/JCLI-D-14-00046.1.
Grimm, A. M., and Tedeschi, R. G. (2009). ENSO and Extreme Rainfall Events in South America. *J. Clim.* 22, 1589–1609. doi:10.1175/2008JCLI2429.1.
Grimmond, C. S. B., Blackett, M., Best, M. J., Baik, J.-J., Belcher, S. E., Beringer, J., et al. (2011). Initial results from Phase 2 of the international urban energy balance model comparison. *Int. J. Climatol.* 31, 244–272. doi:10.1002/joc.2227.
Grimmond, C. S. B., Blackett, M., Best, M. J., Barlow, J., Baik, J.-J., Belcher, S. E., et al. (2010). The International Urban Energy Balance Models Comparison Project: First Results from Phase 1. *J. Appl. Meteorol. Climatol.* 49, 1268–1292. doi:10.1175/2010JAMC2354.1.
Grise, K. M., Davis, S. M., Simpson, I. R., Waugh, D. W., Fu, Q., Allen, R. J., et al. (2019). Recent Tropical Expansion: Natural Variability or Forced Response? *J. Clim.* 32, 1551–1571. doi:10.1175/JCLI-D-18-0444.1.
Grise, K. M., Davis, S. M., Staten, P. W., and Adam, O. (2018). Regional and Seasonal Characteristics of the Recent Expansion of the Tropics. *J. Clim.* 31, 6839–6856. doi:10.1175/JCLI-D-18-0060.1.
Grose, M., Foster, S., Risbey, J., Osbrough, S., and Wilson, L. (2019). Using indices of atmospheric circulation to refine southern Australian winter rainfall climate projections. *J. Clim.* 53, 5481–5493. doi:10.1007/s00382-019-04880-4.
Grossman-Clarke, S., Schubert, S., and Fenner, D. (2017). Urban effects on summertime air temperature in Germany under climate change. *Int. J. Climatol.* 37, 905–917. doi:10.1002/joc.4748.
Gu, H., Yu, Z., Yang, C., Ju, Q., Yang, T., and Zhang, D. (2018). High-resolution ensemble projections and uncertainty assessment of regional climate change over China in CORDEX East Asia. *Hydrol. Earth Syst. Sci.* 22, 3087–3103. doi:10.5194/hess-22-3087-2018.
Gubler, S., Hunziker, S., Begert, M., Croci-Maspoli, M., Konzelmann, T., Brönnimann, S., et al. (2017). The influence of station density on climate data homogenization. *Int. J. Climatol.* 37, 4670–4683. doi:10.1002/joc.5114.
Guemas, V., Blanchard-Wrigglesworth, E., Chevallier, M., Day, J. J., Déqué, M., Doblas-Reyes, F. J., et al. (2016). A review on Arctic sea-ice predictability and prediction on seasonal to decadal time-scales. *Q. J. R. Meteorol. Soc.* 142. doi:10.1002/qj.2401.
Guerreiro, S. B., Fowler, H. J., Barbero, R., Westra, S., Lenderink, G., Blenkinsop, S., et al. (2018). Detection of continental-scale intensification of hourly rainfall extremes. *Nat. Clim. Chang.* 8, 803–807. doi:10.1038/s41558-018-0245-3.
Guido, Z., Hill, D., Crimmins, M., and Ferguson, D. (2012). Informing Decisions with a Climate Synthesis Product: Implications for Regional Climate Services. *Weather. Clim. Soc.* 5, 83–92. doi:10.1175/WCAS-D-12-00012.1.
Guillod, B. P., Orlowsky, B., Miralles, D. G., Teuling, A. J., and Seneviratne, S. I. (2015). Reconciling spatial and temporal soil moisture effects on afternoon rainfall. *Nat. Commun.* 6. doi:10.1038/ncomms7443.
Guimberteau, M., Laval, K., Perrier, A., and Polcher, J. (2012). Global effect of irrigation and its impact on the onset of the Indian summer monsoon. *Clim. Dyn.* 39, 1329–1348. doi:10.1007/s00382-011-1252-5.
Guiot, J., and Cramer, W. (2016). Climate change: The 2015 Paris Agreement thresholds and Mediterranean basin ecosystems. *Science* 354, 465–468. doi:10.1126/science.aah5015.
Gula, J., and Peltier, W. R. (2012). Dynamical Downscaling over the Great Lakes Basin of North America Using the WRF Regional Climate Model: The Impact of the Great Lakes System on Regional Greenhouse Warming. *J. Clim.* 25, 7723–7742. doi:10.1175/JCLI-D-11-00388.1.
Guldberg, A., Kaas, E., Deque, M., Yang, S., and Thorsen, S. V. (2005). Reduction of systematic errors by empirical model correction: impact on seasonal prediction skill. *Tellus A* 57, 575–588. doi:10.1111/j.1600-0870.2005.00120.x.
Gulizia, C., and Camilloni, I. (2015). Comparative analysis of the ability of a set of CMIP3 and CMIP5 global climate models to represent precipitation in South America. *Int. J. Climatol.* 35, 583–595. doi:10.1002/joc.4005.
Gultepe, I. (2015). “Chapter Three - Mountain Weather: Observation and Modeling,” in *Advances in Geophysics*, ed. R. Dmowska (Elsevier), 229–312. doi:https://doi.org/10.1016/bs.agph.2015.01.001.
Gultepe, I., Isaac, G. A., Joe, P., Kucera, P. A., Theriault, J. M., and Fisico, T. (2014). Roundhouse (RND) Mountain Top Research Site: Measurements and Uncertainties for Winter Alpine Weather Conditions. *Pure Appl. Geophys.* 171, 59–85. doi:10.1007/s00024-012-0582-5.
Guo, H., Bao, A., Ndayisaba, F., Liu, T., Kurban, A., and De Maeyer, P. (2017a). Systematical Evaluation of Satellite Precipitation Estimates Over Central Asia Using an Improved Error-Component Procedure. *J. Geophys. Res. Atmos.* 122, 10,906-910,927. doi:10.1002/2017JD026877.
Guo, J., Su, T., Li, Z., Miao, Y., Li, J., Liu, H., et al. (2017b). Declining frequency of summertime local-scale precipitation over eastern China from 1970 to 2010 and its potential link to aerosols. *Geophys. Res. Lett.* 44, 5700–5708. doi:10.1002/2017GL073533.
Guo, L., Turner, A. G., and Highwood, E. J. (2015). Impacts of 20th century aerosol emissions on the South Asian monsoon in the CMIP5 models. *Atmos. Chem. Phys.* 15, 6367–6378. doi:10.5194/acp-15-6367-2015.
Guo, L., Turner, A. G., and Highwood, E. J. (2016). Local and remote impacts of aerosol species on indian summer

monsoon rainfall in a GCM. *J. Clim.* 29, 6937–6955. doi:10.1175/JCLI-D-15-0728.1.
Guo, R., Deser, C., Terray, L., and Lehner, F. (2019). Human Influence on Winter Precipitation Trends (1921–2015) over North America and Eurasia Revealed by Dynamical Adjustment. *Geophys. Res. Lett.* 46, 3426–3434. doi:10.1029/2018GL081316.
Gustafsson, Ö., and Ramanathan, V. (2016). Convergence on climate warming by black carbon aerosols. *Proc. Natl. Acad. Sci.* 113, 4243–4245. doi:10.1073/pnas.1603570113.
Gutiérrez, J. M., Maraun, D., Widmann, M., Huth, R., Hertig, E., Benestad, R., et al. (2018). An intercomparison of a large ensemble of statistical downscaling methods over Europe: Results from the VALUE perfect predictor cross-validation experiment. *Int. J. Climatol.* doi:10.1002/joc.5462.
Gutiérrez, J. M., San-Martín, D., Brands, S., Manzanas, R., and Herrera, S. (2013). Reassessing Statistical Downscaling Techniques for Their Robust Application under Climate Change Conditions. *J. Clim.* 26, 171–188. doi:10.1175/JCLI-D-11-00687.1.
Gutmann, E. D., Rasmussen, R. M., Liu, C., Ikeda, K., Bruyere, C. L., Done, J. M., et al. (2018). Changes in hurricanes from a 13-Yr convection-permitting pseudo- global warming simulation. *J. Clim.* doi:10.1175/JCLI-D-17-0391.1.
Gutmann, E., Pruitt, T., Clark, M. P., Brekke, L., Arnold, J. R., Raff, D. A., et al. (2014). An intercomparison of statistical downscaling methods used for water resource assessments in the United States. *Water Resour. Res.* 50, 7167–7186. doi:10.1002/2014WR015559.
Gutowski Jr., W. J., Giorgi, F., Timbal, B., Frigon, A., Jacob, D., Kang, H.-S., et al. (2016). WCRP COordinated Regional Downscaling EXperiment (CORDEX): a diagnostic MIP for CMIP6. *Geosci. Model Dev.* 9, 4087–4095. doi:10.5194/gmd-9-4087-2016.
Ha, K.-J., Kim, B.-H., Chung, E.-S., Chan, J. C. L., and Chang, C.-P. (submitted). Disentangling the major factors of monsoon rainfall changes. *Environ. Res. Lett.* (submitted).
Haarsma, R. J., Hazeleger, W., Severijns, C., Vries, H., Sterl, A., Bintanja, R., et al. (2013a). More hurricanes to hit western Europe due to global warming. *Geophys. Res. Lett.* 40, 1783–1788. doi:10.1002/grl.50360.
Haarsma, R. J., Roberts, M. J., Vidale, P. L., Senior, C. A., Bellucci, A., Bao, Q., et al. (2016). High Resolution Model Intercomparison Project (HighResMIP v1.0) for CMIP6. *Geosci. Model Dev.* 9, 4185–4208. doi:10.5194/gmd-9-4185-2016.
Haarsma, R. J., Selten, F. M., and Drijfhout, S. S. (2015). Decelerating Atlantic meridional overturning circulation main cause of future west European summer atmospheric circulation changes. *Environ. Res. Lett.* 10, 094007. doi:10.1088/1748-9326/10/9/094007.
Haarsma, R. J., Selten, F., and van Oldenborgh, G. J. (2013b). Anthropogenic changes of the thermal and zonal flow structure over Western Europe and Eastern North Atlantic in CMIP3 and CMIP5 models. *Clim. Dyn.* 41, 2577–2588. doi:10.1007/s00382-013-1734-8.
Haberlie, A. M., Ashley, W. S., and Pingel, T. J. (2015). The effect of urbanisation on the climatology of thunderstorm initiation. *Q. J. R. Meteorol. Soc.* 141, 663–675. doi:10.1002/qj.2499.
Haeffelin, M., Barthès, L., Bock, O., Boitel, C., Bony, S., Bouniol, D., et al. (2005). SIRTA, a ground-based atmospheric observatory for cloud and aerosol research. *Ann. Geophys.* 23, 253–275. doi:10.5194/angeo-23-253-2005.
Haerter, J. O., Hagemann, S., Moseley, C., and Piani, C. (2011). Climate model bias correction and the role of timescales. *Hydrol. Earth Syst. Sci.* 15, 1065–1079. doi:10.5194/hess-15-1065-2011.
Hagemann, S., Chen, C., Clark, D. B., Folwell, S., Gosling, S. N., Haddeland, I., et al. (2013). Climate change impact on available water resources obtained using multiple global climate and hydrology models. *Earth Syst. Dyn.* 4, 129–144. doi:10.5194/esd-4-129-2013.
Hagishima, A., Tanimoto, J., and Narita, K. I. (2005). Intercomparisons of experimental convective heat transfer coefficients and mass transfer coefficients of urban surfaces. *Boundary-Layer Meteorol.* 117, 551–576. doi:10.1007/s10546-005-2078-7.
Hahn, A., Compton, J. S., Meyer-Jacob, C., Kirsten, K. L., Lucasssen, F., Pérez Mayo, M., et al. (2016). Holocene paleo-climatic record from the South African Namaqualand mudbelt: A source to sink approach. *Quat. Int.* 404, 121–135. doi:10.1016/j.quaint.2015.10.017.
Haiden, T., Kann, A., Wittmann, C., Pistotnik, G., Bica, B., and Gruber, C. (2011). The Integrated Nowcasting through Comprehensive Analysis (INCA) System and Its Validation over the Eastern Alpine Region. *Weather Forecast.* 26, 166–183. doi:10.1175/2010WAF2222451.1.
Haines, S. (2019). Managing expectations: articulating expertise in climate services for agriculture in Belize. *Clim. Change* 157, 43–59. doi:10.1007/s10584-018-2357-1.
Hakim, G. J., Emile-Geay, J., Steig, E. J., Noone, D., Anderson, D. M., Tardif, R., et al. (2016). The last millennium climate reanalysis project: Framework and first results. *J. Geophys. Res. Atmos.* 121, 6745–6764. doi:10.1002/2016JD024751.
Halenka, T., Belda, M., Huszar, P., Karlicky, J., Novakova, T., and Zak, M. (2019). On the comparison of urban canopy effects parameterisation. *Int. J. Environ. Pollut.* 65, 177–194. doi:10.1504/IJEP.2019.101840.
Hall, A. (2014). Projecting regional change. *Science* 346, 1461–1462. doi:10.1126/science.aaa0629.
Hall, A., Cox, P., Huntingford, C., and Klein, S. (2019). Progressing emergent constraints on future climate change.

Nat. Clim. Chang. 9, 269–278. doi:10.1038/s41558-019-0436-6.
Hallegatte, S. (2014). Modeling the Role of Inventories and Heterogeneity in the Assessment of the Economic Costs of Natural Disasters. *Risk Anal.* 34, 152–167. doi:10.1111/risa.12090.
Hallegatte, S., Green, C., Nicholls, R. J., and Corfee-Morlot, J. (2013). Future flood losses in major coastal cities. *Nat. Clim. Chang.* 3, 802–806. doi:10.1038/nclimate1979.
Hamada, A., and Takayabu, Y. N. (2018). Large-Scale Environmental Conditions Related to Midsummer Extreme Rainfall Events around Japan in the TRMM Region. *J. Clim.* 31, 6933–6945. doi:10.1175/JCLI-D-17-0632.1.
Hamada, A., Takayabu, Y. N., Liu, C., and Zipser, E. J. (2015a). Weak linkage between the heaviest rainfall and tallest storms. *Nat. Commun.* 6, 6213. doi:10.1038/ncomms7213.
Hamada, A., Takayabu, Y. N., Liu, C., and Zipser, E. J. (2015b). Weak linkage between the heaviest rainfall and tallest storms. *Nat. Commun.* 6, 6213. doi:10.1038/ncomms7213.
Hamdi, R. (2010). Estimating Urban Heat Island Effects on the Temperature Series of Uccle (Brussels, Belgium) Using Remote Sensing Data and a Land Surface Scheme. *Remote Sens.* 2, 2773–2784. doi:10.3390/rs2122773.
Hamdi, R., Duchêne, F., Berckmans, J., Delcloo, A., Vanpoucke, C., and Termonia, P. (2016). Evolution of urban heat wave intensity for the Brussels Capital Region in the ARPEGE-Climat A1B scenario. *Urban Clim.* 17, 176–195. doi:10.1016/J.UCLIM.2016.08.001.
Hamdi, R., and Masson, V. (2008). Inclusion of a Drag Approach in the Town Energy Balance (TEB) Scheme: Offline 1D Evaluation in a Street Canyon. *J. Appl. Meteorol. Climatol.* 47, 2627–2644. doi:10.1175/2008JAMC1865.1.
Hamdi, R., Van de Vyver, H., De Troch, R., and Termonia, P. (2014). Assessment of three dynamical urban climate downscaling methods: Brussels's future urban heat island under an A1B emission scenario. *Int. J. Climatol.* 34, 978–999. doi:10.1002/joc.3734.
Hamdi, R., Van de Vyver, H., and Termonia, P. (2012). New cloud and microphysics parameterisation for use in high-resolution dynamical downscaling: application for summer extreme temperature over Belgium. *Int. J. Climatol.* 32, 2051–2065. doi:10.1002/joc.2409.
Hamilton, L. C. (2011). Education, politics and opinions about climate change evidence for interaction effects. *Clim. Change* 104, 231–242. doi:10.1007/s10584-010-9957-8.
Hanna, E., Fettweis, X., and Hall, R. J. (2018). Recent changes in summer Greenland blocking captured by none of the CMIP5 models. *Cryosph. Discuss.*, 1–8. doi:10.5194/tc-2018-91.
Hansen, J., Ruedy, R., Sato, M., and Lo, K. (2010). GLOBAL SURFACE TEMPERATURE CHANGE. *Rev. Geophys.* 48. doi:10.1029/2010RG000345.
Haren, R. van, Oldenborgh, G. J. van, Lenderink, G., and Hazeleger, W. (2013). Evaluation of modeled changes in extreme precipitation in Europe and the Rhine basin. *Environ. Res. Lett.* 8, 014053. doi:10.1088/1748-9326/8/1/014053.
Harris, I., Jones, P. D., Osborn, T. J., and Lister, D. H. (2014). Updated high-resolution grids of monthly climatic observations - the CRU TS3.10 Dataset. *Int. J. Climatol.* 34, 623–642. doi:10.1002/joc.3711.
Harris, L. M., and Lin, S.-J. (2013). A Two-Way Nested Global-Regional Dynamical Core on the Cubed-Sphere Grid. *Mon. Weather Rev.* 141, 283–306. doi:10.1175/MWR-D-11-00201.1.
Hart, P. S., and Nisbet, E. C. (2012). Boomerang Effects in Science Communication: How Motivated Reasoning and Identity Cues Amplify Opinion Polarization About Climate Mitigation Policies. *Communic. Res.* 39, 701–723. doi:10.1177/0093650211416646.
Hassanzadeh, P., Kuang, Z., and Farrell, B. F. (2014). Responses of midlatitude blocks and wave amplitude to changes in the meridional temperature gradient in an idealized dry GCM. *Geophys. Res. Lett.* 41, 5223–5232. doi:10.1002/2014GL060764.
Hassim, M. E. E., Lane, T. P., and Grabowski, W. W. (2016). The diurnal cycle of rainfall over New Guinea in convection-permitting WRF simulations. *Atmos. Chem. Phys.* 16, 161–175. doi:10.5194/acp-16-161-2016.
Hasson, S. ul, Böhner, J., and Chishtie, F. (2019). Low fidelity of CORDEX and their driving experiments indicates future climatic uncertainty over Himalayan watersheds of Indus basin. *Clim. Dyn.* 52, 777–798. doi:10.1007/s00382-018-4160-0.
Hasson, S. ul, Pascale, S., Lucarini, V., and Böhner, J. (2016). Seasonal cycle of precipitation over major river basins in South and Southeast Asia: A review of the CMIP5 climate models data for present climate and future climate projections. *Atmos. Res.* 180, 42–63. doi:10.1016/j.atmosres.2016.05.008.
Hastenrath, S. (1966). On general circulation and energy budget in the area of the Central American seas. *J. Atmos. Sci.* 23, 694–711.
Hatchett, B. J., Koračin, D., Mejía, J. F., and Boyle, D. P. (2016). Assimilating urban heat island effects into climate projections. *J. Arid Environ.* 128, 59–64. doi:10.1016/j.jaridenv.2016.01.007.
Hauser, M., Orth, R., and Seneviratne, S. I. (2016). Role of soil moisture versus recent climate change for the 2010 heat wave in western Russia. *Geophys. Res. Lett.* 43, 2819–2826. doi:10.1002/2016GL068036.
Hauser, M., Orth, R., and Seneviratne, S. I. (2017). Investigating soil moisture–climate interactions with prescribed soil moisture experiments: an assessment with the Community Earth System Model (version 1.2). *Geosci. Model Dev.* 10, 1665–1677. doi:10.5194/gmd-10-1665-2017.
Hausfather, Z., Cowtan, K., Menne, M. J., and Williams Jr., C. N. (2016). Evaluating the impact of U.S. Historical

Climatology Network homogenization using the U.S. Climate Reference Network. *Geophys. Res. Lett.* 43, 1695–1701. doi:10.1002/2015GL067640.
Hausfather, Z., Menne, M. J., Williams, C. N., Masters, T., Broberg, R., and Jones, D. (2013). Quantifying the effect of urbanization on u.s. Historical climatology network temperature records. *J. Geophys. Res. Atmos.* 118, 481–494. doi:10.1029/2012JD018509.
Hawkins, E., Frame, D., Harrington, L., Joshi, M., King, A., Rojas, M., et al. (submitted). Observed emergence of the climate change signal: from the familiar to the unknown. *Geophys. Res. Lett.* (submitted).
Hawkins, E., Smith, R. S., Gregory, J. M., and Stainforth, D. A. (2016). Irreducible uncertainty in near-term climate projections. *Clim. Dyn.* 46, 3807–3819. doi:10.1007/s00382-015-2806-8.
Hawkins, E., and Sutton, R. (2012). Time of emergence of climate signals. *Geophys. Res. Lett.* 39, n/a-n/a. doi:10.1029/2011GL050087.
Haylock, M. R., Hofstra, N., Klein Tank, A. M. G., Klok, E. J., Jones, P. D., and New, M. (2008). A European daily high-resolution gridded data set of surface temperature and precipitation for 1950–2006. *J. Geophys. Res.* 113, D20119. doi:10.1029/2008JD010201.
Haywood, J. M., Jones, A., Bellouin, N., and Stephenson, D. (2013). Asymmetric forcing from stratospheric aerosols impacts Sahelian rainfall. *Nat. Clim. Chang.* 3, 660–665. doi:10.1038/nclimate1857.
Hazeleger, W., Van Den Hurk, B. J. J. M., Min, E., Van Oldenborgh, G. J., Petersen, A. C., Stainforth, D. A., et al. (2015). Tales of future weather. *Nat. Clim. Chang.* 5, 107–113. doi:10.1038/nclimate2450.
Hegerl, G., Hoegh-Guldberg, O., Casassa, G., Hoerling, M., Kovats, S., Parmesan, C., et al. (2010). Good Practice Guidance Paper on Detection and Attribution Related to Anthropogenic Climate Change. *Meet. Rep. Intergov. Panel Clim. Chang. Expert Meet. Detect. Attrib. Anthropog. Clim. Chang.*, 1–9. Available at: http://nova.wh.whoi.edu/palit/Stocker et al_2009_Report_IPCC Expert Meeting on Detection and Attribution Related to Anthropogenic Climate Change.
Heinrich, G., Gobiet, A., and Mendlik, T. (2014). Extended regional climate model projections for Europe until the mid-twentyfirst century: combining ENSEMBLES and CMIP3. *Clim. Dyn.* 42, 521–535. doi:10.1007/s00382-013-1840-7.
Held, I. M., and Soden, B. J. (2006). Robust Responses of the Hydrological Cycle to Global Warming. *J. Clim.* 19, 5686–5699. doi:10.1175/JCLI3990.1.
Hellwig, J., Stahl, K., Ziese, M., and Becker, A. (2018). The impact of the resolution of meteorological data sets on catchment-scale precipitation and drought studies. *Int. J. Climatol.* 38, 3069–3081. doi:10.1002/joc.5483.
Hempel, S., Frieler, K., Warszawski, L., Schewe, J., and Piontek, F. (2013). A trend-preserving bias correction – the ISI-MIP approach. *Earth Syst. Dyn.* 4, 219–236. doi:10.5194/esd-4-219-2013.
Henderson, S. A., Maloney, E. D., and Barnes, E. A. (2016). The Influence of the Madden–Julian Oscillation on Northern Hemisphere Winter Blocking. *J. Clim.* 29, 4597–4616. doi:10.1175/JCLI-D-15-0502.1.
Hendon, H. H., Lim, E.-P., and Nguyen, H. (2014a). Seasonal Variations of Subtropical Precipitation Associated with the Southern Annular Mode. *J. Clim.* 27, 3446–3460. doi:10.1175/JCLI-D-13-00550.1.
Hendon, H. H., Lim, E., Arblaster, J. M., and Anderson, D. L. T. (2014b). Causes and predictability of the record wet east Australian spring 2010. *Clim. Dyn.* 42, 1155–1174. doi:10.1007/s00382-013-1700-5.
Hendon, H., Thompson, D., and Wheeler, M. (2007). Australian Rainfall and Surface Temperature Variations Associated with the Southern Hemisphere Annular Mode. *J. Clim.* 20, 2452–2465.
Hennessy, K., Fitzharris, B., Bates, B. C., Harvey, N., Howden, S. M., Hughes, L., et al. (2007). "Australia and New Zealand," in *Climate Change 2007: Impacts, Adaptation and Vulnerability. Contribution of Working Group II to the Fourth Assessment Report of the Intergovernmental Panel on Climate Change*, eds. M. L. Parry, O. F. Canziani, J. P. Palutikof, P. J. van der Linden, and C. E. Hanson (Cambridge, UK: Cambridge University Press), 507–540. Available at: https://www.ipcc.ch/site/assets/uploads/2018/03/ar4_wg2_full_report.pdf.
Henrich, J., Heine, S. J., and Norenzayan, A. (2010a). The weirdest people in the world? *Behav. Brain Sci.* 33, 61–83. doi:10.1017/S0140525X0999152X.
Henrich, J., Heine, S., and Norenzayan, A. (2010b). Beyond WEIRD: Towards a broad-based behavioral science. *Behav. Brain Sci.* 33, 111–135. doi:10.1017/S0140525X10000725.
Hernández-Díaz, L., Laprise, R., Sushama, L., Martynov, A., Winger, K., and Dugas, B. (2013). Climate simulation over CORDEX Africa domain using the fifth-generation Canadian Regional Climate Model (CRCM5). *Clim. Dyn.* 40, 1415–1433. doi:10.1007/s00382-012-1387-z.
Hernández-Díaz, L., Nikiéma, O., Laprise, R., Winger, K., and Dandoy, S. (2019). Effect of empirical correction of sea-surface temperature biases on the CRCM5-simulated climate and projected climate changes over North America. *Clim. Dyn.* 53, 453–476. doi:10.1007/s00382-018-4596-2.
Herrera, D., and Ault, T. (2017). Insights from a New High-Resolution Drought Atlas for the Caribbean Spanning 1950–2016. *J. Clim.* 30, 7801–7825. doi:10.1175/JCLI-D-16-0838.1.
Herrera, D., Ault, T. R., Carrillo, C. M., and Cook, B. I. (2018a). Exacerbation of the 2013-2016 Pan-Caribbean Drought by Anthropogenic Warming. *Geophys. Res. Lett.* 45, 10,619-10,626. doi:10.1029/2018GL079408.
Herrera, S., Kotlarski, S., Soares, P. M. M., Cardoso, R. M., Jaczewski, A., Gutiérrez, J. M., et al. (2018b). Uncertainty in gridded precipitation products: Influence of station density, interpolation method and grid resolution. *Int. J.*

Climatol. doi:10.1002/joc.5878.
Herrmann, M., Somot, S., Calmanti, S., Dubois, C., and Sevault, F. (2011). Representation of spatial and temporal variability of daily wind speed and of intense wind events over the Mediterranean Sea using dynamical downscaling: impact of the regional climate model configuration. *Nat. Hazards Earth Syst. Sci.* 11, 1983–2001. doi:10.5194/nhess-11-1983-2011.
Hertig, E., Beck, C., Wanner, H., and Jacobeit, J. (2015). A review of non-stationarities in climate variability of the last century with focus on the North Atlantic–European sector. *Earth-Science Rev.* 147, 1–17. doi:10.1016/j.earscirev.2015.04.009.
Hertig, E., Maraun, D., Bartholy, J., Pongracz, R., Vrac, M., Mares, I., et al. (2018). Comparison of statistical downscaling methods with respect to extreme events over Europe: Validation results from the perfect predictor experiment of the COST Action VALUE. *Int. J. Climatol.* doi:10.1002/joc.5469.
Hertig, E., and Tramblay, Y. (2017). Regional downscaling of Mediterranean droughts under past and future climatic conditions. *Glob. Planet. Change* 151, 36–48. doi:10.1016/j.gloplacha.2016.10.015.
Hewitson, B. C., and Crane, R. G. (2006). Consensus between GCM climate change projections with empirical downscaling: precipitation downscaling over South Africa. *Int. J. Climatol.* 26, 1315–1337. doi:10.1002/joc.1314.
Hewitson, B. C., Daron, J., Crane, R. G., Zermoglio, M. F., and Jack, C. (2014a). Interrogating empirical-statistical downscaling. *Clim. Change* 122, 539–554. doi:10.1007/s10584-013-1021-z.
Hewitson, B., Janetos, A. C., Carter, T. R., Giorgi, F., Jones, R. G., Kwon, W.-T., et al. (2014b). "Regional context," in *Climate Change 2014: Impacts, Adaptation, and Vulnerability. Part B: Regional Aspects. Contribution of Working Group II to the Fifth Assessment Report of the Intergovernmental Panel on Climate Change*, eds. V. R. Barros, C. B. Field, D. J. Dokken, M. D. Mastrandrea, K. J. Mach, T. E. Bilir, et al. (Cambridge, United Kingdom and New York, NY, USA: Cambridge University Press), 1133–1197.
Hewitson, B., Waagsaether, K., Wohland, J., Kloppers, K., and Kara, T. (2017). Climate information websites: an evolving landscape. *Wiley Interdiscip. Rev. Clim. Chang.* 8, e470. doi:10.1002/wcc.470.
Hewitt, C. D., and Lowe, J. A. (2018). Toward a European Climate Prediction System. *Bull. Am. Meteorol. Soc.* 99, 1997–2001. doi:10.1175/BAMS-D-18-0022.1.
Hewitt, C., Mason, S., and Walland, D. (2012). The Global Framework for Climate Services. *Nat. Clim. Chang.* 2, 831. Available at: http://dx.doi.org/10.1038/nclimate1745.
Hibino, K., Takayabu, I., Wakazuki, Y., and Ogata, T. (2018). Physical Responses of Convective Heavy Rainfall to Future Warming Condition: Case Study of the Hiroshima Event. *Front. Earth Sci.* 6, 35. doi:10.3389/feart.2018.00035.
Hiebl, J., and Frei, C. (2016). Daily temperature grids for Austria since 1961 — concept , creation and applicability. *Theor Appl Clim.*, 161–178. doi:10.1007/s00704-015-1411-4.
Hill, S. A. (2019). Theories for Past and Future Monsoon Rainfall Changes. *Curr. Clim. Chang. Reports* 5, 160–171. doi:10.1007/s40641-019-00137-8.
Hinkel, K. M., and Nelson, F. E. (2007). Anthropogenic heat island at Barrow, Alaska, during winter: 2001–2005. *J. Geophys. Res. Atmos.* 112. doi:10.1029/2006JD007837.
Hirose, M., Takayabu, Y. N., Hamada, A., Shige, S., and Yamamoto, M. K. (2017). Impact of Long-Term Observation on the Sampling Characteristics of TRMM PR Precipitation. *J. Appl. Meteorol. Climatol.* 56, 713–723. doi:10.1175/JAMC-D-16-0115.1.
Hirsch, A. L., Prestele, R., Davin, E. L., Seneviratne, S. I., Thiery, W., and Verburg, P. H. (2018). Modelled biophysical impacts of conservation agriculture on local climates. *Glob. Chang. Biol.* 0. doi:10.1111/gcb.14362.
Hirsch, A. L., Wilhelm, M., Davin, E. L., Thiery, W., and Seneviratne, S. I. (2017). Can climate-effective land management reduce regional warming? *J. Geophys. Res. Atmos.* 122, 2269–2288. doi:10.1002/2016JD026125.
Ho-Hagemann, H. T. M., Gröger, M., Rockel, B., Zahn, M., Geyer, B., and Meier, H. E. M. (2017). Effects of air-sea coupling over the North Sea and the Baltic Sea on simulated summer precipitation over Central Europe. *Clim. Dyn.* 49, 3851–3876. doi:10.1007/s00382-017-3546-8.
Hobaek Haff, I., Frigessi, A., and Maraun, D. (2015). How well do regional climate models simulate the spatial dependence of precipitation? An application of pair-copula constructions. *J. Geophys. Res. Atmos.* 120, 2624–2646. doi:10.1002/2014JD022748.
Hock, R., Rasul, G., Adler, C., Cáceres, B., Gruber, S., Hirabayshi, Y., et al. (2019). "High Mountain Areas," in *IPCC Special Report on the Ocean and Cryosphere in a Changing Climate*, eds. H.-O. Pörtner, D. C. Roberts, V. Masson-Delmotte, P. Zhai, M. Tignor, E. Poloczanska, et al. (In Press), 131–202. doi:in press.
Hoegh-Guldberg, O., Jacob, D., Taylor, M., Bindi, M., Abdul Halim, S., Achlatis Australia, M., et al. (2018). "Impacts of 1.5°C of Global Warming on Natural and Human Systems," in *Global Warming of 1.5°C. An IPCC Special Report on the impacts of global warming of 1.5°C above pre-industrial levels and related global greenhouse gas emission pathways, in the context of strengthening the global response to the threat of climate change,* eds. V. Masson-Delmotte, P. Zhai, H.-O. Pörtner, D. Roberts, J. Skea, P. R. Shukla, et al., 175–311.
Hoell, A., Hoerling, M., Eischeid, J., Quan, X.-W., and Liebmann, B. (2017). Reconciling Theories for Human and Natural Attribution of Recent East Africa Drying. *J. Clim.* 30, 1939–1957. doi:10.1175/JCLI-D-16-0558.1.
Hoffmann, P., Schoetter, R., and Schlünzen, K. H. (2018). Statistical-dynamical downscaling of the urban heat island in

Hamburg, Germany. *Meteorol. Zeitschrift* 27, 89–109. doi:10.1127/metz/2016/0773.
Hollmann, R., Merchant, C. J., Saunders, R., Downy, C., Buchwitz, M., Cazenave, A., et al. (2013). The ESA Climate Change Initiative: Satellite Data Records for Essential Climate Variables. *Bull. Am. Meteorol. Soc.* 94, 1541–1552. doi:10.1175/BAMS-D-11-00254.1.
Hong, S.-Y., and Kanamitsu, M. (2014). Dynamical downscaling: Fundamental issues from an NWP point of view and recommendations. *Asia-Pacific J. Atmos. Sci.* 50, 83–104. doi:10.1007/s13143-014-0029-2.
Hope, P., Grose, M. R., Timbal, B., Dowdy, A. J., Bhend, J., Katzfey, J. J., et al. (2015). Seasonal and regional signature of the projected southern Australian rainfall reduction. *Aust. Meteorol. Oceanogr. J.* 65, 54–71. doi:10.22499/2.6501.005.
Hope, P. K., Drosdowsky, W., and Nicholls, N. (2006). Shifts in the synoptic systems influencing southwest Western Australia. *Clim. Dyn.* 26, 751–764. doi:10.1007/s00382-006-0115-y.
Hope, P., Keay, K., Pook, M., Catto, J., Simmonds, I., Mills, G., et al. (2014). A Comparison of Automated Methods of Front Recognition for Climate Studies: A Case Study in Southwest Western Australia. *Mon. Weather Rev.* 142, 343–363. doi:10.1175/MWR-D-12-00252.1.
Hope, P., Lim, E.-P., Hendon, H., and Wang, G. (2018). The Effect of Increasing CO2 on the Extreme September 2016 Rainfall Across Southeastern Australia. *Bull. Am. Meteorol. Soc.* 99, S133–S138. doi:10.1175/BAMS-D-17-0094.1.
Hope, P., Timbal, B., and Fawcett, R. (2009). Associations between rainfall variability in the southwest and southeast of Australia and their evolution through time. *Int. J. Climatol.* 30, 1360–1371. doi:10.1002/joc.1964.
Hope, P., Timbal, B., Hendon, H., Ekström, M., and Potter, N. (2017). A Synthesis of Findings from the Victorian Climate Initiative. Australia: Bureau of Meteorology.
Hope, P., Wang, G., Lim, E.-P., Hendon, H. H., and Arblaster, J. M. (2016). What caused the record-breaking heat across Australia in October 2015? *Bull. Am. Meteorol. Soc.* 96, S1–S172. doi:10.1175/BAMS-D-15-00157.1.
Hope, P., and Watterson, I. (2018). Persistence of cool conditions after heavy rain in Australia. *J. South. Hemisph. Earth Syst. Sci.* 68. doi:10.22499/3.6801.004.
Horton, D. E., Johnson, N. C., Singh, D., Swain, D. L., Rajaratnam, B., and Diffenbaugh, N. S. (2015). Contribution of changes in atmospheric circulation patterns to extreme temperature trends. *Nature* 522, 465–469. doi:10.1038/nature14550.
Hoskins, B. (2013). The potential for skill across the range of the seamless weather-climate prediction problem: A stimulus for our science. *Q. J. R. Meteorol. Soc.* 139, 573–584. doi:10.1002/qj.1991.
Hoskins, B., and Woollings, T. (2015). Persistent Extratropical Regimes and Climate Extremes. *Curr. Clim. Chang. Reports* 1, 115–124. doi:10.1007/s40641-015-0020-8.
Hsu, H.-H., Zhou, T., and Matsumoto, J. (2014). East Asian, Indochina and Western North Pacific Summer Monsoon - An Update. *Asia-Pac. J. Atmos. Sci.* 50, 45–68. doi:10.1007/13143-014-0027-4.
Hu, A., and Deser, C. (2013). Uncertainty in future regional sea level rise due to internal climate variability. *Geophys. Res. Lett.* 40, 2768–2772. doi:10.1002/grl.50531.
Hu, Y., Maskey, S., and Uhlenbrook, S. (2013a). Downscaling daily precipitation over the Yellow River source region in China: a comparison of three statistical downscaling methods. *Theor. Appl. Climatol.* 112, 447–460. doi:10.1007/s00704-012-0745-4.
Hu, Y., Tao, L., and Liu, J. (2013b). Poleward expansion of the Hadley circulation in CMIP5 simulations. *Adv. Atmos. Sci.* 30, 790–795. doi:10.1007/s00376-012-2187-4.
Huang, B., Banzon, V. F., Freeman, E., Lawrimore, J., Liu, W., Peterson, T. C., et al. (2015). Extended Reconstructed Sea Surface Temperature Version 4 (ERSST.v4). Part I: Upgrades and Intercomparisons. *J. Clim.* 28, 911–930. doi:10.1175/JCLI-D-14-00006.1.
Huang, J., Li, Y., Fu, C., Chen, F., Fu, Q., Dai, A., et al. (2017). Dryland climate change: Recent progress and challenges. *Rev. Geophys.* 55, 719–778. doi:10.1002/2016RG000550.
Huang, X., Rhoades, A. M., Ullrich, P. A., and Zarzycki, C. M. (2016). An evaluation of the variable-resolution CESM for modeling California's climate. *J. Adv. Model. Earth Syst.* 8, 345–369. doi:10.1002/2015MS000559.
Huang, X., Zhou, T., Dai, A., Li, H., Li, C., Chen, X., et al. (submitted, a). South Asian summer monsoon projections constrained by the Interdecadal Pacific Oscillation. *Sci. Adv.* (submitted).
Huang, X., Zhou, T., Turner, A., Dai, A., Chen, X., Clark, R., et al. (submitted, b). The recent decline and recovery of Indian summer monsoon rainfall: relative roles of external forcing and internal variability. *J. Clim.* (submitted).
Huffman, G. J., Adler, R. F., Bolvin, D. T., and Gu, G. (2009). Improving the global precipitation record: GPCP Version 2.1. *Geophys. Res. Lett.* 36, L17808. doi:10.1029/2009GL040000.
Huffman, G. J., Bolvin, D. T., Braithwaite, D., Hsu, K., Joyce, R., Xie, P., et al. (2014). Algorithm Theoretical Basis Document (ATBD) NASA Global Precipitation Measurement (GPM) Integrated Multi-satellitE Retrievals for GPM (IMERG).
Huffman, G. J., Bolvin, D. T., Nelkin, E. J., Wolff, D. B., Adler, R. F., Gu, G., et al. (2007). The TRMM Multisatellite Precipitation Analysis (TMPA): Quasi-Global, Multiyear, Combined-Sensor Precipitation Estimates at Fine Scales. *J. Hydrometeorol.* 8, 38–55. doi:10.1175/JHM560.1.
Hughes, J. D., Petrone, K. C., and Silberstein, R. P. (2012). Drought, groundwater storage and stream flow decline in

southwestern Australia. *Geophys. Res. Lett.* 39. doi:10.1029/2011GL050797.
Hulme, M. (2001). Climatic perspectives on Sahelian desiccation: 1973–1998. *Glob. Environ. Chang.* 11, 19–29. doi:10.1016/S0959-3780(00)00042-X.
Hung, M.-P., Lin, J.-L., Wang, W., Kim, D., Shinoda, T., and Weaver, S. J. (2013). MJO and Convectively Coupled Equatorial Waves Simulated by CMIP5 Climate Models. *J. Clim.* 26, 6185–6214. doi:10.1175/JCLI-D-12-00541.1.
Hunt, K. M. R., Turner, A. G., and Shaffrey, L. C. (2018). Extreme Daily Rainfall in Pakistan and North India: Scale Interactions, Mechanisms, and Precursors. *Mon. Weather Rev.* 146, 1005–1022. doi:10.1175/MWR-D-17-0258.1.
Hunt, K. M. R., Turner, A. G., and Shaffrey, L. C. (2019). Falling Trend of Western Disturbances in Future Climate Simulations. *J. Clim.* 32, 5037–5051. doi:10.1175/JCLI-D-18-0601.1.
Hurley, J. V., and Boos, W. R. (2015). A global climatology of monsoon low-pressure systems. *Q. J. R. Meteorol. Soc.* 141, 1049–1064. doi:10.1002/qj.2447.
Hurrell, J., Bader, D., Delworth, T., Kirtman, B., Pan, J. M. H., and Wielicki, B. (2006). White Paper on Seamless Prediction.
Hurrell, J., Meehl, G. A., Bader, D., Delworth, T. L., Kirtman, B., and Wielicki, B. (2009). A Unified Modeling Approach to Climate System Prediction. *Bull. Am. Meteorol. Soc.* 90, 1819–1832. doi:10.1175/2009BAMS2752.1.
Hurwitz, M. M., Calvo, N., Garfinkel, C. I., Butler, A. H., Ineson, S., Cagnazzo, C., et al. (2014). Extra-tropical atmospheric response to ENSO in the CMIP5 models. *Clim. Dyn.* 43, 3367–3376. doi:10.1007/s00382-014-2110-z.
Huth, R., Mikšovský, J., Štěpánek, P., Belda, M., Farda, A., Chládová, Z., et al. (2015). Comparative validation of statistical and dynamical downscaling models on a dense grid in central Europe: temperature. *Theor. Appl. Climatol.* 120, 533–553. doi:10.1007/s00704-014-1190-3.
Hwang, Y.-T., Frierson, D. M. W., and Kang, S. M. (2013). Anthropogenic sulfate aerosol and the southward shift of tropical precipitation in the late 20th century. *Geophys. Res. Lett.* 40, 2845–2850. doi:10.1002/grl.50502.
Ichii, K., Ueyama, M., Kondo, M., Saigusa, N., Kim, J., Alberto, M. C., et al. (2017). New data-driven estimation of terrestrial CO 2 fluxes in Asia using a standardized database of eddy covariance measurements, remote sensing data, and support vector regression. *J. Geophys. Res. Biogeosciences* 122, 767–795. doi:10.1002/2016JG003640.
Ichinose, T., Shimodozono, K., and Hanaki, K. (1999). Impact of anthropogenic heat on urban climate in Tokyo. *Atmos. Environ.* 33, 3897–3909. doi:10.1016/S1352-2310(99)00132-6.
Iizumi, T., Semenov, M. A., Nishimori, M., Ishigooka, Y., and Kuwagata, T. (2012). ELPIS-JP: a dataset of local-scale daily climate change scenarios for Japan. *Philos. Trans. R. Soc. A Math. Phys. Eng. Sci.* 370, 1121–1139. doi:10.1098/rsta.2011.0305.
Iles, C., and Hegerl, G. (2017). Role of the North Atlantic Oscillation in decadal temperature trends. *Environ. Res. Lett.* 12, 114010. doi:10.1088/1748-9326/aa9152.
Illing, S., Kadow, C., Pohlmann, H., and Timmreck, C. (2018). Assessing the impact of a~future volcanic eruption on decadal predictions. *Earth Syst. Dyn.* 9, 701–715. doi:10.5194/esd-9-701-2018.
Immerzeel, W. W., Petersen, L., Ragettli, S., and Pellicciotti, F. (2014). The importance of observed gradients of air temperature and precipitation for modeling runoff from a glacierized watershed in the Nepalese Himalayas. *Water Resour. Res.* 50, 2212–2226. doi:10.1002/2013WR014506.
Immerzeel, W. W., Wanders, N., Lutz, A. F., Shea, J. M., and Bierkens, M. F. P. (2015). Reconciling high-altitude precipitation in the upper Indus basin with glacier mass balances and runoff. *Hydrol. Earth Syst. Sci.* 19, 4673–4687. doi:10.5194/hess-19-4673-2015.
Inatsu, M., Sato, T., Yamada, T. J., Kuno, R., Sugimoto, S., Farukh, M. A., et al. (2015). Multi-GCM by multi-RAM experiments for dynamical downscaling on summertime climate change in Hokkaido. *Atmos. Sci. Lett.* 16, 297–304. doi:10.1002/asl2.557.
Inoue, J., Hori, M. E., and Takaya, K. (2012). The Role of Barents Sea Ice in the Wintertime Cyclone Track and Emergence of a Warm-Arctic Cold-Siberian Anomaly. *J. Clim.* 25, 2561–2568. doi:10.1175/JCLI-D-11-00449.1.
Inoue, T., Ngo-Duc, T., Matsumoto, J., Phan-Van, T., Nguyen-Xuan, T., Trinh-Tuan, L., et al. (2016). The Vietnam Gridded Precipitation (VnGP) Dataset: Construction and Validation. *SOLA*. doi:10.2151/sola.2016-057.
IPCC (2018). Global Warming of 1.5°C. An IPCC Special Report on the impacts of global warming of 1.5°C above pre-industrial levels and related global greenhouse gas emission pathways, in the context of strengthening the global response to the threat of climate change,. , eds. V. Masson-Delmotte, P. Zhai, H.-O. Pörtner, D. Roberts, J. Skea, P. R. Shukla, et al. In Press.
IPCC (2019a). Climate Change and Land: an IPCC special report on climate change, desertification, land degradation, sustainable land management, food security, and greenhouse gas fluxes in terrestrial ecosystems. , eds. P. R. Shukla, J. Skea, E. C. Buendia, V. Masson-Delmotte, H.-O. Pörtner, D. C. Roberts, et al. In Press.
IPCC (2019b). *IPCC Special Report on the Ocean and Cryosphere in a Changing Climate*. , eds. H.-O. Pörtner, D. C. Roberts, V. Masson-Delmotte, P. Zhai, M. Tignor, E. Poloczanska, et al. In press.
Ishizaki, N., and Takayabu, I. (2009). On the Warming Events over Toyama Plain by Using NHRCM. *SOLA* 5, 129–132. doi:10.2151/sola.2009-033.

Isotta, F. A., Frei, C., Weilguni, V., Perčec Tadić, M., Lass, P., Rudolf, B., et al. (2014). The climate of daily precipitation in the Alps : development and analysis of a high-resolution grid dataset from pan-Alpine rain-gauge data. *Int. J. Climatol.* 1675, 1657–1675. doi:10.1002/joc.3794.

Isotta, F. A., Vogel, R., and Frei, C. (2015). Evaluation of European regional reanalyses and downscalings for precipitation in the Alpine region. *Meteorol. Zeitschrift* 24, 15–37. doi:10.1127/metz/2014/0584.

Ivanov, M., Warrach-Sagi, K., and Wulfmeyer, V. (2017). Field significance of performance measures in the context of regional climate model evaluation. Part 1: temperature. *Theor. Appl. Climatol.*, 1–19. doi:10.1007/s00704-017-2100-2.

Ivanov, M., Warrach-Sagi, K., and Wulfmeyer, V. (2018). Field significance of performance measures in the context of regional climate model evaluation. Part 2: precipitation. *Theor. Appl. Climatol.* 132, 239–261. doi:10.1007/s00704-017-2077-x.

Jacob, D., Kotova, L., Teichmann, C., Sobolowski, S. P., Vautard, R., Donnelly, C., et al. (2018). Climate Impacts in Europe Under +1.5°C Global Warming. *Earth's Futur.* 6, 264–285. doi:10.1002/2017EF000710.

Jacob, D., Petersen, J., Eggert, B., Alias, A., Christensen, O. B., Bouwer, L. M., et al. (2014). EURO-CORDEX: new high-resolution climate change projections for European impact research. *Reg. Environ. Chang.* 14, 563–578. doi:10.1007/s10113-013-0499-2.

Jacobeit, J., Hertig, E., Seubert, S., and Lutz, K. (2014). Statistical downscaling for climate change projections in the Mediterranean region: methods and results. *Reg. Environ. Chang.* 14, 1891–1906. doi:10.1007/s10113-014-0605-0.

Jaeger, E. B., and Seneviratne, S. I. (2011). Impact of soil moisture–atmosphere coupling on European climate extremes and trends in a regional climate model. *Clim. Dyn.* 36, 1919–1939. doi:10.1007/s00382-010-0780-8.

Jaiser, R., Nakamura, T., Handorf, D., Dethloff, K., Ukita, J., and Yamazaki, K. (2016). Atmospheric winter response to Arctic sea ice changes in reanalysis data and model simulations. *J. Geophys. Res. Atmos.* 121, 7564–7577. doi:10.1002/2015JD024679.

Jänicke, B., Meier, F., Fenner, D., Fehrenbach, U., Holtmann, A., and Scherer, D. (2017). Urban-rural differences in near-surface air temperature as resolved by the Central Europe Refined analysis (CER): sensitivity to planetary boundary layer schemes and urban canopy models. *Int. J. Climatol.* 37, 2063–2079. doi:10.1002/joc.4835.

Jåuregui, E., and Tejeda, A. (1997). Urban–rural humidity contrasts in Mexico City. *Int. J. Climatol.* 17, 187–196. doi:10.1002/(SICI)1097-0088(199702)17:2<187::AID-JOC114>3.0.CO;2-P.

Jenkner, J., Sprenger, M., Schwenk, I., Schwierz, C., Dierer, S., and Leuenberger, D. (2009). Detection and climatology of fronts in a high-resolution model reanalysis over the Alps. *Meteorol. Appl.*, n/a-n/a. doi:10.1002/met.142.

Jeong, J.-H., Ou, T., Linderholm, H. W., Kim, B.-M., Kim, S.-J., Kug, J.-S., et al. (2011). Recent recovery of the Siberian High intensity. *J. Geophys. Res. Atmos.* 116, n/a-n/a. doi:10.1029/2011JD015904.

Jerez, S., López-Romero, J. M., Turco, M., Jiménez-Guerrero, P., Vautard, R., and Montávez, J. P. (2018). Impact of evolving greenhouse gas forcing on the warming signal in regional climate model experiments. *Nat. Commun.* 9, 1304. doi:10.1038/s41467-018-03527-y.

Ji, F., Wu, Z., Huang, J., and Chassignet, E. P. (2014). Evolution of land surface air temperature trend. *Nat. Clim. Chang.* 4, 462–466. doi:10.1038/nclimate2223.

Jia, G., Shevliakova, E., Artaxo, P., de Noblet-Ducoudré, N., Houghton, R., House, J., et al. (2019). "Land-climate interactions," in *Climate Change and Land: an IPCC special report on climate change, desertification, land degradation, sustainable land management, food security, and greenhouse gas fluxes in terrestrial ecosystems*, eds. P. R. Shukla, J. Skea, E. Calvo Buendia, V. Masson-Delmotte, H.-O. Pörtner, D. C. Roberts, et al. (In Press), 131–248.

Jiang, X., Waliser, D. E., Xavier, P. K., Petch, J., Klingaman, N. P., Woolnough, S. J., et al. (2015). Vertical structure and physical processes of the Madden-Julian oscillation: Exploring key model physics in climate simulations. *J. Geophys. Res. Atmos.* 120, 4718–4748. doi:10.1002/2014JD022375.

Jiang, Y., Liu, X., Yang, X.-Q., and Wang, M. (2013). A numerical study of the effect of different aerosol types on East Asian summer clouds and precipitation. *Atmos. Environ.* 70, 51–63. doi:10.1016/j.atmosenv.2012.12.039.

Jiang, Z., Feldstein, S. B., and Lee, S. (2017). The relationship between the Madden-Julian Oscillation and the North Atlantic Oscillation. *Q. J. R. Meteorol. Soc.* 143, 240–250. doi:10.1002/qj.2917.

Jiménez-Guerrero, P., Montávez, J., Domínguez, M., Romera, R., Fita, L., Fernández, J., et al. (2013). Mean fields and interannual variability in RCM simulations over Spain: the ESCENA project. *Clim. Res.* 57, 201–220. doi:10.3354/cr01165.

Jin, Q., and Wang, C. (2017). A revival of Indian summer monsoon rainfall since 2002. *Nat. Clim. Chang.* 7, 587–594. doi:10.1038/NCLIMATE3348.

Jin, Q., Yang, Z.-L., and Wei, J. (2016). High sensitivity of Indian summer monsoon to Middle East dust absorptive properties. *Sci. Rep.* 6, 30690. doi:10.1038/srep30690.

Johnson, F., and Sharma, A. (2012). A nesting model for bias correction of variability at multiple time scales in general circulation model precipitation simulations. *Water Resour. Res.* 48. doi:10.1029/2011WR010464.

Johnson, S. J., Levine, R. C., Turner, A. G., Martin, G. M., Woolnough, S. J., Schiemann, R., et al. (2016). The resolution sensitivity of the South Asian monsoon and Indo-Pacific in a global 0.35° AGCM. *Clim. Dyn.* 46, 807–

831. doi:10.1007/s00382-015-2614-1.

Jones, A. D., Collins, W. D., and Torn, M. S. (2013). On the additivity of radiative forcing between land use change and greenhouse gases. *Geophys. Res. Lett.* 40, 4036–4041. doi:10.1002/grl.50754.

Jones, P. D., and Moberg, A. (2003). Hemispheric and Large-Scale Surface Air Temperature Variations: An Extensive Revision and an Update to 2001. *J. Clim.* 16, 206–223. doi:10.1175/1520-0442(2003)016<0206:HALSSA>2.0.CO;2.

Joshi, M. M., Gregory, J. M., Webb, M. J., Sexton, D. M. H., and Johns, T. C. (2008). Mechanisms for the land/sea warming contrast exhibited by simulations of climate change. *Clim. Dyn.* 30, 455–465. doi:10.1007/s00382-007-0306-1.

Journée, M., Delvaux, C., and Bertrand, C. (2015). Precipitation climate maps of Belgium. *Adv. Sci. Res.* 12, 73–78. doi:10.5194/asr-12-73-2015.

Joyce, R. J., Janowiak, J. E., Arkin, P. A., and Xie, P. (2004). CMORPH: A Method that Produces Global Precipitation Estimates from Passive Microwave and Infrared Data at High Spatial and Temporal Resolution. *J. Hydrometeorol.* 5, 487–503. doi:10.1175/1525-7541(2004)005<0487:CAMTPG>2.0.CO;2.

Junquas, C., Li, L., Vera, C. S., Le Treut, H., and Takahashi, K. (2016). Influence of South America orography on summertime precipitation in Southeastern South America. *Clim. Dyn.* 46, 3941–3963. doi:10.1007/s00382-015-2814-8.

Junquas, C., Vera, C. S., Li, L., and Le Treut, H. (2013). Impact of projected SST changes on summer rainfall in southeastern South America. *Clim. Dyn.* 40, 1569–1589. doi:10.1007/s00382-013-1695-y.

Jury, M. W., Herrera, S., Gutiérrez, J. M., and Barriopedro, D. (2018). Blocking representation in the ERA-Interim driven EURO-CORDEX RCMs. *Clim. Dyn.* 52, 3291–3306. doi:10.1007/s00382-018-4335-8.

Kaczmarska, J., Isham, V., and Onof, C. (2014). Point process models for fine-resolution rainfall. *Hydrol. Sci. J.* 59, 1972–1991. doi:10.1080/02626667.2014.925558.

Kahan, D. (2012a). Why we are poles apart on climate change. *Nature* 488, 255–255. doi:10.1038/488255a.

Kahan, D. M. (2012b). Ideology, Motivated Reasoning, and Cognitive Reflection: An Experimental Study. *SSRN Electron. J.* 8, 407–424. doi:10.2139/ssrn.2182588.

Kahan, D. M. (2013). Making Climate-Science Communication Evidence-Based — All the Way Down. *SSRN Electron. J.* doi:10.2139/ssrn.2216469.

Kahn, B. H., Nasiri, S. L., Schreier, M. M., and Baum, B. A. (2011). Impacts of subpixel cloud heterogeneity on infrared thermodynamic phase assessment. *J. Geophys. Res. Atmos.* 116. doi:10.1029/2011JD015774.

Kajino, M., Ueda, H., Han, Z., Kudo, R., Inomata, Y., and Kaku, H. (2017). Synergy between air pollution and urban meteorological changes through aerosol-radiation-diffusion feedback―A case study of Beijing in January 2013. *Atmos. Environ.* 171, 98–110. doi:https://doi.org/10.1016/j.atmosenv.2017.10.018.

Kalnay, E., Kanamitsu, M., Kistler, R., Collins, W., Deaven, D., Gandin, L., et al. (1996). The NCEP/NCAR 40-Year Reanalysis Project. *Bull. Am. Meteorol. Soc.* 77, 437–471. doi:10.1175/1520-0477(1996)077<0437:TNYRP>2.0.CO;2.

Kanada, S., Tsuboki, K., Aiki, H., Tsujino, S., and Takayabu, I. (2017). Future Enhancement of Heavy Rainfall Events Associated with a Typhoon in the Midlatitude Regions. *SOLA* 13, 246–251. doi:10.2151/sola.2017-045.

Kanamaru, H., and Kanamitsu, M. (2007). Scale-Selective Bias Correction in a Downscaling of Global Analysis Using a Regional Model. *Mon. Weather Rev.* 135, 334–350. doi:10.1175/MWR3294.1.

Kang, S. M., Deser, C., and Polvani, L. M. (2013). Uncertainty in Climate Change Projections of the Hadley Circulation: The Role of Internal Variability. *J. Clim.* 26, 7541–7554. doi:10.1175/JCLI-D-12-00788.1.

Kaplan, A., Cane, M. A., Kushnir, Y., Clement, A. C., Benno Blumenthal, M., and Rajagopalan, B. (1998). Analyses of global sea surface temperature 1856-1991. *J. Geophys. Res.* doi:10.1029/97JC01736.

Kaplan, S., Georgescu, M., Alfasi, N., and Kloog, I. (2017). Impact of future urbanization on a hot summer: a case study of Israel. *Theor. Appl. Climatol.* 128, 325–341. doi:10.1007/s00704-015-1708-3.

Kaskaoutis, D. G., Singh, R. P., Gautam, R., Sharma, M., Kosmopoulos, P. G., and Tripathi, S. N. (2012). Variability and trends of aerosol properties over Kanpur, northern India using AERONET data (2001–10). *Environ. Res. Lett.* 7, 024003. doi:10.1088/1748-9326/7/2/024003.

Kasoar, M., Shawki, D., and Voulgarakis, A. (2018). Similar spatial patterns of global climate response to aerosols from different regions. *npj Clim. Atmos. Sci.* 1, 12. doi:10.1038/s41612-018-0022-z.

Kawase, H., Hara, M., Yoshikane, T., Ishizaki, N. N., Uno, F., Hatsushika, H., et al. (2013). Altitude dependency of future snow cover changes over Central Japan evaluated by a regional climate model. *J. Geophys. Res. Atmos.* doi:10.1002/2013JD020429.

Kawase, H., Yoshikane, T., Hara, M., Fujita, M., Ishizaki, N. N., Kimura, F., et al. (2012). Downscaling of Snow Cover Changes in the Late 20th Century Using a Past Climate Simulation Method over Central Japan. *SOLA* 8, 61–64. doi:10.2151/sola.2012-016.

Kawazoe, S., and Gutowski, W. J. (2013). Regional, Very Heavy Daily Precipitation in NARCCAP Simulations. *J. Hydrometeorol.* 14, 1212–1227. doi:10.1175/JHM-D-12-068.1.

Kay, J. E., Deser, C., Phillips, A., Mai, A., Hannay, C., Strand, G., et al. (2015). The Community Earth System Model (CESM) Large Ensemble Project: A Community Resource for Studying Climate Change in the Presence of

Internal Climate Variability. *Bull. Am. Meteorol. Soc.* 96, 1333–1349. doi:10.1175/BAMS-D-13-00255.1.
Kayano, M. T., and Andreoli, R. V. (2007). Relations of South American summer rainfall interannual variations with the Pacific Decadal Oscillation. *Int. J. Climatol.* 27, 531–540. doi:10.1002/joc.1417.
Kayano, M. T., and Capistrano, V. B. (2014). How the Atlantic multidecadal oscillation (AMO) modifies the ENSO influence on the South American rainfall. *Int. J. Climatol.* 34, 162–178. doi:10.1002/joc.3674.
Keller, D. E., Fischer, A. M., Frei, C., Liniger, M. A., Appenzeller, C., and Knutti, R. (2015). Implementation and validation of a Wilks-type multi-site daily precipitation generator over a typical Alpine river catchment. *Hydrol. Earth Syst. Sci.* 19, 2163–2177. doi:10.5194/hess-19-2163-2015.
Keller, M., Fuhrer, O., Schmidli, J., Stengel, M., Stöckli, R., and Schär, C. (2016). Evaluation of convection-resolving models using satellite data: The diurnal cycle of summer convection over the Alps. *Meteorol. Zeitschrift* 25, 165–179. doi:10.1127/metz/2015/0715.
Keller, M., Kröner, N., Fuhrer, O., Lüthi, D., Schmidli, J., Stengel, M., et al. (2018). The sensitivity of Alpine summer convection to surrogate climate change: an intercomparison between convection-parameterizing and convection-resolving models. *Atmos. Chem. Phys.* 18, 5253–5264. doi:10.5194/acp-18-5253-2018.
Kelley, C. P., Mohtadi, S., Cane, M. A., Seager, R., and Kushnir, Y. (2015). Climate change in the Fertile Crescent and implications of the recent Syrian drought. *PNAS* 112, 3241–3246. doi:10.1073/pnas.1421533112.
Kendon, E. J., Ban, N., Roberts, N. M., Fowler, H. J., Roberts, M. J., Chan, S. C., et al. (2017). Do Convection-Permitting Regional Climate Models Improve Projections of Future Precipitation Change? *Bull. Am. Meteorol. Soc.* 98, 79–93. doi:10.1175/BAMS-D-15-0004.1.
Kendon, E. J., Roberts, N. M., Fowler, H. J., Roberts, M. J., Chan, S. C., and Senior, C. A. (2014). Heavier summer downpours with climate change revealed by weather forecast resolution model. *Nat. Clim. Chang.* 4, 570. Available at: http://dx.doi.org/10.1038/nclimate2258.
Kerkhoff, C., Künsch, H. R., and Schär, C. (2014). Assessment of Bias Assumptions for Climate Models. *J. Clim.* 27, 6799–6818. doi:10.1175/JCLI-D-13-00716.1.
Kerr, Y. H., Waldteufel, P., Richaume, P., Wigneron, J. P., Ferrazzoli, P., Mahmoodi, A., et al. (2012). The SMOS Soil Moisture Retrieval Algorithm. *IEEE Trans. Geosci. Remote Sens.* 50, 1384–1403. doi:10.1109/TGRS.2012.2184548.
Kharin, V. V., Boer, G. J., Merryfield, W. J., Scinocca, J. F., and Lee, W.-S. (2012). Statistical adjustment of decadal predictions in a changing climate. *Geophys. Res. Lett.* 39, n/a-n/a. doi:10.1029/2012GL052647.
Kida, H., Koide, T., Sasaki, H., and Chiba, M. (1991). A New Approach for Coupling a Limited Area Model to a GCM for Regional Climate Simulations. *J. Meteorol. Soc. Japan. Ser. II* 69, 723–728. doi:10.2151/jmsj1965.69.6_723.
Kidd, C., Becker, A., Huffman, G. J., Muller, C. L., Joe, P., Skofronick-Jackson, G., et al. (2017). So, How Much of the Earth's Surface Is Covered by Rain Gauges? *Bull. Am. Meteorol. Soc.* 98, 69–78. doi:10.1175/BAMS-D-14-00283.1.
Kikegawa, Y., Genchi, Y., Yoshikado, H., and Kondo, H. (2003). Development of a numerical simulation system toward comprehensive assessments of urban warming countermeasures including their impacts upon the urban buildings' energy-demands. *Appl. Energy* 76, 449–466. doi:10.1016/S0306-2619(03)00009-6.
Kim, B.-M., Son, S.-W., Min, S.-K., Jeong, J.-H., Kim, S.-J., Zhang, X., et al. (2014). Weakening of the stratospheric polar vortex by Arctic sea-ice loss. *Nat. Commun.* 5, 4646. doi:10.1038/ncomms5646.
Kim, D., Ahn, M.-S., Kang, I.-S., and Del Genio, A. D. (2015a). Role of Longwave Cloud–Radiation Feedback in the Simulation of the Madden–Julian Oscillation. *J. Clim.* 28, 6979–6994. doi:10.1175/JCLI-D-14-00767.1.
Kim, D., and Maloney, E. D. (2017). "Simulation of the Madden-Julian Oscillation Using General Circulation Models," in, 119–130. doi:10.1142/9789813200913_0009.
Kim, H., Kim, Y. K., Song, S. K., and Lee, H. W. (2016). Impact of future urban growth on regional climate changes in the Seoul Metropolitan Area, Korea. *Sci. Total Environ.* 571, 355–363. doi:10.1016/j.scitotenv.2016.05.046.
Kim, J., and Park, S. K. (2016). Uncertainties in calculating precipitation climatology in East Asia. *Hydrol. Earth Syst. Sci.* 20, 651–658. doi:10.5194/hess-20-651-2016.
Kim, J., Sanjay, J., Mattmann, C., Boustani, M., Ramarao, M. V. S., Krishnan, R., et al. (2015b). Uncertainties in estimating spatial and interannual variations in precipitation climatology in the India-Tibet region from multiple gridded precipitation datasets. *Int. J. Climatol.* 35, 4557–4573. doi:10.1002/joc.4306.
Kim, Y. H., Min, S. K., Stone, D. A., Shiogama, H., and Wolski, P. (2018). Multi-model event attribution of the summer 2013 heat wave in Korea. *Weather Clim. Extrem.* 20, 33–44. doi:10.1016/j.wace.2018.03.004.
King, A. D., Donat, M. G., Fischer, E. M., Hawkins, E., Alexander, L. V, Karoly, D. J., et al. (2015). The timing of anthropogenic emergence in simulated climate extremes. *Environ. Res. Lett.* 10, 094015. doi:10.1088/1748-9326/10/9/094015.
Kirchengast, G., Kabas, T., Leuprecht, A., Bichler, C., and Truhetz, H. (2014). WegenerNet: A Pioneering High-Resolution Network for Monitoring Weather and Climate. *Bull. Am. Meteorol. Soc.* 95, 227–242. doi:10.1175/BAMS-D-11-00161.1.
Kirillin, G., Leppäranta, M., Terzhevik, A., Granin, N., Bernhardt, J., Engelhardt, C., et al. (2012). Physics of seasonally ice-covered lakes: a review. *Aquat. Sci.* 74, 659–682. doi:10.1007/s00027-012-0279-y.
Kirtman, B., Power, S., Adedoyin, J., Boer, G., Bojariu, R., Camilloni, I., et al. (2014). IPCC Assessment Report 2014.

Near-term Climate Change Projections and Predictability. 982–985. doi:10.1017/CBO9781107415324.023.
Kitoh, A. (2017). The Asian Monsoon and its Future Change in Climate Models: A Review. *J. Meteorol. Soc. Japan. Ser. II* 95, 7–33. doi:10.2151/jmsj.2017-002.
Kitoh, A., Endo, H., Krishna Kumar, K., Cavalcanti, I. F. A., Goswami, P., and Zhou, T. (2013). Monsoons in a changing world: A regional perspective in a global context. *J. Geophys. Res. Atmos.* 118, 3053–3065. doi:10.1002/jgrd.50258.
Kjellström, E., Bärring, L., Nikulin, G., Nilsson, C., Persson, G., and Strandberg, G. (2016). Production and use of regional climate model projections – A Swedish perspective on building climate services. *Clim. Serv.* 2–3, 15–29. doi:10.1016/j.cliser.2016.06.004.
Kjellström, E., Döscher, R., and Meier, H. E. M. (2005). Atmospheric response to different sea surface temperatures in the Baltic Sea: coupled versus uncoupled regional climate model experiments. *Hydrol. Res.* 36, 397–409. doi:10.2166/nh.2005.0030.
Kjellström, E., Nikulin, G., Strandberg, G., Christensen, O. B., Jacob, D., Keuler, K., et al. (2018). European climate change at global mean temperature increases of 1.5 and 2 °C above pre-industrial conditions as simulated by the EURO-CORDEX regional climate models. *Earth Syst. Dyn.* 9, 459–478. doi:10.5194/esd-9-459-2018.
Kjellström, E., Thejll, P., Rummukainen, M., Christensen, J., Boberg, F., Christensen, O., et al. (2013). Emerging regional climate change signals for Europe under varying large-scale circulation conditions. *Clim. Res.* 56, 103–119. doi:10.3354/cr01146.
Klaver, R., Haarsma, R., and Hazeleger, W. (submitted). Effective resolution in high resolution global atmospheric models for climate studies. *Atmos. Sci. Lett.* (submitted).
Klein, F., and Goosse, H. (2018). Reconstructing East African rainfall and Indian Ocean sea surface temperatures over the last centuries using data assimilation. *Clim. Dyn.* 50, 3909–3929. doi:10.1007/s00382-017-3853-0.
Knaff, J. (1997). Implications of Summertime Sea Level Pressure Anomalies in the Tropical Atlantic Region. 789–804.
Knist, S., Goergen, K., Buonomo, E., Christensen, O. B., Colette, A., Cardoso, R. M., et al. (2017). Land-atmosphere coupling in EURO-CORDEX evaluation experiments. *J. Geophys. Res. Atmos.* 122, 79–103. doi:10.1002/2016JD025476.
Knutson, T. R., and Zeng, F. (2018). Model assessment of observed precipitation trends over land regions: Detectable human influences and possible low bias in model trends. *J. Clim.* doi:10.1175/JCLI-D-17-0672.1.
Knutson, T. R., Zeng, F., and Wittenberg, A. T. (2013). Multimodel Assessment of Regional Surface Temperature Trends: CMIP3 and CMIP5 Twentieth-Century Simulations. *J. Clim.* 26, 8709–8743. doi:10.1175/JCLI-D-12-00567.1.
Knutti, R., Furrer, R., Tebaldi, C., Cermak, J., and Meehl, G. A. (2010). Challenges in combining projections from multiple climate models. *J. Clim.* 23, 2739–2758. doi:10.1175/2009JCLI3361.1.
Knutti, R., Masson, D., and Gettelman, A. (2013). Climate model genealogy: Generation CMIP5 and how we got there. *Geophys. Res. Lett.* 40, 1194–1199. doi:10.1002/grl.50256.
Kobayashi, C., and Iwasaki, T. (2016). Brewer-Dobson circulation diagnosed from JRA-55. *J. Geophys. Res. Atmos.* 121, 1493–1510. doi:10.1002/2015JD023476.
Kobayashi, S., Ota, Y., Harada, Y., Ebita, A., Moriya, M., Onoda, H., et al. (2015). The JRA-55 Reanalysis: General Specifications and Basic Characteristics. *J. Meteorol. Soc. Japan. Ser. II* 93, 5–48. doi:10.2151/jmsj.2015-001.
Kochendorfer, J., Rasmussen, R., Wolff, M., Baker, B., Hall, M. E., Meyers, T., et al. (2017). The quantification and correction of wind-induced precipitation measurement errors. *Hydrol. Earth Syst. Sci.* 21, 1973–1989. doi:10.5194/hess-21-1973-2017.
Kok, K., Bärlund, I., Flörke, M., Holman, I., Gramberger, M., Sendzimir, J., et al. (2014). European participatory scenario development: strengthening the link between stories and models. *Clim. Change* 128, 187–200. doi:10.1007/s10584-014-1143-y.
Kornhuber, K., Petoukhov, V., Petri, S., Rahmstorf, S., and Coumou, D. (2017). Evidence for wave resonance as a key mechanism for generating high-amplitude quasi-stationary waves in boreal summer. *Clim. Dyn.* 49, 1961–1979. doi:10.1007/s00382-016-3399-6.
Kosaka, Y., and Xie, S.-P. (2016). The tropical Pacific as a key pacemaker of the variable rates of global warming. *Nat. Geosci.* 9, 669–673. doi:10.1038/ngeo2770.
Kosaka, Y., and Xie, S. P. (2013). Recent global-warming hiatus tied to equatorial Pacific surface cooling. *Nature*. doi:10.1038/nature12534.
Koster, R. D., Dirmeyer, P. A., Guo, Z., Bonan, G., Chan, E., Cox, P., et al. (2004). Regions of strong coupling between soil moisture and precipitation. *Science* 305, 1138–1140. doi:10.1126/science.1100217.
Kotlarski, S., Jacob, D., Podzun, R., and Paul, F. (2010). Representing glaciers in a regional climate model. *Clim. Dyn.* 34, 27–46. doi:10.1007/s00382-009-0685-6.
Kotlarski, S., Keuler, K., Christensen, O. B., Colette, A., Déqué, M., Gobiet, A., et al. (2014). Regional climate modeling on European scales: a joint standard evaluation of the EURO-CORDEX RCM ensemble. *Geosci. Model Dev.* 7, 1297–1333. doi:10.5194/gmd-7-1297-2014.
Kotlarski, S., Lüthi, D., and Schär, C. (2015). The elevation dependency of 21st century European climate change: an RCM ensemble perspective. *Int. J. Climatol.* 35, 3902–3920. doi:10.1002/joc.4254.

Kotlarski, S., Szabó, P., Herrera, S., Räty, O., Keuler, K., Soares, P. M., et al. (2017). Observational uncertainty and regional climate model evaluation: a pan-European perspective. *Int. J. Climatol.* 0. doi:10.1002/joc.5249.
Kotlarski, S., Szabó, P., Herrera, S., Räty, O., Keuler, K., Soares, P. M., et al. (2019). Observational uncertainty and regional climate model evaluation: A pan-European perspective. *Int. J. Climatol.* 39, 3730–3749. doi:10.1002/joc.5249.
Krähenmann S., and Walter, A., and Brienen S., and Imbery F., and and Matzarakis A (2018). High-resolution grids of hourly meteorological variables for Germany. *Theor. Appl. Climatol.* 131, 899–926. doi:10.1007/s00704-016-2003-7.
Kretschmer, M., Coumou, D., Agel, L., Barlow, M., Tziperman, E., and Cohen, J. (2018). More-Persistent Weak Stratospheric Polar Vortex States Linked to Cold Extremes. *Bull. Am. Meteorol. Soc.* 99, 49–60. doi:10.1175/BAMS-D-16-0259.1.
Kretschmer, M., Coumou, D., Donges, J. F., and Runge, J. (2016). Using Causal Effect Networks to Analyze Different Arctic Drivers of Midlatitude Winter Circulation. *J. Clim.* 29, 4069–4081. doi:10.1175/JCLI-D-15-0654.1.
Krinner, G., Beaumet, J., Favier, V., Déqué, M., and Brutel-Vuilmet, C. (2019). Empirical Run-Time Bias Correction for Antarctic Regional Climate Projections With a Stretched-Grid AGCM. *J. Adv. Model. Earth Syst.* 11, 64–82. doi:10.1029/2018MS001438.
Krinner, G., and Flanner, M. G. (2018). Striking stationarity of large-scale climate model bias patterns under strong climate change. *Proc. Natl. Acad. Sci.* 115, 9462–9466. doi:10.1073/pnas.1807912115.
Krinner, G., and Genthon, C. (1998). GCM simulations of the Last Glacial Maximum surface climate of Greenland and Antarctica. *Clim. Dyn.* 14, 741–758. doi:10.1007/s003820050252.
Krinner, G., Largeron, C., Ménégoz, M., Agosta, C., and Brutel-Vuilmet, C. (2014). Oceanic Forcing of Antarctic Climate Change: A Study Using a Stretched-Grid Atmospheric General Circulation Model. *J. Clim.* 27, 5786–5800. doi:10.1175/JCLI-D-13-00367.1.
Krishnamurthy, L., and Krishnamurthy, V. (2016). Teleconnections of Indian monsoon rainfall with AMO and Atlantic tripole. *Clim. Dyn.* 46, 2269–2285. doi:10.1007/s00382-015-2701-3.
Krishnan, R., Sabin, T. P., Madhura, R. K., Vellore, R. K., Mujumdar, M., Sanjay, J., et al. (2019a). Non-monsoonal precipitation response over the Western Himalayas to climate change. *Clim. Dyn.* 52, 4091–4109. doi:10.1007/s00382-018-4357-2.
Krishnan, R., Sabin, T. P., Vellore, R., Mujumdar, M., Sanjay, J., Goswami, B. N., et al. (2016). Deciphering the desiccation trend of the South Asian monsoon hydroclimate in a warming world. *Clim. Dyn.* 47, 1007–1027. doi:10.1007/s00382-015-2886-5.
Krishnan, R., Shrestha, A. B., Ren, G., Rajbhandari, R., Saeed, S., Sanjay, J., et al. (2019b). "Unravelling Climate Change in the Hindu Kush Himalaya: Rapid Warming in the Mountains and Increasing Extremes," in *The Hindu Kush Himalaya Assessment*, eds. P. Wester, A. Mishra, A. Mukherji, and A. B. Shrestha (Cham: Springer International Publishing), 57–97. doi:10.1007/978-3-319-92288-1_3.
Krishnan, R., and Sugi, M. (2003). Pacific decadal oscillation and variability of the Indian summer monsoon rainfall. *Clim. Dyn.* 21, 233–242. doi:10.1007/s00382-003-0330-8.
Kröner, N., Kotlarski, S., Fischer, E., Lüthi, D., Zubler, E., and Schär, C. (2017). Separating climate change signals into thermodynamic, lapse-rate and circulation effects: theory and application to the European summer climate. *Clim. Dyn.* 48, 3425–3440. doi:10.1007/s00382-016-3276-3.
Kruger, A. C., and Nxumalo, M. P. (2017). Historical rainfall trends in South Africa: 1921–2015. *Water SA* 43, 285. doi:10.4314/wsa.v43i2.12.
Kruk, M. C., Parker, B., Marra, J. J., Werner, K., Heim, R., Vose, R., et al. (2017). Engaging with Users of Climate Information and the Coproduction of Knowledge. *Weather. Clim. Soc.* 9, 839–849. doi:10.1175/WCAS-D-16-0127.1.
Kuang, W. (2019). New evidences on anomalous phenomenon of buildings in regulating urban climate from observations in Beijing , China. *Earth Sp. Sci.* minor revi.
Kubota, T., Shige, S., Hashizume, H., Aonashi, K., Takahashi, N., Seto, S., et al. (2007). Global Precipitation Map Using Satellite-Borne Microwave Radiometers by the GSMaP Project: Production and Validation. *IEEE Trans. Geosci. Remote Sens.* doi:10.1109/TGRS.2007.895337.
Kucharski, F., Kang, I.-S., Straus, D., and King, M. P. (2010). Teleconnections in the Atmosphere and Oceans. *Bull. Am. Meteorol. Soc.* 91, 381–383. doi:10.1175/2009BAMS2834.1.
Kug, J.-S., Jeong, J.-H., Jang, Y.-S., Kim, B.-M., Folland, C. K., Min, S.-K., et al. (2015). Two distinct influences of Arctic warming on cold winters over North America and East Asia. *Nat. Geosci.* 8, 759–762. doi:10.1038/ngeo2517.
Kulp, S. A., and Strauss, B. H. (2019). New elevation data triple estimates of global vulnerability to sea-level rise and coastal flooding. *Nat. Commun.* 10, 4844. doi:10.1038/s41467-019-12808-z.
Kumar, S., Kinter, J. L., Pan, Z., and Sheffield, J. (2016). Twentieth century temperature trends in CMIP3, CMIP5, and CESM-LE climate simulations: Spatial-temporal uncertainties, differences, and their potential sources. *J. Geophys. Res. Atmos.* 121, 9561–9575. doi:10.1002/2015JD024382.
Kuppel, S., Houspanossian, J., Nosetto, M. D., and Jobbágy, E. G. (2015). What does it take to flood the Pampas?:

Lessons from a decade of strong hydrological fluctuations. *Water Resour. Res.* 51, 2937–2950. doi:10.1002/2015WR016966.
Kurihara, Y., Murakami, H., and Kachi, M. (2016). Sea surface temperature from the new Japanese geostationary meteorological Himawari-8 satellite. *Geophys. Res. Lett.* 43, 1234–1240. doi:10.1002/2015GL067159.
Kusaka, H., Chen, F., Tewari, M., Dudhia, J., Gill, D. O., Duda, M. G., et al. (2012a). Numerical Simulation of Urban Heat Island Effect by the WRF Model with 4-km Grid Increment: An Inter-Comparison Study between the Urban Canopy Model and Slab Model. *J. Meteorol. Soc. Japan. Ser. II*. doi:10.2151/jmsj.2012-B03.
Kusaka, H., Hara, M., and Takane, Y. (2012b). Urban Climate Projection by the WRF Model at 3-km Horizontal Grid Increment: Dynamical Downscaling and Predicting Heat Stress in the 2070's August for Tokyo, Osaka, and Nagoya Metropolises. *J. Meteorol. Soc. Japan. Ser. II* 90B, 47–63. doi:10.2151/jmsj.2012-B04.
Kusaka, H., Kondo, H., Kikegawa, Y., and Kimura, F. (2001). A simple single-layer urban canopy model for atmospheric models: Comparison with multi-layer and slab models. *Boundary-Layer Meteorol.* 101, 329–358. doi:10.1023/A:1019207923078.
Kusaka, H., Suzuki-Parker, A., Aoyagi, T., Adachi, S. A., and Yamagata, Y. (2016). Assessment of RCM and urban scenarios uncertainties in the climate projections for August in the 2050s in Tokyo. *Clim. Change* 137, 427–438. doi:10.1007/s10584-016-1693-2.
Kushnir, Y., Scaife, A. A., Arritt, R., Balsamo, G., Boer, G., Doblas-Reyes, F., et al. (2019). Towards operational predictions of the near-term climate. *Nat. Clim. Chang.* 9, 94–101. doi:10.1038/s41558-018-0359-7.
Kuttler, W., Weber, S., Schonnefeld, J., and Hesselschwerdt, A. (2007). Urban/rural atmospheric water vapour pressure differences and urban moisture excess in Krefeld, Germany. *Int. J. Climatol.* 27, 2005–2015. doi:10.1002/joc.1558.
Kwon, M. H., Jhun, J. G., and Ha, K. J. (2007). Decadal change in east Asian summer monsoon circulation in the mid-1990s. *Geophys. Res. Lett.* 34. doi:10.1029/2007GL031977.
Laaha, G., Parajka, J., Viglione, A., Koffler, D., Haslinger, K., Schöner, W., et al. (2016). A three-pillar approach to assessing climate impacts on low flows. *Hydrol. Earth Syst. Sci.* 20, 3967–3985. doi:10.5194/hess-20-3967-2016.
Lackmann, G. M. (2015). Hurricane Sandy before 1900 and after 2100. *Bull. Am. Meteorol. Soc.* 96, 547–560. doi:10.1175/BAMS-D-14-00123.1.
Lafaysse, M., Hingray, B., Mezghani, A., Gailhard, J., and Terray, L. (2014). Internal variability and model uncertainty components in future hydrometeorological projections: The Alpine Durance basin. *Water Resour. Res.* 50, 3317–3341. doi:10.1002/2013WR014897.
Lagabrielle, E., Lombard, A. T., Harris, J. M., and Livingstone, T. C. (2018). Multi-scale multi-level marine spatial planning: A novel methodological approach applied in south africa. *PLoS One* 13, 1–29. doi:10.1371/journal.pone.0192582.
LaJoie, E., and DelSole, T. (2016). Changes in Internal Variability due to Anthropogenic Forcing: A New Field Significance Test. *J. Clim.* 29, 5547–5560. doi:10.1175/JCLI-D-15-0718.1.
Laloyaux, P., de Boisseson, E., Balmaseda, M., Bidlot, J.-R., Broennimann, S., Buizza, R., et al. (2018). CERA-20C: A Coupled Reanalysis of the Twentieth Century. *J. Adv. Model. Earth Syst.* 10, 1172–1195. doi:10.1029/2018MS001273.
Lamb, M. (2017). *Ethics for Climate Change Communicators*. Oxford University Press doi:10.1093/acrefore/9780190228620.013.564.
Lange, M. A. (2019a). Impacts of Climate Change on the Eastern Mediterranean and the Middle East and North Africa Region and the Water–Energy Nexus. *Atmosphere (Basel).* 10, 455. doi:10.3390/atmos10080455.
Lange, S. (2019b). EartH2Observe, WFDEI and ERA-Interim data Merged and Bias-corrected for ISIMIP (EWEMBI). V. 1.1. doi:10.5880/pik.2019.004.
Lange, S. (2019c). Trend-preserving bias adjustment and statistical downscaling with ISIMIP3BASD (v1.0). *Geosci. Model Dev.* 12, 3055–3070. doi:10.5194/gmd-12-3055-2019.
Langenbrunner, B., and Neelin, J. D. (2013). Analyzing ENSO Teleconnections in CMIP Models as a Measure of Model Fidelity in Simulating Precipitation. *J. Clim.* 26, 4431–4446. doi:10.1175/JCLI-D-12-00542.1.
Langendijk, G. S., Aubry-Wake, C., Osman, M., Gulizia, C., Attig-Bahar, F., Behrens, E., et al. (2019). Three Ways Forward to Improve Regional Information for Extreme Events: An Early Career Perspective. *Front. Environ. Sci.* 7. doi:10.3389/fenvs.2019.00006.
Langhans, W., Schmidli, J., Fuhrer, O., Bieri, S., and Schär, C. (2013). Long-Term Simulations of Thermally Driven Flows and Orographic Convection at Convection-Parameterizing and Cloud-Resolving Resolutions. *J. Appl. Meteorol. Climatol.* 52, 1490–1510. doi:10.1175/JAMC-D-12-0167.1.
Langodan, S., Cavaleri, L., Vishwanadhapalli, Y., Pomaro, A., Bertotti, L., and Hoteit, I. (2017). The climatology of the Red Sea – part 1: the wind. *Int. J. Climatol.* 37, 4509–4517. doi:10.1002/joc.5103.
Laprise, R. (2014). Comment on "The added value to global model projections of climate change by dynamical downscaling: A case study over the continental U.S. using the GISS-ModelE2 and WRF models" by Racherla et al. *J. Geophys. Res. Atmos.* 119, 3877–3881. doi:10.1002/2013JD019945.
Laprise, R., Hernández-Díaz, L., Tete, K., Sushama, L., Šeparović, L., Martynov, A., et al. (2013). Climate projections over CORDEX Africa domain using the fifth-generation Canadian Regional Climate Model (CRCM5). *Clim.*

Dyn. 41, 3219–3246. doi:10.1007/s00382-012-1651-2.
Latif, M., Hannachi, A., and Syed, F. S. (2018). Analysis of rainfall trends over Indo-Pakistan summer monsoon and related dynamics based on CMIP5 climate model simulations. *Int. J. Climatol.* 38, e577–e595. doi:10.1002/joc.5391.
Lau, K.-M., and Kim, K.-M. (2006). Observational relationships between aerosol and Asian monsoon rainfall, and circulation. *Geophys. Res. Lett.* 33, L21810. doi:10.1029/2006GL027546.
Lau, W. (2014). Desert dust and monsoon rain. *Nat. Geosci.* 7, 255–256. doi:10.1038/ngeo2115.
Lau, W. K. M., and Kim, K. M. (2018). Impact of snow darkening by deposition of light-absorbing aerosols on snow cover in the Himalayas-Tibetan Plateau and influence on the Asian summer monsoon: A possible mechanism for the blanford hypothesis. *Atmosphere (Basel).* 9. doi:10.3390/atmos9110438.
Lauwaet, D., Hooyberghs, H., Maiheu, B., Lefebvre, W., Driesen, G., Van Looy, S., et al. (2015). Detailed Urban Heat Island Projections for Cities Worldwide: Dynamical Downscaling CMIP5 Global Climate Models. *Climate* 3, 391–415. doi:10.3390/cli3020391.
Lavaysse, C., Flamant, C., Evan, A., Janicot, S., and Gaetani, M. (2016). Recent climatological trend of the Saharan heat low and its impact on the West African climate. *Clim. Dyn.* doi:10.1007/s00382-015-2847-z.
Lawal, K. A., Abatan, A. A., Angélil, O., Olaniyan, E., Olusoji, V. H., Oguntunde, P. G., et al. (2016). 13. The late onset of the 2015 wet season in Nigeria. *Bull. Am. Meteorol. Soc.* 97, S63–S69. doi:10.1175/BAMS-D-16-0131.1.
Lawrimore, J. H., Menne, M. J., Gleason, B. E., Williams, C. N., Wuertz, D. B., Vose, R. S., et al. (2011). An overview of the Global Historical Climatology Network monthly mean temperature data set, version 3. *J. Geophys. Res. Atmos.* 116. doi:10.1029/2011JD016187.
Lebel, T., and Ali, A. (2009). Recent trends in the Central and Western Sahel rainfall regime (1990-2007). *J. Hydrol.* 375, 52–64. doi:10.1016/j.jhydrol.2008.11.030.
Leduc, M., Mailhot, A., Frigon, A., Martel, J.-L., Ludwig, R., Brietzke, G. B., et al. (2019). The ClimEx Project: A 50-Member Ensemble of Climate Change Projections at 12-km Resolution over Europe and Northeastern North America with the Canadian Regional Climate Model (CRCM5). *J. Appl. Meteorol. Climatol.* 58, 663–693. doi:10.1175/JAMC-D-18-0021.1.
Lee, C., and Whitely Binder, L. (2010). Assessing Pacific Northwest Water Resources Stakeholder Data Needs. Seattle, Washington, USA.
Lee, D. H. K. (1980). Seventy-five years of searching for a heat index. *Environ. Res.* 22, 331–356. doi:10.1016/0013-9351(80)90146-2.
Lee, H. T., Gruber, A., Ellingson, R. G., and Laszlo, I. (2007). Development of the HIRS outgoing longwave radiation climate dataset. *J. Atmos. Ocean. Technol.* 24, 2029–2047. doi:10.1175/2007JTECHA989.1.
Lee, J.-W., and Hong, S.-Y. (2014). Potential for added value to downscaled climate extremes over Korea by increased resolution of a regional climate model. *Theor. Appl. Climatol.* 117, 667–677. doi:10.1007/s00704-013-1034-6.
Lee, J.-W., Hong, S.-Y., Kim, J.-E. E., Yoshimura, K., Ham, S., and Joh, M. (2015). Development and implementation of river-routing process module in a regional climate model and its evaluation in Korean river basins. *J. Geophys. Res. Atmos.* 120, 4613–4629. doi:10.1002/2014JD022698.
Lee, J., Sperber, K. R., Gleckler, P. J., Bonfils, C. J. W., and Taylor, K. E. (2019). Quantifying the agreement between observed and simulated extratropical modes of interannual variability. *Clim. Dyn.* 52, 4057–4089. doi:10.1007/s00382-018-4355-4.
Lee, S. (2014). A theory for polar amplification from a general circulation perspective. *Asia-Pacific J. Atmos. Sci.* 50, 31–43. doi:10.1007/s13143-014-0024-7.
LeGrande, A. N., Tsigaridis, K., and Bauer, S. E. (2016). Role of atmospheric chemistry in the climate impacts of stratospheric volcanic injections. *Nat. Geosci.* 9, 652–655. doi:10.1038/ngeo2771.
Lehner, F., Deser, C., Maher, N., Marotzke, J., Fischer, E., Brunner, L., et al. (submitted). Partitioning climate projection uncertainty with multiple Large Ensembles and CMIP5/6. *Earth Syst. Dyn.* (submitted).
Lehner, F., Deser, C., and Sanderson, B. M. (2018a). Future risk of record-breaking summer temperatures and its mitigation. *Clim. Change* 146, 363–375. doi:10.1007/s10584-016-1616-2.
Lehner, F., Deser, C., Simpson, I. R., and Terray, L. (2018b). Attributing the U.S. Southwest's Recent Shift Into Drier Conditions. *Geophys. Res. Lett.* 45, 6251–6261. doi:10.1029/2018GL078312.
Lehner, F., Deser, C., and Terray, L. (2017a). Toward a New Estimate of "Time of Emergence" of Anthropogenic Warming: Insights from Dynamical Adjustment and a Large Initial-Condition Model Ensemble. *J. Clim.* 30, 7739–7756. doi:10.1175/JCLI-D-16-0792.1.
Lehner, F., Wahl, E. R., Wood, A. W., Blatchford, D. B., and Llewellyn, D. (2017b). Assessing recent declines in Upper Rio Grande runoff efficiency from a paleoclimate perspective. *Geophys. Res. Lett.* 44, 4124–4133. doi:10.1002/2017GL073253.
Lelieveld, J., Proestos, Y., Hadjinicolaou, P., Tanarhte, M., Tyrlis, E., and Zittis, G. (2016). Strongly increasing heat extremes in the Middle East and North Africa (MENA) in the 21st century. *Clim. Change* 137, 245–260. doi:10.1007/s10584-016-1665-6.
Lemonsu, A., Kounkou-Arnaud, R., Desplat, J., Salagnac, J. L., and Masson, V. (2013). Evolution of the Parisian urban climate under a global changing climate. *Clim. Change* 116, 679–692. doi:10.1007/s10584-012-0521-6.

Lemos, M. C., Kirchhoff, C. J., and Ramprasad, V. (2012). Narrowing the climate information usability gap. *Nat. Clim. Chang.* 2, 789–794. doi:10.1038/nclimate1614.
Lempert, R. J., and Collins, M. T. (2007). Managing the Risk of Uncertain Threshold Responses: Comparison of Robust, Optimum, and Precautionary Approaches. *Risk Anal.* 27, 1009–1026. doi:10.1111/j.1539-6924.2007.00940.x.
Lempert, R. J., Groves, D. G., Popper, S. W., and Bankes, S. C. (2006). A General, Analytic Method for Generating Robust Strategies and Narrative Scenarios. *Manage. Sci.* 52, 514–528. doi:10.1287/mnsc.1050.0472.
Lenssen, N. J. L., Schmidt, G. A., Hansen, J. E., Menne, M. J., Persin, A., Ruedy, R., et al. (2019). Improvements in the GISTEMP Uncertainty Model. *J. Geophys. Res. Atmos.* doi:10.1029/2018JD029522.
Lenton, T. M., Held, H., Kriegler, E., Hall, J. W., Lucht, W., Rahmstorf, S., et al. (2008). Tipping elements in the Earth's climate system. *Proc. Natl. Acad. Sci.* 105, 1786–1793. doi:10.1073/pnas.0705414105.
Lenz, C. J., Früh, B., and Adalatpanah, F. D. (2017). Is there potential added value in COSMO–CLM forced by ERA reanalysis data? *Clim. Dyn.* 49, 4061–4074. doi:10.1007/s00382-017-3562-8.
León, L., Lam, D., Schertzer, W., Swayne, D., Imberger, and J (2007). Towards coupling a 3D hydrodynamic lake model with the Canadian Regional Climate Model: Simulation on Great Slave Lake. *Environ. Model. Softw.* 22, 787–796. doi:10.1016/j.envsoft.2006.03.005.
Leonard, M., Westra, S., Phatak, A., Lambert, M., van den Hurk, B., McInnes, K., et al. (2014). A compound event framework for understanding extreme impacts. *Wiley Interdiscip. Rev. Clim. Chang.* 5, 113–128. doi:10.1002/wcc.252.
Letcher, T. W., and Minder, J. R. (2017). The Simulated Response of Diurnal Mountain Winds to Regionally Enhanced Warming Caused by the Snow Albedo Feedback. *J. Atmos. Sci.* 74, 49–67. doi:10.1175/JAS-D-16-0158.1.
Levine, P. A., Randerson, J. T., Swenson, S. C., and Lawrence, D. M. (2016). Evaluating the strength of the land-atmosphere moisture feedback in Earth system models using satellite observations. *Hydrol. Earth Syst. Sci.* 20, 4837–4856. doi:10.5194/hess-20-4837-2016.
Levy, A. A. L., Ingram, W., Jenkinson, M., Huntingford, C., Hugo Lambert, F., and Allen, M. (2013). Can correcting feature location in simulated mean climate improve agreement on projected changes? *Geophys. Res. Lett.* 40, 354–358. doi:10.1002/2012GL053964.
Levy, A. A. L., Jenkinson, M., Ingram, W., and Allen, M. (2014a). Correcting precipitation feature location in general circulation models. *J. Geophys. Res. Atmos.* 119, 13,350-13,369. doi:10.1002/2014JD022357.
Levy, A. A. L., Jenkinson, M., Ingram, W., Lambert, F. H., Huntingford, C., and Allen, M. (2014b). Increasing the detectability of external influence on precipitation by correcting feature location in GCMs. *J. Geophys. Res. Atmos.* 119, 12,466-12,478. doi:10.1002/2014JD022358.
Li, B., Gasser, T., Ciais, P., Piao, S., Tao, S., Balkanski, Y., et al. (2016a). The contribution of China's emissions to global climate forcing. *Nature* 531, 357–361. doi:10.1038/nature17165.
Li, C., Stevens, B., and Marotzke, J. (2015). Eurasian winter cooling in the warming hiatus of 1998-2012. *Geophys. Res. Lett.* 42, 8131–8139. doi:10.1002/2015GL065327.
Li, C., Zhao, T., and Ying, K. (2017a). Quantifying the contributions of anthropogenic and natural forcings to climate changes over arid-semiarid areas during 1946–2005. *Clim. Change* 144, 505–517. doi:10.1007/s10584-017-2028-7.
Li, D., and Xiao, Z. (2018). Can solar cycle modulate the ENSO effect on the Pacific/North American pattern? *J. Atmos. Solar-Terrestrial Phys.* 167, 30–38. doi:https://doi.org/10.1016/j.jastp.2017.10.007.
Li, F., Orsolini, Y. J., Wang, H., Gao, Y., and He, S. (2018a). Atlantic Multidecadal Oscillation Modulates the Impacts of Arctic Sea Ice Decline. *Geophys. Res. Lett.* 45, 2497–2506. doi:10.1002/2017GL076210.
Li, G., Xie, S.-P., He, C., and Chen, Z. (2017b). Western Pacific emergent constraint lowers projected increase in Indian summer monsoon rainfall. *Nat. Clim. Chang.* 7, 708–712. doi:10.1038/nclimate3387.
Li, H., Dai, A., Zhou, T., and Lu, J. (2010). Responses of East Asian summer monsoon to historical SST and atmospheric forcing during 1950–2000. *Clim. Dyn.* 34, 501–514. doi:10.1007/s00382-008-0482-7.
Li, H., Haugen, J. E., and Xu, C. Y. (2018b). Precipitation pattern in the Western Himalayas revealed by four datasets. *Hydrol. Earth Syst. Sci.* 22, 5097–5110. doi:10.5194/hess-22-5097-2018.
Li, H., Zhou, Y., Li, X., Meng, L., Wang, X., Wu, S., et al. (2018c). A new method to quantify surface urban heat island intensity. *Sci. Total Environ.* 624, 262–272. doi:10.1016/j.scitotenv.2017.11.360.
Li, K., Liao, H., Mao, Y., and Ridley, D. A. (2016b). Source sector and region contributions to concentration and direct radiative forcing of black carbon in China. *Atmos. Environ.* 124, 351–366. doi:10.1016/j.atmosenv.2015.06.014.
Li, X., Mitra, C., Dong, L., and Yang, Q. (2018d). Understanding land use change impacts on microclimate using Weather Research and Forecasting (WRF) model. *Phys. Chem. Earth, Parts A/B/C* 103, 115–126. doi:https://doi.org/10.1016/j.pce.2017.01.017.
Li, X., and Ting, M. (2017). Understanding the Asian summer monsoon response to greenhouse warming: the relative roles of direct radiative forcing and sea surface temperature change. *Clim. Dyn.* 49, 2863–2880. doi:10.1007/s00382-016-3470-3.
Li, Y., Ding, Y., and Li, W. (2017c). Interdecadal variability of the Afro-Asian summer monsoon system. *Adv. Atmos. Sci.* 34, 833–846. doi:10.1007/s00376-017-6247-7.

Li, Z.-X. (1999). Ensemble Atmospheric GCM Simulation of Climate Interannual Variability from 1979 to 1994. *J. Clim.* 12, 986–1001. doi:10.1175/1520-0442(1999)012<0986:EAGSOC>2.0.CO;2.
Li, Z., Lau, W. K.-M., Ramanathan, V., Wu, G., Ding, Y., Manoj, M. G., et al. (2016c). Aerosol and monsoon climate interactions over Asia. *Rev. Geophys.* 54, 866–929. doi:10.1002/2015RG000500.
Liang, P., and Ding, Y. (2017). The long-term variation of extreme heavy precipitation and its link to urbanization effects in Shanghai during 1916–2014. *Adv. Atmos. Sci.* 34, 321–334. doi:10.1007/s00376-016-6120-0.
Liao, W., Wang, D., Liu, X., Wang, G., and Zhang, J. (2017). Estimated influence of urbanization on surface warming in Eastern China using time-varying land use data. *Int. J. Climatol.* 37, 3197–3208. doi:10.1002/joc.4908.
Lim, E.-P., Hendon, H. H., Arblaster, J. M., Chung, C., Moise, A. F., Hope, P., et al. (2016a). Interaction of the recent 50 year SST trend and La Niña 2010: amplification of the Southern Annular Mode and Australian springtime rainfall. *Clim. Dyn.* 47, 2273–2291. doi:10.1007/s00382-015-2963-9.
Lim, E.-P., Hendon, H. H., Arblaster, J. M., Delage, F., Nguyen, H., Min, S.-K., et al. (2016b). The impact of the Southern Annular Mode on future changes in Southern Hemisphere rainfall. *Geophys. Res. Lett.* 43, 7160–7167. doi:10.1002/2016GL069453.
Lim, E.-P., Hendon, H. H., and Thompson, D. W. J. (2018). On the Seasonal Evolution and Impacts of Stratosphere-Troposphere Coupling in the Southern Hemisphere. *J. Geophys. Res. Atmos.* doi:10.1029/2018JD029321.
Lim, E.-P. P., and Hendon, H. H. (2015). Understanding and predicting the strong Southern Annular Mode and its impact on the record wet east Australian spring 2010. *Clim. Dyn.* 44, 2807–2824. doi:10.1007/s00382-014-2400-5.
Lim, H.-G., Yeh, S.-W., Kug, J.-S., Park, Y.-G., Park, J.-H., Park, R., et al. (2016c). Threshold of the volcanic forcing that leads the El Niño-like warming in the last millennium: results from the ERIK simulation. *Clim. Dyn.* 46, 3725–3736. doi:10.1007/s00382-015-2799-3.
Lima, D. C. A., Soares, P. M. M., Semedo, A., Cardoso, R. M., Cabos, W., and Sein, D. V. (2019). How Will a Warming Climate Affect the Benguela Coastal Low-Level Wind Jet? *J. Geophys. Res. Atmos.* 124, 5010–5028. doi:10.1029/2018JD029574.
Lin, H., Brunet, G., and Derome, J. (2009). An Observed Connection between the North Atlantic Oscillation and the Madden–Julian Oscillation. *J. Clim.* 22, 364–380. doi:10.1175/2008JCLI2515.1.
Lin, M., and Huybers, P. (2019). If Rain Falls in India and No One Reports It, Are Historical Trends in Monsoon Extremes Biased? *Geophys. Res. Lett.* doi:10.1029/2018GL079709.
Lin, N., and Emanuel, K. (2016). Grey swan tropical cyclones. *Nat. Clim. Chang.* 6, 106–111. doi:10.1038/nclimate2777.
Lindau, R., and Venema, V. (2018a). On the reduction of trend errors by the ANOVA joint correction scheme used in homogenization of climate station records. *Int. J. Climatol.* 38, 5255–5271. doi:10.1002/joc.5728.
Lindau, R., and Venema, V. K. C. (2018b). The joint influence of break and noise variance on the break detection capability in time series homogenization. *Adv. Stat. Climatol. Meteorol. Oceanogr.* 4, 1–18. doi:10.5194/ascmo-4-1-2018.
Lionello, P., Abrantes, F., Congedi, L., Dulac, F., Gacic, M., Gomis, D., et al. (2012). "Introduction: Mediterranean Climate—Background Information," in *The Climate of the Mediterranean Region* (Elsevier), xxxv–xc. doi:10.1016/B978-0-12-416042-2.00012-4.
Lionello, P., and Scarascia, L. (2018). The relation between climate change in the Mediterranean region and global warming. *Reg. Environ. Chang.* 18, 1481–1493. doi:10.1007/s10113-018-1290-1.
Lipson, M. J., Thatcher, M., Hart, M. A., and Pitman, A. (2018). A building energy demand and urban land surface model. *Q. J. R. Meteorol. Soc.* 144, 1572–1590. doi:10.1002/qj.3317.
Liu, F., Chai, J., Wang, B., Liu, J., Zhang, X., and Wang, Z. (2016a). Global monsoon precipitation responses to large volcanic eruptions. *Sci. Rep.* 6, 24331. doi:10.1038/srep24331.
Liu, F., Li, J., Wang, B., Liu, J., Li, T., Huang, G., et al. (2018a). Divergent El Niño responses to volcanic eruptions at different latitudes over the past millennium. *Clim. Dyn.* 50, 3799–3812. doi:10.1007/s00382-017-3846-z.
Liu, F., Xing, C., Sun, L., Wang, B., Chen, D., and Liu, J. (2018b). How Do Tropical, Northern Hemispheric, and Southern Hemispheric Volcanic Eruptions Affect ENSO Under Different Initial Ocean Conditions? *Geophys. Res. Lett.*, 2018GL080315. doi:10.1029/2018GL080315.
Liu, L., Shawki, D., Voulgarakis, A., Kasoar, M., Samset, B. H., Myhre, G., et al. (2018c). A PDRMIP Multimodel Study on the Impacts of Regional Aerosol Forcings on Global and Regional Precipitation. *J. Clim.* 31, 4429–4447. doi:10.1175/JCLI-D-17-0439.1.
Liu, L., Zhang, R., and Zuo, Z. (2016b). The Relationship between Soil Moisture and LAI in Different Types of Soil in Central Eastern China. *J. Hydrometeorol.* 17, 2733–2742. doi:10.1175/JHM-D-15-0240.1.
Liu, Y., Cai, W., Sun, C., Song, H., Cobb, K. M., Li, J., et al. (2019). Anthropogenic Aerosols Cause Recent Pronounced Weakening of Asian Summer Monsoon Relative to Last Four Centuries. *Geophys. Res. Lett.* 46, 5469–5479. doi:10.1029/2019GL082497.
Liu, Y., Chen, F., Warner, T., and Basara, J. (2006). Verification of a Mesoscale Data-Assimilation and Forecasting System for the Oklahoma City Area during the Joint Urban 2003 Field Project. *J. Appl. Meteorol. Climatol.* 45, 912–929. doi:10.1175/JAM2383.1.

Liu, Y., Wang, L., Zhou, W., and Chen, W. (2014a). Three Eurasian teleconnection patterns: spatial structures, temporal variability, and associated winter climate anomalies. *Clim. Dyn.* 42, 2817–2839. doi:10.1007/s00382-014-2163-z.
Liu, Z., Yoshimura, K., Buenning, N. H., and He, X. (2014b). Solar cycle modulation of the Pacific–North American teleconnection influence on North American winter climate. *Environ. Res. Lett.* 9, 24004. doi:10.1088/1748-9326/9/2/024004.
Livezey, R. E., Vinnikov, K. Y., Timofeyeva, M. M., Tinker, R., and van den Dool, H. M. (2007). Estimation and Extrapolation of Climate Normals and Climatic Trends. *J. Appl. Meteorol. Climatol.* 46, 1759–1776. doi:10.1175/2007JAMC1666.1.
Lokoshchenko, M. A. (2017). Urban Heat Island and Urban Dry Island in Moscow and Their Centennial Changes. *J. Appl. Meteorol. Climatol.* 56, 2729–2745. doi:10.1175/JAMC-D-16-0383.1.
Lorenz, P., and Jacob, D. (2005). Influence of regional scale information on the global circulation: A two-way nesting climate simulation. *Geophys. Res. Lett.* 32, n/a-n/a. doi:10.1029/2005GL023351.
Lorenz, P., and Jacob, D. (2010). Validation of temperature trends in the ENSEMBLES regional climate model runs driven by ERA40. *Clim. Res.* 44, 167–177. doi:10.3354/cr00973.
Lorenz, R., Argüeso, D., Donat, M. G., Pitman, A. J., van den Hurk, B., Berg, A., et al. (2016). Influence of land-atmosphere feedbacks on temperature and precipitation extremes in the GLACE-CMIP5 ensemble. *J. Geophys. Res. Atmos.* 121, 607–623. doi:10.1002/2015JD024053.
Lourenço, T. C., Swart, R., Goosen, H., and Street, R. (2016). The rise of demand-driven climate services. *Nat. Clim. Chang.* 6, 13–14. doi:10.1038/nclimate2836.
Lovino, M. A., Müller, O. V, Berbery, E. H., and Müller, G. V (2018). Evaluation of CMIP5 retrospective simulations of temperature and precipitation in northeastern Argentina. *Int. J. Climatol.* 38, e1158–e1175. doi:10.1002/joc.5441.
Lowry, D. P., and Morrill, C. (2019). Is the Last Glacial Maximum a reverse analog for future hydroclimate changes in the Americas? *Clim. Dyn.* 52, 4407–4427. doi:10.1007/s00382-018-4385-y.
Lucas-Picher, P., Christensen, J. H., Saeed, F., Kumar, P., Asharaf, S., Ahrens, B., et al. (2011). Can Regional Climate Models Represent the Indian Monsoon? *J. Hydrometeorol.* 12, 849–868. doi:10.1175/2011JHM1327.1.
Lucas-Picher, P., Laprise, R., and Winger, K. (2017). Evidence of added value in North American regional climate model hindcast simulations using ever-increasing horizontal resolutions. *Clim. Dyn.* 48, 2611–2633. doi:10.1007/s00382-016-3227-z.
Lucas, C., Timbal, B., and Nguyen, H. (2014). The expanding tropics: a critical assessment of the observational and modeling studies. *Wiley Interdiscip. Rev. Clim. Chang.* 5, 89–112. doi:10.1002/wcc.251.
Luo, D., Yao, Y., Dai, A., Simmonds, I., and Zhong, L. (2017). Increased quasi stationarity and persistence of winter ural blocking and Eurasian extreme cold events in response to arctic warming. Part II: A theoretical explanation. *J. Clim.* 30, 3569–3587. doi:10.1175/JCLI-D-16-0262.1.
Luterbacher, J., Werner, J. P., Smerdon, J. E., Fernández-Donado, L., González-Rouco, F. J., Barriopedro, D., et al. (2016). European summer temperatures since Roman times. *Environ. Res. Lett.* 11, 024001. doi:10.1088/1748-9326/11/2/024001.
Lyu, K., Zhang, X., Church, J. A., and Hu, J. (2015). Quantifying internally generated and externally forced climate signals at regional scales in CMIP5 models. *Geophys. Res. Lett.* 42, 9394–9403. doi:10.1002/2015GL065508.
Ma, S., Pitman, A., Hart, M., Evans, J. P., Haghdadi, N., and MacGill, I. (2017). The impact of an urban canopy and anthropogenic heat fluxes on Sydney's climate. *Int. J. Climatol.* 37, 255–270. doi:10.1002/joc.5001.
Macias, D., Garcia-Gorriz, E., Dosio, A., Stips, A., and Keuler, K. (2018). Obtaining the correct sea surface temperature: bias correction of regional climate model data for the Mediterranean Sea. *Clim. Dyn.* 51, 1095–1117. doi:10.1007/s00382-016-3049-z.
Macias, D., Garcia-Gorriz, E., and Stips, A. (2013). Understanding the Causes of Recent Warming of Mediterranean Waters. How Much Could Be Attributed to Climate Change? *PLoS One* 8, e81591. doi:10.1371/journal.pone.0081591.
MacKellar, N., New, M., and Jack, C. (2014). Observed and modelled trends in rainfall and temperature for South Africa: 1960–2010. *S. Afr. J. Sci.* 110, 1–13. doi:10.1590/sajs.2014/20130353.
MacLeod, D. A., Cloke, H. L., Pappenberger, F., and Weisheimer, A. (2016). Improved seasonal prediction of the hot summer of 2003 over Europe through better representation of uncertainty in the land surface. *Q. J. R. Meteorol. Soc.* 142, 79–90. doi:10.1002/qj.2631.
Madhusoodhanan, C. G., Shashikanth, K., Eldho, T. I., and Ghosh, S. (2018). Can statistical downscaling improve consensus among CMIP5 models for Indian summer monsoon rainfall projections? *Int. J. Climatol.* 38, 2449–2461. doi:10.1002/joc.5352.
Madsen, M. S., Langen, P. L., Boberg, F., and Christensen, J. H. (2017). Inflated Uncertainty in Multimodel-Based Regional Climate Projections. *Geophys. Res. Lett.* 44, 11,606-11,613. doi:10.1002/2017GL075627.
Magana, V., Amador, J., and Medina, S. (1999). The Midsummer Drought over Mexico and Central America. *J. Clim.* 12, 1577–1588. doi:10.1175/1520-0442(1999)012<1577:TMDOMA>2.0.CO;2.
Maher, N., Milinski, S., Suarez-Gutierrez, L., Botzet, M., Dobrynin, M., Kornblueh, L., et al. (2019). The Max Planck

Institute Grand Ensemble: Enabling the Exploration of Climate System Variability. *J. Adv. Model. Earth Syst.* 11, 2050–2069. doi:10.1029/2019MS001639.
Mahlalela, P. T., Blamey, R. C., and Reason, C. J. C. (2019). Mechanisms behind early winter rainfall variability in the southwestern Cape, South Africa. *Clim. Dyn.* 53, 21–39. doi:10.1007/s00382-018-4571-y.
Mahlstein, I., Hegerl, G., and Solomon, S. (2012). Emerging local warming signals in observational data. *Geophys. Res. Lett.* 39, n/a-n/a. doi:10.1029/2012GL053952.
Mahmood, R., Pielke, R. A., Hubbard, K. G., Niyogi, D., Dirmeyer, P. A., Mcalpine, C., et al. (2014). Land cover changes and their biogeophysical effects on climate. *Int. J. Climatol.* 34, 929–953. doi:10.1002/joc.3736.
Mahmood, S., Davie, J., Jermey, P., Renshaw, R., George, J. P., Rajagopal, E. N., et al. (2018). Indian monsoon data assimilation and analysis regional reanalysis: Configuration and performance. *Atmos. Sci. Lett.* 19, e808. doi:10.1002/asl.808.
Maidment, R. I., Allan, R. P., and Black, E. (2015). Recent observed and simulated changes in precipitation over Africa. *Geophys. Res. Lett.* 42, 8155–8164. doi:10.1002/2015GL065765.
Maidment, R. I., Grimes, D., Allan, R. P., Tarnavsky, E., Stringer, M., Hewison, T., et al. (2014). The 30 year TAMSAT African Rainfall Climatology And Time series (TARCAT) data set. *J. Geophys. Res. Atmos.* 119, 10, 610–619, 644. doi:10.1002/2014JD021927.
Maldonado, T., Rutgersson, A., Alfaro, E., Amador, J., and Claremar, B. (2016). Interannual variability of the midsummer drought in Central America and the connection with sea surface temperatures. *Adv. Geosci.* 42, 35–50. doi:10.5194/adgeo-42-35-2016.
Mallard, M. S., Nolte, C. G., Bullock, O. R., Spero, T. L., and Gula, J. (2014). Using a coupled lake model with WRF for dynamical downscaling. *J. Geophys. Res. Atmos.* 119, 7193–7208. doi:10.1002/2014JD021785.
Mallet, M., Dulac, F., Formenti, P., Nabat, P., Sciare, J., Roberts, G., et al. (2016). Overview of the Chemistry-Aerosol Mediterranean Experiment/Aerosol Direct Radiative Forcing on the Mediterranean Climate (ChArMEx/ADRIMED) summer 2013 campaign. *Atmos. Chem. Phys.* 16, 455–504. doi:10.5194/acp-16-455-2016.
Man, W., and Zhou, T. (2014). Response of the East Asian summer monsoon to large volcanic eruptions during the last millennium. *Chinese Sci. Bull.* 59, 4123–4129. doi:10.1007/s11434-014-0404-5.
Mann, M. E., Rahmstorf, S., Kornhuber, K., Steinman, B. A., Miller, S. K., and Coumou, D. (2017). Influence of Anthropogenic Climate Change on Planetary Wave Resonance and Extreme Weather Events. *Sci. Rep.* 7, 45242. doi:10.1038/srep45242.
Mann, M. E., Rahmstorf, S., Kornhuber, K., Steinman, B. A., Miller, S. K., Petri, S., et al. (2018). Projected changes in persistent extreme summer weather events: The role of quasi-resonant amplification. *Sci. Adv.* 4, eaat3272. doi:10.1126/sciadv.aat3272.
Manz, B., Buytaert, W., Zulkafli, Z., Lavado, W., Willems, B., Robles, L. A., et al. (2016). High-resolution satellite-gauge merged precipitation climatologies of the Tropical Andes. *J. Geophys. Res. Atmos.* 121, 1190–1207. doi:10.1002/2015JD023788.
Manzanas, R., Amekudzi, L. K., Preko, K., Herrera, S., and Gutiérrez, J. M. (2014). Precipitation variability and trends in Ghana: An intercomparison of observational and reanalysis products. *Clim. Change* 124, 805–819. doi:10.1007/s10584-014-1100-9.
Manzanas, R., and Gutiérrez, J. M. (2019). Process-conditioned bias correction for seasonal forecasting: a case-study with ENSO in Peru. *Clim. Dyn.* 52, 1673–1683. doi:10.1007/s00382-018-4226-z.
Manzini, E., Karpechko, A. Y., Anstey, J., Baldwin, M. P., Black, R. X., Cagnazzo, C., et al. (2014). Northern winter climate change: Assessment of uncertainty in CMIP5 projections related to stratosphere-troposphere coupling. *J. Geophys. Res. Atmos.* 119, 7979–7998. doi:10.1002/2013JD021403.
Maraun, D. (2012). Nonstationarities of regional climate model biases in European seasonal mean temperature and precipitation sums. *Geophys. Res. Lett.* 39, n/a-n/a. doi:10.1029/2012GL051210.
Maraun, D. (2013a). Bias Correction, Quantile Mapping, and Downscaling: Revisiting the Inflation Issue. *J. Clim.* 26, 2137–2143. doi:10.1175/JCLI-D-12-00821.1.
Maraun, D. (2013b). When will trends in European mean and heavy daily precipitation emerge? *Environ. Res. Lett.* 8, 014004. doi:10.1088/1748-9326/8/1/014004.
Maraun, D., Huth, R., Gutiérrez, J. M., Martín, D. S., Dubrovsky, M., Fischer, A., et al. (2017a). The VALUE perfect predictor experiment: evaluation of temporal variability. *Int. J. Climatol.* doi:10.1002/joc.5222.
Maraun, D., Shepherd, T. G., Widmann, M., Zappa, G., Walton, D., Gutiérrez, J. M., et al. (2017b). Towards process-informed bias correction of climate change simulations. *Nat. Clim. Chang.* 7, 664–773. doi:10.1038/nclimate3418.
Maraun, D., and Widmann, M. (2015). The representation of location by a regional climate model in complex terrain. *Hydrol. Earth Syst. Sci.* 19, 3449–3456. doi:10.5194/hess-19-3449-2015.
Maraun, D., and Widmann, M. (2018a). Cross-validation of bias-corrected climate simulations is misleading. *Hydrol. Earth Syst. Sci.* 22, 4867–4873. doi:10.5194/hess-22-4867-2018.
Maraun, D., and Widmann, M. (2018b). *Statistical Downscaling and Bias Correction for Climate Research*. Cambridge: Cambridge University Press doi:10.1017/9781107588783.

Maraun, D., Widmann, M., and Gutiérrez, J. M. (2018). Statistical downscaling skill under present climate conditions: A synthesis of the VALUE perfect predictor experiment. *Int. J. Climatol.* doi:10.1002/joc.5877.
Maraun, D., Widmann, M., Gutiérrez, J. M., Kotlarski, S., Chandler, R. E., Hertig, E., et al. (2015). VALUE: A framework to validate downscaling approaches for climate change studies. *Earth's Futur.* 3, 1–14. doi:10.1002/2014EF000259.
Marengo, J. A., Rusticucci, M., Penalba, O., and Renom, M. (2010). An intercomparison of observed and simulated extreme rainfall and temperature events during the last half of the twentieth century: part 2: historical trends. *Clim. Change* 98, 509–529. doi:10.1007/s10584-009-9743-7.
Mariotti, A., Pan, Y., Zeng, N., and Alessandri, A. (2015). Long-term climate change in the Mediterranean region in the midst of decadal variability. *Clim. Dyn.* 44, 1437–1456. doi:10.1007/s00382-015-2487-3.
Marteau, R., Richard, Y., Pohl, B., Smith, C. C., and Castel, T. (2015). High-resolution rainfall variability simulated by the WRF RCM: application to eastern France. *Clim. Dyn.* 44, 1093–1107. doi:10.1007/s00382-014-2125-5.
Martilli, A., Clappier, A., and Rotach, M. W. (2002). An urban surface exchange parameterisation for mesoscale models. *Boundary-Layer Meteorol.* 104, 261–304. doi:10.1023/A:1016099921195.
Martín-Gómez, V., and Barreiro, M. (2016). Analysis of oceans' influence on spring time rainfall variability over Southeastern South America during the 20th century. *Int. J. Climatol.* 36, 1344–1358. doi:10.1002/joc.4428.
Martín-Gómez, V., and Barreiro, M. (2017). Effect of future climate change on the coupling between the tropical oceans and precipitation over Southeastern South America. *Clim. Change* 141, 315–329. doi:10.1007/s10584-016-1888-6.
Martin, E. R., Thorncroft, C., and Booth, B. B. B. (2014). The multidecadal atlantic SST-Sahel rainfall teleconnection in CMIP5 simulations. *J. Clim.* 27, 784–806. doi:10.1175/JCLI-D-13-00242.1.
Martin, E. R., and Thorncroft, C. D. (2014). The impact of the AMO on the West African monsoon annual cycle. *Q. J. R. Meteorol. Soc.* 140, 31–46. doi:10.1002/qj.2107.
Martin, G. M., Milton, S. F., Senior, C. A., Brooks, M. E., Ineson, S., Reichler, T., et al. (2010). Analysis and Reduction of Systematic Errors through a Seamless Approach to Modeling Weather and Climate. *J. Clim.* 23, 5933–5957. doi:10.1175/2010JCLI3541.1.
Martin, G. M., Peyrillé, P., Roehrig, R., Rio, C., Caian, M., Bellon, G., et al. (2017). Understanding the West African Monsoon from the analysis of diabatic heating distributions as simulated by climate models. *J. Adv. Model. Earth Syst.* 9, 239–270. doi:10.1002/2016MS000697.
Martius, O., Pfahl, S., and Chevalier, C. (2016). A global quantification of compound precipitation and wind extremes. *Geophys. Res. Lett.* 43, 7709–7717. doi:10.1002/2016GL070017.
Martynov, A., Sushama, L., and Laprise, R. (2010). Simulation of temperate freezing lakes by one-dimensional lake models: performance assessment for interactive coupling with regional climate models. *Boreal Environ. Res.* 15, 143–164.
Martynov, A., Sushama, L., Laprise, R., Winger, K., and Dugas, B. (2012). Interactive lakes in the Canadian Regional Climate Model, version 5: the role of lakes in the regional climate of North America. *Tellus A Dyn. Meteorol. Oceanogr.* 64, 16226. doi:10.3402/tellusa.v64i0.16226.
Marvel, K., Schmidt, G. A., Shindell, D., Bonfils, C., LeGrande, A. N., Nazarenko, L., et al. (2015). Do responses to different anthropogenic forcings add linearly in climate models? *Environ. Res. Lett.* 10, 104010. doi:10.1088/1748-9326/10/10/104010.
Masato, G., Hoskins, B. J., and Woollings, T. (2013). Winter and Summer Northern Hemisphere Blocking in CMIP5 Models. *J. Clim.* 26, 7044–7059. doi:10.1175/JCLI-D-12-00466.1.
Masson, D., and Frei, C. (2014). Spatial analysis of precipitation in a high-mountain region : exploring methods with multi-scale topographic predictors and circulation types. *Hydrol. Earth Syst. Sci.,* 18, 4543–4563. doi:10.5194/hess-18-4543-2014.
Masson, V. (2000). A physically-based scheme for the urban energy budget in atmospheric models. *Boundary-Layer Meteorol.* 94, 357–397. doi:10.1023/A:1002463829265.
Masson, V. (2006). Urban surface modeling and the meso-scale impact of cities. *Theor. Appl. Climatol.* 84, 35–45. doi:10.1007/s00704-005-0142-3.
Masson, V., Marchadier, C., Adolphe, L., Aguejdad, R., Avner, P., Bonhomme, M., et al. (2014). Adapting cities to climate change: A systemic modelling approach. *Urban Clim.* 10, 407–429. doi:10.1016/j.uclim.2014.03.004.
Massonnet, F., Bellprat, O., Guemas, V., and Doblas-Reyes, F. J. (2016). Using climate models to estimate the quality of global observational data sets. *Science* 354, 452–455. doi:10.1126/science.aaf6369.
Matte, D., Larsen, M. A. D., Christensen, O. B., and Christensen, J. H. (2019). Robustness and Scalability of Regional Climate Projections Over Europe. *Front. Environ. Sci.* 6, 163. doi:10.3389/fenvs.2018.00163.
Maule, C. F., Mendlik, T., and Christensen, O. B. (2017). The effect of the pathway to a two degrees warmer world on the regional temperature change of Europe. *Clim. Serv.* 7, 3–11. doi:10.1016/j.cliser.2016.07.002.
Maúre, G., Pinto, I., Ndebele-Murisa, M., Muthige, M., Lennard, C., Nikulin, G., et al. (2018). The southern African climate under 1.5 °C and 2 °C of global warming as simulated by CORDEX regional climate models. *Environ. Res. Lett.* 13, 065002. doi:10.1088/1748-9326/aab190.
Maurer, E. P., and Pierce, D. W. (2014). Bias correction can modify climate model simulated precipitation changes

without adverse effect on the ensemble mean. *Hydrol. Earth Syst. Sci.* 18, 915–925. doi:10.5194/hess-18-915-2014.
May, W. (2011). The sensitivity of the Indian summer monsoon to a global warming of 2°C with respect to pre-industrial times. *Clim. Dyn.* 37, 1843–1868. doi:10.1007/s00382-010-0942-8.
McCarthy, M. P., Best, M. J., and Betts, R. A. (2010). Climate change in cities due to global warming and urban effects. *Geophys. Res. Lett.* 37. doi:10.1029/2010GL042845.
McCarthy, M. P., Harpham, C., Goodess, C. M., and Jones, P. D. (2012). Simulating climate change in UK cities using a regional climate model, HadRM3. *Int. J. Climatol.* 32, 1875–1888. doi:10.1002/joc.2402.
McCusker, K. E., Fyfe, J. C., and Sigmond, M. (2016). Twenty-five winters of unexpected Eurasian cooling unlikely due to Arctic sea-ice loss. *Nat. Geosci.* 9, 838–842. doi:10.1038/ngeo2820.
McCusker, K. E., Kushner, P. J., Fyfe, J. C., Sigmond, M., Kharin, V. V., and Bitz, C. M. (2017). Remarkable separability of circulation response to Arctic sea ice loss and greenhouse gas forcing. *Geophys. Res. Lett.* 44, 7955–7964. doi:10.1002/2017GL074327.
McDermid, S. S., Mearns, L. O., and Ruane, A. C. (2017). Representing agriculture in Earth System Models: Approaches and priorities for development. *J. Adv. Model. Earth Syst.* 9, 2230–2265. doi:10.1002/2016MS000749.
McDonald, R. I., Chai, H. Y., and Newell, B. R. (2015). Personal experience and the ‘psychological distance’ of climate change: An integrative review. *J. Environ. Psychol.* 44, 109–118. doi:10.1016/j.jenvp.2015.10.003.
McGraw, M. C., and Barnes, E. A. (2020). New Insights on Subseasonal Arctic–Midlatitude Causal Connections from a Regularized Regression Model. *J. Clim.* 33, 213–228. doi:10.1175/JCLI-D-19-0142.1.
McGregor, J. L. (2015). Recent developments in variable-resolution global climate modelling. *Clim. Change* 129, 369–380. doi:10.1007/s10584-013-0866-5.
McGregor, S., Timmermann, A., Stuecker, M. F., England, M. H., Merrifield, M., Jin, F.-F., et al. (2014). Recent Walker circulation strengthening and Pacific cooling amplified by Atlantic warming. *Nat. Clim. Chang.* 4, 888–892. doi:10.1038/nclimate2330.
McKinnon, K. A., and Deser, C. (2018). Internal Variability and Regional Climate Trends in an Observational Large Ensemble. *J. Clim.* 31, 6783–6802. doi:10.1175/JCLI-D-17-0901.1.
McKinnon, K. A., Poppick, A., Dunn-Sigouin, E., and Deser, C. (2017). An “Observational Large Ensemble” to Compare Observed and Modeled Temperature Trend Uncertainty due to Internal Variability. *J. Clim.* 30, 7585–7598. doi:10.1175/JCLI-D-16-0905.1.
McLandress, C., Jonsson, A. I., Plummer, D. A., Reader, M. C., Scinocca, J. F., and Shepherd, T. G. (2010). Separating the Dynamical Effects of Climate Change and Ozone Depletion. Part I: Southern Hemisphere Stratosphere. *J. Clim.* 23, 5002–5020. doi:10.1175/2010JCLI3586.1.
McLeod, J., Shepherd, M., and Konrad, C. E. (2017). Spatio-temporal rainfall patterns around Atlanta, Georgia and possible relationships to urban land cover. *Urban Clim.* 21, 27–42. doi:10.1016/j.uclim.2017.03.004.
McNeall, D., Williams, J., Booth, B., Betts, R., Challenor, P., Wiltshire, A., et al. (2016). The impact of structural error on parameter constraint in a climate model. *Earth Syst. Dyn.* 7, 917–935. doi:10.5194/esd-7-917-2016.
McPherson, R. A. (2013). “High-Resolution Surface Observations for Climate Monitoring,” in *Climate Variability - Regional and Thematic Patterns* (InTech). doi:10.5772/56044.
McSweeney, C. F., Jones, R. G., Lee, R. W., and Rowell, D. P. (2015). Selecting CMIP5 GCMs for downscaling over multiple regions. *Clim. Dyn.* 44, 3237–3260. doi:10.1007/s00382-014-2418-8.
Mearns, L. O., Arritt, R., Biner, S., Bukovsky, M. S., McGinnis, S., Sain, S., et al. (2012). The North American Regional Climate Change Assessment Program. *Bull. Am. Meteorol. Soc.* 93, 1337–1362. doi:10.1175/BAMS-D-11-00223.1.
Mearns, L. O., Sain, S., Leung, L. R., Bukovsky, M. S., McGinnis, S., Biner, S., et al. (2013). Climate change projections of the North American Regional Climate Change Assessment Program (NARCCAP). *Clim. Change* 120. doi:10.1007/s10584-013-0831-3.
Meehl, G. A., Hu, A., Arblaster, J. M., Fasullo, J., and Trenberth, K. E. (2013). Externally Forced and Internally Generated Decadal Climate Variability Associated with the Interdecadal Pacific Oscillation. *J. Clim.* 26, 7298–7310. doi:10.1175/JCLI-D-12-00548.1.
Meher, J. K., Das, L., Benestad, R. E., and Mezghani, A. (2018). Analysis of winter rainfall change statistics over the Western Himalaya: the influence of internal variability and topography. *Int. J. Climatol.* 38, e475–e496. doi:10.1002/joc.5385.
Mehrotra, R., Evans, J. P., Sharma, A., and Sivakumar, B. (2014). Evaluation of downscaled daily rainfall hindcasts over Sydney, Australia using statistical and dynamical downscaling approaches. *Hydrol. Res.* 45, 226–249. doi:10.2166/nh.2013.094.
Meier, F., Fenner, D., Grassmann, T., Otto, M., and Scherer, D. (2017). Crowdsourcing air temperature from citizen weather stations for urban climate research. *Urban Clim.* 19, 170–191. doi:https://doi.org/10.1016/j.uclim.2017.01.006.
Meinke, H., Nelson, R., Kokic, P., Stone, R., and Selvaraju, R. (2006). Actionable climate knowledge: from analysis to synthesis. *Clim. Res.* 33, 101–110. doi:10.3354/cr033101.

Menary, M. B., Kuhlbrodt, T., Ridley, J., Andrews, M. B., Dimdore-Miles, O. B., Deshayes, J., et al. (2018). Preindustrial Control Simulations With HadGEM3-GC3.1 for CMIP6. *J. Adv. Model. Earth Syst.* 10, 3049–3075. doi:10.1029/2018MS001495.

Méndez-Lázaro, P. A., Nieves-Santiago, A., and Miranda, J. (2014). Trends in total rainfall , heavy rain events , and number of dry days in San Juan, Puerto Rico, 1955-2009. *Ecol. Soc.* 19. doi:10.5751/ES-06464-190250.

Mendlik, T., and Gobiet, A. (2016). Selecting climate simulations for impact studies based on multivariate patterns of climate change. *Clim. Change* 135, 381–393. doi:10.1007/s10584-015-1582-0.

Ménégoz, M., Bilbao, R., Bellprat, O., Guemas, V., and Doblas-Reyes, F. J. (2018a). Forecasting the climate response to volcanic eruptions: prediction skill related to stratospheric aerosol forcing. *Environ. Res. Lett.* 13, 64022. doi:10.1088/1748-9326/aac4db.

Ménégoz, M., Cassou, C., Swingedouw, D., Ruprich-Robert, Y., Bretonnière, P.-A., and Doblas-Reyes, F. (2018b). Role of the Atlantic Multidecadal Variability in modulating the climate response to a Pinatubo-like volcanic eruption. *Clim. Dyn.* 51, 1863–1883. doi:10.1007/s00382-017-3986-1.

Menne, M. J., Williams, C. N., Gleason, B. E., Rennie, J. J., and Lawrimore, J. H. (2018). The Global Historical Climatology Network Monthly Temperature Dataset, Version 4. *J. Clim.* 31, 9835–9854. doi:10.1175/JCLI-D-18-0094.1.

Merchant, C. J., Paul, F., Popp, T., Ablain, M., Bontemps, S., Defourny, P., et al. (2017). Uncertainty information in climate data records from Earth observation. *Earth Syst. Sci. Data* 9, 511–527. doi:10.5194/essd-9-511-2017.

Meredith, E. P., Maraun, D., Semenov, V. A., and Park, W. (2015a). Evidence for added value of convection-permitting models for studying changes in extreme precipitation. *J. Geophys. Res. Atmos.* 120, 12500–12513. doi:10.1002/2015JD024238.

Meredith, E. P., Semenov, V. A., Maraun, D., Park, W., and Chernokulsky, A. V. (2015b). Crucial role of Black Sea warming in amplifying the 2012 Krymsk precipitation extreme. *Nat. Geosci.* 8, 615–619. doi:10.1038/ngeo2483.

Mestre, O., Gruber, C., Prieur, C., Caussinus, H., and Jourdain, S. (2011). SPLIDHOM: A Method for Homogenization of Daily Temperature Observations. *J. Appl. Meteorol. Climatol.* 50, 2343–2358. doi:10.1175/2011JAMC2641.1.

Mezghani, A., and Hingray, B. (2009). A combined downscaling-disaggregation weather generator for stochastic generation of multisite hourly weather variables over complex terrain: Development and multi-scale validation for the Upper Rhone River basin. *J. Hydrol.* 377, 245–260. doi:10.1016/j.jhydrol.2009.08.033.

Michel, S., Swingedouw, D., Chavent, M., Ortega, P., Mignot, J., and Khodri, M. (2018). Reconstructing climatic modes of variability from proxy records: sensitivity to the methodological approach. *Geosci. Model Dev. Discuss.* 2018, 1–48. doi:10.5194/gmd-2018-211.

Migliavacca, M., Dosio, A., Camia, A., Hobourg, R., Houston-Durrant, T., Kaiser, J. W., et al. (2013). Modeling biomass burning and related carbon emissions during the 21st century in Europe. *J. Geophys. Res. Biogeosciences* 118, 1732–1747. doi:10.1002/2013JG002444.

Miller, R. L., Knippertz, P., Pérez García-Pando, C., Perlwitz, J. P., and Tegen, I. (2014). "Impact of dust radiative forcing upon climate BT - Mineral Dust: A Key Player in the Earth System," in, eds. P. Knippertz and J.-B. W. Stuut (Dordrecht, the Netherlands: Springer), 327–357. doi:10.1007/978-94-017-8978-3_13.

Minder, J. R., Letcher, T. W., and Skiles, S. M. (2016). An evaluation of high-resolution regional climate model simulations of snow cover and albedo over the Rocky Mountains, with implications for the simulated snow-albedo feedback. *J. Geophys. Res. Atmos.* 121, 9069–9088. doi:10.1002/2016JD024995.

Mindlin, J., Shepherd, T. G., Vera, C. S., Osman, M., Zappa, G., Lee, R. W., et al. (submitted). Storyline description of Southern Hemisphere midlatitude circulation and precipitation response to greenhouse gas forcing. *Clim. Dyn.* (submitted).

Ming, Y., and Ramaswamy, V. (2011). A Model Investigation of Aerosol-Induced Changes in Tropical Circulation. *J. Clim.* 24, 5125–5133. doi:10.1175/2011JCLI4108.1.

Miralles, D. G., Teuling, A. J., van Heerwaarden, C. C., and Vilà-Guerau de Arellano, J. (2014). Mega-heatwave temperatures due to combined soil desiccation and atmospheric heat accumulation. *Nat. Geosci.* 7, 345. doi:10.1038/ngeo2141.

Mironov, D., Heise, E., Kourzeneva, E., Ritter, B., Schneider, N., and Terzhevik, A. (2010). Implementation of the lake parameterisation scheme FLake into numerical weather prediction model COSMO. *Boreal Environ. Res.* 15, 218–230.

Mishra, V. (2015). Climatic uncertainty in Himalayan water towers. *J. Geophys. Res. Atmos.* 120, 2689–2705. doi:10.1002/2014JD022650.

Mizuta, R., Murata, A., Ishii, M., Shiogama, H., Hibino, K., Mori, N., et al. (2017). Over 5,000 Years of Ensemble Future Climate Simulations by 60-km Global and 20-km Regional Atmospheric Models. *Bull. Am. Meteorol. Soc.* 98, 1383–1398. doi:10.1175/BAMS-D-16-0099.1.

MJO Working Group (2009). MJO Simulation Diagnostics. *J. Clim.* 22, 3006–3030. doi:10.1175/2008JCLI2731.1.

Moezzi, M., Janda, K. B., and Rotmann, S. (2017). Using stories, narratives, and storytelling in energy and climate change research. *Energy Res. Soc. Sci.* 31, 1–10. doi:https://doi.org/10.1016/j.erss.2017.06.034.

Mohino, E., Keenlyside, N., and Pohlmann, H. (2016). Decadal prediction of Sahel rainfall: where does the skill (or lack thereof) come from? *Clim. Dyn.* 47, 3593–3612. doi:10.1007/s00382-016-3416-9.

Monerie, P.-A., Robson, J., Dong, B., Hodson, D. L. R., and Klingaman, N. P. (2019). Effect of the Atlantic Multidecadal Variability on the Global Monsoon. *Geophys. Res. Lett.* 46, 1765–1775. doi:10.1029/2018GL080903.
Monerie, P. A., Robson, J., Dong, B., and Dunstone, N. (2018). A role of the Atlantic Ocean in predicting summer surface air temperature over North East Asia? *Clim. Dyn.* 51, 473–491. doi:10.1007/s00382-017-3935-z.
Montroull, N. B., Saurral, R. I., and Camilloni, I. A. (2018). Hydrological impacts in La Plata basin under 1.5, 2 and 3 °C global warming above the pre-industrial level. *Int. J. Climatol.* 38, 3355–3368. doi:10.1002/joc.5505.
Mori, M., Kosaka, Y., Watanabe, M., Nakamura, H., and Kimoto, M. (2019a). A reconciled estimate of the influence of Arctic sea-ice loss on recent Eurasian cooling. *Nat. Clim. Chang.* 9, 123–129. doi:10.1038/s41558-018-0379-3.
Mori, M., Kosaka, Y., Watanabe, M., Taguchi, B., Nakamura, H., and Kimoto, M. (2019b). Reply to: Is sea-ice-driven Eurasian cooling too weak in models? *Nat. Clim. Chang.* 9, 937–939. doi:10.1038/s41558-019-0636-0.
Mori, M., Watanabe, M., Shiogama, H., Inoue, J., and Kimoto, M. (2014). Robust Arctic sea-ice influence on the frequent Eurasian cold winters in past decades. *Nat. Geosci.* 7, 869–873. doi:10.1038/ngeo2277.
Morice, C. P., Kennedy, J. J., Rayner, N. A., and Jones, P. D. (2012). Quantifying uncertainties in global and regional temperature change using an ensemble of observational estimates: The HadCRUT4 data set. *J. Geophys. Res. Atmos.* 117. doi:10.1029/2011JD017187.
Morrill, C., Lowry, D. P., and Hoell, A. (2018). Thermodynamic and Dynamic Causes of Pluvial Conditions During the Last Glacial Maximum in Western North America. *Geophys. Res. Lett.* 45, 335–345. doi:10.1002/2017GL075807.
Morton, T. A., Rabinovich, A., Marshall, D., and Bretschneider, P. (2011). The future that may (or may not) come: How framing changes responses to uncertainty in climate change communications. *Glob. Environ. Chang.* 21, 103–109. doi:10.1016/j.gloenvcha.2010.09.013.
Moss, R. H. (2016). Assessing decision support systems and levels of confidence to narrow the climate information "usability gap." *Clim. Change* 135, 143–155. doi:10.1007/s10584-015-1549-1.
Mueller, N. D., Gerber, J. S., Johnston, M., Ray, D. K., Ramankutty, N., and Foley, J. A. (2012). Closing yield gaps through nutrient and water management. *Nature* 490, 254–257. doi:10.1038/nature11420.
Muerth, M. J., Gauvin St-Denis, B., Ricard, S., Velázquez, J. A., Schmid, J., Minville, M., et al. (2013). On the need for bias correction in regional climate scenarios to assess climate change impacts on river runoff. *Hydrol. Earth Syst. Sci.* 17, 1189–1204. doi:10.5194/hess-17-1189-2013.
Mukheibir, P., and Ziervogel, G. (2007). Developing a Municipal Adaptation Plan (MAP) for climate change: the city of Cape Town. *Environ. Urban.* 19, 143–158. doi:10.1177/0956247807076912.
Muller, C. L., Chapman, L., Grimmond, C. S. B., Young, D. T., and Cai, X. (2013). Sensors and the city: a review of urban meteorological networks. *Int. J. Climatol.* 33, 1585–1600. doi:10.1002/joc.3678.
Muller, C. L., Chapman, L., Johnston, S., Kidd, C., Illingworth, S., Foody, G., et al. (2015). Crowdsourcing for climate and atmospheric sciences: current status and future potential. *Int. J. Climatol.* 35, 3185–3203. doi:10.1002/joc.4210.
Muller, M. (2018). Cape Town's drought: don't blame climate change. *Nature* 559, 174–176. doi:10.1038/d41586-018-05649-1.
Mulwa, C., Marenya, P., Rahut, D. B., and Kassie, M. (2017). Response to climate risks among smallholder farmers in Malawi: A multivariate probit assessment of the role of information, household demographics, and farm characteristics. *Clim. Risk Manag.* 16, 208–221. doi:10.1016/j.crm.2017.01.002.
Mundhenk, B. D., Barnes, E. A., and Maloney, E. D. (2016). All-Season Climatology and Variability of Atmospheric River Frequencies over the North Pacific. *J. Clim.* 29, 4885–4903. doi:10.1175/JCLI-D-15-0655.1.
Muñoz, A. G., Goddard, L., Robertson, A. W., Kushnir, Y., and Baethgen, W. (2015). Cross-time scale interactions and rainfall extreme events in southeastern South America for the austral summer. Part I: Potential predictors. *J. Clim.* 28, 7894–7913. doi:10.1175/JCLI-D-14-00693.1.
Myhre, G., Samset, B. H., Schulz, M., Balkanski, Y., Bauer, S., Berntsen, T. K., et al. (2013). Radiative forcing of the direct aerosol effect from AeroCom Phase II simulations. *Atmos. Chem. Phys.* 13, 1853–1877. doi:10.5194/acp-13-1853-2013.
Nabat, P., Somot, S., Mallet, M., Michou, M., Sevault, F., Driouech, F., et al. (2015). Dust aerosol radiative effects during summer 2012 simulated with a coupled regional aerosol–atmosphere–ocean model over the Mediterranean. *Atmos. Chem. Phys.* 15, 3303–3326. doi:10.5194/acp-15-3303-2015.
Nabat, P., Somot, S., Mallet, M., Sanchez-Lorenzo, A., and Wild, M. (2014). Contribution of anthropogenic sulfate aerosols to the changing Euro-Mediterranean climate since 1980. *Geophys. Res. Lett.* 41, 5605–5611. doi:10.1002/2014GL060798.
Nakamura, T., Yamazaki, K., Iwamoto, K., Honda, M., Miyoshi, Y., Ogawa, Y., et al. (2015). A negative phase shift of the winter AO/NAO due to the recent Arctic sea-ice reduction in late autumn. *J. Geophys. Res. Atmos.* 120, 3209–3227. doi:10.1002/2014JD022848.
Naranjo-Diaz, L. R., and Centella, A. (1998). Recent trends in the climate of Cuba. *Weather* 53, 78–85. doi:10.1002/j.1477-8696.1998.tb03964.x.
Nath, R., Luo, Y., and Chen, W. (2019). Future projection of summer surface air temperature trend over central India:

Role of external forcing and internal variability. *Int. J. Climatol.*, 1–11. doi:10.1002/joc.6258.
Nath, R., Luo, Y., Chen, W., and Cui, X. (2018). On the contribution of internal variability and external forcing factors to the Cooling trend over the Humid Subtropical Indo-Gangetic Plain in India. *Sci. Rep.* 8, 18047. doi:10.1038/s41598-018-36311-5.
Nazemi, A., and Wheater, H. S. (2015). On inclusion of water resource management in Earth system models – Part 1: Problem definition and representation of water demand. *Hydrol. Earth Syst. Sci.* 19, 33–61. doi:10.5194/hess-19-33-2015.
Neelin, J. D., Chou, C., and Su, H. (2003). Tropical drought regions in global warming and El Niño teleconnections. *Geophys. Res. Lett.* 30, 1–4. doi:10.1029/2003GL018625.
Neelin, J. D., Münnich, M., Su, H., Meyerson, J. E., and Holloway, C. E. (2006). Tropical drying trends in global warming models and observations. *Proc. Natl. Acad. Sci. U. S. A.* 103, 6110–6115. doi:10.1073/pnas.0601798103.
Nelson, B. R., Prat, O. P., Seo, D.-J., and Habib, E. (2016). Assessment and Implications of NCEP Stage IV Quantitative Precipitation Estimates for Product Intercomparisons. *Weather Forecast.* 31, 371–394. doi:10.1175/waf-d-14-00112.1.
Nengker, T., Choudhary, A., and Dimri, A. P. (2018). Assessment of the performance of CORDEX-SA experiments in simulating seasonal mean temperature over the Himalayan region for the present climate: Part I. *Clim. Dyn.* 50, 2411–2441. doi:10.1007/s00382-017-3597-x.
Neu, U., Akperov, M. G., Bellenbaum, N., Benestad, R., Blender, R., Caballero, R., et al. (2013). IMILAST: A Community Effort to Intercompare Extratropical Cyclone Detection and Tracking Algorithms. *Bull. Am. Meteorol. Soc.* 94, 529–547. doi:10.1175/BAMS-D-11-00154.1.
Neukom, R., Steiger, N., Gómez-Navarro, J. J., Wang, J., and Werner, J. P. (2019). No evidence for globally coherent warm and cold periods over the preindustrial Common Era. *Nature* 571, 550–554. doi:10.1038/s41586-019-1401-2.
New, M., Todd, M., Hulme, M., and Jones, P. (2001). PRECIPITATION MEASUREMENTS AND TRENDS IN THE TWENTIETH CENTURY. *Int. J. Climatol.* 21, 1899–1922. doi:10.1002/joc.680.
Nguyen, P., Shearer, E. J., Tran, H., Ombadi, M., Hayatbini, N., Palacios, T., et al. (2019). The CHRS Data Portal, an easily accessible public repository for PERSIANN global satellite precipitation data. *Sci. Data* 6, 180296. doi:10.1038/sdata.2018.296.
Nicholson, S. E. (2013). The West African Sahel: A Review of Recent Studies on the Rainfall Regime and Its Interannual Variability. *ISRN Meteorol.* 2013, 1–32. doi:10.1155/2013/453521.
Nigam, S., and Bollasina, M. (2010). "Elevated heat pump" hypothesis for the aerosol-monsoon hydroclimate link: "Grounded" in observations? *J. Geophys. Res.* 115, D16201. doi:10.1029/2009JD013800.
Nikiema, P. M., Sylla, M. B., Ogunjobi, K., Kebe, I., Gibba, P., and Giorgi, F. (2017). Multi-model CMIP5 and CORDEX simulations of historical summer temperature and precipitation variabilities over West Africa. *Int. J. Climatol.* 37, 2438–2450. doi:10.1002/joc.4856.
Nikulin, G., Asharaf, S., Magariño, M. E., Calmanti, S., Cardoso, R. M., Bhend, J., et al. (2018). Dynamical and statistical downscaling of a global seasonal hindcast in eastern Africa. *Clim. Serv.* 9, 72–85. doi:10.1016/j.cliser.2017.11.003.
Nikulin, G., Jones, C., Giorgi, F., Asrar, G., Büchner, M., Cerezo-Mota, R., et al. (2012). Precipitation Climatology in an Ensemble of CORDEX-Africa Regional Climate Simulations. *J. Clim.* 25, 6057–6078. doi:10.1175/JCLI-D-11-00375.1.
Nitu, R., Roulet, Y., Wolff, M., Earle, M., Reverdin, A., Smith, C., et al. (2018). WMO Solid Precipitation Intercomparison Experiment (SPICE) (2012 - 2015).
Nosetto, M. D., Paez, R. A., Ballesteros, S. I., and Jobbágy, E. G. (2015). Higher water-table levels and flooding risk under grain vs. livestock production systems in the subhumid plains of the Pampas. *Agric. Ecosyst. Environ.* 206, 60–70. doi:10.1016/j.agee.2015.03.009.
Notaro, M., Holman, K., Zarrin, A., Fluck, E., Vavrus, S., and Bennington, V. (2013). Influence of the Laurentian Great Lakes on Regional Climate*. *J. Clim.* 26, 789–804. doi:10.1175/JCLI-D-12-00140.1.
Notz, D. (2015). How well must climate models agree with observations? *Philos. Trans. R. Soc. A Math. Phys. Eng. Sci.* 373, 20140164. doi:10.1098/rsta.2014.0164.
O'Higgins, T., Nogueira, A. A., and Lillebø, A. I. (2019). A simple spatial typology for assessment of complex coastal ecosystem services across multiple scales. *Sci. Total Environ.* 649, 1452–1466. doi:10.1016/j.scitotenv.2018.08.420.
O'Reilly, C. H., Minobe, S., and Kuwano-Yoshida, A. (2016). The influence of the Gulf Stream on wintertime European blocking. *Clim. Dyn.* 47, 1545–1567. doi:10.1007/s00382-015-2919-0.
O'Reilly, C. H., Woollings, T., and Zanna, L. (2017). The Dynamical Influence of the Atlantic Multidecadal Oscillation on Continental Climate. *J. Clim.* 30, 7213–7230. doi:10.1175/JCLI-D-16-0345.1.
O, S., and Foelsche, U. (2018). Assessment of spatial uncertainty of heavy local rainfall using a dense gauge network. *Hydrol. Earth Syst. Sci. Discuss.*, 1–21. doi:10.5194/hess-2018-517.
Obermann, A., Bastin, S., Belamari, S., Conte, D., Gaertner, M. A., Li, L., et al. (2018). Mistral and Tramontane wind

speed and wind direction patterns in regional climate simulations. *Clim. Dyn.* 51, 1059–1076. doi:10.1007/s00382-016-3053-3.

Ochsner, T. E., Cosh, M. H., Cuenca, R. H., Dorigo, W. A., Draper, C. S., Hagimoto, Y., et al. (2013). State of the Art in Large-Scale Soil Moisture Monitoring. *Soil Sci. Soc. Am. J.* 77, 1888. doi:10.2136/sssaj2013.03.0093.

Ogawa, F., Keenlyside, N., Gao, Y., Koenigk, T., Yang, S., Suo, L., et al. (2018). Evaluating Impacts of Recent Arctic Sea Ice Loss on the Northern Hemisphere Winter Climate Change. *Geophys. Res. Lett.* 45, 3255–3263. doi:10.1002/2017GL076502.

Okamoto, K. i., Ushio, T., Iguchi, T., Takahashi, N., and Iwanami, K. (2005). The global satellite mapping of precipitation (GSMaP) project. in *Proceedings. 2005 IEEE International Geoscience and Remote Sensing Symposium, 2005. IGARSS '05.* (IEEE), 3414–3416. doi:10.1109/IGARSS.2005.1526575.

Oke, T. R., Mills, G., Christen, A., and Voogt, J. A. (2017). *Urban Climates*. Cambridge: Cambridge University Press doi:10.1017/9781139016476.

Oleson, K. (2012). Contrasts between Urban and rural climate in CCSM4 CMIP5 climate change scenarios. *J. Clim.* 25, 1390–1412. doi:10.1175/JCLI-D-11-00098.1.

Oleson, K. W., Bonan, G. B., Feddema, J., and Jackson, T. (2011). An examination of urban heat island characteristics in a global climate model. *Int. J. Climatol.* 31, 1848–1865. doi:10.1002/joc.2201.

Olonscheck, D., Mauritsen, T., and Notz, D. (2019). Arctic sea-ice variability is primarily driven by atmospheric temperature fluctuations. *Nat. Geosci.* 12, 430–434. doi:10.1038/s41561-019-0363-1.

Olonscheck, D., and Notz, D. (2017). Consistently Estimating Internal Climate Variability from Climate Model Simulations. *J. Clim.* 30, 9555–9573. doi:10.1175/JCLI-D-16-0428.1.

Orlanski, I. (1975). A Rational Subdivision of Scales for Atmospheric Processes. *Bull. Am. Meteorol. Soc.* 56, 527–530. Available at: http://www.jstor.org/stable/26216020.

Ortega, P., Lehner, F., Swingedouw, D., Masson-Delmotte, V., Raible, C. C., Casado, M., et al. (2015). A model-tested North Atlantic Oscillation reconstruction for the past millennium. *Nature* 523, 71–74. doi:10.1038/nature14518.

Osborn, T. J., and Jones, P. D. (2014). The CRUTEM4 land-surface air temperature data set: construction, previous versions and dissemination via Google Earth. *Earth Syst. Sci. Data* 6, 61–68. doi:10.5194/essd-6-61-2014.

Otto, F. E. L., Haustein, K., Uhe, P., Coelho, C. A. S., Aravequia, J. A., Almeida, W., et al. (2015). Factors Other Than Climate Change, Main Drivers of 2014/15 Water Shortage in Southeast Brazil. *Bull. Am. Meteorol. Soc.* 96, S35–S40. doi:10.1175/BAMS-D-15-00120.1.

Otto, F. E. L., van Oldenborgh, G. J., Eden, J., Stott, P. A., Karoly, D. J., and Allen, M. R. (2016a). The attribution question. *Nat. Clim. Chang.* 6, 813–816. doi:10.1038/nclimate3089.

Otto, F. E. L., Wolski, P., Lehner, F., Tebaldi, C., van Oldenborgh, G. J., Hogesteeger, S., et al. (2018). Anthropogenic influence on the drivers of the Western Cape drought 2015–2017. *Environ. Res. Lett.* 13, 124010. doi:10.1088/1748-9326/aae9f9.

Otto, J., Brown, C., Buontempo, C., Doblas-Reyes, F., Jacob, D., Juckes, M., et al. (2016b). Uncertainty: Lessons Learned for Climate Services. *Bull. Am. Meteorol. Soc.* 97, ES265–ES269. doi:10.1175/BAMS-D-16-0173.1.

Oueslati, B., and Bellon, G. (2015). The double ITCZ bias in CMIP5 models: interaction between SST, large-scale circulation and precipitation. *Clim. Dyn.* 44, 585–607. doi:10.1007/s00382-015-2468-6.

Overland, J. E. (2016). A difficult Arctic science issue: Midlatitude weather linkages. *Polar Sci.* 10, 210–216. doi:10.1016/j.polar.2016.04.011.

Overland, J. E., Dethloff, K., Francis, J. A., Hall, R. J., Hanna, E., Kim, S.-J., et al. (2016). Nonlinear response of mid-latitude weather to the changing Arctic. *Nat. Clim. Chang.* 6, 992–999. doi:10.1038/nclimate3121.

Overland, J., Francis, J. A., Hall, R., Hanna, E., Kim, S.-J., and Vihma, T. (2015). The Melting Arctic and Midlatitude Weather Patterns: Are They Connected?*. *J. Clim.* 28, 7917–7932. doi:10.1175/JCLI-D-14-00822.1.

Oyler, J. W., Ballantyne, A., Jencso, K., Sweet, M., and Running, S. W. (2015). Creating a topoclimatic daily air temperature dataset for the conterminous United States using homogenized station data and remotely sensed land skin temperature. *Int. J. Climatol.* 35, 2258–2279. doi:10.1002/joc.4127.

Ozturk, T., Turp, M. T., Türkeş, M., and Kurnaz, M. L. (2018). Future projections of temperature and precipitation climatology for CORDEX-MENA domain using RegCM4.4. *Atmos. Res.* 206, 87–107. doi:10.1016/j.atmosres.2018.02.009.

Paegle, J. N., and Mo, K. C. (2002). Linkages between Summer Rainfall Variability over South America and Sea Surface Temperature Anomalies. *J. Clim.* 15, 1389–1407. doi:10.1175/1520-0442(2002)015<1389:LBSRVO>2.0.CO;2.

Pai, D. S., Sridhar, L., Badwaik, M. R., and Rajeevan, M. (2015). Analysis of the daily rainfall events over India using a new long period (1901–2010) high resolution (0.25° × 0.25°) gridded rainfall data set. *Clim. Dyn.* 45, 755–776. doi:10.1007/s00382-014-2307-1.

Pai, D. S., Sridhar, L., Rajeevan, M., Sreejith, O. P., Satbhai, N. S., and Mukhopadhyay, B. (2014). Development of a new high spatial resolution (0.25° × 0.25°) long period (1901-2010) daily gridded rainfall data set over India and its comparison with existing data sets over the region. *Mausam* 65, 1–18.

Palazzi, E., Von Hardenberg, J., and Provenzale, A. (2013). Precipitation in the hindu-kush karakoram himalaya: Observations and future scenarios. *J. Geophys. Res. Atmos.* 118, 85–100. doi:10.1029/2012JD018697.

Pall, P., Patricola, C. M., Wehner, M. F., Stone, D. A., Paciorek, C. J., and Collins, W. D. (2017). Diagnosing conditional anthropogenic contributions to heavy Colorado rainfall in September 2013. *Weather Clim. Extrem.* 17, 1–6. doi:10.1016/j.wace.2017.03.004.
Palmer, T. N. (2016). A personal perspective on modelling the climate system. *Proc. R. Soc. A Math. Phys. Eng. Sci.* 472, 20150772. doi:10.1098/rspa.2015.0772.
Pandey, A., Patel, S., Pervez, S., Tiwari, S., Yadama, G., Chow, J. C., et al. (2017). Aerosol emissions factors from traditional biomass cookstoves in India: insights from field measurements. *Atmos. Chem. Phys.* 17, 13721–13729. doi:10.5194/acp-17-13721-2017.
Panthou, G., Lebel, T., Vischel, T., Quantin, G., Sane, Y., Ba, A., et al. (2018a). Rainfall intensification in tropical semi-arid regions: the Sahelian case. *Environ. Res. Lett.* 13, 064013. doi:10.1088/1748-9326/aac334.
Panthou, G., Vischel, T., and Lebel, T. (2014). Recent trends in the regime of extreme rainfall in the Central Sahel. *Int. J. Climatol.* 34, 3998–4006. doi:10.1002/joc.3984.
Panthou, G., Vrac, M., Drobinski, P., Bastin, S., and Li, L. (2018b). Impact of model resolution and Mediterranean sea coupling on hydrometeorological extremes in RCMs in the frame of HyMeX and MED-CORDEX. *Clim. Dyn.* 51, 915–932. doi:10.1007/s00382-016-3374-2.
Panziera, L., Gabella, M., Germann, U., and Martius, O. (2018). A 12-year radar-based climatology of daily and sub-daily extreme precipitation over the Swiss Alps. *Int. J. Climatol.* 38, 3749–3769. doi:10.1002/joc.5528.
Park, B.-J., Kim, Y.-H., Min, S.-K., Kim, M.-K., Choi, Y., Boo, K.-O., et al. (2017). Long-Term Warming Trends in Korea and Contribution of Urbanization: An Updated Assessment. *J. Geophys. Res. Atmos.* 122, 10,610-637,654. doi:10.1002/2017JD027167.
Park, D.-S. R., Lee, S., and Feldstein, S. B. (2015a). Attribution of the Recent Winter Sea Ice Decline over the Atlantic Sector of the Arctic Ocean*. *J. Clim.* 28, 4027–4033. doi:10.1175/JCLI-D-15-0042.1.
Park, J.-Y., Bader, J., and Matei, D. (2015b). Northern-hemispheric differential warming is the key to understanding the discrepancies in the projected Sahel rainfall. *Nat. Commun.* 6, 5985. doi:10.1038/ncomms6985.
Park, J. Y., Bader, J., and Matei, D. (2016). Anthropogenic Mediterranean warming essential driver for present and future Sahel rainfall. *Nat. Clim. Chang.* doi:10.1038/nclimate3065.
Parker, D. E. (1994). Effects of changing exposure of thermometers at land stations. *Int. J. Climatol.* 14, 1–31. doi:10.1002/joc.3370140102.
Parker, D. E. (2006). A Demonstration That Large-Scale Warming Is Not Urban. *J. Clim.* 19, 2882–2895. doi:10.1175/JCLI3730.1.
Parker, D. E. (2010). Urban heat island effects on estimates of observed climate change. *WIREs Clim. Chang.* 1, 123–133. doi:10.1002/wcc.21.
Parker, W. S. (2009). II–Confirmation and Adequacy-for-Purpose in Climate Modelling. *Aristot. Soc. Suppl. Vol.* 83, 233–249. doi:10.1111/j.1467-8349.2009.00180.x.
Parker, W. S., and Lusk, G. (2019). Incorporating User Values into Climate Services. *Bull. Am. Meteorol. Soc.* 100, 1643–1650. doi:10.1175/BAMS-D-17-0325.1.
Parsons, S., Renwick, J. A., and McDonald, A. J. (2016). An Assessment of Future Southern Hemisphere Blocking Using CMIP5 Projections from Four GCMs. *J. Clim.* 29, 7599–7611. doi:10.1175/JCLI-D-15-0754.1.
Patil, N., Venkataraman, C., Muduchuru, K., Ghosh, S., and Mondal, A. (2019). Disentangling sea-surface temperature and anthropogenic aerosol influences on recent trends in South Asian monsoon rainfall. *Clim. Dyn.* 52, 2287–2302. doi:10.1007/s00382-018-4251-y.
Patricola, C. M., and Wehner, M. F. (2018). Anthropogenic influences on major tropical cyclone events. *Nature* 563, 339–346. doi:10.1038/s41586-018-0673-2.
Patterson, M., Bracegirdle, T., and Woollings, T. (2019). Southern Hemisphere Atmospheric Blocking in CMIP5 and Future Changes in the Australia-New Zealand Sector. *Geophys. Res. Lett.* 46, 9281–9290. doi:10.1029/2019GL083264.
Paul, S., Ghosh, S., Oglesby, R., Pathak, A., Chandrasekharan, A., and Ramsankaran, R. (2016). Weakening of Indian Summer Monsoon Rainfall due to Changes in Land Use Land Cover. *Sci. Rep.* 6. doi:10.1038/srep32177.
Pausata, F. S. R., Chafik, L., Caballero, R., and Battisti, D. S. (2015). Impacts of high-latitude volcanic eruptions on ENSO and AMOC. *Proc. Natl. Acad. Sci.* 112, 13784–13788. doi:10.1073/pnas.1509153112.
Pedro, J. B., Martin, T., Steig, E. J., Jochum, M., Park, W., and Rasmussen, S. O. (2016). Southern Ocean deep convection as a driver of Antarctic warming events. *Geophys. Res. Lett.* 43, 2192–2199. doi:10.1002/2016GL067861.
Peings, Y. (2019). Ural Blocking as a Driver of Early-Winter Stratospheric Warmings. *Geophys. Res. Lett.* 46, 5460–5468. doi:10.1029/2019GL082097.
Peings, Y., Cattiaux, J., Vavrus, S. J., and Magnusdottir, G. (2018). Projected squeezing of the wintertime North-Atlantic jet. *Environ. Res. Lett.* 13, 074016. doi:10.1088/1748-9326/aacc79.
Peings, Y., Douville, H., Colin, J., Martin, D. Saint, and Magnusdottir, G. (2017). Snow–(N)AO Teleconnection and Its Modulation by the Quasi-Biennial Oscillation. *J. Clim.* 30, 10211–10235. doi:10.1175/JCLI-D-17-0041.1.
Peings, Y., and Magnusdottir, G. (2014). Response of the Wintertime Northern Hemisphere Atmospheric Circulation to Current and Projected Arctic Sea Ice Decline: A Numerical Study with CAM5. *J. Clim.* 27, 244–264.

doi:10.1175/JCLI-D-13-00272.1.
Peña-Ortiz, C., Barriopedro, D., and García-Herrera, R. (2015). Multidecadal Variability of the Summer Length in Europe*. *J. Clim.* 28, 5375–5388. doi:10.1175/JCLI-D-14-00429.1.
Penalba, O. C., and Robledo, F. A. (2010). Spatial and temporal variability of the frequency of extreme daily rainfall regime in the La Plata Basin during the 20th century. *Clim. Change* 98, 531–550. doi:10.1007/s10584-009-9744-6.
Peng, D., Zhou, T., Zhang, L., and Zou, L. (2019). Detecting human influence on the temperature changes in Central Asia. *Clim. Dyn.* 53, 4553–4568. doi:10.1007/s00382-019-04804-2.
Pepin, N., Bradley, R. S., Diaz, H. F., Baraer, M., Caceres, E. B., Forsythe, N., et al. (2015). Elevation-dependent warming in mountain regions of the world. *Nat. Clim. Chang.* 5, 424–430. doi:10.1038/nclimate2563.
Pepler, A., Coutts-Smith, A., and Timbal, B. (2014). The role of East Coast Lows on rainfall patterns and inter-annual variability across the East Coast of Australia. *Int. J. Climatol.* 34, 1011–1021. doi:10.1002/joc.3741.
Pepler, A., Dowdy, A., and Hope, P. (2019). A global climatology of surface anticyclones, their variability, associated drivers and long-term trends. *Clim. Dyn.* 52, 5397–5412. doi:10.1007/s00382-018-4451-5.
Pepler, A. S., Alexander, L. V., Evans, J. P., and Sherwood, S. C. (2017). The influence of topography on midlatitude cyclones on Australia's east coast. *J. Geophys. Res. Atmos.* 122, 9173–9184. doi:10.1002/2017JD027345.
Petoukhov, V., Rahmstorf, S., Petri, S., and Schellnhuber, H. J. (2013). Quasiresonant amplification of planetary waves and recent Northern Hemisphere weather extremes. *Proc. Natl. Acad. Sci.* 110, 5336–5341. doi:10.1073/pnas.1222000110.
Petrie, R. E., Shaffrey, L. C., and Sutton, R. T. (2015). Atmospheric Impact of Arctic Sea Ice Loss in a Coupled Ocean–Atmosphere Simulation*. *J. Clim.* 28, 9606–9622. doi:10.1175/JCLI-D-15-0316.1.
Pettenger, M. E. (2016). *The Social Construction of Climate Change*. Routledge doi:10.4324/9781315552842.
Pfahl, S. (2014). Characterising the relationship between weather extremes in Europe and synoptic circulation features. *Nat. Hazards Earth Syst. Sci.* 14, 1461–1475. doi:10.5194/nhess-14-1461-2014.
Pfahl, S., and Wernli, H. (2012). Quantifying the relevance of atmospheric blocking for co-located temperature extremes in the Northern Hemisphere on (sub-)daily time scales. *Geophys. Res. Lett.* 39, n/a-n/a. doi:10.1029/2012GL052261.
Pfeifer, S., Rechid, D., Reuter, M., Viktor, E., and Jacob, D. (2019). 1.5°, 2°, and 3° global warming: visualizing European regions affected by multiple changes. *Reg. Environ. Chang.* 19, 1777–1786. doi:10.1007/s10113-019-01496-6.
Pfeifroth, U., Bojanowski, J. S., Clerbaux, N., Manara, V., Sanchez-Lorenzo, A., Trentmann, J., et al. (2018). Satellite-based trends of solar radiation and cloud parameters in Europe. *Adv. Sci. Res.* 15, 31–37. doi:10.5194/asr-15-31-2018.
Pham, T. Van, Brauch, J., Früh, B., and Ahrens, B. (2017). Simulation of snowbands in the Baltic Sea area with the coupled atmosphere-ocean-ice model COSMO-CLM/NEMO. *Meteorol. Zeitschrift* 26, 71–82. doi:10.1127/metz/2016/0775.
Pham, T. Van, Brauch, J., Früh, B., and Ahrens, B. (2018). Added decadal prediction skill with the coupled regional climate model COSMO-CLM/NEMO. *Meteorol. Zeitschrift* 27, 391–399. doi:10.1127/metz/2018/0872.
Philip, S., Sparrow, S., Kew, S. F., van der Wiel, K., Wanders, N., Singh, R., et al. (2018). Attributing the 2017 Bangladesh floods from meteorological and hydrological perspectives. *Hydrol. Earth Syst. Sci. Discuss.*, 1–32. doi:10.5194/hess-2018-379.
Philipona, R., Behrens, K., and Ruckstuhl, C. (2009). How declining aerosols and rising greenhouse gases forced rapid warming in Europe since the 1980s. *Geophys. Res. Lett.* 36, L02806. doi:10.1029/2008GL036350.
Philippon, N., Rouault, M., Richard, Y., and Favre, A. (2012). The influence of ENSO on winter rainfall in South Africa. *Int. J. Climatol.* 32, 2333–2347. doi:10.1002/joc.3403.
Piennaar, L., and Boonzaaier, J. (2018). DROUGHT POLICY BRIEF WESTERN CAPE AGRICULTURE. Die Wilgers, South Africa Available at: www.bfap.co.za.
Pierce, D. W., Cayan, D. R., Maurer, E. P., Abatzoglou, J. T., and Hegewisch, K. C. (2015). Improved Bias Correction Techniques for Hydrological Simulations of Climate Change*. *J. Hydrometeorol.* 16, 2421–2442. doi:10.1175/JHM-D-14-0236.1.
Pierce, D. W., Cayan, D. R., and Thrasher, B. L. (2014). Statistical Downscaling Using Localized Constructed Analogs (LOCA). *J. Hydrometeorol.* 15, 2558–2585. doi:10.1175/JHM-D-14-0082.1.
Pietikäinen, J.-P., Markkanen, T., Sieck, K., Jacob, D., Korhonen, J., Räisänen, P., et al. (2018). The regional climate model REMO (v2015) coupled with the 1-D freshwater lake model FLake (v1): Fenno-Scandinavian climate and lakes. *Geosci. Model Dev.* 11, 1321–1342. doi:10.5194/gmd-11-1321-2018.
Pinto, I., Jack, C., and Hewitson, B. (2018). Process-based model evaluation and projections over southern Africa from Coordinated Regional Climate Downscaling Experiment and Coupled Model Intercomparison Project Phase 5 models. *Int. J. Climatol.* 38, 4251–4261. doi:10.1002/joc.5666.
Pinto, J. G., Reyers, M., and Ulbrich, U. (2011). The variable link between PNA and NAO in observations and in multi-century CGCM simulations. *Clim. Dyn.* 36, 337–354. doi:10.1007/s00382-010-0770-x.
Pithan, F., and Mauritsen, T. (2014). Arctic amplification dominated by temperature feedbacks in contemporary climate

models. *Nat. Geosci.* 7, 181–184. doi:10.1038/ngeo2071.
Pithan, F., Shepherd, T. G., Zappa, G., and Sandu, I. (2016). Climate model biases in jet streams, blocking and storm tracks resulting from missing orographic drag. *Geophys. Res. Lett.* 43, 7231–7240. doi:10.1002/2016GL069551.
Plant, R. S., and Yano, J.-I. (2015). *Parameterization of Atmospheric Convection*. IMPERIAL COLLEGE PRESS doi:10.1142/p1005.
Poan, E. D., Gachon, P., Laprise, R., Aider, R., and Dueymes, G. (2018). Investigating added value of regional climate modeling in North American winter storm track simulations. *Clim. Dyn.* 50, 1799–1818. doi:10.1007/s00382-017-3723-9.
Pokhrel, Y. N., Hanasaki, N., Wada, Y., and Kim, H. (2016). Recent progresses in incorporating human land-water management into global land surface models toward their integration into Earth system models. *Wiley Interdiscip. Rev. Water* 3, 548–574. doi:10.1002/wat2.1150.
Polade, S. D., Gershunov, A., Cayan, D. R., Dettinger, M. D., and Pierce, D. W. (2013). Natural climate variability and teleconnections to precipitation over the Pacific-North American region in CMIP3 and CMIP5 models. *Geophys. Res. Lett.* 40, 2296–2301. doi:10.1002/grl.50491.
Polcher, J., Piles, M., Gelati, E., Barella-Ortiz, A., and Tello, M. (2016). Comparing surface-soil moisture from the SMOS mission and the ORCHIDEE land-surface model over the Iberian Peninsula. *Remote Sens. Environ.* 174, 69–81. doi:https://doi.org/10.1016/j.rse.2015.12.004.
Poli, P., Dee, D. P., Saunders, R., John, V. O., Rayer, P., Schulz, J., et al. (2016a). Recent Advances in Satellite Data Rescue. *Bull. Am. Meteorol. Soc.* 98, 1471–1484. doi:10.1175/BAMS-D-15-00194.1.
Poli, P., Hersbach, H., Dee, D. P., Berrisford, P., Simmons, A. J., Vitart, F., et al. (2016b). ERA-20C: An Atmospheric Reanalysis of the Twentieth Century. *J. Clim.* 29, 4083–4097. doi:10.1175/JCLI-D-15-0556.1.
Polk, E. (2018). "Communicating Climate Change: Where Did We Go Wrong, How Can We Do Better?," in *Handbook of Communication for Development and Social Change* (Singapore: Springer Singapore), 1–19. doi:10.1007/978-981-10-7035-8_26-1.
Polson, D., Bollasina, M., Hegerl, G. C., and Wilcox, L. J. (2014). Decreased monsoon precipitation in the Northern Hemisphere due to anthropogenic aerosols. *Geophys. Res. Lett.* 41, 6023–6029. doi:10.1002/2014GL060811.
Polydoros, A., Mavrakou, T., and Cartalis, C. (2018). Quantifying the Trends in Land Surface Temperature and Surface Urban Heat Island Intensity in Mediterranean Cities in View of Smart Urbanization. *Urban Sci.* 2, 16. doi:10.3390/urbansci2010016.
Pontoppidan, M., Kolstad, E. W., Sobolowski, S. P., Sorteberg, A., Liu, C., and Rasmussen, R. (2019). Large-scale regional model biases in the extratropical North Atlantic storm track and impacts on downstream precipitation. *Q. J. R. Meteorol. Soc.*, qj.3588. doi:10.1002/qj.3588.
Pook, M. J., Risbey, J. S., and McIntosh, P. C. (2012). The Synoptic Climatology of Cool-Season Rainfall in the Central Wheatbelt of Western Australia. *Mon. Weather Rev.* 140, 28–43. doi:10.1175/MWR-D-11-00048.1.
Porter, J. J., and Dessai, S. (2017). Mini-me: Why do climate scientists' misunderstand users and their needs? *Environ. Sci. Policy* 77, 9–14. doi:10.1016/j.envsci.2017.07.004.
Prakash, S., Mitra, A. K., Momin, I. M., Rajagopal, E. N., Basu, S., Collins, M., et al. (2015). Seasonal intercomparison of observational rainfall datasets over India during the southwest monsoon season. *Int. J. Climatol.* 35, 2326–2338. doi:10.1002/joc.4129.
Prasanna, V. (2016). Assessment of South Asian Summer Monsoon Simulation in CMIP5-Coupled Climate Models During the Historical Period (1850--2005). *Pure Appl. Geophys.* 173, 1379–1402. doi:10.1007/s00024-015-1126-6.
Prein, A. F., Bukovsky, M. S., Mearns, L. O., Bruyère, C. L., and Done, J. M. (2019). Simulating North American Weather Types With Regional Climate Models. *Front. Environ. Sci.* 7, 36. doi:10.3389/fenvs.2019.00036.
Prein, A. F., and Gobiet, A. (2017). Impacts of uncertainties in European gridded precipitation observations on regional climate analysis. *Int. J. Climatol.* 37, 305–327. doi:10.1002/joc.4706.
Prein, A. F., Gobiet, A., Suklitsch, M., Truhetz, H., Awan, N. K., Keuler, K., et al. (2013a). Added value of convection permitting seasonal simulations. *Clim. Dyn.* 41, 2655–2677. doi:10.1007/s00382-013-1744-6.
Prein, A. F., Gobiet, A., Truhetz, H., Keuler, K., Goergen, K., Teichmann, C., et al. (2016a). Precipitation in the EURO-CORDEX 0.11° and 0.44° simulations: high resolution, high benefits? *Clim. Dyn.* 46, 383–412. doi:10.1007/s00382-015-2589-y.
Prein, A. F., Holland, G. J., Rasmussen, R. M., Clark, M. P., and Tye, M. R. (2016b). Running dry: The U.S. Southwest's drift into a drier climate state. *Geophys. Res. Lett.* 43, 1272–1279. doi:10.1002/2015GL066727.
Prein, A. F., Holland, G. J., Rasmussen, R. M., Done, J., Ikeda, K., Clark, M. P., et al. (2013b). Importance of Regional Climate Model Grid Spacing for the Simulation of Heavy Precipitation in the Colorado Headwaters. *J. Clim.* 26, 4848–4857. doi:10.1175/JCLI-D-12-00727.1.
Prein, A. F., Langhans, W., Fosser, G., Ferrone, A., Ban, N., Goergen, K., et al. (2015). A review on regional convection-permitting climate modeling: Demonstrations, prospects, and challenges. *Rev. Geophys.* 53, 323–361. doi:10.1002/2014RG000475.
Prein, A. F., Liu, C., Ikeda, K., Trier, S. B., Rasmussen, R. M., Holland, G. J., et al. (2017). Increased rainfall volume from future convective storms in the US. *Nat. Clim. Chang.* 7, 880–884. doi:10.1038/s41558-017-0007-7.

Priya, P., Krishnan, R., Mujumdar, M., and Houze, R. A. (2017). Changing monsoon and midlatitude circulation interactions over the Western Himalayas and possible links to occurrences of extreme precipitation. *Clim. Dyn.* 49, 2351–2364. doi:10.1007/s00382-016-3458-z.
Prodhomme, C., Batté, L., Massonnet, F., Davini, P., Bellprat, O., Guemas, V., et al. (2016). Benefits of increasing the model resolution for the seasonal forecast quality in EC-earth. *J. Clim.* 29. doi:10.1175/JCLI-D-16-0117.1.
Prospero, J. M., Ginoux, P., Torres, O., Nicholson, S. E., and Gill, T. E. (2002). ENVIRONMENTAL CHARACTERIZATION OF GLOBAL SOURCES OF ATMOSPHERIC SOIL DUST IDENTIFIED WITH THE NIMBUS 7 TOTAL OZONE MAPPING SPECTROMETER (TOMS) ABSORBING AEROSOL PRODUCT. *Rev. Geophys.* 40, 2–31. doi:10.1029/2000RG000095.
Prudhomme, C., Wilby, R. L., Crooks, S., Kay, A. L., and Reynard, N. S. (2010). Scenario-neutral approach to climate change impact studies: Application to flood risk. *J. Hydrol.* 390, 198–209. doi:10.1016/j.jhydrol.2010.06.043.
Pryor, S. C., and Hahmann, A. N. (2019). "Downscaling Wind," in *Oxford Research Encyclopedia of Climate Science* (Oxford University Press). doi:10.1093/acrefore/9780190228620.013.730.
Pu, B., and Ginoux, P. (2018). How reliable are CMIP5 models in simulating dust optical depth? *Atmos. Chem. Phys.* 18, 12491–12510. doi:10.5194/acp-18-12491-2018.
Purich, A., Cowan, T., Min, S.-K., and Cai, W. (2013). Autumn Precipitation Trends over Southern Hemisphere Midlatitudes as Simulated by CMIP5 Models. *J. Clim.* 26, 8341–8356. doi:10.1175/JCLI-D-13-00007.1.
Qian, C. (2016). Disentangling the urbanization effect, multi-decadal variability, and secular trend in temperature in eastern China during 1909-2010. *Atmos. Sci. Lett.* 17, 177–182. doi:10.1002/asl.640.
Qian, C., and Zhou, T. (2014). Multidecadal variability of North China aridity and its relationship to PDO during 1900-2010. *J. Clim.* 27, 1210–1222. doi:10.1175/JCLI-D-13-00235.1.
Qiao, L., Hong, Y., McPherson, R., Shafer, M., Gade, D., Williams, D., et al. (2014). Climate Change and Hydrological Response in the Trans-State Oologah Lake Watershed–Evaluating Dynamically Downscaled NARCCAP and Statistically Downscaled CMIP3 Simulations with VIC Model. *Water Resour. Manag.* 28, 3291–3305. doi:10.1007/s11269-014-0678-z.
Qin, J., Yang, K., Liang, S., and Guo, X. (2009). The altitudinal dependence of recent rapid warming over the Tibetan Plateau. *Clim. Change* 97, 321. doi:10.1007/s10584-009-9733-9.
Racherla, P. N., Shindell, D. T., and Faluvegi, G. S. (2012). The added value to global model projections of climate change by dynamical downscaling: A case study over the continental U.S. using the GISS-ModelE2 and WRF models. *J. Geophys. Res. Atmos.* 117, D20118. doi:10.1029/2012JD018091.
Rackow, T., Goessling, H. F., Jung, T., Sidorenko, D., Semmler, T., Barbi, D., et al. (2018). Towards multi-resolution global climate modeling with ECHAM6-FESOM. Part II: climate variability. *Clim. Dyn.* 50, 2369–2394. doi:10.1007/s00382-016-3192-6.
Rafael, S., Martins, H., Marta-Almeida, M., Sá, E., Coelho, S., Rocha, A., et al. (2017). Quantification and mapping of urban fluxes under climate change: Application of WRF-SUEWS model to Greater Porto area (Portugal). *Environ. Res.* 155, 321–334. doi:10.1016/j.envres.2017.02.033.
Räisänen, J., and Palmer, T. N. (2001). A probability and decision-model analysis of a multimodel ensemble of climate change simulations. *J. Clim.* 14, 3212–3226. doi:10.1175/1520-0442(2001)014<3212:APADMA>2.0.CO;2.
Rajczak, J., and Schär, C. (2017). Projections of Future Precipitation Extremes Over Europe: A Multimodel Assessment of Climate Simulations. *J. Geophys. Res. Atmos.* 122, 10,773-10,800. doi:10.1002/2017JD027176.
Rajeevan, M., and Bhate, J. (2009). A High Resolution Daily Gridded rainfall dataset (1971–2005) for Mesoscale Meteorological Studies. *Curr. Sci.* 96, 558–562.
Rajeevan, M., Bhate, J., Kale, J. D., and Lal, B. (2006). High resolution daily gridded rainfall data for the Indian region: Analysis of break and active monsoon spells. *Curr. Sci.* doi:10.1007/s12040-007-0019-1.
Ramarao, M. V. S., Krishnan, R., Sanjay, J., and Sabin, T. P. (2015). Understanding land surface response to changing South Asian monsoon in a warming climate. *Earth Syst. Dyn.* 6, 569–582. doi:10.5194/esd-6-569-2015.
Ramos, A. M., Blamey, R. C., Algarra, I., Nieto, R., Gimeno, L., Tomé, R., et al. (2019). From Amazonia to southern Africa: atmospheric moisture transport through low-level jets and atmospheric rivers. *Ann. N. Y. Acad. Sci.* 1436, 217–230. doi:10.1111/nyas.13960.
Rasmijn, L. M., van der Schrier, G., Bintanja, R., Barkmeijer, J., Sterl, A., and Hazeleger, W. (2018). Future equivalent of 2010 Russian heatwave intensified by weakening soil moisture constraints. *Nat. Clim. Chang.* 8, 381–385. doi:10.1038/s41558-018-0114-0.
Rasmussen, R., Baker, B., Kochendorfer, J., Meyers, T., Landolt, S., Fischer, A. P., et al. (2012). How Well Are We Measuring Snow: The NOAA/FAA/NCAR Winter Precipitation Test Bed. *Bull. Am. Meteorol. Soc.* 93, 811–829. doi:10.1175/BAMS-D-11-00052.1.
Räty, O., Räisänen, J., and Ylhäisi, J. S. (2014). Evaluation of delta change and bias correction methods for future daily precipitation: intermodel cross-validation using ENSEMBLES simulations. *Clim. Dyn.* 42, 2287–2303. doi:10.1007/s00382-014-2130-8.
Rauscher, S. A., Giorgi, F., Diffenbaugh, N. S., and Seth, A. (2008). Extension and Intensification of the Meso-American mid-summer drought in the twenty-first century. *Clim. Dyn.* 31, 551–571. doi:10.1007/s00382-007-0359-1.

Rauscher, S. A., Kucharski, F., and Enfield, D. B. (2011). The Role of Regional SST Warming Variations in the Drying of Meso-America in Future Climate Projections *. *J. Clim.* 24, 2003–2016. doi:10.1175/2010JCLI3536.1.
Re, M., and Barros, V. R. (2009). Extreme rainfalls in SE South America. *Clim. Change* 96, 119–136. doi:10.1007/s10584-009-9619-x.
Reason, C. J. C., and Jagadheesha, D. (2005). Relationships between South Atlantic SST Variability and Atmospheric Circulation over the South African Region during Austral Winter. *J. Clim.* 18, 3339–3355. doi:10.1175/JCLI3474.1.
Reason, C. J. C., and Rouault, M. (2005). Links between the Antarctic Oscillation and winter rainfall over western South Africa. *Geophys. Res. Lett.* 32, L07705. doi:10.1029/2005GL022419.
Reboita, M. S., da Rocha, R. P., de Souza, M. R., and Llopart, M. (2018). Extratropical cyclones over the southwestern South Atlantic Ocean: HadGEM2-ES and RegCM4 projections. *Int. J. Climatol.* 38, 2866–2879. doi:10.1002/joc.5468.
Rehman, I. H., Ahmed, T., Praveen, P. S., Kar, A., and Ramanathan, V. (2011). Black carbon emissions from biomass and fossil fuels in rural India. *Atmos. Chem. Phys.* 11, 7289–7299. doi:10.5194/acp-11-7289-2011.
Reichstein, M., Camps-Valls, G., Stevens, B., Jung, M., Denzler, J., Carvalhais, N., et al. (2019). Deep learning and process understanding for data-driven Earth system science. *Nature* 566, 195–204. doi:10.1038/s41586-019-0912-1.
Ren, Y., Song, L., Xiao, Y., and Du, L. (2019). Underestimated interannual variability of East Asian summer rainfall under climate change. *Theor. Appl. Climatol.* 135, 911–920. doi:10.1007/s00704-018-2398-4.
Ren, Y. Y., Ren, G. Y., Sun, X. B., Shrestha, A. B., You, Q. L., Zhan, Y. J., et al. (2017). Observed changes in surface air temperature and precipitation in the Hindu Kush Himalayan region over the last 100-plus years. *Adv. Clim. Chang. Res.* 8, 148–156. doi:10.1016/j.accre.2017.08.001.
Reszler, C., Switanek, M. B., and Truhetz, H. (2018). Convection-permitting regional climate simulations for representing floods in small- and medium-sized catchments in the Eastern Alps. *Nat. Hazards Earth Syst. Sci.* 18, 2653–2674. doi:10.5194/nhess-18-2653-2018.
Ribes, A., and Terray, L. (2013). Application of regularised optimal fingerprinting to attribution. Part II: application to global near-surface temperature. *Clim. Dyn.* 41, 2837–2853. doi:10.1007/s00382-013-1736-6.
Rice, J. L., Woodhouse, C. A., and Lukas, J. J. (2009). Science and Decision Making: Water Management and Tree-Ring Data in the Western United States. *JAWRA J. Am. Water Resour. Assoc.* 45, 1248–1259. doi:10.1111/j.1752-1688.2009.00358.x.
Ridley, D. A., Heald, C. L., and Prospero, J. M. (2014). What controls the recent changes in African mineral dust aerosol across the Atlantic? *Atmos. Chem. Phys.* 14, 5735–5747. doi:10.5194/acp-14-5735-2014.
Rienecker, M. M., Suarez, M. J., Gelaro, R., Todling, R., Bacmeister, J., Liu, E., et al. (2011). MERRA: NASA's Modern-Era Retrospective Analysis for Research and Applications. *J. Clim.* 24, 3624–3648. doi:10.1175/JCLI-D-11-00015.1.
Rimi, R. H., Haustein, K., Allen, M. R., and Barbour, E. J. (2019). Risks of Pre-Monsoon Extreme Rainfall Events of Bangladesh: Is Anthropogenic Climate Change Playing a Role? *Bull. Am. Meteorol. Soc.* 100, S61–S65. doi:10.1175/BAMS-D-18-0152.1.
Risbey, J. S., Pook, M. J., McIntosh, P. C., Wheeler, M. C., and Hendon, H. H. (2009). On the Remote Drivers of Rainfall Variability in Australia. *Mon. Weather Rev.* 137, 3233–3253. doi:10.1175/2009MWR2861.1.
Robaa, S. M. (2003). Urban-suburban / rural differences over Greater Cairo, Egypt. *Atmosfera*, 157–171.
Robaa, S. M. (2013). Some aspects of the urban climates of Greater Cairo Region, Egypt. *Int. J. Climatol.* 33, 3206–3216. doi:10.1002/joc.3661.
Robeson, S. M. (2015). Revisiting the recent California drought as an extreme value. *Geophys. Res. Lett.* 42, 6771–6779. doi:10.1002/2015GL064593.
Robin, Y., Vrac, M., Naveau, P., and Yiou, P. (2019). Multivariate stochastic bias corrections with optimal transport. *Hydrol. Earth Syst. Sci.* 23, 773–786. doi:10.5194/hess-23-773-2019.
Robins, S. (2019). 'Day Zero', Hydraulic Citizenship and the Defence of the Commons in Cape Town: A Case Study of the Politics of Water and its Infrastructures (2017–2018). *J. South. Afr. Stud.*, 1–25. doi:10.1080/03057070.2019.1552424.
Robledo, F. A., Vera, C., and Penalba, O. C. (2016). Influence of the large-scale climate variability on daily rainfall extremes over Argentina. *Int. J. Climatol.* 36, 412–423. doi:10.1002/joc.4359.
Robledo, F., Vera, C., and Penalba, O. (2019). Multi-scale features of the co-variability between global sea surface temperature anomalies and daily extreme rainfall in Argentina. *Int. J. Climatol.* doi:10.1002/joc.6462.
Robock, A., and Mao, J. (1992). Winter warming from large volcanic eruptions. *Geophys. Res. Lett.* 19, 2405–2408. doi:10.1029/92GL02627.
Robson, J., Ortega, P., and Sutton, R. (2016). A reversal of climatic trends in the North Atlantic since 2005. *Nat. Geosci.* 9, 513–517. doi:10.1038/ngeo2727.
Rodríguez-Fonseca, B., Mohino, E., Mechoso, C. R., Caminade, C., Biasutti, M., Gaetani, M., et al. (2015). Variability and Predictability of West African Droughts: A Review on the Role of Sea Surface Temperature Anomalies. *J. Clim.* 28, 4034–4060. doi:10.1175/JCLI-D-14-00130.1.

Rodwell, M. J., and Hoskins, B. J. (1996). Monsoons and the dynamics of deserts. *Q. J. R. Meteorol. Soc.* 122, 1385–1404. doi:10.1002/qj.49712253408.
Roehrig, R., Bouniol, D., Guichard, F., Hourdin, F., and Redelsperger, J. L. (2013). The present and future of the west african monsoon: A process-oriented assessment of CMIP5 simulations along the AMMA transect. *J. Clim.* 26, 6471–6505. doi:10.1175/JCLI-D-12-00505.1.
Rohde, R., Muller, R., Jacobsen, R., Muller, E., and Wickham, C. (2013). A New Estimate of the Average Earth Surface Land Temperature Spanning 1753 to 2011. *Geoinformatics Geostatistics An Overv.* 1. doi:10.4172/2327-4581.1000101.
Rojas, R., Feyen, L., Dosio, A., and Bavera, D. (2011). Improving pan-European hydrological simulation of extreme events through statistical bias correction of RCM-driven climate simulations. *Hydrol. Earth Syst. Sci.* 15, 2599–2620. doi:10.5194/hess-15-2599-2011.
Ropelewski, C. F., and Halpert, M. S. (1987). Global and Regional Scale Precipitation Patterns Associated with the El Niño/Southern Oscillation. *Mon. Weather Rev.* 115, 1606–1626. doi:10.1175/1520-0493(1987)115<1606:GARSPP>2.0.CO;2.
Rosenzweig, C., and Neofotis, P. (2013). Detection and attribution of anthropogenic climate change impacts. *Wiley Interdiscip. Rev. Clim. Chang.* 4, 121–150. doi:10.1002/wcc.209.
Rössler, O., Fischer, A. M., Huebener, H., Maraun, D., Benestad, R. E., Christodoulides, P., et al. (2019a). Challenges to link climate change data provision and user needs: Perspective from the COST-action VALUE. *Int. J. Climatol.* 39, 3704–3716. doi:10.1002/joc.5060.
Rössler, O., Kotlarski, S., Fischer, A. M., Keller, D., Liniger, M., and Weingartner, R. (2019b). Evaluating the added value of the new Swiss climate scenarios for hydrology: An example from the Thur catchment. *Clim. Serv.* 13, 1–13. doi:10.1016/j.cliser.2019.01.001.
Rostkier-Edelstein, D., Liu, Y., Wu, W., Kunin, P., Givati, A., and Ge, M. (2014). Towards a high-resolution climatography of seasonal precipitation over Israel. *Int. J. Climatol.* 34, 1964–1979. doi:10.1002/joc.3814.
Rotstayn, L. D., Collier, M. A., Shindell, D. T., and Boucher, O. (2015). Why Does Aerosol Forcing Control Historical Global-Mean Surface Temperature Change in CMIP5 Models? *J. Clim.* 28, 6608–6625. doi:10.1175/JCLI-D-14-00712.1.
Rouault, M., Pohl, B., and Penven, P. (2010). Coastal oceanic climate change and variability from 1982 to 2009 around South Africa. *African J. Mar. Sci.* 32, 237–246. doi:10.2989/1814232X.2010.501563.
Routson, C. C., McKay, N. P., Kaufman, D. S., Erb, M. P., Goosse, H., Shuman, B. N., et al. (2019). Mid-latitude net precipitation decreased with Arctic warming during the Holocene. *Nature* 568, 83–87. doi:10.1038/s41586-019-1060-3.
Rowell, D. P., and Jones, R. G. (2006). Causes and uncertainty of future summer drying over Europe. *Clim. Dyn.* 27, 281–299. doi:10.1007/s00382-006-0125-9.
Roxy, M. K., Ritika, K., Terray, P., Murtugudde, R., Ashok, K., and Goswami, B. N. (2015). Drying of Indian subcontinent by rapid Indian Ocean warming and a weakening land-sea thermal gradient. *Nat. Commun.* 6, 7423. doi:10.1038/ncomms8423.
Ruckstuhl, C., Philipona, R., Behrens, K., Collaud Coen, M., Dürr, B., Heimo, A., et al. (2008). Aerosol and cloud effects on solar brightening and the recent rapid warming. *Geophys. Res. Lett.* 35, L12708. doi:10.1029/2008GL034228.
Ruiz-Ramos, M., Rodríguez, A., Dosio, A., Goodess, C. M., Harpham, C., Mínguez, M. I., et al. (2016). Comparing correction methods of RCM outputs for improving crop impact projections in the Iberian Peninsula for 21st century. *Clim. Change* 134, 283–297. doi:10.1007/s10584-015-1518-8.
Rummukainen, M. (2016). Added value in regional climate modeling. *Wiley Interdiscip. Rev. Clim. Chang.* 7, 145–159. doi:10.1002/wcc.378.
Ruprich-Robert, Y., Delworth, T., Msadek, R., Castruccio, F., Yeager, S., and Danabasoglu, G. (2018). Impacts of the Atlantic Multidecadal Variability on North American Summer Climate and Heat Waves. *J. Clim.* 31, 3679–3700. doi:10.1175/JCLI-D-17-0270.1.
Ruprich-Robert, Y., Msadek, R., Castruccio, F., Yeager, S., Delworth, T., and Danabasoglu, G. (2017). Assessing the Climate Impacts of the Observed Atlantic Multidecadal Variability Using the GFDL CM2.1 and NCAR CESM1 Global Coupled Models. *J. Clim.* 30, 2785–2810. doi:10.1175/JCLI-D-16-0127.1.
Russo, A., Gouveia, C. M., Dutra, E., Soares, P. M. M., and Trigo, R. M. (2019). The synergy between drought and extremely hot summers in the Mediterranean. *Environ. Res. Lett.* 14, 014011. doi:10.1088/1748-9326/aaf09e.
Russo, S., Sillmann, J., and Fischer, E. M. (2015). Top ten European heatwaves since 1950 and their occurrence in the coming decades. *Environ. Res. Lett.* 10, 124003. doi:10.1088/1748-9326/10/12/124003.
Rusticucci, M., and Penalba, O. (2000). Interdecadal changes in the precipitation seasonal cycle over Southern South America and their relationship with surface temperature. *Clim. Res.* 16, 1–15. doi:10.3354/cr016001.
Ruti, P. M., Somot, S., Giorgi, F., Dubois, C., Flaounas, E., Obermann, A., et al. (2016). Med-CORDEX Initiative for Mediterranean Climate Studies. *Bull. Am. Meteorol. Soc.* 97, 1187–1208. doi:10.1175/BAMS-D-14-00176.1.
Saadi, S., Todorovic, M., Tanasijevic, L., Pereira, L. S., Pizzigalli, C., and Lionello, P. (2015). Climate change and Mediterranean agriculture: Impacts on winter wheat and tomato crop evapotranspiration, irrigation requirements

and yield. *Agric. Water Manag.* 147, 103–115. doi:10.1016/j.agwat.2014.05.008.
Sabeerali, C. T., and Ajayamohan, R. S. (2018). On the shortening of Indian summer monsoon season in a warming scenario. *Clim. Dyn.* 50, 1609–1624. doi:10.1007/s00382-017-3709-7.
Sabin, T. P., Krishnan, R., Ghattas, J., Denvil, S., Dufresne, J.-L., Hourdin, F., et al. (2013). High resolution simulation of the South Asian monsoon using a variable resolution global climate model. *Clim. Dyn.* 41, 173–194. doi:10.1007/s00382-012-1658-8.
Sachindra, D. A., Ng, A. W. M., Muthukumaran, S., and Perera, B. J. C. (2016). Impact of climate change on urban heat island effect and extreme temperatures: a case-study. *Q. J. R. Meteorol. Soc.* 142, 172–186. doi:10.1002/qj.2642.
Saeed, F., Hagemann, S., Saeed, S., and Jacob, D. (2013). Influence of mid-latitude circulation on upper Indus basin precipitation: the explicit role of irrigation. *Clim. Dyn.* 40, 21–38. doi:10.1007/s00382-012-1480-3.
Saggioro, E., and Shepherd, T. G. (2019). Quantifying the Timescale and Strength of Southern Hemisphere Intraseasonal Stratosphere-troposphere Coupling. *Geophys. Res. Lett.* 46, 13479–13487. doi:10.1029/2019GL084763.
Saha, A., Ghosh, S., Sahana, A. S., and Rao, E. P. (2014). Failure of CMIP5 climate models in simulating post-1950 decreasing trend of Indian monsoon. *Geophys. Res. Lett.* 41, 7323–7330. doi:10.1002/2014GL061573.
Salazar, E., Hammerling, D., Wang, X., Sansó, B., Finley, A. O., and Mearns, L. O. (2016). Observation-based blended projections from ensembles of regional climate models. *Clim. Change* 138, 55–69. doi:10.1007/s10584-016-1722-1.
Salvi, K., Kannan, S., and Ghosh, S. (2013). High-resolution multisite daily rainfall projections in India with statistical downscaling for climate change impacts assessment. *J. Geophys. Res. Atmos.* 118, 3557–3578. doi:10.1002/jgrd.502802013.
Salzmann, M., Weser, H., and Cherian, R. (2014). Robust response of Asian summer monsoon to anthropogenic aerosols in CMIP5 models. *J. Geophys. Res. Atmos.* 119, 11,321-11,337. doi:10.1002/2014JD021783.
Samaniego, L., Thober, S., Kumar, R., Wanders, N., Rakovec, O., Pan, M., et al. (2018). Anthropogenic warming exacerbates European soil moisture droughts. *Nat. Clim. Chang.* 8, 421–426. doi:10.1038/s41558-018-0138-5.
Samset, B. H., Lund, M. T., Bollasina, M., Myhre, G., and Wilcox, L. (2019). Emerging Asian aerosol patterns. *Nat. Geosci.* 12, 582–584. doi:10.1038/s41561-019-0424-5.
Samset, B. H., Sand, M., Smith, C. J., Bauer, S. E., Forster, P. M., Fuglestvedt, J. S., et al. (2018). Climate Impacts From a Removal of Anthropogenic Aerosol Emissions. *Geophys. Res. Lett.* 45, 1020–1029. doi:10.1002/2017GL076079.
Samson, G., Masson, S., Lengaigne, M., Keerthi, M. G., Vialard, J., Pous, S., et al. (2014). The NOW regional coupled model: Application to the tropical Indian Ocean climate and tropical cyclone activity. *J. Adv. Model. Earth Syst.* 6, 700–722. doi:10.1002/2014MS000324.
Samuelsson, P., Kourzeneva, E., and Mironov, D. (2010). The impact of lakes on the European climate as simulated by a regional climate model. *Boreal Environ. Res.* 15, 113–129.
San-Martín, D., Manzanas, R., Brands, S., Herrera, S., and Gutiérrez, J. M. (2017). Reassessing Model Uncertainty for Regional Projections of Precipitation with an Ensemble of Statistical Downscaling Methods. *J. Clim.* 30, 203–223. doi:10.1175/JCLI-D-16-0366.1.
Sanchez-Gomez, E., and Somot, S. (2018). Impact of the internal variability on the cyclone tracks simulated by a regional climate model over the Med-CORDEX domain. *Clim. Dyn.* 51, 1005–1021. doi:10.1007/s00382-016-3394-y.
Sanchez-Gomez, E., Somot, S., and Déqué, M. (2009). Ability of an ensemble of regional climate models to reproduce weather regimes over Europe-Atlantic during the period 1961–2000. *Clim. Dyn.* 33, 723–736. doi:10.1007/s00382-008-0502-7.
Sanderson, B. M., Knutti, R., and Caldwell, P. (2015). Addressing Interdependency in a Multimodel Ensemble by Interpolation of Model Properties. *J. Clim.* 28, 5150–5170. doi:10.1175/JCLI-D-14-00361.1.
Sanderson, M., Arbuthnott, K., Kovats, S., Hajat, S., and Falloon, P. (2017). The use of climate information to estimate future mortality from high ambient temperature: A systematic literature review. *PLoS One* 12, e0180369. doi:10.1371/journal.pone.0180369.
Sanjay, J., Krishnan, R., Shrestha, A. B., Rajbhandari, R., and Ren, G.-Y. (2017). Downscaled climate change projections for the Hindu Kush Himalayan region using CORDEX South Asia regional climate models. *Adv. Clim. Chang. Res.* 8, 185–198. doi:10.1016/j.accre.2017.08.003.
Sanogo, S., Fink, A. H., Omotosho, J. A., Ba, A., Redl, R., and Ermert, V. (2015). Spatio-temporal characteristics of the recent rainfall recovery in West Africa. *Int. J. Climatol.* 35, 4589–4605. doi:10.1002/joc.4309.
Sarewitz, D. (2004). How science makes environmental controversies worse. *Environ. Sci. Policy* 7, 385–403. doi:10.1016/j.envsci.2004.06.001.
Sarojini, B. B., Stott, P. A., and Black, E. (2016). Detection and attribution of human influence on regional precipitation. *Nat. Clim. Chang.* 6, 669–675. doi:10.1038/nclimate2976.
Sato, K., Inoue, J., and Watanabe, M. (2014). Influence of the Gulf Stream on the Barents Sea ice retreat and Eurasian coldness during early winter. *Environ. Res. Lett.* 9, 084009. doi:10.1088/1748-9326/9/8/084009.
Saurral, R. I., Barros, V. R., and Lettenmaier, D. P. (2008). Land use impact on the Uruguay River discharge. *Geophys.*

Res. Lett. 35, L12401. doi:10.1029/2008GL033707.
Saurral, R. I., Camilloni, I. A., and Barros, V. R. (2017). Low-frequency variability and trends in centennial precipitation stations in southern South America. *Int. J. Climatol.* 37, 1774–1793. doi:10.1002/joc.4810.
Saurral, R. I., Kucharski, F., and Raggio, G. A. (2019). Variations in ozone and greenhouse gases as drivers of Southern Hemisphere climate in a medium-complexity global climate model. *Clim. Dyn.* doi:10.1007/s00382-019-04950-7.
Sayles, J. S. (2018). Effects of social-ecological scale mismatches on estuary restoration at the project and landscape level in Puget Sound, USA. *Ecol. Restor.* 36, 62–75. doi:10.3368/er.36.1.62c.
Scannell, C., Booth, B. B. B., Dunstone, N. J., Rowell, D. P., Bernie, D. J., Kasoar, M., et al. (2019). The Influence of Remote Aerosol Forcing from Industrialized Economies on the Future Evolution of East and West African Rainfall. *J. Clim.* 32, 8335–8354. doi:10.1175/JCLI-D-18-0716.1.
Schaaf, B., and Feser, F. (2018). Is there added value of convection-permitting regional climate model simulations for storms over the German Bight and Northern Germany? *Meteorol. Hydrol. Water Manag.* 6, 21–37. doi:10.26491/mhwm/85507.
Schaller, N., Cermak, J., Wild, M., and Knutti, R. (2013). The sensitivity of the modeled energy budget and hydrological cycle to CO2 and solar forcing. *Earth Syst. Dyn.* 4, 253–266. doi:10.5194/esd-4-253-2013.
Schär, C., Frei, C., Lüthi, D., and Davies, H. C. (1996). Surrogate climate-change scenarios for regional climate models. *Geophys. Res. Lett.* 23, 669–672. doi:10.1029/96GL00265.
Scheff, J., Seager, R., Liu, H., and Coats, S. (2017). Are Glacials Dry? Consequences for Paleoclimatology and for Greenhouse Warming. *J. Clim.* 30, 6593–6609. doi:10.1175/JCLI-D-16-0854.1.
Schemm, S., Nisi, L., Martinov, A., Leuenberger, D., and Martius, O. (2016). On the link between cold fronts and hail in Switzerland. *Atmos. Sci. Lett.* 17, 315–325. doi:10.1002/asl.660.
Schemm, S., Rudeva, I., and Simmonds, I. (2015). Extratropical fronts in the lower troposphere-global perspectives obtained from two automated methods. *Q. J. R. Meteorol. Soc.* 141, 1686–1698. doi:10.1002/qj.2471.
Schiemann, R., Demory, M.-E., Mizielinski, M. S., Roberts, M. J., Shaffrey, L. C., Strachan, J., et al. (2014). The sensitivity of the tropical circulation and Maritime Continent precipitation to climate model resolution. *Clim. Dyn.* 42, 2455–2468. doi:10.1007/s00382-013-1997-0.
Schiemann, R., Demory, M.-E., Shaffrey, L. C., Strachan, J., Vidale, P. L., Mizielinski, M. S., et al. (2017). The Resolution Sensitivity of Northern Hemisphere Blocking in Four 25-km Atmospheric Global Circulation Models. *J. Clim.* 30, 337–358. doi:10.1175/JCLI-D-16-0100.1.
Schlünzen, K. H., Hoffmann, P., Rosenhagen, G., and Riecke, W. (2010). Long-term changes and regional differences in temperature and precipitation in the metropolitan area of Hamburg. *Int. J. Climatol.* 30, 1121–1136. doi:10.1002/joc.1968.
Schmetz, J., Pili, P., Tjemkes, S., Just, D., Kerkmann, J., Rota, S., et al. (2002). An Introduction to Meteosat Second Generation (MSG). *Bull. Am. Meteorol. Soc.* 83, 977–992. doi:10.1175/1520-0477(2002)083<0977:AITMSG>2.3.CO;2.
Schneider, S. H. (2001). What is "dangerous" climate change? *Nature* 411, 17–19. doi:10.1038/35075167.
Schneider, U., Finger, P., Meyer-Christoffer, A., Rustemeier, E., Ziese, M., Becker, A., et al. (2017). Evaluating the Hydrological Cycle over Land Using the Newly-Corrected Precipitation Climatology from the Global Precipitation Climatology Centre (GPCC). *Atmosphere (Basel).* 8, 52. doi:10.3390/atmos8030052.
Schneider, U., Ziese, M., Meyer-Christoffer, A., Finger, P., Rustemeier, E., and Becker, A. (2016). The new portfolio of global precipitation data products of the Global Precipitation Climatology Centre suitable to assess and quantify the global water cycle and resources. *Proc. Int. Assoc. Hydrol. Sci.* 374, 29–34. doi:10.5194/piahs-374-29-2016.
Schoof, J. T. (2013). Statistical Downscaling in Climatology. *Geogr. Compass* 7, 249–265. doi:10.1111/gec3.12036.
Schubert, S., Grossman-Clarke, S., and Martilli, A. (2012). A Double-Canyon Radiation Scheme for Multi-Layer Urban Canopy Models. *Boundary-Layer Meteorol.* doi:10.1007/s10546-012-9728-3.
Schurer, A. P., Hegerl, G. C., Luterbacher, J., Brönnimann, S., Cowan, T., Tett, S. F. B., et al. (2019). Disentangling the causes of the 1816 European year without a summer. *Environ. Res. Lett.* 14, 94019. doi:10.1088/1748-9326/ab3a10.
Schwartz, S. H., Cieciuch, J., Vecchione, M., Davidov, E., Fischer, R., Beierlein, C., et al. (2012). Refining the theory of basic individual values. *J. Pers. Soc. Psychol.* 103, 663–688. doi:10.1037/a0029393.
Scott, D., Iipinge, K. N., Mfune, J. K. E., Muchadenyika, D., Makuti, O. V, and Ziervogel, G. (2018). The Story of Water in Windhoek: A Narrative Approach to Interpreting a Transdisciplinary Process. *Water* 10. doi:10.3390/w10101366.
Screen, J. A. (2014). Arctic amplification decreases temperature variance in northern mid- to high-latitudes. *Nat. Clim. Chang.* 4, 577–582. doi:10.1038/nclimate2268.
Screen, J. A., and Blackport, R. (2019). Is sea-ice-driven Eurasian cooling too weak in models? *Nat. Clim. Chang.* 9, 934–936. doi:10.1038/s41558-019-0635-1.
Screen, J. A., Deser, C., Simmonds, I., and Tomas, R. (2014). Atmospheric impacts of Arctic sea-ice loss, 1979–2009: separating forced change from atmospheric internal variability. *Clim. Dyn.* 43, 333–344. doi:10.1007/s00382-013-1830-9.
Screen, J. A., and Simmonds, I. (2013). Exploring links between Arctic amplification and mid-latitude weather.

Geophys. Res. Lett. 40, 959–964. doi:10.1002/grl.50174.

Seager, R., and Hoerling, M. (2014). Atmosphere and Ocean Origins of North American Droughts. *J. Clim.* 27, 4581–4606. doi:10.1175/JCLI-D-13-00329.1.

Seager, R., Liu, H., Henderson, N., Simpson, I., Kelley, C., Shaw, T., et al. (2014). Causes of Increasing Aridification of the Mediterranean Region in Response to Rising Greenhouse Gases. *J. Clim.* 27, 4655–4676. doi:10.1175/JCLI-D-13-00446.1.

Seager, R., Naik, N., Baethgen, W., Robertson, A., Kushnir, Y., Nakamura, J., et al. (2010). Tropical Oceanic Causes of Interannual to Multidecadal Precipitation Variability in Southeast South America over the Past Century*. *J. Clim.* 23, 5517–5539. doi:10.1175/2010JCLI3578.1.

Seager, R., Osborn, T. J., Kushnir, Y., Simpson, I. R., Nakamura, J., and Liu, H. (2019). Climate Variability and Change of Mediterranean-Type Climates. *J. Clim.* 32, 2887–2915. doi:10.1175/JCLI-D-18-0472.1.

Seager, R., and Ting, M. (2017). Decadal Drought Variability Over North America: Mechanisms and Predictability. *Curr. Clim. Chang. Reports* 3, 141–149. doi:10.1007/s40641-017-0062-1.

Seaman, N. L., Ludwig, F. L., Donall, E. G., Warner, T. T., and Bhumralkar, C. M. (1989). Numerical Studies of Urban Planetary Boundary-Layer Structure under Realistic Synoptic Conditions. *J. Appl. Meteorol.* 28, 760–781. doi:10.1175/1520-0450(1989)028<0760:NSOUPB>2.0.CO;2.

Sein, D. V., Mikolajewicz, U., Gröger, M., Fast, I., Cabos, W., Pinto, J. G., et al. (2015). Regionally coupled atmosphere-ocean-sea ice-marine biogeochemistry model ROM: 1. Description and validation. *J. Adv. Model. Earth Syst.* 7, 268–304. doi:10.1002/2014MS000357.

Seneviratne, S. I., Corti, T., Davin, E. L., Hirschi, M., Jaeger, E. B., Lehner, I., et al. (2010). Investigating soil moisture–climate interactions in a changing climate: A review. *Earth-Science Rev.* 99, 125–161. doi:10.1016/j.earscirev.2010.02.004.

Seneviratne, S. I., Donat, M. G., Pitman, A. J., Knutti, R., and Wilby, R. L. (2016). Allowable CO_2 emissions based on regional and impact-related climate targets. *Nature* 529, 477–483. doi:10.1038/nature16542.

Seneviratne, S. I., Lüthi, D., Litschi, M., and Schär, C. (2006). Land-atmosphere coupling and climate change in Europe. *Nature* 443, 205–209. doi:10.1038/nature05095.

Seneviratne, S. I., Nicholls, N., Easterling, D., Goodess, C. M., Kanae, S., Kossin, J., et al. (2012). "Changes in climate extremes and their impacts on the natural physical environment," in *Managing the Risks of Extreme Events and Disasters to Advance Climate Change Adaptation: Special Report of the Intergovernmental Panel on Climate Change*, 109–230. doi:10.1017/CBO9781139177245.006.

Seneviratne, S. I., Phipps, S. J., Pitman, A. J., Hirsch, A. L., Davin, E. L., Donat, M. G., et al. (2018). Land radiative management as contributor to regional-scale climate adaptation and mitigation. *Nat. Geosci.* 11, 88–96. doi:10.1038/s41561-017-0057-5.

Seneviratne, S. I., Wilhelm, M., Stanelle, T., van den Hurk, B., Hagemann, S., Berg, A., et al. (2013). Impact of soil moisture-climate feedbacks on CMIP5 projections: First results from the GLACE-CMIP5 experiment. *Geophys. Res. Lett.* 40, 5212–5217. doi:10.1002/grl.50956.

Seo, K.-H., Lee, H.-J., and Frierson, D. M. W. (2016). Unraveling the Teleconnection Mechanisms that Induce Wintertime Temperature Anomalies over the Northern Hemisphere Continents in Response to the MJO. *J. Atmos. Sci.* 73, 3557–3571. doi:10.1175/JAS-D-16-0036.1.

Sevault, F., Somot, S., Alias, A., Dubois, C., Lebeaupin-Brossier, C., Nabat, P., et al. (2014). A fully coupled Mediterranean regional climate system model: design and evaluation of the ocean component for the 1980–2012 period. *Tellus A Dyn. Meteorol. Oceanogr.* 66, 23967. doi:10.3402/tellusa.v66.23967.

Sexton, D. M. H., Karmalkar, A. V, Murphy, J. M., Williams, K. D., Boutle, I. A., Morcrette, C. J., et al. (2019). Finding plausible and diverse variants of a climate model. Part 1: establishing the relationship between errors at weather and climate time scales. *Clim. Dyn.* doi:10.1007/s00382-019-04625-3.

Shaevitz, D. A., Camargo, S. J., Sobel, A. H., Jonas, J. A., Kim, D., Kumar, A., et al. (2014). Characteristics of tropical cyclones in high-resolution models in the present climate. *J. Adv. Model. Earth Syst.* 6, 1154–1172. doi:10.1002/2014MS000372.

Shalev, I. (2015). The climate change problem: promoting motivation for change when the map is not the territory. *Front. Psychol.* 6. doi:10.3389/fpsyg.2015.00131.

Sharma, D., and Miller, R. L. (2017). Revisiting the observed correlation between weekly averaged Indian monsoon precipitation and Arabian Sea aerosol optical depth. *Geophys. Res. Lett.* 44, 6-10,10,16. doi:10.1002/2017GL074373.

Sharma, E., Molden, D., Rahman, A., Khatiwada, Y. R., Zhang, L., Singh, S. P., et al. (2019). *The Hindu Kush Himalaya Assessment*. , eds. P. Wester, A. Mishra, A. Mukherji, and A. B. Shrestha Cham: Springer International Publishing doi:10.1007/978-3-319-92288-1.

Shastri, H., Paul, S., Ghosh, S., and Karmakar, S. (2015). Impacts of urbanization on Indian summer monsoon rainfall extremes. *J. Geophys. Res. Atmos.* 120, 496–516. doi:10.1002/2014JD022061.

Shaw, T. A., Baldwin, M., Barnes, E. A., Caballero, R., Garfinkel, C. I., Hwang, Y.-T., et al. (2016). Storm track processes and the opposing influences of climate change. *Nat. Geosci.* 9, 656. doi:10.1038/ngeo2783.

Shawki, D., Voulgarakis, A., Chakraborty, A., Kasoar, M., and Srinivasan, J. (2018). The South Asian Monsoon

Response to Remote Aerosols: Global and Regional Mechanisms. *J. Geophys. Res. Atmos.* 123, 11,585-11,601. doi:10.1029/2018JD028623.
Shea, J. M., Wagnon, P., Immerzeel, W. W., Biron, R., Brun, F., and Pellicciotti, F. (2015). A comparative high-altitude meteorological analysis from three catchments in the Nepalese Himalaya. *Int. J. Water Resour. Dev.* 31, 174–200. doi:10.1080/07900627.2015.1020417.
Sheen, K. L., Smith, D. M., Dunstone, N. J., Eade, R., Rowell, D. P., and Vellinga, M. (2017). Skilful prediction of Sahel summer rainfall on inter-annual and multi-year timescales. *Nat. Commun.* 8, 14966. doi:10.1038/ncomms14966.
Sheikh, M. M., Manzoor, N., Ashraf, J., Adnan, M., Collins, D., Hameed, S., et al. (2015). Trends in extreme daily rainfall and temperature indices over South Asia. *Int. J. Climatol.* 35, 1625–1637. doi:10.1002/joc.4081.
Shen, Y., Hong, Z., Pan, Y., Yu, J., and Maguire, L. (2018). China's 1 km Merged Gauge, Radar and Satellite Experimental Precipitation Dataset. *Remote Sens.* 10. doi:10.3390/rs10020264.
Shepard, D. (1968). A two-dimensional interpolation function for irregularly-spaced data. in *Proceedings of the 1968 23rd ACM national conference on* - (New York, New York, USA: ACM Press), 517–524. doi:10.1145/800186.810616.
Shepherd, T. G. (2014). Atmospheric circulation as a source of uncertainty in climate change projections. *Nat. Geosci.* 7, 703. Available at: http://dx.doi.org/10.1038/ngeo2253.
Shepherd, T. G. (2016). A Common Framework for Approaches to Extreme Event Attribution. *Curr. Clim. Chang. Reports* 2, 28–38. doi:10.1007/s40641-016-0033-y.
Shepherd, T. G. (2019). Storyline approach to the construction of regional climate change information. *Proc. R. Soc. A Math. Phys. Eng. Sci.* 475, 20190013. doi:10.1098/rspa.2019.0013.
Shepherd, T. G., Boyd, E., Calel, R. A., Chapman, S. C., Dessai, S., Dima-West, I. M., et al. (2018). Storylines: an alternative approach to representing uncertainty in physical aspects of climate change. *Clim. Change* 151, 555–571. doi:10.1007/s10584-018-2317-9.
Sherwood, S. C., Bony, S., Boucher, O., Bretherton, C., Forster, P. M., Gregory, J. M., et al. (2015). Adjustments in the Forcing-Feedback Framework for Understanding Climate Change. *Bull. Am. Meteorol. Soc.* 96, 217–228. doi:10.1175/BAMS-D-13-00167.1.
Shige, S., Kida, S., Ashiwake, H., Kubota, T., and Aonashi, K. (2013). Improvement of TMI Rain Retrievals in Mountainous Areas. *J. Appl. Meteorol. Climatol.* 52, 242–254. doi:10.1175/JAMC-D-12-074.1.
Shige, S., Takayabu, Y. N., KIDA, S., Tao, W. K., Zeng, X., Yokoyama, C., et al. (2009). Spectral retrieval of latent heating profiles from TRMM PR data. Part IV: comparisons of lookup tables from two-and three-dimensional cloud-resolving model simulations. *J. Clim.* 22, 5577–5594. doi:10.1175/2009JCLI2919.1.
Shimpo, A., Takemura, K., Wakamatsu, S., Togawa, H., Mochizuki, Y., Takekawa, M., et al. (2019). Primary factors behind the Heavy Rain Event of July 2018 and the subsequent heat wave in Japan. *Sci. Online Lett. Atmos.* 15, 13–18. doi:10.2151/sola.15A-003.
Shindell, D., and Faluvegi, G. (2009). Climate response to regional radiative forcing during the twentieth century. *Nat. Geosci.* 2, 294–300. doi:10.1038/ngeo473.
Shiogama, H., Stone, D. A., Nagashima, T., Nozawa, T., and Emori, S. (2013). On the linear additivity of climate forcing-response relationships at global and continental scales. *Int. J. Climatol.* 33, 2542–2550. doi:10.1002/joc.3607.
Shonk, J., Turner, A. G., Chevuturi, A., Wilcox, L. J., Dittus, A. J., and Hawkins, E. (submitted). Uncertainty in aerosol radiative forcing impacts the simulated global monsoon in the 20th century. *Geophys. Res. Lett.* (submitted).
Shrestha, S., Yao, T., and Adhikari, T. R. (2019). Analysis of rainfall trends of two complex mountain river basins on the southern slopes of the Central Himalayas. *Atmos. Res.* 215, 99–115. doi:10.1016/j.atmosres.2018.08.027.
Shukla, S. P., Puma, M. J., and Cook, B. I. (2014). The response of the South Asian Summer Monsoon circulation to intensified irrigation in global climate model simulations. *Clim. Dyn.* 42, 21–36. doi:10.1007/s00382-013-1786-9.
Si, D., and Ding, Y. (2013). Decadal change in the correlation pattern between the tibetan plateau winter snow and the East Asian summer precipitation during 1979-2011. *J. Clim.* 26, 7622–7634. doi:10.1175/JCLI-D-12-00587.1.
Sigl, M., Winstrup, M., McConnell, J. R., Welten, K. C., Plunkett, G., Ludlow, F., et al. (2015). Timing and climate forcing of volcanic eruptions for the past 2,500 years. *Nature* 523, 543–549. doi:10.1038/nature14565.
Sigmond, M., and Fyfe, J. C. (2016). Tropical Pacific impacts on cooling North American winters. *Nat. Clim. Chang.* 6, 970–974. doi:10.1038/nclimate3069.
Sillmann, J., Kharin, V. V., Zhang, X., Zwiers, F. W., and Bronaugh, D. (2013). Climate extremes indices in the CMIP5 multimodel ensemble: Part 1. Model evaluation in the present climate. *J. Geophys. Res. Atmos.* 118, 1716–1733. doi:10.1002/jgrd.50203.
Simmonds, I., and Govekar, P. D. (2014). What are the physical links between Arctic sea ice loss and Eurasian winter climate? *Environ. Res. Lett.* 9, 101003. doi:10.1088/1748-9326/9/10/101003.
Simpson, I. R., Hitchcock, P., Seager, R., Wu, Y., and Callaghan, P. (2018). The Downward Influence of Uncertainty in the Northern Hemisphere Stratospheric Polar Vortex Response to Climate Change. *J. Clim.* 31, 6371–6391. doi:10.1175/JCLI-D-18-0041.1.
Simpson, I. R., and Polvani, L. M. (2016). Revisiting the relationship between jet position, forced response, and annular

mode variability in the southern midlatitudes. *Geophys. Res. Lett.* 43, 2896–2903. doi:10.1002/2016GL067989.
Simpson, I. R., Seager, R., Shaw, T. A., and Ting, M. (2015). Mediterranean Summer Climate and the Importance of Middle East Topography*. *J. Clim.* 28, 1977–1996. doi:10.1175/JCLI-D-14-00298.1.
Simpson, I. R., Seager, R., Ting, M., and Shaw, T. A. (2016). Causes of change in Northern Hemisphere winter meridional winds and regional hydroclimate. *Nat. Clim. Chang.* 6, 65–70. doi:10.1038/nclimate2783.
Simpson, I. R., Shepherd, T. G., Hitchcock, P., and Scinocca, J. F. (2013). Southern Annular Mode Dynamics in Observations and Models. Part II: Eddy Feedbacks. *J. Clim.* 26, 5220–5241. doi:10.1175/JCLI-D-12-00495.1.
Simpson, J., Kummerow, C., Tao, W.-K., and Adler, R. F. (1996). On the Tropical Rainfall Measuring Mission (TRMM). *Meteorol. Atmos. Phys.* 60, 19–36. doi:10.1007/BF01029783.
Singh, H. K. A., Hakim, G. J., Tardif, R., Emile-Geay, J., and Noone, D. C. (2018). Insights into Atlantic multidecadal variability using the Last Millennium Reanalysis framework. *Clim. Past* 14, 157–174. doi:10.5194/cp-14-157-2018.
Singh, J., Vittal, H., Karmakar, S., Ghosh, S., and Niyogi, D. (2016). Urbanization causes nonstationarity in Indian Summer Monsoon Rainfall extremes. *Geophys. Res. Lett.* 43, 11,269-11,277. doi:10.1002/2016GL071238.
Singh, R., and AchutaRao, K. (2018). Quantifying uncertainty in twenty-first century climate change over India. *Clim. Dyn.* doi:10.1007/s00382-018-4361-6.
Singh, S., Ghosh, S., Sahana, A. S., Vittal, H., and Karmakar, S. (2017). Do dynamic regional models add value to the global model projections of Indian monsoon? *Clim. Dyn.* 48, 1375–1397. doi:10.1007/s00382-016-3147-y.
Sippel, S., Otto, F. E. L., Flach, M., and van Oldenborgh, G. J. (2016). The Role of Anthropogenic Warming in 2015 Central European Heat Waves. *Bull. Am. Meteorol. Soc.* 97, S51–S56. doi:10.1175/BAMS-D-16-0150.1.
Sippel, S., Zscheischler, J., Mahecha, M. D., Orth, R., Reichstein, M., Vogel, M., et al. (2017). Refining multi-model projections of temperature extremes by evaluation against land–atmosphere coupling diagnostics. *Earth Syst. Dyn.* 8, 387–403. doi:10.5194/esd-8-387-2017.
Sjolte, J., Sturm, C., Adolphi, F., Vinther, B. M., Werner, M., Lohmann, G., et al. (2018). Solar and volcanic forcing of North Atlantic climate inferred from a process-based reconstruction. *Clim. Past* 14, 1179–1194. doi:10.5194/cp-14-1179-2018.
Skiles, S. M., Painter, T. H., Deems, J. S., Bryant, A. C., and Landry, C. C. (2012). Dust radiative forcing in snow of the Upper Colorado River Basin: 2. Interannual variability in radiative forcing and snowmelt rates. *Water Resour. Res.* 48, W07522. doi:10.1029/2012WR011986.
Skofronick-Jackson, G., Petersen, W. A., Berg, W., Kidd, C., Stocker, E. F., Kirschbaum, D. B., et al. (2017). The Global Precipitation Measurement (GPM) Mission for Science and Society. *Bull. Am. Meteorol. Soc.* 98, 1679–1695. doi:10.1175/BAMS-D-15-00306.1.
Slivinski, L. C., Compo, G. P., Whitaker, J. S., Sardeshmukh, P. D., Giese, B. S., McColl, C., et al. (2019). Towards a more reliable historical reanalysis: Improvements for version 3 of the Twentieth Century Reanalysis system. *Q. J. R. Meteorol. Soc.* 145, 2876–2908. doi:10.1002/qj.3598.
Slovic, P., Finucane, M. L., Peters, E., and MacGregor, D. G. (2004). Risk as Analysis and Risk as Feelings: Some Thoughts about Affect, Reason, Risk, and Rationality. *Risk Anal.* 24, 311–322. doi:10.1111/j.0272-4332.2004.00433.x.
Smith, A. B., and Matthews, J. L. (2015). Quantifying uncertainty and variable sensitivity within the US billion-dollar weather and climate disaster cost estimates. *Nat. Hazards* 77, 1829–1851. doi:10.1007/s11069-015-1678-x.
Smith, D. M., Scaife, A. A., and Kirtman, B. P. (2012). What is the current state of scientific knowledge with regard to seasonal and decadal forecasting? *Environ. Res. Lett.* 7, 015602. doi:10.1088/1748-9326/7/1/015602.
Smith, I., and Power, S. (2014). Past and future changes to inflows into Perth (Western Australia) dams. *J. Hydrol. Reg. Stud.* 2, 84–96. doi:10.1016/j.ejrh.2014.08.005.
Smith, K. L., and Polvani, L. M. (2017). Spatial patterns of recent Antarctic surface temperature trends and the importance of natural variability: lessons from multiple reconstructions and the CMIP5 models. *Clim. Dyn.* 48, 2653–2670. doi:10.1007/s00382-016-3230-4.
Smoliak, B. V., Wallace, J. M., Lin, P., and Fu, Q. (2015). Dynamical Adjustment of the Northern Hemisphere Surface Air Temperature Field: Methodology and Application to Observations*. *J. Clim.* 28, 1613–1629. doi:10.1175/JCLI-D-14-00111.1.
Soares, P. M. M., and Cardoso, R. M. (2018). A simple method to assess the added value using high-resolution climate distributions: application to the EURO-CORDEX daily precipitation. *Int. J. Climatol.* 38, 1484–1498. doi:10.1002/joc.5261.
Soares, P. M. M., Cardoso, R. M., Semedo, Ál., Chinita, M. J., and Ranjha, R. (2014). Climatology of the Iberia coastal low-level wind jet: weather research forecasting model high-resolution results. *Tellus A Dyn. Meteorol. Oceanogr.* 66, 22377. doi:10.3402/tellusa.v66.22377.
Soares, P. M. M., Lima, D. C. A., Semedo, A., Cardoso, R. M., Cabos, W., and Sein, D. V. (2019a). Assessing the climate change impact on the North African offshore surface wind and coastal low-level jet using coupled and uncoupled regional climate simulations. *Clim. Dyn.* 52, 7111–7132. doi:10.1007/s00382-018-4565-9.
Soares, P. M. M., Maraun, D., Brands, S., Jury, M. W., Gutiérrez, J. M., San-Martín, D., et al. (2019b). Process-based evaluation of the VALUE perfect predictor experiment of statistical downscaling methods. *Int. J. Climatol.* 39,

3868–3893. doi:10.1002/joc.5911.
Sohn, B. J., Ryu, G.-H., Song, H.-J., Ou, M.-L., Sohn, B. J., Ryu, G.-H., et al. (2013). Characteristic Features of Warm-Type Rain Producing Heavy Rainfall over the Korean Peninsula Inferred from TRMM Measurements. *Mon. Weather Rev.* 141, 3873–3888. doi:10.1175/MWR-D-13-00075.1.
Solmon, F., Nair, V. S., and Mallet, M. (2015). Increasing Arabian dust activity and the Indian summer monsoon. *Atmos. Chem. Phys.* 15, 8051–8064. doi:10.5194/acp-15-8051-2015.
Somot, S., Ruti, P., Ahrens, B., Coppola, E., Jordà, G., Sannino, G., et al. (2018). Editorial for the Med-CORDEX special issue. *Clim. Dyn.* 51, 771–777. doi:10.1007/s00382-018-4325-x.
Somot, S., Sevault, F., Déqué, M., and Crépon, M. (2008). 21st century climate change scenario for the Mediterranean using a coupled atmosphere–ocean regional climate model. *Glob. Planet. Change* 63, 112–126. doi:10.1016/j.gloplacha.2007.10.003.
Song, F., Zhou, T., and Qian, Y. (2014). Responses of East Asian summer monsoon to natural and anthropogenic forcings in the 17 latest CMIP5 models. *Geophys. Res. Lett.* 41, 596–603. doi:10.1002/2013GL058705.
Sontakke, N. A., Singh, N., and Singh, H. N. (2008). Instrumental period rainfall series of the Indian region (AD 1813—2005): revised reconstruction, update and analysis. *The Holocene* 18, 1055–1066. doi:10.1177/0959683608095576.
Sooraj, K. P., Terray, P., and Mujumdar, M. (2015). Global warming and the weakening of the Asian summer monsoon circulation: assessments from the CMIP5 models. *Clim. Dyn.* 45, 233–252. doi:10.1007/s00382-014-2257-7.
Sörensson, A. A., and Ruscica, R. C. (2018). Intercomparison and Uncertainty Assessment of Nine Evapotranspiration Estimates Over South America. *Water Resour. Res.* 54, 2891–2908. doi:10.1002/2017WR021682.
Sørland, S. L., Schär, C., Lüthi, D., and Kjellström, E. (2018). Bias patterns and climate change signals in GCM-RCM model chains. *Environ. Res. Lett.* 13, 074017. doi:10.1088/1748-9326/aacc77.
Sørland, S. L., and Sorteberg, A. (2016). Low-pressure systems and extreme precipitation in central India: sensitivity to temperature changes. *Clim. Dyn.* 47, 465–480. doi:10.1007/s00382-015-2850-4.
Sørland, S. L., Sorteberg, A., Liu, C., and Rasmussen, R. (2016). Precipitation response of monsoon low-pressure systems to an idealized uniform temperature increase. *J. Geophys. Res. Atmos.* 121, 6258–6272. doi:10.1002/2015JD024658.
Sorokina, S. A., Li, C., Wettstein, J. J., and Kvamstø, N. G. (2016). Observed Atmospheric Coupling between Barents Sea Ice and the Warm-Arctic Cold-Siberian Anomaly Pattern. *J. Clim.* 29, 495–511. doi:10.1175/JCLI-D-15-0046.1.
Sosko, S., and Dalyot, S. (2017). Crowdsourcing User-Generated Mobile Sensor Weather Data for Densifying Static Geosensor Networks. *ISPRS Int. J. Geo-Information* 6, 61. doi:10.3390/ijgi6030061.
Sousa, P. M., Blamey, R. C., Reason, C. J. C., Ramos, A. M., and Trigo, R. M. (2018a). The ‘Day Zero’ Cape Town drought and the poleward migration of moisture corridors. *Environ. Res. Lett.* 13, 124025. doi:10.1088/1748-9326/aaebc7.
Sousa, P. M., Trigo, R. M., Barriopedro, D., Soares, P. M. M., Ramos, A. M., and Liberato, M. L. R. (2017). Responses of European precipitation distributions and regimes to different blocking locations. *Clim. Dyn.* 48, 1141–1160. doi:10.1007/s00382-016-3132-5.
Sousa, P. M., Trigo, R. M., Barriopedro, D., Soares, P. M. M., and Santos, J. A. (2018b). European temperature responses to blocking and ridge regional patterns. *Clim. Dyn.* 50, 457–477. doi:10.1007/s00382-017-3620-2.
Spence, A., Poortinga, W., and Pidgeon, N. (2012). The Psychological Distance of Climate Change. *Risk Anal.* 32, 957–972. doi:10.1111/j.1539-6924.2011.01695.x.
Sperber, K. R., Annamalai, H., Kang, I.-S., Kitoh, A., Moise, A., Turner, A., et al. (2013). The Asian summer monsoon: an intercomparison of CMIP5 vs. CMIP3 simulations of the late 20th century. *Clim. Dyn.* 41, 2711–2744. doi:10.1007/s00382-012-1607-6.
Spero, T. L., Nolte, C. G., Bowden, J. H., Mallard, M. S., and Herwehe, J. A. (2016). The Impact of Incongruous Lake Temperatures on Regional Climate Extremes Downscaled from the CMIP5 Archive Using the WRF Model. *J. Clim.* 29, 839–853. doi:10.1175/JCLI-D-15-0233.1.
Spinoni, J., Barbosa, P., Bucchignani, E., Cassano, J., Cavazos, T., Christensen, J. H., et al. (2019). Future global meteorological drought hotspots: a study based on CORDEX data. *J. Clim.* doi:10.1175/JCLI-D-19-0084.1.
Spinoni, J., Vogt, J. V., Naumann, G., Barbosa, P., and Dosio, A. (2018). Will drought events become more frequent and severe in Europe? *Int. J. Climatol.* 38, 1718–1736. doi:10.1002/joc.5291.
Stager, J. C., Mayewski, P. A., White, J., Chase, B. M., Neumann, F. H., Meadows, M. E., et al. (2012). Precipitation variability in the winter rainfall zone of South Africa during the last 1400 yr linked to the austral westerlies. *Clim. Past* 8, 877–887. doi:10.5194/cp-8-877-2012.
Staten, P. W., Lu, J., Grise, K. M., Davis, S. M., and Birner, T. (2018). Re-examining tropical expansion. *Nat. Clim. Chang.* 8, 768–775. doi:10.1038/s41558-018-0246-2.
Stegehuis, A. I., Vautard, R., Ciais, P., Teuling, A. J., Miralles, D. G., and Wild, M. (2015). An observation-constrained multi-physics WRF ensemble for simulating European mega heat waves. *Geosci. Model Dev.* 8, 2285–2298. doi:10.5194/gmd-8-2285-2015.
Steiger, N. J., Smerdon, J. E., Cook, E. R., and Cook, B. I. (2018). A reconstruction of global hydroclimate and

dynamical variables over the Common Era. *Sci. Data* 5, 180086. doi:10.1038/sdata.2018.86.
Sterl, A., van Oldenborgh, G. J., Hazeleger, W., and Burgers, G. (2007). On the robustness of ENSO teleconnections. *Clim. Dyn.* 29, 469–485. doi:10.1007/s00382-007-0251-z.
Stevens, B., Fiedler, S., Kinne, S., Peters, K., Rast, S., Müsse, J., et al. (2017). MACv2-SP: a parameterization of anthropogenic aerosol optical properties and an associated Twomey effect for use in CMIP6. *Geosci. Model Dev.* 10, 433–452. doi:10.5194/gmd-10-433-2017.
Stevenson, S., Fasullo, J. T., Otto-Bliesner, B. L., Tomas, R. A., and Gao, C. (2017). Role of eruption season in reconciling model and proxy responses to tropical volcanism. *Proc. Natl. Acad. Sci.* 114, 1822 LP – 1826. doi:10.1073/pnas.1612505114.
Stevenson, S., Otto-Bliesner, B., Fasullo, J., and Brady, E. (2016). "El Niño Like" Hydroclimate Responses to Last Millennium Volcanic Eruptions. *J. Clim.* 29, 2907–2921. doi:10.1175/JCLI-D-15-0239.1.
Stillinger, T., Roberts, D. A., Collar, N. M., and Dozier, J. (2019). Cloud Masking for Landsat 8 and MODIS Terra Over Snow-Covered Terrain: Error Analysis and Spectral Similarity Between Snow and Cloud. *Water Resour. Res.* 55, 6169–6184. doi:10.1029/2019WR024932.
Stocker, T. F., Dahe, Q., Plattner, G.-K., and Tignor, M. (2015). IPCC Workshop on Regional Climate Projections and their Use in Impacts and Risk Analysis Studies. Sao Jose dos Campos.
Stoffel, M., Khodri, M., Corona, C., Guillet, S., Poulain, V., Bekki, S., et al. (2015). Estimates of volcanic-induced cooling in the Northern Hemisphere over the past 1,500 years. *Nat. Geosci.* 8, 784–788. doi:10.1038/ngeo2526.
Stott, P. A., and Kettleborough, J. A. (2002). Origins and estimates of uncertainty in predictions of twenty-first century temperature rise. *Nature* 416, 723–726. doi:10.1038/416723a.
Stott, P., Good, P., Jones, G., Gillett, N., and Hawkins, E. (2013). The upper end of climate model temperature projections is inconsistent with past warming. *Environ. Res. Lett.* 8, 014024. doi:10.1088/1748-9326/8/1/014024.
Strasser, U., Förster, K., Formayer, H., Hofmeister, F., Marke, T., Meißl, G., et al. (2019). Storylines of combined future land use and climate scenarios and their hydrological impacts in an Alpine catchment (Brixental/Austria). *Sci. Total Environ.* 657, 746–763. doi:10.1016/j.scitotenv.2018.12.077.
Stratton, R. A., Senior, C. A., Vosper, S. B., Folwell, S. S., Boutle, I. A., Earnshaw, P. D., et al. (2018). A Pan-African Convection-Permitting Regional Climate Simulation with the Met Office Unified Model: CP4-Africa. *J. Clim.* 31, 3485–3508. doi:10.1175/JCLI-D-17-0503.1.
Street, R. B. (2016). Towards a leading role on climate services in Europe: A research and innovation roadmap. *Clim. Serv.* 1, 2–5. doi:10.1016/j.cliser.2015.12.001.
Strobach, E., and Bel, G. (2019). Regional decadal climate predictions using an ensemble of WRF parameterizations driven by the MIROC5 GCM. *J. Appl. Meteorol. Climatol.* 58, 527–549. doi:10.1175/JAMC-D-18-0051.1.
Strømmen, K., Christensen, H. M., Berner, J., and Palmer, T. N. (2018). The impact of stochastic parametrisations on the representation of the Asian summer monsoon. *Clim. Dyn.* 50, 2269–2282. doi:10.1007/s00382-017-3749-z.
Strong, J. D. O., Vecchi, G. A., and Ginoux, P. (2015). The Response of the Tropical Atlantic and West African Climate to Saharan Dust in a Fully Coupled GCM. *J. Clim.* 28, 7071–7092. doi:10.1175/JCLI-D-14-00797.1.
Su, C.-H., Eizenberg, N., Steinle, P., Jakob, D., Fox-Hughes, P., White, C. J., et al. (2018). BARRA v1.0: The Bureau of Meteorology Atmospheric high-resolution Regional Reanalysis for Australia. *Geosci. Model Dev. Discuss.*, 1–33. doi:10.5194/gmd-2018-277.
Sugimoto, S., Ito, R., Dairaku, K., Kawase, H., Sasaki, H., Watanabe, S., et al. (2018). Impact of Spatial Resolution on Simulated Consecutive Dry Days and Near-Surface Temperature over the Central Mountains in Japan. *SOLA* 14, 46–51. doi:10.2151/sola.2018-008.
Sun, L., Deser, C., and Tomas, R. A. (2015). Mechanisms of Stratospheric and Tropospheric Circulation Response to Projected Arctic Sea Ice Loss. *J. Clim.* 28, 7824–7845. doi:10.1175/JCLI-D-15-0169.1.
Sun, L., Perlwitz, J., and Hoerling, M. (2016a). What caused the recent "Warm Arctic, Cold Continents" trend pattern in winter temperatures? *Geophys. Res. Lett.* 43, 5345–5352. doi:10.1002/2016GL069024.
Sun, W., Liu, J., Wang, B., Chen, D., Liu, F., Wang, Z., et al. (2019a). A "La Niña-like" state occurring in the second year after large tropical volcanic eruptions during the past 1500 years. *Clim. Dyn.* 52, 7495–7509. doi:10.1007/s00382-018-4163-x.
Sun, W., Wang, B., Liu, J., Chen, D., Gao, C., Ning, L., et al. (2019b). How Northern High-Latitude Volcanic Eruptions in Different Seasons Affect ENSO. *J. Clim.* 32, 3245–3262. doi:10.1175/JCLI-D-18-0290.1.
Sun, Y., Zhang, X., Ren, G., Zwiers, F. W., and Hu, T. (2016b). Contribution of urbanization to warming in China. *Nat. Clim. Chang.* 6, 706–709. doi:10.1038/nclimate2956.
Sutton, R. T. (2018). Ideas: a simple proposal to improve the contribution of IPCC WG1 to the assessment and communication of climate change risks. *Earth Syst. Dyn. Discuss.*, 1–3. doi:10.5194/esd-2018-36.
Sutton, R. T., and Dong, B. (2012). Atlantic Ocean influence on a shift in European climate in the 1990s. *Nat. Geosci.* 5, 788. doi:10.1038/ngeo1595.
Sutton, R. T., Dong, B., and Gregory, J. M. (2007). Land/sea warming ratio in response to climate change: IPCC AR4 model results and comparison with observations. *Geophys. Res. Lett.* 34, L02701. doi:10.1029/2006GL028164.
Suzuki-Parker, A., Kusaka, H., Takayabu, I., Dairaku, K., Ishizaki, N. N., and Ham, S. (2018). Contributions of GCM/RCM Uncertainty in Ensemble Dynamical Downscaling for Precipitation in East Asian Summer Monsoon

Season. *SOLA* 14, 97–104. doi:10.2151/sola.2018-017.
Swain, D. L., Singh, D., Horton, D. E., Mankin, J. S., Ballard, T. C., and Diffenbaugh, N. S. (2017). Remote Linkages to Anomalous Winter Atmospheric Ridging Over the Northeastern Pacific. *J. Geophys. Res. Atmos.* 122, 12,194-12,209. doi:10.1002/2017JD026575.
Swingedouw, D., Mignot, J., Ortega, P., Khodri, M., Menegoz, M., Cassou, C., et al. (2017). Impact of explosive volcanic eruptions on the main climate variability modes. *Glob. Planet. Change* 150, 24–45. doi:https://doi.org/10.1016/j.gloplacha.2017.01.006.
Switanek, M. B., Troch, P. A., Castro, C. L., Leuprecht, A., Chang, H.-I., Mukherjee, R., et al. (2017). Scaled distribution mapping: a bias correction method that preserves raw climate model projected changes. *Hydrol. Earth Syst. Sci.* 21, 2649–2666. doi:10.5194/hess-21-2649-2017.
Sylla, M. B., Faye, A., Giorgi, F., Diedhiou, A., and Kunstmann, H. (2018). Projected Heat Stress Under 1.5 °C and 2 °C Global Warming Scenarios Creates Unprecedented Discomfort for Humans in West Africa. *Earth's Futur.* 6, 1029–1044. doi:10.1029/2018EF000873.
Sylla, M. B., Giorgi, F., Coppola, E., and Mariotti, L. (2013). Uncertainties in daily rainfall over Africa: assessment of gridded observation products and evaluation of a regional climate model simulation. *Int. J. Climatol.* 33, 1805–1817. doi:10.1002/joc.3551.
Tabari, H., De Troch, R., Giot, O., Hamdi, R., Termonia, P., Saeed, S., et al. (2016). Local impact analysis of climate change on precipitation extremes: are high-resolution climate models needed for realistic simulations? *Hydrol. Earth Syst. Sci.* 20, 3843–3857. doi:10.5194/hess-20-3843-2016.
Takahashi, H. G., Watanabe, S., Nakata, M., and Takemura, T. (2018). Response of the atmospheric hydrological cycle over the tropical Asian monsoon regions to anthropogenic aerosols and its seasonality. *Prog. Earth Planet. Sci.* 5, 44. doi:10.1186/s40645-018-0197-2.
Takayabu, I., Hibino, K., Sasaki, H., Shiogama, H., Mori, N., Shibutani, Y., et al. (2015). Climate change effects on the worst-case storm surge: a case study of Typhoon Haiyan. *Environ. Res. Lett.* 10, 064011. doi:10.1088/1748-9326/10/6/064011.
Takayabu, I., Kanamaru, H., DAIRAKU, K., Benestad, R., Storch, H. von, and CHRISTENSEN, J. H. (2016). Reconsidering the Quality and Utility of Downscaling. *J. Meteorol. Soc. Japan. Ser. II* 94A, 31–45. doi:10.2151/jmsj.2015-042.
Takayabu, Y. N., Shige, S., Tao, W. K., and Hirota, N. (2010). Shallow and deep latent heating modes over tropical oceans observed with TRMM PR spectral latent heating data. *J. Clim.* 23, 2030–2046. doi:10.1175/2009JCLI3110.1.
Takayabu, Y. N., and Tao, W.-K. (submitted). "Latent heating retrievals from satellite observations," in *Satellite Precipitation Measurement*, eds. V. Levizzani, C. Kidd, D. Kirschbaum, C. Kummerow, K. Nakamura, and F. J. Turk (Springer International Publishing). doi:10.1007/978-3-030-24568-9.
Talchabhadel, R., Karki, R., Thapa, B. R., Maharjan, M., and Parajuli, B. (2018). Spatio-temporal variability of extreme precipitation in Nepal. *Int. J. Climatol.* 38, 4296–4313. doi:10.1002/joc.5669.
Tang, Q., Zhang, X., Yang, X., and Francis, J. A. (2013). Cold winter extremes in northern continents linked to Arctic sea ice loss. *Environ. Res. Lett.* 8, 014036. doi:10.1088/1748-9326/8/1/014036.
Tang, Z., Wang, X., Wang, J., Wang, X., Li, H., and Jiang, Z. (2017). Spatiotemporal Variation of Snow Cover in Tianshan Mountains, Central Asia, Based on Cloud-Free MODIS Fractional Snow Cover Product, 2001–2015. *Remote Sens.* 9. doi:10.3390/rs9101045.
Tao, W.-K., Takayabu, Y. N., Lang, S., Shige, S., Olson, W., Hou, A., et al. (2016). TRMM Latent Heating Retrieval: Applications and Comparisons with Field Campaigns and Large-Scale Analyses. *Meteorol. Monogr.* doi:10.1175/AMSMONOGRAPHS-D-15-0013.1.
Tapper, N. J. (1990). Urban influences on boundary layer temperature and humidity: Results from Christchurch, New Zealand. *Atmos. Environ. Part B. Urban Atmos.* 24, 19–27. doi:https://doi.org/10.1016/0957-1272(90)90005-F.
Taylor, C. M., Belušić, D., Guichard, F., Parker, D. J., Vischel, T., Bock, O., et al. (2017). Frequency of extreme Sahelian storms tripled since 1982 in satellite observations. *Nature* 544, 475–478. doi:10.1038/nature22069.
Taylor, C. M., Birch, C. E., Parker, D. J., Dixon, N., Guichard, F., Nikulin, G., et al. (2013a). Modeling soil moisture-precipitation feedback in the Sahel: Importance of spatial scale versus convective parameterization. *Geophys. Res. Lett.* 40, 6213–6218. doi:10.1002/2013GL058511.
Taylor, C. M., de Jeu, R. A. M., Guichard, F., Harris, P. P., and Dorigo, W. A. (2012). Afternoon rain more likely over drier soils. *Nature* 489, 423–426. doi:10.1038/nature11377.
Taylor, M. A., Clarke, L. A., Centella, A., Bezanilla, A., Stephenson, T. S., Jones, J. J., et al. (2018). Future Caribbean Climates in a World of Rising Temperatures : The 1.5 vs 2.0 Dilemma. *J. Clim.* 31, 2907–2926. doi:10.1175/JCLI-D-17-0074.1.
Taylor, M. A., Stephenson, T. S., Chen, A. A., and Stephenson, K. A. (2013b). Climate Change and the Caribbean: Review and Response. *Caribb. Stud.* 40, 169–200. doi:10.1353/crb.2012.0020.
Tencer, B., Bettolli, M., and Rusticucci, M. (2016). Compound temperature and precipitation extreme events in southern South America: associated atmospheric circulation, and simulations by a multi-RCM ensemble. *Clim. Res.* 68, 183–199. doi:10.3354/cr01396.

Termonia, P., Fischer, C., Bazile, E., Bouyssel, F., Brožková, R., Bénard, P., et al. (2018a). The ALADIN System and its canonical model configurations AROME CY41T1 and ALARO CY40T1. *Geosci. Model Dev.* 11, 257–281. doi:10.5194/gmd-11-257-2018.
Termonia, P., Van Schaeybroeck, B., De Cruz, L., De Troch, R., Caluwaerts, S., Giot, O., et al. (2018b). The CORDEX.be initiative as a foundation for climate services in Belgium. *Clim. Serv.* 11, 49–61. doi:10.1016/J.CLISER.2018.05.001.
Teutschbein, C., and Seibert, J. (2013). Is bias correction of regional climate model (RCM) simulations possible for non-stationary conditions? *Hydrol. Earth Syst. Sci.* 17, 5061–5077. doi:10.5194/hess-17-5061-2013.
Thiéblemont, R., Matthes, K., Omrani, N.-E., Kodera, K., and Hansen, F. (2015). Solar forcing synchronizes decadal North Atlantic climate variability. *Nat. Commun.* 6, 8268. doi:10.1038/ncomms9268.
Thiery, W., Davin, E. L., Panitz, H.-J., Demuzere, M., Lhermitte, S., and van Lipzig, N. (2015). The Impact of the African Great Lakes on the Regional Climate. *J. Clim.* 28, 4061–4085. doi:10.1175/JCLI-D-14-00565.1.
Thober, S., Mai, J., Zink, M., and Samaniego, L. (2014). Stochastic temporal disaggregation of monthly precipitation for regional gridded data sets. *Water Resour. Res.* 50, 8714–8735. doi:10.1002/2014WR015930.
Thompson, D. W. J., Barnes, E. A., Deser, C., Foust, W. E., and Phillips, A. S. (2015). Quantifying the Role of Internal Climate Variability in Future Climate Trends. *J. Clim.* 28, 6443–6456. doi:10.1175/JCLI-D-14-00830.1.
Thompson, D. W. J., Solomon, S., Kushner, P. J., England, M. H., Grise, K. M., and Karoly, D. J. (2011). Signatures of the Antarctic ozone hole in Southern Hemisphere surface climate change. *Nat. Geosci.* 4, 741–749. doi:10.1038/ngeo1296.
Thompson, E., Frigg, R., and Helgeson, C. (2016). Expert Judgment for Climate Change Adaptation. *Philos. Sci.* 83, 1110–1121. doi:10.1086/687942.
Thornhill, G. D., Ryder, C. L., Highwood, E. J., Shaffrey, L. C., and Johnson, B. T. (2018). The effect of South American biomass burning aerosol emissions on the regional climate. *Atmos. Chem. Phys.* 18, 5321–5342. doi:10.5194/acp-18-5321-2018.
Tian, F., Dong, B., Robson, J., and Sutton, R. (2018). Forced decadal changes in the East Asian summer monsoon: the roles of greenhouse gases and anthropogenic aerosols. *Clim. Dyn.* 51, 3699–3715. doi:10.1007/s00382-018-4105-7.
Timmreck, C. (2012). Modeling the climatic effects of large explosive volcanic eruptions. *WIREs Clim. Chang.* 3, 545–564. doi:10.1002/wcc.192.
Toohey, M., Krüger, K., Bittner, M., Timmreck, C., and Schmidt, H. (2014). The impact of volcanic aerosol on the Northern Hemisphere stratospheric polar vortex: mechanisms and sensitivity to forcing structure. *Atmos. Chem. Phys.* 14, 13063–13079. doi:10.5194/acp-14-13063-2014.
Torma, C., Giorgi, F., and Coppola, E. (2015). Added value of regional climate modeling over areas characterized by complex terrain-Precipitation over the Alps. *J. Geophys. Res. Atmos.* 120, 3957–3972. doi:10.1002/2014JD022781.
Torralba, V., Doblas-Reyes, F. J., and Gonzalez-Reviriego, N. (2017). Uncertainty in recent near-surface wind speed trends: A global reanalysis intercomparison. *Environ. Res. Lett.* 12, 114019. doi:10.1088/1748-9326/aa8a58.
Torres-Valcárcel, Á. R., Harbor, J., Torres-Valcárcel, A. L., and González-Avilés, C. J. (2015). Historical differences in temperature between urban and non-urban areas in Puerto Rico. *Int. J. Climatol.* 35, 1648–1661. doi:10.1002/joc.4083.
Trapp, R. J., Robinson, E. D., Baldwin, M. E., Diffenbaugh, N. S., and Schwedler, B. R. J. (2011). Regional climate of hazardous convective weather through high-resolution dynamical downscaling. *Clim. Dyn.* 37, 677–688. doi:10.1007/s00382-010-0826-y.
Trenberth, K. E., Fasullo, J. T., Branstator, G., and Phillips, A. S. (2014). Seasonal aspects of the recent pause in surface warming. *Nat. Clim. Chang.* 4, 911–916. doi:10.1038/nclimate2341.
Trenberth, K. E., Fasullo, J. T., and Shepherd, T. G. (2015). Attribution of climate extreme events. *Nat. Clim. Chang.* 5, 725–730. doi:10.1038/nclimate2657.
Trewin, B. (2010). Exposure, instrumentation, and observing practice effects on land temperature measurements. *Wiley Interdiscip. Rev. Clim. Chang.* 1, 490–506. doi:10.1002/wcc.46.
Trewin, B. (2013). A daily homogenized temperature data set for Australia. *Int. J. Climatol.* 33, 1510–1529. doi:10.1002/joc.3530.
Trusilova, K., Schubert, S., Wouters, H., Früh, B., Grossman-Clarke, S., Demuzere, M., et al. (2016). The urban land use in the COSMO-CLM model: a comparison of three parameterizations for Berlin. *Meteorol. Zeitschrift* 25, 231–244. doi:10.1127/metz/2015/0587.
Tsanis, I., and Tapoglou, E. (2019). Winter North Atlantic Oscillation impact on European precipitation and drought under climate change. *Theor. Appl. Climatol.* 135, 323–330. doi:10.1007/s00704-018-2379-7.
Tschakert, P., Barnett, J., Ellis, N., Lawrence, C., Tuana, N., New, M., et al. (2017). Climate change and loss, as if people mattered: values, places, and experiences. *Wiley Interdiscip. Rev. Clim. Chang.* 8, 1–19. doi:10.1002/wcc.476.
Tschakert, P., Tuana, N., Westskog, H., Koelle, B., and Afrika, A. (2016). TCHANGE: The role of values and visioning in transformation science. *Curr. Opin. Environ. Sustain.* 20, 21–25. doi:10.1016/j.cosust.2016.04.003.

Tucker, S., Jones, R. G., Buonomo, E., Burgin, L., and Gallo, F. (2018). Dynamical downscaling of GloSea5 over Ethiopia. *Clim. Serv.* 9, 57–71. doi:10.1016/J.CLISER.2018.02.001.

Tuinenburg, O. A., Hutjes, R. W. A., Stacke, T., Wiltshire, A., and Lucas-Picher, P. (2014). Effects of Irrigation in India on the Atmospheric Water Budget. *J. Hydrometeorol.* 15, 1028–1050. doi:10.1175/JHM-D-13-078.1.

Tuomenvirta, H. (2001). Homogeneity adjustments of temperature and precipitation series—Finnish and Nordic data. *Int. J. Climatol.* 21, 495–506. doi:10.1002/joc.616.

Turner, A. G., and Annamalai, H. (2012). Climate change and the South Asian summer monsoon. *Nat. Clim. Chang.* 2, 587–595. doi:10.1038/nclimate1495.

Turnock, S. T., Butt, E. W., Richardson, T. B., Mann, G. W., Reddington, C. L., Forster, P. M., et al. (2016). The impact of European legislative and technology measures to reduce air pollutants on air quality, human health and climate. *Environ. Res. Lett.* 11, 24010. doi:10.1088/1748-9326/11/2/024010.

Turnock, S. T., Spracklen, D. V, Carslaw, K. S., Mann, G. W., Woodhouse, M. T., Forster, P. M., et al. (2015). Modelled and observed changes in aerosols and surface solar radiation over Europe between 1960 and 2009. *Atmos. Chem. Phys.* 15, 9477–9500. doi:10.5194/acp-15-9477-2015.

Turuncoglu, U. U., Giuliani, G., Elguindi, N., and Giorgi, F. (2012). Modeling the Caspian Sea and its catchment area using a coupled regional atmosphere-ocean model (RegCM-ROMS): model design and preliminary results. *Geosci. Model Dev. Discuss.* 5, 3907–3955. doi:10.5194/gmdd-5-3907-2012.

Tuttle, S., and Salvucci, G. (2016). Empirical evidence of contrasting soil moisture-precipitation feedbacks across the United States. *Science* 352, 825–828. doi:10.1126/science.aaa7185.

Udall, B., and Overpeck, J. (2017). The twenty-first century Colorado River hot drought and implications for the future. *Water Resour. Res.* 53, 2404–2418. doi:10.1002/2016WR019638.

Ueda, H., Iwai, A., Kuwako, K., and Hori, M. E. (2006). Impact of anthropogenic forcing on the Asian summer monsoon as simulated by eight GCMs. *Geophys. Res. Lett.* 33, L06703. doi:10.1029/2005GL025336.

Ukkola, A. M., Pitman, A. J., Donat, M. G., De Kauwe, M. G., and Angélil, O. (2018). Evaluating the Contribution of Land-Atmosphere Coupling to Heat Extremes in CMIP5 Models. *Geophys. Res. Lett.* 45, 9003–9012. doi:10.1029/2018GL079102.

Undorf, S., Polson, D., Bollasina, M. A., Ming, Y., Schurer, A., and Hegerl, G. C. (2018). Detectable Impact of Local and Remote Anthropogenic Aerosols on the 20th Century Changes of West African and South Asian Monsoon Precipitation. *J. Geophys. Res. Atmos.* 123, 4871–4889. doi:10.1029/2017JD027711.

Unger, J. (1999). Urban–rural air humidity differences in Szeged, Hungary. *Int. J. Climatol.* 19, 1509–1515. doi:10.1002/(SICI)1097-0088(19991115)19:13<1509::AID-JOC453>3.0.CO;2-P.

Unkašević, M., Jovanović, O., and Popović, T. (2001). Urban-suburban/rural vapour pressure and relative humidity differences at fixed hours over the area of Belgrade city. *Theor. Appl. Climatol.* 68, 67–73. doi:10.1007/s007040170054.

Uppala, S. M., KÅllberg, P. W., Simmons, A. J., Andrae, U., Bechtold, V. D. C., Fiorino, M., et al. (2006). The ERA-40 re-analysis. *Q. J. R. Meteorol. Soc.* 131, 2961–3012. doi:10.1256/qj.04.176.

Vaittinada Ayar, P., Vrac, M., Bastin, S., Carreau, J., Déqué, M., and Gallardo, C. (2016). Intercomparison of statistical and dynamical downscaling models under the EURO- and MED-CORDEX initiative framework: present climate evaluations. *Clim. Dyn.* 46, 1301–1329. doi:10.1007/s00382-015-2647-5.

Van Den Besselaar, E. J. M., Klein Tank, A. M. G., Van Der Schrier, G., Abass, M. S., Baddour, O., Van Engelen, A. F. V., et al. (2015). International Climate Assessment & Dataset: Climate Services across Borders. *Bull. Am. Meteorol. Soc.* 96, 16–21. doi:10.1175/BAMS-D-13-00249.1.

van den Besselaar, E. J. M. M., van der Schrier, G., Cornes, R. C., Iqbal, A. S., and Klein Tank, A. M. G. (2017). SA-OBS: A Daily Gridded Surface Temperature and Precipitation Dataset for Southeast Asia. *J. Clim.* 30, 5151–5165. doi:10.1175/JCLI-D-16-0575.1.

van der Schrier, G., van den Besselaar, E. J. M., Klein Tank, A. M. G., and Verver, G. (2013). Monitoring European average temperature based on the E-OBS gridded data set. *J. Geophys. Res. Atmos.* 118, 5120–5135. doi:10.1002/jgrd.50444.

van Haren, R., Haarsma, R. J., de Vries, H., van Oldenborgh, G. J., and Hazeleger, W. (2015). Resolution dependence of circulation forced future central European summer drying. *Environ. Res. Lett.* 10, 55002. Available at: http://stacks.iop.org/1748-9326/10/i=5/a=055002.

van Oldenborgh, G. J., Drijfhout, S., van Ulden, A., Haarsma, R., Sterl, A., Severijns, C., et al. (2009). Western Europe is warming much faster than expected. *Clim. Past* 5, 1–12. doi:10.5194/cp-5-1-2009.

Van Pham, T., Brauch, J., Dieterich, C., Frueh, B., and Ahrens, B. (2014). New coupled atmosphere-ocean-ice system COSMO-CLM/NEMO: assessing air temperature sensitivity over the North and Baltic Seas. *Oceanologia* 56, 167–189. doi:10.5697/oc.56-2.167.

Vanden Broucke, S., Wouters, H., Demuzere, M., and van Lipzig, N. P. M. (2018). The influence of convection-permitting regional climate modeling on future projections of extreme precipitation: dependency on topography and timescale. *Clim. Dyn.* 52, 1–22. doi:10.1007/s00382-018-4454-2.

Vannitsem, S. (2011). Bias correction and post-processing under climate change. *Nonlinear Process. Geophys.* 18, 911–924. doi:10.5194/npg-18-911-2011.

Varikoden, H., Mujumdar, M., Revadekar, J. V., Sooraj, K. P., Ramarao, M. V. S., Sanjay, J., et al. (2018). Assessment of regional downscaling simulations for long term mean, excess and deficit Indian Summer Monsoons. *Glob. Planet. Change* 162, 28–38. doi:10.1016/j.gloplacha.2017.12.002.
Vautard, R., Gobiet, A., Jacob, D., Belda, M., Colette, A., Déqué, M., et al. (2013). The simulation of European heat waves from an ensemble of regional climate models within the EURO-CORDEX project. *Clim. Dyn.* 41, 2555–2575. doi:10.1007/s00382-013-1714-z.
Vautard, R., and Yiou, P. (2009). Control of recent European surface climate change by atmospheric flow. *Geophys. Res. Lett.* 36, L22702. doi:10.1029/2009GL040480.
Vavrus, S. J., Wang, F., Martin, J. E., Francis, J. A., Peings, Y., and Cattiaux, J. (2017). Changes in North American Atmospheric Circulation and Extreme Weather: Influence of Arctic Amplification and Northern Hemisphere Snow Cover. *J. Clim.* 30, 4317–4333. doi:10.1175/JCLI-D-16-0762.1.
Vellinga, M., Roberts, M., Vidale, P. L., Mizielinski, M. S., Demory, M., Schiemann, R., et al. (2016). Sahel decadal rainfall variability and the role of model horizontal resolution. *Geophys. Res. Lett.* 43, 326–333. doi:10.1002/2015GL066690.
Venema, V. K. C., Mestre, O., Aguilar, E., Auer, I., Guijarro, J. A., Domonkos, P., et al. (2012). Benchmarking homogenization algorithms for monthly data. *Clim. Past* 8, 89–115. doi:10.5194/cp-8-89-2012.
Vera, C. S., and Díaz, L. (2015). Anthropogenic influence on summer precipitation trends over South America in CMIP5 models. *Int. J. Climatol.* 35, 3172–3177. doi:10.1002/joc.4153.
Vergara-Temprado, J., Ban, N., Panosetti, D., Schlemmer, L., and Schär, C. (2019). Climate models permit convection at much coarser resolutions than previously considered. *J. Clim.*, JCLI-D-19-0286.1. doi:10.1175/JCLI-D-19-0286.1.
Vernier, J.-P., Thomason, L. W., Pommereau, J.-P., Bourassa, A., Pelon, J., Garnier, A., et al. (2011). Major influence of tropical volcanic eruptions on the stratospheric aerosol layer during the last decade. *Geophys. Res. Lett.* 38. doi:10.1029/2011GL047563.
Verrax, F. (2017). Engineering ethics and post-normal science: A French perspective. *Futures* 91, 76–79. doi:10.1016/j.futures.2017.01.009.
Vezér, M., Bakker, A., Keller, K., and Tuana, N. (2018). Epistemic and ethical trade-offs in decision analytical modelling: A case study of flood risk management in New Orleans. *Clim. Change* 147, 1–10. doi:10.1007/s10584-017-2123-9.
Vidal, J.-P., Martin, E., Franchistéguy, L., Baillon, M., and Soubeyroux, J.-M. (2010). A 50-year high-resolution atmospheric reanalysis over France with the Safran system. *Int. J. Climatol.* 30, 1627–1644. doi:10.1002/joc.2003.
Vigaud, N., Vrac, M., and Caballero, Y. (2013). Probabilistic downscaling of GCM scenarios over southern India. *Int. J. Climatol.* 33, 1248–1263. doi:10.1002/joc.3509.
Villamayor, J., and Mohino, E. (2015). Robust Sahel drought due to the Interdecadal Pacific Oscillation in CMIP5 simulations. *Geophys. Res. Lett.* doi:10.1002/2014GL062473.
Vincent, K., Daly, M., Scannell, C., and Leathes, B. (2018). What can climate services learn from theory and practice of co-production? *Clim. Serv.* 12, 48–58. doi:https://doi.org/10.1016/j.cliser.2018.11.001.
Vincent, K., Dougill, A. J., Dixon, J. L., Stringer, L. C., and Cull, T. (2017). Identifying climate services needs for national planning: insights from Malawi. *Clim. Policy* 17, 189–202. doi:10.1080/14693062.2015.1075374.
Vinoj, V., Rasch, P. J., Wang, H., Yoon, J.-H., Ma, P.-L., Landu, K., et al. (2014). Short-term modulation of Indian summer monsoon rainfall by West Asian dust. *Nat. Geosci.* 7, 308–313. doi:10.1038/ngeo2107.
Visser, W. P. (2018). A perfect storm: The ramifications of Cape Town's drought crisis. *J. Transdiscipl. Res. South. Africa* 14, 1–10. doi:10.4102/td.v14i1.567.
Vitart, F., Ardilouze, C., Bonet, A., Brookshaw, A., Chen, M., Codorean, C., et al. (2017). The Subseasonal to Seasonal (S2S) Prediction Project Database. *Bull. Am. Meteorol. Soc.* 98, 163–173. doi:10.1175/BAMS-D-16-0017.1.
Vizy, E. K., and Cook, K. H. (2017). Seasonality of the Observed Amplified Sahara Warming Trend and Implications for Sahel Rainfall. *J. Clim.* 30, 3073–3094. doi:10.1175/JCLI-D-16-0687.1.
Vogel, M. M., Orth, R., Cheruy, F., Hagemann, S., Lorenz, R., van den Hurk, B. J. J. M., et al. (2017). Regional amplification of projected changes in extreme temperatures strongly controlled by soil moisture-temperature feedbacks. *Geophys. Res. Lett.* 44, 1511–1519. doi:10.1002/2016GL071235.
Volosciuk, C., Maraun, D., Vrac, M., and Widmann, M. (2017). A combined statistical bias correction and stochastic downscaling method for precipitation. *Hydrol. Earth Syst. Sci.* 21, 1693–1719. doi:10.5194/hess-21-1693-2017.
Von Clarmann, T. (2014). Smoothing error pitfalls. *Atmos. Meas. Tech.* 7, 3023–3034. doi:10.5194/amt-7-3023-2014.
von Storch, H., Langenberg, H., and Feser, F. (2000). A Spectral Nudging Technique for Dynamical Downscaling Purposes. *Mon. Weather Rev.* 128, 3664–3673. doi:10.1175/1520-0493(2000)128<3664:ASNTFD>2.0.CO;2.
von Trentini, F., Aalbers, E. E., Fischer, E. M., and Ludwig, R. (2019a). Comparing internal variabilities in three regional single model initial-condition large ensembles (SMILE) over Europe. *Earth Syst. Dyn. Discuss.* doi:10.5194/esd-2019-67.
von Trentini, F., Leduc, M., and Ludwig, R. (2019b). Assessing natural variability in RCM signals: comparison of a multi model EURO-CORDEX ensemble with a 50-member single model large ensemble. *Clim. Dyn.* 53, 1963–

1979. doi:10.1007/s00382-019-04755-8.
Vose, R. S., Arndt, D., Banzon, V. F., Easterling, D. R., Gleason, B., Huang, B., et al. (2012). NOAA's Merged Land–Ocean Surface Temperature Analysis. *Bull. Am. Meteorol. Soc.* 93, 1677–1685. doi:10.1175/BAMS-D-11-00241.1.
Vrac, M. (2018). Multivariate bias adjustment of high-dimensional climate simulations: the Rank Resampling for Distributions and Dependences (R^2D^2) bias correction. *Hydrol. Earth Syst. Sci.* 22, 3175–3196. doi:10.5194/hess-22-3175-2018.
Vrac, M., and Friederichs, P. (2015). Multivariate—Intervariable, Spatial, and Temporal—Bias Correction*. *J. Clim.* 28, 218–237. doi:10.1175/JCLI-D-14-00059.1.
Wada, Y., Wisser, D., and Bierkens, M. F. P. (2014). Global modeling of withdrawal, allocation and consumptive use of surface water and groundwater resources. *Earth Syst. Dyn.* doi:10.5194/esd-5-15-2014.
Waha, K., Krummenauer, L., Adams, S., Aich, V., Baarsch, F., Coumou, D., et al. (2017). Climate change impacts in the Middle East and Northern Africa (MENA) region and their implications for vulnerable population groups. *Reg. Environ. Chang.* doi:10.1007/s10113-017-1144-2.
Wahl, S., Bollmeyer, C., Crewell, S., Figura, C., Friederichs, P., Hense, A., et al. (2017). A novel convective-scale regional reanalysis COSMO-REA2: Improving the representation of precipitation. *Meteorol. Zeitschrift* 26, 345–361. doi:10.1127/metz/2017/0824.
Wahl, T., Jain, S., Bender, J., Meyers, S. D., and Luther, M. E. (2015). Increasing risk of compound flooding from storm surge and rainfall for major US cities. *Nat. Clim. Chang.* 5, 1093. Available at: https://doi.org/10.1038/nclimate2736.
Waldron, K. M., Paegle, J., and Horel, J. D. (1996). Sensitivity of a Spectrally Filtered and Nudged Limited-Area Model to Outer Model Options. *Mon. Weather Rev.* 124, 529–547. doi:10.1175/1520-0493(1996)124<0529:SOASFA>2.0.CO;2.
Walker, W., Haasnoot, M., and Kwakkel, J. (2013). Adapt or Perish: A Review of Planning Approaches for Adaptation under Deep Uncertainty. *Sustainability* 5, 955–979. doi:10.3390/su5030955.
Wallace, J. M., Held, I. M., Thompson, D. W. J., Trenberth, K. E., and Walsh, J. E. (2014). Global Warming and Winter Weather. *Science* 343, 729–730. doi:10.1126/science.343.6172.729.
Wallack, J. S., and Ramanathan, V. (2009). The Other Climate Changers. *Foreign Aff.*
Walsh, J. E. (2014). Intensified warming of the Arctic: Causes and impacts on middle latitudes. *Glob. Planet. Change* 117, 52–63. doi:10.1016/j.gloplacha.2014.03.003.
Walton, D. B., Sun, F., Hall, A., and Capps, S. (2015). A Hybrid Dynamical–Statistical Downscaling Technique. Part I: Development and Validation of the Technique. *J. Clim.* 28, 4597–4617. doi:10.1175/JCLI-D-14-00196.1.
Wan, H., Zhang, X., and Zwiers, F. (2019). Human influence on Canadian temperatures. *Clim. Dyn.* 52, 479–494. doi:10.1007/s00382-018-4145-z.
Wan, H., Zhang, X., Zwiers, F., and Min, S.-K. (2015). Attributing northern high-latitude precipitation change over the period 1966–2005 to human influence. *Clim. Dyn.* 45, 1713–1726. doi:10.1007/s00382-014-2423-y.
Wang, B., Biasutti, M., Byrne, M., Castro, C., Chang, C.-P., Cook, K., et al. (submitted). Monsoon climate change assessment. *Bull. Am. Meteorol. Soc.* (submtted).
Wang, C. (2007). Variability of the Caribbean Low-Level Jet and its relations to climate. *Clim. Dyn.* 29, 411–422. doi:10.1007/s00382-007-0243-z.
Wang, C., and Lee, S. (2007). Atlantic warm pool, Caribbean low-level jet, and their potential impact on Atlantic hurricanes. *Geophys. Res. Lett.* 34, L02703. doi:10.1029/2006GL028579.
Wang, J., Yan, Z., Quan, X. W., and Feng, J. (2017a). Urban warming in the 2013 summer heat wave in eastern China. *Clim. Dyn.* 48, 3015–3033. doi:10.1007/s00382-016-3248-7.
Wang, K., Deser, C., Sun, L., and Tomas, R. A. (2018a). Fast Response of the Tropics to an Abrupt Loss of Arctic Sea Ice via Ocean Dynamics. *Geophys. Res. Lett.* 45, 4264–4272. doi:10.1029/2018GL077325.
Wang, K., Li, Y., Luo, Z., Yin, S., and Chan, P. W. (2018b). Harmonic analysis of 130-year hourly air temperature in Hong Kong: detecting urban warming from the perspective of annual and daily cycles. *Clim. Dyn.* 51, 613–625. doi:10.1007/s00382-017-3944-y.
Wang, L., and Chen, W. (2014). The East Asian winter monsoon: re-amplification in the mid-2000s. *Chinese Sci. Bull.* 59, 430–436. doi:10.1007/s11434-013-0029-0.
Wang, L., Liu, Y., Zhang, Y., Chen, W., and Chen, S. (2019). Time-varying structure of the wintertime Eurasian pattern: role of the North Atlantic sea surface temperature and atmospheric mean flow. *Clim. Dyn.* 52, 2467–2479. doi:10.1007/s00382-018-4261-9.
Wang, L., Xu, P., Chen, W., and Liu, Y. (2017b). Interdecadal variations of the Silk Road pattern. *J. Clim.* 30, 9915–9932. doi:10.1175/JCLI-D-17-0340.1.
Wang, Q., Wang, Z., and Zhang, H. (2017c). Impact of anthropogenic aerosols from global, East Asian, and non-East Asian sources on East Asian summer monsoon system. *Atmos. Res.* 183, 224–236. doi:10.1016/j.atmosres.2016.08.023.
Wang, T. J., Zhuang, B. L., Li, S., Liu, J., Xie, M., Yin, C. Q., et al. (2015a). The interactions between anthropogenic aerosols and the East Asian summer monsoon using RegCCMS. *J. Geophys. Res. Atmos.* 120, 5602–5621.

doi:10.1002/2014JD022877.

Wang, T., Wang, H. J., Otterå, O. H., Gao, Y. Q., Suo, L. L., Furevik, T., et al. (2013). Anthropogenic forcing of shift in precipitation in Eastern China in late 1970s. *Atmos. Chem. Phys. Discuss.* 13, 11997–12032. doi:10.5194/acpd-13-11997-2013.

Wang, W., Evan, A. T., Flamant, C., and Lavaysse, C. (2015b). On the decadal scale correlation between African dust and Sahel rainfall: The role of Saharan heat low–forced winds. *Sci. Adv.* 1, e1500646. doi:10.1126/sciadv.1500646.

Wang, Y., Sun, Y., Hu, T., Qin, D., and Song, L. (2018c). Attribution of temperature changes in Western China. *Int. J. Climatol.* 38, 742–750. doi:10.1002/joc.5206.

Wang, Z., Li, Y., Liu, B., and Liu, J. (2015c). Global climate internal variability in a 2000-year control simulation with Community Earth System Model (CESM). *Chinese Geogr. Sci.* 25. doi:10.1007/s11769-015-0754-1.

Wang, Z., Lin, L., Yang, M., Xu, Y., and Li, J. (2017d). Disentangling fast and slow responses of the East Asian summer monsoon to reflecting and absorbing aerosol forcings. *Atmos. Chem. Phys.* 17, 11075–11088. doi:10.5194/acp-17-11075-2017.

Ward, K., Lauf, S., Kleinschmit, B., and Endlicher, W. (2016). Heat waves and urban heat islands in Europe: A review of relevant drivers. *Sci. Total Environ.* 569–570, 527–539. doi:10.1016/j.scitotenv.2016.06.119.

Warner, J. L., Screen, J. A., and Scaife, A. A. (2019). Links between Barents-Kara sea ice and the Extratropical Atmospheric Circulation explained by internal variability and tropical forcing. *Geophys. Res. Lett.* 46. doi:10.1029/2019GL085679.

Warszawski, L., Frieler, K., Huber, V., Piontek, F., Serdeczny, O., and Schewe, J. (2014). The Inter-Sectoral Impact Model Intercomparison Project (ISI–MIP): Project framework. *Proc. Natl. Acad. Sci.* 111, 3228–3232. doi:10.1073/pnas.1312330110.

Waugh, D. W., Garfinkel, C. I., and Polvani, L. M. (2015). Drivers of the Recent Tropical Expansion in the Southern Hemisphere: Changing SSTs or Ozone Depletion? *J. Clim.* 28, 6581–6586. doi:10.1175/JCLI-D-15-0138.1.

Waylen, P. R., Caviedes, C. N., and Quesada, M. E. (1996). Interannual Variability of Monthly Precipitation in Costa Rica. *J. Clim.* 9, 2606–2613. doi:10.1175/1520-0442(1996)009<2606:IVOMPI>2.0.CO;2.

Weaver, C. P., Lempert, R. J., Brown, C., Hall, J. A., Revell, D., and Sarewitz, D. (2013). Improving the contribution of climate model information to decision making: the value and demands of robust decision frameworks. *Wiley Interdiscip. Rev. Clim. Chang.* 4, 39–60. doi:10.1002/wcc.202.

Webber, H., Ewert, F., Olesen, J. E., Müller, C., Fronzek, S., Ruane, A. C., et al. (2018). Diverging importance of drought stress for maize and winter wheat in Europe. *Nat. Commun.* 9, 4249. doi:10.1038/s41467-018-06525-2.

Webber, S., and Donner, S. D. (2017). Climate service warnings: cautions about commercializing climate science for adaptation in the developing world. *Wiley Interdiscip. Rev. Clim. Chang.* 8, e424. doi:10.1002/wcc.424.

Weedon, G. P., Balsamo, G., Bellouin, N., Gomes, S., Best, M. J., and Viterbo, P. (2014). The WFDEI meteorological forcing data set: WATCH Forcing data methodology applied to ERA-Interim reanalysis data. *Water Resour. Res.* doi:10.1002/2014WR015638.

Weldeab, S., Stuut, J.-B. W., Schneider, R. R., and Siebel, W. (2013). Holocene climate variability in the winter rainfall zone of South Africa. *Clim. Past* 9, 2347–2364. doi:10.5194/cp-9-2347-2013.

Westervelt, D. M., Conley, A. J., Fiore, A. M., Lamarque, J.-F., Shindell, D. T., Previdi, M., et al. (2018). Connecting regional aerosol emissions reductions to local and remote precipitation responses. *Atmos. Chem. Phys.* 18, 12461–12475. doi:10.5194/acp-18-12461-2018.

Westra, S., Varley, I., Jordan, P., Nathan, R., Ladson, A., Sharma, A., et al. (2010). Addressing Climatic Non-Stationarity in the Assessment of Flood Risk. *Australas. J. Water Resour.* 14, 1–16. doi:10.1080/13241583.2010.11465370.

Wettstein, J. J., and Deser, C. (2014). Internal Variability in Projections of Twenty-First-Century Arctic Sea Ice Loss: Role of the Large-Scale Atmospheric Circulation. *J. Clim.* 27, 527–550. doi:10.1175/JCLI-D-12-00839.1.

Whan, K., Zscheischler, J., Orth, R., Shongwe, M., Rahimi, M., Asare, E. O., et al. (2015). Impact of soil moisture on extreme maximum temperatures in Europe. *Weather Clim. Extrem.* 9, 57–67. doi:10.1016/j.wace.2015.05.001.

Whan, K., and Zwiers, F. (2017). The impact of ENSO and the NAO on extreme winter precipitation in North America in observations and regional climate models. *Clim. Dyn.* 48, 1401–1411. doi:10.1007/s00382-016-3148-x.

White, R. H., and Toumi, R. (2013). The limitations of bias correcting regional climate model inputs. *Geophys. Res. Lett.* 40, 2907–2912. doi:10.1002/grl.50612.

Whyte, F. S., Taylor, M. A., Stephenson, T. S., and Campbell, J. D. (2008). Features of the Caribbean low level jet. *Int. J. Climatol.* 28, 119–128. doi:10.1002/joc.1510.

Widmann, M., Bedia, J., Gutiérrez, J. M., Bosshard, T., Hertig, E., Maraun, D., et al. (2019). Validation of spatial variability in downscaling results from the VALUE perfect predictor experiment. *Int. J. Climatol.* 39, 3819–3845. doi:10.1002/joc.6024.

Widmann, M., Goosse, H., van der Schrier, G., Schnur, R., and Barkmeijer, J. (2010). Using data assimilation to study extratropical Northern Hemisphere climate over the last millennium. *Clim. Past* 6, 627–644. doi:10.5194/cp-6-627-2010.

Wiest, S. L., Raymond, L., and Clawson, R. A. (2015). Framing, partisan predispositions, and public opinion on climate change. *Glob. Environ. Chang.* 31, 187–198. doi:10.1016/J.GLOENVCHA.2014.12.006.

Wilby, R. L., and Dessai, S. (2010). Robust adaptation to climate change. *Weather* 65, 180–185. doi:10.1002/wea.543.

Wilby, R. L., and Yu, D. (2013). Rainfall and temperature estimation for a data sparse region. *Hydrol. Earth Syst. Sci.* 17, 3937–3955. doi:10.5194/hess-17-3937-2013.

Wilcke, R. A. I., and Bärring, L. (2016). Selecting regional climate scenarios for impact modelling studies. *Environ. Model. Softw.* 78, 191–201. doi:10.1016/j.envsoft.2016.01.002.

Wilcox, L. J., Highwood, E. J., and Dunstone, N. J. (2013). The influence of anthropogenic aerosol on multi-decadal variations of historical global climate. *Environ. Res. Lett.* 8, 024033. doi:10.1088/1748-9326/8/2/024033.

Wilcox, L. J., Liu, Z., Samset, B. H., Hawkins, E., Lund, M. T., Nordling, K., et al. (submitted). Aerosol reductions accelerate near-term changes in the Asian summer monsoon. *Atmos. Chem. Phys.* (submitted).

Wildschut, D. (2017). The need for citizen science in the transition to a sustainable peer-to-peer-society. *Futures* 91, 46–52. doi:10.1016/j.futures.2016.11.010.

Wilks, D. S. (2016). "The Stippling Shows Statistically Significant Grid Points": How Research Results are Routinely Overstated and Overinterpreted, and What to Do about It. *Bull. Am. Meteorol. Soc.* 97, 2263–2273. doi:10.1175/BAMS-D-15-00267.1.

Willems, P., and Vrac, M. (2011). Statistical precipitation downscaling for small-scale hydrological impact investigations of climate change. *J. Hydrol.* 402, 193–205. doi:10.1016/j.jhydrol.2011.02.030.

Williams, A. P., Seager, R., Abatzoglou, J. T., Cook, B. I., Smerdon, J. E., and Cook, E. R. (2015). Contribution of anthropogenic warming to California drought during 2012-2014. *Geophys. Res. Lett.* 42, 6819–6828. doi:10.1002/2015GL064924.

Williams, C. N., Menne, M. J., and Thorne, P. W. (2012). Benchmarking the performance of pairwise homogenization of surface temperatures in the United States. *J. Geophys. Res. Atmos.* 117, D05116. doi:10.1029/2011JD016761.

Williams, K. D., Copsey, D., Blockley, E. W., Bodas-Salcedo, A., Calvert, D., Comer, R., et al. (2018). The Met Office Global Coupled Model 3.0 and 3.1 (GC3.0 and GC3.1) Configurations. *J. Adv. Model. Earth Syst.* 10, 357–380. doi:10.1002/2017MS001115.

Willison, J., Robinson, W. A., and Lackmann, G. M. (2013). The Importance of Resolving Mesoscale Latent Heating in the North Atlantic Storm Track. *J. Atmos. Sci.* 70, 2234–2250. doi:10.1175/JAS-D-12-0226.1.

Willmott, C. J., and Matsuura, K. (1995). Smart Interpolation of Annually Averaged Air Temperature in the United States. *J. Appl. Meteorol.* 34, 2577–2586. doi:10.1175/1520-0450(1995)034<2577:SIOAAA>2.0.CO;2.

Willyard, C., Scudellari, M., and Nordling, L. (2018). How three research groups are tearing down the ivory tower. *Nature* 562, 24–28. doi:10.1038/d41586-018-06858-4.

Winter, K. J.-P. M., Kotlarski, S., Scherrer, S. C., and Schär, C. (2017). The Alpine snow-albedo feedback in regional climate models. *Clim. Dyn.* 48, 1109–1124. doi:10.1007/s00382-016-3130-7.

WMO (2017). WMO Guidelines on Generating a Defined Set of National Climate Monitoring Products 2017.

WMO (2019). *Guide to the WMO Integrated Global Observing System 2019*.

Wolski, P. (2018). How severe is Cape Town's "Day Zero" drought? *Significance* 15, 24–27. doi:10.1111/j.1740-9713.2018.01127.x.

Wolski, P., Jack, C., and Conradie, S. (submitted). Rainfall trends and anomalies underlying 2015-2017 Cape Town drought and water crisis. *Int. J. Climatol.* (submitted).

Wolski, P., Jack, C., Tadross, M., van Aardenne, L., and Lennard, C. (2018). Interannual rainfall variability and SOM-based circulation classification. *Clim. Dyn.* 50, 479–492. doi:10.1007/s00382-017-3621-1.

Woodhouse, C. A., Meko, D. M., MacDonald, G. M., Stahle, D. W., and Cook, E. R. (2010). A 1,200-year perspective of 21st century drought in southwestern North America. *Proc. Natl. Acad. Sci.* 107, 21283–21288. doi:10.1073/pnas.0911197107.

Woodhouse, C. A., and Pederson, G. T. (2018). Investigating Runoff Efficiency in Upper Colorado River Streamflow Over Past Centuries. *Water Resour. Res.* 54, 286–300. doi:10.1002/2017WR021663.

Woodhouse, C. A., Pederson, G. T., Morino, K., McAfee, S. A., and McCabe, G. J. (2016). Increasing influence of air temperature on upper Colorado River streamflow. *Geophys. Res. Lett.* 43, 2174–2181. doi:10.1002/2015GL067613.

Woods, C., and Caballero, R. (2016). The Role of Moist Intrusions in Winter Arctic Warming and Sea Ice Decline. *J. Clim.* 29, 4473–4485. doi:10.1175/JCLI-D-15-0773.1.

Woods, C., Caballero, R., and Svensson, G. (2013). Large-scale circulation associated with moisture intrusions into the Arctic during winter. *Geophys. Res. Lett.* 40, 4717–4721. doi:10.1002/grl.50912.

Woollings, T., Harvey, B., and Masato, G. (2014). Arctic warming, atmospheric blocking and cold European winters in CMIP5 models. *Environ. Res. Lett.* 9, 014002. doi:10.1088/1748-9326/9/1/014002.

World Bank Group (2017). Middle East & North Africa Data. Available at: Middle East & North Africa Data [Accessed September 3, 2017].

Wright, D. M., Posselt, D. J., and Steiner, A. L. (2013). Sensitivity of Lake-Effect Snowfall to Lake Ice Cover and Temperature in the Great Lakes Region. *Mon. Weather Rev.* 141, 670–689. doi:10.1175/MWR-D-12-00038.1.

Wright, E. E., Sutton, J. R. P., Luchetti, N. T., Kruk, M. C., and Marra, J. J. (2016). Closing the Pacific Rainfall Data Void. *Eos (Washington. DC).* 97. doi:10.1029/2016EO055053.

Wu, B., Lin, J., and Zhou, T. (2016a). Interdecadal circumglobal teleconnection pattern during boreal summer. *Atmos. Sci. Lett.* 17, 446–452. doi:10.1002/asl.677.

Wu, B., Zhou, T., and Li, T. (2016b). Impacts of the Pacific–Japan and Circumglobal Teleconnection Patterns on the Interdecadal Variability of the East Asian Summer Monsoon. *J. Clim.* 29, 3253–3271. doi:10.1175/JCLI-D-15-0105.1.

Wu, G., Li, Z., Fu, C., Zhang, X., Zhang, R., Zhang, R., et al. (2016c). Advances in studying interactions between aerosols and monsoon in China. *Sci. China Earth Sci.* 59, 1–16. doi:10.1007/s11430-015-5198-z.

Wu, J., Zha, J., and Zhao, D. (2017). Evaluating the effects of land use and cover change on the decrease of surface wind speed over China in recent 30 years using a statistical downscaling method. *Clim. Dyn.* 48, 131–149. doi:10.1007/s00382-016-3065-z.

Wu, Y., and Polvani, L. M. (2017). Recent Trends in Extreme Precipitation and Temperature over Southeastern South America: The Dominant Role of Stratospheric Ozone Depletion in the CESM Large Ensemble. *J. Clim.* 30, 6433–6441. doi:10.1175/JCLI-D-17-0124.1.

Wu, Z., and Huang, N. E. (2009). Ensemble empirical mode decomposition: a noise-assisted data analysis method. *Adv. Adapt. Data Anal.* 01, 1–41. doi:10.1142/S1793536909000047.

Wulder, M. A., White, J. C., Loveland, T. R., Woodcock, C. E., Belward, A. S., Cohen, W. B., et al. (2016). The global Landsat archive: Status, consolidation, and direction. *Remote Sens. Environ.* 185, 271–283. doi:10.1016/j.rse.2015.11.032.

Xavier, A. C., King, C. W., and Scanlon, B. R. (2016). Daily gridded meteorological variables in Brazil (1980–2013). *Int. J. Climatol.* 36, 2644–2659. doi:10.1002/joc.4518.

Xiao, C., Lofgren, B. M., Wang, J., and Chu, P. Y. (2016). Improving the lake scheme within a coupled WRF-lake model in the Laurentian Great Lakes. *J. Adv. Model. Earth Syst.* 8, 1969–1985. doi:10.1002/2016MS000717.

Xie, P., and Arkin, P. A. (1997). Global Precipitation: A 17-Year Monthly Analysis Based on Gauge Observations, Satellite Estimates, and Numerical Model Outputs. *Bull. Am. Meteorol. Soc.* 78, 2539–2558. doi:10.1175/1520-0477(1997)078<2539:GPAYMA>2.0.CO;2.

Xie, S.-P., Deser, C., Vecchi, G. A., Collins, M., Delworth, T. L., Hall, A., et al. (2015). Towards predictive understanding of regional climate change. *Nat. Clim. Chang.* 5, 921. doi:10.1038/nclimate2689.

Xie, S., McCoy, R. B., Klein, S. A., Cederwall, R. T., Wiscombe, W. J., Jensen, M. P., et al. (2010). CLOUDS AND MORE: ARM Climate Modeling Best Estimate Data. *Bull. Am. Meteorol. Soc.* 91, 13–20. doi:10.1175/2009BAMS2891.1.

Xie, X., Wang, H., Liu, X., Li, J., Wang, Z., and Liu, Y. (2016). Distinct effects of anthropogenic aerosols on the East Asian summer monsoon between multidecadal strong and weak monsoon stages. *J. Geophys. Res. Atmos.* 121, 7026–7040. doi:10.1002/2015JD024228.

Xu, W., Li, Q., Wang, X. L., Yang, S., Cao, L., and Feng, Y. (2013). Homogenization of Chinese daily surface air temperatures and analysis of trends in the extreme temperature indices. *J. Geophys. Res. Atmos.* 118, 9708–9720. doi:10.1002/jgrd.50791.

Xu, Y., Ramanathan, V., and Washington, W. M. (2016). Observed high-altitude warming and snow cover retreat over Tibet and the Himalayas enhanced by black carbon aerosols. *Atmos. Chem. Phys.* 16, 1303–1315. doi:10.5194/acp-16-1303-2016.

Xue, Y., Janjic, Z., Dudhia, J., Vasic, R., and De Sales, F. (2014). A review on regional dynamical downscaling in intraseasonal to seasonal simulation/prediction and major factors that affect downscaling ability. *Atmos. Res.* 147–148, 68–85. doi:10.1016/j.atmosres.2014.05.001.

Yamada, T. J., Lee, M.-I., Kanamitsu, M., and Kanamaru, H. (2012). Diurnal Characteristics of Rainfall over the Contiguous United States and Northern Mexico in the Dynamically Downscaled Reanalysis Dataset (US10). *J. Hydrometeorol.* 13, 1142–1148. doi:10.1175/JHM-D-11-0121.1.

Yan, L., Liu, Z., Chen, G., Kutzbach, J. E., and Liu, X. (2016). Mechanisms of elevation-dependent warming over the Tibetan plateau in quadrupled CO2 experiments. *Clim. Change* 135, 509–519. doi:10.1007/s10584-016-1599-z.

Yan, Z., Li, Z., li, Q., and Jones, P. (2010). Effects of site change and urbanisation in the Beijing temperature series 1977–2006. *Int. J. Climatol.* 30, 1226–1234. doi:10.1002/joc.1971.

Yang, F., and Lau, K. M. (2004). Trend and variability of China precipitation in spring and summer: Linkage to sea-surface temperatures. *Int. J. Climatol.* 24, 1625–1644. doi:10.1002/joc.1094.

YANG, K., WATANABE, T., KOIKE, T., LI, X., FUJII, H., TAMAGAWA, K., et al. (2007). Auto-calibration System Developed to Assimilate AMSR-E Data into a Land Surface Model for Estimating Soil Moisture and the Surface Energy Budget. *J. Meteorol. Soc. Japan* 85A, 229–242. doi:10.2151/jmsj.85A.229.

Yang, M., Li, X., Zuo, R., Chen, X., and Wang, L. (2018). Climatology and Interannual Variability of Winter North Pacific Storm Track in CMIP5 Models. *Atmosphere (Basel).* 9, 79. doi:10.3390/atmos9030079.

Yang, Q., Ma, Z., Fan, X., Yang, Z.-L., Xu, Z., and Wu, P. (2017a). Decadal Modulation of Precipitation Patterns over Eastern China by Sea Surface Temperature Anomalies. *J. Clim.* 30, 7017–7033. doi:10.1175/JCLI-D-16-0793.1.

Yang, W., John, V., Zhao, X., Lu, H., and Knapp, K. (2016a). Satellite Climate Data Records: Development, Applications, and Societal Benefits. *Remote Sens.* 8, 331. doi:10.3390/rs8040331.

Yang, W., Vecchi, G. A., Fueglistaler, S., Horowitz, L. W., Luet, D. J., Muñoz, Á. G., et al. (2019). Climate Impacts

From Large Volcanic Eruptions in a High-Resolution Climate Model: The Importance of Forcing Structure. *Geophys. Res. Lett.* 46, 7690–7699. doi:10.1029/2019GL082367.
Yang, X.-Y., Yuan, X., and Ting, M. (2016b). Dynamical Link between the Barents–Kara Sea Ice and the Arctic Oscillation. *J. Clim.* 29, 5103–5122. doi:10.1175/JCLI-D-15-0669.1.
Yang, Z., Hsu, K., Sorooshian, S., Xu, X., Braithwaite, D., Zhang, Y., et al. (2017b). Merging high-resolution satellite-based precipitation fields and point-scale rain gauge measurements-A case study in Chile. *J. Geophys. Res. Atmos.* 122, 5267–5284. doi:10.1002/2016JD026177.
Yano, J.-I., Ziemiański, M. Z., Cullen, M., Termonia, P., Onvlee, J., Bengtsson, L., et al. (2018). Scientific Challenges of Convective-Scale Numerical Weather Prediction. *Bull. Am. Meteorol. Soc.* 99, 699–710. doi:10.1175/BAMS-D-17-0125.1.
Yao, T., Thompson, L. G., Mosbrugger, V., Zhang, F., Ma, Y., Luo, T., et al. (2012a). Third Pole Environment (TPE). *Environ. Dev.* 3, 52–64. doi:10.1016/j.envdev.2012.04.002.
Yao, T., Thompson, L., Yang, W., Yu, W., Gao, Y., Guo, X., et al. (2012b). Different glacier status with atmospheric circulations in Tibetan Plateau and surroundings. *Nat. Clim. Chang.* 2, 663–667. doi:10.1038/nclimate1580.
Yasutomi, N., Hamada, A., and Yatagai, A. (2011). Development of a Long-term Daily Gridded Temperature Dataset and Its Application to Rain/Snow Discrimination of Daily Precipitation. Available at: http://hydro.iis.u-tokyo.ac.jp/GAME-T.
Yatagai, A., Kamiguchi, K., Arakawa, O., Hamada, A., Yasutomi, N., and Kitoh, A. (2012). APHRODITE: Constructing a Long-Term Daily Gridded Precipitation Dataset for Asia Based on a Dense Network of Rain Gauges. *Bull. Am. Meteorol. Soc.* 93, 1401–1415. doi:10.1175/BAMS-D-11-00122.1.
Yokoi, S., Mori, S., Katsumata, M., Geng, B., Yasunaga, K., Syamsudin, F., et al. (2017). Diurnal cycle of precipitation observed in the western coastal area of Sumatra Island: Offshore preconditioning by gravity waves. *Mon. Weather Rev.* 145, 3745–3761. doi:10.1175/MWR-D-16-0468.1.
You, Q.-L., Ren, G.-Y., Zhang, Y.-Q., Ren, Y.-Y., Sun, X.-B., Zhan, Y.-J., et al. (2017). An overview of studies of observed climate change in the Hindu Kush Himalayan (HKH) region. *Adv. Clim. Chang. Res.* 8, 141–147. doi:10.1016/j.accre.2017.04.001.
You, Q., Min, J., and Kang, S. (2016). Rapid warming in the Tibetan Plateau from observations and CMIP5 models in recent decades. *Int. J. Climatol.* 36, 2660–2670. doi:10.1002/joc.4520.
Yu, Y., Notaro, M., Liu, Z., Wang, F., Alkolibi, F., Fadda, E., et al. (2015). Climatic controls on the interannual to decadal variability in Saudi Arabian dust activity: Toward the development of a seasonal dust prediction model. *J. Geophys. Res. Atmos.* 120, 1739–1758. doi:10.1002/2014JD022611.
Zak, M. R., Cabido, M., Cáceres, D., and Díaz, S. (2008). What Drives Accelerated Land Cover Change in Central Argentina? Synergistic Consequences of Climatic, Socioeconomic, and Technological Factors. *Environ. Manage.* 42, 181–189. doi:10.1007/s00267-008-9101-y.
Zakey, A. S., Solmon, F., and Giorgi, F. (2006). Implementation and testing of a desert dust module in a regional climate model. *Atmos. Chem. Phys.* 6, 4687–4704. doi:10.5194/acp-6-4687-2006.
Zampieri, M., D'Andrea, F., Vautard, R., Ciais, P., de Noblet-Ducoudré, N., and Yiou, P. (2009). Hot European Summers and the Role of Soil Moisture in the Propagation of Mediterranean Drought. *J. Clim.* 22, 4747–4758. doi:10.1175/2009JCLI2568.1.
Zanchettin, D., Khodri, M., Timmreck, C., Toohey, M., Schmidt, A., Gerber, E. P., et al. (2016). The Model Intercomparison Project on the climatic response to Volcanic forcing (VolMIP): experimental design and forcing input data for CMIP6. *Geosci. Model Dev.* 9, 2701–2719. doi:10.5194/gmd-9-2701-2016.
Zanchettin, D., Timmreck, C., Bothe, O., Lorenz, S. J., Hegerl, G., Graf, H.-F., et al. (2013). Delayed winter warming: A robust decadal response to strong tropical volcanic eruptions? *Geophys. Res. Lett.* 40, 204–209. doi:10.1029/2012GL054403.
Zanchettin, D., Timmreck, C., Toohey, M., Jungclaus, J. H., Bittner, M., Lorenz, S. J., et al. (2019). Clarifying the Relative Role of Forcing Uncertainties and Initial-Condition Unknowns in Spreading the Climate Response to Volcanic Eruptions. *Geophys. Res. Lett.* 46, 1602–1611. doi:10.1029/2018GL081018.
Zandler, H., Haag, I., and Samimi, C. (2019). Evaluation needs and temporal performance differences of gridded precipitation products in peripheral mountain regions. *Sci. Rep.* 9, 15118. doi:10.1038/s41598-019-51666-z.
Zängl, G. (2004). A reexamination of the valley wind system in the Alpine Inn Valley with numerical simulations. *Meteorol. Atmos. Phys.* 87, 241–256. doi:10.1007/s00703-003-0056-5.
Zanna, L., Brankart, J. M., Huber, M., Leroux, S., Penduff, T., and Williams, P. D. (2019). Uncertainty and scale interactions in ocean ensembles: From seasonal forecasts to multidecadal climate predictions. *Q. J. R. Meteorol. Soc.* 145, 160–175. doi:10.1002/qj.3397.
Zanna, L., Porta Mana, P., Anstey, J., David, T., and Bolton, T. (2017). Scale-aware deterministic and stochastic parametrizations of eddy-mean flow interaction. *Ocean Model.* 111, 66–80. doi:https://doi.org/10.1016/j.ocemod.2017.01.004.
Zappa, G., Lucarini, V., and Navarra, A. (2011). Baroclinic Stationary Waves in Aquaplanet Models. *J. Atmos. Sci.* 68, 1023–1040. doi:10.1175/2011JAS3573.1.
Zappa, G., Pithan, F., and Shepherd, T. G. (2018). Multimodel Evidence for an Atmospheric Circulation Response to

Arctic Sea Ice Loss in the CMIP5 Future Projections. *Geophys. Res. Lett.* 45, 1011–1019. doi:10.1002/2017GL076096.
Zappa, G., Shaffrey, L. C., and Hodges, K. I. (2013). The Ability of CMIP5 Models to Simulate North Atlantic Extratropical Cyclones*. *J. Clim.* 26, 5379–5396. doi:10.1175/JCLI-D-12-00501.1.
Zappa, G., and Shepherd, T. G. (2017). Storylines of Atmospheric Circulation Change for European Regional Climate Impact Assessment. *J. Clim.* 30, 6561–6577. doi:10.1175/JCLI-D-16-0807.1.
Zeng, Z., Chen, A., Ciais, P., Li, Y., Li, L. Z. X., Vautard, R., et al. (2015). Regional air pollution brightening reverses the greenhouse gases induced warming-elevation relationship. *Geophys. Res. Lett.* 42, 4563–4572. doi:10.1002/2015GL064410.
Zerenner, T., Venema, V., Friederichs, P., and Simmer, C. (2016). Downscaling near-surface atmospheric fields with multi-objective Genetic Programming. *Environ. Model. Softw.* 84, 85–98. doi:10.1016/j.envsoft.2016.06.009.
Zhai, P., Zhou, B., and Chen, Y. (2018). A Review of Climate Change Attribution Studies. *J. Meteorol. Res.* 32, 671–692. doi:10.1007/s13351-018-8041-6.
Zhan, Y.-J., Ren, G.-Y., Shrestha, A. B., Rajbhandari, R., Ren, Y.-Y., Sanjay, J., et al. (2017). Changes in extreme precipitation events over the Hindu Kush Himalayan region during 1961–2012. *Adv. Clim. Chang. Res.* 8, 166–175. doi:10.1016/j.accre.2017.08.002.
Zhang, C., Wang, Y., Hamilton, K., and Lauer, A. (2016a). Dynamical downscaling of the climate for the Hawaiian islands. Part II: Projection for the late twenty-first century. *J. Clim.* 29, 8333–8354. doi:10.1175/JCLI-D-16-0038.1.
Zhang, G. J., Cai, M., and Hu, A. (2013). Energy consumption and the unexplained winter warming over northern Asia and North America. *Nat. Clim. Chang.* 3, 466–470. doi:10.1038/nclimate1803.
Zhang, H., Delworth, T. L., Zeng, F., Vecchi, G., Paffendorf, K., and Jia, L. (2016b). Detection, Attribution, and Projection of Regional Rainfall Changes on (Multi-) Decadal Time Scales: A Focus on Southeastern South America. *J. Clim.* 29, 8515–8534. doi:10.1175/JCLI-D-16-0287.1.
Zhang, H., Xie, B., and Wang, Z. (2018a). Effective Radiative Forcing and Climate Response to Short-Lived Climate Pollutants Under Different Scenarios. *Earth's Futur.* 6, 857–866. doi:10.1029/2018EF000832.
Zhang, K., Kimball, J. S., and Running, S. W. (2016c). A review of remote sensing based actual evapotranspiration estimation. *Wiley Interdiscip. Rev. Water* 3, 834–853. doi:10.1002/wat2.1168.
Zhang, L., and Li, T. (2016). Relative roles of anthropogenic aerosols and greenhouse gases in land and oceanic monsoon changes during past 156 years in CMIP5 models. *Geophys. Res. Lett.* 43, 5295–5301. doi:10.1002/2016GL069282.
Zhang, P., Wu, Y., Simpson, I. R., Smith, K. L., Zhang, X., De, B., et al. (2018b). A stratospheric pathway linking a colder Siberia to Barents-Kara Sea sea ice loss. *Sci. Adv.* 4. doi:10.1126/sciadv.aat6025.
Zhang, R. (2015a). Changes in East Asian summer monsoon and summer rainfall over eastern China during recent decades. *Sci. Bull.* 60, 1222–1224. doi:10.1007/s11434-015-0824-x.
Zhang, R. H. (2015b). Natural and human-induced changes in summer climate over the East Asian monsoon region in the last half century: A review. *Adv. Clim. Chang. Res.* 6, 131–140. doi:10.1016/j.accre.2015.09.009.
Zhang, T., Hoerling, M. P., Perlwitz, J., and Xu, T. (2016d). Forced Atmospheric Teleconnections during 1979–2014. *J. Clim.* 29, 2333–2357. doi:10.1175/JCLI-D-15-0226.1.
Zhang, X., Alexander, L., Hegerl, G. C., Jones, P., Tank, A. K., Peterson, T. C., et al. (2011). Indices for monitoring changes in extremes based on daily temperature and precipitation data. *Wiley Interdiscip. Rev. Clim. Chang.* 2, 851–870. doi:10.1002/wcc.147.
Zhang, Y., Kang, S., Sprenger, M., Cong, Z., Gao, T., Li, C., et al. (2018c). Black carbon and mineral dust in snow cover on the Tibetan Plateau. *Cryosph.* 12, 413–431. doi:10.5194/tc-12-413-2018.
Zhao, A. D., Stevenson, D. S., and Bollasina, M. A. (2019). The role of anthropogenic aerosols in future precipitation extremes over the Asian Monsoon Region. *Clim. Dyn.* 52, 6257–6278. doi:10.1007/s00382-018-4514-7.
Zhao, D., and Wu, J. (2017). The impact of land use and land cover changes on East Asian summer monsoon precipitation using the WRF-mosaic approach. *Atmos. Sci. Lett.* 18, 450–457. doi:10.1002/asl.788.
Zhao, L., Lee, X., Smith, R. B., and Oleson, K. (2014). Strong contributions of local background climate to urban heat islands. *Nature* 511, 216–219. doi:10.1038/nature13462.
Zheng, F., Tao, R., Maier, H. R., See, L., Savic, D., Zhang, T., et al. (2018). Crowdsourcing Methods for Data Collection in Geophysics: State of the Art, Issues, and Future Directions. *Rev. Geophys.* 56, 698–740. doi:10.1029/2018RG000616.
Zhou, B., Rybski, D., and Kropp, J. P. (2017a). The role of city size and urban form in the surface urban heat island. *Sci. Rep.* 7, 4791. doi:10.1038/s41598-017-04242-2.
Zhou, D., Zhang, L., Hao, L., Sun, G., Liu, Y., and Zhu, C. (2016a). Spatiotemporal trends of urban heat island effect along the urban development intensity gradient in China. *Sci. Total Environ.* 544, 617–626. doi:10.1016/j.scitotenv.2015.11.168.
Zhou, T., Gong, D., Li, J., and Li, B. (2009a). Detecting and understanding the multi-decadal variability of the East Asian Summer Monsoon Recent progress and state of affairs. *Meteorol. Zeitschrift* 18, 445–467. doi:10.1127/0941-2948/2009/0396.

Zhou, T., Song, F., Ha, K. J., and Chen, X. (2017b). "Decadal changes of East Asian summer monsoon: Contributions of internal variability and external forcing," in *The Global Monsoon System: Research and Forecasting*, ed. M. C. Chang, C. P., Kuo, H. C., Lau, N. C., Johnson, Richard H., Wang, Bin, Wheeler (World Scientific), 327–336. Available at: https://doi.org/10.1142/10305.
Zhou, T., Turner, A. G., Kinter, J. L., Wang, B., Qian, Y., Chen, X., et al. (2016b). GMMIP (v1.0) contribution to CMIP6: Global Monsoons Model Inter-comparison Project. *Geosci. Model Dev.* 9, 3589–3604. doi:10.5194/gmd-9-3589-2016.
Zhou, T., Yu, R., Zhang, J., Drange, H., Cassou, C., Deser, C., et al. (2009b). Why the Western Pacific Subtropical High Has Extended Westward since the Late 1970s. *J. Clim.* 22, 2199–2215. doi:10.1175/2008JCLI2527.1.
Zhu, P., Dudhia, J., Field, P. R., Wapler, K., Fridlind, A., Varble, A., et al. (2012). A limited area model (LAM) intercomparison study of a TWP-ICE active monsoon mesoscale convective event. *J. Geophys. Res. Atmos.* 117, n/a-n/a. doi:10.1029/2011JD016447.
Zhu, X.-C., Guo, Y.-Y., and Zhang, Hai-Yan, LI, Xiu-Zhen, Chen, Rui-Dan, Wen, Z.-P. (2018). A southward withdrawal of the northern edge of the East Asian summer monsoon around the early 1990s. *Atmos. Ocean. Sci. Lett.* 11, 136–142. doi:10.1080/16742834.2018.1410058.
Zhu, Y., Wang, H., Zhou, W., and Ma, J. (2011). Recent changes in the summer precipitation pattern in East China and the background circulation. *Clim. Dyn.* 36, 1463–1473. doi:10.1007/s00382-010-0852-9.
Zhuo, Z., Gao, C., and Pan, Y. (2014). Proxy evidence for China's monsoon precipitation response to volcanic aerosols over the past seven centuries. *J. Geophys. Res. Atmos.* 119, 6638–6652. doi:10.1002/2013JD021061.
Zia, A., and Todd, A. M. (2010). Evaluating the effects of ideology on public understanding of climate change science: How to improve communication across ideological divides? *Public Underst. Sci.* 19, 743–761. doi:10.1177/0963662509357871.
Zickfeld, K., Knopf, B., Petoukhov, V., and Schellnhuber, H. J. (2005). Is the Indian summer monsoon stable against global change? *Geophys. Res. Lett.* 32, L15707. doi:10.1029/2005GL022771.
Zittis, G., Bruggeman, A., Camera, C., Hadjinicolaou, P., and Lelieveld, J. (2017). The added value of convection permitting simulations of extreme precipitation events over the eastern Mediterranean. *Atmos. Res.* 191, 20–33. doi:10.1016/j.atmosres.2017.03.002.
Zittis, G., and Hadjinicolaou, P. (2017). The effect of radiation parameterization schemes on surface temperature in regional climate simulations over the MENA-CORDEX domain. *Int. J. Climatol.* 37, 3847–3862. doi:10.1002/joc.4959.
Zou, L., and Zhou, T. (2016). Future summer precipitation changes over CORDEX-East Asia domain downscaled by a regional ocean-atmosphere coupled model: A comparison to the stand-alone RCM. *J. Geophys. Res. Atmos.* 121, 2691–2704. doi:10.1002/2015JD024519.
Zou, L., and Zhou, T. (2017). Dynamical downscaling of East Asian winter monsoon changes with a regional ocean-atmosphere coupled model. *Q. J. R. Meteorol. Soc.* 143, 2245–2259. doi:10.1002/qj.3082.
Zscheischler, J., Michalak, A. M., Schwalm, C., Mahecha, M. D., Huntzinger, D. N., Reichstein, M., et al. (2014). Impact of large-scale climate extremes on biospheric carbon fluxes: An intercomparison based on MsTMIP data. *Global Biogeochem. Cycles* 28, 585–600. doi:10.1002/2014GB004826.
Zscheischler, J., and Seneviratne, S. I. (2017). Dependence of drivers affects risks associated with compound events. *Sci. Adv.* 3, e1700263. doi:10.1126/sciadv.1700263.
Zscheischler, J., Westra, S., van den Hurk, B. J. J. M., Seneviratne, S. I., Ward, P. J., Pitman, A., et al. (2018). Future climate risk from compound events. *Nat. Clim. Chang.* 8, 469–477. doi:10.1038/s41558-018-0156-3.
Zubler, E. M., Folini, D., Lohmann, U., Lüthi, D., Schär, C., and Wild, M. (2011). Simulation of dimming and brightening in Europe from 1958 to 2001 using a regional climate model. *J. Geophys. Res.* 116, D18205. doi:10.1029/2010JD015396.
Zulkafli, Z., Buytaert, W., Onof, C., Manz, B., Tarnavsky, E., Lavado, W., et al. (2014). A Comparative Performance Analysis of TRMM 3B42 (TMPA) Versions 6 and 7 for Hydrological Applications over Andean–Amazon River Basins. *J. Hydrometeorol.* 15, 581–592. doi:10.1175/JHM-D-13-094.1.
Zuo, Z., Yang, S., Kumar, A., Zhang, R., Xue, Y., and Jha, B. (2012). Role of thermal condition over Asia in the weakening Asian summer monsoon under global warming background. *J. Clim.* doi:10.1175/JCLI-D-11-00742.1.
Zuo, Z., Yang, S., Xu, K., Zhang, R., He, Q., Zhao, T., et al. (2018). Land surface air temperature variations over Eurasia and possible causes in the past century. *Int. J. Climatol.* 38, 1925–1937. doi:10.1002/joc.5306.
Zuo, Z., Yang, S., Zhang, R., Jiang, P., Zhang, L., and Wang, F. (2013). Long-term variations of broad-scale Asian summer monsoon circulation and possible causes. *J. Clim.* doi:10.1175/JCLI-D-12-00691.1.

Figures

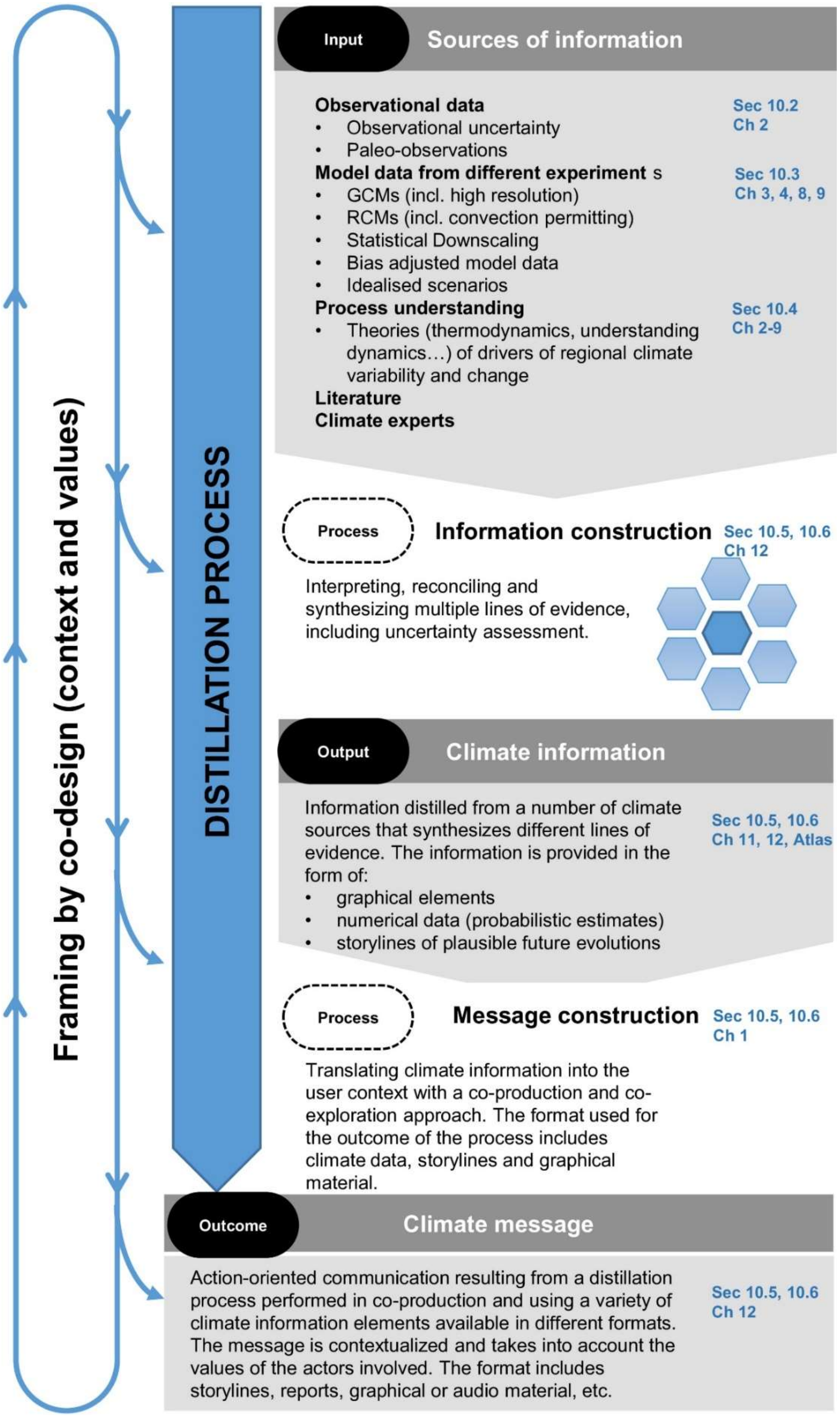

Figure 10.1: Simplified view of the construction of a regional climate message including sources, context, values and storylines, with the processes that lead to the distillation of the message. The chapters and sections where the elements entering the message construction are assessed are indicated.

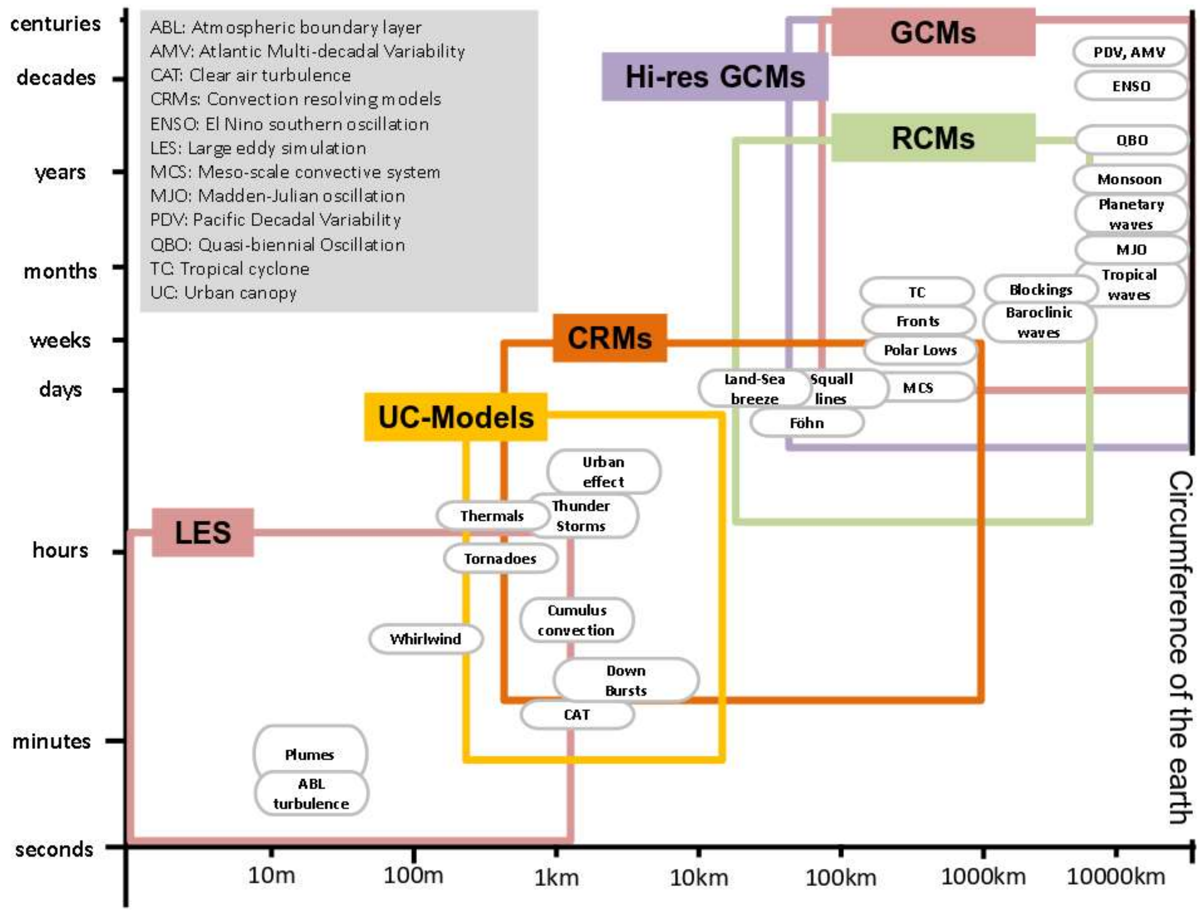

Figure 10.2: Schematic diagram derived from the inventive way of (Orlanski, 1975) displaying relevant interacting space and time scales to regional climate change information. Also indicated are the processes included in the different models and model components considered in Chapter 10 as a function of time and space scales. This figure is a companion of Figure 1.14 in Chapter 1 where the region sets adopted in the report are illustrated as a function of time and space scales.

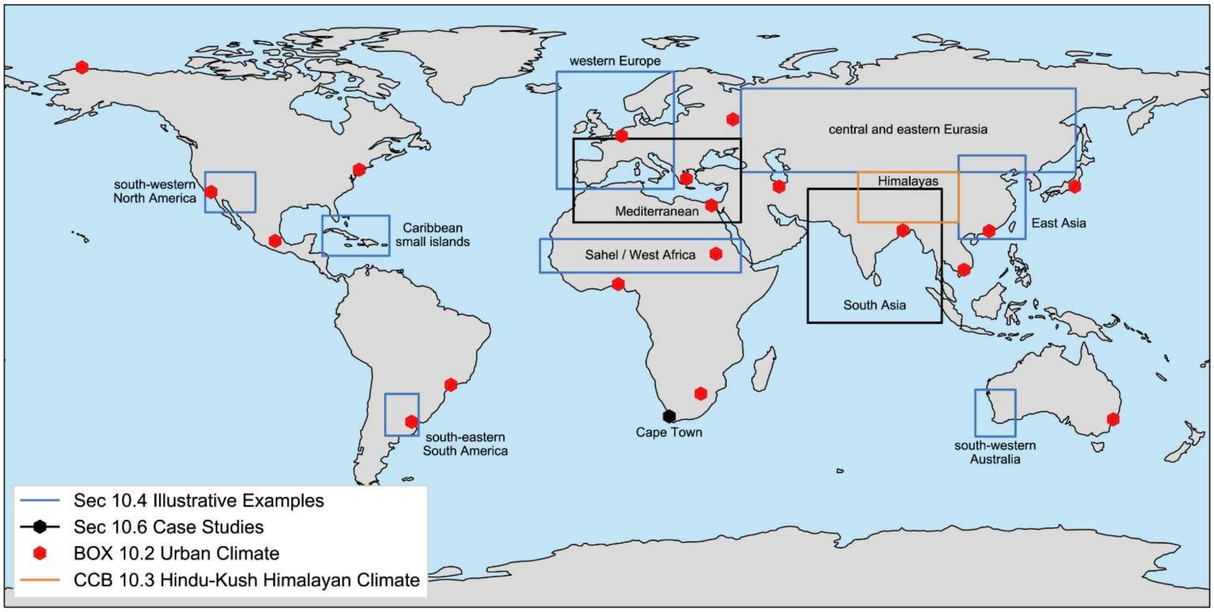

Figure 10.3: Regions used in the chapter. The regions for Section 10.4, illustrative regional attribution examples are in blue: Caribbean small islands, central and eastern Eurasia, East Asia, western Europe, south-western Australia, south-eastern South America, Sahel/West African monsoon region, and south-western North America (AR6 region SWN). The regions for Section 10.6, the comprehensive case studies of constructing regional climate messages, are in black: Cape Town, Mediterranean and South Asian monsoon. The urban areas used in Box 10.2 (urban climate) and the region used in Cross-Chapter Box 10.3 (Hindu-Kush Himalayan climate) are in red and orange, respectively.

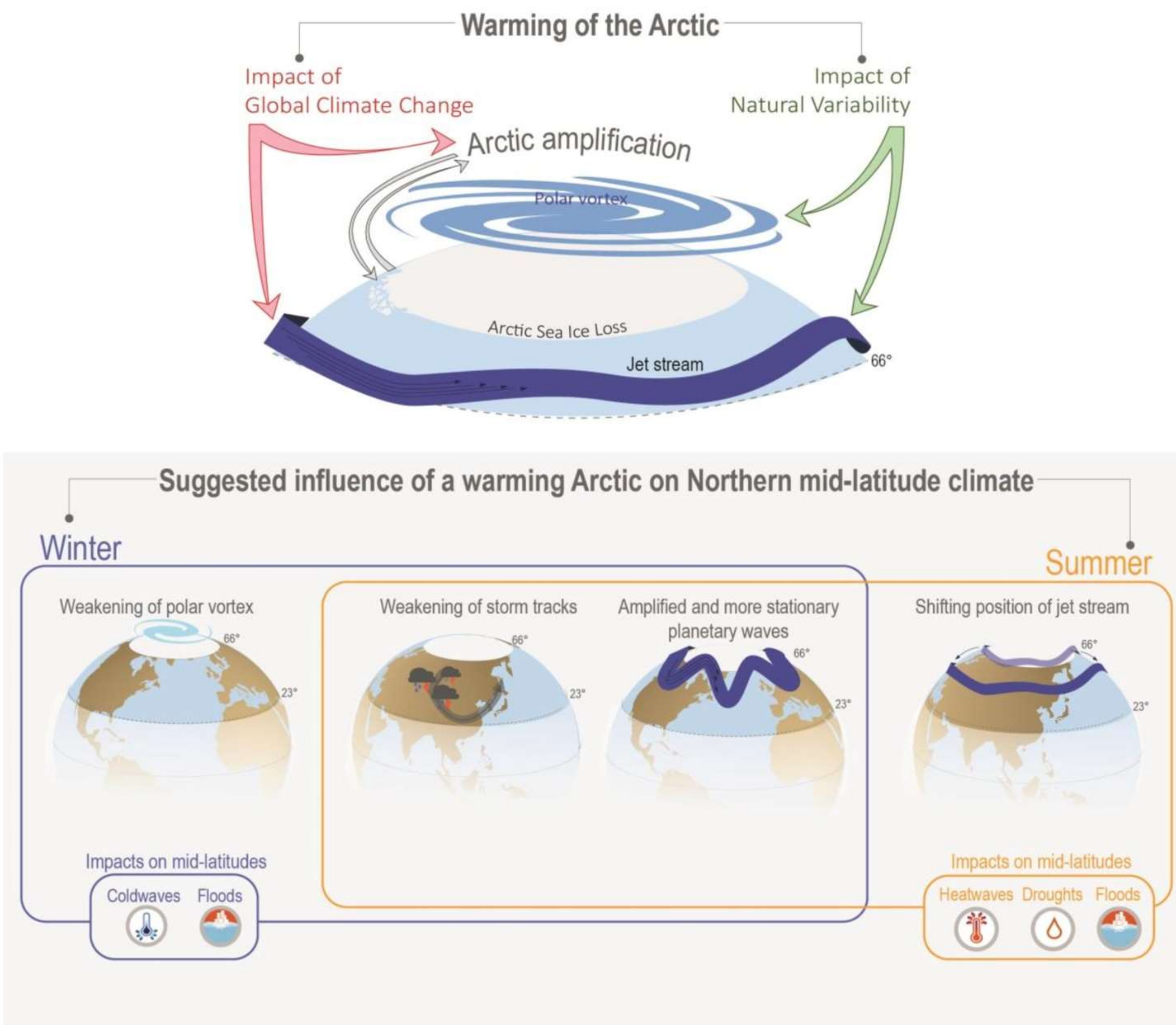

Cross-Chapter Box 10.1, Figure 1: Mechanisms of potential impacts of Arctic warming on mid-latitude climate. Mechanisms are different for winter and summer with different associated impacts on mid-latitudes. The mechanisms involve changes in the polar vortex, storm tracks, planetary waves and jet stream.

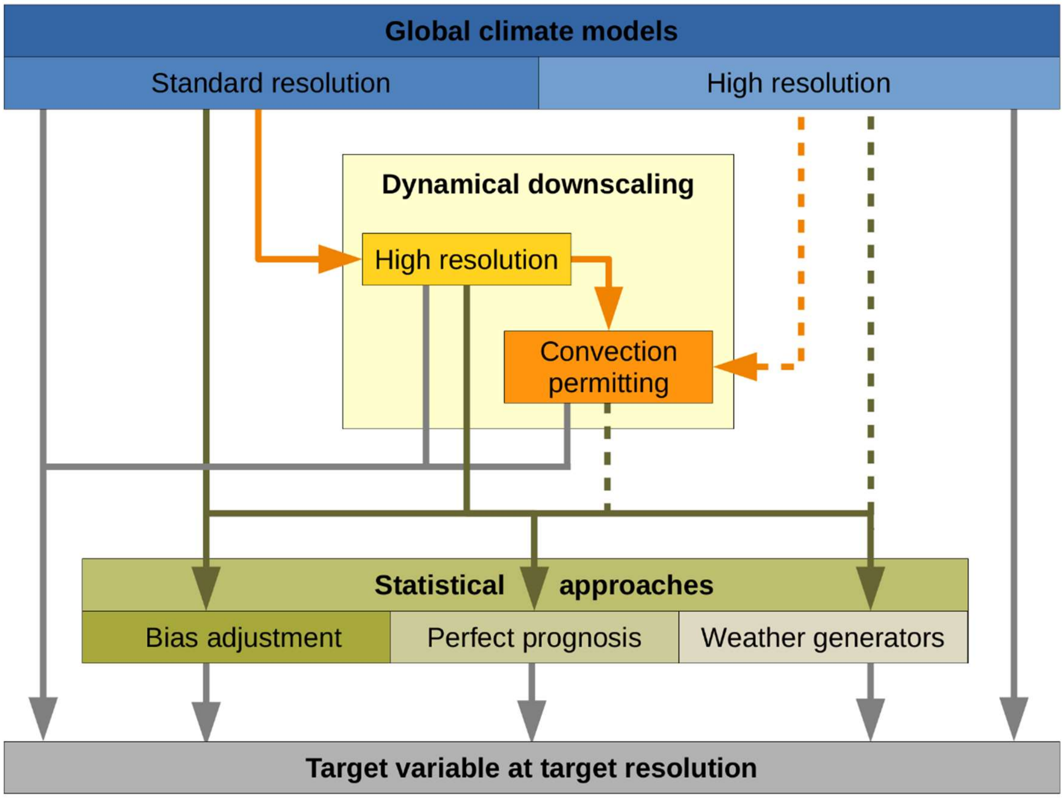

Figure 10.4: Typical model types and chains used in modelling regional climate. Grey lines: upstream model output is used without further post-processing. Orange lines: upstream model output is dynamically downscaled. Green lines: upstream model output is further statistically post-processed. The dashed lines indicate model chains that might prove useful but have not or only rarely been used.

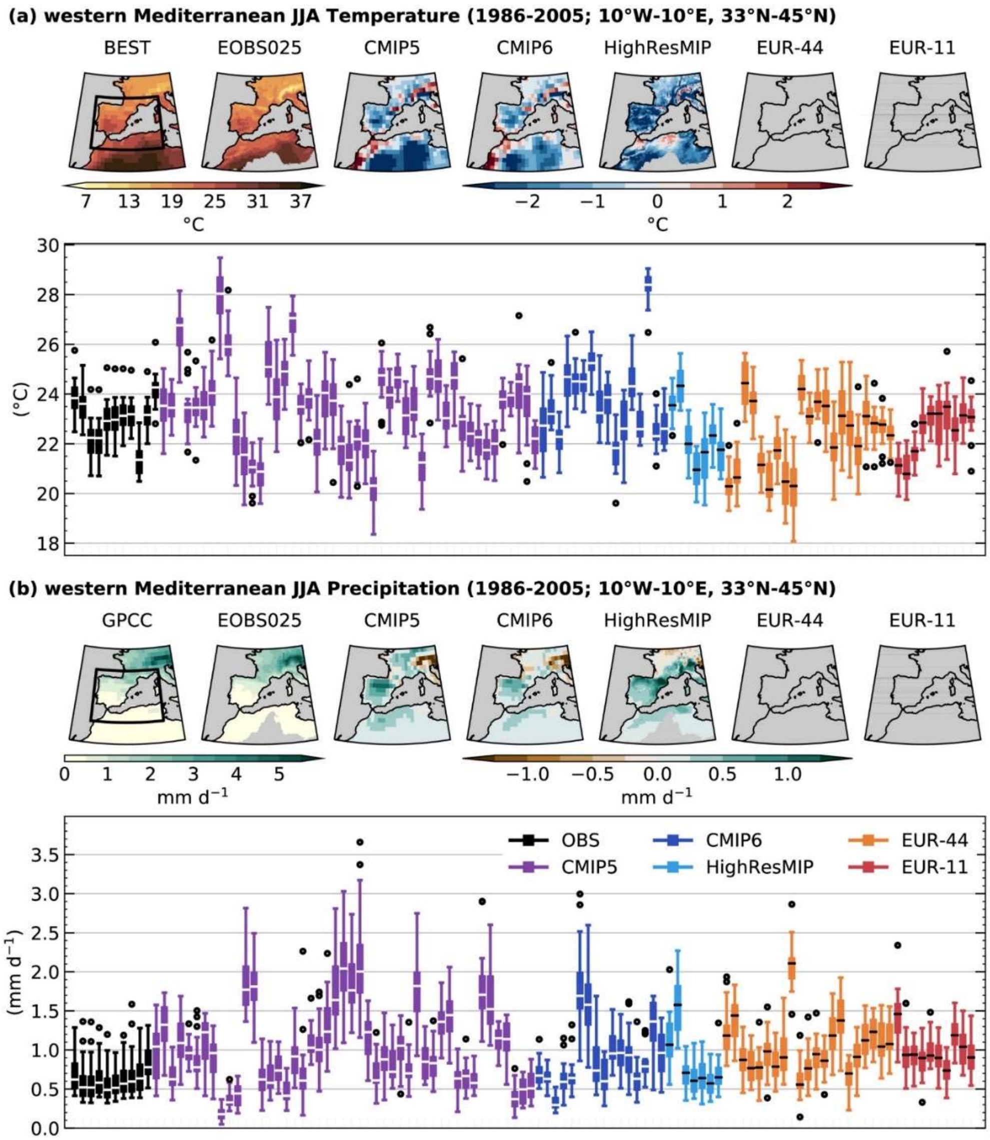

Figure 10.5: Illustration of some systematic errors in simulations performed with dynamical models. (a) Top row: Mean summer (June to August) near-surface air temperature (in °C) over the Mediterranean area in two observational datasets with the first panel for Berkeley surface temperature dataset (BEST) (Rohde et al., 2013) and the second panel for E-OBS v19.0e (Cornes et al., 2018), and mean bias for five multi-model experiments with GCMs (CMIP5, CMIP6 and HighResMIP) and RCMs (CORDEX EUR-44 and EUR-11). Biases of the CMIP ensembles are shown with respect to BEST, HighResMIP and CORDEX ensembles with respect to E-OBS. Bottom row: Box-and-whisker plot of the yearly mean summer near-surface temperature averaged over the western Mediterranean area (33°N–45°N, 10°W–10°E, black quadrilateral in the first panel of the top row) for a set of references and single model runs of the five multi-model experiments (one simulation per model). Additional observation and reanalysis data included in the bottom row are CRU TS v4.02, E-OBS v17, ERA-Interim, EWEMBI, HadCRUT4, JRA-55, NCEP/NCAR (Kalnay et al., 1996; Dee et al., 2011; Morice et al., 2012; Harris et al., 2014; Kobayashi and Iwasaki, 2016; Cornes et al., 2018; Lange, 2019). As (a) but for precipitation rate (mm day^{-1}) and showing Global Precipitation Climatology Centre (GPCC) version 2018 (Schneider et al., 2017) in the first panel of the top row. Biases of the CMIP ensembles are shown in respect to GPCC. Additional observation and reanalysis data included in the bottom row are CRU TS v4.02, E-OBS v17, ERA-Interim, EWEMBI, GHCN (Jones and Moberg, 2003; Dee et al., 2011; Harris et al., 2014; Cornes et al., 2018; Lange, 2019b). All results correspond to the period 1986–2005. **[Placeholder: The maps for EUR-44 and EUR-11 need to be completed]**

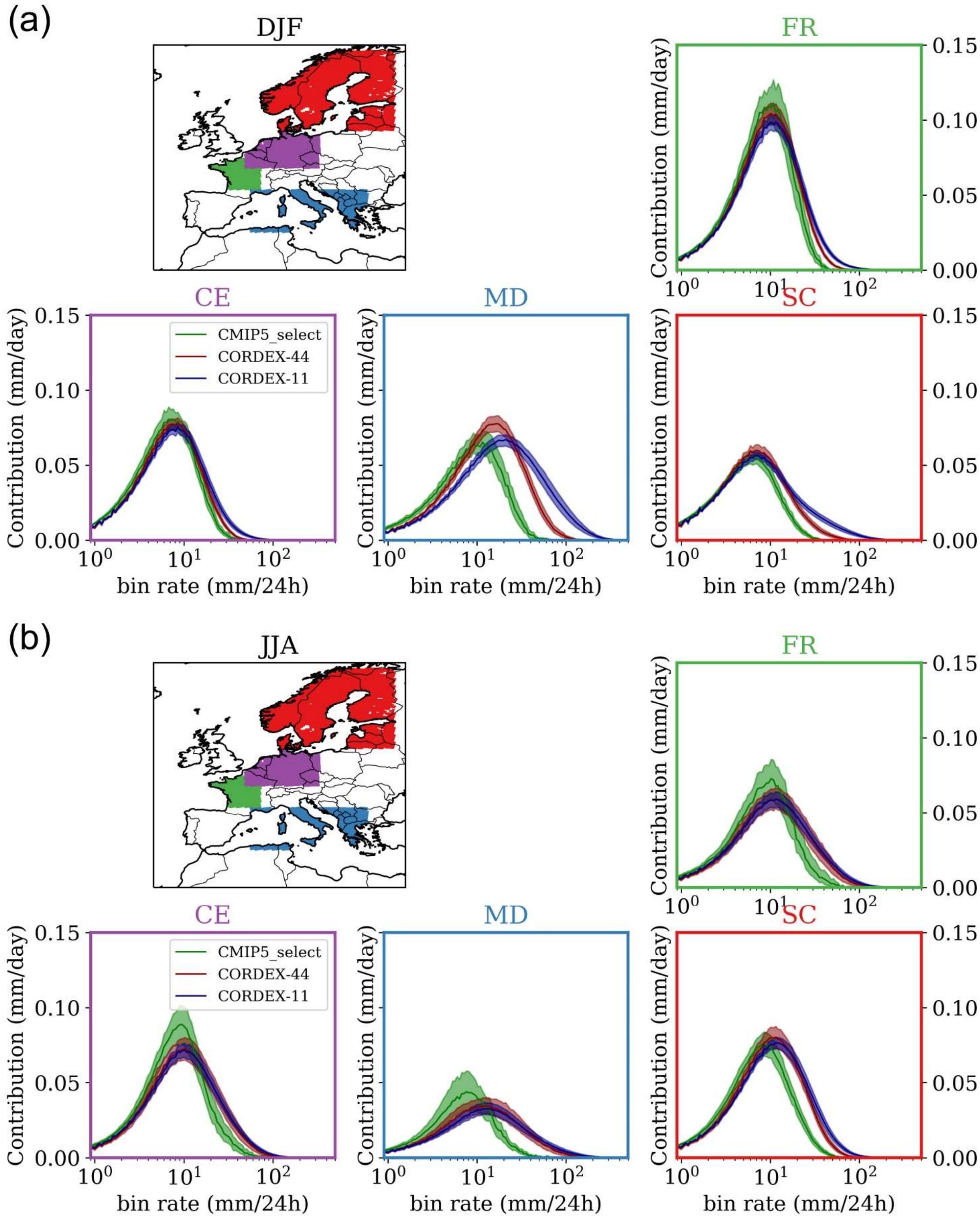

Figure 10.6: Probability density function of the winter (December to February, top) and summer (June to August, bottom) daily precipitation in the HighResMIP, CMIP5 (eight models), CORDEX EUR-44 (27 models) and EUR-11 (36 models) multi-model simulations for different European regions: France (FR), Central Europe (CE), Mediterranean (MD) and Scandinavia (SC). **[Placeholder: Observations will be added]**

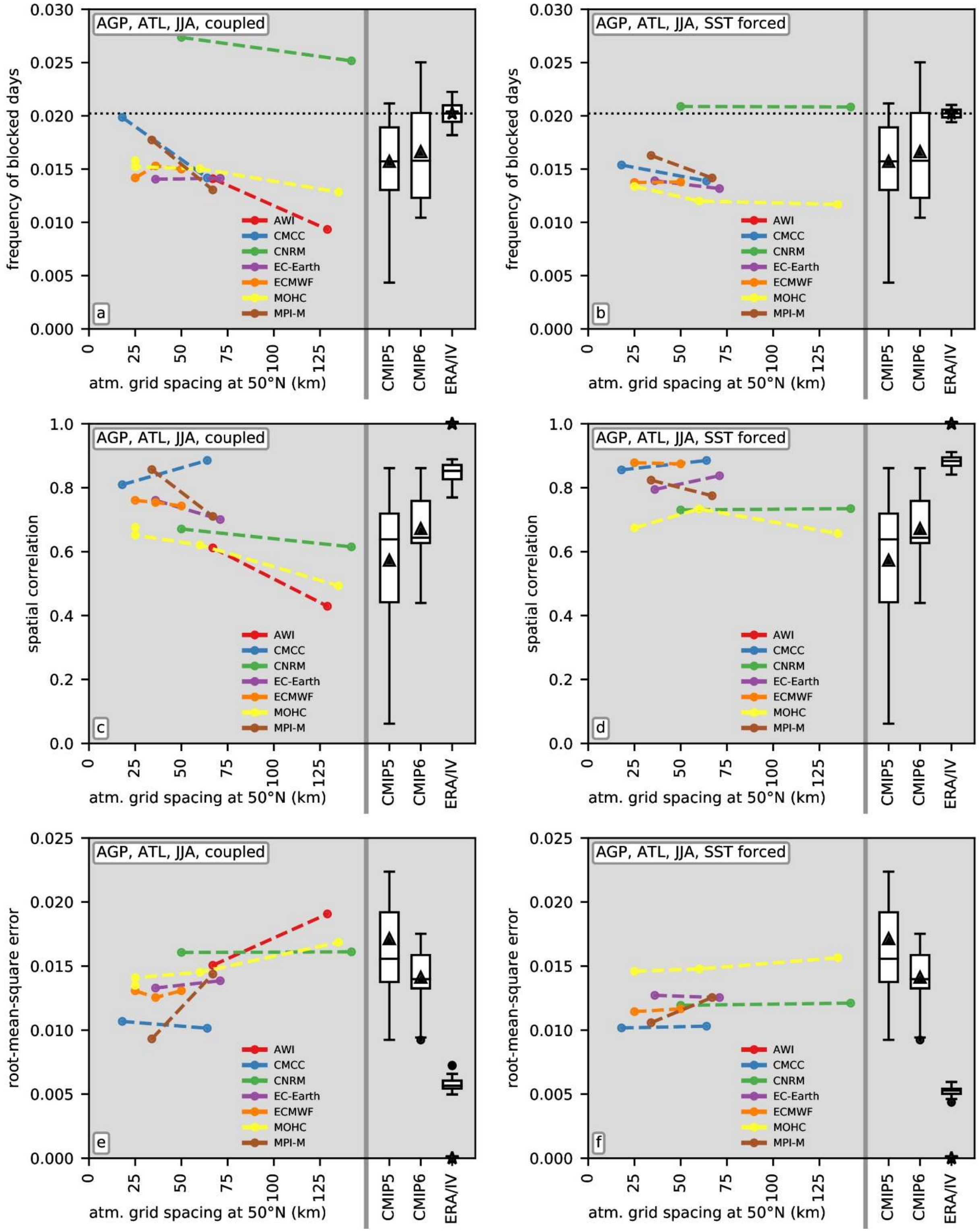

Figure 10.7: **[Placeholder**: Characteristics of summer (June to August) blocking over the North Atlantic in the HighResMIP experiment (seven models) as a function of resolution along with the CMIP5 and CMIP6 multi-model results and a reference from ERA-Interim for (left) global climate model and (right) atmospheric global climate model simulations using observed sea surface temperature and sea ice. Top row: area mean blocking frequency; middle row: spatial correlation between simulated and observed frequencies; bottom row: root mean squared error between simulated and observed frequencies.**]**

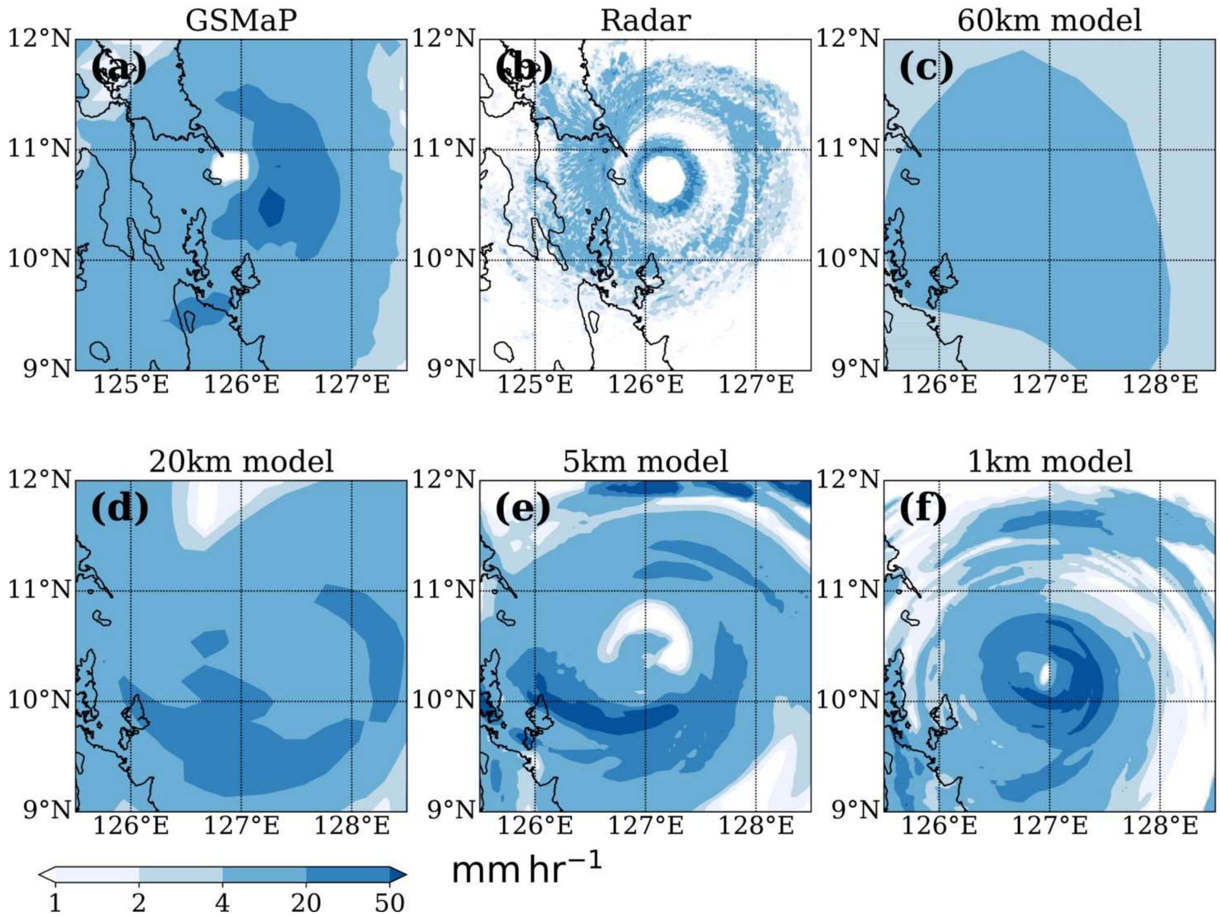

Figure 10.8: Hourly accumulated precipitation profiles (mm hour^{-1}) around the eye of Typhoon Haiyan, represented by (a) GSMaP satellite observation data, (b) Guiuan radar (PAGASA), (c) meso-ensemble forecast (60 km), (d) NHRCM (20 km), (e) NHRCM (5 km), and (f) WRF (1 km) models. Adapted from Takayabu et al. (2015).

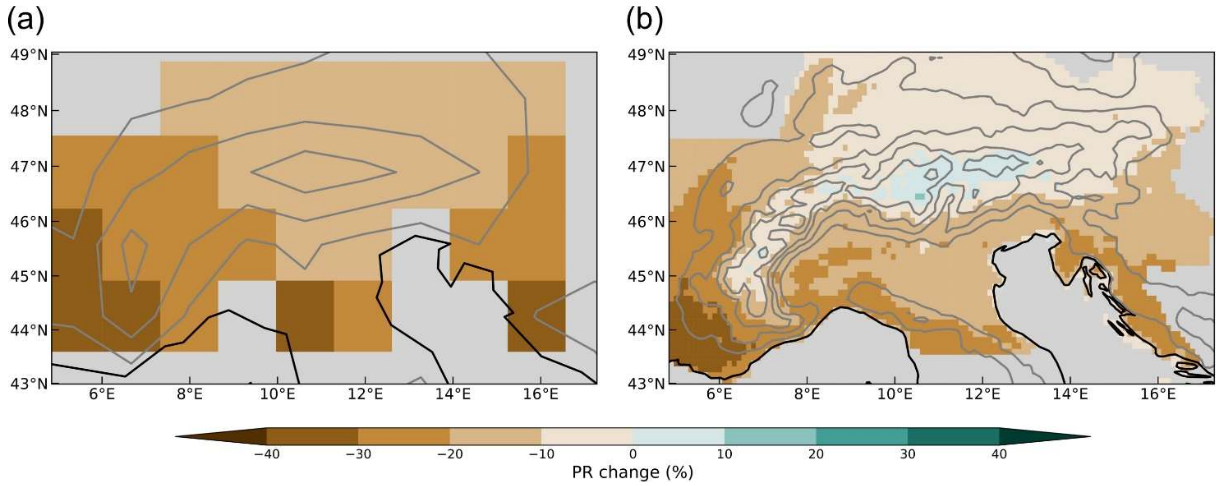

Figure 10.9: Projected changes in summer (June to August) precipitation (in percent with respect to the mean precipitation) over the Alps between the periods 2070–2099 and 1975–2004. (a) Mean of four GCMs regridded to a common 1.32°x1.32° grid resolution; (b) mean of six RCMs driven with these GCMs. The grey contours show elevation at 500 m intervals from the digital elevation model of the SMHI-RCA EUR11, regridded to the GCM resolution for panel b. Adapted from Giorgi et al. (2016).

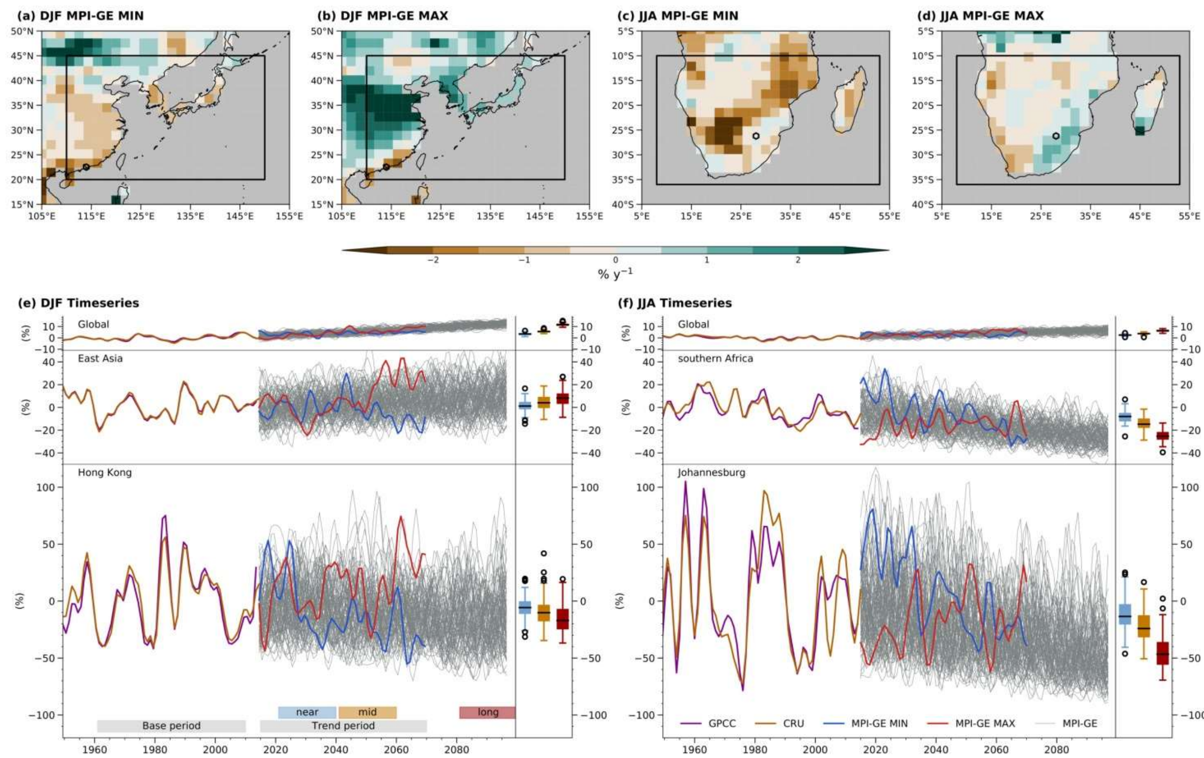

Figure 10.10: Observed and projected changes in seasonal mean (December to February in the left column and June to August in the right one) precipitation. Observations based on Global Precipitation Climatology Centre (GPCC) version 2018 (Schneider et al., 2017) and Climate Research Unit (CRU TS) version 4.02 (Harris et al., 2014) datasets, projections based on the Max-Planck Institute Grand-Ensemble (MPI-GE) (Maher et al., 2019) with 100 simulations starting from different initial conditions. (a)-(d) 55-year trends (2016–2070) from ensemble members with the minimum (a,c) and maximum (b,d) area mean change in the trend. (e) and (f) Time series of seasonal mean precipitation with the red (blue) lines corresponding to the ensemble member with strongest (weakest) 55-year trend and the grey lines to all remaining ensemble members. Box-and-whisker plots show changes relative to the base period across all ensemble members for three future time slices (near, mid, and long term). The top panels show global averages, the middle panels averages across the domains marked in (a)-(d), and the bottom panels results for grid boxes close to the cities mentioned.

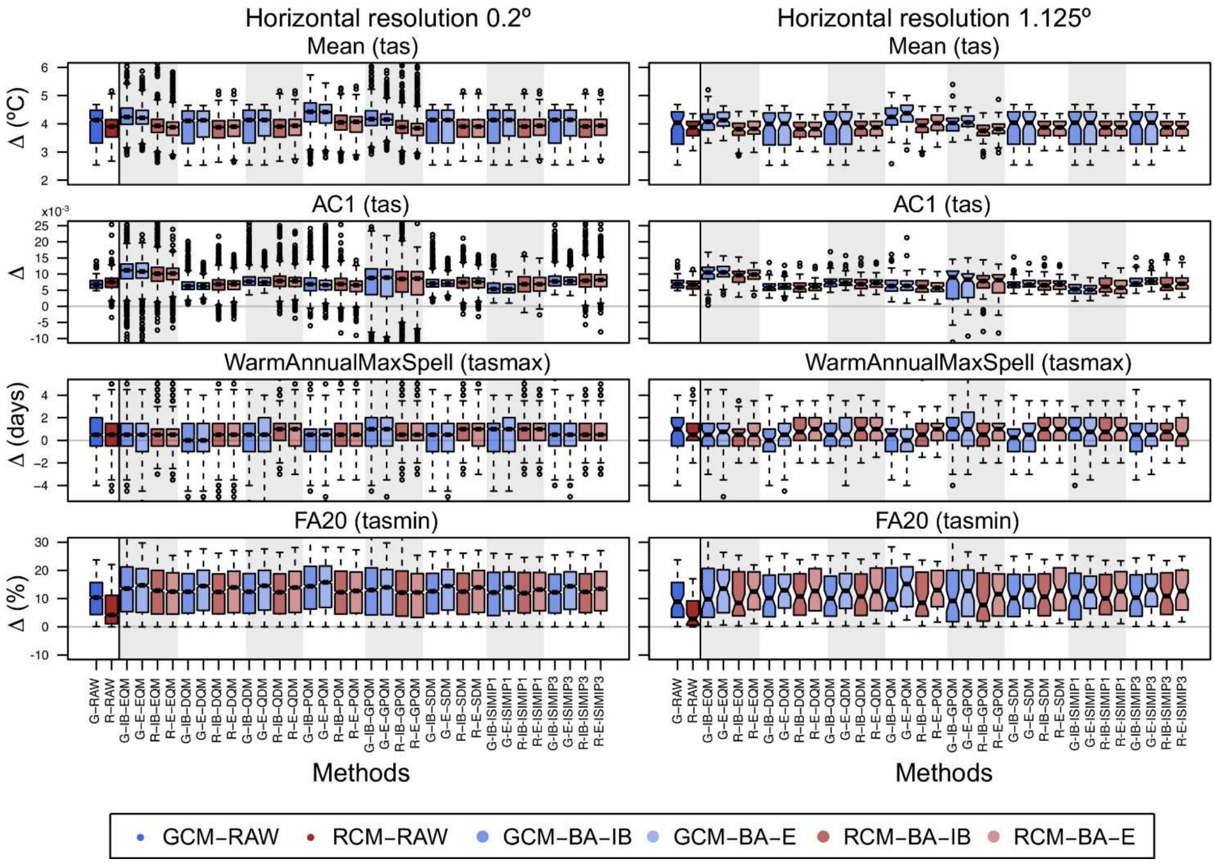

Cross-Chapter Box 10.2, Figure 1: Modification of simulated climate change signals by different bias-adjustment methods in different settings over the Iberian Peninsula. Climate change signal (deltas, Δ) for the 2071–2100 (RCP8.5) period with respect to the baseline 1971–2000 for global (G-RAW, 1.125º horizontal resolution) and regional (R-RAW, 0.2º) model outputs (first two boxplots in each panel) together with bias-adjusted results (rest of boxplots). Results are shown for two similar bias-adjustment experiments with high-resolution (0.2º, left column) and coarse (1.125º, right column) observational reference data from two different datasets: Iberia01 (IB) and E-OBS (E). In the left column the GCM outputs are "downscaled" to the high resolution, whereas the RCM outputs have the same target resolution (so there is no associated downscaling). However, in the right column all datasets are upscaled to the GCM resolution (no downscaling effect). Results are shown for seven bias-adjustment methods with four results (boxplots) for each method (G-IB-code, G-E-code, R-IB-code, R-E-code, for global 'G' and regional 'R' model outputs adjusted using Iberia01 'IB' or E-OBS 'E' observational references). Adapted from Casanueva et al. (submitted).

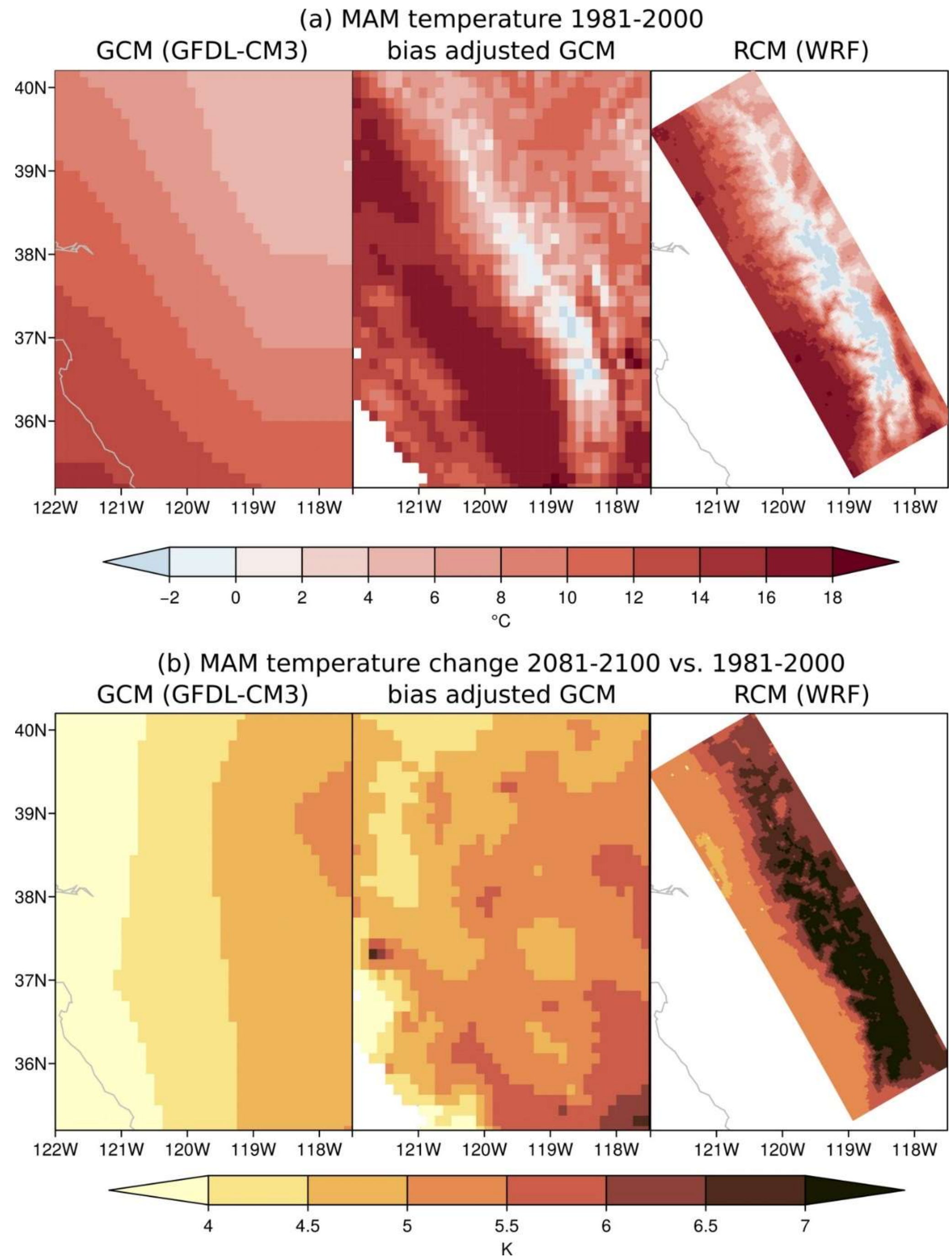

Cross-Chapter Box 10.2, Figure 2: Boreal spring (March to May) daily mean temperature in the Sierra Nevada region in California. (a) Present climate (1981–2000 average) in the GFDL-CM3 GCM, interpolated to 8 km (left), GCM bias adjusted (using quantile mapping) to observations at 8 km resolution (middle) and WRF RCM at 3 km horizontal resolution (right). (b) Climate change signal (2081–2100 average minus 1981–2000 average according to RCP8.5) in the GCM (left), the bias adjusted GCM (middle) and the RCM (right). As the GCM does not resolve the snow-albedo feedback, it simulates an implausible regional warming signal. The bias adjustment cannot improve the missing feedback. Only the high-resolution RCM simulation simulates a plausible elevation-dependent climate change signal. Adapted from Maraun et al. (2017b).

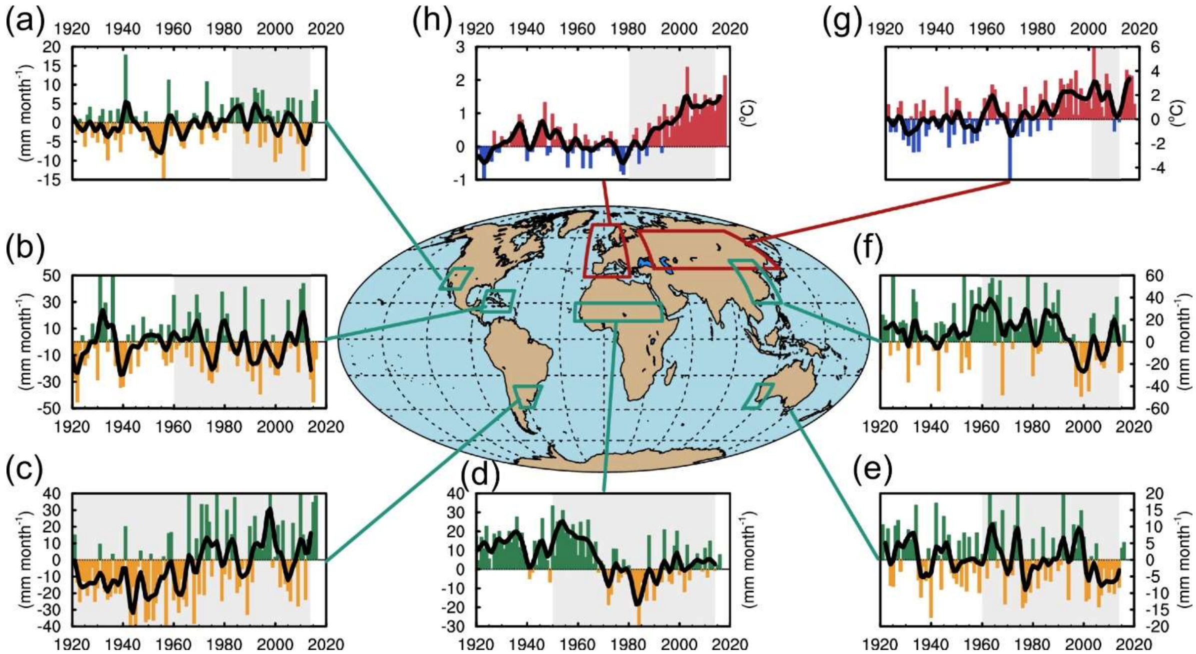

Figure 10.11: Time series of surface air temperature (in °C, blue and red colours) or precipitation (in mm per month, green and ochre colours) anomalies (relative to the 1951–1980 period) area-averaged over appropriate regions of the selected illustrative examples. The regions are broadly defined by the green (precipitation) and magenta (temperature) rectangles. The precise region boundaries and examples are from top to bottom and left to right: (a) The south-western North America (28°N–40°N, 105°W–120°W) drought. (b) The Caribbean small islands (15°N–27°N, 65°W–85°W) summer (June to August) drought. (c) The south-eastern South America (26.25°S–38.75°S, 56.25°W–66.25°W) Austral summer (December to February) drought. (d) The Sahel and the West African summer (June to September) monsoon (10°N–20°N, 20°W–40°E) drought and recovery. (e) The south-western Australia (25°S–39°S, 110°E–122°E) Austral autumn and winter rainfall decline. (f) The East Asia summer (June to August) monsoon weakening and recovery; here the time series is the difference of mean precipitation between two regions: (110°E–125°E, 35°N–45°N) – (105°E–125°E, 20°N–35°N). (g) The central and eastern Eurasia (40°N–65°N, 40°E–140°E) winter (January to March) cooling. (h) The western Europe (35°N–70°N, 15°W–20°E) summer (June to August) warming. Temperature data is from the Berkeley surface temperature dataset (BEST) (Rohde et al., 2013) and precipitation from Global Precipitation Climatology Centre (GPCC) version 2018 (Becker et al., 2013; Schneider et al., 2017). The light-grey area on each graphic represents the period of interest for attribution. The black line is a simple low-pass filter that has been used in AR4, Chapter 3, Appendix 3.A. It has five weights 1/12 [1-3-4-3-1] and for annual data, its half-amplitude point is for a six-year period, and the half-power point is near 8.4 years.

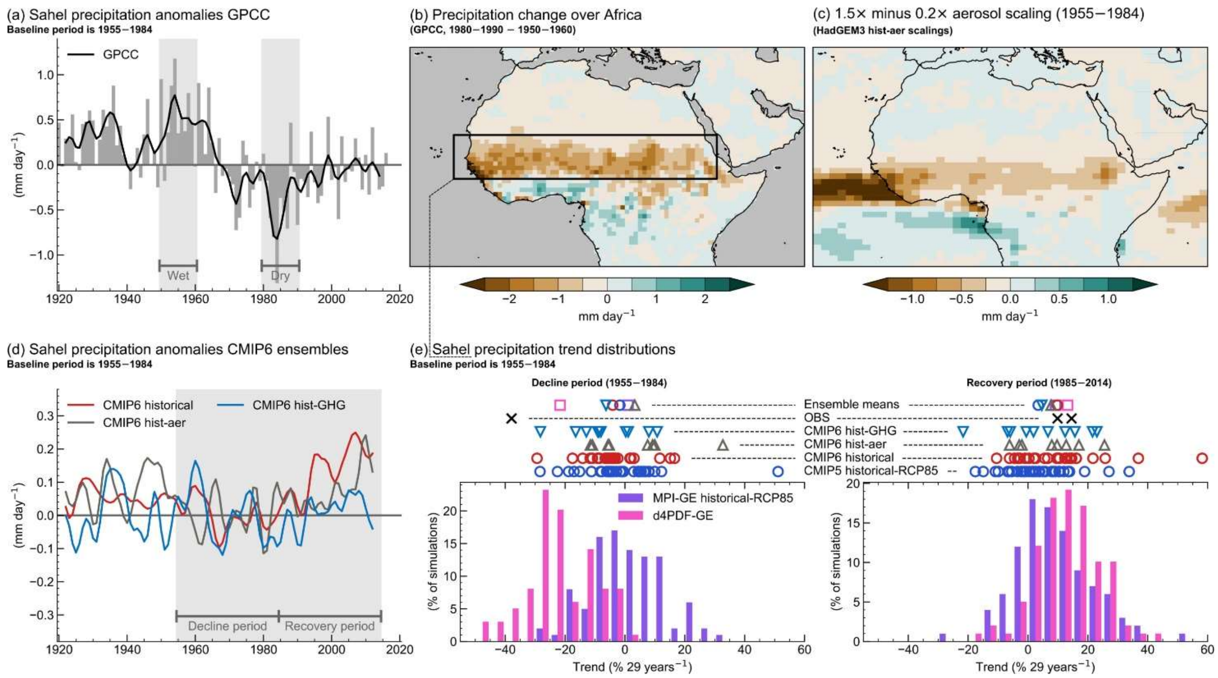

Figure 10.12: Attribution of historic precipitation change in the West African monsoon and Sahel region during June to August: (a) Time series of GPCC version 2018 (Schneider et al., 2017) precipitation anomalies (mm day^{-1}, baseline 1955–1984) in the Sahel box (10°N–20°N, 20°W–40°E) indicated in panel (b) (same as Figure 10.11) with a five-year weighted mean applied (see Figure 10.11). The two periods used for difference diagnostics are shown in grey columns. (b) Precipitation change (mm day^{-1}) in GPCC data for the 1980–1990 minus the 1950–1960 periods. (c) Precipitation difference (mm day^{-1}) averaged over 1955–1984 and four ensemble members of HadGEM3 experiments between 1.5x and 0.2x historical aerosol emissions scaling factors after Shonk et al. (2019). (d) Precipitation anomaly time series (mm day^{-1}, baseline 1955–1984) over the Sahel in the CMIP6 multi-model database for 26 historical simulations with all forcings (in red), ten with greenhouse gas-only forcing (in light blue) and eight with aerosol-only forcing (in grey). (e) Precipitation change (% (29 years)$^{-1}$) for the (left) decline period (1955–1984) and (right) recovery period (1985–2014) for ensemble means and in 26 individual models of the CMIP6 historical experiment, ten with greenhouse gas-only forcing, eight with aerosol-only forcing, 34 CMIP5 models (in dark blue) and in individual members of the Database for Policy Decision Making for Future Climate Change Grand-Ensemble (d4PDF-GE) (Mizuta et al., 2017) (pink histogram) and the Max-Planck Institute Grand-Ensemble (MPI-GE) (Maher et al., 2019) (violet histogram). The two black crosses represent observational estimates from GPCC and the Climate Research Unit Time-Series (CRU TS) version 4.02 (Harris et al., 2014). Trends are estimated using ordinary least squares.

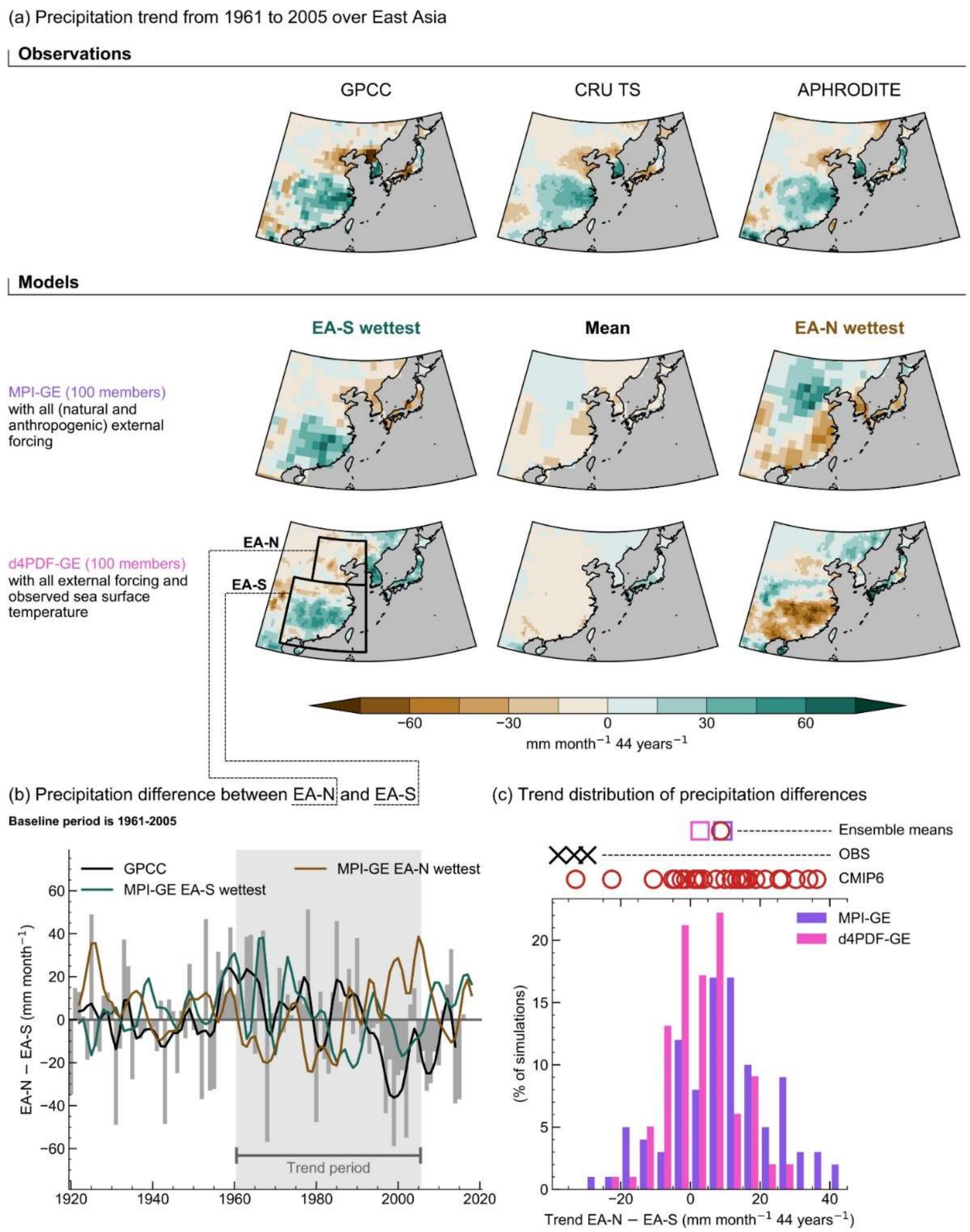

Figure 10.13: (a) Mean boreal summer (from June to August) precipitation spatial linear trend (mm month^{-1} (44 years)$^{-1}$) over the East Asia Summer Monsoon (EASM) region from 1961 to 2005. Trends are estimated using ordinary least squares. Top row: Observed trends from GPCC version 2018 (Schneider et al., 2017), CRU TS version 4.02 (Harris et al., 2014) and the Asian Precipitation-Highly Resolved Observational Data Integration Towards Evaluation of Water Resources (APHRODITE V1101) (Yatagai et al., 2012). Middle and bottom rows: Simulated trends corresponding to the East Asia-South (105°E–125°E, 20°N–35°N) wettest (left) and mean (middle) and East Asia-North (110°E–125°E, 35°N–45°N) wettest (right) over the EASM region using the 100 ensemble simulations of the MPI-GE (Maher et al., 2019) (middle row) and from the 100 members of the d4PDF-GE (Mizuta et al., 2017) (bottom row). (b) Precipitation difference (mm month^{-1}, baseline 1961–2005) between East Asia-North and East Asia-South for GPCC (grey bar charts). The lines show low-pass filtered time series of this difference for GPCC (in black) and for the East Asia-South wettest (in green) and East Asia-North wettest (in brown) MPI-GE members. The filter is the same as the one used in Figure 10.11. (c) Distribution of trends of the summer precipitation difference between the two regions in panel (b) for MPI-GE (violet histogram), d4PDF-GE (pink histogram), observations (back crosses), historical simulations from a set of 26 CMIP6 models (red circles) and ensemble mean trends.

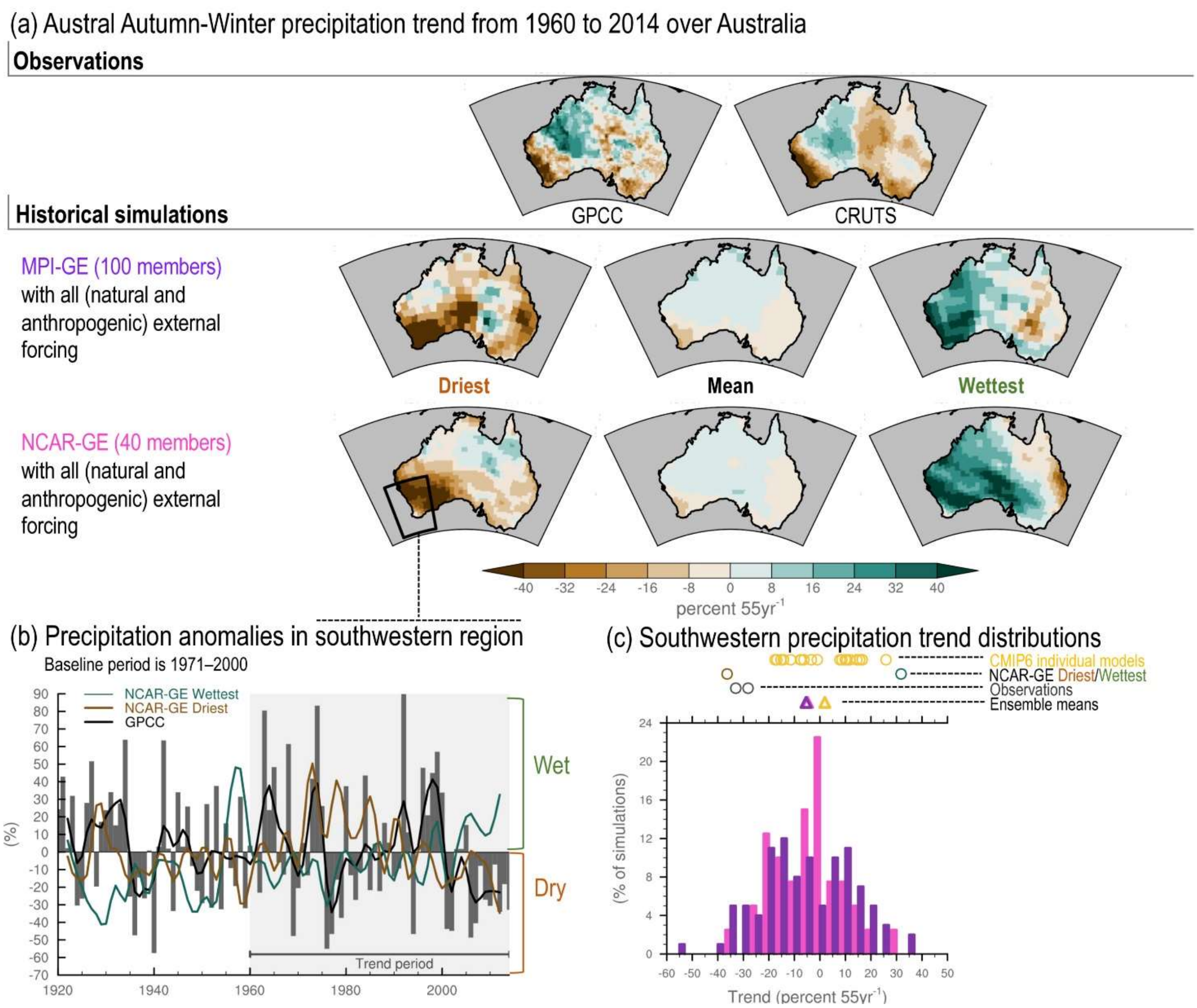

Figure 10.14:(a) Mean austral autumn and winter (March to August) precipitation spatial linear trend (% (55 year)$^{-1}$) over Australia from 1960 to 2014. Trends are estimated using ordinary least squares. Top row: Observed trends from the GPCC version 2018 (Schneider et al., 2017) and CRU TS version 4.00 (Harris et al., 2014). Middle row: Driest, mean and wettest trends (relative to the region enclosed in the black quadrilateral, left panel of bottom row) from the 100 members of the MPI-GE (Maher et al., 2019). Bottom row: Driest, mean and wettest trends (relative to the above region from the 40 members of the National Center for Atmospheric Research grand ensemble (NCAR-GE) (Kay et al., 2015). (b) Time series of austral autumn and winter precipitation anomalies (%, baseline 1971–2000) over the south-western Australia region delimited by the black quadrilateral for GPCC (grey bar charts). Black, brown and green lines show low-pass filtered time series for GPCC, driest and wettest members of NCAR-GE, respectively. The filter is the same as the one used in Figure 10.11. (c) Distribution of south-western Australia region-averaged austral autumn and winter precipitation 1960–2014 trends (% (55 year)$^{-1}$) for MPI-GE (violet histogram), NCAR-GE (pink histogram), observations (GPCC and CRUTS, dark grey open-filled circles) and historical simulations from a set of 22 CMIP6 models (yellow open-filled circles). Coloured triangles refer to ensemble mean trends of their respective ensemble. Brown and green open-filled circles refer to the driest and wettest NCAR-GE ensemble members.

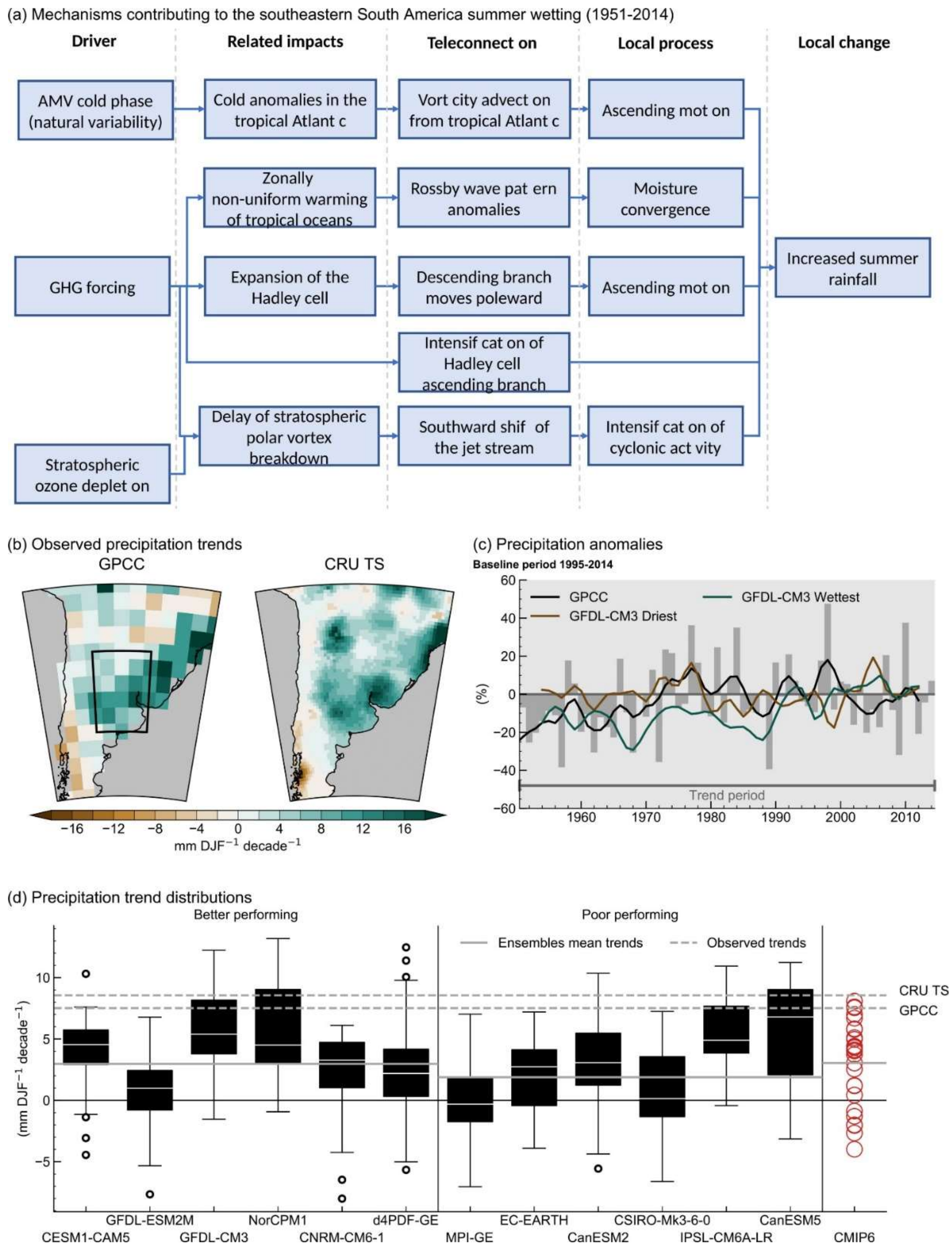

Figure 10.15: (a) Mechanisms that have been suggested to contribute to south-eastern South America summer wetting since the beginning of the 20th century. (b) Mean austral summer (December to February) precipitation spatial linear 1951–2014 trends (mm per season and decade) from GPCC version 2018 (Schneider et al., 2017) and CRU TS version 4.02 (Harris et al., 2014). Trends are estimated using ordinary least squares. (c) Time series of austral summer precipitation anomalies (%, baseline 1995–2014) over the south-eastern South American region (black in (b)) for GPCC (bar charts). Black, brown and green lines show low-pass filtered time series for GPCC, driest and wettest members of GFDL-CM3, respectively. The filter is the same as the one used in Figure 10.11. (d) Distribution of precipitation 1951–2014 trends over south-eastern South America from 12 grand ensembles (adapted from Díaz et al. (submitted)). The six grand ensembles to the left reproduce reasonably well the observed spatial patterns of mean precipitation and interannual variability (better performing), while the six grand ensembles to the right have a considerably worse performance (poor performing) (Díaz et al., submitted). The grey horizontal lines show the mean trend of each of these two subsets of grand ensembles. Dashed grey lines show GPCC and CRU TS trends and the red circles to the right show trends of 26 individual CMIP6 models.

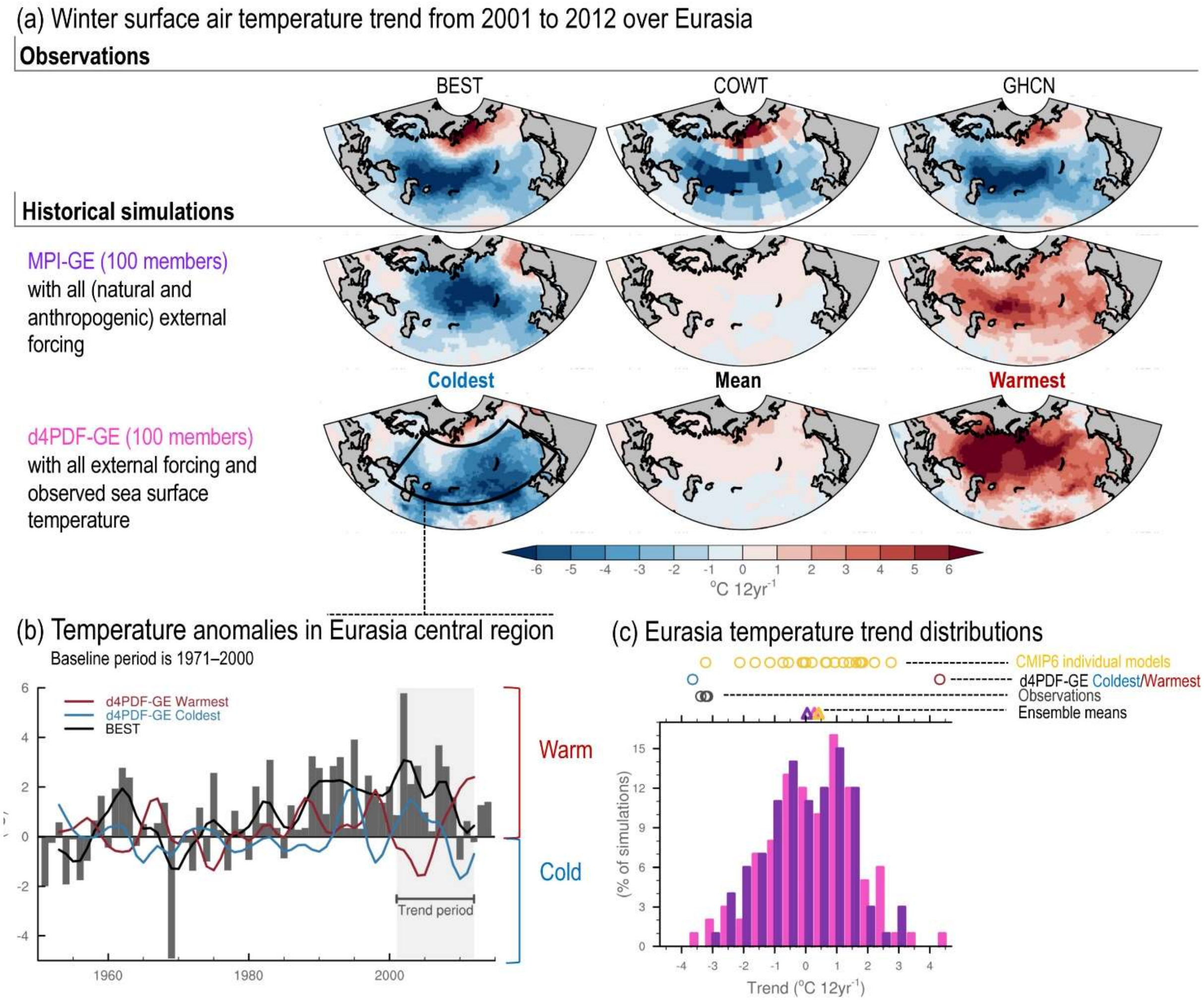

Figure 10.16: (a) Winter (January to March) near-surface air temperature spatial linear trend (in °C (12 year)$^{-1}$) over Eurasia from 2001 to 2012. Trends are estimated using ordinary least squares. Top row: Observed trends from the BEST dataset (Rohde et al., 2013), the Cowtan and Way dataset (Cowtan and Way, 2014) and the Global Historical Climatology Network version 2 and the Climate Anomaly Monitoring System (GHCN-CAMS) dataset (Fan and van den Dool, 2008). Middle row: Coldest, mean and warmest trends (relative to the region enclosed in the black quadrilateral, left panel of middle row) from the 100 members of the MPI-GE (Maher et al., 2019). Bottom row: coldest, mean and warmest trends relative to the above region from the 100 members of the d4PDF-GE (Mizuta et al., 2017). (b) Time series of BEST winter temperature anomalies (%, baseline 1971–2000) over the Eurasian region delimited by the black quadrilateral in (a) (grey bar charts). Black, brown and green lines show low-pass filtered time series for BEST, coldest and warmest members of d4PDF-GE, respectively. The filter is the same as the one used in Figure 10.11. (c) Distribution of Eurasia region-averaged winter temperature 2001-2012 trends (in °C (12 year)$^{-1}$) for MPI-GE (violet histogram), d4PDF (pink histogram), four observational datasets (BEST, GHCN-CAMS, Cowtan and Way and National Oceanic and Atmospheric Administration Merged land ocean global surface temperature analysis version 5 (Vose et al., 2012; Huang et al., 2015; Menne et al., 2018), dark grey open-filled circles) and historical simulations from a set of 22 CMIP6 models (yellow open-filled circles). Coloured triangles refer to ensemble mean trends of their respective ensemble. Blue and dark-red open-filled circles refer to the coldest and warmest d4PDF-GE ensemble members.

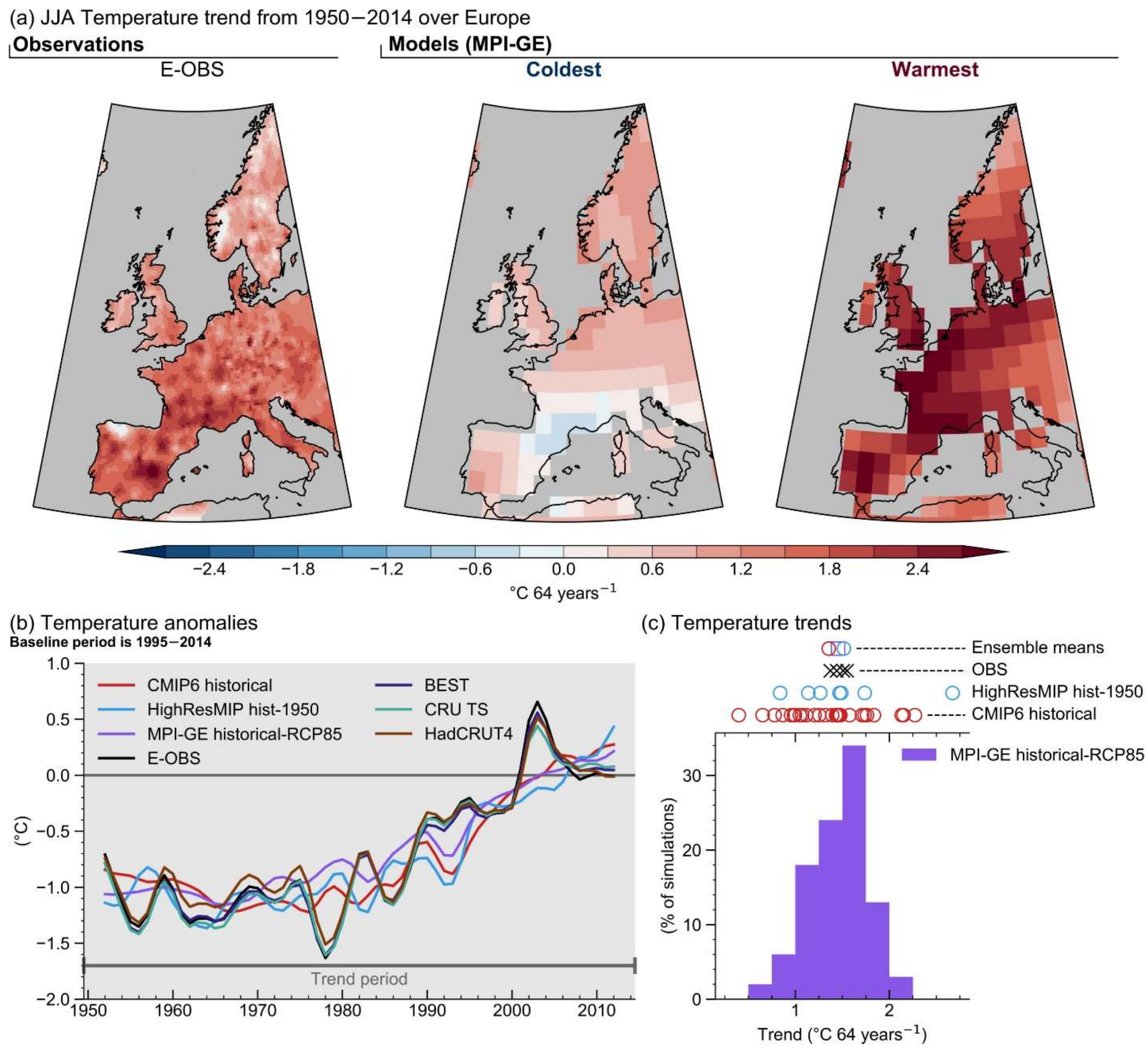

Figure 10.17: (a) European historical summer (June to August) near-surface air temperature spatial linear trend (in °C (64 years)$^{-1}$) from 1950 to 2014. Trends are estimated using ordinary least squares. Observed trends from E-OBS v19.0e (Cornes et al., 2018) (left) and the coldest (middle) and warmest (right) trends from the 100 members of the MPI-GE (Maher et al., 2019). Trends are estimated using ordinary least-squares. (b) Time series of European area mean (15ºW–20ºE, 35ºN–70ºN) summer temperature anomalies (in °C, baseline 1995–2014) applying the same filter used in Figure 10.11 for different observational datasets: E-OBS, BEST (Rohde et al., 2013), CRU TS v4.02 (Harris et al., 2014) and HadCRUT4 (Morice et al., 2012) (black, dark blue, turquois and brown line, respectively) and model ensemble means of CMIP6, HighResMIP and the MPI-GE (red, light blue and violet line, respectively). (c) European area mean summer 1950–2014 warming trends (in °C (64 years)$^{-1}$) for ensemble means and individual members of CMIP6 (28 members, red circles), HighResMIP (7 members, blue circles) and MPI-GE (violet histogram). The observational data sets are indicated by black crosses.

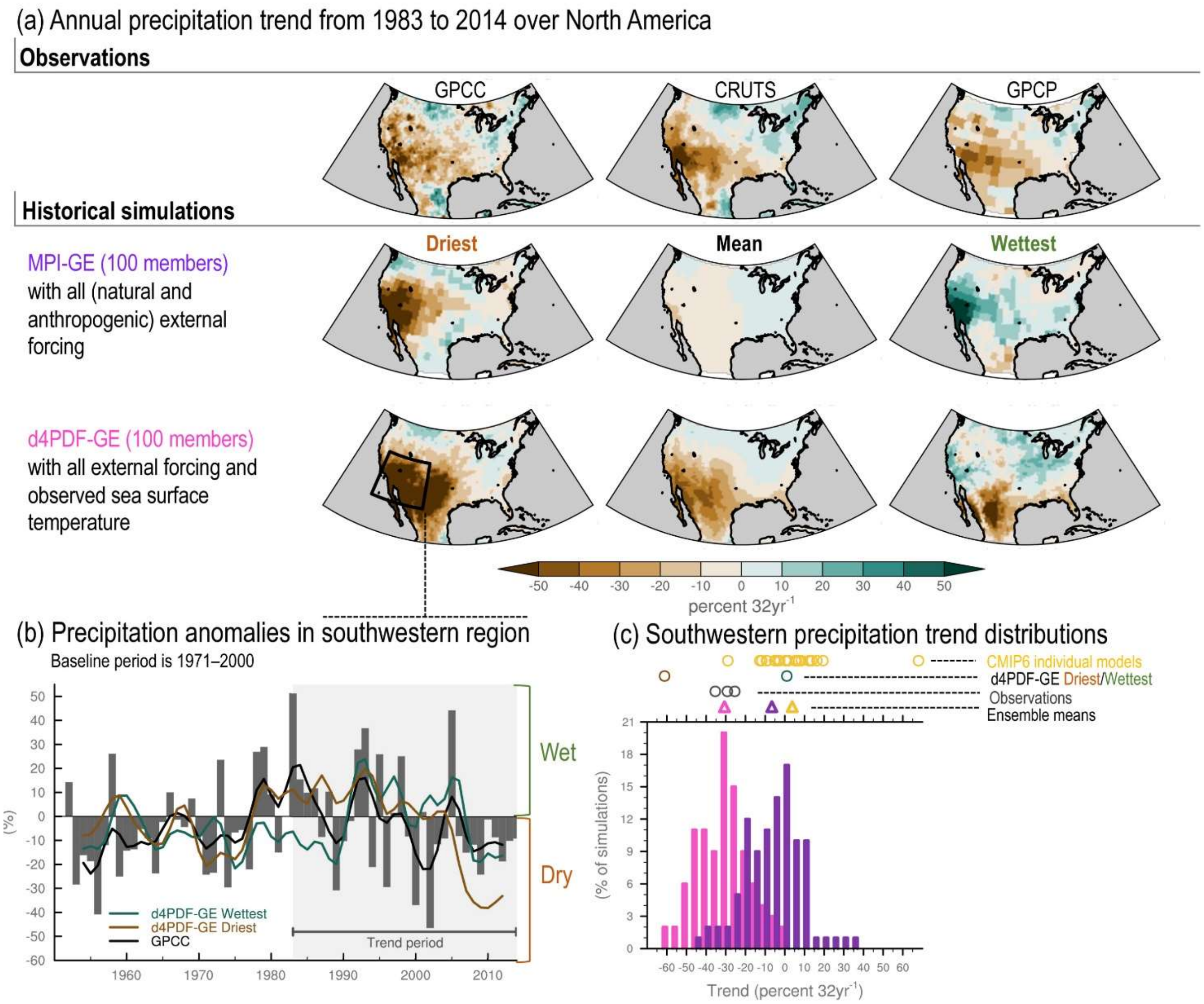

Figure 10.18: (a) Water year (October to September) precipitation spatial linear trend (in percent (32 year)$^{-1}$) over North America from 1983 to 2014. Trends are estimated using ordinary least squares. Top row: Observed trends from GPCC version 2018 (Schneider et al., 2017), CRU TS version 4.00 (Harris et al., 2014) and the Global Precipitation Climatology Project (GPCP) (Huffman et al., 2009) version 2.3. Middle row: Driest, mean and wettest trends (relative to the region enclosed in the black quadrilateral, middle row) from the 100 members of the MPI-GE (Maher et al., 2019). Bottom row: Driest, mean and wettest trends relative to the above region from the 100 members of the d4PDF-GE (Mizuta et al., 2017). (b) Time series of water year precipitation anomalies (%, baseline 1971–2000) over the above south-western North America region for GPCC (grey bar charts). Black, brown and green lines show low-pass filtered time series for GPCC, driest and wettest members of d4PDF-GE, respectively. The filter is the same as the one used in Figure 10.11. (c) Distribution of south-western region-averaged water-year precipitation 1983–2014 trends (in percent (32 year)$^{-1}$) for MPI-GE (violet histogram), d4PDF (pink histogram), observations (GPCC, CRUTS and GPCP, dark grey open-filled circles) and historical simulations from a set of 22 CMIP6 models (yellow open-filled circles). Coloured triangles refer to ensemble mean trends of their respective ensemble. Brown and green open-filled circles refer to the driest and wettest d4PDF-GE ensemble members.

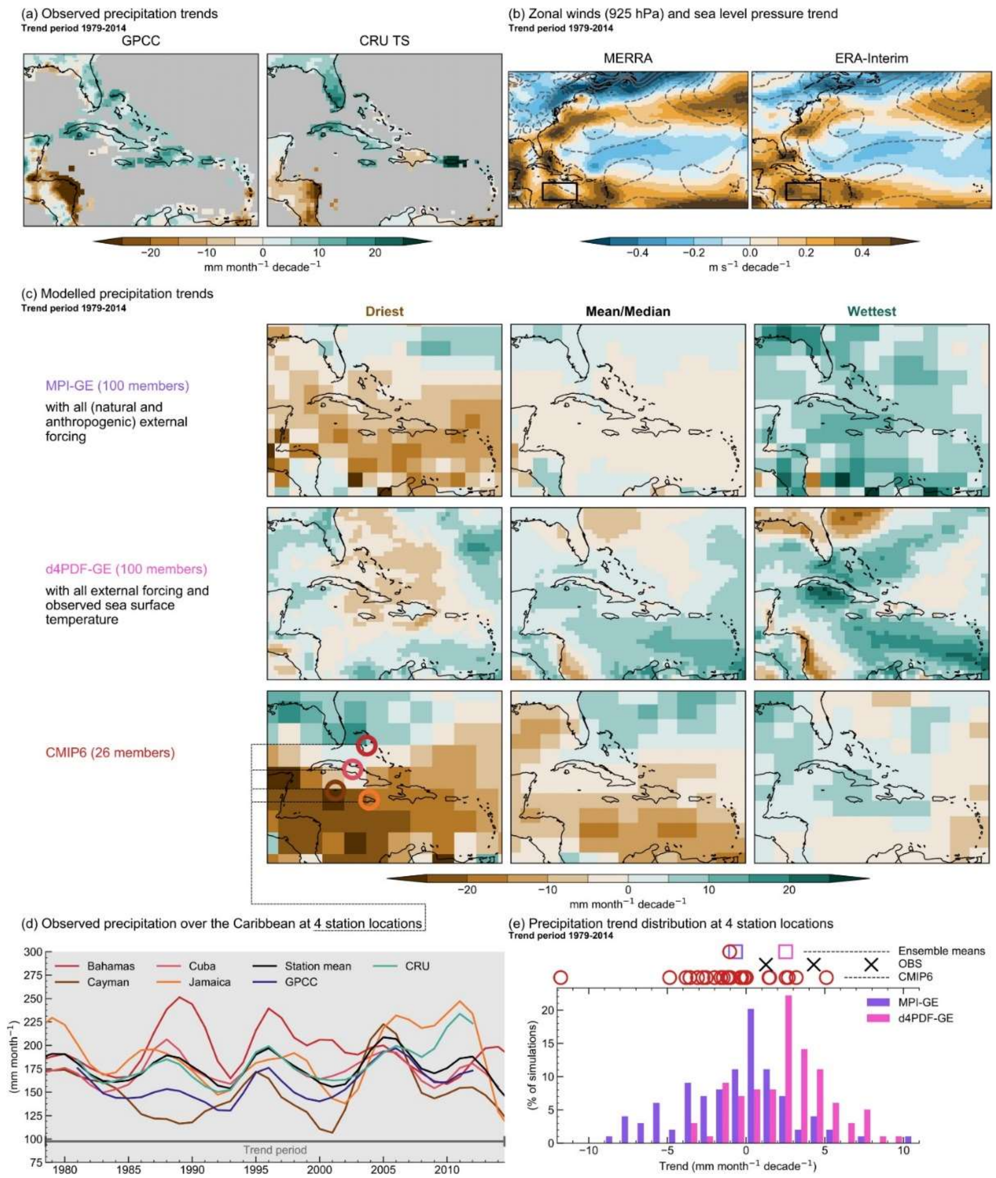

Figure 10.19: (a) Observed trends in June to August precipitation (mm day^{-1} decade^{-1}) from GPCC version 2018 (Schneider et al., 2017) and CRU TS version 4.02 (Harris et al., 2014) over the Caribbean from 1979 to 2014. (b) Trends in June to August zonal winds at 925 hPa (m s^{-1} decade^{-1}, in colour) and sea level pressure (solid (dashed) line contours indicate positive (negative) trends in 0.1 hPa decade^{-1} steps) over the tropical North Atlantic from MERRA (Rienecker et al., 2011) and ERA-Interim (Dee et al., 2011) with the area for the Caribbean low-level jet highlighted (12.5°N–17.5°N, 70°W–80°W). (c) As (a) but for model simulations. Top row: Driest, mean and wettest trends (in the mean over the four indicated station locations in the bottom left panel) from the 100 members of the MPI-GE (Maher et al., 2019). Middle row: Driest, mean and wettest trends relative to the above station locations from the 100 members of the d4PDF-GE (Mizuta et al., 2017). Bottom row: Driest, median and wettest trends relative to the above station locations from historical simulations of 26 CMIP6 models. (d) Time series of average June to August precipitation for four stations (Bahamas in dark red, Cuba in light red, Cayman in brown, Jamaica in orange) and the mean over this four stations (in black) as well as the station location mean extracted from GPCC and CRU TS gridded data. The filter is the same as the one used in Figure 10.11. (e) Distribution of mean precipitation trends for the four station locations between 1979 and 2014 for MPI-GE (violet histogram), d4PDF-GE (pink histogram), historical simulations from a set of 26 CMIP6 models (red circles), observations (means over station observations, GPCC and CRU TS, black crosses) and ensemble mean trends. All trends are estimated using ordinary least squares.

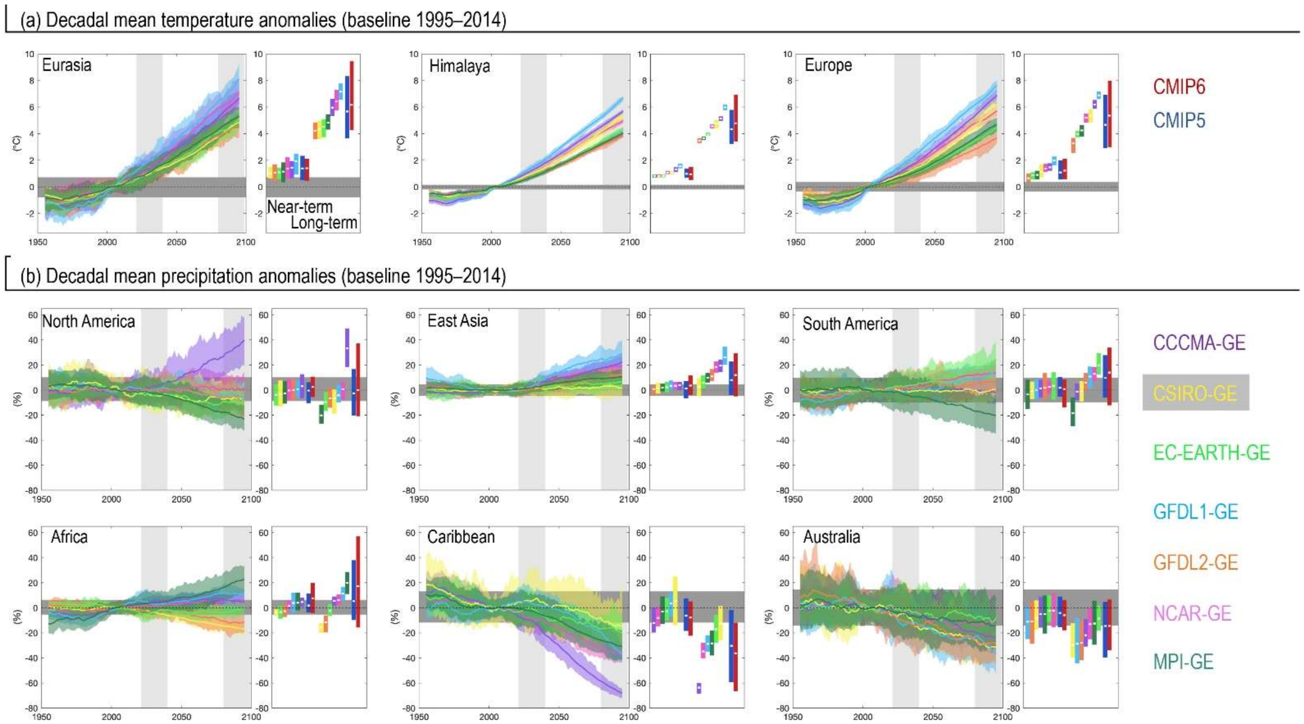

Figure 10.20: (a) Time series of simulated decadal mean air temperature anomalies (baseline 1995–2014) for regions of Eurasia, Himalaya and western Europe (see Figure 10.11 for the exact regional boundaries). Box plots indicate simulated decadal mean temperature anomalies averaged over near-term (2021–2040) and long-term (2081–2100) future periods. Models include seven initial-condition large ensembles, as in (Deser et al., submitted), 39 CMIP5 and 22 CMIP6 models that all have pre-industrial, historical and scenario simulations (RCP8.5 for CMIP5 and SSP5-8.5 for CMIP6 models). (b) As in (a) but for precipitation anomalies. The regions are sub-regions of North America, East Asia, South America, Africa, Caribbean and Australia (as in Figure 10.11).

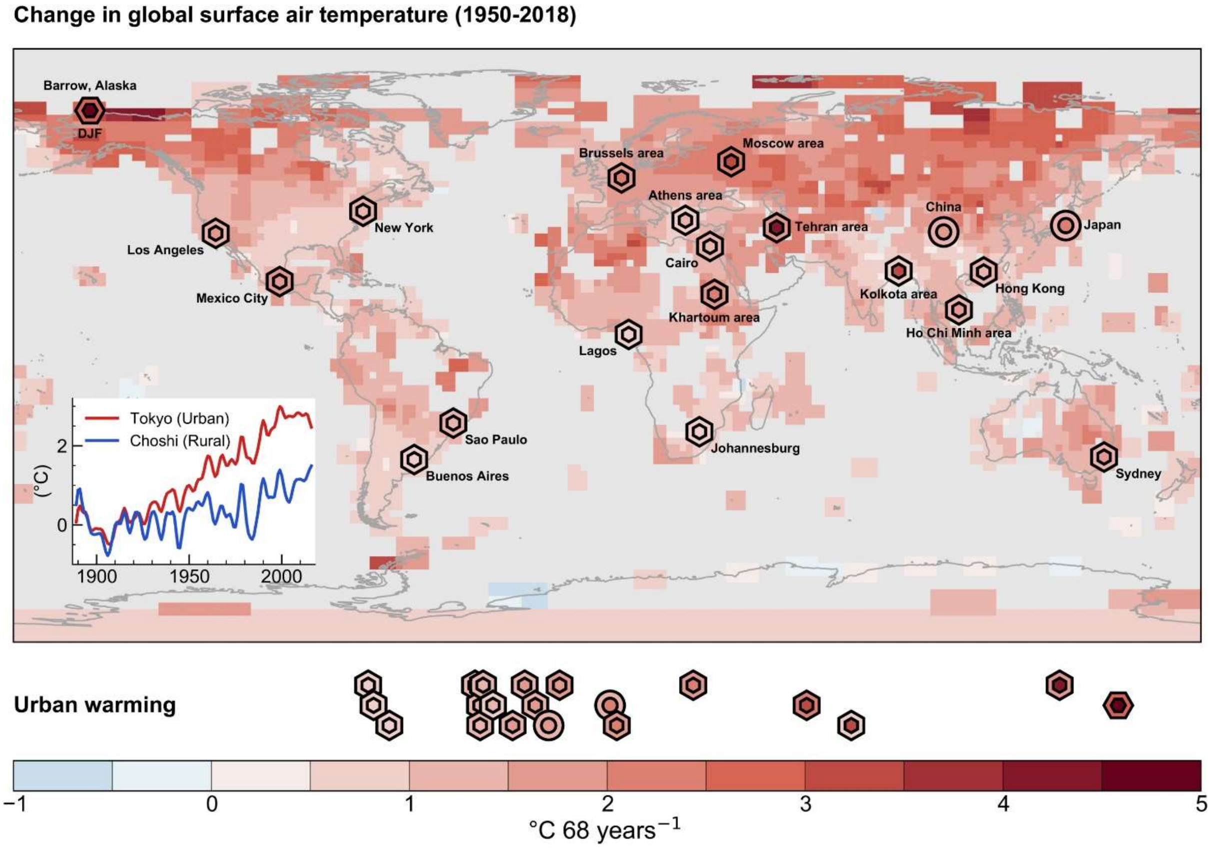

Box 10.2, Figure 1: Change in the annual mean surface temperature over the period 1950–2018 based on local linear trend retrieved from the GISTEMP data (Lenssen et al., 2019). This background warming is added to the local warming that has been reported during 1950–2018 in the literature from historical urbanization in different cities and plotted on top of the background as hexagon for each city. The colour of the circles refers to the magnitude of the urban warming calculated as the background warming plus the historical urbanization warming. This map has been compiled using the following studies: (Ajaaj et al., 2018; Alizadeh-Choobari et al., 2016; Bader et al., 2018; Chen et al., 2016; Chrysanthou et al., 2014; Doan et al., 2016; Dou et al., 2015; Elagib, 2011; Founda et al., 2015; Fujibe, 2009; Gaffin et al., 2008; Hinkel and Nelson, 2007; ; Li et al., 2018; Liao et al., 2017; Lokoshchenko, 2017; Polydoros et al., 2018; Sun et al., 2016; ; Wang et al., 2018; Zhou et al., 2016, 2017). The bottom left panel shows the low-pass filtered time series of the annual mean temperature anomalies observed in the urban station of Tokyo and the rural reference station in Choshi (Japan) (°C, baseline 1887-1917). The filter is the same as the one used in Figure 10.11.

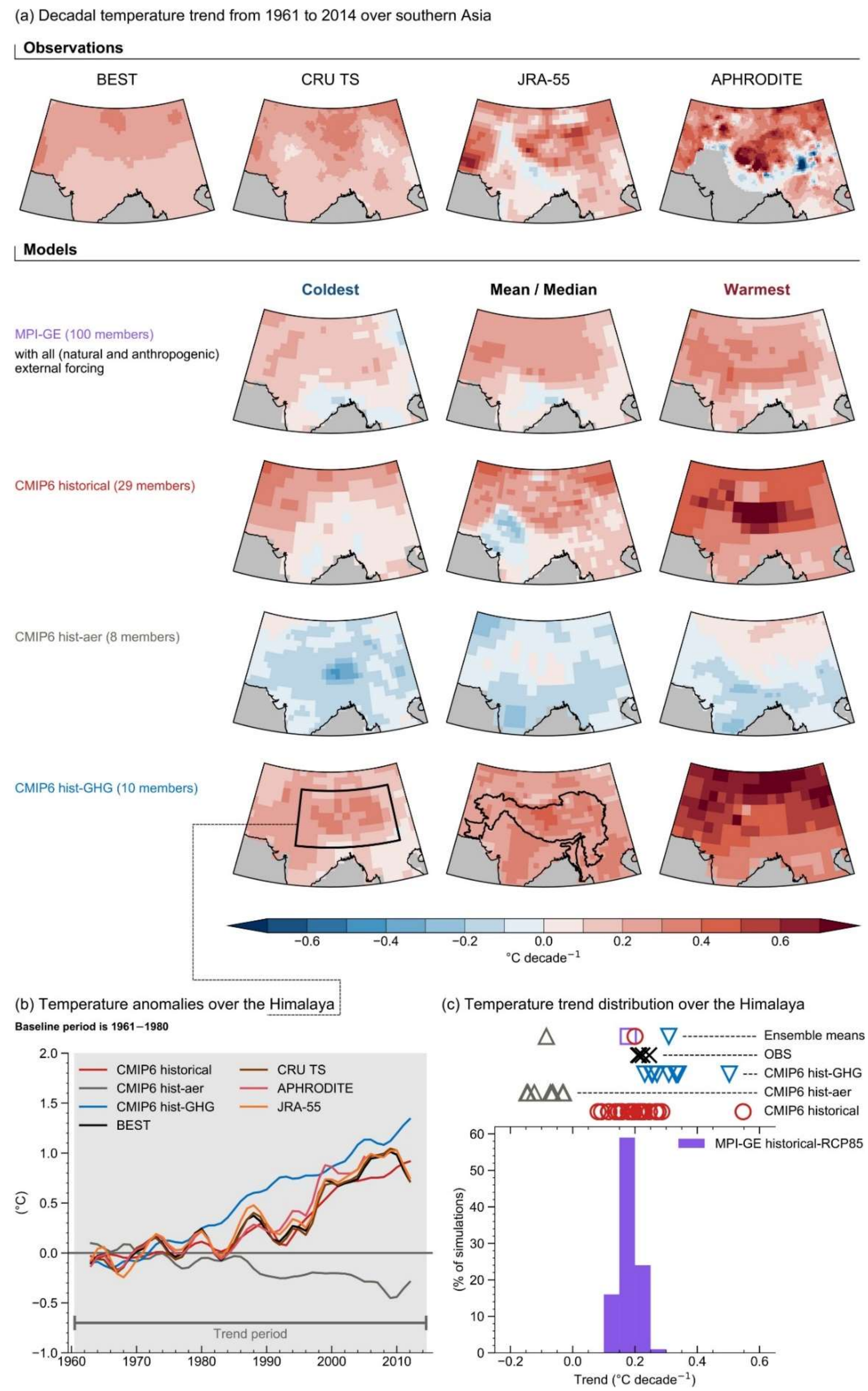

Cross-Chapter Box 10.3, Figure 1: Historical annual-mean surface air temperature linear trend (°C decade^{-1}) and its attribution over the Hindu Kush Himalaya (HKH) region. (a) Top row: Observed trends from the Berkeley surface temperature (BEST) dataset (Rohde et al., 2013), Climatic Research Unit Time Series (CRU TS) version 4.02 (Harris et al., 2014), the Japanese 55-year Reanalysis (JRA-55) (Kobayashi and Iwasaki, 2016) for 1961–2014 and from Asian Precipitation-Highly-Resolved Observational Data Integration Towards Evaluation (APHRODITE) V1204R1 (Yasutomi et al., 2011) for 1961–2007. Second row: Coldest, mean, and warmest trends (relative to the region enclosed in the black quadrilateral, fifth row) from the 100 members of the Max-Planck Institute grand ensemble (MPI-GE) (Maher et al., 2019). Third row: coldest, median, and warmest trends from CMIP6 historical 29 members. Fourth and fifth rows: coldest, median, and warmest trends from CMIP6 aerosol-only nine members and greenhouse gas-only ten members, respectively. The black shape in the last row second column map is the HKH boundary. (b) Time series of annual-mean surface air temperature anomalies (°C, baseline 1961–1980) over the region enclosed in the black quadrilateral (25°N–40°N, 75°E–105°E) in (a) bottom left map. Black, brown, orange, red, dark red, grey, and blue lines show low-pass filtered time series for BEST, CRU TS, JRA-55, APHRODITE, CMIP6 all-forcing historical mean, CMIP6 aerosol-only mean, and CMIP6 greenhouse gas-only mean, respectively. The filter is the same as the one used in Figure 10.11. (c) Distribution of annual mean surface air temperature trends (°C decade^{-1}) over the region enclosed in the black quadrilateral (25°N–40°N, 75°E–105°E) from 1961 to 2017 for ensemble means, the MPI-GE (violet histogram), and individual members of CMIP6 all-forcing historical (red circles), CMIP6 greenhouse gas-only (blue triangles), CMIP6 aerosols-only (grey triangles), and observations (black cross).

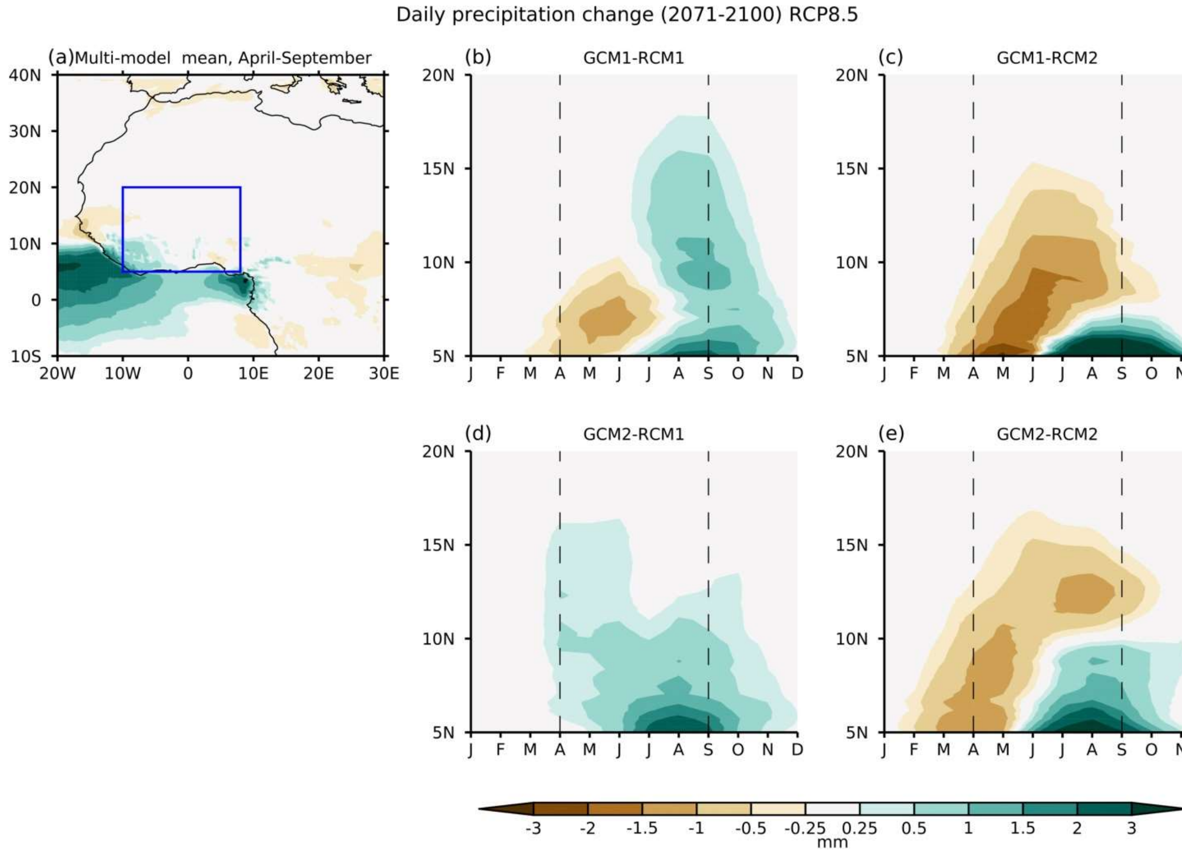

Figure 10.21: Illustration of how using different tools can result in different and potentially conflicting information. Change in daily precipitation (2071–2100 RCP8.5 relative to 1981–2010) over West Africa as simulated by an ensemble of GCM-driven RCMs. (a) Change in daily precipitation (mm) for April to September, as mean of 17 CORDEX models (Dosio et al., submitted) (b-e) Time-latitude diagram of daily precipitation change for four selected RCM-GCM combinations. For each month and latitude, model results are averaged along the longitude between 10°W–10°E (blue box in a). Different CGM-RCM combinations can produce substantially different and contrasting results, when the same RCM is used to downscale different GCMs (b, d), or the same GCM is downscaled by different RCMs (d, e). GCM1=IPSL-IPSL-CM5A, GCM2=ICHEC-EC-EARTH, RCM1=RCA4, RCM2=REMO2009.

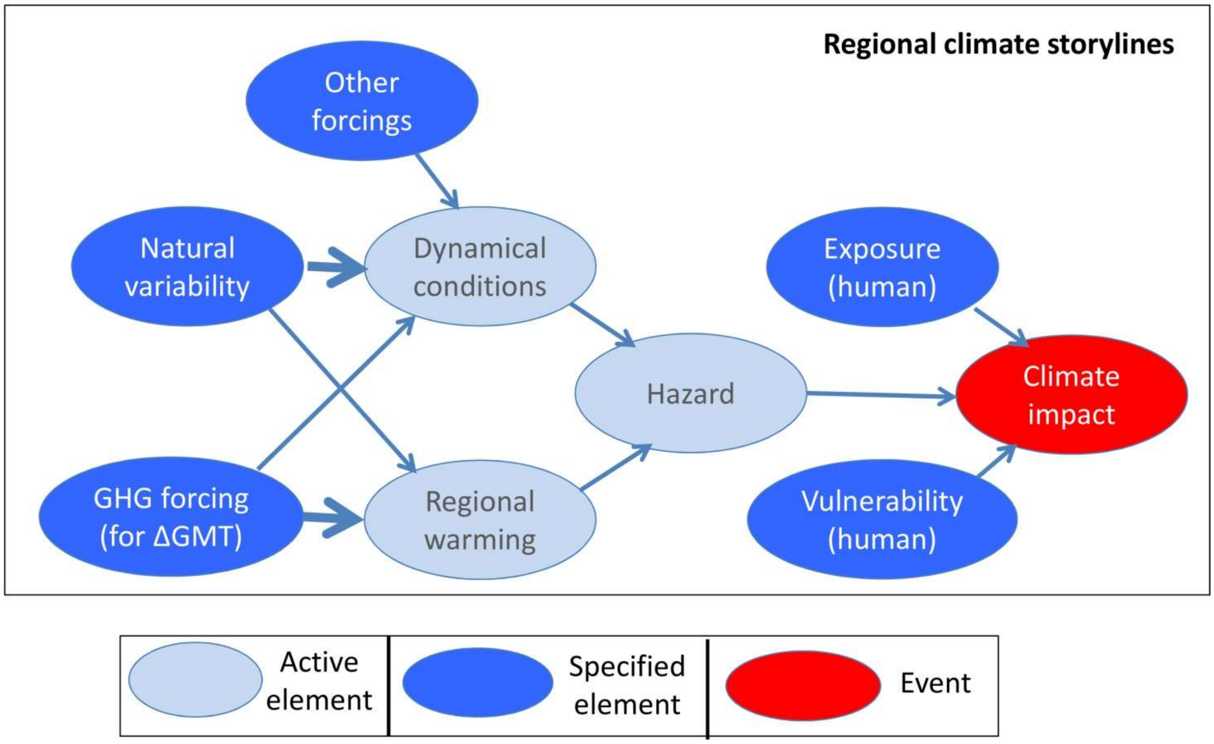

Figure 10.22: Schematic of regional climate storylines consistent with a particular climate impact of concern (red), which is associated with a meteorological hazard such as a long-term trend or a short-term event. The hazard involves a combination of thermodynamic factors linked to regional warming and particular dynamical conditions. Storylines express the fact that the same antecedent conditions could have more than one explanation in terms of the role of greenhouse gas forcing, other forcings affecting the dynamical conditions that do not scale with global-mean warming (e.g. ozone depletion, regional aerosol forcing), and natural variability. The dark blue elements represent the specified elements that define the storyline. The thicker arrows indicate that regional warming is mainly determined by greenhouse gas forcing, whilst the dynamical conditions are mainly determined by natural variability. Adapted from Shepherd (2019).

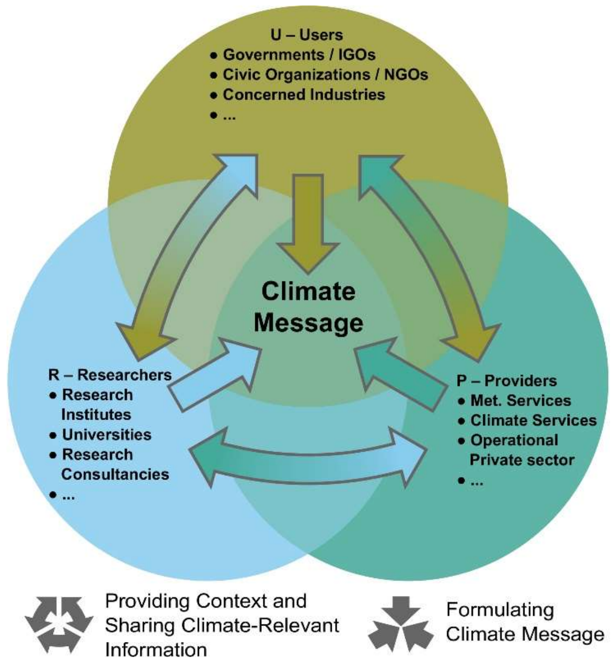

Figure 10.23: Effective messaging requires shared development of the actionable information that engages all parties involved and the values that guide their engagement. Participants in the development of climate messages come from varying perspectives, based in part on their professions and communities. Each of the three broad categories shown in the Venn diagram (U, P, R) is not a homogenous group, and often has a diversity of perspectives, values and interests among its members. The subheadings in each category are illustrative and not all-inclusive. The arrows connecting those categories represent the distillation process of providing context and sharing climate relevant information. The arrows that point toward the centre represent the distillation of climate messages that involves all three categories.

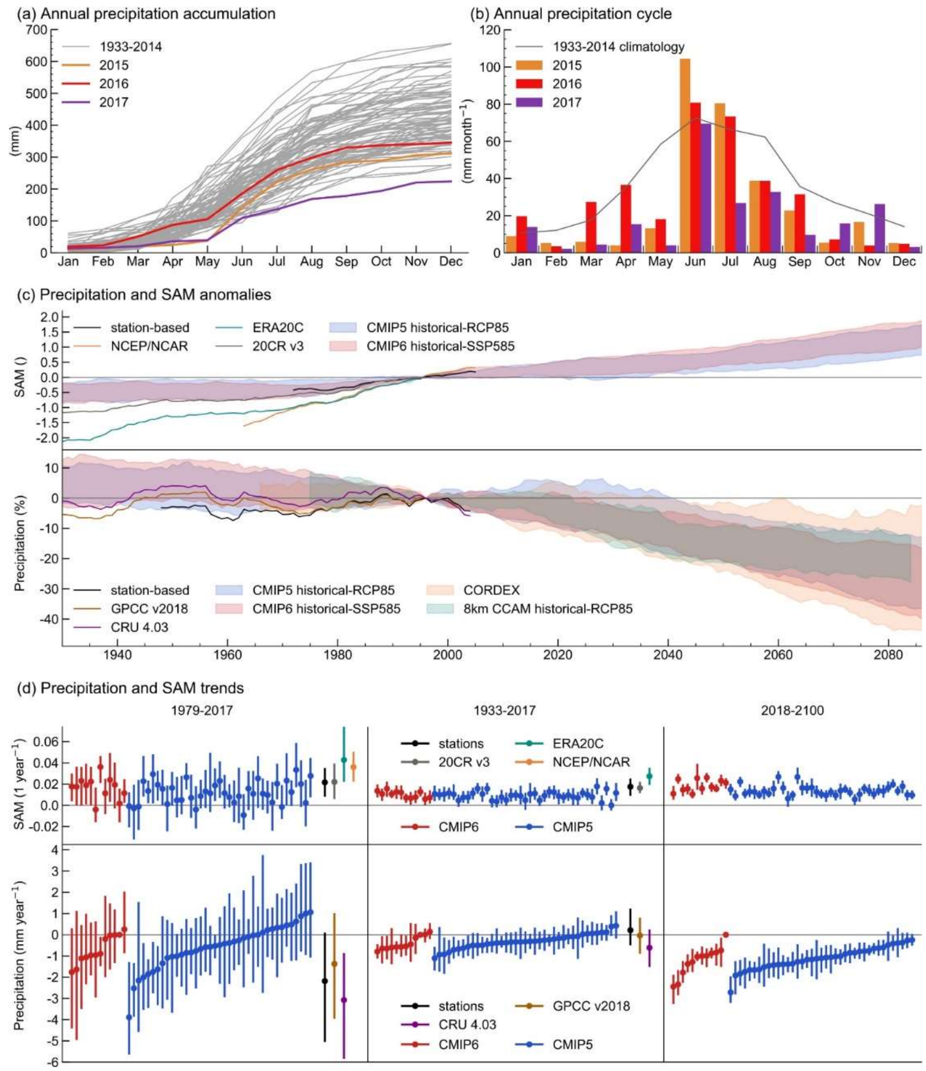

Figure 10.24: Historical and projected rainfall and Southern Annular Mode (SAM) over the Cape Town region. (a) Yearly accumulation of rainfall (in mm) obtained by summing monthly totals between January and December, with the drought years 2015–2017 highlighted in colour. (b) Monthly rainfall for the drought years (in colour) compared with the 1981–2014 climatology (grey line). Rainfall in (a) and (b) is the average of 20 quality controlled and gap-filled series from stations within the Cape Town region (31ºS–35ºS, 18ºW–20.5ºW). (c) Time series of historical and projected rainfall anomalies (%, baseline 1980–2010) over Cape Town region and SAM index. Observed data presented as 30-year running means of relative total annual rainfall over the Cape Town region for station-based data (black line, average of 20 stations as in (a) and (b)), and gridded data (average of all grid cells falling within 31ºS–35ºS, 18ºW–20.5ºW): the Global Precipitation Climatology Centre (GPCC) version 2018 (Schneider et al., 2017) (brown line) and the Climate Research Unit (CRU TS) version 4.03 (Harris et al., 2014) (green line). Model ensemble results presented as the 90th-percentile range of relative 30-year running means of 39 CMIP5 (blue shading), 12 CMIP6 (red shading), 6 COREX driven by 1 to 10 GCMs (orange shading) and 6 CCAM (green shading) individual ensemble member's rainfall, respectively. SAM calculated from sea-level pressure reanalysis and GCM data as per Gong and Wang (1999) and averaged over the aforementioned bounding box. The orange, green and grey lines correspond to NCEP/NCAR (Kalnay et al., 1996), ERA20C (Poli et al., 2016b) and 20CR v3 (Slivinski et al., 2019), respectively. (d) Historical and projected trends in rainfall over the Cape Town region and in SAM index. Observations and gridded data processed as in (c). Trends calculated as Theil-Sen trend with block-bootstrap confidence interval estimate. Markers show median trend, bars 95% confidence interval. GCMs in each CMIP group ordered according to the magnitude of trend in rainfall, and the same order is maintained in panels showing trends in SAM.

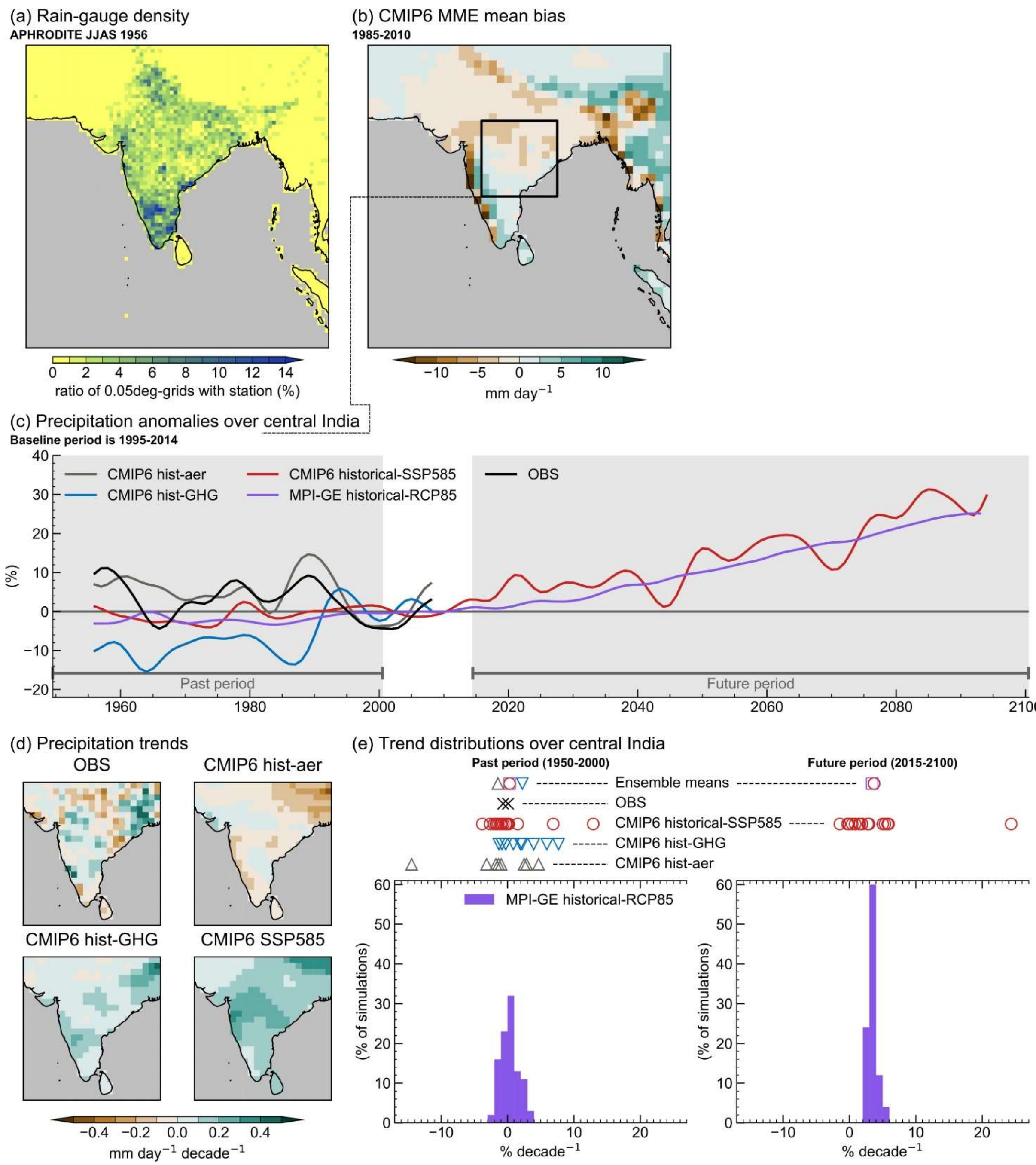

Figure 10.25: Changes in the Indian monsoon in the historical and future periods: (a) Observational uncertainty demonstrated by a snapshot of rain-gauge density in the APHRODITE V1101 (Yatagai et al., 2012) 0.5°-daily precipitation dataset for June to September 1956. (b) Multi-model ensemble (MME) mean bias of 16 CMIP6 models for June to September precipitation (mm day^{-1}) compared to GPCC v2018 (Schneider et al., 2017; doi:10.5676/DWD_GPCC/FD_M_V2018_100) observations for the 1985-2010 period. (c) Time series of June to September precipitation averaged over the central India box (15°N–25°N, 75°E–85°E) shown in panel (b) in GPCC (black line) since 1950 in comparison with the MME-mean from the all-forcings historical experiments in 16 CMIP6 models (red line), and with changes in aerosol-only (hist-aer, 8 models, blue line) and greenhouse gas-only (hist-GHG, 9 models, grey line). MME-mean change in the SSP5-8.5 experiment for future projections out to 2100. CMIP6 results are compared with historical and future simulations of the MPI Grand Ensemble (MPI-GE historical-RCP85, violet line) (Maher et al.,

2019). Anomalies are computed with respect to the 1995–2014 baseline and a weighted 13-year low-pass filter is applied. The low-pass filter has been used in AR4, Chapter 3, Appendix 3.A. It has 13 weights 1/576 [1-6-19-42-71-96-106-96-71-42-19-6-1] and for annual data, its half-amplitude point is about a 12-year period, and the half-power point is 16 years. (d) Maps of rainfall trends (mm day^{-1} decade^{-1}) in GPCC observations, the CMIP6 MME-mean of hist-aer runs, the CMIP6 MME-mean of greenhouse gas-only runs over the 1950–2000 period and an example MME-mean future projection from CMIP6 SSP5-8.5 for 2015–2100. (e) Histogram to illustrate the role of internal variability for historical 1950–2000 (left) and future 2015–2100 (right) trends in South Asian monsoon rainfall (% decade^{-1}) in the MPI-GE (expressed as percentage of simulations showing a trend in each bin, violet histogram). Individual members as well as ensemble means of CMIP6 historical-SSP5-8.5 (all-forcings, red circles), hist-aer (grey triangles) and hist-GHG (light blue triangles) are also shown, along with observed estimates from GPCC and CRU TS v4 (doi: 10.5285/edf8febfdaad48abb2cbaf7d7e846a86). All trends are estimated using ordinary least squares.

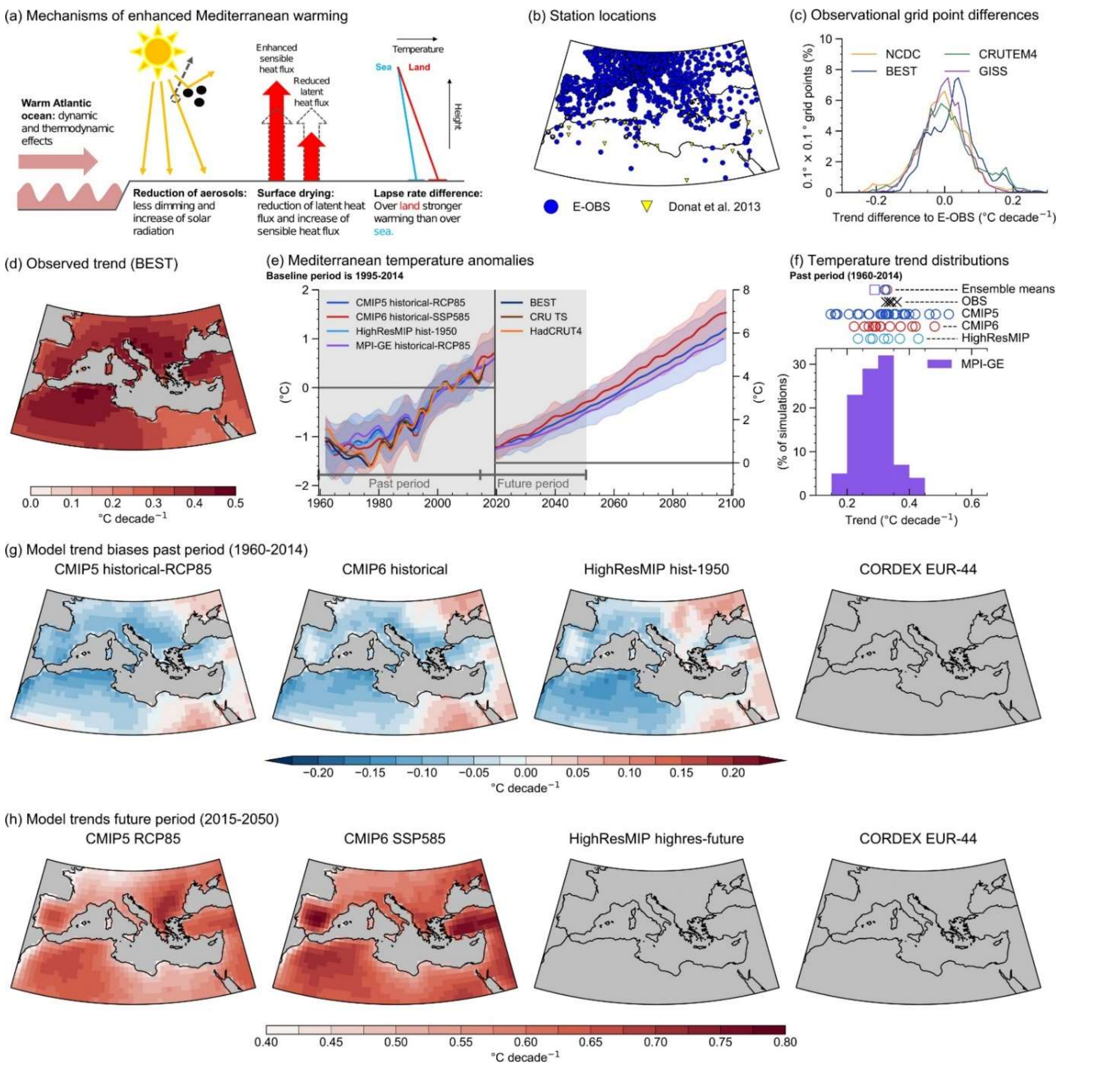

Figure 10.26: Aspects of Mediterranean summer warming. (a) Mechanisms and feedbacks involved in enhanced Mediterranean summer warming. (b) Locations of observing stations in E-OBS v19e (Cornes et al., 2018) and Donat et al. (2014). (c) Differences in temperature observational data sets with respect to E-OBS for the land points between the Mediterranean Sea and 46°N and west of 30°E. (d) Observed summer (June to August) surface air temperature trends (°C decade^{-1}) over the 1960–2014 period from BEST (Rohde et al., 2013) dataset. (e) Time series of area averaged (25°N–50°N, 10°W–40°E) land point summer temperature anomalies (°C, baseline 1995–2014). Black, brown, orange and violet lines show low-pass filtered temperature of BEST, CRU TS v4.02 (Harris et al., 2014), HadCRUT4 (Morice et al., 2012) and the MPI-GE (Maher et al., 2019), respectively. Dark blue, red and light blue lines and shadings show low-pass filtered ensemble means and standard deviations of CMIP5 (30 members), CMIP6 (15 members) and HighResMIP (7 members), respectively. The filter is the same as the one used in Figure 10.11. (f) Distribution of 1960–2014 summer temperature trends (°C decade^{-1}) for observations (black crosses), the MPI-GE (violet histogram) and for ensemble means and single runs of CMIP5 (dark blue circles), CMIP6 (red circles) and HighResMIP (light blue circles). (g) Bias in ensemble mean 1960–2014 trends (°C decade^{-1}) of CMIP5, CMIP6, HighResMIP and CORDEX in reference to BEST. (h) Projections of ensemble mean 2014–2050 trends (°C decade^{-1}) of CMIP5, CMIP6, HighResMIP and CORDEX. All trends are estimated using ordinary least-squares. **[Placeholder: The CORDEX and HighResMIP panels need to be completed.]**

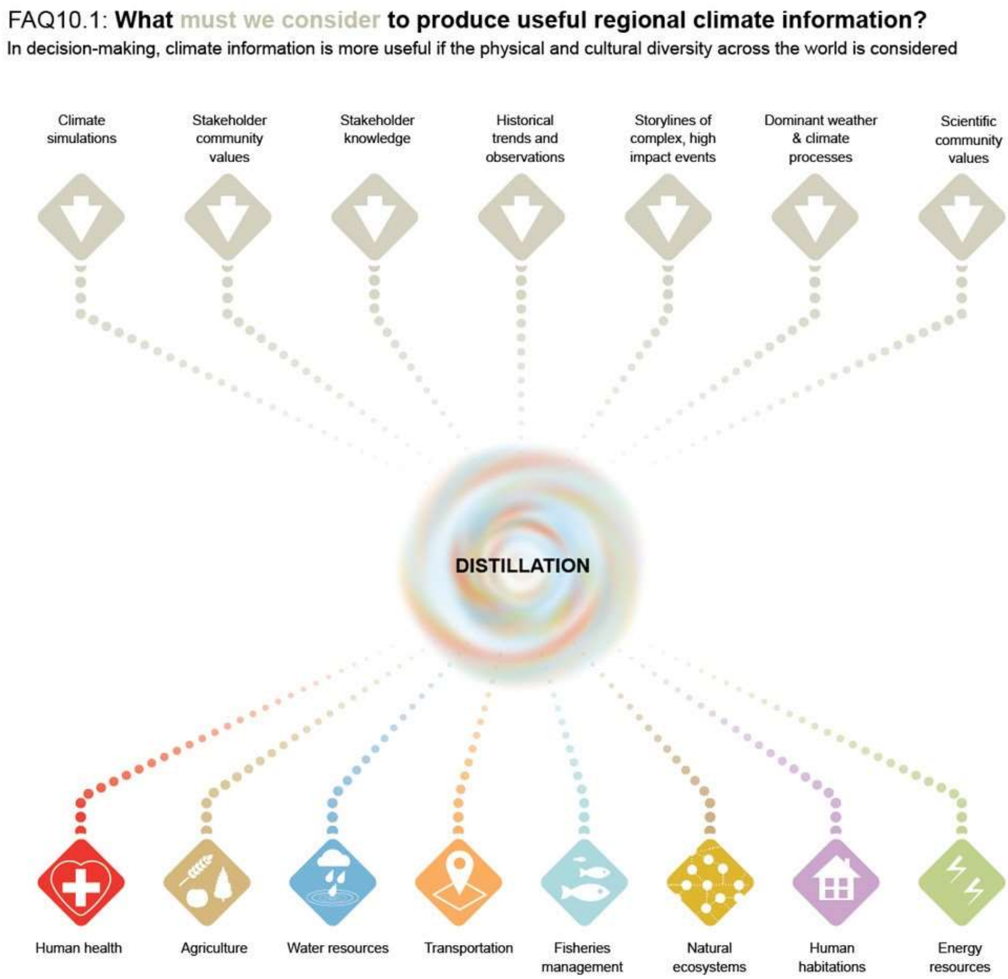

FAQ 10.1, Figure 1: Climate information for decision makers is more useful if the physical and cultural diversity across the world is considered. The figure illustrates schematically the broad range of knowledge that must be blended with the diversity of users to distil information that will have relevance and credibility.

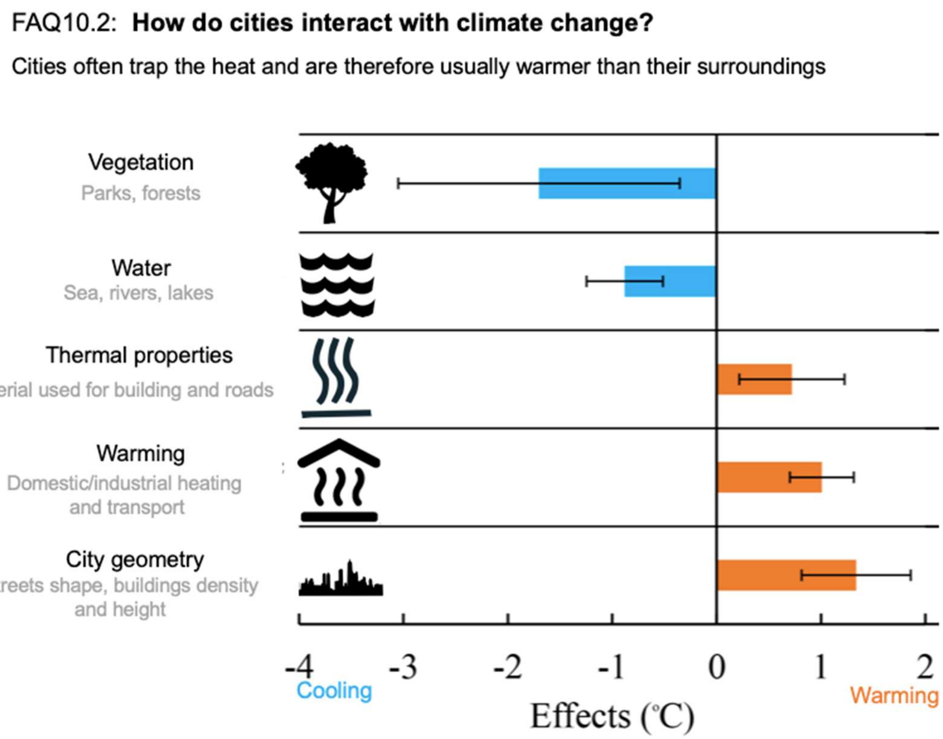

FAQ 10.1, Figure 2: Various factors contribute to either warm up or cool down urban areas, compared to their surroundings. Overall, cities tend to be warmer than their surroundings. This is called the "urban heat island" effect. Values are taken from the recent literature.